Engineering Bioorthogonal Chemistries: Copper-Free Click Chemistry and the Quadricyclane Ligation

By

Chelsea Gloria Gordon

A dissertation submitted in partial satisfaction of the

requirements of the degree of

Doctor of Philosophy

in

Chemistry

in the

Graduate Division

of the

University of California, Berkeley

Committee in charge:

Professor Carolyn R. Bertozzi, Chair
Professor Robert G. Bergman
Professor Gerard Marriott

Spring 2015

Engineering Bioorthogonal Chemistries: Copper-Free Click Chemistry and the Quadricyclane Ligation

© 2015

By Chelsea Gloria Gordon

Abstract

Engineering Bioorthogonal Chemistries: Copper-Free Click Chemistry and the Quadricyclane Ligation

by

Chelsea Gloria Gordon

Doctor of Philosophy in Chemistry

University of California, Berkeley

Professor Carolyn R. Bertozzi, Chair

Bioorthogonal chemistries are reactions that are designed to proceed in living environments without perturbing endogenous biological functionalities. These reactions are valuable tools for labeling and studying biomolecules both *in vitro* and *in vivo,* often providing unique insights into dynamic, living processes. For a reaction to be considered bioorthogonal, it must proceed in aqueous solvents at physiological pH and temperature. The reaction must also be rapid and selective, generating a stable, covalent adduct that is not reactive towards biological functionalities. Finally, one of the reaction partners must be capable of installation onto the biomolecule of interest.

A major motivator in the development of bioorthogonal chemistries is their potential utility in imaging and studying biomolecules in living animals. Chapter one chronicles advancements in the use of bioorthogonal reactions to tag biomolecules in multicellular organisms, focusing on the most prevalent reactions developed to date — the Staudinger ligation, copper-click chemistry, copper-free click chemistry, and the tetrazine ligation. Examples are provided to highlight the importance of fast reaction kinetics as well as pharmacokinetics on the success of a ligation *in vivo*. Chapter one also provides commentary on unmet challenges in the field as well as an outlook on future advancements.

The *in vivo* applications of bioorthogonal chemistry discussed in chapter one serve as motivation for the experimental work presented in chapter two. Here, we describe our efforts to understand the factors that contribute to the kinetic profile of the copper-free click reaction. Copper-free click chemistry is a bioorthogonal 1,3-dipolar cycloaddition between azides and strained cyclooctynes to form triazoles. The reaction has seen widespread use in selectively tagging biomolecules both *in vitro* and *in vivo*. These successes have prompted the development of cyclooctyne analogs with improved reactivity toward the azide. However, predicting a cyclooctyne's reactivity is challenging, requiring researchers to design and undertake lengthy syntheses of alkynes that may or may not prove successful bioorthogonal reagents. In chapter two, we discuss our work towards defining and predicting the effects of strain and electronics on the reactivity of a cyclooctyne reagent. Through synthesis of analogs of biarylazacyclooctynone (BARAC), the fastest cyclooctyne developed to date, and subsequent reactivity measurements, we

gain new insights into the effects of cyclooctyne strain and electronics on reactivity. As well, through computational modeling of our BARAC analogs we conclude that the distortion/interaction model of 1,3-dipolar cycloaddition kinetics serves as a valuable predictor of cyclooctyne reactivity in the copper-free click reaction.

Chapter three describes our motivation to develop new bioorthogonal ligations, highlighting the dearth of mutually orthogonal reactions capable of achieving multiplexed imaging. In addition, we discuss the need for bioorthogonal chemistries with new functional capabilities (i.e. polymerizations, reversible reactions, etc.). We then introduce the quadricyclane (QC) ligation, a new bioorthogonal reaction developed in the Bertozzi lab. The QC ligation is a formal [2σ+2σ+2π] reaction between QC and nickel bis(dithiolene). The reaction has been shown to fulfill many of the requirements of bioorthogonality, but no method of incorporating the QC functionality into a biomolecule of interest has been demonstrated. In chapter three, we discuss our use of the pyrrolysine synthetase/$tRNA_{CUA}$ system for site-specific incorporation of a QC amino acid into a protein and subsequent tagging of this QC functionality with a nickel bis(dithiolene) reagent.

In chapter four we discuss efforts to further develop the QC ligation, exploring new chemical transformations accessible through this unique reaction. Specifically, we analyze the photodissociation of the QC/nickel bis(dithiolene) adduct to form nickel bis(dithiolene) and norbornadiene, a transformation that has the potential to make the QC ligation a "click-unclick" reaction. In addition, we have begun to analyze possible secondary reaction partners for the norbornadiene product of the photodissociation. Chapter four chronicles our ongoing work to optimize these unique chemical transformations for reversible tagging of model proteins.

This dissertation is dedicated to my family.

Engineering Bioorthogonal Chemistries: Copper-Free Click Chemistry and the Quadricyclane Ligation

Table of Contents

List of Figures……... iv
List of Schemes……. vi
List of Tables……. vi
Acknowledgements……vii

Chapter 1. A Review of Bioorthogonal Chemistries and Their Applications *In Vivo*
Introduction……... 1
Methods of Incorporating Bioorthogonal Functional Groups into Biomolecules in Living Animals…….. 2
Metabolic Glycan Engineering……. 2
Pre-Targeting…… 4
Bioorthogonal Chemistries for Imaging and Labeling Biomolecules *In Vivo*……... 5
The Staudinger Ligation…… 5
The Staudinger Ligation in Mice…….. 5
Copper-Click Chemistry……... 7
Cu(I) Ligands to Reduce Toxicity…… 8
Copper-Click Chemistry in Zebrafish…….. 9
Copper-Free Click Chemistry…….. 11
Copper-Free Click Chemistry in Zebrafish…….. 13
Copper-Free Click Chemistry in *C. Elegans*…… 15
Copper-Free Click Chemistry in Mice……. 16
Background Reactivity of Cyclooctynes…….. 20
The Tetrazine Ligation……. 20
The Tetrazine Ligation in Mice…… 23
The Future of *In Vivo* Bioorthogonal Chemistry…….. 28
In Vivo Self-Assembling Drugs…… 28
Bioorthogonal Prodrugs…… 30
Conclusion…… 31
References……. 32

Chapter 2. Reactivity of Biarylazacyclooctynones in Copper-Free Click Chemistry
Introduction……... 39
The Distortion/Interaction Model…… 41
Design of Cyclooctyne Analogs…… 43
Analog Synthesis…….. 44
BARAC's Structure…….. 47
Reactivity of BARAC and Analogs…….. 48
Alkyne Bond Angles as a Measure of Reactivity……. 52

Effects of BARAC's Amide Bond Structure on Reactivity and Regioselectivity…… 54
Conclusion…… 57
Future Directions…….. 58
Materials and Methods……. 59
General Procedures……... 59
Synthetic Procedures……. 59
2D NOESY Analysis of Triazole Adducts of **2.10** and **2.11**……. 82
NMR Kinetic Analysis…….. 84
General Procedures…… 84
Kinetics Analysis Procedures…… 85
Computational Methods…… 96
References……. 100

Chapter 3. The Quadricyclane (QC) Ligation: Protein Labeling via Site-Specific Incorporation of a QC Amino Acid
Introduction……104
The Quadricyclane Ligation…….. 107
Site-Selective Incorporation of QC Into a Protein……111
Components of a QC Amino Acid Incorporation Experiment…….. 114
QC-sfGFP Expression……116
Labeling QC-sfGFP-His_6 via the Quadricyclane Ligation…… 118
Eliminating the His_6 Tag……... 120
Conclusion……. 122
Materials and Methods……...122
Synthesis of Quadricyclane Amino Acid (QCaa) **3.18** and Nickel Bis(dithiolene) Biotin **3.19**……122
General Procedures……... 122
Synthetic Procedures……..123
Non-Natural Amino Acid Incorporation and QC Ligation Labeling Experiments……125
Materials and Equipment……125
General Procedure for Transformation of *E. coli* with plasmids *psfGFP150TAGHis6PylT* or *psfGFP150TAGFLAGPylT* and/or *pBkPylRS*……126
Expression of QC- and Boc-sfGFP-His_6 or QC- and Boc-sfGFP-FLAG……..126
General QC Ligation Procedure…….129
General Western Blotting Procedure……..129
Cloning to Exchange His_6 Tag for FLAG Tag…….....130
References……..135

Chapter 4: A "Click-Unclick" Quadricyclane Ligation
Introduction……140
Reversible Bioconjugations…….. 140
Bioconjugations That Are Responsive to Environmental Cues……142

A "Click-Unclick" Quadricyclane Ligation……...144
Background……144
^{1}H NMR Analysis of Photolysis……146
Proof-of-Concept Photolysis on a Model Protein……..147
Towards a "Click-Unclick-Click" Quadricyclane Ligation……...150
Conclusion……154
Materials and Methods……...154
Compound Synthesis……154
General Procedures……154
Synthetic Procedures……...155
Photolysis Experiments and Norbornadiene Model Reactions……..156
General Procedures……156
^{1}H NMR Analysis of the Photolysis of Adduct **4.4**……... 157
Photodissociation of Adduct **4.5**……159
Optimization of the Photodissociation Reaction via Addition of Excess QCOAc to Scavenge Released **3.19**……...159
Optimization of the Photodissociation Reaction via 1) Addition of Excess QCOAc to Scavenge Released **3.19** and 2) Reduced Protein Concentration……160
General Western Blotting Procedure……161
"Click-Unclick-Click" Experiments With Tetrazine and Tetrazole……..161
Analysis of the Reaction of Tetrazine with Norbornadiene on a Model Protein……161
Photo-Click Chemistry on a Model Norbornadiene-Tagged Protein……162
References……...163

Appendix A: ^{1}H and ^{13}C NMR Spectra……..166
Compounds from Chapter 2……...167
Compounds from Chapter 3……...249
Compounds from Chapter 4……...256

Appendix B: X-Ray Crystallography Data……260
Monofluorinated Cyclooctyne (MOFO, **2.21**)……...261
Biarylazacyclooctynone (BARAC, **2.1**)…… 268
Dimethoxyazacyclooctyne (DIMAC, **2.20**)……...274
Second Generation Difluorinated Cyclooctyne (DIFO2, **2.22**)…… 281

Appendix C: Cartesian Coordinates of B3LYP/6-31G9d) Stationary Points.... 293
B3LYP/6-31G(d) and MeCN Solvation Energetics…….. 294
Reactants: *Cis* Lactam Compounds……... 294
Reactants: *Trans* Lactam Compounds……... 302
Transition States: *Cis* Lactam *Syn* Regioisomers…….. 311
Transition States: *Trans* Lactam *Syn* Regioisomers…….. 321
Transition States: *Cis* Lactam *Anti* Regioisomers……. 331
Transition States: *Trans* Lactam *Anti* Regioisomers……. 342

Isomerization Transition States……. 352

List of Figures

Figure 1.1 The bioorthogonal reaction between X and Y proceeds in physiological environments without perturbing native chemical functionalities…… 1
Figure 1.2 Metabolic glycan engineering…….. 3
Figure 1.3 Bioorthogonal pre-targeting……. 4
Figure 1.4 Mechanism of the Staudinger Ligation…… 5
Figure 1.5 *In vivo* labeling of cell-surface sialic acid residues via the Staudinger ligation…… 6
Figure 1.6 Pre-targeting approach to *in vivo* labeling via the Staudinger ligation…….. 7
Figure 1.7 The copper-click reaction……. 7
Figure 1.8 Cu(I) ligands used to accelerate the copper-click reaction…….. 8
Figure 1.9 Copper-click chemistry *in vivo*..... 10
Figure 1.10 Imaging the glycome of developing zebrafish embryos using copper-click chemistry and BTTAA or BTTES……... 10
Figure 1.11 Copper-free click chemistry…….. 11
Figure 1.12 Cyclooctyne analogs for copper-free click chemistry……... 12
Figure 1.13 Copper-free click chemistry for labeling the glycome of living zebrafish…….. 13
Figure 1.14 Imaging reorganization of glycans at cleavage furrows of mitotic cells in developing zebrafish……. 14
Figure 1.15 Additional azidosugars used in zebrafish labeling experiments with copper-free click chemistry…….. 14
Figure 1.16 Two color imaging of glycan dynamics in *C. elegans*…….. 15
Figure 1.17 Copper-free click chemistry and the Staudinger ligation *in vitro* and *in vivo*……. 16
Figure 1.18 Pre-targeting experiment using copper-free click chemistry in mice……... 17
Figure 1.19 Imaging tumors in mice via pre-targeting with cyclooctyne-functionalized mesoporous nanoparticles……. 18
Figure 1.20 Copper-free click chemistry in mice using metabolic glycan labeling and a DIBAC-conjugated liposome…… 19
Figure 1.21 The tetrazine ligation…… 21
Figure 1.22 Analysis of tetrazine reactivity and stability…… 21
Figure 1.23 Dienophiles used in the tetrazine ligation…… 22
Figure 1.24 Labeling tumors in mice via the tetrazine ligation…….. 23
Figure 1.25 Labeling TCO-antibodies *in vivo* using a tetrazine-functionalized dextran polymer…… 24
Figure 1.26 Imaging tumors in mice via the tetrazine ligation using tetrazine-functionalized dextran polymers…… 25

Figure 1.27 Computational model predicting the effects of reaction rate and secondary clearance rate (AUC) on % reaction……. 26
Figure 1.28 Imaging tumors in mice via the tetrazine ligation using tetrazine-functionalized pHLIP peptides and TCO-liposomes……. 26
Figure 1.29 Optimization of TCO-antibody connectivity for *in vivo* tetrazine ligation…… 27
Figure 1.30 Self-assembling chemotherapeutic agents…… 29
Figure 1.31 Dinuclear ruthenium cytotoxin assembled via tetrazine/ cyclooctyne cycloaddition.…… 30
Figure 1.32 Doxorubicin prodrug activated via Staudinger reduction……. 30
Figure 1.33 Doxorubicin prodrug activated via tetrazine ligation…… 31
Figure 2.1 The copper-free click reaction……... 39
Figure 2.2 Reagent development for copper-free click chemistry…….. 40
Figure 2.3 Distortion/interaction model…….. 42
Figure 2.4 BARAC analogs designed for subsequent reactivity studies…… 44
Figure 2.5 BARAC analogs designed to analyze the effects of sterics on reaction rate……... 44
Figure 2.6 Structural analysis of BARAC…….. 47
Figure 2.7 Bond angles and reactivities of BARAC analogs……..49
Figure 2.8 Measuring the second order rate constant for the reaction between BARAC analogs and benzyl azide — a representative analysis with analog **2.3**…… 50
Figure 2.9 Flagpole methyl substituents sterically hinder the transition state…… 52
Figure 2.10 Strain modulation through rehybridization……55
Figure 2.11 Under Curtin-Hammett conditions, BARAC's amide conformation influences reactivity and regioselectivity…… 56
Figure 3.1 Cross-reactivity of bioorthogonal ligations……... 105
Figure 3.2 Modulating reactivity between two bioorthogonal reagents via (a) electronic or (b) steric modulation……..106
Figure 3.3 The quadricyclane (QC) ligation……107
Figure 3.4 Crystal structure of QC…….. 108
Figure 3.5 The redox non-innocence of nickel bis(dithiolene) ligands……...109
Figure 3.6 Stability of nickel bis(dithiolene) and its adduct with QC……109
Figure 3.7 Model QC labeling experiments on Bovine Serum Albumin (BSA)……..110
Figure 3.8 Pyrrolysine and analogs…….112
Figure 3.9 Selected non-natural amino acids incorporated into proteins via the pyrrolysine synthetase/$tRNA_{CUA}$ system……....113
Figure 3.10 Components of a non-natural amino acid incorporation experiment……..114
Figure 3.11 Plasmid *psfGFP150TAGHis$_6$PylT*……. 115
Figure 3.12 QC-sfGFP-His_6 expression…… 117
Figure 3.13 High-resolution mass spectrometry analysis of non-natural amino acid incorporation products……118
Figure 3.14 Labeling QC-sfGFP-His_6 via the quadricyclane ligation……...119

Figure 3.15 Labeling QC-sfGFP-His_6 in *E. coli* lysate via the QC ligation……..120
Figure 3.16 FLAG versus His_6 tag on sfGFP……121
Figure 4.1 Examples of reversible conjugation chemistries for modification of proteins and peptides……140
Figure 4.2 Reversible bioconjugation chemistries for amino-acid dependent peptide enrichment……... 141
Figure 4.3 "Photo-click" chemistries…….. 143
Figure 4.4 Oxidation-controlled click chemistry…… 144
Figure 4.5 Photodissociation of the QC/nickel bis(dithiolene) adduct……... 144
Figure 4.6 Mechanistic analysis of photolytic cleavage of nickel bis(dithiolene) adducts……... 145
Figure 4.7 ^{1}H NMR analysis of the photolytic cleavage of QC/nickel bis(dithiolene) adduct **4.4** to norbornadiene **3.13** and nickel bis(dithiolene) **4.2**……....146
Figure 4.8 Photodissociation of the QC adduct on a protein…….. 148
Figure 4.9 Optimization of the photodissociation reaction……. 149
Figure 4.10 Proposed bioorthogonal reaction of norbornadiene with tetrazine……..150
Figure 4.11 Analysis of the reaction of tetrazine with norbornadiene on a model protein…….. 151
Figure 4.12 Retro-Diels—Alder reaction of norbornadiene-tetrazine adduct…….152
Figure 4.13 1,3-dipolar cycloaddition between norbornadiene and nitrile imine……152
Figure 4.14 Photo-click chemistry on a model norbornadiene-tagged protein…… 153

List of Schemes

Scheme 2.1 Retrosynthetic Analysis of BARAC and Analogs…… 45
Scheme 2.2 Synthesis of BARAC and Analogs……... 46
Scheme 3.1 Synthesis of QCaa **3.18**……. 115
Scheme 3.2 Incorporation of QCaa into sfGFP in DH10β *E. coli*……..... 116

List of Tables

Table 2.1 Reactivity and alkyne bond angles…… 53

Acknowledgements

There are many people without whom this dissertation would not be possible. First and foremost, a huge thank you to Carolyn who has been an inspiring and encouraging mentor over the past six years. Throughout my time in her lab it has become clear that she is not only a brilliant scientist, she also truly cares about her students. She has provided so much support over the course of my graduate career in the form of scientific instruction and advice on life and careers. I am truly grateful for all of her efforts.

The Bertozzi lab would not run without the daily efforts of Asia Avelino, Olga Martinez, Cheryl McVaugh, and Sia Kruschke. They make sure we all have what we need to do our experiments, and worry about stocking lab supplies, balancing the budget, getting grants, and autoclaving media so we don't have to. They also organize all of the lab social activities like the holiday party, summer picnic, and spontaneous lab bakeoffs. I am so grateful to the hard work these amazing women do every day. I wouldn't be here without them.

I'm thankful to Professor Bob Bergman who has been a supportive mentor throughout my graduate career. Bob taught me physical organic chemistry in my first year of graduate school and I had the opportunity to GSI for the same course as a third year student. Bob is an amazing mentor because of how much effort he puts into teaching. I learned so much from him, both in his class, and while a GSI for his course. He has since served as a strong advocate for my future career in science.

I also have been fortunate to have amazing labmates in the Bertozzi lab. The sense of camaraderie and respect that I have felt as a member of the Bertozzi community since my first day in lab has been overwhelming. For everything that I've wanted to do in my experiments, I've been able to find an expert in the lab willing to teach me new skills. The breadth of this dissertation was only possible because of the kindness of my colleagues.

Ellen Sletten and John Jewett were my first mentors in the lab. John helped me get up and running with the BARAC project and let me share his hood for my first few months. He taught me a ton of chemistry and his love of reactions was contagious. He also played some great April fool's day pranks, ranging from hiding Hitomi (Ellen's undergrad at the time) in a giant box and telling me my new vacuum manifold had arrived to stuffing my desk drawers with liquid nitrogen frozen balloons that slowly warmed up and expanded… Ellen was and still is my science role model. She's brilliant and hard working, and her scientific intuition is amazing. She guided me through my first project and helped me make some difficult science decisions. She is also a great friend, and we've had a lot of fun over the years going to parties, training for half marathons, and just hanging out.

Yisu Han was an undergraduate student who worked with me for a few years on the BARAC project and also on the QC project. I learned a ton by teaching Yisu how to do experiments, and am so grateful for all of her help synthesizing compounds over the years. She is a talented scientist, and is currently pursuing her PhD at MIT. I also have to thank Bastiaan Buddingh, a visiting Master's student from the Netherlands who worked with me for ~6 months on the QC project. Bastiaan's questions and insights proved

invaluable to the progress of the project, and I learned a lot by working with him. He is also an amazing scientist, and is soon starting his PhD at Radboud University in the Netherlands.

I have to thank those in my year: Lauren Wagner, Gabriela de Almeida, Paresh Agarwal and Brendan Beahm. All of us have been together from the beginning, and I can't imagine a better support network. Lauren is an impeccable scientist, always available to help troubleshoot or analyze data. She taught me how to run Western blots, express protein, work with bacteria, and clone. Aside from the science, she's been one of my closest friends throughout graduate school, constantly providing emotional support during the roller coaster that is inevitably the PhD. We've also been exercise buddies throughout the years and she helps me get outside of lab for runs and yoga. Thank you Lauren for you generous time, support, and friendship. Paresh and I have been together in Latimer 810 from the beginning, and I can't think of a better colleague and friend to spend the years with. Paresh is an amazing scientist and he's helped me work through countless scientific challenges. He's kind and understanding, and an overall amazing person. Gaby has been a great friend throughout the years, always providing sound perspective and helping to calm me down with reason and logic. She also provided Bogie therapy and frequent barbeques. And on top of it all, she was a reliable running buddy. Thank you Gaby for all of your help through the years! Brendan brings up everyone's spirits because his happiness is contagious. He's been such a fun person to be around and he is always willing to help with anything.

I also have to thank the members of room 810 Latimer. For my first few years of graduate school, 810 was inhabited by me, Kim Sogi, Kanna Palaniappan, and Paresh Agarwal. These people made coming to lab every day fun. I got so much science advice from all three of them over the years, and am very appreciative for their perspective and insights. We also had a lot of fun going on lab outings to the Exploratorium, Hangar One, and Cal Academy of Sciences. Gary Tong was an honorary member of room 810 at the time, and I always appreciated his company. We all had a lot of fun together, and I am grateful for these amazing labmates. New members of 810 Latimer include Justin Kim and Neil Rumachik, both of whom have been amazing additions to the lab. Justin knows everything and is always willing to answer questions. Neil is generally gregarious and brings up everyone's happiness level. He also knows everything about mass spec and answers all of my questions.

Ellie Smith has been a great friend throughout the years, and I am grateful for her advice and support. She was a great running buddy while she was still in the lab, and I'm happy that we still keep in touch now that she's on to bigger and better things. I first met Marjoke Debets in 2011 when she came to the lab as a visiting scholar from the Netherlands. We have remained friends since, and I am happy that she is now a full-time member of the lab. She's been so supportive and helpful, and also a lot of fun to hang out with. Jessica Kramer is a new friend in the lab, and I am grateful for her scientific advice, friendship, and her puppies, which routinely provide puppy therapy during hard days. We have a lot of fun running together on the fire trails.

Other members of the Bertozi lab, past and present, who have provided valuable insights and advice include Brian Belardi, Jason Hudak, Sloan Siegrist, Peter Robinson, David Spiciarich, Peyton Shieh, Mason Appel, Douglas Fox, and Lissette Andrés. Thank you all for making my experiments possible and for being amazing co-workers.

None of the work in this dissertation would have been possible without the help of numerous collaborators. Professor Ken Houk and Joel Mackey were instrumental in providing computational insights for the BARAC project. Their work using the distortion/interaction model made it possible for us to understand cyclooctyne reactivity. They are amazing collaborators and fantastic scientists. I am grateful to Professor Houk for his continued investment in my scientific career. I am also thankful to Professor Jason Chin and Fiona Townsley who provided the plasmids that I used in the QC amino acid incorporation project.

I've been lucky to have the opportunity to live with amazing roommates. Particularly, thank you to Jessica Kisunzu and Stephanie Jones who I lived with on Virginia St. for four years. We were together through everything: GRS, qualifying exams, grad school stresses, and finally, graduation. These two helped me get through the hard times, and provided countless fun times. I am so grateful for their friendship. I'm also grateful to Isha Agarwal, my roommate through all four years of college. She has always been a strong supporter of my career in science and is also an amazing friend.

I also have to thank my undergraduate research advisor, Professor Andy Myers, who gave me the opportunity to learn synthetic chemistry. In the Myers lab, Simon Lewis and Landy Blasdel taught me all of the skills necessary to do reactions from the ground up. I am grateful for their patience, time, and mentorship.

I owe a huge thanks to Professor Miriam Rafailovich at SUNY Stony Brook, whose selfless efforts to promote science education amongst high school students made me the scientist I am today. Every year, Miriam hosts upwards of 50 high school students in her materials engineering lab at Stony Brook and gives them the freedom to pursue their passions. Miriam gave me my first real taste of academic research, and inspired me to pursue a career as a scientist. She has done the same for hundreds of other students. I'm also thankful to my science partner-in-crime during my years in the Rafailovich lab – Sylvia Qu. She was and still is one of my best friends, and we bonded over polymers, thin films, and supercritical carbon dioxide.

Of course I wouldn't be where I am today without the constant support of my family. Thank you to my parents, Douglas Gordon and Linette Robins, for giving me everything I've ever needed to learn and grow as both a scientist and a person. There aren't sufficient words to express how grateful I am to you both. Thank you to my sister, Michelle Gordon, for always being there for me and for being my best friend. Thank you to my aunt, Martha Relyea, for her unwavering encouragement and support. And thank you to Howard Robins, who has become an important part of my family and a constant supporter of my goals.

And last but definitely not least, thank you to my boyfriend Douglas Waters for helping me to get where I am today. These years would not have been the same without all the great times we've had together. From trips to Hawaii to hiking in Montclair, you're friendship has been a constant source of support and encouragement, and you've made it possible for me to achieve my goals.

Chapter 1:
A Review of Bioorthogonal Chemistries and Their Applications *In Vivo*[*]

Introduction

Bioorthogonal reactions are chemistries that are designed to proceed in physiological environments without interfering with the myriad biological processes occurring in living systems. Over the past 15 years, bioorthogonal tools have provided powerful methods for visualizing biomolecules *in vitro* and *in vivo*. These reactions are able to successfully proceed in complex, living environments because they are carefully designed to be non-perturbing to native biological functionalities such primary amines, thiols, carboxylic acids, phosphates, oxygen, and most importantly, water (Figure 1.1).[1] Development of a bioorthogonal reaction begins with rigorous screening to identify water-compatible chemistries that employ abiotic reagents.[2] Selection of a promising reaction is followed by mechanistic analysis and assessment of reactivity in model physiological environments, on proteins, and on cells. After thorough optimization, the true test of a bioorthogonal ligation is its ability to proceed *in vivo*.[2]

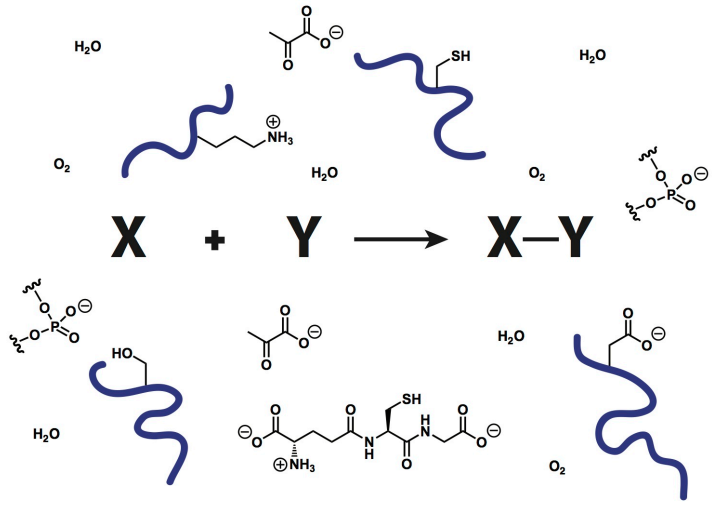


Figure 1.1. The bioorthogonal reaction between X and Y proceeds in physiological environments without perturbing native chemical functionalities.

In this chapter, we review the development and optimization of four bioorthogonal reactions: the Staudinger ligation, copper-catalyzed azide-alkyne cycloaddition (hereafter referred to as copper-click chemistry), copper-free click chemistry, and the tetrazine ligation. We then discuss the efforts of various researchers to transition these reactions to the complex environments of multicellular organisms, limiting the discussion to

[*] This chapter is adapted from Gordon, C. G.; Bertozzi, C. R. *In Vivo* Bioorthogonal Chemistry. In *Chemoselective and Bioorthogonal Ligation Reactions - Concepts and Applications;* Medintz, I. L.; Algar, W. R.; Dawson, P. E., Ed.; Wiley-VCH. Copyright Wiley-VCH. ISBN 9783527334360.

examples in which the organism is alive during the entire ligation process. Finally, we discuss future applications of bioorthogonal chemistry in biomedicine.

Initial work optimizing bioorthogonal reagents for use *in vivo* has focused on increasing the reactivity between the two ligation partners used in the reaction. Faster reactions enable use of lower concentrations of reagent, thereby offsetting the effects of any low-level toxicity associated with the reactive partners. In addition, faster ligations facilitate tagging of biomolecules prior to clearance of the probes from the animal. Thus, considerable effort has been placed on the development of new, rapid bioorthogonal reactions. Indeed, the tetrazine ligation, one of the fastest known bioorthogonal reactions, has been used most extensively and with the most success *in vivo* when compared to other chemistries. However, researchers are beginning to realize that reaction kinetics is not the only factor at play in determining the success of a reaction in a living animal. Equally if not more important are the pharmacokinetic properties of the reagents used. As a result, focus has been shifting towards the optimization of the pharmacokinetic properties of bioorthogonal reagents, with particular emphasis on aqueous solubility and circulation time. Throughout this chapter, we highlight the efforts of researchers to enhance the pharmacokinetic properties of bioorthogonal reagents, thereby enabling their use *in vivo* and opening the door for exciting new applications of these unique chemistries.

Methods of Incorporating Bioorthogonal Functional Groups Into Biomolecules in Living Animals

In order for a bioorthogonal reaction to be successful *in vivo*, one of the reaction partners must be somehow integrated into the target biomolecule. Often, this incorporated functional group is referred to as a bioorthogonal handle. A number of methods of installing non-natural functional groups into native biomolecules have been developed. Here, we discuss the two methods that have been most widely used in living, multicellular organisms.

Metabolic Glycan Engineering

Metabolic glycan engineering is a method of incorporating a bioorthogonal functional group into a component of the glycome – the totality of glycans in an organism.[3] Using this method, a non-natural monosaccharide containing the reactive chemical group is introduced into a cell or animal via injection, feeding, or bathing. The organism's own metabolic machinery then processes the analog as though it were the natural substrate, leading to incorporation of the bioorthogonal functionality into the glycome (Figure 1.2a).[4] A complementary reaction partner can then be introduced into the system to append a label onto the non-natural sugar via bioorthogonal ligation.

The metabolic glycan engineering technique is valuable because it enables the study of a class of molecules that are not templated by DNA, and so are not amenable to traditional labeling techniques such as fusion to a genetically-encoded protein fluorophore or tag. The technology has enabled the study of the dynamics of the glycome – an area of

growing interest because of reports that glycosylation patterns change upon transition from a healthy to a diseased state.[5,6] Thus, tools such as non-natural sugar incorporation via metabolic glycan engineering have implications in the detection and treatment of diseases such as cancer.

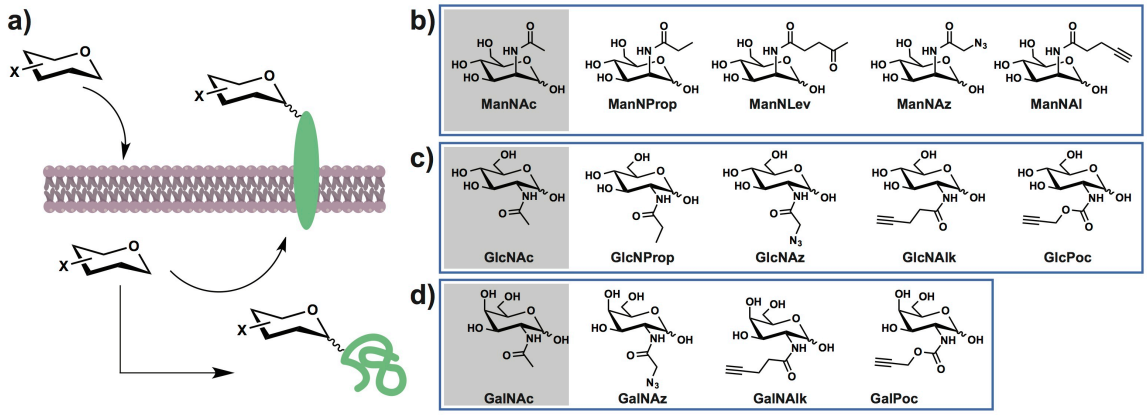


Figure 1.2. Metabolic glycan engineering. (a) A functionalized monosaccharide analog is administered to cells or animals, and the organism's metabolic machinery incorporates it into cell surface or cytosolic glycoproteins and glycolipids. Structures of (b) *N*-acetylmannosamine (ManNAc), (c) *N*-acetylglucosamine (GlcNAc), and (d) *N*-acetylgalactosamine (GalNAc) and examples of non-natural analogs used in metabolic glycan engineering experiments.

The idea to introduce a non-natural monosaccharide into the glycome was first proposed by Werner Reutter and coworkers in the early 1990s.[7] These researchers showed that *N*-propanoylmannosamine (ManNProp, Figure 1.2b), an analog of *N*-acetylmannosamine (ManNAc), and *N*-propanoylglucosamine (GlcNProp, Figure 1.2c), an analog of *N*-acetylglucosamine (GlcNAc), are converted to the corresponding sialic acid analogs and incorporated into glycoconjugates in rats upon intraperitoneal (IP) injection. These results demonstrated that the sialic acid biosynthetic enzymes accept structurally altered substrates.

Inspired by this work, Bertozzi and coworkers took advantage of the promiscuity of the sialic acid biosynthetic enzymes to introduce a reactive, bioorthogonal handle into the glycome. For example, treatment of cells with *N*-levulinoylmannosamine (ManNLev, Figure 1.2b), an analog of ManNAc bearing a ketone group, led to incorporation of the corresponding sialic acid (SiaLev) into cell surface glycoconjugates, where they could be further treated with hydrazide probes.[8] It was later shown that the azide-bearing ManNAc analog *N*-azidoacetylmannosamine[9,10] (ManNAz, Figure 1.2b) and the alkyne-bearing *N*-(4-pentynoyl)mannosamine[11,12] (ManNAl, Figure 1.2b) are also processed by the biosynthetic machinery of vertebrate cells, enabling further modification through bioorthogonal reaction with phosphines, alkynes, or azides.

The sialic acid biosynthetic pathway is not the only metabolic pathway amenable to metabolic engineering. Non-natural analogs of GlcNAc, such as GlcNAz[13] GlcNAlk[14] and GlcPoc[15] (Figure 1.2c), and analogs of *N*-acetylgalactosamine (GalNAc, Figure 1.2d), such as GalNAz,[16] GalNAlk[14] and GalPoc[15] are incorporated into various

glycoconjugates in living animals. Considerable work has been done to understand the metabolic fates of these monosaccharide analogs in cells. [14,15,17,18]

In this chapter, we present examples in which metabolic glycan engineering is used to install reactive bioorthogonal handles into the glycomes of living animals. Most of the *in vivo* metabolic labeling experiments presented in this chapter employ peracetylated versions of the sugar analogs, which readily penetrate cell membranes and are deacetylated by cytosolic esterases. [19]

Pre-Targeting

A second approach used to introduce bioorthogonal handles into biomolecules of interest is the pre-targeting approach. This method was initially developed as a tool to enhance the efficiency of targeted radioimmunotherapy for cancer treatment. Targeted radioimmunotherapy is a technique in which a radionuclide is targeted to a tumor by conjugation to a monoclonal antibody (mAb) specific for a tumor antigen, leading to directed attack of the tumor with minimal off target damage. [20]

Unfortunately, due to their pharmacokinetic properties, mAbs accumulate slowly at the tumor site and have high circulation residence times resulting in high levels of off-target damage, particularly in the bone marrow. Pre-targeting can obviate these problems. In this approach, an unlabeled mAb is injected into the body and allowed to accumulate at the tumor site over the course of days. Because the mAb is not conjugated to a radionuclide, its long residence time is not harmful to other tissues in the body. Once the mAb has accumulated at the tumor site and unbound mAb has cleared, a radionuclide conjugated to a secondary agent that is specific for the mAb is injected. This radionuclide-conjugated molecule is designed to have a strong affinity for the mAb and also to rapidly clear from the body so as to minimize off target damage. [20]

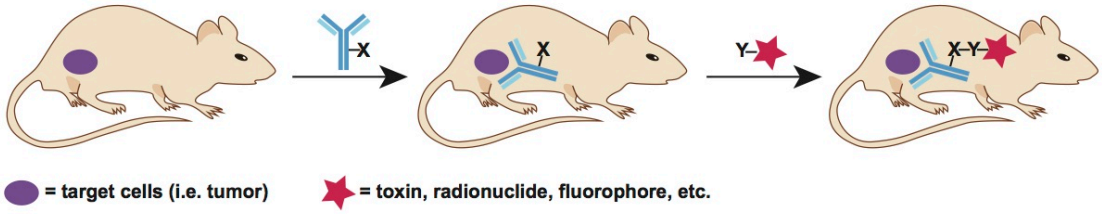


Figure 1.3. Bioorthogonal pre-targeting.

Bioorthogonal reactions are ideal for pre-targeting approaches *in vivo*. Figure 1.3 shows a typical pre-targeting experiment using a bioorthogonal reaction. Here, a mAb harboring a bioorthogonal reactive group X is introduced into the animal and accumulates at the tumor site. Then, a radionuclide conjugated to a complementary reactive group Y is injected, and Y rapidly ligates with its partner via bioorthogonal reaction at the tumor site. Because the radionuclide is appended to a small molecule rather than a large antibody, its pharmacokinetic properties enable rapid clearance and reduced off-target damage. Numerous studies discussed in this chapter aim to further develop this bioorthogonal pre-targeting approach to develop cancer detection and treatment methods.

Bioorthogonal Chemistries for Imaging and Labeling Biomolecules *In Vivo*

The Staudinger Ligation

The Staudinger ligation is one of the first bioorthogonal reactions developed. It is a modified version of the classic Staudinger reduction, and proceeds between an azide and a carbomethoxy-substituted triphenylphosphine derivative to form a stable amide bond linkage as shown in Figure 1.4. Both the phosphine and the azide are abiotic and relatively unreactive toward biological functionalities, making the Staudinger ligation ideal for use in living systems. [9] Since its initial introduction, the reaction has been used in many successful *in vitro* labeling experiments. [9,19] However, its transition to use *in vivo* has proven a challenge, in part because the reaction is sluggish. Its second order rate constant is $k = 2.5 \pm 0.2 \times 10^{-3}$ M^{-1} s^{-1} at room temperature, which translates to a reaction half-life of ~9 days when both the azide and the alkyne are used at a concentration of 0.5 mM. [21]

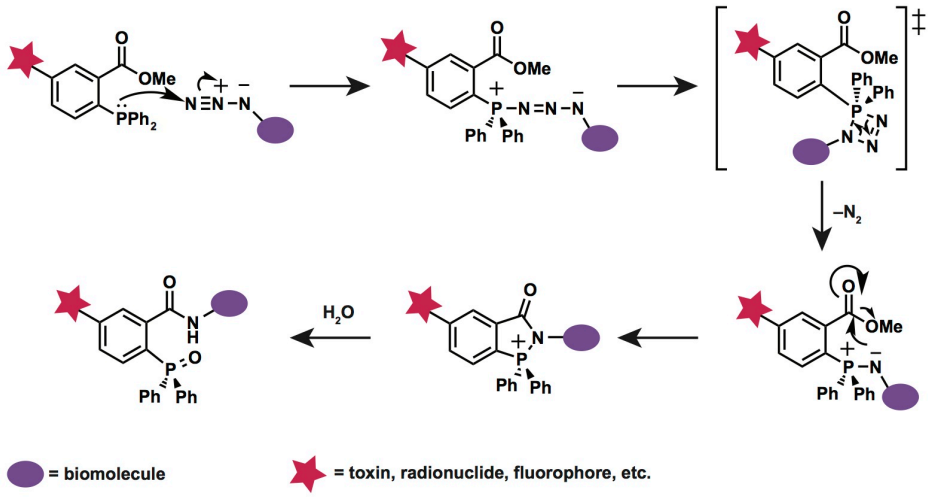


Figure 1.4. Mechanism of the Staudinger ligation.

The Staudinger Ligation in Mice

In 2004, Bertozzi and co-workers reported the first attempt to label an azide-containing biomolecule via the Staudinger ligation inside a living mouse. [22] They aimed to study protein sialylation, incorporating the azide functionality into the mouse glycome using the strategy of metabolic labeling. Mice were treated with Ac_4ManNAz via IP injection one time daily for seven days (Figure 1.5a). On the eighth day, mice were injected IP with FLAG-conjugated phosphine (phos-FLAG, Figure 1.5a) after which their splenocytes were harvested and labeled with a fluorophore-conjugated α-FLAG antibody. Analysis by flow cytometry revealed significant labeling of splenocyte cells in mice that were injected with azidosugar versus those that were not, suggesting that the reaction proceeded *in vivo* (Figure 1.5b). Interestingly, when splenocytes from mice that had been treated with both azidosugar and Phos-FLAG were re-exposed to additional Phos-FLAG

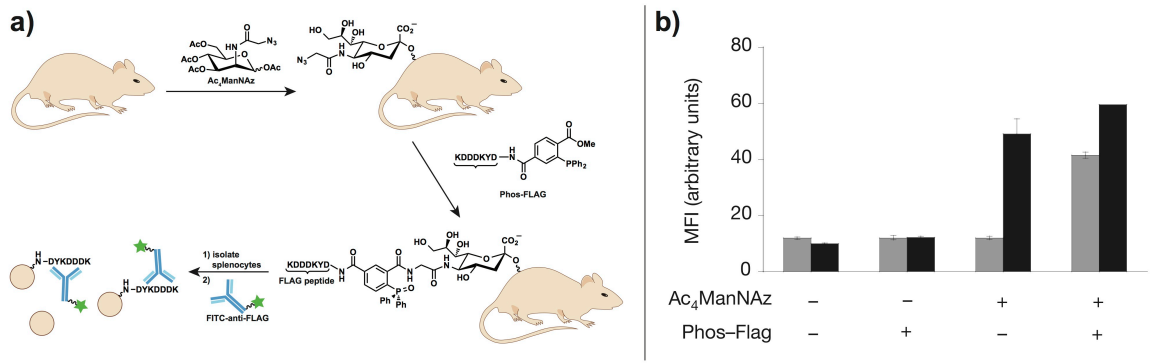


Figure 1.5. *In vivo* labeling of cell-surface sialic acid residues via the Staudinger ligation. (a) Mice were injected IP with $Ac_4ManNAz$ once daily for seven days and were injected IP with phosphine-FLAG probe on the eighth day. Splenocytes were harvested, labeled with fluorescein isothiocyanate (FITC) α-FLAG and analyzed by flow cytometry. (b) Flow cytometry analysis of splenocytes isolated from mice injected with $Ac_4ManNAz$ or vehicle and phosphine-FLAG or vehicle. Black bars represent data from splenocytes that were re-exposed to phosphine-FLAG *ex-vivo* after harvesting. Figure 1.5b is adapted with permission from Macmillan Publishers Ltd: Nature, reference 22, Copyright 2004.

ex-vivo, fluorescence labeling increased, revealing that not all available azides reacted with the phosphine reagent in the live mouse.

Later, Brindle and co-workers used the metabolic labeling strategy followed by Staudinger ligation to image tumor sialylation in mice bearing a subcutaneous xenograft of a murine tumor cell line.[23] After treatment with $Ac_4ManNAz$ (IP injection) followed by a biotin-conjugated phosphine probe (IP injection) and neutravidin fluorophore (IV injection), imaging revealed labeling at the tumor site. The maximum tumor/tissue mean fluorescence intensity ratio was ~3 for $Ac_4ManNAz$ treated mice and ~2 for vehicle treated mice. This statistically significant 50% signal increase in treated mice suggests that the Staudinger ligation proceeded *in vivo*. However, the authors state that for clinical use, the technique will require a faster ligation chemistry.[23]

In 2011, Vugts and co-workers tested the *in vivo* utility of the Staudinger ligation in combination with pre-targeting.[24] Deferoxamine phosphine probe **1.1** (Figure 1.6a) was prepared and chelated to ^{67}Ga for use as the radiolabeling agent. As the targeting agent, α-CD44v6 chimeric mAb U36, a monoclonal antibody that binds the CD44 antigen in head and neck squamous cell carcinoma cell lines, was conjugated to triazide probe **1.2** via lysines (Figure 1.6b). However, upon introduction of these reagents into the mouse, no ligation product was detected.

In vitro studies of probe reactivity provide some clues as to why the reaction failed in mice. For example, product formation showed a dependence on reaction medium – the reaction between ^{67}Ga-**1.1** and **1.3** proceeded to 20-25% completion after 2 h at 37 ºC in PBS, but generated no product when the reaction was performed in 50% mouse serum due to generation of a phosphine-based side-product, the structure of which was not elucidated. This side reactivity, if relevant *in vivo*, would reduce the effective

concentration of probe **1.1**, thereby reducing product formation inside the mouse. Interestingly, however, Western Blot analysis of the *in vitro* reaction between ^{67}Ga-**1.1**

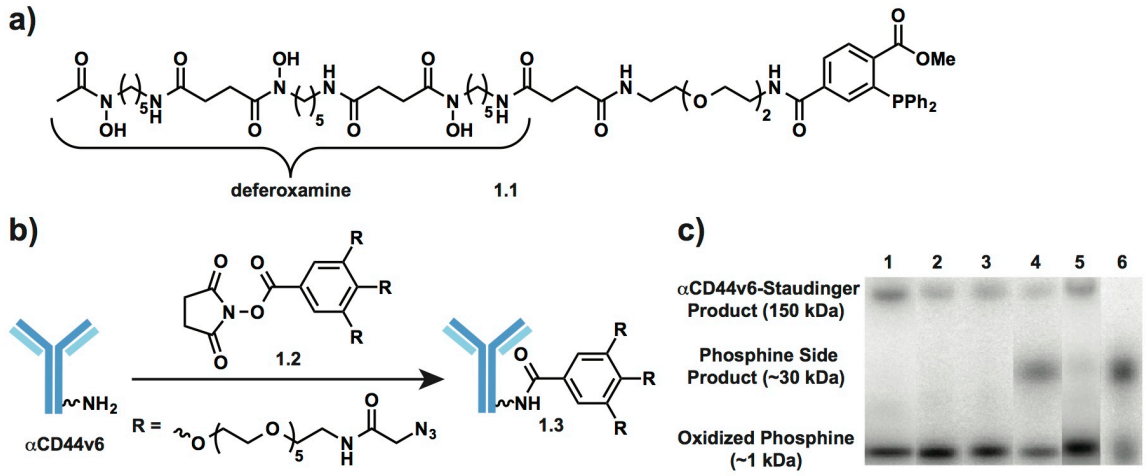


Figure 1.6. Pre-targeting approach to *in vivo* labeling via the Staudinger ligation. (a) Deferoxamine-conjugated phosphine **1.1**. (b) a-CD44v6 chimeric mAb U36 was conjugated via lysine residues to triazide 1.**2** yielding azide-functionalized antibody 1.**3**. c) *In vitro* studies of reactivity between 1.**3** and ^{67}Ga-**1.1**. **1.3** and ^{67}Ga-**1.1** were combined in a 1:1 ratio in (lane 1) PBS, (lane 2) 50% pig serum in PBS, (lane 3) 50% goat serum in PBS, (lane 4) 50% rabbit serum in PBS, (lane 5) 50% human serum in PBS, and (lane 6) 50% mouse serum in PBS. Samples were incubated at 37 ºC for 2 h then analyzed by SDS-PAGE. Figure 1.6c is adapted with permission from reference 24. Copyright 2011, American Chemical Society.

and **1.3** did not show formation of the side product in the presence of 50% human serum (Figure 1.6c), the most relevant conditions for use of the Staudinger ligation for therapeutics and diagnostics in the clinic.

Efforts to improve *in vivo* labeling via optimization of the Staudinger ligation chemistry have proven challenging. [10] Instead, the field has moved toward the development of new bioorthogonal chemistries with faster rates and improved *in vivo* results.

Copper-Click Chemistry

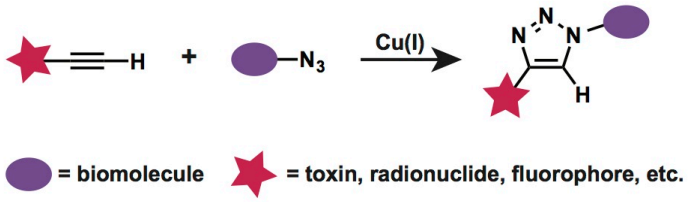


Figure 1.7. The copper-click reaction.

The copper-click reaction, a Cu(I)-catalyzed 1,3-dipolar cycloaddition between the azide and a terminal alkyne to form a triazole (Figure 1.7), was independently reported by both Sharpless and Meldal in 2002. [25,26] The reaction between azides and alkynes has been known for decades, but in its uncatalyzed form requires heating to proceed at observable rates. The Cu(I) catalyst increases the rate of the reaction by roughly seven orders of

magnitude,[27] enabling its use at room temperature. Sharpless recognized the utility of this reaction for rapid, facile ligations between molecules, classifying it as a "click reaction" – a reaction that is simple, derived from readily available starting materials, is exquisitely selective, and is high yielding.[28]

In 2003, Finn and co-workers reported the first use of the reaction in a biological system, showing that it proceeds efficiently on the protein coat of a cowpea mosaic virus.[29] After this report, biological applications of the copper-click reaction grew exponentially.

Cu(I) Ligands to Reduce Toxicity

One of the major liabilities of the copper-click reaction for use *in vivo* is the toxicity of the copper catalyst. Cu(I) has been shown to damage iron-sulfur clusters leading to deactivation of dehydratases.[30] As well, Cu(I) is prone to biological redox chemistry, readily being oxidized to Cu(II) or undergoing disproportionation to both Cu(0) and Cu(II) – species which are not active catalysts of the click reaction.[31] This problem can be circumvented by producing Cu(I) *in situ* from Cu(II) using a reducing agent such as sodium ascorbate.[25] However, when combined, copper and ascorbate readily generate reactive oxygen species (ROS) capable of inducing biological damage.[32,33] As a result, researchers have developed stabilizing ligands for Cu(I).[31] By enabling the Cu(I) species to persist in solution, these ligands promote considerable rate enhancements.

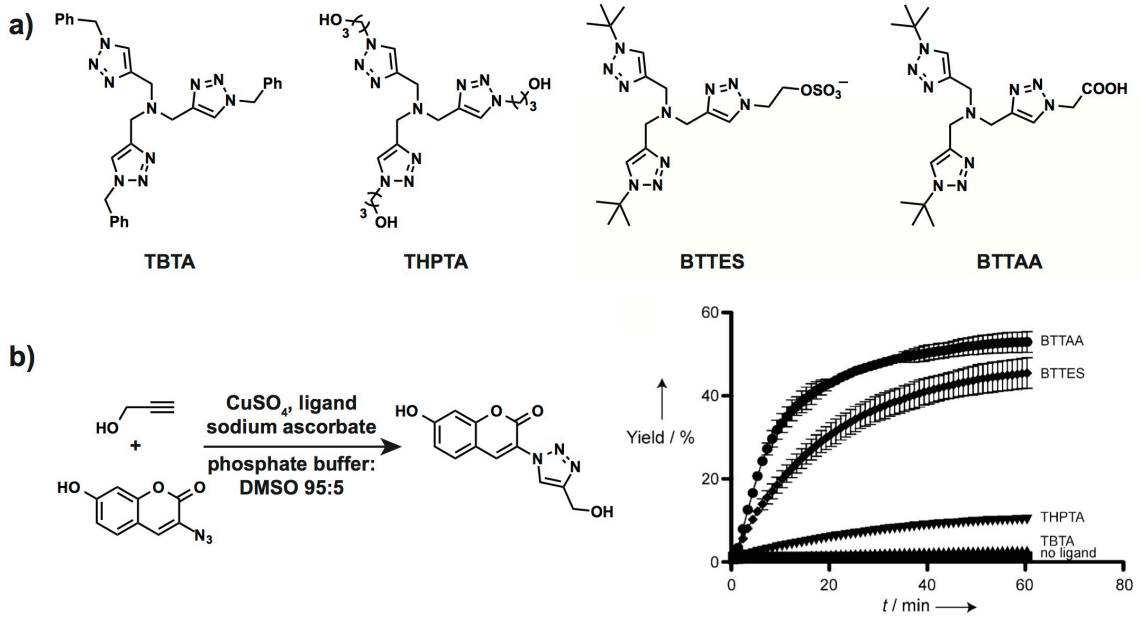


Figure 1.8. Cu(I) ligands used to accelerate the copper-click reaction. (a) Structures of various rate accelerating ligands. (b) The progress of the reaction between propargyl alcohol (50 μM) and 3-azido-7-hydroxycoumarin (100 μM) in the presence of $CuSO_4$ (50 μM), ligand (300 μM), and sodium ascorbate (2.5 mM) in 95:5 potassium phosphate buffer:DMSO at room temperature was measured by monitoring the fluorescence of the product at 477 nm. Lines through data points represent error bars. Figure 1.8b is adapted with permission from reference 36. Copyright 2011, John Wiley and Sons.

Additionally, the ligands reduce ROS accumulation by acting as sacrificial reductants, [33] and may also reduce damage to enzymes by sequestering Cu(I) and preventing it from passing through the cell membrane, [27] a process which typically occurs via active or facilitated diffusion. [30,34]

One of the first ligands designed for catalysis of the copper-click reaction was tris-(benzyltriazolylmethyl)amine (TBTA, Figure 1.8a), introduced by Finn, Fokin and Sharpless in 2003. [29] TBTA's rate-enhancing abilities were discovered fortuitously – when using the Cu-Click reaction to synthesize the ligand, Finn and co-workers found that the reaction was autocatalytic. [29,31] Indeed, studies show that TBTA significantly increases the rate of the click reaction relative to the no ligand control. [35] But despite this rate accelerating effect, TBTA has poor aqueous solubility, requiring high levels of Cu(I) (0.2–1 mM) for labeling experiments, exacerbating the toxicity problem. [27]

The solubility challenge is overcome by modifying the structure of the ligand. Tris(3-hydroxypropyltriazolyl methyl)amine (THPTA, Figure 1.8a), [33] and *bis*(tert-butyltriazolyl) ligands BTTES [27] and BTTAA [36] (Figure 1.8a) are more water soluble variants of TBTA that also increase the rate of the click reaction relative to the parent compound (1.8b). In the case of BTTES, an appended sulfate group serves to reduce the amount of Cu(I) that traverses the cell membrane while simultaneously enhancing solubility. [27] In BTTAA, an appended acetate functionality is thought to coordinate Cu(I), acting as an electron donor to further increase the rate of the reaction. [36] These and other [37–39] Cu(I)-chelating agents have enabled translation of the copper-click reaction to live cells and animals by reducing Cu(I) toxicity and enabling its use at lower concentrations.

Copper-Click Chemistry in Zebrafish

After testing the biocompatibility of the BTTES-Cu(I) catalyzed reaction on mammalian cells in culture, Wu and co-workers used the technology to successfully label alkyne-containing sugars on the cell-surfaces of developing zebrafish embryos. [27] The researchers employed the metabolic glycan engineering approach to incorporate an alkyne-modified GDP-fucose (GDP-FucAl, Figure 1.9a) into the zebrafish glycome. In this case, the nucleotide sugar was used instead of the free sugar because fucose biosynthetic enzymes may not efficiently process analogs of fucose. [40] Because nucleotide sugars do not readily pass through the cell membrane due to their charged structure, GDP-FucAl was introduced into the zebrafish embryos at the one or two cell stage via microinjection – a commonly used method of overcoming the cell permeability challenge.

After microinjection of GDP-FucAl, the embryos were labeled with an azidofluorophore in the presence of BTTES and $CuSO_4$. Upon imaging, robust signal was observed on embryos treated with GDP-FucAl and azidofluorophore, whereas minimal signal was observed in the GDP-Fuc control embryos (Figure 1.9b). Interestingly, when comparing the *in vivo* labeling ability of BTTES and THPTA, considerably more signal was observed with the former, suggesting that reaction rate and labeling efficacy are

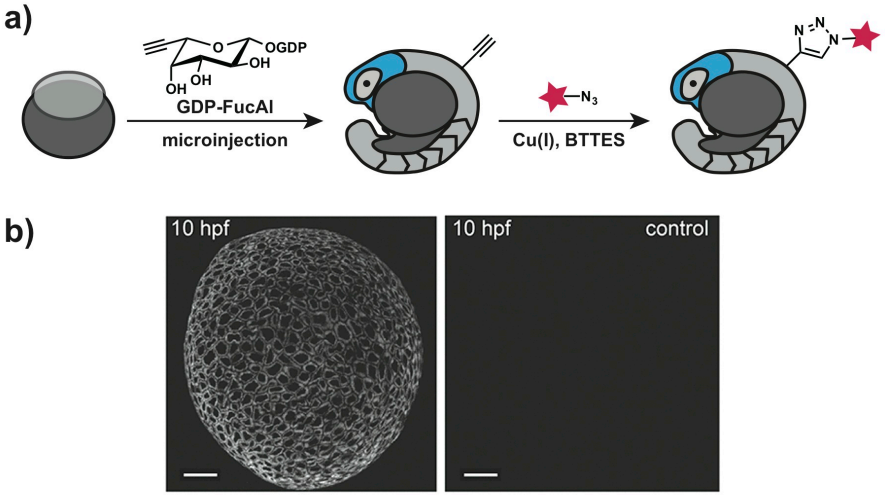


Figure 1.9. Copper-click chemistry *in vivo*. (a) Zebrafish were microinjected with GDP-FucAl at the one- or two-cell stage and allowed to develop for 10 hrs. Embryos were then bathed in Alexa Fluor 488–azide in the presence of BTTES, $CuSO_4$, and sodium ascorbate. (b) Embryos were imaged via confocal microscopy. Left – embryos treated as described. Right – embryos injected with GDP-Fuc rather than GDP-FucAl. Scale bar 100 μm. Figure 1.9b reprinted with permission from reference 27. Copyright 2010, American Chemical Society.

correlated.[27] As well, the Cu(I)-BTTES reagents generated minimal toxicity and developmental abnormalities in the treated fish.[27] In later experiments, Wu took advantage of the low toxicity and labeling efficiency of the BTTES-Cu(I) click technique to study and image *N*-acetyllactosamine (LacNAc) residues in zebrafish.[41]

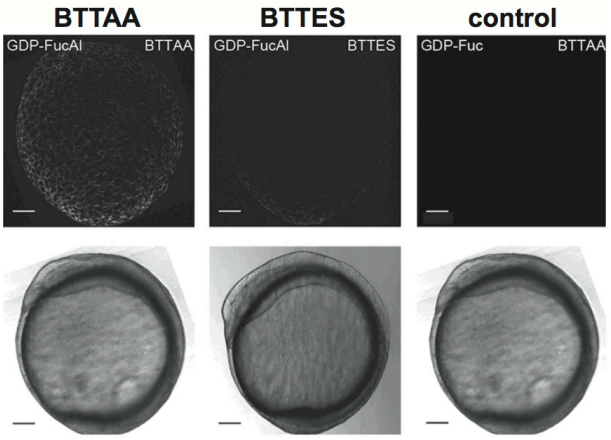


Figure 1.10. Imaging the glycome of developing zebrafish embryos using copper-click chemistry and BTTAA or BTTES. Embryos were injected with GDP-FucAl or GDP-Fuc (control), developed to 9 hpf, and bathed in azido-Alexa Fluor 488 in the presence of $CuSO_4$, sodium ascorbate, and BTTAA or BTTES. The fish were imaged via confocal microscopy. Top: 488 channel; bottom: brightfield; scale bar 100 μm. Figure reprinted with permission from reference 36. Copyright 2011, John Wiley and Sons.

Upon development of BTTAA, Wu and co-workers transitioned to using this new, faster ligand to image FucAl in zebrafish. In these studies, robust labeling was observed on treated embryos when compared to the minus alkyne control. In addition, considerably more labeling was achieved using BTTAA versus BTTES, again suggesting correlation between reaction rate and labeling efficiency (Figure 1.10). Importantly, the researchers report no observable developmental defects in the treated embryos for 5 days after labeling. [36]

To date, copper-click chemistry has seen some success in labeling azide- or alkyne-containing sugars on live zebrafish embryos. The development of triazolyl Cu(I) chelating ligands has made this success possible. However, the toxicity of copper still limits use of the chemistry in living systems, and to date, copper-click chemistry has not been used to label biomolecules in mice. Thus, researchers have focused on developing metal-free bioorthogonal chemistries with reaction kinetics that exceed those of the Staudinger ligation.

Copper-Free Click Chemistry

The challenges of the Staudinger ligation and copper-click chemistry were recognized early on, and researchers set out to identify new reactions that were both mild enough to avoid toxicity and fast enough to enhance labeling efficiency *in vivo*.

In 2004, Bertozzi and co-workers reported a new bioorthogonal reaction – the 1,3-dipolar cycloaddition between azides and strained cyclooctynes, which they termed "copper-free click chemistry" (Figure 1.11). [10] Inspired by a report from Wittig and Krebs in 1961 detailing the "explosive" reactivity between azides and cyclooctynes, [42] Bertozzi realized that the ring strain inherent to cyclooctynes had the potential to increase the rate of the azide/alkyne cycloaddition without the use of the toxic Cu(I) catalyst.

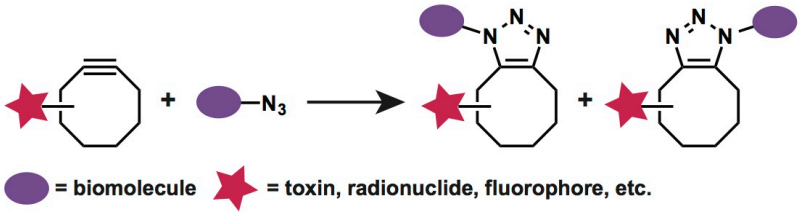


Figure 1.11. Copper-free click chemistry.

Their first rendition of this reaction employed the cyclooctyne shown in Figure 1.12, referred to as OCT. OCT reacts with benzyl azide with a rate constant of $k = 2.4 \times 10^{-3}$ M^{-1} s^{-1}, similar to the rate of the Staudinger ligation. [10] A related derivative, ALO (Figure 1.12) had better water solubility and reacted with benzyl azide at roughly the same rate. [43]

Given the importance of kinetics for *in vivo* chemistry, a significant effort has been directed toward enhancing the reactivities of cyclooctyne reagents. Two approaches have taken center stage: modulation of electronics and enhancing ring strain.

To modify cyclooctyne electronics, electron-withdrawing fluorine atoms have been installed at the propargylic position. Computational studies have demonstrated that such groups proximal to the alkyne reduce the activation energy by promoting interaction between the azide and the alkyne.[44,45] In agreement with this prediction, the monofluorinated cyclooctyne (MOFO, Figure 1.12) with one fluorine atom at the

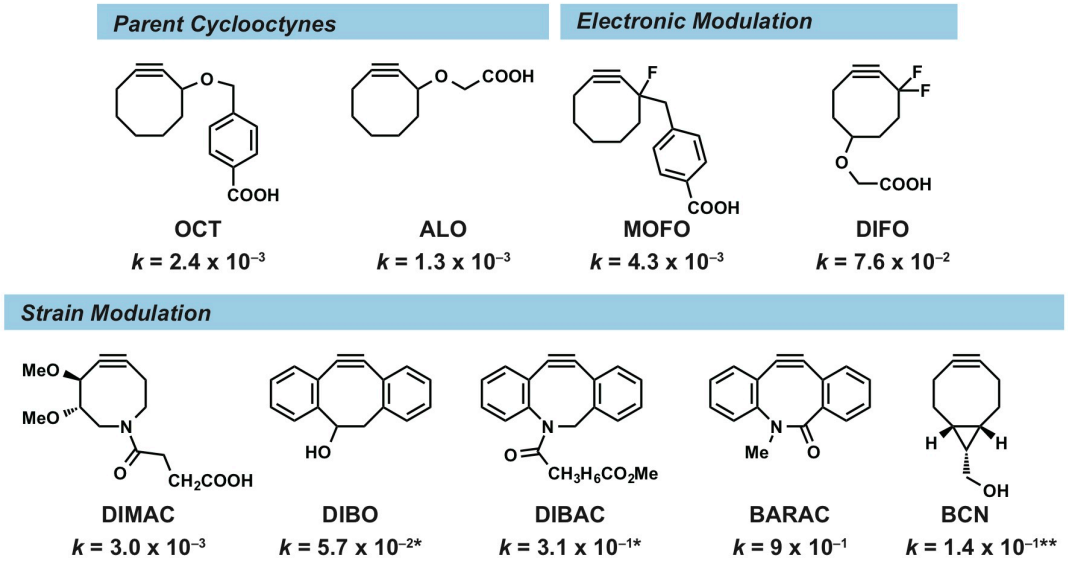


Figure 1.12. Cyclooctyne analogs for copper-free click chemistry. The rate of the cycloaddition between cyclooctyne and azide can be modified via electronic and strain modulation of the parent compounds. Shown are select cyclooctynes that exemplify these approaches to rate enhancement. All rates are second order (M^{-1} s^{-1}), and were measured for the reaction with benzyl azide in CD_3CN at room temperature. One asterisk * denotes rates measured in CD_3OD and two asterisks ** denotes rates measured in 3:1 CD_3CN:D_2O

propargylic position reacts ~2-fold faster than OCT,[43] and the difluorinated cyclooctyne (DIFO, Figure 1.12), with two fluorine atoms at the propargylic position, reacts ~32-fold faster.[46,47] Due to its superior kinetics, DIFO has been used in many labeling experiments, both *in vivo* and *ex vivo*.

The second approach to increasing cyclooctyne reactivity is strain modulation.[44,45] For example, 6,7-dimethoxyazacyclooct-4-yne (DIMAC, Figure 1.12)[48] possesses an exocyclic amide bond that is predicted to increase overall ring strain due to the sp^2 character of the nitrogen atom. As well, C—N bonds are shorter than C—C bonds, further adding to ring strain. DIMAC reacts with benzyl azide with a second order rate constant of 3 x 10^{-3} M^{-1} s^{-1}, slightly faster than the parent cyclooctyne, OCT.[48] Aside from increased reactivity due to enhanced ring strain, DIMAC's amide nitrogen atom, along with its pendant methoxy groups, improve the aqueous solubility of the molecule, leading to superior pharmacokinetic properties for *in vivo* experiments.[48,49] Indeed, the effects of DIMAC's excellent solubility are borne out in *in vivo* experiments, as discussed later in the chapter.

In 2008, Boons and co-workers introduced 4-dibenzocyclooctynol (DIBO, Figure 1.12).[50,51] DIBO has a second order rate constant of 5.7 x 10^{-2} M^{-1} s^{-1} for the reaction with benzyl azide, roughly 24-fold faster than OCT.[51] Boons hypothesized that the additional strain imparted by the fused benzene rings was responsible for the molecule's enhanced reactivity. Soon thereafter, Van Delft and coworkers introduced aza-dibenzocyclooctyne (DIBAC), a benzene-fused cyclooctyne that incorporates additional strain via an exocyclic amide nitrogen bond.[52] DIBAC reacts with azides roughly 130-fold faster (k = 3.1 x 10^{-1} M^{-1} s^{-1}) than OCT. The most reactive cyclooctyne developed to date, biarylazacyclooctynone (BARAC, Figure 1.12), possesses the fused benzene rings in addition to an endocyclic amide bond.[53] BARAC reacts with benzyl azide nearly 375 times faster than OCT with a second order rate constant of 9 x 10^{-1} M^{-1} s^{-1}.

A liability of DIBO, DIBAC and BARAC is their requirement of two bulky aryl rings for enhanced reactivity. These bulky appendages make incorporation of the cyclooctyne into biomolecules via methods such as metabolic labeling more challenging. As a result, there has been some focus on developing less bulky yet still highly reactive cyclooctynes. Bicyclononyne (BCN, Figure 1.12), a cyclooctyne with a strain enhancing fused cyclopropane ring, fulfills this need.[54] BCN achieves faster rates than some of the aryl functionalized cycloocytynes, and is considerably less bulky, opening the door to new modes of incorporation into biomolecules *in vivo*.[55,56]

Copper-Free Click Chemistry in Zebrafish

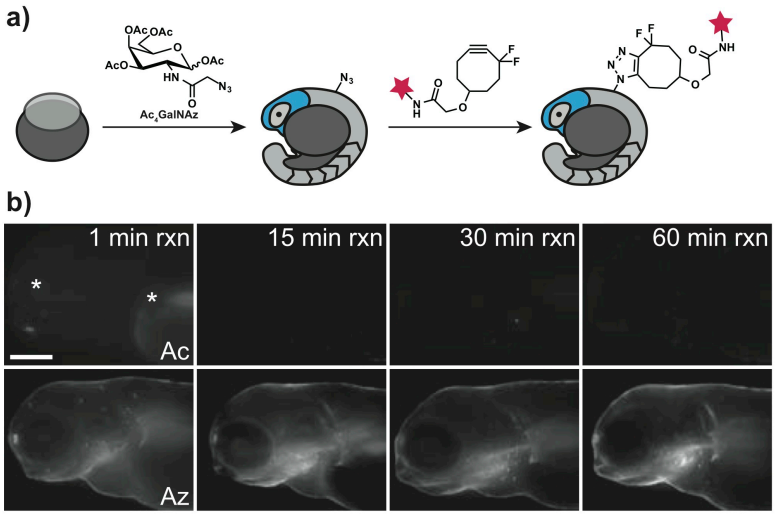


Figure 1.13. Copper-free click chemistry for labeling the glycome of living zebrafish. (a) Zebrafish were bathed in $Ac_4GalNAz$ or $Ac_4GalNAc$ for three days, then reacted with DIFO-Alexa Fluor 647. (b) Images of control embryos (Ac) and labeled embryos (Az) after reaction with DIFO-Alexa Fluor 488 for 1– 60 min. Asterisk * indicates autofluorescence. Scale bar is 200 μm. Figure 1.13b reprinted with permission from reference 57. Copyright 2008, American Association for the Advancement of Science.

The first application of copper-free click chemistry in live animals was toward imaging glycans in developing zebrafish.[57] This organism has a well understood developmental program, is increasingly considered a viable model for human diseases, and is

translucent, which enables optical imaging of chemically labeled species. Via metabolic labeling, GalNAz residues were introduced into glycans of zebrafish embryos and larvae. This was achieved by bathing the embryos in a solution of Ac_4GalNAz for three days followed by reaction with DIFO-Alexa Fluor 647 (Figure 1.13a). Subsequent imaging revealed robust labeling of cell-surface glycans (Figure 1.13b). Control zebrafish that were bathed in Ac_4GalNAc instead of Ac_4GalNAz did not display fluorescence above background, underscoring the bioorthogonality of copper-free click chemistry. [57]

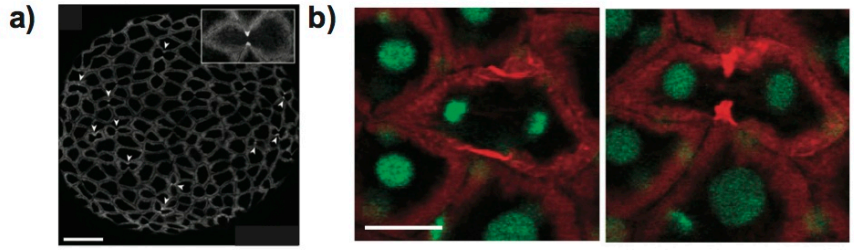


Figure 1.14. Imaging reorganization of glycans at cleavage furrows of mitotic cells in developing zebrafish. (a) Embryos were microinjected with GalNAz, developed to 10 hpf, labeled with DIFO-Alexa Fluor 488, and imaged via confocal microscopy. Arrows designate locations of high fluorescence signal. (b) Embryos from H2A-GFP transgenic zebrafish expressing a GFP-tagged histone for visualization of the nucleus were microinjected with GalNAz, developed to 10 hpf, and labeled with DIFO-Alexa Fluor 647. Images at 10 min (left) and 1 h (right) post-labeling. Scale bars: (a) 100 μm; (b) 20 μm. Figure adapted with permission from reference 58.

To image very early embryos (e.g., 7-10 hpf), azidosugars or their nucleotide sugar analogs can be microinjected at the one or two cell stage. [58] Applying this technique, it was discovered that mucin-type O-glycans undergo spatial reorganization during the cell cycle, transiently concentrating at the cleavage furrow during cytokinesis (Figure 1.14). Microinjection was later used to introduce SiaNAz [59] (Figure 1.15) and also Ac_3-4-Az-ManNAc [60] into developing zebrafish embryos or larvae, revealing temporal changes in distribution of the sialome throughout the course of development. To image fucosylated glycans, GDP-FucAz (Figure 1.15) was microinjected into embryos, enabling visualization of fucosylation as early as 7 hpf. [40] The nucleotide sugar was used in these studies as opposed to FucAz because, as mentioned earlier, FucAz may not be efficiently processed by fucose biosynthetic enzymes. In related example, Beahm *et al.* used UDP-4-XylAz (Figure 1.15) to label sites of glycosaminoglycan (GAG) synthesis and as a chain-terminating inhibitor of GAG elaboration. [61]

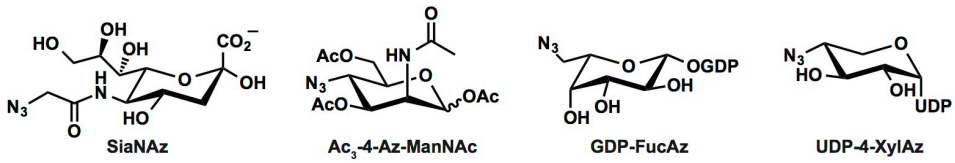


Figure 1.15. Additional azidosugars used in zebrafish labeling experiments with copper-free click chemistry.

Copper Free Click Chemistry in *C. Elegans*

The Cu-free click reaction has also been used to label and image sugars in *Caenorhabditis elegans*, again using the method of metabolic engineering. [62] Similar to zebrafish, *C. elegans* is a transparent organism with a well-understood developmental program. In the experiment, worms were grown on nematode growth medium (NGM) agar plates containing $Ac_4GalNAz$ for 24 hrs, after which they were labeled with DIFO-Alexa Fluor 488. The reaction produced robust, azide-dependent fluorescence on the surfaces of the worms. Labeling the azidosugars at different time points with different colored dyes enabled visualization of changes in glycan biosynthesis at various larval stages (Figure 1.16). For example, DIFO-labeling revealed continuous production of new glycans in portions of the worm implicated in motility. The glycans may be related to motility-enabling lubrication of these structures. [62]

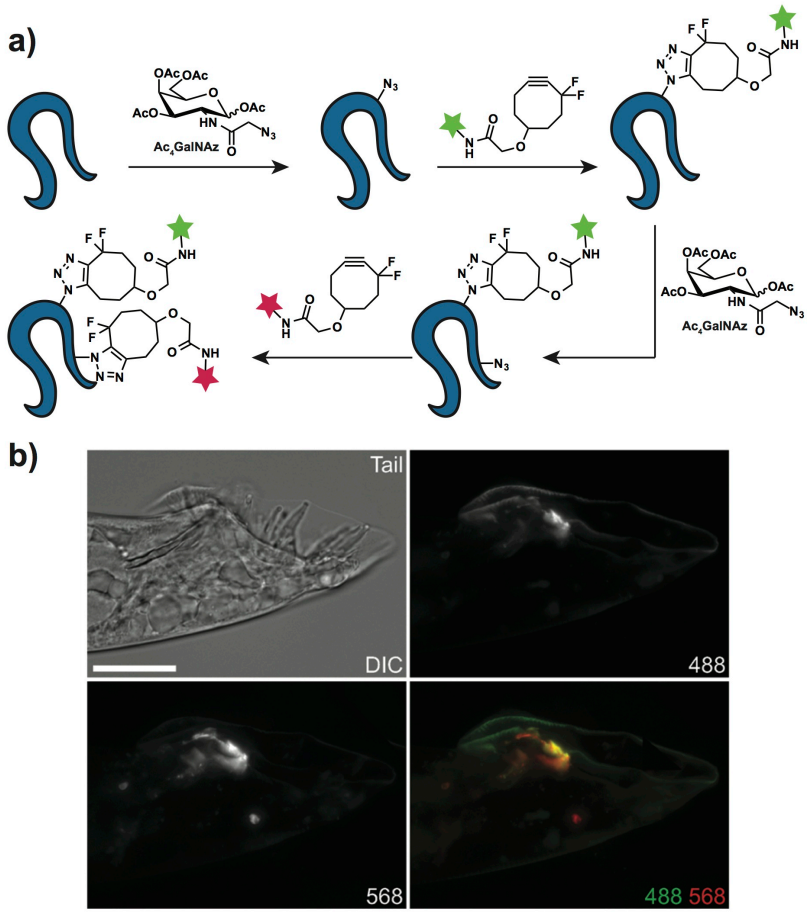


Figure 1.16. Two color imaging of glycan dynamics in *C. elegans*. (a) Worms were grown on NGM agar containing $Ac_4GalNAz$ for 24 hrs and then were labeled with DIFO-Alexa Fluor 488. Subsequently, the worms were re-exposed to $Ac_4GalNAz$ for 12 hrs and labeled with DIFO-Alexa Fluor 568. (b) Images of a dual-labeled *C. elegans* tail. Green (488) represents old glycans and red (568) represents the newer glycans. Scale bar is 25 μm. Figure 1.16b reprinted with permission from reference 62.

Zebrafish and *C. elegans* are both excellent models for evaluation of bioorthogonal chemistries *in vivo*. Their transparency, and in the case of zebrafish, amenability to microinjection, overcome many of the hurdles associated with *in vivo* imaging. However, an important step toward translation of bioorthogonal chemistries to clinical diagnostics and therapeutics is their application to mammalian organisms such as the mouse.

In an early mouse study, the reaction of cyclooctynes and metabolically incorporated azidosugars was performed *in vivo*, but analysis of cyclooctyne/azide conjugates was performed *ex vivo* on tissue homogenates due to the challenges of imaging in an opaque organism.[49] This study is of particular interest because it provides a comprehensive comparison of *in vitro* and *in vivo* labeling performance across cyclooctyne structures. When Jurkat cells with azide-modified sialic acid residues (installed via metabolic glycan

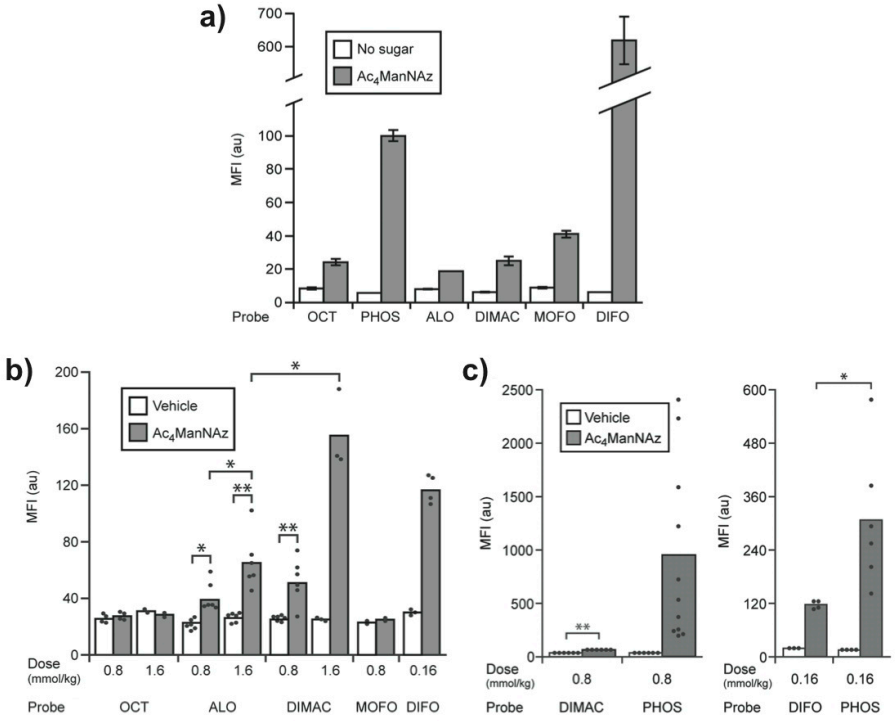


Figure 1.17. Copper-free click chemistry and the Staudinger ligation *in vitro* and *in vivo*. (a) Cells were grown in medium supplemented with or without $Ac_4ManNAz$ for three days and incubated with various FLAG-conjugated cyclooctynes or phosphine-FLAG at 250 μM for 1 h at rt. Cells were then labeled with fluorescein isothiocyanate (FITC) conjugated α-FLAG antibody and analyzed by flow cytometry. (b), (c) Mice were injected IP with $Ac_4ManNAz$ or vehicle for seven days and then injected IP with the indicated concentrations of (b), (c) cyclooctyne-FLAG conjugate or (c) phosphine-FLAG. After 3 h, mice were sacrificed, splenocytes were harvested, and FLAG peptide was labeled with FITC-α-FLAG antibody. Cells were analyzed by flow cytometry. MFI = mean fluorescence intensity. Figure adapted with permission from reference 49.

engineering with Ac_4ManNAz) were labeled with various cyclooctynes or the Staudinger ligation phosphine probe, labeling efficiency paralleled reactivity, with faster reagents generating the most signal (Figure 1.17a). The Staudinger phosphine probe was a notable exception, generating more signal than all cyclooctynes tested except DIFO despite its slow reaction rate.

This correlation between reactivity and labeling efficiency did not hold in the complex environment of the mouse. *In vivo*, DIMAC outperformed the other cyclooctynes despite being one of the less reactive reagents (Figure 1.17b) – perhaps a result of DIMAC's superior aqueous solubility. Surprisingly, the slow reacting, hydrophobic phosphine probe generated more signal than DIMAC (Figure 1.17c). These data suggest that the success of a bioorthogonal ligation *in vivo* is the result of a complicated combination of factors.[49] Much work remains to fully understand the fate of bioorthogonal reagents in the body of a live animal, but such information is crucial for future applications in therapeutics and diagnostics in humans.

Building on this work, Robillard and co-workers further explored the efficacy of the copper-free click reaction in living mice, this time using the pre-targeting approach to introduce the azide.[63] Rituximab, a monoclonal antibody that binds CD20 antigen on B-cells, was functionalized with azides as shown in Figure 1.18a to generate Rtx-N_3. In addition, probes **1.4**–**1.6** were synthesized, each bearing a radionuclide-chelating moiety (Figure 1.18b).[63] Rtx-N_3 was introduced into mice via intravenous (IV) injection followed by probes **1.4**, **1.5**, or **1.6** chelated to radionuclide ^{177}Lu as a bolus injection.

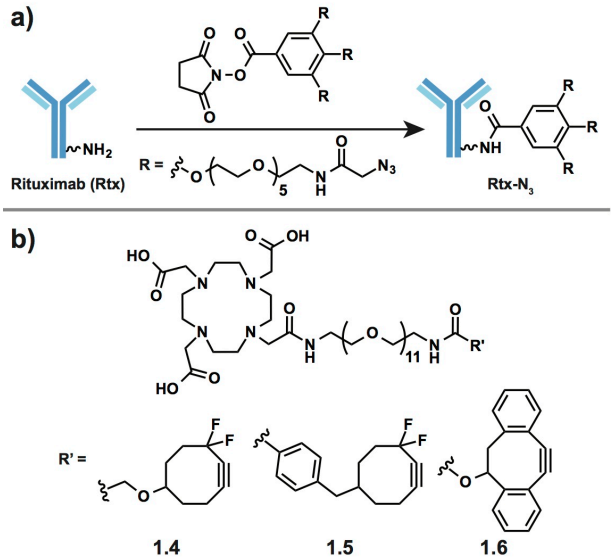


Figure 1.18. Pre-targeting experiment using copper-free click chemistry in mice. (a) Rituximab (Rtx) was functionalized on lysine residues with the triazide probe shown. (b) Cyclooctynes **1.4**–**1.6** were conjugated to DOTA, a metal chelator.

Mice were sacrificed 3 hrs later and biodistribution of the probes was analyzed. No evidence of ligation between the Rtx-N_3 probe and cyclooctynes **1.4**–**1.6** was observed,

perhaps due to the fast clearance times of the probes relative to the rate of the copper-free click reaction. These results suggest that a faster bioorthogonal reaction is necessary for the pre-targeting approach to be a viable therapeutic option. [63]

Lee, Kim and co-workers took a different approach to the pre-targeting system. [64] Instead of using antibodies to deliver a bioorthogonal handle to a target, they used mesoporous silica nanoparticles (MSNs), which accrue at tumor sites *in vivo* via the enhanced permeability and retention (EPR) effect. [65] Kim took advantage of this property to selectively deliver DIBAC-functionalized MSNs to tumors. Mice bearing subcutaneous tumors were injected IV with DIBAC-MSN **1.7** followed 24 hrs later by IV injection of ^{18}F-azide **1.8** (Figure 1.19a). PET imaging at various time-points after injection of the azide indicated significant buildup of signal at the tumor site in MSN treated mice relative to the no MSN control (Figure 1.19b), suggesting that the copper-free click reaction proceeded *in vivo*. [64]

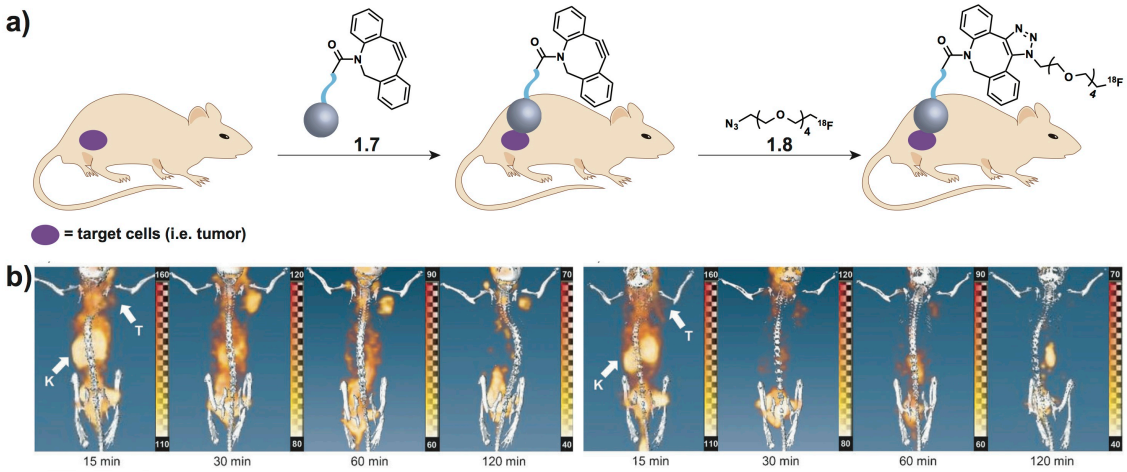


Figure 1.19. Imaging tumors in mice via pre-targeting with cyclooctyne-functionalized mesoporous nanoparticles. (a) Schematic of labeling experiment. (b) Mice bearing a subcutaneous U87 MG tumor were injected IV with DIBAC-functionalized MSN **1.7** (first four images) or were not injected with **1.7** (second four images) followed 24 hrs later by IV injection of ^{18}F-azide **1.8**. Mice were then imaged at multiple time points following injection of **1.8** via PET-CT. K = kidneys, T = tumor. Figure 1.19b adapted with permission from reference 64. Copyright 2013, John Wiley and Sons.

Building on this approach, Koo, Kim and co-workers designed an experiment in which an azide-bearing tumor modified via metabolic glycan engineering was labeled with a cyclooctyne/fluorophore liposome probe. [66] The researchers hypothesized that introducing the cyclooctyne/fluorophore probe as a liposome conjugate rather than as a small molecule would enhance *in vivo* labeling for three reasons: 1) similar to Lee and Kim's experiments, [64] the EPR effect would increase accumulation of the liposome at the tumor site, 2) the multivalent effect would increase the likelihood of successful ligation, and 3) liposomes have longer circulation times than do small molecules, enabling generation of more ligation product.

In their experiments, mice bearing two subcutaneous xenograft tumors were directly injected with Ac_4ManNAz at one tumor site and the other tumor was injected with

vehicle. Mice were then injected IV with DIBAC-Cy5-lipo, Cy5-lipo (no DIBAC), or DIBAC-Cy5 (Figure 1.20a). As a control, tris(2-carboxyethyl)phosphine (TCEP) was injected into the Ac_4ManNAz treated tumor of one of the mice to reduce azide moieties prior to introduction of the cyclooctyne reagent. Subsequent imaging revealed increased fluorescence in the tumors that were treated with Ac_4ManNAZ as compared to those treated with vehicle or TCEP (Figure 1.20b). Across azide labeled tumors, fluorescence signal was highest in those dosed with DIBAC-Cy5-lipo as compared to those injected

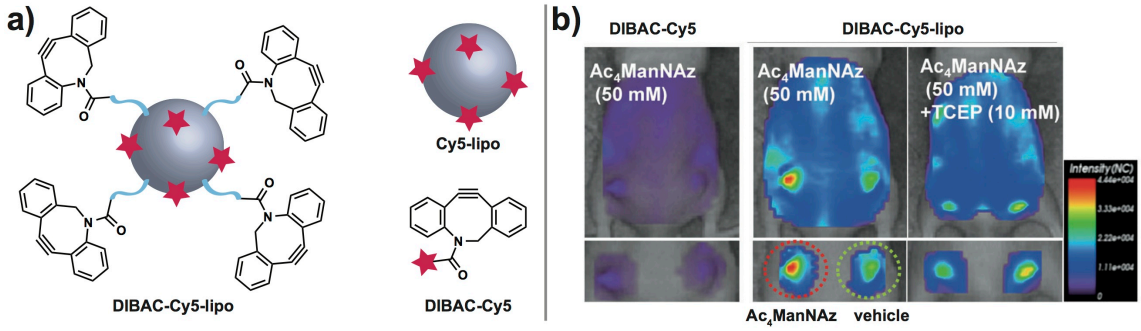


Figure 1.20. Copper-free click chemistry in mice using metabolic glycan labeling and a DIBAC-conjugated liposome. (a) PEGylated liposomes were synthesized using DIBAC-conjugated PEG lipids and Cy-5 conjugated lipids. A Cy5-liposome, without conjugated DIBAC molecules, as well as a Cy-5 conjugated DIBAC small molecule were prepared as controls. (b) Mice bearing two subcutaneous xenograft tumors were injected with Ac_4ManNAz in one tumor site and with saline in the other daily for three days. Mice were then injected IV with solutions of DIBAC-Cy5 or DIBAC-Cy5-lipo (both solutions at the same NIRF intensities) and analyzed via optical imaging. TCEP treated tumors were injected with TCEP (via intratumoral injection) to reduce azides 1 hr before IV injection of DIBAC reagents. Figure 1.20b adapted with permission from reference 66. Copyright 2012, John Wiley and Sons.

with Cy5-lipo and DIBAC-Cy5. These results suggests that labeling is cyclooctyne dependent, and that liposome-conjugated cyclooctynes are more effective labeling reagents than their small molecule counterparts. [66]

Notably, this approach requires direct injection of azidosugar into the tumor, which, for use in humans, would require knowledge of the exact tumor site and negate many of the benefits of this imaging approach. To overcome this challenge, Choi and Kim worked to develop a new method of tumor-selective azidosugar delivery, choosing to encapsulate Ac_4ManNAz in a glycol chitosan nanoparticle (CNP). [67] These nanoparticles selectively accumulate at the tumor site upon IV injection by the EPR effect, delivering Ac_4ManNAz to the tumor without the need for direct intratumoral injection. Upon successfully implementing this sugar delivery method, Kim introduced a second CNP conjugated to the cyclooctyne BCN and the photosensitizer Ce6, again via IV injection. Using this method, the researchers were able to achieve roughly 2-fold increased fluorescence (Ce6 is fluorescent in the near IR region) in mice treated with the Ac_4ManNAz nanoparticle relative to treatment with free Ac_4ManNAz or vehicle. As well, the nanoparticle-conjugated Ce6 photosensitizer was able to kill target cells by photodynamic therapy. [67]

To further improve on this azidosugar delivery method, Chen and co-workers engineered a system in which the azidosugar nanocarrier is directed to tumors using a tumor-

targeting peptide.[68] They functionalized PEGylated-liposome nanocarriers with the cRGDyK pentapeptide, a cyclic peptide that selectively binds the $\alpha_V\beta_3$ integrin, which is overexpressed on B16-F10 mouse melanoma cells, and used these nanocarriers to deliver various azidosugars to tumors via IV injection. Subsequent tail-vein injection of a DIBAC-Cy5 conjugate enabled tumor imaging.[68] This work represents an important development in the use of metabolic glycan engineering and copper-free click chemistry in living animals.

Background Reactivity of Cyclooctynes

One of the recurring themes in bioorthogonal chemistry is that increased reactivity often leads to unwanted side reactions in biological settings. It is widely recognized that a major challenge in the use of copper-free click chemistry is the off-target reactivity of the cyclooctyne with sulfhydryl groups. This reactivity was first reported by Bertozzi and co-workers in 2010 when use of the reaction in mice persistently and in an azide-independent manner produced cyclooctyne-labeled mouse serum albumin (MSA).[49] The researchers hypothesized that the azide-independent labeling of MSA was a result of thiol addition into the strained alkyne.

Later, Hanover and co-workers confirmed that cyclooctynes react with cysteine residues when they found that Nup62, a human nuclear pore protein with three cysteine residues, is labeled by DIFO-biotin in the absence of azides.[69] When the cysteine residues on Nup62 were capped with maleimides, the DIFO-biotin signal was eliminated. Similarly, Boelens and co-workers demonstrated that capping thiols with iodoacetimide reduces background reactivity of DIBO, DIBAC, and BCN.[70] However, these methods of global thiol capping cannot be used *in vivo*.

The Tetrazine Ligation

The tetrazine ligation, shown in Figure 1.21, is an inverse electron demand Diels-Alder reaction between tetrazine and a strained alkene to form intermediate **1.9**, followed by loss of N_2 and isomerization to give the ligation product shown. The reaction was independently reported by Blackman *et al.* and Devaraj *et al.* in 2008 – Blackman used transcyclooctene as the dienophile and Devaraj used norbornene.[71,72]

This tetrazine ligation has rapidly grown in popularity since Blackman and Devaraj's first reports. It has the fastest intrinsic kinetics of any bioorthogonal reaction developed to date, with second-order rate constants ranging from 10^{-2} to 10^6 $M^{-1}s^{-1}$ depending on the diene/dienophile combination used.[73–76] As a result of its superior kinetics, the tetrazine ligation is one of the most successful bioorthogonal reactions to be used in living animals.

Considerable work has been done to optimize both the reactivity and stability of the tetrazine probe to increase labeling efficiency. Whereas faster reacting tetrazines have potential to perform better *in vivo*, they also are more susceptible to attack by water and

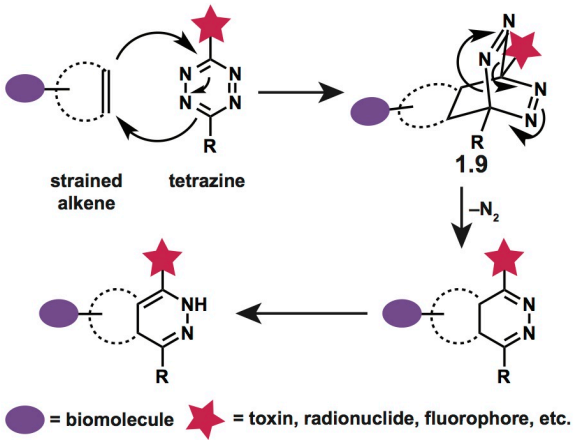
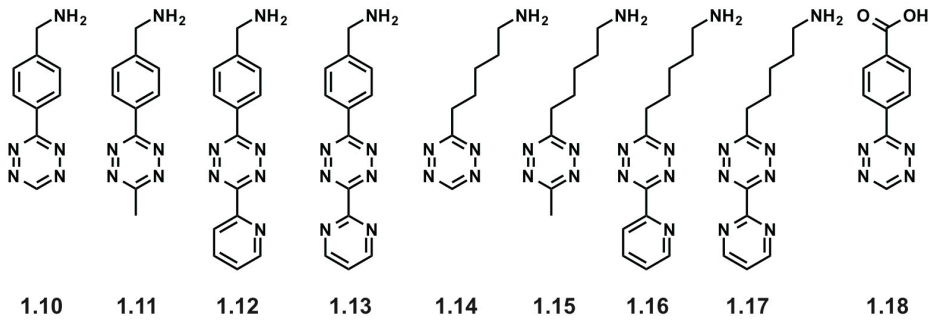


Figure 1.21. The tetrazine ligation.

other nucleophiles.[77] In 2011, Hilderbrand and co-workers performed a systematic study of the reactivities and stabilities of a panel of tetrazine analogs (Figure 1.22).[78] They measured the second order rate constant of the reaction of each analog with *trans*-cyclooctene and found that electron withdrawing groups on the tetrazine scaffold (**1.13** and **1.17**, Figure 1.22a) enhance reactivity, whereas electron donating groups (**1.11** and

a)



b)

tetrazine	k (M^{-1} s^{-1})	error
1.10	26000	500
1.11	820	70
1.12	5300	400
1.13	22000	2000
1.14	4900	100
1.15	210	20
1.16	2300	300
1.17	4400	300
1.18	30000	3000

c)

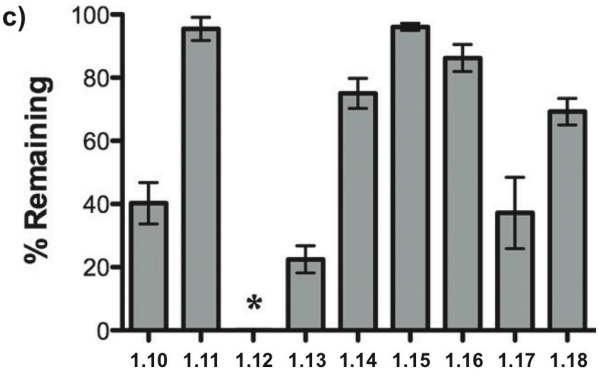


Figure 1.22. Analysis of tetrazine reactivity and stability. (a) Panel of tetrazine analogs. (b) The second order rate constant of the reaction between tetrazine analog and *trans*-cyclooctene was measured in FBS at 37 ºC. (c) The stability of tetrazine in aqueous conditions was measured by incubating each analog in FBS at 37 ºC for 10 h. Asterisk (*) represents compound that precipitated out of solution after 1.5–2 h. Figure 1.22c adapted with permission from reference 78. Copyright 2011, American Chemical Society.

1.15, Figure 1.22a) decrease reactivity. Interestingly, analogs with a hydrogen atom on one side of the tetrazine core (**1.10**, **1.14**, and **1.18**, Figure 1.22a) displayed faster kinetics than expected considering the hydrogen atom is less electron withdrawing than some of the other functionalities studied. The authors hypothesize that this high reactivity is a result of reduced steric congestion around the diene core.

The stability of each analog under aqueous conditions was also analyzed by incubating tetrazines in FBS at 37 ºC for 10 h and then measuring the amount of tetrazine remaining. Results show that high reactivity often corresponds with aqueous instability: some of the fastest analogs analyzed during this study (e.g. **1.10** and **1.13**, Figure 1.22a) are also some of the least stable in FBS (Figure 1.22c). Ultimately, Hilderbrand and co-workers opted for stability over reactivity in their on-cell studies, selecting analog **1.15** (~96% remaining after a 10 hr incubation in FBS) as the workhorse for their *in vitro* experiments. [78]

In addition to kinetics and stability optimization studies, considerable work has been done on the development of fluorogenic tetrazine probes that show enhancement in fluorescence upon reacting with a dienophile, [79–83] These probes rely on the ability of the tetrazine core to quench fluorescence in the 400-600 nm range. The ligation product, on the other hand, does not quench efficiently at these wavelengths. [79] Fluorogenic tetrazines are of value in cases where washing out excess probe is not a possibility, such as in the body of a living animal.

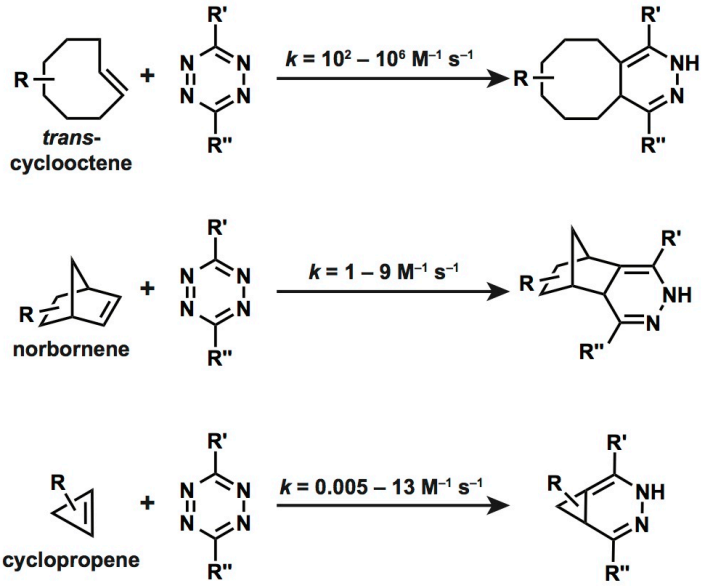


Figure 1.23. Dienophiles used in the tetrazine ligation.

The dienophile reaction partner has also been the subject of considerable optimization. *Trans*-cyclooctene (TCO, Figure 1.23) is the fastest reaction partner, reacting with tetrazine with a second order rate constant between 10^2 and 10^6 M^{-1} s^{-1} depending on its substituents and the tetrazine employed. [73,75,76,78] Due to its rapid reactivity, TCO is the most widely used diene, however, its high strain corresponds with instability under

various conditions used in biological experiments. TCO is known to isomerize to the orders of magnitude less reactive *cis*-cyclooctene over time. [75,84] Another strained alkene often used as a reaction partner for tetrazine is norbornene (Figure 1.23). [71] Norbornene is considerably more stable than TCO, but it also is many orders of magnitude less reactive with second order rate constants between 1– 9 M^{-1} s^{-1} in 95:5 H_2O:MeOH. [73,81] Along the same lines, Presher and Devaraj introduced cyclopropene (Figure 1.23) as a suitable reaction partner for tetrazine. [85,86] Though also much slower than TCO with second order rate constants between 0.005 M^{-1} s^{-1} (25% DMF in MOPS buffer) and 13 M^{-1} s^{-1} (12% DMSO in water), [86,87] cyclopropene's small size and relative stability are distinct advantages, enabling its facile incorporation into biomolecules via metabolic engineering and other methods. [73,85,86,88]

The Tetrazine Ligation in Mice

The majority of the work done to date to apply the tetrazine ligation *in vivo* has been performed via the pre-targeting approach. A major goal of this work is to optimize the tetrazine ligation pre-targeting technique as a therapeutic tool for cancer radioimaging and radioimmunotherapy.

In 2010, Robillard and co-workers showed that the tetrazine ligation proceeds in a living mouse and can be combined with pre-targeting to selectively label cancer cells. [89] They prepared α-TAG72 mAb CC49-TCO (Figure 1.24a) and Rituximab-TCO (Rtx-TCO, Figure 1.24a). CC49 binds TAG72, an antigen that is overexpressed on various tumors including the colorectal cancer model used in this study, whereas Rtx is not specific for TAG72 and served as a control. As well, Robillard prepared DOTA-tetrazine **19** (Figure 1.24b), which was later chelated to ^{111}In for single photon emission computed tomography/computed tomography SPECT/CT imaging of labeled mice.

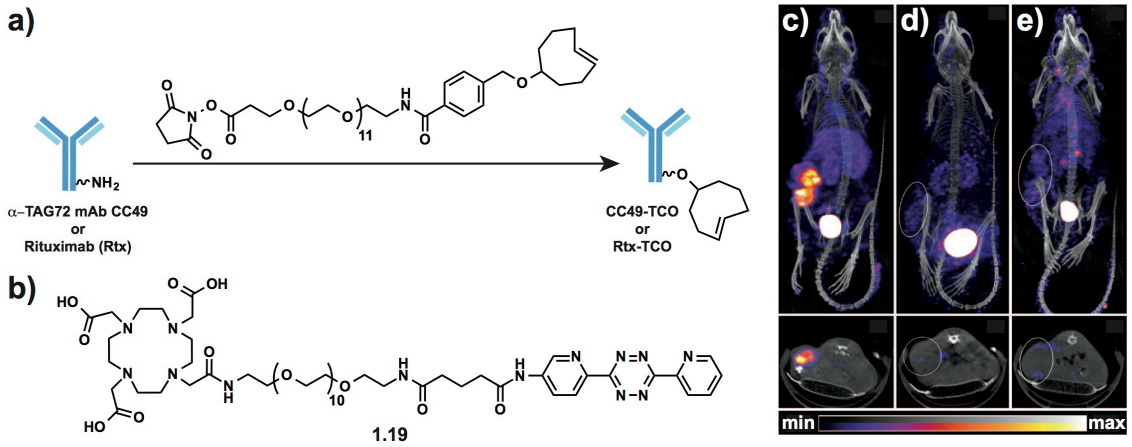


Figure 1.24. Labeling tumors in mice via the tetrazine ligation. (a) a-TAG72 mAb CC49 or Rituximab was conjugated to TCO via reaction of lysines with the TCO-NHS-ester shown to produce CC49-TCO or Rtx-TCO. (b) Tetrazine-DOTA conjugate **1.19** was prepared for use in *in vivo* labeling. Mice were injected IV with CC49-TCO (c), non-functionalized CC49 (d) and Rtx–TCO (e) and 24 hrs later were injected with ^{111}In-**1.19**. Mice were imaged 3 hrs after injection of **1.19** via SPECT/CT. Figures 1.24c,d, and e adapted with permission from reference 89. Copyright 2010, John Wiley and Sons.

Mice bearing xenografts of colon cancer tumors were injected with the CC49-TCO or Rtx-TCO and later with ^{111}In-tetrazine **1.19**. SPECT/CT imaging after tetrazine injection showed significant buildup of signal in the tumor area in mice injected with CC49-TCO (Figure 1.24c) and not in mice injected with antibody control (unlabeled α-TAG72 mAb CC49, Figure 1.24d). As well, mice injected with Rtx-TCO and ^{111}In-tetrazine **1.19** showed retention of ^{111}In in the blood and various organs (Figure 1.24e). This may be the result of the increased circulation time of ^{111}In-**1.19** conjugated to Rtx-TCO relative to the circulation time of ^{111}In-**1.19** alone, and is consistent with the lack of specificity of Rtx for the tumor cells. Overall, these results suggest successful conjugation between tetrazine and TCO in the mouse. [89] Of note is that a similar experiment in mice in which Rtx-N_3 was injected followed by injection of cyclooctynes **1.4**–**1.6** (Figure 1.18b) chelated to ^{177}Lu yielded no detectable retention of ^{177}Lu in blood, suggesting that the copper-free click reaction does not proceed efficiently *in vivo*. [63] The superior performance of the tetrazine ligation relative to copper-free click is in part attributable to the orders of magnitude rate difference between the two reactions. Later work supports Robillard's findings, affirming the utility of the tetrazine ligation *in vivo* using both the pre-targeting approach as well as metabolic glycan engineering. [90,91]

Since these initial studies, several groups have begun analyzing the effects of pharmacokinetics on reaction performance *in vivo*. Similar to previously described work in copper-free click chemistry, there has been a trend towards appending the tetrazine or alkene reagent to a macromolecular scaffold such as a polymer or a liposome. The increased circulation times of these large compounds as well as the benefits of the multivalent effect often enable superior *in vivo* labeling. Despite these benefits, however, the tradeoff is the increased potential for off-target damage if this scaffold is also appended to a radionuclide or toxin.

In 2011, Weissleder and co-workers performed a systematic study of the tetrazine ligation in living mice, emphasizing the importance of pharmacokinetics on ligation efficiency. [92] The authors studied the reactivity of two tetrazine-conjugated dextran polymers – one 10kDa polymer and one 40kDa polymer. Each polymer contained one fluorophore and approximately two or eleven tetrazines (10kDa and 40 kDa polymers respectively). They aimed to use the pre-targeting strategy along with these tetrazine-polymers to label tumors in living mice (Figure 1.25).

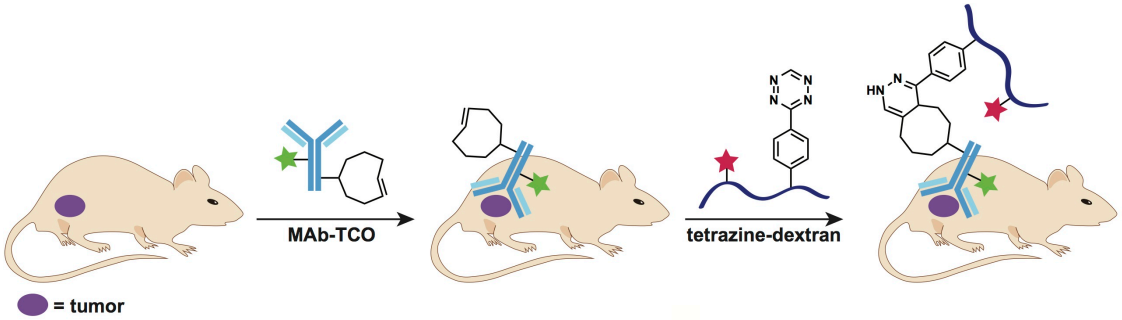


Figure 1.25. Labeling TCO-antibodies *in vivo* using a tetrazine-functionalized dextran polymer.

Weissleder hypothesized that the polymer-conjugated tetrazine would have longer *in vivo* circulation times than the small molecule variant, enabling more efficient labeling. Indeed, *in vivo* studies of probe clearance were consistent with this hypothesis. In tumor-bearing mice pre-targeted with a tumor-specific TCO-antibody, the polymer-bound tetrazines performed better than the corresponding small molecule tetrazine probe. Figure 1.26 shows fluorescence and PET/CT images of tumors labeled using the 10 kDa polymer after treatment with TCO-conjugated antibody (MAb-TCO) or with an unlabeled antibody (MAb). Signal is only present in TCO-MAb treated mice, highlighting the bioorthogonality of the technique. Building on this success, Devaraj and co-workers in 2014 performed a similar pre-targeting experiment using a ^{68}Ga-tetrazine-dextran polymer in mice. [93]

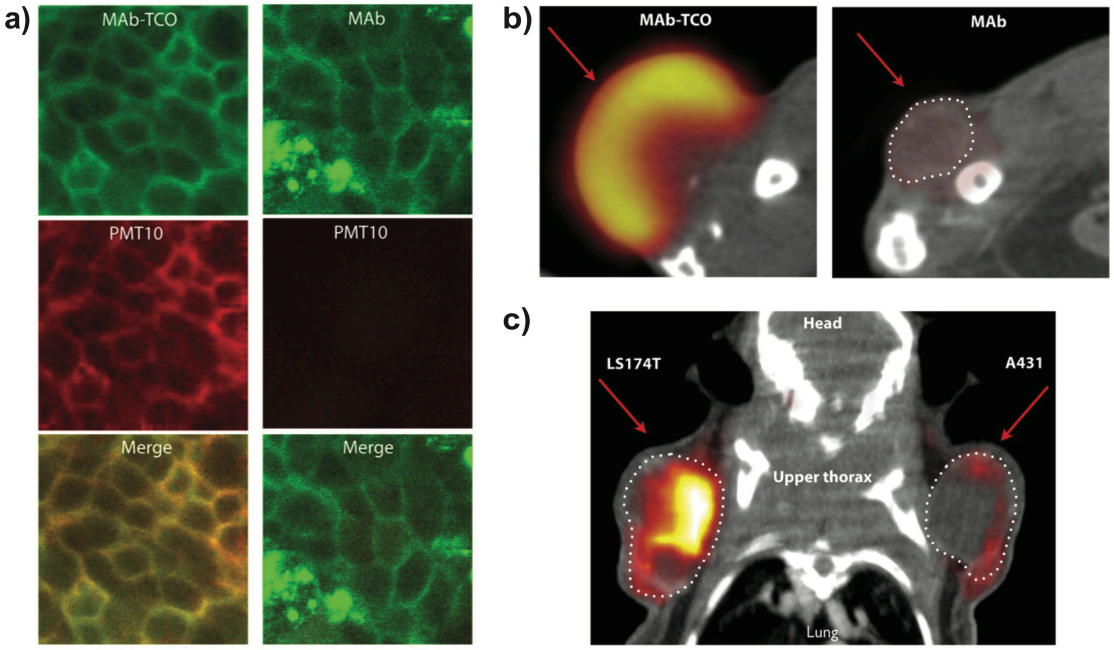


Figure 1.26. Imaging tumors in mice via the tetrazine ligation using tetrazine-functionalized dextran polymers. (a) Window chamber mice bearing subcutaneous colorectal cancer xenograft tumors (LS174T cells) were injected via tail vein with α-A33-TCO conjugated to VT-680 fluorophore (MAb-TCO) or α-A33 conjugated to VT-680 fluorophore (MAb) followed 24 hrs later by tail vein injection of 10 kDa tetrazine polymer conjugated to Alexa Fluor 750. Fluorescence at both 680 nm (top row) and 750 nm (middle row) were imaged. Bottom row is a merge. (b) Mice bearing LS147T xenograft tumors were injected via tail vein with α-A33-TCO (MAb-TCO) or unlabeled α-A33 (MAb) followed by tail vein injection of ^{18}F-tetrazine-dextran polymer (10 kDa) and imaged via PET/CT fusion. (c) A mouse bearing one LS147T tumor and one A431 tumor was injected via tail vein with TCO-conjugated α-A33 followed by tail vein injection of ^{18}F-tetrazine-dextran polymer an imaged via PET/CT.

Inspired by these results and realizing the immense importance of pharmacokinetics in addition to reaction kinetics in the success of an *in vivo* reaction, Weissleder and co-workers developed a model to predict the utility of a reaction based on its kinetic rate and the *in vivo* retention time of its components, quantified by the area under the concentration curve (AUC). [92] Figure 1.27 shows a heat map resulting from this model. It

is clear that the combination of a fast reaction rate and a long *in vivo* retention time generates successful labeling *in vivo*, whereas either component alone is not sufficient.

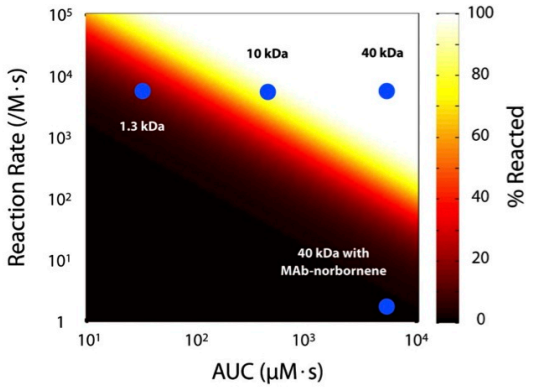


Figure 1.27. Computational model predicting the effects of reaction rate and secondary clearance rate (AUC) on % reaction. The point at 1.3 kDa represents a small molecule tetrazine-fluorophore. The points labeled 10 kDa and 40 kDa represent the corresponding dextran-tetrazine polymers. The point labeled 40 kDa with MAb-norbornene represents the reaction between the 40 kDa tetrazine polymer and a norbornene-labeled antibody.

Further highlighting the utility of macromolecule-bound reagents for *in vivo* bioconjugation experiments, Reiner and co-workers chose to use TCO-bound liposomes instead of polymers to label a tetrazine-tagged tumor in mice. [94] Aside from taking advantage of the pharmacokinetic properties of the liposome for improved labeling, this technology also has potential implications in the targeted delivery of toxic cargos to cancerous cells.

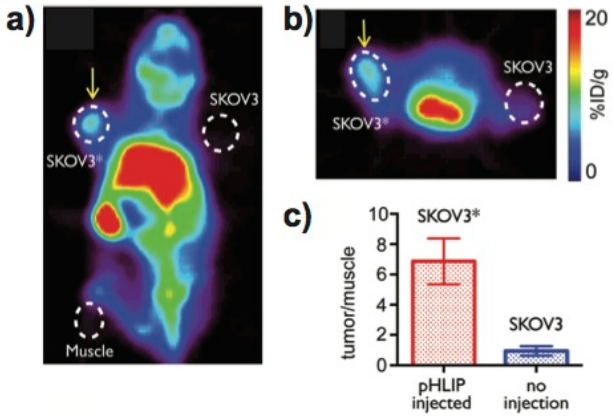
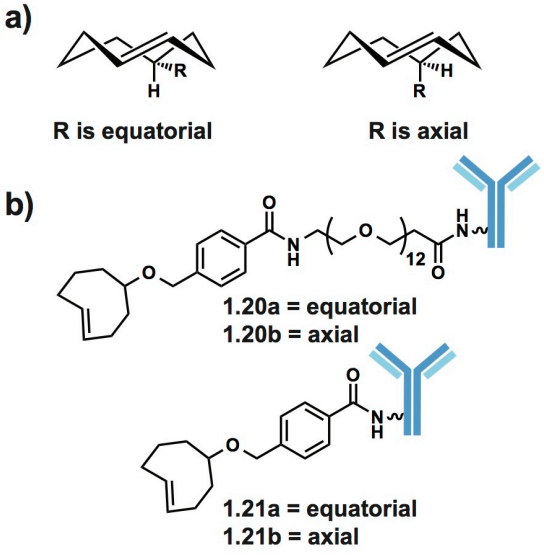


Figure 1.28. Imaging tumors in mice via the tetrazine ligation using tetrazine-functionalized pHLIP peptides and TCO-liposomes. (a), (b) Mice bearing two SKOV3 tumors (one on left shoulder and one on right shoulder) were injected with tetrazine-pHLIP peptide directly into the left tumor. The right tumor was not treated. 10 min later, ^{18}F-TCO-liposome was injected IV, and 2 h post liposome injection the mice were imaged via PET. (c) Tumor/muscle ratios measured 2 h after liposome injection. Figure adapted with permission from reference 94. Copyright 2013, American Chemical Society.

In the experiment, a tetrazine labeled pHLIP peptide (capable of targeting tumors via a pH dependent mechanism [95]) was delivered to tumors in mice via injection directly into the tumor. Upon subsequent IV injection of an ^{18}F labeled TCO-liposome, PET imaging revealed significant signal at the tumor sites of treated mice (Figure 1.28). [94] Again, these results highlight the utility of polymers and liposomes as reactive group carriers in the development of *in vivo* bioorthogonal chemistries. However, optimization of this approach is necessary because the pHLIP peptide required direct injection into the tumor for successful labeling.

In efforts to further optimize *in vivo* labeling via the pre-targeting strategy, Robillard and co-workers worked to increase the stability of the TCO reagent under physiological conditions. They did so by identifying a key liability of TCO – *in vivo* isomerization to *cis*-cyclooctene (CCO), a considerably less reactive substrate. [75] In the presence of certain copper-containing serum proteins, TCO moieties on a TCO-modified antibody are isomerized to *cis*-cyclooctene (CCO) with a half-life between 0.65–1.39 hrs, considerably shorter than TCO's >7 day half-life in PBS.

To overcome this challenge, the linker between TCO and its antibody carrier can be shortened, impeding isomerization via steric protection of TCO's double bond without altering reactivity toward tetrazine (Figure 1.29). [75] Robillard also discovered that TCO connected to a linker via the axial position is roughly ten-fold more reactive than the same TCO connected via the equatorial position (Figure 1.29). Combining the effects of axial connectivity with a shorter linker, compound **1.21b** achieves an ideal balance between reactivity and stability. In mice, **1.21b**'s superior reactivity and stability generated improved labeling compared to other TCO constructs. [75]



c)

TCO	*k* (x10⁴ M^{-1} s^{-1})	*in vivo* stability half-life (days)
1.20a	2.7 ± 0.2	2.62
1.20b	26.1 ± 0.5	1.12
1.21a	3.2 ± 0.2	6.19
1.21b	27.3 ± 0.5	3.94

Figure 1.29. Optimization of TCO-antibody connectivity for *in vivo* tetrazine ligation. (a) Equatorial versus axial connectivity of TCO. (b) TCO was conjugated to a CC49 antibody via the two different linkers shown and via the axial and equatorial positions. (c) The second order rate constant for the reaction of each TCO-antibody variant with a ^{177}Lu-conjugated tetrazine was measured in PBS at 37 ºC. The *in vivo* stability of each TCO-antibody variant was also measured (see reference 75 for a detailed description of the methods used to measure half-lives).

A liability of pre-targeting in general is residual circulation of functionalized antibodies, which generate off target signal upon introduction of a secondary probe. In the past, this challenge has been addressed by introduction of a pre-clearing agent capable to directing non-tumor bound antibody probe to the liver for clearance. [20] In 2014, Robillard and co-workers introduced a galactose- and tetrazine-functionalized albumin scaffold for use as a clearing agent. [96] This clearing agent rapidly reacts with any TCO-antibody in circulation and subsequently directs it to the liver. Using the clearing agent, a tumor/blood labeling ratio of 250 was achieved in mice versus a ratio of 2 when the clearing agent was not used.

Efforts to improve the tetrazine ligation for clinical applications are ongoing, as researchers work to optimize the pharmacokinetic properties of labeling reagents for *in vivo* use. [97–101] Others are working to expand the scope of the pre-targeting strategy, employing microbubbles [102] and implantable biomaterials [103] to deliver TCO or tetrazine to a target site. These studies pave the way for clinical diagnostic and therapeutic applications of the tetrazine ligation.

The Future of *In Vivo* Bioorthogonal Chemistry

As bioorthogonal chemistries continue to be optimized for performance in living systems, we foresee the applications of these uniquely selective reactions expanding to clinical therapeutics and diagnostics. Two opportunities for such expansion include the development of *in vivo* self-assembling drugs, and the advancement of prodrug design.

In Vivo Self-Assembling Drugs

In the 1990s, a decade prior to the introduction of the concept of bioorthogonality, Rideout and coworkers proposed the idea of "self-assembling chemotherapeutic agents," in which non-toxic fragments of a drug react *in vivo* to form the full toxin. [104–106] Ideally, these fragments would display "target selective synergism," meaning the environment around or in the target cells (i.e., tumor or pathogen) would enable the fragments to react faster than they would in nonpathogenic settings. This way, off target effects of the drug would be minimized.

The idea may well be realized using bioorthogonal chemistries. Indeed, Rideout's original description of the concept seemed to foreshadow the developments of the coming decade. Figure 1.30a shows an image from one of Rideout's early publications. [106] The figure depicts selective accumulation of two drug fragments, X and Y, in a target cell followed by their reaction to form X—Y. The 3-fold enhanced concentration of the fragments in the target relative to the normal cell then leads to increased reactivity, generating a 9-fold higher concentration of X—Y product in the target (assuming a second order reaction between X and Y). Aside from concentration gradients, Rideout also discusses the possibility of enhanced reactivity due to environmental effects near the target (i.e. pH, reduction potential, etc.).

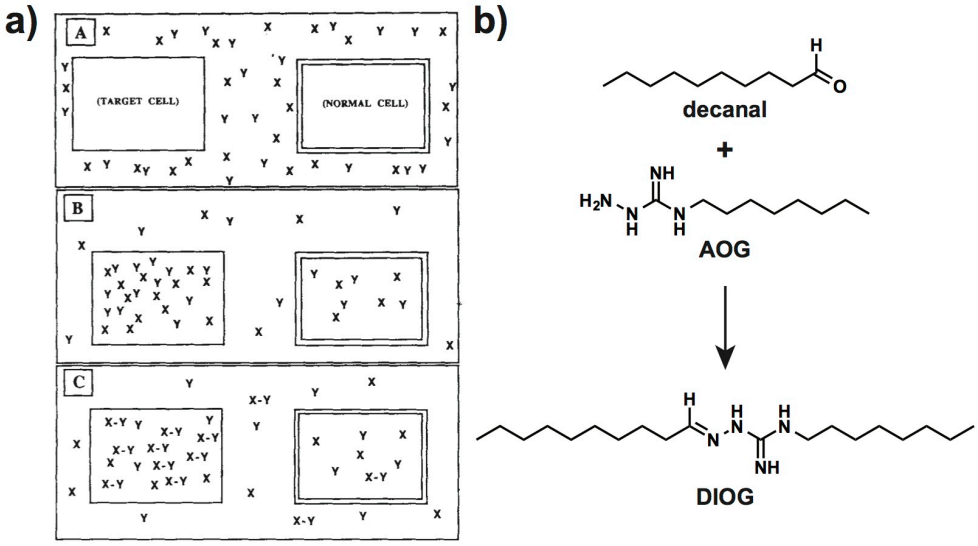


Figure 1.30. Self-assembling chemotherapeutic agents. (a) Rideout's original proposal of self-assembling drugs where assembly is promoted by the environment in or around a target cell. b) An example of a self-assembling chemotherapeutic. Decanal and *N*-amino-*N*′-octyl guanidine (AOG) react to form the cytolytic agent *N*-(1-decylidenimino)-*N*′-1-octylguanidine (DIOG). Figure 1.30a adapted with permission from reference 106. Copyright 2004, John Wiley and Sons.

In his original publications, Rideout used aldehyde/hydrazide condensation chemistry to assemble drugs *in vivo*. In one example, he achieved enhanced reactivity between decanal and *N*-amino-*N*′-octyl guanidine (AOG) in low serum environments versus high serum (Figure 1.30b). [106] Decanal and AOG react to form the cytolytic agent *N*-(1-decylidenimino)-*N*′-1-octylguanidine (DIOG), which kills cells by damaging the membrane. DIOG is much more cytotoxic than either AOG or decanal alone. The reactivity differential in low versus high serum is caused by sequestration of decanal via binding to serum proteins, a process that is magnified under high serum conditions. As well, the toxicity of DIOG is reduced in high serum environments, also due sequestration, which reduces DIOG's access to the cell membrane. [106]

Rideout's work sets the stage for more recent work in self-assembling drugs. Given the considerable expansion of the bioorthogonal toolbox since his early publications, the concept of self-assembling drugs can now be revisited through the lens of modern reactions. In a recent example, Dyson and co-workers used the reaction between BCN and tetrazine (tetrazine is known to react with some strained alkynes [107,108]) to form a cytotoxic dinuclear ruthenium drug for cancer treatment (Figure 1.31). [109] They showed that mononuclear ruthenium compound **1.22** (IC_{50} in A2780 cell line is 12 ± 1 μM) is considerably less cytotoxic than dinuclear complex **1.24** (IC_{50} in A2780 cell line is 2.6 ± 0.2 μM) formed by the tetrazine/BCN reaction. Though considerable research is required to determine a method of co-localizing **1.22** and **1.23** at target cells *in vivo*, the work is a promising demonstration of the viability of Rideout's original proposal.

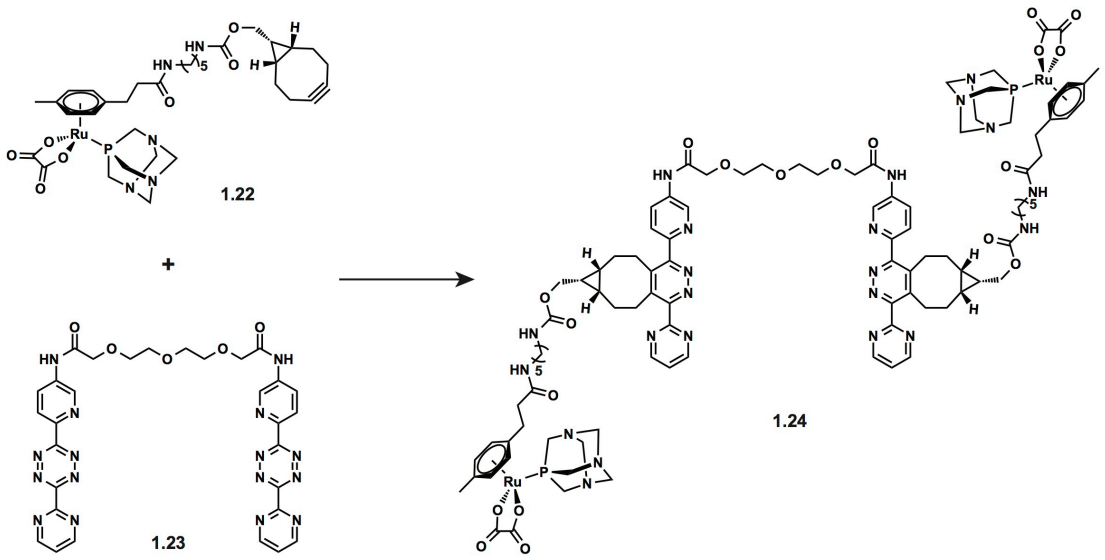


Figure 1.31. Dinuclear ruthenium cytotoxin assembled via tetrazine/cyclooctyne cycloaddition.

Bioorthogonal Prodrugs

Another exciting new application of bioorthogonal reactions is their use in the development of prodrugs that are activated only in target environments. In 2008, Robillard and co-workers published an example of doxorubicin prodrug activation via Staudinger reduction. [110] Caged doxorubicin **1.25** was designed for activation via reduction of its azide to an amine using triphenylphosphine **1.26** followed by release of free doxorubicin **1.27** via the mechanism shown in Figure 1.32. For future applications of this system *in vivo*, Robillard proposes appending prodrug **1.25** to a polymer capable of targeting tumors via the EPR effect. Upon buildup of the polymer at the tumor site, triphenylphosphine **1.26** is injected to achieve release of free doxorubicin. While use of **1.25** *in vivo* has not yet been published, the idea holds promise as an application of bioorthogonal chemistry for targeted therapies.

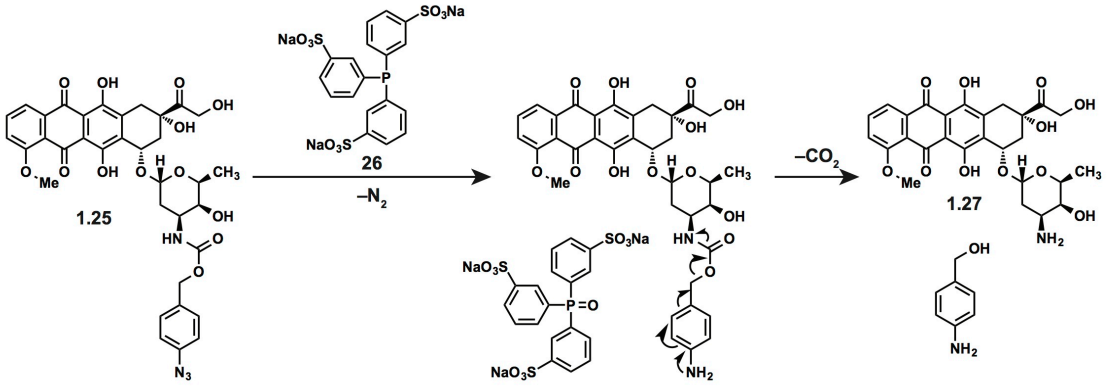


Figure 1.32. Doxorubicin prodrug activated via Staudinger reduction.

In another example of prodrug activation via bioorthogonal chemistry, Robillard and co-workers developed the tetrazine ligation prodrug strategy shown in Figure 1.33. Here, doxorubicin is appended to TCO via a carbamate linkage to form prodrug **1.28**. Upon reaction of TCO with an appropriate tetrazine, doxorubicin **1.27** is released. Though the mechanism of release has not been fully investigated, one possibility is depicted in Figure 1.33. The researchers propose using this new prodrug strategy as a method of cleaving toxins from antibody drug conjugates (ADCs). [111]

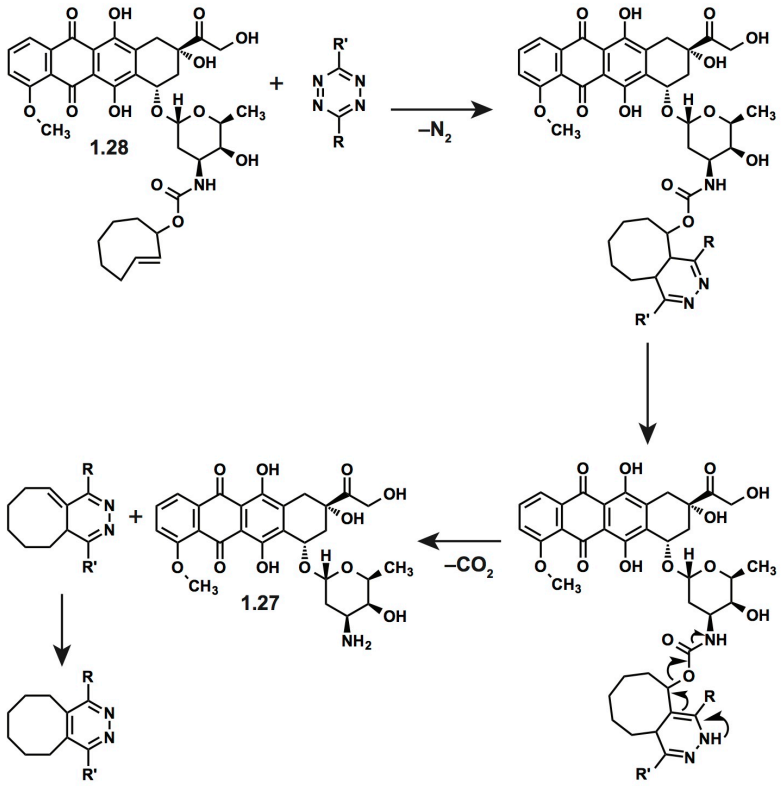


Figure 1.33. Doxorubicin prodrug activated via tetrazine ligation.

In addition to these two examples from Robillard, others have published use of the Staudinger ligation [112] and strain-promoted 1,3-dipolar cycloaddition between TCO and azide [113] as methods of prodrug activation.

Conclusion

Though much work has already been done towards the development of bioorthgoonal chemistry as a valuable tool for both chemists and biologists, we are only just starting to realize the full potential of these uniquely mild and selective reactions. As the field continues to mature, so too will the scope of its applications. New opportunities are bound to arise as researchers push toward new methods of incorporating bioorthogonal handles into molecules in living systems. For example, non-natural amino acid incorporation is a rapidly progressing technique used to site selectively install functional

groups into proteins for subsequent chemical modification.[114] Recently, Chin and co-workers have published use of the pyrrolysine synthetase method of non-natural amino acid incorporation in live animals such as fruit flies.[115] Though modification of these tagged proteins via bioorthogonal ligation has thus far only been achieved *ex vivo*, in time bioorthogonal tagging of non-natural amino acid-containing proteins in multicellular organisms will be realized.

Opportunities for *in vivo* bioorthogonal ligations will also expand as researchers continue to optimize reaction kinetics as well as pharmacokinetics of reagents. Considerable work must be done to better understand the fate of bioorthogonal reagents in living systems. As well, engineering to optimize tissue access, blood circulation time, and aqueous solubility must be performed.

Finally, additional opportunities will arise as new bioorthogonal reactions are developed. Most of the ligation chemistries developed to date are designed to generate a stable covalent bond *in vivo*. However, one can imagine myriad other functionalities embedded in the reaction. For example, Lin and co-workers have introduced a series of light-induced bioorthogonal reactions.[116,117] These reactions, referred to as "photo-click" chemistries, can afford exquisite spatial and temporal control of the ligation.

Thus, this chapter reflects only the beginning of what will be a continuously growing and evolving field with exciting and impactful applications.

References

1. Sletten, E. M.; Bertozzi, C. R. Bioorthogonal chemistry: Fishing for selectivity in a sea of functionality. *Angew. Chem. Int. Ed.* **2009**, *48*, 6974-6998.
2. Sletten, E. M.; Bertozzi, C. R. From mechanism to mouse: A tale of two bioorthogonal reactions. *Acc. Chem. Res.* **2011**, *44*, 666-676.
3. Varki, A.; Cummings, R. D.; Esko, J. D.; Freeze, H. H.; Stanley, P.; Bertozzi, C. R.; Hart, G. W.; Etzler, M. E. *Essentials of Glycobiology, 2nd edition;* Cold Spring Harbor Laboratory Press: Cold Spring Harbor, NY, **2009**.
4. Dube, D. H.; Bertozzi, C. R. Metabolic oligosaccharide engineering as a tool for glycobiology. *Curr. Opin. Chem. Biol.* **2003**, *7*, 616-625.
5. Dube, D. H.; Bertozzi, C. R. Glycans in cancer and inflammation—potential for therapeutics and diagnostics. *Nat Rev Drug Discov* **2005**, *4*, 477-488.
6. Christiansen, M. N.; Chik, J.; Lee, L.; Anugraham, M.; Abrahams, J. L.; Packer, N. H. Cell surface protein glycosylation in cancer. *Proteomics* **2014**, *14*, 525-546.
7. Kayser, H.; Zeitler, R.; Kannicht, C.; Grunow, D.; Nuck, R.; Reutter, W. Biosynthesis of a nonphysiological sialic acid in different rat organs using N-propanoyl-D-hexosamines as precursors. *J. Biol. Chem.* **1992**, *267*, 16934-16938.
8. Mahal, L. K.; Yarema, K. J.; Bertozzi, C. R. Engineering chemical reactivity on cell surfaces through oligosaccharide biosynthesis. *Science* **1997**, *276*, 1125-1128.
9. Saxon, E.; Bertozzi, C. R. Cell surface engineering by a modified staudinger reaction. *Science* **2000**, *287*, 2007-2010.
10. Agard, N. J.; Prescher, J. A.; Bertozzi, C. R. A strain-promoted [3 + 2] azide-alkyne cycloaddition for covalent modification of biomolecules in living systems. *J. Am. Chem. Soc.* **2004**, *126*, 15046-15047.

11. Chang, P. V.; Chen, X.; Smyrniotis, C.; Xenakis, A.; Hu, T.; Bertozzi, C. R.; Wu, P. Metabolic labeling of sialic acids in living animals with alkynyl sugars. *Angew. Chem. Int. Ed.* **2009**, *48*, 4030-4033.
12. Hsu, T.; Hanson, S. R.; Kishikawa, K.; Wang, S.; Sawa, M.; Wong, C. Alkynyl sugar analogs for the labeling and visualization of glycoconjugates in cells. *Proc. Natl. Acad. Sci. USA* **2007**, *104*, 2614-2619.
13. Vocadlo, D. J.; Hang, H. C.; Kim, E.; Hanover, J. A.; Bertozzi, C. R. A chemical approach for identifying *O*-GlcNAc-modified proteins in cells. *Proc. Natl. Acad. Sci. USA* **2003**, *100*, 9116-9121.
14. Zaro, B. W.; Yang, Y.; Hang, H. C.; Pratt, M. R. Chemical reporters for fluorescent detection and identification of O-GlcNAc-modified proteins reveal glycosylation of the ubiquitin ligase NEDD4-1. *Proc. Natl. Acad. Sci. USA* **2011**, *108*, 8146-8151.
15. Bateman, L. A.; Zaro, B. W.; Chuh, K. N.; Pratt, M. R. N-propargyloxycarbamate monosaccharides as metabolic chemical reporters of carbohydrate salvage pathways and protein glycosylation. *Chem. Commun.* **2013**, *49*, 4328-4330.
16. Hang, H. C.; Yu, C.; Kato, D. L.; Bertozzi, C. R. A metabolic labeling approach toward proteomic analysis of mucin-type *O*-linked glycosylation. *Proc. Natl. Acad. Sci. USA* **2003**, *100*, 14846-14851.
17. Boyce, M.; Carrico, I. S.; Ganguli, A. S.; Yu, S.; Hangauer, M. J.; Hubbard, S. C.; Kohler, J. J.; Bertozzi, C. R. Metabolic cross-talk allows labeling of *O*-linked ß-*N*-acetylglucosamine-modified proteins via the *N*-acetylgalactosamine salvage pathway. *Proc. Natl. Acad. Sci. USA* **2011**, *108*, 3141-3146.
18. Chuh, K. N.; Zaro, B. W.; Piller, F.; Piller, V.; Pratt, M. R. Changes in metabolic chemical reporter structure yield a selective probe of *O*-GlcNAc modification. *J. Am. Chem. Soc.* **2014**, *136*, 12283-12295.
19. Saxon, E.; Luchansky, S. J.; Hang, H. C.; Yu, C.; Lee, S. C.; Bertozzi, C. R. Investigating cellular metabolism of synthetic azidosugars with the staudinger ligation. *J. Am. Chem. Soc.* **2002**, *124*, 14893-14902.
20. Boerman, O. C.; van Schaijk, F. G.; Oyen, W. J. G.; Corstens, F. H. M. Pretargeted radioimmunotherapy of cancer: Progress step by step. *J. Nucl. Med.* **2003**, *44*, 400-411.
21. Lin, F. L.; Hoyt, H. M.; van Halbeek, H.; Bergman, R. G.; Bertozzi, C. R. Mechanistic investigation of the staudinger ligation. *J. Am. Chem. Soc.* **2005**, *127*, 2686-2695.
22. Prescher, J. A.; Dube, D. H.; Bertozzi, C. R. Chemical remodelling of cell surfaces in living animals. *Nature* **2004**, *430*, 873-877.
23. Neves, A. A.; Stöckmann, H.; Harmston, R. R.; Pryor, H. J.; Alam, I. S.; Ireland-Zecchini, H.; Lewis, D. Y.; Lyons, S. K.; Leeper, F. J.; Brindle, K. M. Imaging sialylated tumor cell glycans in vivo. *FASEB J.* **2011**, *25*, 2528-2537.
24. Vugts, D. J.; Vervoort, A.; Stigter-van Walsum, M.; Visser, G. W. M.; Robillard, M. S.; Versteegen, R. M.; Vulders, R. C. M.; Herscheid, J. K.; van Dongen, Guus A. M. S. Synthesis of phosphine and antibody-azide probes for in vivo staudinger ligation in a pretargeted imaging and therapy approach. *Bioconjugate Chem.* **2011**, *22*, 2072-2081.
25. Rostovtsev, V. V.; Green, L. G.; Fokin, V. V.; Sharpless, K. B. A stepwise huisgen cycloaddition process: Copper(I)-catalyzed regioselective "ligation" of azides and terminal alkynes. *Angew. Chem. Int. Ed.* **2002**, *41*, 2596-2599.
26. Tornoe, C. W.; Christensen, C.; Meldal, M. Peptidotriazoles on solid phase: [1,2,3]-triazoles by regiospecific copper(I)-catalyzed 1,3-dipolar cycloadditions of terminal alkynes to azides. *J. Org. Chem.* **2002**, *67*, 3057-3064.
27. Soriano, d. A.; Wang, W.; Jiang, H.; Besanceney, C.; Yan, A. C.; Levy, M.; Liu, Y.; Marlow, F. L.; Wu, P. Biocompatible copper(I) catalysts for in vivo imaging of glycans. *J. Am. Chem. Soc.* **2010**, *132*, 16893-16899.

28. Kolb, H. C.; Finn, M. G.; Sharpless, K. B. Click chemistry: Diverse chemical function from a few good reactions. *Angew. Chem. Int. Ed.* **2001**, *40*, 2004-2021.
29. Wang, Q.; Chan, T. R.; Hilgraf, R.; Fokin, V. V.; Sharpless, K. B.; Finn, M. G. Bioconjugation by copper(I)-catalyzed azide-alkyne [3 + 2] cycloaddition. *J. Am. Chem. Soc.* **2003**, *125*, 3192-3193.
30. Macomber, L.; Imlay, J. A. The iron-sulfur clusters of dehydratases are primary intracellular targets of copper toxicity. *Proc. Natl. Acad. Sci. USA* **2009**, *106*, 8344-8349.
31. Chan, T. R.; Hilgraf, R.; Sharpless, K. B.; Fokin, V. V. Polytriazoles as copper(I)-stabilizing ligands in catalysis. *Org. Lett.* **2004**, *6*, 2853-2855.
32. Hong, V.; Steinmetz, N. F.; Manchester, M.; Finn, M. G. Labeling live cells by copper-catalyzed alkyne-azide click chemistry. *Bioconjugate Chem.* **2010**, *21*, 1912-1916.
33. Hong, V.; Presolski, S. I.; Ma, C.; Finn, M. G. Analysis and optimization of copper-catalyzed azide-alkyne cycloaddition for bioconjugation. *Angew. Chem. Int. Ed.* **2009**, *48*, 9879-9883.
34. Harris, E. D. Copper homeostasis: The role of cellular transporters. *Nutr. Rev.* **2001**, *59*, 281-285.
35. Rodionov, V. O.; Presolski, S. I.; Gardinier, S.; Lim, Y.; Finn, M. G. Benzimidazole and related ligands for cu-catalyzed azide-alkyne cycloaddition. *J. Am. Chem. Soc.* **2007**, *129*, 12696-12704.
36. Besanceney-Webler, C.; Jiang, H.; Zheng, T.; Feng, L.; Soriano del Amo, D.; Wang, W.; Klivansky, L. M.; Marlow, F. L.; Liu, Y.; Wu, P. Increasing the efficacy of bioorthogonal click reactions for bioconjugation: A comparative study. *Angew. Chem. Int. Ed.* **2011**, *50*, 8051-8056.
37. Uttamapinant, C.; Tangpeerachaikul, A.; Grecian, S.; Clarke, S.; Singh, U.; Slade, P.; Gee, K. R.; Ting, A. Y. Fast, cell-compatible click chemistry with copper-chelating azides for biomolecular labeling. *Angew. Chem. Int. Ed.* **2012**, *51*, 5852-5856.
38. Uttamapinant, C.; Sanchez, M. I.; Liu, D. S.; Yao, J. Z.; Ting, A. Y. Site-specific protein labeling using PRIME and chelation-assisted click chemistry. *Nat. Protocols* **2013**, *8*, 1620-1634.
39. Jiang, H.; Zheng, T.; Lopez-Aguilar, A.; Feng, L.; Kopp, F.; Marlow, F. L.; Wu, P. Monitoring dynamic glycosylation in vivo using supersensitive click chemistry. *Bioconjugate Chem.* **2014**, *25*, 698-706.
40. Dehnert, K. W.; Beahm, B. J.; Huynh, T. T.; Baskin, J. M.; Laughlin, S. T.; Wang, W.; Wu, P.; Amacher, S. L.; Bertozzi, C. R. Metabolic labeling of fucosylated glycans in developing zebrafish. *ACS Chem. Biol.* **2011**, *6*, 547-552.
41. Zheng, T.; Jiang, H.; Gros, M.; Soriano del Amo, D.; Sundaram, S.; Lauvau, G.; Marlow, F.; Liu, Y.; Stanley, P.; Wu, P. Tracking *N*-acetyllactosamine on cell-surface glycans in vivo. *Angew. Chem.* **2011**, *123*, 4199-4204.
42. Wittig, G.; Krebs, A. Zur existenz niedergliedriger cycloalkine, I. *Chem. Ber.* **1961**, *94*, 3260-3275.
43. Agard, N. J.; Baskin, J. M.; Prescher, J. A.; Lo, A.; Bertozzi, C. R. A comparative study of bioorthogonal reactions with azides. *ACS Chem. Biol.* **2006**, *1*, 644-648.
44. Schoenebeck, F.; Ess, D. H.; Jones, G. O.; Houk, K. N. Reactivity and regioselectivity in 1,3-dipolar cycloadditions of azides to strained alkynes and alkenes: A computational study. *J. Am. Chem. Soc.* **2009**, *131*, 8121-8133.
45. Gordon, C. G.; Mackey, J. L.; Jewett, J. C.; Sletten, E. M.; Houk, K. N.; Bertozzi, C. R. Reactivity of biarylazacyclooctynones in copper-free click chemistry. *J. Am. Chem. Soc.* **2012**, *134*, 9199-9208.
46. Baskin, J. M.; Prescher, J. A.; Laughlin, S. T.; Agard, N. J.; Chang, P. V.; Miller, I. A.; Lo, A.; Codelli, J. A.; Bertozzi, C. R. Copper-free click chemistry for dynamic in vivo imaging. *Proc. Natl. Acad. Sci. USA* **2007**, *104*, 16793-16797.

47. Codelli, J. A.; Baskin, J. M.; Agard, N. J.; Bertozzi, C. R. Second-generation difluorinated cyclooctynes for copper-free click chemistry. *J. Am. Chem. Soc.* **2008**, *130*, 11486-11493.
48. Sletten, E. M.; Bertozzi, C. R. A hydrophilic azacyclooctyne for cu-free click chemistry. *Org. Lett.* **2008**, *10*, 3097-3099.
49. Chang, P. V.; Prescher, J. A.; Sletten, E. M.; Baskin, J. M.; Miller, I. A.; Agard, N. J.; Lo, A.; Bertozzi, C. R. Copper-free click chemistry in living animals. *Proc. Natl. Acad. Sci. USA* **2010**, *107*, 1821-1826.
50. Ning, X.; Guo, J.; Wolfert, M.; Boons, G. Visualizing metabolically labeled glycoconjugates of living cells by copper-free and fast huisgen cycloadditions. *Angewandte Chemie* **2008**, *120*, 2285-2287.
51. Mbua, N. E.; Guo, J.; Wolfert, M. A.; Steet, R.; Boons, G. Strain-promoted alkyne-azide cycloadditions (SPAAC) reveal new features of glycoconjugate biosynthesis. *ChemBioChem* **2011**, *12*, 1912-1921.
52. Debets, M. F.; van Berkel, S. S.; Schoffelen, S.; Rutjes, F. P. J. T.; van Hest, Jan C. M.; van Delft, F. L. Aza-dibenzocyclooctynes for fast and efficient enzyme PEGylation via copper-free (3+2) cycloaddition. *Chem. Commun.* **2010**, *46*, 97-99.
53. Jewett, J. C.; Sletten, E. M.; Bertozzi, C. R. Rapid cu-free click chemistry with readily synthesized biarylazacyclooctynones. *J. Am. Chem. Soc.* **2010**, *132*, 3688-3690.
54. Dommerholt, J.; Schmidt, S.; Temming, R.; Hendriks, L. J. A.; Rutjes, F. P. J. T.; van Hest, J. C. M.; Lefeber, D. J.; Friedl, P.; van Delft, F. L. Readily accessible bicyclononynes for bioorthogonal labeling and three-dimensional imaging of living cells. *Angew. Chem. Int. Ed.* **2010**, *49*, 9422-9425.
55. Shieh, P.; Siegrist, M. S.; Cullen, A. J.; Bertozzi, C. R. Imaging bacterial peptidoglycan with near-infrared fluorogenic azide probes. *Proc. Natl. Acad. Sci. USA* **2014**, *111*, 5456-5461.
56. Lang, K.; Davis, L.; Wallace, S.; Mahesh, M.; Cox, D. J.; Blackman, M. L.; Fox, J. M.; Chin, J. W. Genetic encoding of bicyclononynes and trans-cyclooctenes for site-specific protein labeling in vitro and in live mammalian cells via rapid fluorogenic diels-alder reactions. *J. Am. Chem. Soc.* **2012**, *134*, 10317-10320.
57. Laughlin, S. T.; Baskin, J. M.; Amacher, S. L.; Bertozzi, C. R. In vivo imaging of membrane-associated glycans in developing zebrafish. *Science* **2008**, *320*, 664-667.
58. Baskin, J. M.; Dehnert, K. W.; Laughlin, S. T.; Amacher, S. L.; Bertozzi, C. R. Visualizing enveloping layer glycans during zebrafish early embryogenesis. *Proc. Natl. Acad. Sci. USA* **2010**, *107*, 10360-10365.
59. Dehnert, K. W.; Baskin, J. M.; Laughlin, S. T.; Beahm, B. J.; Naidu, N. N.; Amacher, S. L.; Bertozzi, C. R. Imaging the sialome during zebrafish development with copper-free click chemistry. *ChemBioChem* **2012**, *13*, 353-357.
60. Möller, H.; Böhrsch, V.; Bentrop, J.; Bender, J.; Hinderlich, S.; Hackenberger, C. P. R. Glycan-specific metabolic oligosaccharide engineering of C7-substituted sialic acids. *Angew. Chem. Int. Ed.* **2012**, *51*, 5986-5990.
61. Beahm, B. J.; Dehnert, K. W.; Derr, N. L.; Kuhn, J.; Eberhart, J. K.; Spillmann, D.; Amacher, S. L.; Bertozzi, C. R. A visualizable chain-terminating inhibitor of glycosaminoglycan biosynthesis in developing zebrafish. *Angew. Chem. Int. Ed.* **2014**, *53*, 3347-3352.
62. Laughlin, S. T.; Bertozzi, C. R. In vivo imaging of caenorhabditis elegans glycans. *ACS Chem. Biol.* **2009**, *4*, 1068-1072.
63. van den Bosch, S. M.; Rossin, R.; Renart Verkerk, P.; ten Hoeve, W.; Janssen, H. M.; Lub, J.; Robillard, M. S. Evaluation of strained alkynes for cu-free click reaction in live mice. *Nucl. Med. Biol.* **2013**, *40*, 415-423.
64. Lee, S. B.; Kim, H. L.; Jeong, H.; Lim, S. T.; Sohn, M.; Kim, D. W. Mesoporous silica nanoparticle pretargeting for PET imaging based on a rapid bioorthogonal reaction in a living body. *Angew. Chem. Int. Ed.* **2013**, *52*, 10549-10552.

65. Lu, J.; Liong, M.; Li, Z.; Zink, J. I.; Tamanoi, F. Biocompatibility, biodistribution, and drug-delivery efficiency of mesoporous silica nanoparticles for cancer therapy in animals. *Small* **2010**, *6*, 1794-1805.
66. Koo, H.; Lee, S.; Na, J. H.; Kim, S. H.; Hahn, S. K.; Choi, K.; Kwon, I. C.; Jeong, S. Y.; Kim, K. Bioorthogonal copper-free click chemistry in-vivo for tumor-targeted delivery of nanoparticles. *Angew. Chem. Int. Ed.* **2012**, *51*, 11836-11840.
67. Lee, S.; Koo, H.; Na, J. H.; Han, S. J.; Min, H. S.; Lee, S. J.; Kim, S. H.; Yun, S. H.; Jeong, S. Y.; Kwon, I. C.; Choi, K.; Kim, K. Chemical tumor-targeting of nanoparticles based on metabolic glycoengineering and click chemistry. *ACS Nano* **2014**, *8*, 2048-2063.
68. Xie, R.; Dong, L.; Huang, R.; Hong, S.; Lei, R.; Chen, X. Targeted imaging and proteomic analysis of tumor-associated glycans in living animals. *Angew. Chem. Int. Ed.* **2014**, *53*, 14082-14086.
69. Kim, E. J.; Kang, D. W.; Leucke, H. F.; Bond, M. R.; Ghosh, S.; Love, D. C.; Ahn, J.; Kang, D.; Hanover, J. A. Optimizing the selectivity of DIFO-based reagents for intracellular bioorthogonal applications. *Carbohydr. Res.* **2013**, *377*, 18-27.
70. van Geel, R.; Pruijn, G. J. M.; van Delft, F. L.; Boelens, W. C. Preventing thiol-yne addition improves the specificity of strain-promoted azide-alkyne cycloaddition. *Bioconjugate Chem.* **2012**, *23*, 392-398.
71. Devaraj, N. K.; Weissleder, R.; Hilderbrand, S. A. Tetrazine-based cycloadditions: Application to pretargeted live cell imaging. *Bioconjugate Chem.* **2008**, *19*, 2297-2299.
72. Blackman, M. L.; Royzen, M.; Fox, J. M. Tetrazine ligation: Fast bioconjugation based on inverse-electron-demand diels-alder reactivity. *J. Am. Chem. Soc.* **2008**, *130*, 13518-13519.
73. Patterson, D. M.; Nazarova, L. A.; Prescher, J. A. Finding the right (bioorthogonal) chemistry. *ACS Chem. Biol.* **2014**, *9*, 592-605.
74. Kamber, D. N.; Nazarova, L. A.; Liang, Y.; Lopez, S. A.; Patterson, D. M.; Shih, H.; Houk, K. N.; Prescher, J. A. Isomeric cyclopropenes exhibit unique bioorthogonal reactivities. *J. Am. Chem. Soc.* **2013**, *135*, 13680-13683.
75. Rossin, R.; van, d. B.; ten Hoeve, W.; Carvelli, M.; Versteegen, R. M.; Lub, J.; Robillard, M. S. Highly reactive trans-cyclooctene tags with improved stability for diels-alder chemistry in living systems. *Bioconjugate Chem.* **2013**, *24*, 1210-1217.
76. Selvaraj, R.; Fox, J. M. Trans-cyclooctene — a stable, voracious dienophile for bioorthogonal labeling. *Curr. Opin. Chem. Biol.* **2013**, *17*, 753-760.
77. Kämpchen, T.; Massa, W.; Overheu, W.; Schmidt, R.; Seitz, G. Zur kenntnis von reaktionen des 1,2,4,5-tetrazin-3,6-dicarbonsäure-dimethylesters mit nucleophilen. *Chem. Ber.* **1982**, *115*, 683-694.
78. Karver, M. R.; Weissleder, R.; Hilderbrand, S. A. Synthesis and evaluation of a series of 1,2,4,5-tetrazines for bioorthogonal conjugation. *Bioconjugate Chem.* **2011**, *22*, 2263-2270.
79. Devaraj, N. K.; Hilderbrand, S.; Upadhyay, R.; Mazitschek, R.; Weissleder, R. Bioorthogonal turn-on probes for imaging small molecules inside living cells. *Angew. Chem. Int. Ed.* **2010**, *49*, 2869-2872.
80. Carlson, J. C. T.; Meimetis, L. G.; Hilderbrand, S. A.; Weissleder, R. BODIPY-tetrazine derivatives as superbright bioorthogonal turn-on probes. *Angew. Chem. Int. Ed.* **2013**, *52*, 6917-6920.
81. Lang, K.; Davis, L.; Torres-Kolbus, J.; Chou, C.; Deiters, A.; Chin, J. W. Genetically encoded norbornene directs site-specific cellular protein labelling via a rapid bioorthogonal reaction. *Nat Chem* **2012**, *4*, 298-304.
82. Meimetis, L. G.; Carlson, J. C. T.; Giedt, R. J.; Kohler, R. H.; Weissleder, R. Ultrafluorogenic coumarin-tetrazine probes for real-time biological imaging. *Angew. Chem. Int. Ed.* **2014**, *53*, 7531-7534.

83. Wu, H.; Yang, J.; Seckute, J.; Devaraj, N. K. In situ synthesis of alkenyl tetrazines for highly fluorogenic bioorthogonal live-cell imaging probes. *Angew. Chem. Int. Ed.* **2014**, *53*, 5805-5809.
84. Thalhammer, F.; Wallfahrer, U.; Sauer, J. Reaktivität einfacher offenkettiger und cyclischer dienophile bei diels-alder-reaktionen mit inversem elektronenbedarf. *Tetrahedron Lett.* **1990**, *31*, 6851-6854.
85. Patterson, D. M.; Nazarova, L. A.; Xie, B.; Kamber, D. N.; Prescher, J. A. Functionalized cyclopropenes as bioorthogonal chemical reporters. *J. Am. Chem. Soc.* **2012**, *134*, 18638-18643.
86. Yang, J.; Seckute, J.; Cole, C. M.; Devaraj, N. K. Live-cell imaging of cyclopropene tags with fluorogenic tetrazine cycloadditions. *Angew. Chem.* **2012**, *124*, 7594-7597.
87. Yang, J.; Liang, Y.; Seckute, J.; Houk, K. N.; Devaraj, N. K. Synthesis and reactivity comparisons of 1-methyl-3-substituted cyclopropene mini-tags for tetrazine bioorthogonal reactions. *Chem. Eur. J.* **2014**, *20*, 3365-3375.
88. Cole, C. M.; Yang, J.; Seckute, J.; Devaraj, N. K. Fluorescent live-cell imaging of metabolically incorporated unnatural cyclopropene-mannosamine derivatives. *ChemBioChem* **2013**, *14*, 205-208.
89. Rossin, R.; Renart Verkerk, P.; van den Bosch, S. M.; Vulders, R. C. M.; Verel, I.; Lub, J.; Robillard, M. S. In vivo chemistry for pretargeted tumor imaging in live mice. *Angew. Chem. Int. Ed.* **2010**, *49*, 3375-3378.
90. Zeglis, B. M.; Sevak, K. K.; Reiner, T.; Mohindra, P.; Carlin, S. D.; Zanzonico, P.; Weissleder, R.; Lewis, J. S. A pretargeted PET imaging strategy based on bioorthogonal Diels–Alder click chemistry. *J. Nucl. Med.* **2013**, *54*, 1389-1396.
91. Neves, A. A.; Stockmann, H.; Wainman, Y. A.; Kuo, J. C. -.; Fawcett, S.; Leeper, F. J.; Brindle, K. M. Imaging cell surface glycosylation in vivo using "double click" chemistry. *Bioconjugate Chem.* **2013**, *24*, 934-941.
92. Devaraj, N. K.; Thurber, G. M.; Keliher, E. J.; Marinelli, B.; Weissleder, R. Reactive polymer enables efficient in vivo bioorthogonal chemistry. *Proc. Natl. Acad. Sci. USA* **2012**, *109*, 4762-4767.
93. Nichols, B.; Qin, Z.; Yang, J.; Vera, D. R.; Devaraj, N. K. 68Ga chelating bioorthogonal tetrazine polymers for the multistep labeling of cancer biomarkers. *Chem. Commun.* **2014**, *50*, 5215-5217.
94. Emmetiere, F.; Irwin, C.; Viola-Villegas, N.; Longo, V.; Cheal, S. M.; Zanzonico, P.; Pillarsetty, N.; Weber, W. A.; Lewis, J. S.; Reiner, T. 18F-labeled-bioorthogonal liposomes for in vivo targeting. *Bioconjugate Chem.* **2013**, *24*, 1784-1789.
95. Reshetnyak, Y. K.; Segala, M.; Andreev, O. A.; Engelman, D. M. A monomeric membrane peptide that lives in three worlds: In solution, attached to, and inserted across lipid bilayers. *Biophys. J.* **2007**, *93*, 2363-2372.
96. Rossin, R.; Läppchen, T.; van den Bosch, S. M.; Laforest, R.; Robillard, M. S. Diels–Alder reaction for tumor pretargeting: In vivo chemistry can boost tumor radiation dose compared with directly labeled antibody. *J. Nucl. Med.* **2013**, *54*, 1989-1995.
97. Rossin, R.; van Duijnhoven, Sander M. J.; Lappchen, T.; van, d. B.; Robillard, M. S. Trans-cyclooctene tag with improved properties for tumor pretargeting with the diels-alder reaction. *Mol. Pharm.* **2014**, *11*, 3090-3096.
98. Denk, C.; Svatunek, D.; Filip, T.; Wanek, T.; Lumpi, D.; Fröhlich, J.; Kuntner, C.; Mikula, H. Development of a 18F-labeled tetrazine with favorable pharmacokinetics for bioorthogonal PET imaging. *Angew. Chem. Int. Ed.* **2014**, *53*, 9655-9659.
99. wyffels, L.; Thomae, D.; Waldron, A.; Fissers, J.; Dedeurwaerdere, S.; Van, d. V.; Joossens, J.; Stroobants, S.; Augustyns, K.; Staelens, S. In vivo evaluation of 18F-labeled TCO for pre-targeted PET imaging in the brain. *Nucl. Med. Biol.* **2014**, *41*, 513-523.

100. Li, Z.; Cai, H.; Hassink, M.; Blackman, M. L.; Brown, R. C. D.; Conti, P. S.; Fox, J. M. Tetrazine-trans-cyclooctene ligation for the rapid construction of 18F labeled probes. *Chem. Commun.* **2010**, *46*, 8043-8045.
101. Knight, J. C.; Richter, S.; Wuest, M.; Way, J. D.; Wuest, F. Synthesis and evaluation of an 18F-labelled norbornene derivative for copper-free click chemistry reactions. *Org. Biomol. Chem.* **2013**, *11*, 3817-3825.
102. Zlitni, A.; Janzen, N.; Foster, F. S.; Valliant, J. F. Catching bubbles: Targeting ultrasound microbubbles using bioorthogonal inverse-electron-demand diels-alder reactions. *Angew. Chem. Int. Ed.* **2014**, *53*, 6459-6463.
103. Mejía Oneto, J. M.; Gupta, M.; Leach, J. K.; Lee, M.; Sutcliffe, J. L. Implantable biomaterial based on click chemistry for targeting small molecules. *Acta Biomater.* **2014**, *10*, 5099-5105.
104. Rideout, D. Self-assembling cytotoxins. *Science* **1986**, *233*, 561-563.
105. Rideout, D.; Jaworski, J.; Dagnino Jr., R. Environment-selective synergism using self-assembling cytotoxic and antimicrobial agents. *Biochem. Pharmacol.* **1988**, *37*, 4505-4512.
106. Rideout, D.; Calogeropoulou, T.; Jaworski, J.; McCarthy, M. Synergism through direct covalent bonding between agents: A strategy for rational design of chemotherapeutic combinations. *Biopolymers* **1990**, *29*, 247-262.
107. Liang, Y.; Mackey, J. L.; Lopez, S. A.; Liu, F.; Houk, K. N. Control and design of mutual orthogonality in bioorthogonal cycloadditions. *J. Am. Chem. Soc.* **2012**, *134*, 17904-17907.
108. Chen, W.; Wang, D.; Dai, C.; Hamelberg, D.; Wang, B. Clicking 1,2,4,5-tetrazine and cyclooctynes with tunable reaction rates. *Chem. Commun.* **2012**, *48*, 1736-1738.
109. Murray, B. S.; Crot, S.; Siankevich, S.; Dyson, P. J. Potential of cycloaddition reactions to generate cytotoxic metal drugs in vitro. *Inorg. Chem.* **2014**, *53*, 9315-9321.
110. Brakel, R., van; Vulders, R. C. M.; Bokdam, R. J.; Grull, H.; Robillard, M. S. A doxorubicin prodrug activated by the staudinger reaction. *Bioconjugate Chem.* **2008**, *19*, 714-718.
111. Versteegen, R. M.; Rossin, R.; ten Hoeve, W.; Janssen, H. M.; Robillard, M. S. Click to release: Instantaneous doxorubicin elimination upon tetrazine ligation. *Angew. Chem. Int. Ed.* **2013**, *52*, 14112-14116.
112. Azoulay, M.; Tuffin, G.; Sallem, W.; Florent, J. A new drug-release method using the staudinger ligation. *Bioorg. Med. Chem. Lett.* **2006**, *16*, 3147-3149.
113. Matikonda, S. S.; Orsi, D. L.; Staudacher, V.; Jenkins, I. A.; Fiedler, F.; Chen, J.; Gamble, A. B. Bioorthogonal prodrug activation driven by a strain-promoted 1,3-dipolar cycloaddition. *Chem. Sci.* **2015**.
114. Lang, K.; Chin, J. W. Cellular incorporation of unnatural amino acids and bioorthogonal labeling of proteins. *Chem. Rev.* **2014**, *114*, 4764-4806.
115. Bianco, A.; Townsley, F. M.; Greiss, S.; Lang, K.; Chin, J. W. Expanding the genetic code of drosophila melanogaster. *Nat Chem Biol* **2012**, *8*, 748-750.
116. Song, W.; Wang, Y.; Qu, J.; Madden, M. M.; Lin, Q. A photoinducible 1,3-dipolar cycloaddition reaction for rapid, selective modification of tetrazole-containing proteins. *Angew. Chem. Int. Ed.* **2008**, *47*, 2832-2835.
117. Lim, R. K. V.; Lin, Q. Azirine ligation: Fast and selective protein conjugation via photoinduced azirine-alkene cycloaddition. *Chem. Commun.* **2010**, *46*, 7993-7995.

Chapter 2:
Reactivity of Biarylazacyclooctynones in Copper-Free Click Chemistry[†]

Introduction

As highlighted in the previous chapter, the kinetic profile of a bioorthogonal ligation is one of the major factors contributing to its success *in vivo*. As a result, once a new bioorthogonal reaction is developed, considerable effort is invested to optimize its rate. Unlike conventional synthetic transformations in which reaction rate can be easily increased by raising temperatures or reagent concentrations, bioorthogonal ligations have much more stringent requirements. *In vivo*, all reactions must be performed at 37 ºC, and the concentrations of bioorthogonal probes must be as low as possible to avoid background reactivity and toxicity issues. As a result, researchers have focused on increasing the inherent reactivity between the two probes, usually through iterative synthesis of reagent analogs followed by kinetic analysis.

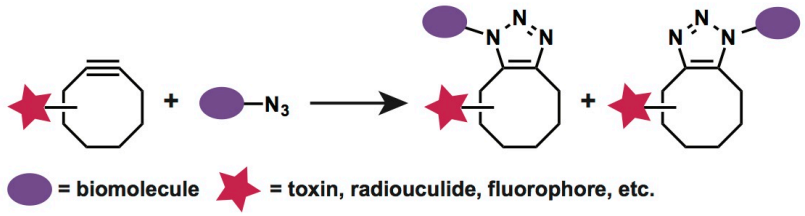


Figure 2.1. The copper-free click reaction.

The copper-free click reaction between strained cyclooctynes and azides to form triazoles (Figure 2.1) is a widely used bioorthoonal ligation for *in vivo* and in *vitro* experiments and for applications in materials science.[1–3] As described in the previous chapter, several groups have contributed to a series of structurally varied cyclooctyne scaffolds that display differential reactivities toward the azide. A selection of these compounds is shown in Figure 1.12, reproduced here as Figure 2.2 for ease of reference. All were designed on the basis of assuming that one can alter the reactivity of a cyclooctyne through modulation either of strain or electronics.

OCT and ALO (Figure 2.2), the first cyclooctynes developed specifically as bioorthogonal reagents, display second-order rate constants of 2.4×10^{-3} M^{-1} s^{-1} and 1.3×10^{-3} M^{-1} s^{-1} respectively for the reaction with benzyl azide.[4,5] It was later shown that this rate can be enhanced through installation of fluorine atoms at the propargylic position. Monofluorinated cyclooctyne (MOFO, Figure 2.2) displays a second-order rate

[†] This chapter is adapted from: Gordon, C. G.; Mackey, J. L.; Jewett, J. C.; Sletten, E. M.; Houk, K. N.; Bertozzi, C. R. Reactivity of biarylazacyclooctynones in copper-free click chemistry. *J. Am. Chem. Soc.* **2012**, *134*, 9199–9208. C. G. Gordon synthesized all compounds, performed kinetic analyses, and helped analyze computational data. J. L. Mackey and K. N. Houk performed computational studies and helped analyze data. C. R. Bertozzi, J. C. Jewett and E. M. Sletten provided valuable insights and suggestions.

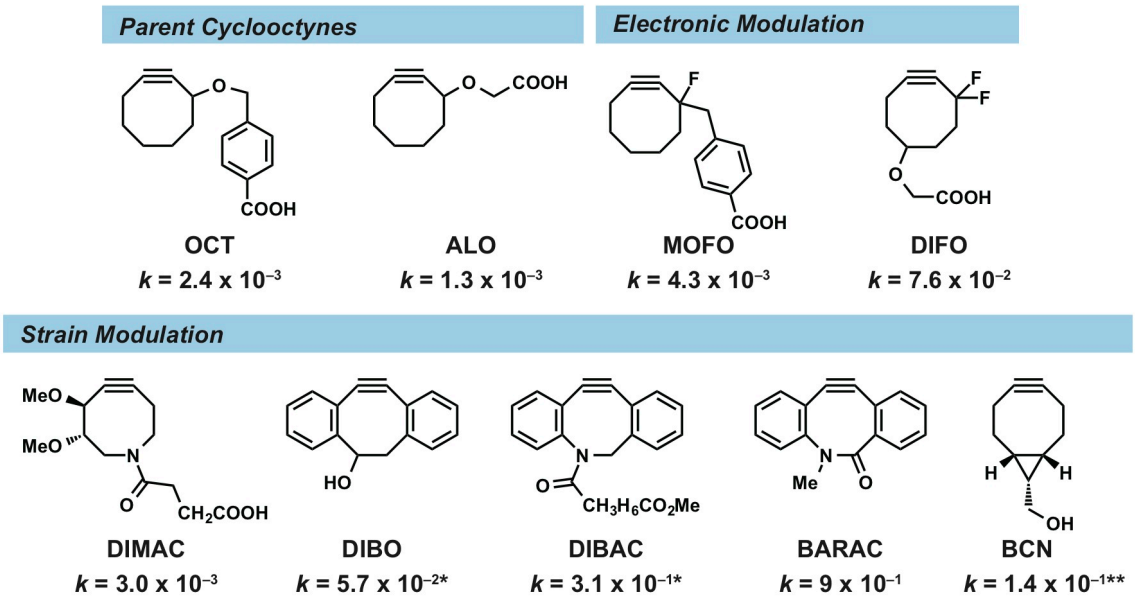


Figure 2.2. Reagent development for copper-free click chemistry. Parent cyclooctynes OCT and ALO were the first cyclooctynes developed as bioorthogonal reagents. Their corresponding second-order rate constants for the reaction with benzyl azide are shown. The reactivity of a cyclooctyne can be altered through electronic and strain modulation as exemplified by the cyclooctyne analogs listed.[4–11] All rate constants are second order (M^{-1} s^{-1}) and were measured at room temperature in CD_3CN except for values noted with an asterisk (*) which were measured in CD_3OD, and those noted with two asterisks (**) which were measured in 3:1 CD_3CN:D_2O.

constant of 4.3×10^{-3} M^{-1} s^{-1}, whereas difluorinated cyclooctyne (DIFO, Figure 2.2) reacts with a rate constant of 7.6×10^{-2} M^{-1} s^{-1} (1.8-fold and 32-fold faster than OCT, respectively).[4,6] The rate-enhancing effects of strain were subsequently demonstrated in the context of dimethoxyazacyclooctyne (DIMAC, Figure 2.2)[12] dibenzocyclooctyne (DIBO, Figure 2.2),[7,8] dibenzoazacyclooctyne (DIBAC, Figure 2.2),[9] biarylazacyclooctynone (BARAC, Figure 2.2),[10] and bicyclononyne (BCN, Figure 22)[11] which respectively react with azides 24-fold to 375-fold faster than is observed for OCT.

The intention implicit in the design of DIBO, DIBAC, and BARAC was to increase strain by adding sp^2 centers to the cyclooctyne ring. However, there may be more subtle consequences of these compounds' structural modifications that actually oppose the desired reactivity outcome. For example, while aryl ring fusion may enhance strain, the "flagpole" hydrogen atoms *ortho* to the aryl/cyclooctyne ring junction were predicted by Goddard and co-workers to decrease reactivity by steric interference with the azide in the transition state.[13] The experimentally observed reactivity of biarylcyclooctynes likely reflects a balance of these rate-enhancing and -diminishing effects. This example underscores the difficulty inherent to rational design of new cyclooctynes with tailored kinetic properties. Many structural perturbations affect more than one contributor to reactivity, e.g., strain, sterics, and electronics. Without a better understanding of their relative influence on transition state activation energies, these parameters cannot be readily optimized to achieve a desired outcome. In principle, one might derive a set of rules that links structure and reactivity solely on the basis of empirical data. However, cyclooctynes are generally challenging synthetic targets that do not lend themselves to

extensive analoging.

In previous work, density functional theory (DFT) models have been employed to analyze reactions of cyclooctynes with azides and have proven to be useful predictors of relative transition state activation energies.[13–15] Here we performed a systematic analysis of the effects of strain and electronics on the reactivity of cyclooctynes with azides, using both empirical data and a DFT-based distortion/interaction transition state model. [14,15] We focused our analysis on a series of differentially substituted BARAC analogs, comparing their second-order rate constants in the cycloaddition reaction with benzyl azide to those predicted by DFT calculations. We also investigated the relationship between alkyne bond angles and reactivity and determined the conformation of BARAC's central lactam, which has significant energetic consequences. The results herein provide a framework for understanding and predicting cycloaddition kinetics.

The Distortion/Interaction Model

The distortion/interaction model deconstructs the activation energy of a reaction into two components: the distortion energy, which is dependent on ground state strain, and the interaction energy, which is governed by transition state electronics.[14,15] In this model, the transition state energy ($\Delta E^{\ddagger}$) of a reaction is defined as the sum of distortion energy ($\Delta E^{\ddagger}_{d}$), the energy required to distort the alkyne and azide into their preferred transition state conformations, and interaction energy ($\Delta E^{\ddagger}_{i}$), the energy change upon orbital overlap between the azide and the alkyne ($\Delta E^{\ddagger} = \Delta E^{\ddagger}_{d} + \Delta E^{\ddagger}_{i}$). Thus, the activation energy of a reaction can be altered by changing either the distortion energy or the interaction energy required to reach the transition state.

In the case of the 1,3-dipolar cycloaddition of 2-butyne with methyl azide (Figure 2.3a), our calculations indicate that 29.9 kcal/mol energy is required to distort the ground state substrates into their preferred transition state conformations. Upon distortion, the alkyne and azide interact, changing the energy of the overall system by −9.0 kcal/mol through a favorable orbital overlap that can only be achieved via the geometry of the distorted state. Combining the effects of distortion and interaction, we calculate an overall transition state activation energy of 20.9 kcal/mol ($\Delta E^{\ddagger} = \Delta E^{\ddagger}_{d} + \Delta E^{\ddagger}_{i}$).[‡] In reality, distortion and interaction are not independent processes but instead occur simultaneously to bring reactants directly to their transition state geometries. However, this model breaks up activation energy into two imaginary distortion and interaction processes to allow a more detailed analysis of reaction strain and electronics.

An example of how electronic perturbation can affect interaction and distortion energies is illustrated by comparing the above reaction coordinate to that for the reaction of 1,1,1,4,4,4-hexafluoro-2-butyne with methyl azide (Figure 2.3b). In this case, the interaction energy is more negative than that calculated for 2-butyne ($\Delta E^{\ddagger}_{i,hexafluoroalkyne}$ =

[‡] Distortion/interaction model calculations are performed by first calculating the activation energy of the reaction and determining the conformations of both reactants in the transition state. These transition state conformations are then used to calculate distortion energies. The transition state interaction energy is calculated as the difference between total distortion energy and transition state activation energy.

−12.2 kcal/mol vs $\Delta E^{\ddagger}_{i,2\text{-butyne}}$ = −9.0 kcal/mol). This change may result from electronic perturbation of the alkyne LUMO energy via mixing of the alkyne π-system with $\sigma^*_{C—F}$. Alabugin and co-workers have shown that the observed acceleration results from hyperconjugative stabilization of the cycloaddition transition state via electron donation

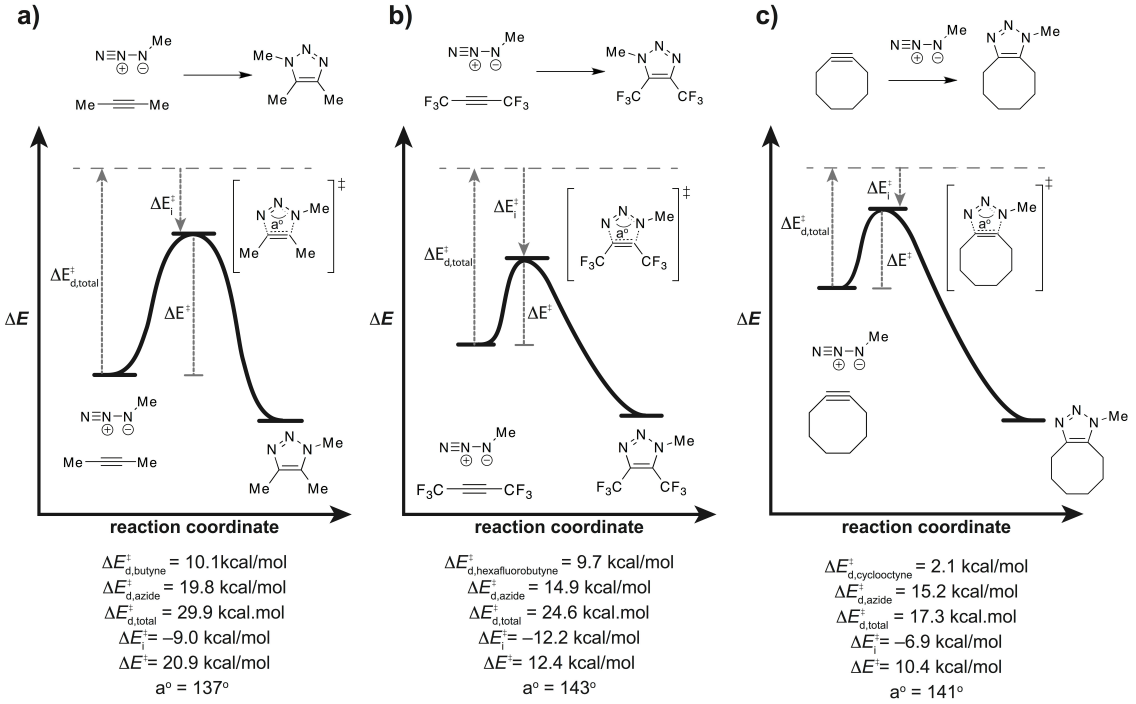


Figure 2.3. Distortion/interaction model. (a) Activation energy ($\Delta E^{\ddagger}$) for the reaction between 2-butyne and methyl azide is the sum of distortion energy ($\Delta E^{\ddagger}_{d}$) and interaction energy ($\Delta E^{\ddagger}_{i}$). (b) Perfluorination of the alkyne reduces $\Delta E^{\ddagger}$ of the reaction by increasing the magnitude of stabilizing interactions in the transition state and decreasing distortion energy. (c) Constraining the alkyne into an eight-membered ring reduces $\Delta E^{\ddagger}$ by decreasing the distortion energy required to bend the starting materials into their preferred transition state conformations. For a−c, calculated values are electronic energies, the potential energy of the molecule on a vibrationless potential energy surface. As all reactions are represented on separate energy diagrams, the depictions are only intended to facilitate comparisons of $\Delta E^{\ddagger}$, $\Delta E^{\ddagger}_{d}$, and $\Delta E^{\ddagger}_{i}$ values and not the overall energies of starting materials or triazole products. Calculations were performed using B3LYP/6-31G(d). See Supporting Information for details.

from the in-plane alkyne π-orbital to the $\sigma^*_{C—F}$-orbital.[16]

As both 1,1,1,4,4,4-hexafluoro-2-butyne and 2-butyne are relatively unstrained molecules, we would expect their distortion energies to be similar for the reaction with methyl azide. However, calculations indicate a larger total distortion energy for the reaction of 2-butyne by 5.3 kcal/mol ($\Delta E^{\ddagger}_{d,total,2\text{-butyne}}$ = 29.9 kcal/mol and $\Delta E^{\ddagger}_{d,total,hexafluoroalkyne}$ = 24.6 kcal/mol). The data in a and b of Figure 2.3 indicate that this difference results both from a change in alkyne transition state distortion energy upon perfluorination as well as from a decrease in azide distortion energy. That both the alkyne and azide undergo shifts in distortion energy in the perfluorinated case indicates that the transition state occurs at an earlier point on the reaction coordinate. Calculated azide bond angles provide further evidence for an early transition state upon perfluorination.

Whereas the azide is bent to 137° in the transition state of the 2-butyne reaction, it is only bent to 143° in the transition state of the perfluorinated-alkyne reaction (Figure 2.3). Thus, the effect of propargylic fluorination is 2-fold when considering the distortion/interaction model; the fluorine atoms enhance transition state interaction energies, which facilitates an early transition state where less distortion is required for both reactants.

The effects of distortion energy modulation in the context of the cyclooctyne have previously been discussed[14,15] and are summarized in Figure 2.3c. The alkyne bond angles in cyclooctyne are bent from linearity, and the molecule is therefore destabilized relative to a linear isomer. Because it is already distorted toward the transition state geometry, the cyclooctyne requires less distortion energy to reach its preferred transition state geometry than does a linear alkyne ($\Delta E^{\ddagger}_{d,2\text{-butyne}}$ = 10.1 kcal/mol and $\Delta E^{\ddagger}_{d,\text{cyclooctyne}}$ = 2.1 kcal/ mol). In addition, calculations show that the distortion energy of methyl azide is lower for the reaction with cyclooctyne than it is for the reaction with 2-butyne. We again attribute this difference to the position of the transition state along the reaction coordinate; here, ground state destabilization of the strained cyclooctyne generates an early transition state, thereby reducing the distortion required for the azide to reach its transition state geometry. This shift in the position of the transition state in response to the greater exothermicity of the strained alkyne reaction is also consistent with the Hammond Postulate. As a result of this significant reduction in distortion energy, cyclooctyne displays a lower overall activation energy for the cycloaddition reaction than does 2-butyne. In this way, strain (i.e., distortion) promotes the cycloaddition.

Because this model is capable of distinguishing the effects of strain and electronics on transition state energies, we chose to apply it to the study of cyclooctyne reactivity. We began by preparing a series of substituted BARAC analogues and analyzing their reactivities experimentally and computationally.

Design of Cyclooctyne Analogs

The modular nature of BARAC's synthesis[10] rendered this scaffold amenable to derivatization with aryl ring substituents. Previous analyses of the difluorinated cyclooctyne DIFO (Figure 2.2) suggested that addition of fluorine atoms at the propargylic position enhances reaction rates by increasing interaction energies and decreasing distortion energies in the transition state.[14,15] We were curious as to whether comparable interaction energy changes might be affected through installation of fluorine atoms on BARAC's aryl rings, and, alternatively, whether electron-donating methoxy groups would affect reaction kinetics in an opposite manner. Accordingly, compounds **2.2**–**2.8** (Figure 2.4) were selected as targets for our study. Compounds **2.2**−**2.5** possess a single fluorine atom variously positioned around BARAC's two aryl rings. Compound **2.6** is doubly fluorinated. On the other end of the spectrum, compounds **2.7** and **2.8** have single methoxy groups on the aryl rings.

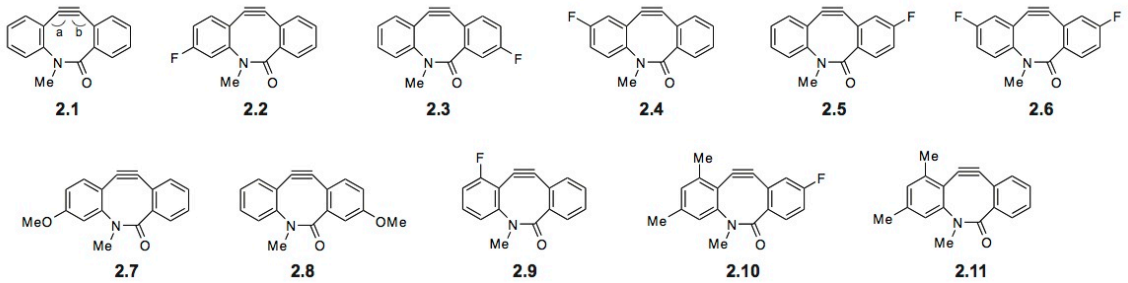


Figure 2.4. BARAC analogs designed for subsequent reactivity studies.

As well, we sought to analyze the steric effects of flagpole substituents on the rate of the cycloaddition reaction. To this end, we designed analogs **2.9**–**2.11** with substituents at the flagpole position. Analog **2.9** possesses a fluorine atom *ortho* to the alkyne. Fluorine is considerably larger than the hydrogen atom present in parent compound **2.1** (Figure 2.5). Its van der Waals radius is 1.51 Å,[17] and the C—F bond in **2.9** is 1.36 Å in length (measured via X-ray crystallography, details in Appendix B). We hypothesized that the fluorine atom would impede access of the azide to BARAC's strained alkyne. However, it is also possible that the fluorine atom is capable of perturbing the electronics of the transition state, and may offset these steric effects.

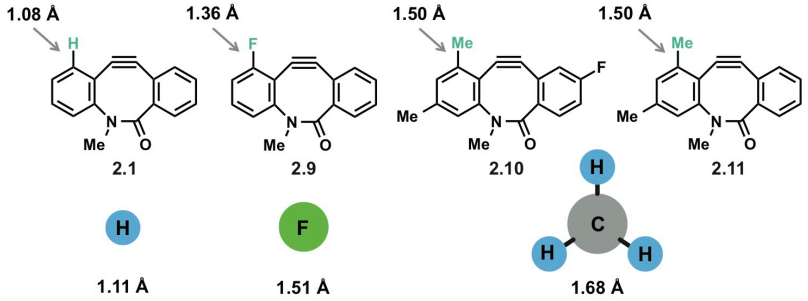


Figure. 2.5. BARAC analogs designed to analyze the effects of sterics on reaction rate.

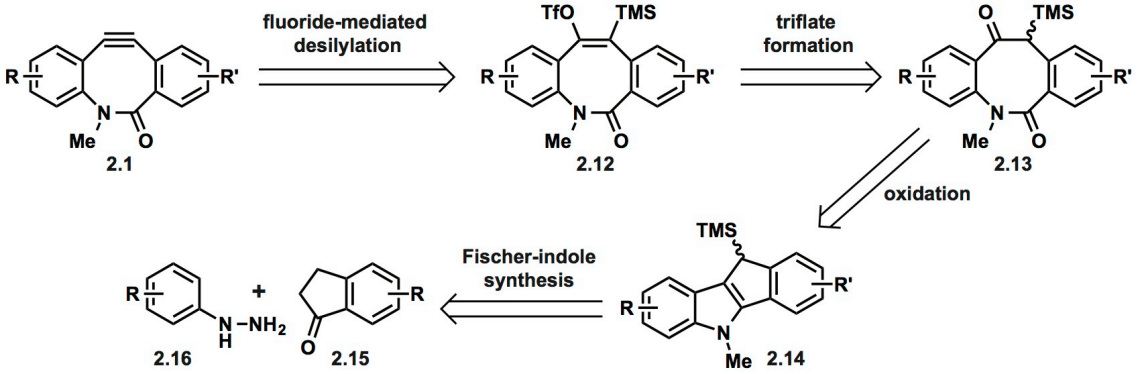
We also designed compounds **2.10** and **2.11**, each with a methyl substituent at the flagpole position. The methyl group is considerably larger than the fluorine atom (2.0 Å van der Waals radius[18] and 1.50 Å C—Me bond length as measured via X-ray crystallography of **2.10**, details in Appendix B), and should further reduce the reactivity of the azide toward the alkyne via sterics. Compound **2.10** also possesses a fluorine atom *meta* to the alkyne on the opposite ring, potentially generating a combination of steric and electronic effects.

Analog Synthesis

All analogs were synthesized according to the route published by Jewett *et al.*[10] A retrosynthetic analysis of Jewett's original route is presented in Scheme 2.1. In

constructing a highly strained cyclooctyne, the most widely used approach is to install strain at the latest possible stage so as to protect the bent alkyne from exposure to harsh conditions and unwanted side reactivity. This is the approach taken in BARAC's synthesis, where the alkyne is installed as the last step via mild, fluoride-mediated desilylation of silyl enol triflate **2.12** followed by loss of triflic acid. This approach to formation of highly strained alkyne bonds has been used in the preparation of reactive cyclohexynes and benzynes,[8,19–21] but BARAC's synthesis represents its first use in the synthesis of a cyclooctyne. The method is valuable because it is mild when compared to other approaches to cyclooctyne formation such as base-mediated *syn*-elimination of a vinyl halide or triflate, dehydrobromination of vicinal bromides with LDA, or thermal cleavage of selenadiazole.[5–8,12] Jewett's mild method of alkyne formation allows for functionalization of the eight-membered ring with sensitive linkers, fluorophores, or other functional groups prior to alkyne installation.

Scheme 2.1. Retrosynthetic analysis of BARAC and analogs.

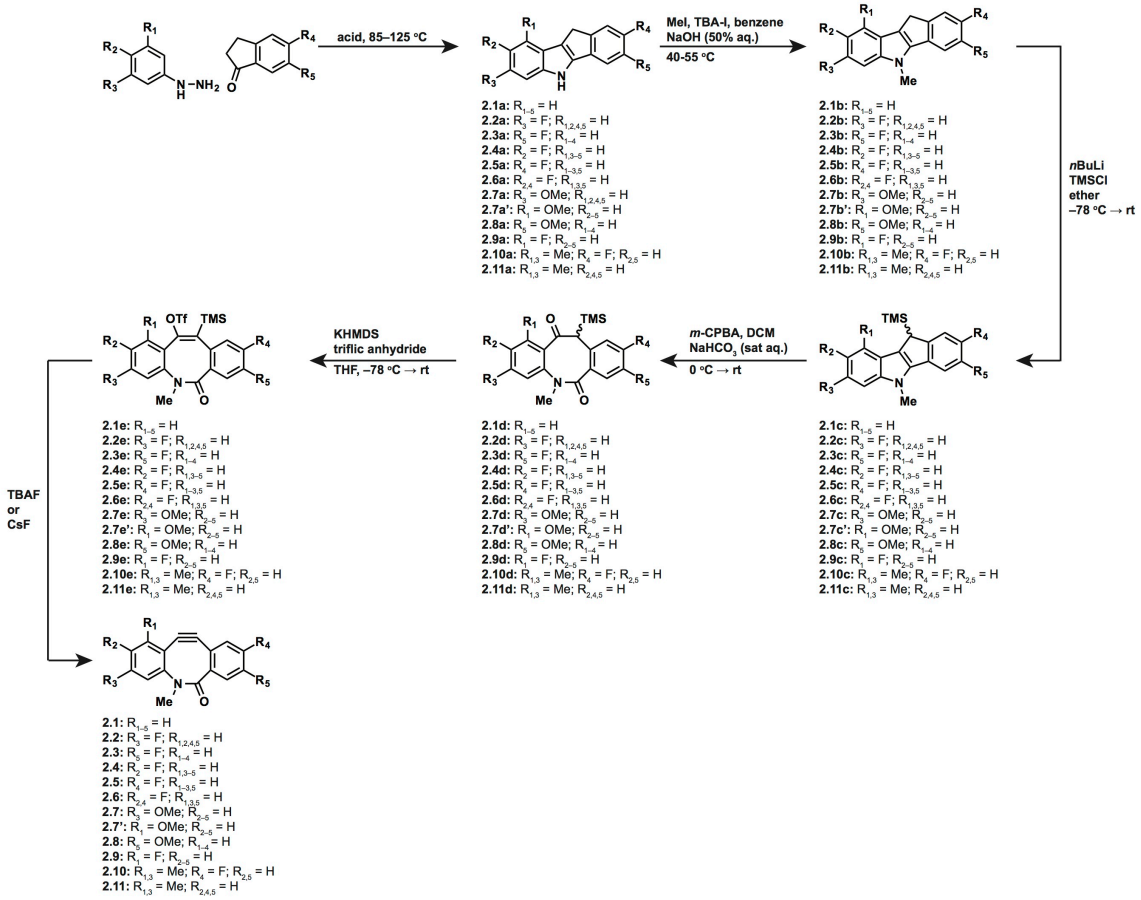


Silyl enol triflate **2.12** is formed from α-silyl ketone **2.13** via treatment with base and triflic anhydride. The α-silyl ketone in **2.13** is a challenging functionality to access due to the oxophilic nature of silicon, which leads to generation of silyl enol ethers upon direct silylation of the ketone.[10,22,23] As a result, Jewett opted to install the silyl group prior to introduction of the ketone via oxidation of silylated indole **2.14**. This unique oxidation, which was originally introduced by Cheung and co-workers,[24] likely proceeds via epoxide formation at the indole double bond followed by addition of a second equivalent of *m*-CPBA and subsequent ring opening. Silylated indole **2.14** is readily formed from its corresponding indole, which is generated from Fisher-indole cyclization of indanone **2.15** and phenyl hydrazine **2.16**. These starting materials are commercially available in substituted forms, providing rapid access to a variety of BARAC analogs.

Scheme 2.2 shows the route to BARAC **2.1** and analogs **2.2**–**2.11** in the forward sense. The Fisher-indole cyclization of phenyl hydrazine and 1-indanone precursors was performed under acidic conditions at temperatures between 85 and 125 ºC. Reaction conditions and product yields varied depending on the starting materials used (see Materials and Methods section). For example, the Fisher-indole cyclization between a 3-substituted phenyl hydrazine and 1-indanone generates a mixture of indole regioisomers, diluting yields of the desired product. As well, the electronics of the starting materials play a role in the rate of the Fisher-indole reaction, sometimes necessitating altered

reaction conditions. For example, phenyl-hydrazine reagents substituted with electron-withdrawing groups generally react more slowly than does unsubstituted phenyl hydrazine.[25] As a result, cyclization of 4-fluoro-phenylhydrazine and 1-indanone required use of a high-pressure vessel and 120–125 ^{o}C temperatures to achieve indole formation.

Scheme 2.2. Synthesis of BARAC and analogs.



The second step of the synthesis is indole N-methylation. In the original route, BARAC's nitrogen atom served as a site of functionalization for biological experiments. Jewett achieved installation of biotin or fluorescein by appending an allyl group via N-alkylation with allyl bromide under phase transfer conditions. The resulting alkene was later tethered to a linker via cyclization with a linker-conjugated nitrile oxide. The linker was then functionalized with a biotin or fluorescein probe.[10] For the purposes of this work, however, we elected to cap BARAC's amide nitrogen atom with a methyl group, thereby providing a convenient ^{1}H signature for later NMR kinetics studies.

Upon formation of N-methylated indoles **2.1b**–**2.11b**, silylation at the benzylic position was achieved using standard conditions. At this stage, silylated indoles were oxidized to unveil the eight-membered ring scaffold via treatment with *m*-CPBA. The α-silyl ketone product of this reaction is unstable to column chromatography, and crude product was immediately converted to the silyl-enol triflate. For some of our BARAC analogs, the silyl enol triflate was also challenging to isolate by column chromatography. As well,

these intermediates are readily converted to the de-silylated ketone in polar protic solvents. As a result, many of the silyl enol triflate intermediates were formed and then immediately converted to the alkyne *in situ* by dilution with diethyl ether followed by addition of tetrabutylammonium fluoride to the reaction mixture. By this route, we synthesized BARAC analogs **2.1**–**2.11** and then set out to analyze their reactivities toward the azide via empirical and computation analyses.

BARAC's Structure

As a platform for our experimental and computational studies, we first analyzed the bond angles and conformation of the parent compound BARAC using X-ray crystallography and DFT calculations. Figure 2.6a shows DFT geometry optimizations performed with B3LYP and the 6-31G(d) basis set. The results indicate that the *trans* conformation of the central amide bond is preferred to the *cis* conformation by $\Delta\Delta G_{solv}$ = 9.4 kcal/mol in acetonitrile. X-ray data support this model, indicating that in crystal form, BARAC preferentially occupies the *trans* conformation (Figure 2.6b).

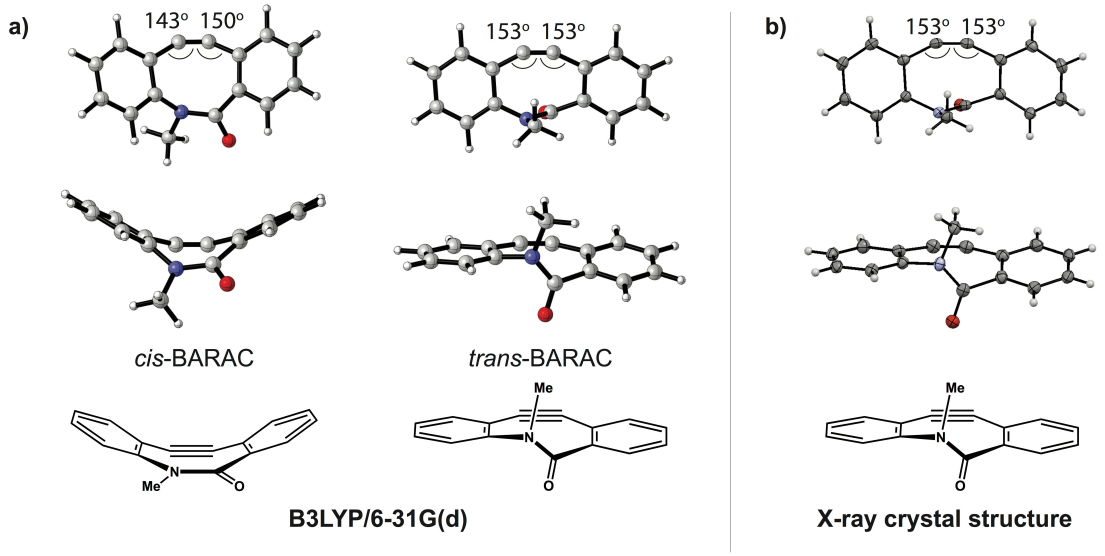


Figure 2.6. Structural analysis of BARAC. (a) DFT calculations (B3LYP/6-31G(d)) of *cis*- and *trans*-BARAC. (b) Front and side view of BARAC obtained via X-ray crystallography. Crystalline BARAC exists as the *trans* conformer. Thermal ellipsoid plots are shown at 50% probability.

Interestingly, DFT calculations show that the conformation of the amide functionality dramatically influences BARAC's alkyne bond angles. As shown in Figure 2.6a, both alkyne angles in *trans*-BARAC are 153°, whereas in *cis*-BARAC the angles are compressed to 143° and 150°. These results suggest that *cis*-BARAC is higher in energy than *trans*-BARAC due to increased alkyne distortion and also imply that *cis*-BARAC would display enhanced reactivity relative to that of *trans*-BARAC in the cycloaddition reaction with azides. DFT calculations of free energies of activation in acetonitrile ($\Delta G^{\ddagger}_{solv}$) for this reaction support our hypothesis. *Trans*-BARAC has a $\Delta G^{\ddagger}_{solv}$ of 24.0 kcal/mol, whereas *cis*-BARAC has a $\Delta G^{\ddagger}_{solv}$ of 18.0 kcal/mol.

We performed energy optimization calculations on substituted BARAC analogs **2.2**–**2.11**

as well, and the results also indicated that the *trans* conformation is preferred to the *cis* conformation by $\Delta\Delta G_{solv}$ = 9.1−9.7 kcal/mol (see Materials and Methods section). We then calculated $\Delta G^{\ddagger}_{solv}$ values for the reactions of compounds **2.2**−**2.11** with methyl azide, and results indicate that for compounds **2.2**−**2.8**, reaction of the *trans*-conformer is a lower-energy process by 3.0−4.5 kcal/mol than is isomerization to the *cis*-conformer followed by reaction to form the triazole. These results suggest that compounds **2.2**−**2.8** react predominantly as the *trans* conformer. Thus, we focus the remainder of the calculations in this section on *trans*-BARAC. As discussed later, $\Delta G^{\ddagger}_{solv}$'s for reactions of the *cis*- and *trans*-conformers are similar in energy for compounds **2.9**−**2.11**, suggesting a Curtin-Hammett controlled reaction.

Reactivity of BARAC and Analogs

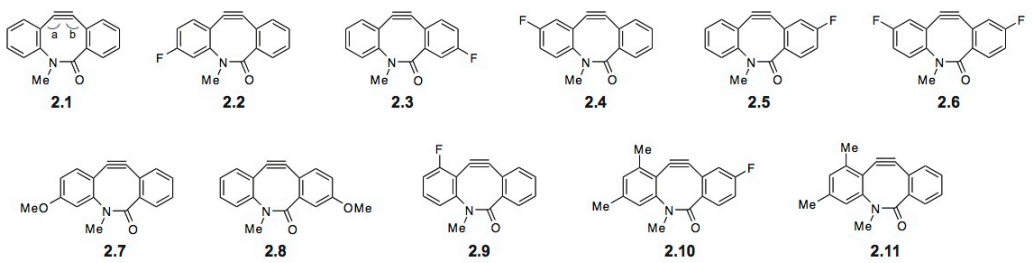
The table shown in Figure 2.7c shows the results of DFT calculations of alkyne bond angles as well as empirical bond angle measurements obtained by X-ray crystallography (shown in parentheses) for select compounds in the *trans* conformation. We conclude from these data that aryl substitution does not impose significant structural changes, as all compounds exhibit alkyne bond angles close to 153°.

We next measured the second-order rate constants of the reactions of **2.1**−**2.11** with benzyl azide. ^{1}H NMR was used to monitor the conversion of each analog to its corresponding triazole, and second order rate constants were obtained by measuring the slope of a plot of 1/[analog] versus time (Figure 2.8). For each analog, this experiment was repeated 4–13 times, and the average rate constant of all trials is reported in Figure 2.7c. Compounds **2.1**−**2.5** and **2.7**−**2.8** exhibited rate constants between 0.9 and 1.2 M^{-1} s^{-1}, with differences that do not lie outside the range of experimental error.[§,**] Compound **2.6**, however, showed a roughly 75% increase in reactivity relative to that of **2.1** ($k_{\mathbf{2.6}}$ = 1.6 ± 0.1 M^{-1} s^{-1} versus $k_{\mathbf{2.1}}$ = 0.9 ± 0.1 M^{-1} s^{-1}). Given the similar reactivities of **2.1**−**2.5**, **2.7**, and **2.8**, we expected these compounds to display transition state distortion and

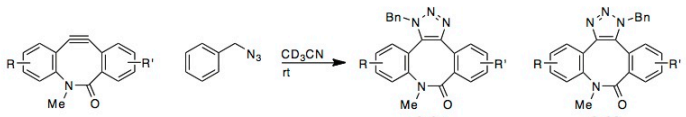
[§] Calculatd *p*-values (two-tailed, unpaired Student's t-test) comparing the second-order rate constants measured for compounds **2.2**−**2.4**, **2.7**, and **2.8** to that measured for **2.1** are $0.5 > p > 0.001$. The *p*-value calculated for compound **2.5** is $p = 0.0001$. *p*-values calculated for compounds **2.6** and **2.9**−**2.11** are $p < 0.0001$.

[**] A disubstituted BARAC analog with a fluorine atom at the position shown in compound **2.3** and a methoxy group at the position shown in compound **2.7** was synthesized, and its reactivity with benzyl azide was analyzed to determine the combined effects of electron- withdrawing and -donating groups on cyclooctyne reactivity. The calculated second-order rate constant was k = 1.1 ± 0.1 M^{-1} s^{-1} for the reaction with benzyl azide in CD_3CN at rt — on par with rate constants observed for compounds **2.1**−**2.5**, **2.7**, and **2.8**.

a)



b)



c)

Compound	angle a (°)	angle b (°)	k_{exp}(M^{-1} s^{-1})	$\Delta G^{\ddagger}_{exp}$ (kcal/mol)	$\Delta E^{\ddagger}_{d,calc}$ (kcal/mol)	$\Delta E^{\ddagger}_{i,calc}$ (kcal/mol)	$\Delta E^{\ddagger}_{calc}$ (kcal/mol)	$\Delta G^{\ddagger}_{calc}$* (kcal/mol)
2.1	152.7 (153)	153.0 (153)	0.9 ± 0.1	17.5	*syn* = 16.5 *anti* = 16.7	*syn* = –8.2 *anti* = –8.8	*syn* = 8.3 *anti* = 8.0	*syn* = 24.0 *anti* = 24.1
2.2	152.4	153.1	1.1 ± 0.1	17.4	*syn* = 16.6 *anti* = 16.6	*syn* = –8.3 *anti* = –8.9	*syn* = 8.2 *anti* = 7.7	*syn* = 24.1 *anti* = 24.0
2.3	153.0	152.7	1.10 ± 0.04	17.4	*syn* = 16.4 *anti* = 16.8	*syn* = –8.4 *anti* = –8.9	*syn* = 8.0 *anti* = 7.9	*syn* = 23.8 *anti* = 24.0
2.4	152.3	153.4	1.0 ± 0.1	17.4	*syn* = 16.6 *anti* = 16.7	*syn* = –8.6 *anti* = –9.0	*syn* = 8.0 *anti* = 7.7	*syn* = 23.7 *anti* = 23.7
2.5	153.0	152.7	1.2 ± 0.1	17.3	*syn* = 16.4 *anti* = 16.8	*syn* = –8.4 *anti* = –9.0	*syn* = 8.0 *anti* = 7.8	*syn* = 23.7 *anti* = 23.9
2.6	152.5	153.1	1.6 ± 0.1	17.1	*syn* = 16.4 *anti* = 16.7	*syn* = –8.7 *anti* = –9.2	*syn* = 7.7 *anti* = 7.5	*syn* = 23.5 *anti* = 23.6
2.7	152.6	152.8	1.0 ± 0.1	17.4	*syn* = 16.2 *anti* = 16.5	*syn* = –8.2 *anti* = –8.7	*syn* = 8.1 *anti* = 7.9	*syn* = 23.9 *anti* = 24.0
2.8	152.5 (154)	153.0 (153)	1.1 ± 0.1	17.4	*syn* = 16.4 *anti* = 16.6	*syn* = –8.1 *anti* = –8.7	*syn* = 8.3 *anti* = 8.0	*syn* = 23.8 *anti* = 23.9
2.9	151.1	153.7	0.058 ± 0.003	19.1	*syn* = 17.3 *anti* = 19.4	*syn* = –8.2 *anti* = –8.3	*syn* = 9.1 *anti* = 11.1	*syn* = 24.7 *anti* = 26.0
2.10	153.6 (155)	152.1 (152)	0.0019 ± 0.0003**	21.1	*syn* = 19.6 *anti* = 21.7	*syn* = –7.9 *anti* = –8.2	*syn* = 11.7 *anti* = 13.4	*syn* = 28.2 *anti* = 30.1
2.11	153.0 (154)	152.7 (152)	0.0009 ± 0.0001**	21.5	*syn* = 19.7 *anti* = 21.6	*syn* = –7.7 *anti* = –8.0	*syn* = 12.0 *anti* = 13.6	*syn* = 28.3 *anti* = 30.2

Figure 2.7. Bond angles and reactivities of BARAC analogs. (a) BARAC analogs targeted for our initial study of distortion/interaction modulation. (b) Reactivity was probed empirically by measuring the second-order rate constant for the reaction of each analog with benzyl azide in CD_3CN at rt by ^1H NMR spectroscopy. (c) Table shows both calculated and measured (X-ray crystallography data shown in parentheses) alkyne bond angles for compounds **2.1**−**2.11** as well as measured second-order rate constants and activation free energies ($\Delta G^{\ddagger}_{exp}$, calculated using the Eyring equation and measured values for *k*) for the model reaction with benzyl azide. Also shown are calculated interaction ($\Delta E^{\ddagger}_{i,calc}$) and total distortion energies ($\Delta E^{\ddagger}_{d,calc}$ = $\Delta E^{\ddagger}_{d,calc,azide}$ + $\Delta E^{\ddagger}_{d,calc,alkyne}$) as well as overall electronic energies of activation ($\Delta E^{\ddagger}_{calc}$) and free energies of activation ($\Delta G^{\ddagger}_{calc}$) for the reaction of each analog with methyl azide. All computational data provided for compounds **2.1**−**2.11** are for the *trans*-BARAC isomer. *Free energies were calculated for the reaction in acetonitrile. **The second-order rate constants shown for **2.10** and **2.11** were measured in $CDCl_3$ due to the limited solubility of **2.10** in CD_3CN.

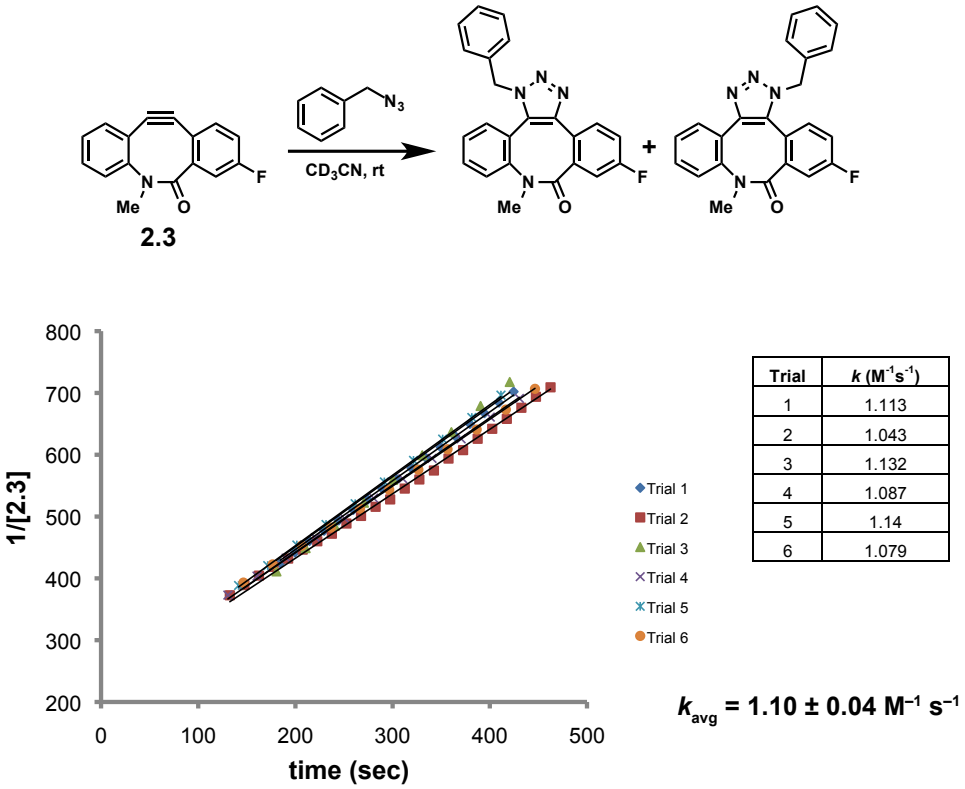


Figure 2.8. Measuring the second order rate constant for the reaction between BARAC analogs and benzyl azide — a representative analysis with analog 2.3. The reaction between fluorinated BARAC (**2.3**) and benzyl azide was monitored by ^{1}H NMR in CD_3CN at room temperature with each reagent at a starting concentration of 5 mM. The second-order rate constant was calculated by plotting 1/[**2.3**] as a function of time. The slope of the resulting line is the rate constant. Data are plotted to within 67% and 69% conversion to the triazole. Shown are the calculated second-order rate constants for each trial; average k = 1.10 ± 0.04 M^{-1} s^{-1}.

interaction energies of similar magnitude. DFT calculations were used to model the reaction of each analog with methyl azide, as calculations show that methyl azide behaves similarly to benzyl azide for the reaction with **2.1** (data provided in the Materials and Methods section). In discussing the results of these calculations, we define triazole **2.17** (Figure 2.7b) as the *syn*-regioisomer and triazole **2.18** as the *anti*-regioisomer.

Computational data indicate that compounds **2.1**−**2.5**, **2.7** and **2.8** do in fact exhibit similar energetics in their transition states, with distortion energies for all seven compounds lying between 16.2 and 16.6 kcal/mol for the *syn*-regioisomer and between 16.5 and 16.8 kcal/mol for the *anti*-regioisomer. These data are consistent with our observations that the compounds have nearly identical alkyne bond angles (additional structural data are provided in the Materials and Methods section). Similarly, calculated interaction energies were alike for these compounds with values between −8.1 and −8.6 kcal/mol for the *syn*-regioisomer and between −8.7 and −9.0 kcal/mol for the *anti*-regioisomer. As a result, overall energies of activation ($\Delta E^{\ddagger} = \Delta E^{\ddagger}_{d} + \Delta E^{\ddagger}_{i}$) for these compounds are quite comparable, falling within the range of 8.0−8.3 kcal/mol for the *syn*-regioisomer and between 7.7−8.0 kcal/mol for the *anti*-regioisomer.

Calculated free energies of activation in acetonitrile ($\Delta G^{\ddagger}_{calc}$) are also similar for compounds **2.1**−**2.5**, **2.7** and **2.8**. For both the *syn*- and *anti*-regioisomers, $\Delta G^{\ddagger}_{calc}$ lies between 23.7 and 24.1 kcal/mol. These calculations systematically overestimate the true free energies of activation by about 6.5 kcal/mol. This error has been previously noted in applications of B3LYP to cycloaddition reactions.[††26,27] Such calculations also overestimate the entropic penalty associated with the transition states of bimolecular reactions.

Compound **2.6** was the only analog with substantially increased reactivity compared to BARAC, and accordingly, its transition state interaction energies ($\Delta E^{\ddagger}_{i,calc}$ values of −8.7 kcal/mol (*syn*) and −9.2 kcal/mol (*anti*)) were the largest measured in this study. Interestingly, we found that the transition state distortion energies for this analog lie within the range of those calculated for the other compounds ($\Delta E^{\ddagger}_{d,calc}$ = 16.4 kcal/mol (*syn*) and $\Delta E^{\ddagger}_{d,calc}$ = 16.7 kcal/mol (*anti*)). As a result, combined activation energies for compound **2.6** are lower than those observed for the other analogs ($\Delta E^{\ddagger}_{calc}$ = 7.7 kcal/mol (*syn*) and $\Delta E^{\ddagger}_{calc}$ = 7.5 kcal/mol (*anti*)). The calculated free energies of activation in acetonitrile ($\Delta G^{\ddagger}_{calc}$) for compound **2.6** follow a similar trend (Figure 2.7c). These data indicate that the enhanced reaction rate observed for **2.6** is a result of electronic modulation that generates enhanced stabilizing interactions in the transition state. Modulation of strain and distortion energy does not appear to play a significant role in the rate enhancement.

Our experimental results also provide insight into the effects of sterics on cyclooctyne reactivity. Compounds **2.9**−**2.11**, which all contain a flagpole substituent *ortho* to the alkyne, exhibit dramatic decreases in their rates relative to the parent BARAC ($k_{\mathbf{2.9}}$ = 5.8 ± 0.3 × 10^{-2} M^{-1} s^{-1} in CD_3CN, $k_{\mathbf{2.10}}$ = 1.9 ± 0.3 × 10^{-3} M^{-1} s^{-1} in $CDCl_3$, and $k_{\mathbf{2.11}}$ = 9 ± 1 × 10^{-4} M^{-1} s^{-1} in $CDCl_3$). Calculations show that these three compounds display corresponding increases in transition state distortion energies relative to analogs **2.1**−**2.8**. This enhanced distortion is due to the close proximity of the substituent to the alkyne and its orientation directly toward the path of the incoming azide, requiring both the azide and the alkyne to distort to a higher degree in the transition state. Figure 2.9 gives both a front and side view of the transition state of the reaction of compounds **2.1** and **2.10** with methyl azide, and it is clear that the methyl group is causing disfavorable steric interactions. Even a relatively small fluorine atom in this position, as in compound **2.9**, causes a significant increase in transition state distortion energy (Figure 2.7c). By contrast, the transition state interaction energies of compounds **2.9**−**2.11** are similar to those of the other BARAC analogs. As a result, **2.9**−**2.11** have higher activation barriers than do the other analogs tested, resulting in the observed orders of magnitude decrease in reactivity.

[††] During the course of this work, a more extensive benchmarking of 1,3-dipolar cycloadditions to ethylene and acetylene was performed by Houk and co-workers (see reference 26). Through this work, more accurate methods and additional functionals for modeling these reactions were identified. The M06-2X functional was found to provide activation barriers that more closely matched higher-accuracy calculations. As a result, in addition to the B3LYP results in Figure 2.7c, M06-2X calculations have been performed on BARAC compounds **2.1** and **2.9**−**2.11** and are given in the materials and methods section. These activation energies deviate by 1.3−4.6 kcal/mol from energies calculated using the B3LYP functional. The conclusions are the same, except that M06-2X predicts all reactions to involve only the *trans*-isomer.

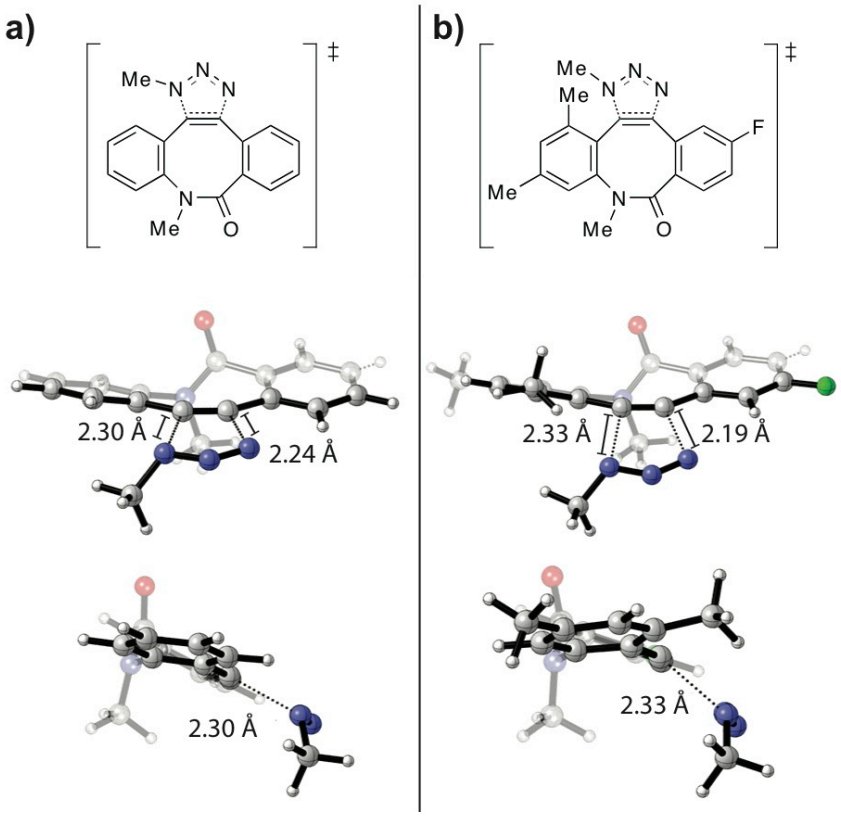


Figure 2.9. Flagpole methyl substituents sterically hinder the transition state. (a) Front and side views of the transition state of the reaction of **2.1** with methyl azide. (b) Front and side views of the transition state of the reaction of **2.10** with methyl azide. Transition states were modeled using B3LYP/6-31G(d).

Overall, our analyses of compounds **2.1**−**2.11** indicate that aryl substitution can affect minor reactivity changes by altering transition state interaction energies (e.g., compound **2.6**) and substantial rate changes by increasing steric hindrance in the transition state (e.g., compounds **2.9**−**2.11**). For compounds **2.1**−**2.8**, we did not observe any changes in reactivity due to modulation of transition state distortion energies, and we hypothesize that the enhanced distortion energies observed for **2.9**−**2.11** are a result of sterics rather than alkyne strain.

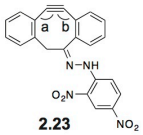
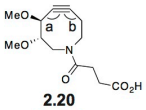
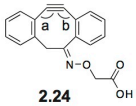
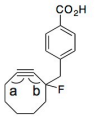
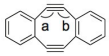
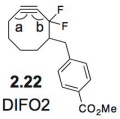
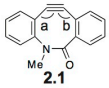
Alkyne Bond Angles as a Measure of Reactivity

Compounds **2.1**−**2.8**, which share similar reactivities and transition state distortion energies, also possess similar structures with alkyne bond angles close to 153° (Figure 2.7c). This observation led us to hypothesize that alkyne bond angles may correlate with transition state activation energies for the cycloaddition with organic azides. If so, one may be able to predict the reactivity of a given cyclooctyne by determining its alkyne bond angles either through X-ray crystallography or DFT geometry optimizations. Table 2.1 shows compiled X-ray structural data for a series of cyclooctynes as well as second-order rate constants for the reaction of each compound with benzyl azide (complete crystallographic data sets for compounds **2.1**, **2.20**, **2.21**, and **2.22** are in the

Materials and Methods section; crystallographic or electron diffraction data for the other compounds are referenced in Table 2.1). Although kinetic parameters for the reaction of cyclooctyne itself (**2.19**) with organic azides have not been reported, we include the average bond angle of cyclooctyne[28] in Table 2.1 as a point of comparison.

The data in Table 2.1 indicate a general correlation between alkyne bond angle distortion and cyclooctyne reactivity. Dimethoxyazacyclooctyne (DIMAC,[12] **2.20**) exhibits bond angles of 158° and 157°, structural deviations of only 1° and 2°, respectively, from the parent cyclooctyne **2.19**. Thus, neither DIMAC's endocyclic nitrogen nor its exocyclic substituents distort the alkyne bond angles to a significant extent. Installation of a fluorine atom at the propargylic position in MOFO[4] (**2.21**) slightly enhances alkyne distortion at angle b through a bond polarization mechanism that has been extensively documented in substituted arynes.[29,30] Angle b in MOFO is 4° more distorted than the average bond angle in cyclooctyne (155° versus 159°, respectively). Conversely, angle a is less distorted in MOFO (160° versus 159°). Overall, the structural differences between MOFO and DIMAC are small, and, correspondingly only minor reactivity differences between the two are observed (k_{MOFO} = 4.3 × 10^{-3} M^{-1} s^{-1} and k_{DIMAC} = 3.0 x 10^{-3} M^{-1} s^{-1}).[4,12]

Table 2.1. Reactivity and alkyne bond angles[a]

cyclooctyne	a (°)	b (°)	rate constant (M^{-1} s^{-1})	ref.	cyclooctyne	a (°)	b (°)	rate constant (M^{-1} s^{-1})	ref.
 **2.19** cyclooctyne	159	N/A	N/A	28	 **2.23**	152	157	N/A	32
 **2.20** DIMAC	158	157	3.0 x 10^{-3}	12, SI	 **2.24**	N/A	N/A	6.1 x 10^{-2}**	8
 **2.21** MOFO	160	155	4.3 x 10^{-3}	4, SI	 **2.25**	156	155	6.3 x 10^{-2}**	28, 33, 34
 **2.22** DIFO2	162	151	4.2 x 10^{-2}*	31, SI	 **2.1** BARAC	153	153	9 x 10^{-1}	10, SI

[a]Cyclooctyne bond angles and second-order rate constants for the reaction with benzyl azide in acetonitrile at rt. All bond angles were measured via X-ray crystallography with the exception of compound **2.19**, which was analyzed by electron diffraction in the gas phase. All data are referenced in the table, and details of the measurements first reported in this publication are located in Appendix B (labeled SI in the table). N/A = data not available. *Rate was measured for the acid form of DIFO2. **Rate constant measured in methanol.

As previously mentioned, installation of an additional fluorine atom at the propargylic position as in DIFO2[31] (**2.22**) further enhances alkyne distortion at angle b (151°) through bond polarization. This additional bending at angle b is accompanied by a reduction in distortion at angle a (162° for DIFO2 vs 160° for MOFO). Despite strain reduction at angle a, however, the data suggest that the highly distorted nature of angle b in DIFO2 may contribute to the order of magnitude rate enhancement observed for this compound relative to that or MOFO (k_{DIFO} = 4.2 x 10^{-2} M^{-1} s^{-1} versus k_{MOFO} = 4.3 x 10^{-3} M^{-1} s^{-1}).[4,31]

The structure/reactivity trend observed for DIMAC, MOFO, and DIFO2 is also evident in the biarylcyclooctyne series. Dibenzocyclooctyne **2.23**, reported by Kornmayer *et al.*, exhibits bond angles of 152° and 157° and therefore is only slightly less distorted than DIFO2 at one angle but significantly more distorted than DIFO2 at the other.[32] Although rate data are not available for this particular compound, a related oxime- substituted dibenzocyclooctyne (**2.24**) has been reported by Boons and co-workers to display a second-order rate constant of k = 6.1 x 10^{-2} M^{-1} s^{-1} for the reaction with benzyl azide in methanol.[8] The enhanced alkyne distortion observed at both alkyne angles in compound **2.23** (vs just one alkyne bond angle in DIFO2) may contribute to its heightened reactivity. Dibenzocyclooctadiyne **2.25**, with alkyne bond angles of 156° and 155°,[28,33,34] seems to distribute alkyne distortion more symmetrically across the bond but overall is not significantly more distorted than **2.24**. The reaction of compound **2.25** with benzyl azide was reported by Kii *et al.* to proceed with a second-order rate constant of k = 6.3 x 10^{-2} M^{-1} s^{-1}.[34] As expected given their similar degrees of overall alkyne distortion, the reactivity of compound **2.25** is similar in magnitude to that measured for compound **2.24** (k = 6.1 x 10^{-2} M^{-1} s^{-1}).

Relative to compounds **2.24** and **2.25**, BARAC (**2.1**) is significantly more distorted. With both alkyne bond angles at 153°, BARAC's structure exhibits the greatest overall deviation from cyclooctyne **2.19** (159°). Accordingly, BARAC exhibits a second-order rate constant that is an order of magnitude greater than that of compound **2.25** (k_{BARAC} = 9 x 10^{-1} M^{-1} s^{-1} vs $k_{\mathbf{2.25}}$ = 6.3 x 10^{-2} M^{-1} s^{-1}).[34] In summary, compounds **2.1** and **2.23**–**2.25** follow the same distortion/reactivity trend observed for DIMAC, MOFO, and DIFO2, with increased overall alkyne bond angle distortion correlating with increased reactivity.

Effects of BARAC's Amide Bond Structure on Reactivity and Regioselectivity

The extreme distortion of BARAC's alkyne bond angles compared to that of bond angles of other dibenzocyclooctynes may reflect adjustments of the cyclooctyne ring geometry to accommodate the lactam functionality. We speculate that BARAC's endocyclic amide bond enhances the overall ring strain of the compound by contributing some partial double bond character to the position directly opposite the alkyne. Semi-empirical calculations by Meier *et al.* predict that the fully unsaturated cyclooctyne **2.26** (Figure 2.10) would possess almost 3-fold more ring strain than the parent cyclooctyne **2.19**.[35] A related dibenzocyclooctenyne (**2.27**, Figure 2.10) has been synthesized but is not bench-stable,[28] consistent with the notion that ring strain increases with cyclooctyne

unsaturation. BARAC shares structural features with compounds **2.26** and **2.27** but is relatively stable, prompting us to investigate the properties of BARAC's central amide bond.

An interesting comparison can be made between the hybridization indices of the nitrogen atoms in BARAC's and DIMAC's (**2.20**, Table 2.1) amide bonds, which we calculated using the sum of the bond angles surrounding the atom.[‡‡17] Whereas the amide nitrogen of DIMAC displays the expected sp^2 hybridization, that of BARAC is slightly pyramidalized with an $sp^{2.2}$ hybridization index. Though deviation from sp^2 hybridization in amides is generally thermodynamically disfavored, such distortion may reduce BARAC's overall ring strain by diminishing the double bond character and planarity of the lactam. This structural flexibility allows BARAC to balance reactivity and stability through amide nitrogen rehybridization.

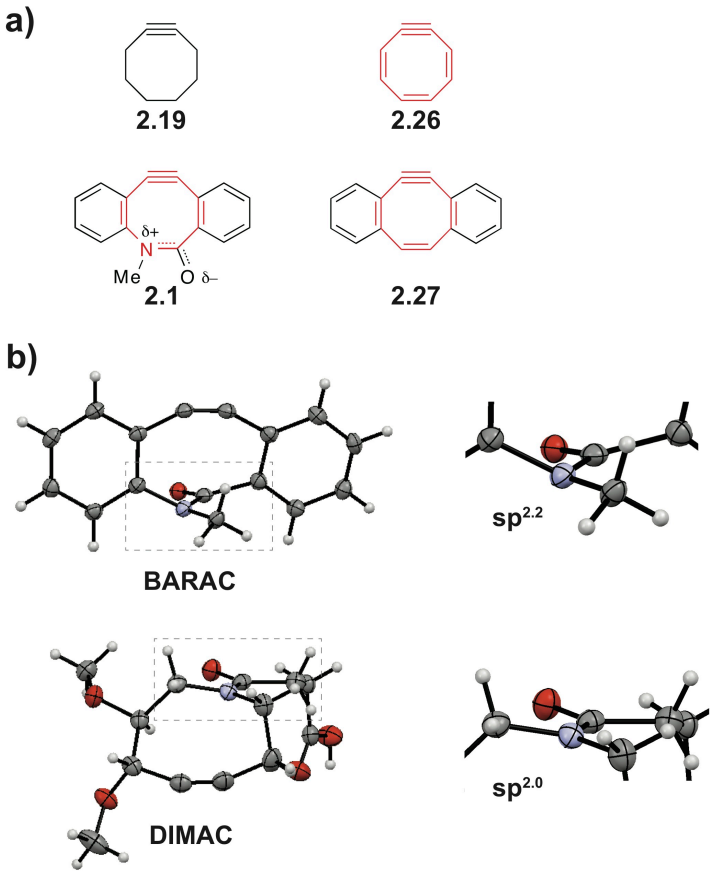


Figure 2.10. Strain modulation through rehybridization. (a) Ring strain in cyclooctynes increases with increased unsaturation. We hypothesize that BARAC's fused aryl rings and central lactam contribute significantly to the compound's ring strain. (b) X-ray crystal structures show that the nitrogen atom of BARAC's central lactam is $sp^{2.2}$ hybridized, whereas DIMAC's amide nitrogen atom is sp^2 hybridized. Thermal ellipsoid plots are shown at 50% probability.

‡‡ $1 + i \cos \theta = 0$ where i = hybridization index (see reference 17)

Another notable feature of BARAC's amide bond is that its conformational state appears to impact regioselectivity in the alkyne−azide cycloaddition reaction. Whereas parent compound **2.1** reacts with benzyl azide to give a 1:1 mixture of *syn*- and *anti*-triazole products, analogs **2.10** and **2.11** generate *syn*-/ *anti*-triazole product ratios of 3:1 and 2:1, respectively, wherein the favored product reflects the more sterically hindered transition state. Though counterintuitive on its face, this observation follows the general trend predicted using the distortion/interaction model.[§§36] However, the magnitude of the regioisomeric preference is strongly affected by the conformation of BARAC's lactam in the ground state. For both **2.10** and **2.11**, our calculations predict a 25:1 preference for the *syn*-regioisomer when BARAC reacts through its lowest-energy *trans*-conformer, but when the calculation was performed using *cis*-BARAC as a substrate, the predicted product ratio was 1.2:1 *syn*/*anti* for **2.10** and 0.8:1 *syn*/*anti* for **2.11**. Our experimentally observed product ratio may therefore reflect the presence of both conformers in solution, which, if interconvertible, would generate a Curtin-Hammett-controlled product distribution.

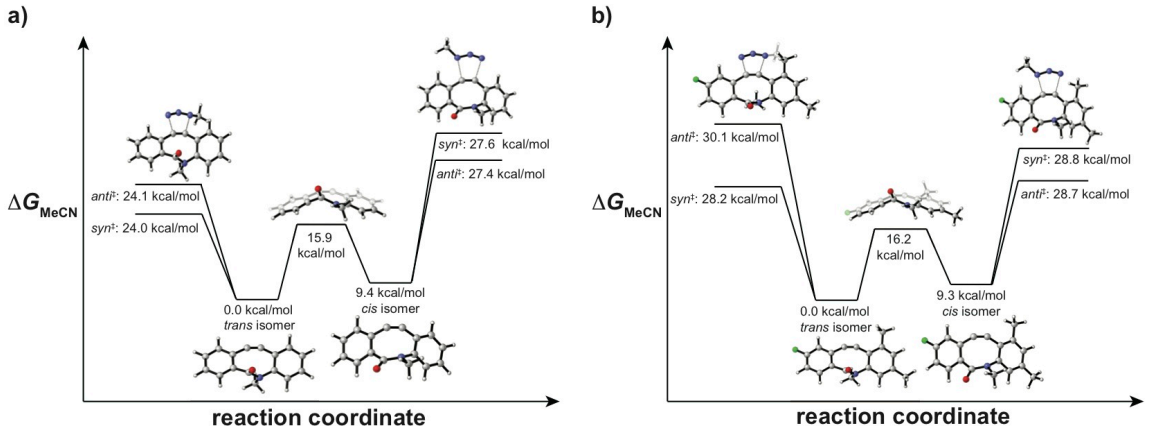


Figure 2.11. Under Curtin-Hammett conditions, BARAC's amide conformation influences reactivity and regioselectivity. (a) The reaction coordinate diagram displays calculated activation free energies for reaction of the parent BARAC compound **2.1** with methyl azide in acetonitrile. Also shown are the relative energies of *cis*-**2.1** and *trans*-**2.1** and the barrier to *cis*/*trans* interconversion. Transition state images show only the lowest-energy regioisomers. (b) Calculated values for the interconversion and reaction of analog **2.10** with methyl azide in acetonitrile. Transition state images show only the lowest-energy regioisomers.

We calculated the barrier to amide bond isomerization for BARAC (**2.1**) and analogs **2.10** and **2.11** (a and b of Figure 2.11). For BARAC, the barrier to *cis*/*trans* isomerization is 15.9 kcal/ mol. With the energy of *trans*-BARAC set to 0 kcal/mol, reaction of the *trans*-conformer with methyl azide has an energetic barrier of 24.0 or 24.1 kcal/mol for formation of the *syn*- and *anti*-regioisomers, respectively. Isomerization to and reaction of the *cis*-conformer have barriers of 27.4 (*anti*) and 27.6 (*syn*) kcal/mol, respectively.

[§§] Notably, Yoshida *et al.* reported that sterically hindered azides react more rapidly with cyclooctynes than unhindered azides. Their explanation for the energetic origins of this observation may also apply to our system. See reference 36.

Because the energetic barrier to isomerization is significantly lower than the barrier to reaction, we hypothesize that BARAC isomerizes during the course of the cycloaddition. However, because the activation energy for reaction of the *trans*-isomer is lower than the activation energy for isomerization to and reaction of the *cis*- isomer, we conclude that BARAC (**2.1**) reacts mainly through the *trans*-isomer. As a result, the energetic barriers shown in Figure 2.11a, which predict a roughly 1:1 ratio of regioisomeric products, accurately predict the experimentally observed ratio of regioisomers (also 1:1).

The calculated barriers to *cis*/*trans* isomerization for both compounds **2.10** and **2.11** are about 16 kcal/mol, on par with that observed for the parent BARAC. Interestingly, however, for **2.10**, the transition state energies of the *trans*- and *cis*-isomers are much closer in energy than they are for those of the parent compound. Reaction of the *trans*-isomer of **2.10** displays activation energies of 28.2 (*syn*) and 30.1 (*anti*) kcal/mol, and reaction of the *cis*-isomer displays similar activation energies of 28.7 (*anti*) and 28.8 (*syn*) kcal/mol. Because the transition state energies of the *cis*- and *trans*-isomers are similar, we hypothesize that **2.10** may undergo the 1,3-dipolar cycloaddition with methyl azide by reacting through both the *cis* and the *trans* pathways. On the basis of this hypothesis and the aforementioned transition state energies, we calculate a *syn*/*anti* product ratio of 3:1 for **2.10**. Compound **2.11** also showed similar *trans* and *cis* transition state energetics, and gave a calculated *syn*/*anti* product ratio of 5:1. These values are close to the observed product ratios (3:1 and 2:1 *syn*/*anti* for **2.10** and **2.11**, respectively).

Of note is the fact that the observed regioselectvities for compounds **2.10** and **2.11** are not what one would predict based on the fundamentals of steric interactions in reaction transition states. Prior to these experiments, we hypothesized that the *anti* regioisomer would be favored for the reactions of **2.10** and **2.11** with benzyl azide. The ability of the distortion/interaction model to predict the alternative (and accurate) outcome is a testament to its utility in understanding cyclooctyne reactivity.

Conclusion

We have performed a systematic analysis of the effects of strain and electronics on the reactivities of various cyclooctynes using the distortion/interaction model. We found that aryl ring substitution with electron-withdrawing and -donating groups produces only minor alterations in reactivity. The majority of the analogs tested did not display significant rate changes relative to that of the parent compound **2.1** for the reaction with benzyl azide. However, we did see a ~75% increase in reactivity for the difluorinated analog **2.6**, which subsequent DFT calculations attributed to increased stabilizing interaction energy in the transition state of the reaction.

We observed more significant rate changes upon aryl substitution with groups capable of imposing steric hindrance in the transition state. Methyl-substituted analogs **2.10** and **2.11** and fluorine-substituted analog **2.9**, which possess substituents at the flagpole position (*ortho* to the alkyne) displayed second-order rate constants between 2 and 3 orders of magnitude lower than that observed for parent BARAC. DFT data confirmed significantly increased transition state distortion energies for the reactions of these

compounds with methyl azide. We also identified a correlation between total alkyne bond angle distortion and reactivity for the series of cyclooctynes shown in Table 2.1. Thus, computed alkyne bond angles as well as transition state distortion and interaction energies may be used in the informed design of cyclooctynes with tailored reactivities.

Analysis of BARAC's amide bond structure provided insight into its reactivity and regioselectivity with azides. X-ray structures of BARAC analogs provided evidence that BARAC is able to modulate stability through amide bond rehybridization. As well, we found that BARAC's lactam has the *trans* configuration in crystal form. Computations confirmed that the *trans* conformation is energetically preferred to the *cis* conformation by 9.4 kcal/mol in acetonitrile and that this significant energetic difference may be in part a result of enhanced alkyne distortion upon isomerization to the *cis*-conformer (Figure 2.6). These data suggest that a *cis*-constrained BARAC analog may display enhanced reactivity toward the azide as a result of enhanced strain.

Overall, our results show that DFT calculations can be a valuable resource in predicting the reactivity of potential new cyclooctynes. Accordingly, tools and trends summarized here should be useful for crafting new bioorthogonal reagents.

Future Directions

The rapid reactivity of difluorinated analog **2.6** and the slow rates of compounds **2.9**–**2.11** are evidence that the copper-free click reaction can be tuned to meet the demands of a range of experiments. Whereas **2.6** may prove useful for *in vivo* labeling where fast ligation rates are essential, **2.9**–**2.11** could be used in situations where slow rates are preferred. A growing trend in bioconjugation chemistry is the use of "proximity-enhanced" ligations — ligations that proceed only when two reactive functionalities are in close proximity. This spatial dependence enables proximity-enhanced ligations to serve as a record of the interactions of tagged biomolecules, and also affords a new degree of control over which substrates are labeled. Proximity enhanced ligations have been used to cross-link protein-receptor complexes,[37] to generate disulfide mimics within proteins,[38] and to label active enzymes via activity based protein profiling.[39]

In proximity-enhanced experiments, slow reactions are deliberately selected such that the ligation only proceeds at high effective concentrations (when the reactive groups are proximal), but does not proceed at low concentrations. To date, most proximity-enhanced methods rely on native biological functionalities such as primary amines or sulfydryl groups as one reactive partner. Examples include ligations between cysteine and a fluoromethyl ketones or haloalkanes,[38,40] reactions of lysines with acrylamides and vinyl sulfonamides,[37] and dimethylaminopyridine (DMAP)-mediated acylation of of lysines or cysteines.[41,42] However, because all of these methods employ a native functional group such as lysine or cysteine as a reaction partner, they are inherently prone to background reactivity with off-target proteins. Use of bioorthogonal reagents as proximity-enhanced ligation partners would mitigate this challenge.

This work provides a platform for designing cyclooctyne reagents with a range of

reactivities, and could therefore be valuable in engineering new proximity-enhanced ligations. In particular, the slow reaction rates of compounds **2.9**–**2.11** may enable their use in the design of new proximity-enhanced ligation systems.

Materials and Methods

General Procedures. Reagents and solvents were obtained commercially and used without further purification with the exception of anhydrous solvents which were prepared by the method developed by Pangborn *et al.*[43] Flash column chromatography was performed according to the method described by Still *et al.* using Silicycle Silica Flash P60 silica (40-63 mm, 230-400 mesh).[44] All high pressure liquid chromatography purifications were performed on a Varian ProStar HPLC equipped with UV/vis detector using a 100 Å C18 column (250 x 21.4 mm) at a flow rate of 20 mL/min. Reactions were monitored by TLC with Analtech Uniplate silica gel plates (250 mm) visualized with ultraviolet light or with potassium permanganate staining followed by brief heating on a hot plate. Unless otherwise noted, anhydrous magnesium sulfate was used to dry organic extracts and solutions were concentrated using a Buchi Rotovapor-114 equipped with a KNF-Neuberger 115-vacuum or a Welch 2026 self- cleaning dry vacuum system. Compounds were dried under reduced pressure on a Schlenk line equipped with an Edwards 8 high vacuum.

All ^{1}H and ^{13}C spectra were obtained with a Bruker AV-600, AV-500, AVB-400, or AVQ-400 spectrometer. Peaks are reported in ppm and referenced to the solvent ($CDCl_3$). Data are presented as follows: chemical shift in ppm, multiplicity (s = singlet, d = doublet, t = triplet, q = quartet, quin = quintet, m =multiplet), coupling constant in Hz, and integration value. All ^{19}F spectra were obtained with a Bruker AVQ-400 NMR spectrometer. High-resolution electrospray ionization (ESI) mass spectrometry data were obtained through the UC Berkeley Mass Spectrometry Facility on a Linear trap quadrupole fourier transform ion cyclotron resonance (LTQ-FT-ICR) mass spectrometer from Thermo Fisher. High-resolution electron ionization (EI) mass spectrometry data were obtained through the UC Berkeley Mass Spectrometry Facility on an AutoSpec mass spectrometer from Waters. X-ray crystallography data was obtained through the UC Berkeley X-ray crystallography facility (see pages S122-S142 for details).

5,10-dihydroindeno[1,2-b]indole (2.1a). To a solution of phenyl hydrazine (2.98 mL, 3.27 g, 30.3 mmol, 1.00 equiv.) and 1-indanone (4.00 g, 30.3 mmol, 1.00 equiv.) in ethanol (21 mL) was added glacial acetic acid (5 drops). The solution was stirred at reflux (85 ^{o}C) for 15 minutes and cooled to room temperature. Upon cooling, long, white crystals precipitated out of solution. The crystals were collected via vacuum filtration and combined with isopropanol (102 mL). Sulfuric acid (36 N, 3.4 mL) was added via syringe and the resulting solution was stirred at reflux (90 ^{o}C) for 16 hours. Upon cooling to room temperature, the solution was basified to pH 10 with aqueous sodium hydroxide (2% NaOH by mass) resulting in the formation of precipitate. The solid was collected by vacuum filtration to yield **2.1a** in 89% yield (5.55 g, 27.1 mmol). R_f = 0.6 in 3:1 hexanes:ethyl acetate; ^{1}H NMR (600 MHz, $CDCl_3$): δ 8.30 (s, 1H), 7.67–7.62 (m, 1H),

7.55 (d, J = 7.4 Hz, 1H), 7.47 (d, J = 7.5 Hz, 1H), 7.45–7.43 (m, 1H), 7.34 (t, J = 7.5 Hz, 1H), 7.25–7.21 (m, 1H), 7.21–7.15 (m, 2H), 3.74 (s, 2H); ^{13}C NMR (151 MHz, $CDCl_3$): δ 147.8, 143.3, 140.6, 135.0, 126.5, 125.5, 124.8, 124.7, 121.8, 121.7, 120.2, 118.9, 117.2, 112.0, 30.3; ESI-HRMS: Calcd. for $C_{15}H_{12}N^+$ $[M+H]^+$: 206.0964, found 206.0964.

5-methyl-5,10-dihydroindeno[1,2-*b*]indole (2.1b). To a solution of **2.1a** (5.40 g, 26.3 mmol, 1.00 equiv.) in benzene (35 mL) was added aqueous sodium hydroxide (50% NaOH by mass, 14 mL), tetrabutylammonium iodide (494 mg, 1.34 mmol, 0.051 equiv.), and iodomethane (13.1 mL, 29.9 g, 210 mmol, 8.00 equiv.). The reaction mixture was stirred vigorously at 40 °C for 17 hours and then at 55 °C for an additional 1.5 hours. Upon cooling to room temperature, the mixture was diluted with benzene (25 mL) and H_2O (25 mL), and the aqueous layer was extracted 2x with 50 mL ethyl acetate. The organic layers were combined, dried over anhydrous magnesium sulfate, and concentrated to yield an orange/brown solid. The crude product was purified by flash column chromatography (15:1, 10:1, 4:1, 0:1 hexanes- ethyl acetate) to give **2.1b** in 86% yield (4.96 g, 22.6 mmol). R_f = 0.7 in 3:1 hexanes:ethyl acetate: ^{1}H NMR (600 MHz, $CDCl_3$): δ7.75 (d, J = 7.7 Hz, 1H), 7.68 (d, J = 7.5 Hz, 1H), 7.62 (d, J = 7.4 Hz, 1H), 7.48–7.40 (m, 2H), 7.40–7.29 (m, 3H), 3.96 (s, 3H), 3.69 (s, 2H); ^{13}C NMR (151 MHz, CDCl3): δ 148.0, 144.5, 141.7, 135.2, 126.3, 125.4, 124.4, 123.9, 121.0, 120.0, 119.3, 118.8, 117.4, 109.5, 30.7, 29.8; ESI-HRMS: Calcd. for $C_{16}H_{13}N$ $[M]^+$: 219.1043, found 219.1042.

5-methyl-10-(trimethylsilyl)-5,10-dihydroindeno[1,2-*b*]indole (2.1c). Methylated indole **2.1b** (357 mg, 1.63 mmol, 1.00 equiv.) was dried by azeotrope (2x with toluene) and then combined with anhydrous ether (14 mL). The reaction flask was immersed in a room temperature water bath, and *n*-BuLi (1.66M in hexanes, 980 µL, 1.63 mmol, 1.00 equiv.) was added dropwise over 30 minutes via syringe pump. Upon addition of base, the reaction mixture acquired a dark red color and the starting material went into solution. The reaction was stirred an additional 1 hour at room temperature and then cooled to –78 °C in a dry ice/acetone bath. TMSCl (830 µL, 6.52 mmol, 4.00 equiv.) was added and the reaction mixture was immediately warmed to room temperature over 1.5 hrs. Upon warming, the reaction was filtered to remove CsF and concentrated *in vacuo* to a brown oil. The product was purified by flash column chromatography (40:1 hexanes-ethyl acetate) to yield **2.1c** in 76% yield (363 mg, 1.25 mmol). R_f = 0.7 in 3:1 hexanes:ethyl acetate; ^{1}H NMR (600 MHz, CDCl3): δ 7.84 (dd, J = 11.3, 7.8 Hz, 2H), 7.68 (d, J = 7.6 Hz, 1H), 7.50 (t, J = 6.9 Hz, 1H), 7.47 (t, J = 7.4 Hz, 1H), 7.37 (dt, J = 14.6, 7.4 Hz, 2H), 7.32 (t, J = 7.4 Hz, 1H), 4.13 (s, 3H), 3.87 (s, 1H), 0.14 (s, 9H); ^{13}C NMR (151 MHz, CDCl3): δ 149.9, 143.2, 141.9, 141.9, 133.5, 124.9, 124.6, 123.5, 123.0, 120.9, 120.1, 118.9, 117.5, 109.5, 36.7, 31.0, -2.4; ESI-HRMS: Calcd. for $C_{19}H_{22}NSi$ $[M+H]^+$: 292.1516, found 292.1516.

BARAC (2.1). To a solution of **2.1c** (714 mg, 2.45 mmol, 1.00 equiv.) in dichloromethane (63 mL) and saturated aqueous $NaHCO_3$ (13 mL) at 0 °C was added *m*-CPBA (77%, 1.23 g, 7.10 mmol, 2.90 equiv.) portionwise over 5 minutes. The reaction mixture was stirred at 0 °C for 30 minutes and then warmed to room temperature over 40 minutes. The reaction was subsequently quenched via addition of 1N NaOH (20 mL) and

the resulting aqueous layer was extracted 2x with 50 mL dichloromethane and 1x with 50 mL ethyl acetate. The organic layers were combined and washed 1x with brine, dried over anhydrous magnesium sulfate, and concentrated *in vacuo* to yield an orange oil (**2.1d**). Crude product was immediately brought on to the next step.

To a solution of **2.1d** (2.45 mmol assuming 100% yield from the previous step) in anhydrous THF (28 mL) at –78 ^{o}C was added potassium hexamethyldisilazide (0.5 M in toluene, 10.7 mL, 5.34 mmol, 2.20 equiv.) dropwise via syringe to give an orange solution which was stirred an additional 30 minutes at –78 ^{o}C. Triflic anhydride (474 μL, 2.82 mmol, 1.15 equiv.) was added and the reaction mixture immediately turned yellow. The solution was stirred for 30 minutes at –78 ^{o}C prior to dilution with 44 mL anhydrous ether and addition of tetrabutyl ammonium fluoride (1M in THF, 24.5 mL, 10.0 equiv.). The reaction mixture was warmed to room temperature over 25 minutes then quenched with saturated aqueous $NaHCO_3$ (60 mL). The aqueous layer was subsequently extracted 2x with 30 mL ethyl acetate and the organic layer was dried over anhydrous magnesium sulfate and concentrated to yield a brown oil. The product was purified by flash column chromatography (20:1, 10:1, 5:1, 4:1, 3:1 hexanes – ethyl acetate) to yield **2.1** in 34% yield (192 mg, 0.823 mmol). The compound was then purified by HPLC for the purposes of characterization and kinetic analysis. A 25 mg sample of **2.1** was dissolved in a solution of water (A) and acetonitrile (B) (2:3 A:B). The compound was injected onto a C18 column and eluted at 20 mL/min using a gradient of 35% B to 75% B over 35 minutes. The product was collected at 16 minutes. Elution was monitored by UV absorption at 210 and 254 nM. R_f = 0.3 in 3:1 hexanes- ethyl acetate; ^{1}H NMR (600 MHz, $CDCl_3$): δ 7.65–7.57 (m, 2H), 7.51–7.40 (m, 4H), 7.40–7.35 (m, 2H), 2.73 (s, 3H); ^{13}C NMR (151 MHz, $CDCl_3$): δ 176.7, 156.6, 149.3, 129.8, 129.3, 129.3, 128.7, 128.0, 127.5, 126.4, 125.5, 122.2, 122.2, 109.4, 108.6, 38.7; ESI-HRMS: Calcd. for $C_{16}H_{12}NO$ $[M+H]^{+}$: 234.0913, found 234.0914.

7-fluoro-5,10-dihydroindeno[1,2-*b*]indole (2.2a) and 9-fluoro- 5,10-dihydroindeno[1,2-*b*]indole (2.9a). 3-fluorophenylhydrazine hydrochloride (2.00g, 12.3 mmol, 1.00 equiv.) and 1-indanone (1.63 g, 12.3 mmol, 1.00 equiv.) were dissolved in ethanol (31 mL) and stirred at reflux (85 ^{o}C) for 12 minutes. Glacial acetic acid (3 drops) was added, and the solution was stirred an additional 5 minutes at 85 ^{o}C, then cooled to room temperature. Ethanol was removed under reduced pressure to yield a brown/red solid which was subsequently dissolved in isopropanol (21 mL). Sulfuric acid (36 N, 1.4 mL) was added to the reaction mixture via syringe and the resulting solution was stirred at reflux (90 ^{o}C) for 16 hours. Upon cooling to room temperature, the solution was basified to pH 10 with aqueous sodium hydroxide (2% NaOH by mass) resulting in the formation of a green precipitate. This solid was collected by vacuum filtration, dissolved in dichloromethane, and diluted with water. The aqueous layer was extracted 3x with 15 mL dichloromethane, and the remaining organic layer was dried over anhydrous magnesium sulfate and concentrated to yield a brown solid as a mixture of regioisomers (2:1.1 **2.2a:2.9a**) in 78% crude yield (2.14 g, 9.59 mmol). This mixture was brought on to the next step without further purification. For purposes of characterization, a small fraction of desired product was purified by numerous passes through a biotage 40M column (20:1 hexanes – ethyl acetate).

2.2a: R_f = 0.64 in 3:1 hexanes-ethyl acetate; ^{1}H NMR (600 MHz, CDCl3): δ 8.32 (s, 1H), 7.53 (m, *J* = 8.4, 5.1 Hz, 2H), 7.45 (d, *J* = 7.5 Hz, 1H), 7.33 (t, *J* = 7.4 Hz, 1H), 7.22 (td, *J* = 7.5, 1.0 Hz, 1H), 7.13 (dd, *J* = 9.7, 2.3 Hz, 1H), 6.93 (ddd, *J* = 9.6, 8.7, 2.3 Hz, 1H), 3.72 (s, 2H); ^{13}C NMR (151 MHz, CDCl3): δ 158.8 (s), 147.4 (s), 143.6 (s), 140.6 (d, *J* = 12.1 Hz), 134.9 (s), 126.58 (s), 125.5 (s), 124.7 (s), 121.7 (s), 121.5 (s), 119.4 (d, *J* = 10.0 Hz), 117.1 (s), 108.7 (d, *J* = 24.2 Hz), 98.6 (d, *J* = 26.2 Hz), 30.3 (s); ^{19}F NMR (376 MHz, CDCl3): δ –120.07 (td, *J* = 9.6, 5.5 Hz); ESI-HRMS: Calcd. for $C_{15}H_{10}FN^+$ $[M]^+$: 223.0792, found 223.0791.

2.9a: R_f = 0.57 in 3:1 hexanes-ethyl acetate; ^{1}H NMR (600 MHz, $CDCl_3$): δ 8.38 (s, 1H), 7.57 (d, *J* = 7.4 Hz, 1H), 7.48 (d, *J* = 7.5 Hz, 1H), 7.35 (t, *J* = 7.4 Hz, 1H), 7.28–7.23 (m, 2H), 7.21 (d, *J* = 8.1 Hz, 1H), 7.09 (td, *J* = 8.0, 5.3 Hz, 1H), 6.85 (dd, *J* = 10.2, 8.0 Hz, 1H), 3.85 (s, 2H); ^{13}C NMR (151 MHz, $CDCl_3$): δ 156.2 (d, *J* = 246.1 Hz), 148.0 (s), 143.1 (s), 143.0 (d, *J* = 11.0 Hz), 134.4 (s), 126.6 (s), 125.5 (s), 125.1 (s), 122.1 (d, *J* = 7.7 Hz), 118.9 (s), 117.4 (s), 114.2 (d, *J* = 22.7 Hz), 108.0 (d, *J* = 3.4 Hz), 105.3 (d, *J* = 18.9 Hz), 31.0 (s); ^{19}F NMR (376 MHz, $CDCl_3$): δ –121.92 – –122.00 (m); ESI-HRMS: Calcd. for $C_{15}H_{11}FN$ $[M+H]^+$: 224.0870, found 224.0875.

7-fluoro-5-methyl-5,10-dihydroindeno[1,2-*b*]indole (2.2b) and 9-fluoro-5-methyl-5,10-dihydroindeno[1,2-b]indole (2.9b). To a solution of **2.2a** and **2.9a** (as a 2:1.1 mixture of regioisomers, 2.14 g, 9.58 mmol, 1.00 equiv.) in benzene (31 mL) was added aqueous sodium hydroxide (50% NaOH by mass, 5.0 mL), tetrabutylammonium iodide (184 mg, 0.463 mmol, 0.048 equiv.), and iodomethane (4.77 mL, 76.6 mmol, 8.00 equiv). The reaction mixture was stirred vigorously at 40 °C for 17.5 hours and subsequently cooled to room temperature. The solution was then diluted with benzene (10 mL) and H_2O (10 mL), and the aqueous layer was extracted 2x with 20 mL ethyl acetate. Organic layers were combined, dried over anhydrous magnesium sulfate and concentrated *in vacuo*. The crude product was purified by flash column chromatography (15:1 to 15:1.5 hexanes-ethyl acetate) to give a solid, inseparable mixture of **2.2b** and **2.9b** in 72% yield (1.63 g, 6.87 mmol). Spectral data are reported for the mixture. R_f= 0.70, 0.74 in 3:1 hexanes-ethyl acetate; ^{1}H NMR (600 MHz, CDCl3): δ 7.54–7.45 (m, 3.8H), 7.38 (dd, *J* = 14.2, 7.1 Hz, 1.5H), 7.33–7.24 (m, 1.6H), 7.15 (tt, *J* = 13.5, 6.8 Hz, 0.5H), 7.05 (d, *J* = 8.2 Hz, 0.5H), 7.03–6.96 (m, 2H), 6.93 (dd, *J* = 10.2, 7.8 Hz, 0.5H), 3.73 (s, 1.4H), 3.68 (s, 3H), 3.60 (d, *J* = 7.5 Hz, 0.9H), 3.42 (s, 2H); ^{13}C NMR (151 MHz, $CDCl_3$): δ 159.2 (d, *J* = 237.2 Hz), 156.0 (d, *J* = 245.7 Hz), 148.1 (s), 147.5 (s), 144.6 (d, *J* = 3.4 Hz), 144.1 (s), 143.9 (d, *J* = 12.0 Hz), 141.5 (d, *J* = 11.7 Hz), 135.0 (s), 134.5 (s), 126.2 (s), 126.1 (s), 125.3 (s), 125.2 (s), 124.5 (s), 124.2 (s), 121.1 (d, *J* = 7.6 Hz), 120.5 (s), 119.8 (s), 119.1 (d, *J* = 10.0 Hz), 117.3 (s), 117.0 (s), 116.8 (s), 113.1 (d, *J* = 23.0 Hz), 107.6 (d, *J* = 24.4 Hz), 105.5 (d, *J* = 3.3 Hz), 104.2 (d, *J* = 18.8 Hz), 96.0 (d, *J* = 26.3 Hz), 30.7 (s), 30.5 (s), 30.3 (s), 29.5 (s); ^{19}F NMR (376 MHz, $CDCl_3$): δ –119.99 (td, *J* = 9.8, 5.6 Hz), –122.18 (dd, *J* = 10.2, 4.9 Hz).

7-fluoro-5-methyl-10-(trimethylsilyl)-5,10-dihydroindeno[1,2- *b*]indole (2.2c) and 9-fluoro-5-methyl-10-(trimethylsilyl)-5,10- dihydroindeno[1,2-b]indole (2.9c). A

mixture of compounds **2.2b** and **2.9b** (as a 1:0.4 mixture of regioisomers, 531 mg, 2.24 mmol, 1.00 equiv.) was dried by azeotrope (2 x 2 mL toluene), dissolved in anhydrous ether (15 mL), and the reaction mixture was immersed in a room temperature water bath. *n*-BuLi (1.70M in hexanes, 1.32 mL, 2.24 mmol, 1.00 equiv.) was added dropwise via syringe pump over one hour. Following addition of base, the reaction mixture was stirred for one hour at room temperature and then cooled to –78 °C. TMSCl (568 μL, 4.48 mmol, 2.00 equiv) was added rapidly via syringe and the resulting mixture was immediately warmed to room temperature. The reaction mixture was diluted ether, filtered, and concentrated *in vacuo* to yield a dark green oil which was subsequently purified by flash column chromatography (20:1 hexanes-ethyl acetate) to **2.2c** and **2.9c** as a mixture of regioisomers in 67% yield (462 mg, 1.49 mmol). Spectral data are reported for the mixture, but do not represent the ratio of regioisomers obtained from this reaction. R_f = 0.75, 0.78 in 3:1 hexanes-ethyl acetate; ^{1}H NMR (600 MHz, $CDCl_3$): δ 7.76 (d, *J* = 7.6 Hz, 1H), 7.72 (d, *J* = 7.6 Hz, 0.7H), 7.60–7.53 (m, 2.4H), 7.36 (dd, *J* = 12.7, 7.2 Hz, 1.7H), 7.29–7.23 (m, 1.8H), 7.20–7.13 (m, 1.9H), 7.08 (dd, *J* = 10.1, 2.3 Hz, 0.7H), 6.95 (ddd, *J* = 9.4, 8.8, 2.3 Hz, 0.7H), 6.87 (ddd, *J* = 10.7, 7.1, 1.4 Hz, 0.9H), 4.08 (s, 3H), 4.02 (s, 2.2H), 3.94 (s, *J* = 5.0 Hz, 1H), 3.74 (s, *J* = 5.1 Hz, 0.7H), -0.01 (m, 6.6H), –0.04 (d, *J* = 0.8 Hz, 9H); ^{13}C NMR (151 MHz, $CDCl_3$): δ 159.3 (d, *J* = 237.5 Hz), 156.0 (d, *J* = 246.4 Hz), 150.4 (s), 149.6 (s), 144.3 (d, *J* = 11.9 Hz), 143.6 (d, *J* = 3.5 Hz), 143.0 (s), 142.0 (d, *J* = 11.5 Hz), 133.4 (s), 132.7 (s), 125.1 (s), 124.9 (s), 124.6 (s), 124.6 (s), 123.8 (s), 123.5 (s), 123.1 (s), 121.3 (d, *J* = 7.9 Hz), 120.6 (d, *J* = 10.0 Hz), 120.4 (s), 120.3 (s), 117.6 (s), 117.3 (s), 113.0 (d, *J* = 22.0 Hz), 107.4 (d, *J* = 24.3 Hz), 105.6 (d, *J* = 3.3 Hz), 104.4 (d, *J* = 19.8 Hz), 96.2 (d, *J* = 26.3 Hz), 37.3 (s), 36.8 (s), 31.5 (s), 31.3 (s), –2.4 (s), –2.5 (d, *J* = 2.6 Hz); ESI-HRMS: Calcd. For $C_{19}H_{21}FNSi^+$ $[M]^+$: 292.1516, found 292.1516.

Fluoro-BARACs (**2.2** and **2.9**)**.** To a stirred solution of **2.2c** and **2.9c** (1:0.55 **2.2c**:**2.9c**, 462 mg, 1.49 mmol total, 1.00 equiv., 0.95 mmol **2.2c**, 0.54 mmol **2.9c**) in dichloromethane (30 mL) and saturated aqueous $NaHCO_3$ (14 mL) at 0 °C was added *m*-CPBA (77%, 1.93 g, 8.61 mmol, 5.78 equiv.) portionwise over 2 minutes. The reaction mixture was stirred at 0 °C for 10 minutes and then warmed to room temperature over 20 minutes. The reaction was quenched via addition of 1N NaOH (30 mL) and the resulting aqueous layer was extracted 2x with 30 mL dichloromethane and 1x with 30 mL ethyl acetate. Organic layers were combined and washed 1x with 40 mL brine, dried over anhydrous magnesium sulfate, and concentrated *in vacuo* to yield a yellow oil (**2.2d** and **2.9d**), which was immediately brought on to the next step in crude form.

To a solution of **2.2d** and **2.9d** (1.49 mmol total assuming 100% yield from the previous step) in anhydrous THF (19 mL) at –78 °C was added potassium hexamethyldisilazide (0.5 M in toluene, 3.28 mL, 1.64 mmol, 1.10 equiv.) dropwise via syringe to give a red solution which was stirred an additional 40 minutes at –78 °C. Triflic anhydride (300 μL, 1.79 mmol, 1.20 equiv.) was then added, and the solution immediately turned yellow. The solution was stirred for 40 minutes at –78 °C prior to dilution with 20 mL anhydrous ether. The reaction was warmed to room temperature over 1 hour then quenched with saturated aqueous $NaHCO_3$ (25 mL). The aqueous layer was subsequently extracted 2x with 25 mL ethyl acetate and the organic layer was dried over anhydrous magnesium

sulfate and concentrated *in vacuo* to yield an orange oil. At this stage, regioisomers were separated by flash column chromatography (10:1, 5:1, 3:1 hexanes – ethyl acetate) to give **2.9e** in 63% yield (yield calculated based on the amount of **2.9d** in the starting mixture; 163 mg, 0.344 mmol). Fractions containing **2.2e** were pooled and purified by a second round of column chromatography to give **2.2e** in 14% yield as a mixture with ~27% impurity (yield calculated based on the amount of **2.2d** in the starting mixture and the amount of **2.2e** in the product mixture; 81 mg total product mixture, 0.17 mmol total product mixture, 62 mg **2.2e**, 0.13 mmol **2.2e**).

This **1:0.27** mixture of **2.2e:impurity** (0.07 mmol **2.2e**, 31 mg) was dissolved in acetonitrile (5 mL). CsF was added (169 mg, 1.11 mmol, 15.9 equiv.) and the reaction mixture was stirred at room temperature for 30 minutes prior to addition of another 97 mg CsF (0.69 mmol, 9.1 equiv). The reaction was stirred for 10 additional minutes at room temperature at which point the CsF was filtered and the resulting solution was concentrated *in vacuuo*. Crude product was purified by flash column chromatography (10:1, 5:1 hexanes–ethyl acetate) to give **2.2** in 57% yield (yield calculated based on the amount of **2.2e** in the starting mixture, 9.5 mg, 0.038 mmol).

To generate cycooctyne **2.9**, **2.9e** (163 mg, 0.34 mmol, 1.00 equiv.) was dissolved in acetonitrile (15 mL) and CsF (382 mg, 2.51 mmol, 7.38 equiv.) was added. The reaction mixture was stirred for 1 h at room temperature and the CsF was filtered off. The resulting solution was concentrated *in vacuuo* to give an orange solid. Crude product was purified by flash column chromatography (7:1, 5:1 hexanes – ethyl acetate) to give **2.9** in 30% yield (65 mg, 0.26 mmol).

For the purposes of characterization and kinetic analysis, **2.9** was further purified by HPLC. The compound was injected onto a C18 preparatory column in a 0.5:2 water(A):acetonitrile(B) solution and eluted at 20 mL/min at using a gradient of 35% B to 75% B over 35 minutes at a flow rate of 20 mL/min. The product was collected at 19 minutes. Elution was monitored at 210 and 254 nM.

2.2: R_f = 0.4 in 3:1 hexanes-ethyl acetate; ^{1}H NMR (600 MHz, $CDCl_3$): δ 7.62–7.56 (m, 1H), 7.49–7.42 (m, 2H), 7.42–7.33 (m, 3H), 7.11 (td, J = 8.4, 2.4 Hz, 1H), 2.73 (s, 3H); ^{13}C NMR (151 MHz, $CDCl_3$): δ 176.5 (s), 162.9 (d, J = 252.7 Hz), 157.9 (d, J = 10.6 Hz), 149.2 (s), 129.5 (s), 128.7 (s), 128.4 (d, J = 9.5 Hz), 126.3 (s), 125.5 (s), 122.1 (s), 118.4 (d, J = 3.7 Hz), 117.8 (d, J = 23.1 Hz), 115.2 (d, J = 22.1 Hz), 109.4 (d, J = 1.9 Hz), 107.6 (s), 38.5 (s); ^{19}F NMR (376 MHz, $CDCl_3$): δ –107.20 (m); ESI-HRMS: Calcd. for $C_{16}H_{11}FNO^+$ $[M+H]^+$: 252.0819, found 252.0820.

2.9: R_f = 0.3 in 3:1 hexanes-ethyl acetate; ^{1}H NMR (600 MHz, $CDCl_3$): δ 7.63–7.57 (m, 1H), 7.50–7.45 (m, 2H), 7.45–7.41 (m, 2H), 7.41–7.37 (m, 1H), 7.18–7.12 (m, 1H), 2.73 (s, 3H); ^{13}C NMR (151 MHz, $CDCl_3$): δ 176.5 (s), 158.9 (d, J = 255.5 Hz), 157.5 (d, J = 3.4 Hz), 149.3 (s), 130.4 (d, J = 9.0 Hz), 129.5 (s), 129.0 (s), 126.4 (s), 125.5 (s), 125.2 (d, J = 3.2 Hz), 121.9 (s), 115.6 (d, J = 20.1 Hz), 113.0 (s), 111.5 (d, J = 16.2 Hz), 103.5 (d, J = 2.6 Hz), 38.6 (s); ^{19}F NMR (376 MHz, $CDCl_3$): δ –105.83 – –105.94 (m); ESI-HRMS: Calcd. for $C_{16}H_{11}FNO^+$ $[M+H]^+$: 252.0819, found 252.0821.

3-fluoro-5,10-dihydroindeno[1,2-*b*]indole (2.3a). To a solution of phenyl hydrazine (1.32 mL, 13.3 mmol, 1.00 equiv.) and 6-fluoro-1-indanone (2.02 g, 13.5 mmol, 1.01equiv.) in ethanol (7.6 mL) was added glacial acetic acid (3 drops). The solution was stirred at reflux (85 ^{o}C) for 17 minutes and cooled to room temperature. Upon cooling, white crystals precipitated out of solution. These crystals were collected by vacuum filtration and dissolved in isopropanol (23 mL). Sulfuric acid (36 N, 1.51 mL) was added via syringe and the resulting solution was stirred at reflux (90 ^{o}C) for 18 hours and subsequently cooled to room temperature. The solution was then basified to pH 10 via addition of aqueous sodium hydroxide (2% NaOH by mass) resulting in the formation of precipitate. The solid was collected by vacuum filtration to yield **2.3a** as a brown solid in 46% crude yield (1.38 g, 6.17 mmol). Crude product was brought on to the next step without further purification. For purposes of characterization, the product was purified by flash column chromatography (20:1 to 20:1.5 hexanes – ethyl acetate). R_f = 0.7 in 3:1 hexanes-ethyl acetate; ^{1}H NMR (600 MHz, $CDCl_3$): δ 8.26 (s, 1H), 7.65 (d, *J* = 7.8 Hz, 1H), 7.44 (dd, *J* = 8.1, 4.4 Hz, 2H), 7.24–7.20 (m, 1H), 7.18 (td, *J* = 7.5, 1.1 Hz, 1H), 7.13 (dt, *J* = 8.3, 4.1 Hz, 1H), 6.90 (ddd, *J* = 9.5, 8.2, 2.4 Hz, 1H), 3.69 (s, 2H); ^{13}C NMR (151 MHz, $CDCl_3$): δ 162.3 (d, *J* = 242.5 Hz), 142.8 (d, *J* = 2.5 Hz), 142.3 (d, *J* = 3.0 Hz), 140.7 (s), 136.5 (d, *J* = 9.6 Hz), 126.0 (d, *J* = 9.2 Hz), 124.5 (s), 123.8 (s), 122.2 (s), 120.4 (s), 119.1 (s), 112.1 (s), 111.0 (d, *J* = 22.8 Hz), 104.7 (d, *J* = 24.5 Hz), 29.7 (s); ^{19}F NMR (376 MHz, $CDCl_3$): δ –119.99 – –120.14 (m); ESI- HRMS: Calcd. for $C_{15}H_{10}FN^{+}$ $[M]^{+}$: 223.0792, found 223.0790.

3-fluoro-5-methyl-5,10-dihydroindeno[1,2-*b*]indole (2.3b). To a solution of **2.3a** (1.38 g, 6.17 mmol, 1.00 equiv.) in benzene (12 mL) was added aqueous sodium hydroxide (33% NaOH by mass, 3.2 mL), tetrabutylammonium iodide (123 mg, 0.310 mmol, 0.050 equiv.), and iodomethane (3.04 mL, 48.8 mmol, 7.91 equiv.). The reaction mixture was stirred vigorously at 40 ^{o}C for 19 hours and then cooled to room temperature. The mixture was diluted with benzene (20 mL) and H_2O (20 mL), and the aqueous layer was extracted 1x with 15 mL ethyl acetate. The organic layers were combined, washed 1x with 25 mL H_2O, dried over anhydrous magnesium sulfate and concentrated to yield an orange/brown solid. Crude product was purified by flash column chromatography (10:1 to 4:1 hexanes-ethyl acetate) to give **2.3b** as a white solid in 71% yield (976 mg, 4.37 mmol). R_f = 0.8 in 3:1 hexanes-ethyl acetate; ^{1}H NMR (600 MHz, $CDCl_3$): δ 7.64 (d, *J* = 7.8 Hz, 1H), 7.40 (dt, *J* = 15.8, 7.9 Hz, 1H), 7.36 (d, *J* = 8.2 Hz, 1H), 7.31–7.24 (m, 2H), 7.21 (t, *J* = 7.4 Hz, 1H), 6.95–6.89 (m, 1H), 3.88 (s, 3H), 3.55 (s, 2H); ^{13}C NMR (151 MHz, $CDCl_3$): δ 162.1 (d, *J* = 241.9 Hz), 143.5 (d, *J* = 2.9 Hz), 143.1 (d, *J* = 2.4 Hz), 141.8 (s), 136.7 (d, *J* = 9.5 Hz), 125.9 (d, *J* = 9.2 Hz), 123.8 (s), 122.1 (s), 121.6 (s), 119.6 (s), 119.1 (s), 110.6 (d, *J* = 22.7 Hz), 109.7 (s), 104.9 (d, *J* = 24.7 Hz), 30.7 (d, *J* = 1.8 Hz), 29.3 (s); ^{19}F NMR (376 MHz, $CDCl_3$): δ –119.99 – –120.14 (m); ESI-HRMS: Calcd. for $C_{16}H_{13}FN^{+}$ $[M+H]^{+}$: 238.1027, found 238.1027.

3-fluoro-5-methyl-10-(trimethylsilyl)-5,10-dihydroindeno[1,2-*b*]indole (2.3c). A round bottom flask containing **2.3b** (976 mg, 4.37 mmol, 1.00 equiv.,) in dry ether (30 mL) was immersed in a room temperature water bath. *n*-BuLi (1.5 M in THF, 3.38 mL 5.07 mmol 1.16 equiv.) was added via syringe pump over one hour, generating a dark red

solution. Following addition of base, the reaction mixture was stirred at room temperature for an additional 50 minutes and then cooled to –78 °C. TMSCl (1.17 mL, 9.18 mmol, 2.10 equiv.) was added rapidly via syringe, and the reaction mixture was stirred an additional 5 minutes at –78 °C and then warmed to room temperature over 1.5 hours. The reaction was subsequently diluted with ether, filtered, and concentrated *in vacuo*. The crude product was purified by flash column chromatography (15:1 hexanes – ethyl acetate) to yield an inseparable mixture of **2.3c** and its corresponding di-silylated indole (disilylation at the benzylic position; 6.8:1 ratio **2.3c**:side product) in 67% yield (1.08 g mixture, 3.39 mmol mixture; 912 mg **2.3c**, 2.95 mmol **2.3c**, 67% yield **2.3c**). **2.3c** was brought on to the next step as a mixture with the di-silylated indole. Spectral data are reported for **2.3c** only. R_f = 0.8 in 3:1 hexanes-ethyl acetate; ^{1}H NMR (600 MHz, $CDCl_3$): δ 7.70 (d, *J* = 7.9 Hz, 1H), 7.49–7.39 (m, 3H), 7.29 (t, *J* = 7.5 Hz, 1H), 7.19 (t, *J* = 7.4 Hz, 1H), 6.94 (t, *J* = 8.8 Hz, 1H), 4.05 (s, 3H), 3.73 (s, 1H), 0.01 (s, 9H); ^{13}C NMR (151 MHz, $CDCl_3$): δ 161.3 (d, *J* = 240.6 Hz), 145.2 (d, *J* = 2.1 Hz), 142.4 (d, *J* = 3.1 Hz), 142.0 (s), 134.6 (d, *J* = 9.7 Hz), 125.2 (s), 125.0 (d, *J* = 9.2 Hz), 123.3 (s), 121.5 (s), 120.3 (s), 119.1 (s), 110.1 (d, *J* = 22.9 Hz), 109.6 (s), 104.5 (d, *J* = 24.3 Hz), 36.3 (s), 31.0 (s), –2.4 (s); ^{19}F NMR (376 MHz, $CDCl_3$): δ –117.37 (dd, *J* = 14.1, 9.0 Hz); ESI-HRMS: Calcd. for $C_{19}H_{21}FNSi^+$ $[M+H]^+$: 310.1422, found 310.1425.

Fluoro-BARAC (2.3). To a solution of **2.3c** as a mixture with 30% methylated indole **2.3b** (165 mg mixture, 0.58 mmol total, 1.0 equiv; 115 mg **2.3c**, 0.372 mmol **2.3c**) in dichloromethane (17 mL) and saturated aqueous $NaHCO_3$ (3.5 mL) at 0 °C was added *m*-CPBA (77%, 401 mg, 1.79 mmol, 3.08 equiv.) portionwise over 5 minutes. The reaction mixture was stirred at 0 °C for 12 minutes and then warmed to room temperature over 20 minutes. The reaction was subsequently quenched via addition of 1N NaOH (10 mL) and the resulting aqueous layer was extracted 2x with 10 mL dichloromethane and 1x with 10 mL ethyl acetate. The organic layers were combined and washed 1x with 40 mL brine, dried over anhydrous magnesium sulfate, and concentrated *in vacuo* to yield an orange oil. The crude product (**2.3d**) was immediately brought on to the next step without further purification.

To a solution of **2.3d** (0.58 mmol total, 1.0 equiv.; 0.37 mmol **2.3d** assuming 100% yield from the previous step) in anhydrous THF (6.6 mL) at –78 °C was added potassium hexamethyldisilazide (0.5 M in toluene, 2.6 mL, 1.3 mmol, 2.2 equiv.) dropwise via syringe to give an orange solution which was stirred an additional 15 minutes at –78 °C. Triflic anhydride (110 μL, 0.67 mmol, 1.2 equiv.) was then added, and the solution was stirred for an additional 30 minutes at –78 °C prior to dilution with 22 mL anhydrous ether and addition of tetrabutyl ammonium fluoride (1M in THF, 11.0 mL, 11.0 mmol, 18.9 equiv.). The reaction mixture was warmed to room temperature over 40 minutes and then quenched with saturated aqueous $NaHCO_3$ (21 mL). The aqueous layer was subsequently extracted 2x with 30 mL ethyl acetate and the organic layer was dried over anhydrous magnesium sulfate and concentrated to yield a brown oil. The product was purified by flash column chromatography (10:1 to 5:1 hexanes – ethyl acetate) to give **2.3** in 22% yield (21 mg, 0.084 mmol).

For the purposes of characterization and kinetic analysis, the compound was then purified

by HPLC. A 10 mg sample of **2.3** was dissolved in a 2.5 mL solution of water (A) and acetonitrile (B) (2:3 A:B). The compound was injected onto a C18 column and eluted at 20 mL/min using a gradient of 35% B to 75% B over 35 minutes The product was collected at 18.5 minutes. Elution was monitored at 210 and 254 nM. Rf = 0.6 in 2:1 hexanes-ethyl acetate; ^{1}H NMR (600 MHz, $CDCl_3$): δ 7.61 (d, *J* = 7.5 Hz, 1H), 7.47 (td, *J* = 7.6, 1.8 Hz, 1H), 7.43–7.32 (m, 4H), 7.16 (td, *J* = 8.6, 2.6 Hz, 1H), 2.74 (s, 3H); ^{13}C NMR (151 MHz, $CDCl_3$): δ 175.0 (s), 162.4 (d, *J* = 252.8 Hz), 156.3 (s), 151.0 (d, *J* = 7.5 Hz), 129.8 (s), 129.3 (s), 128.2 (d, *J* = 8.7 Hz), 128.2 (s), 127.4 (s), 122.1 (s), 118.3 (d, *J* = 3.5 Hz), 116.5 (d, *J* = 22.6 Hz), 113.8 (d, *J* = 24.3 Hz), 108.7 (s), 108.1 (s), 38.6 (s);; ^{19}F NMR (376 MHz, $CDCl_3$): δ –108.01 (dd, *J* = 13.3, 8.2 Hz); ESI-HRMS: Calcd. for $C_{16}H_{11}FNO^+$ $[M+H]^+$: 252.0819, found 252.0821.

8-fluoro-5,10-dihydroindeno[1,2-*b*]indole (2.4a). To a 100 mL cyclindrical, heavy wall, high pressure vessel was added 4-fluorophenylhydrazine (1.00 g, 6.17 mmol, 1.00 eq), 1-indanone (815 mg, 6.17 mmol, 1.00 eq) , isopropanol (31 mL), and sulfuric acid (0.7 mL). The reaction vessel was sealed and heated to 120 ^{o}C. Upon heating, starting material dissolved and the reaction mixture acquired a dark red color. The reaction was stirred at 120 ^{o}C for 4 days and then cooled to room temperature. The resulting dark brown liquid was basified to pH 10 with aqueous sodium hydroxide (2% NaOH by mass). The aqueous layer was subsequently extracted 3x with 10 mL ethyl acetate. Organics were combined, concentrated to yield a red solid, and re-dissolved in ethyl acetate. The solution was then dried over anhydrous magnesium sulfate and concentrated to give **2.4a** as a red solid (1.37 g, 6.14 mmol, 99% crude yield). Crude product was brought on to the next step without purification. R_f= 0.6 in 3:1 hexanes-ethyl acetate; ^{1}H NMR (600 MHz, $CDCl_3$): δ 8.31 (s, 1H), 7.55 (d, *J* = 7.4 Hz, 1H), 7.48 (d, *J* = 7.5 Hz, 1H), 7.36–7.33 (m, 2H), 7.28–7.23 (m, 2H), 6.92 (td, *J* = 9.0, 2.1 Hz, 1H), 3.72 (s, 2H); ^{13}C NMR (151 MHz, $CDCl_3$): δ 158.17 (d, *J* = 235.0 Hz), 147.74, 145.09, 137.02, 134.61, 126.59, 125.54, 125.17, 124.95 (d, *J* = 10.2 Hz), 121.59 (d, *J* = 4.6 Hz), 117.47, 112.37 (d, *J* = 9.8 Hz), 109.63 (d, *J* = 26.2 Hz), 103.98 (d, *J* = 23.8 Hz), 30.22; ^{19}F NMR (376 MHz, $CDCl_3$): δ – 123.1(td, *J* = 9.3, 4.1 Hz); HRMS (EI+) calcd for $C_{15}H_{10}FN$ $[M]^+$: 223.0797; found: 223.0792.

8-fluoro-5-methyl-5,10-dihydroindeno[1,2-*b*]indole (2.4b). To a solution of indole **2.4a**, (1.32 g, 5.92 mmol, 1.00 eq) in benzene (16 mL) was added aqueous sodium hydroxide (50% by mass, 4 mL), tetrabutylammonium iodide (118 mg, 0.297 mmol, 0.0502 eq), and iodomethane (2.9 mL, 47 mmol, 7.9 eq). The reaction mixture was stirred vigorously at 50 ^{o}C for 16 hours and subsequently cooled to room temperature. The solution was then diluted with benzene and water, and the aqueous layer was extracted 2x with ethyl acetate. The organic layers were combined, dried over anhydrous magnesium sulfate and concentrated *in vacuo* to yield a red oil. Crude product was purified by flash column chromatography (20:1 hexanes-ethyl acetate). Mixed fractions were purified in a second round of column chromatography using the same eluent system. The product was isolated in 63% yield (885 mg, 3.73 mmol). R_f = 0.7 in 3:1 hexanes-ethyl acetate; ^{1}H NMR (600 MHz, $CDCl_3$): δ 7.60 (d, *J* = 7.5 Hz, 1H), 7.53 (d, *J* = 7.4 Hz, 1H), 7.36 (t, *J* = 7.5 Hz, 1H), 7.26 (t, *J* = 7.7 Hz, 2H), 7.21 (dd, *J* = 8.8, 4.2 Hz, 1H), 6.98 (t, *J* = 8.9 Hz, 1H), 3.90 (s, 3H), 3.57 (s, 2H); ^{13}C NMR (151 MHz, $CDCl_3$): δ 157.9 (d, *J* = 234.3 Hz),

148.0, 146.1, 138.3, 134.9, 126.4, 125.5, 124.9, 124.0 (d, J = 10.2 Hz), 119.6 (d, J = 4.8 Hz), 117.6, 110.0 (d, J = 10.0 Hz), 108.9 (d, J = 26.3 Hz), 103.7 (d, J = 23.6 Hz), 30.9, 29.8; ^{19}F NMR (376 MHz, $CDCl_3$): δ –124.0 (td, J = 9.4, 4.3 Hz); HRMS (EI+) calcd for $C_{16}H_{12}FN$ $[M]^+$: 237.0954; found: 227.0949.

8-fluoro-5-methyl-10-(trimethylsilyl)-5,10-dihydroindeno[1,2-*b*]indole (2.4c). Methylated indole **2.4b** (581 mg, 2.45 mmol, 1.00 eq) was dissolved in anhydrous ether (15 mL) and the reaction mixture was immersed in a room temperature water bath. *n*-BuLi (1.68 M in hexanes, 1.46 mL, 2.45 mmol) was added dropwise via syringe pump over one hour. Following addition of base, the reaction mixture was stirred for 1.5 hr at room temperature and then cooled to –78 °C. Some precipitate formed upon cooling. After 7 minutes at –78 °C, TMSCl (0.78 mL, 6.1 mmol, 2.5 eq) was added rapidly via syringe and the resulting mixture was immediately warmed to room temperature. The reaction mixture was diluted with ether, filtered, and concentrated *in vacuo* to yield a gray solid, which was subsequently purified by flash column chromatography (20:1 hexanes-ethyl acetate). Mixed fractions were purified in a second round of column chromatography using the same eluent system. The product was isolated in 79 % yield (598 mg, 1.93 mmol). R_f = 0.7 in 3:1 hexanes-ethyl acetate; ^{1}H NMR (600 MHz, $CDCl_3$): δ 7.74 (d, J = 7.6 Hz, 1H), 7.54 (d, J = 7.6 Hz, 1H), 7.35 (t, J = 7.5 Hz, 1H), 7.31–7.23 (m, 3H), 6.98 (td, J = 9.0, 2.0 Hz, 1H), 4.07 (s, 3H), 3.74 (s, 1H), –0.01 (s, 9H); ^{13}C NMR (151 MHz, $CDCl_3$): δ 157.6 (d, J = 233.5 Hz), 150.1, 144.9, 138.6, 133.2, 125.1, 124.7, 124.03, 123.5 (d, J = 10.0 Hz), 122.7 (d, J = 4.7 Hz), 117.8, 109.9 (d, J = 10.0 Hz), 108.8 (d, J = 26.3 Hz), 104.9 (d, J = 23.8 Hz), 36.7, 31.3, –2.4; ^{19}F NMR (376 MHz): δ –124.4 (td, J = 9.5, 4.1 Hz); HRMS (ESI) calcd for $C_{19}H_{20}FNSi$ $[M]^+$: 309.1349; found: 309.1348.

Fluoro-BARAC (2.4). To a solution of silylated indole **2.4c** (311 mg, 1.00 mmol, 1.00 equiv.) in dichloromethane (33 mL) and saturated aqueous $NaHCO_3$ (7 mL) at 0 °C was added *m*-CPBA (77%, 745 mg, 3.32 mmol, 3.32 eq) portionwise over 4 minutes. The reaction mixture was stirred at 0 °C and allowed to warm to room temperature over the course of 1 hr 20 min. The reaction was then quenched via addition of 1N NaOH (30 mL) and the resulting aqueous layer was extracted 2x with dichloromethane and 1x with ethyl acetate. The organic layers were combined and washed 1x with brine, dried over anhydrous magnesium sulfate, and concentrated *in vacuo* to yield an orange oil (**2.4d**) which was immediately brought on to the next step in crude form.

Ketone **2.4d** (1.00 mmol assuming 100% yield from the previous step) was dried on a schlenk line for ~30 minutes and then transferred via syringe to a flame dried round bottom flask as a solution in dry THF (12 mL). The solution was cooled to –78 °C, and potassium hexamethyldisilazide (0.5 M in toluene, 2.2 mL, 1.1 mmol, 1.1 eq) was added dropwise. The solution was stirred for an additional 24 minutes at –78 °C, and then triflic anhydride (200 μL, 1.2 mmol, 1.2 eq) was added. The solution was stirred for 12 minutes at –78 °C prior to dilution with 20 mL anhydrous ether and addition of tetrabutyl ammonium fluoride (1M in THF, 15 mL, 15 mmol, 15 equiv.). After five additional minutes at –78 °C, the reaction mixture was warmed to room temperature and then quenched with saturated aqueous $NaHCO_3$. The aqueous layer was subsequently

extracted 1x with ethyl acetate and the organic layer was dried over anhydrous magnesium sulfate and concentrated to yield a brown oil. The crude product was purified by flash column chromatography (10:1 hexanes-ethyl acetate) to yield **2.4** in 19% yield (47 mg, 0.19 mmol). For the purposes of characterization and kinetic analysis, **2.4** was further purified by HPLC. The compound was injected onto a C18 preparatory column in a 1:2 water(A):acetonitrile(B) solution and eluted at 20 mL/min at using a gradient of 35% B to 75% B over 35 minutes. The product was collected at 19 minutes. Elution was monitored at 210 and 254 nM. Compound **2.4** is not bench stable, and decomposes to a brown oil on the hour timescale at room temperature. R_f = 0.3 in 3:1 hexanes-ethyl acetate; ^{1}H NMR (500 MHz, $CDCl_3$): δ 7.64–7.59 (m, 1H), 7.57 (dd, *J* = 8.6, 5.1 Hz, 1H), 7.51–7.44 (m, 2H), 7.40–7.38(m, 1H), 7.17–7.10(m, 2H), 2.71 (s, 3H); ^{13}C NMR (151 MHz, $CDCl_3$): δ 176.6 (s), 161.5 (d, *J* = 248.4 Hz), 152.5 (s), 149.6 (s), 130.5 (d, *J* = 9.3 Hz), 129.5 (s), 129.1 (s), 126.6 (s), 125.6 (s), 124.0 (d, *J* = 11.0 Hz), 121.7 (s), 116.4 (d, *J* = 22.9 Hz), 114.6 (d, *J* = 24.9 Hz), 110.7 (s), 107.3 (s), 38.7 (s); ^{19}F NMR (376 MHz, $CDCl_3$): δ –111.36 (dd, *J* = 13.4, 8.2 Hz). HRMS (ESI) calcd for $C_{16}H_{11}FNO$ $[M+H]^+$: 252.0819; found: 252.0817.

2-fluoro-5,10-dihydroindeno[1,2-*b*]indole (2.5a). To a solution of phenyl hydrazine (1.30 mL, 13.2 mmol, 1.00 equiv.) and 5-fluoro-1-indanone (2.03 g, 13.5 mmol, 1.02 equiv.) in ethanol (9.5 mL) was added glacial acetic acid (10 drops). The solution was stirred at reflux (85 ^{o}C) for 12 minutes and cooled to room temperature. Once cooled, the reaction flask was immersed in an ice water bath to induce product precipitation. White crystals were collected by vacuum filtration and combined with isopropanol (22 mL). Sulfuric acid (36N, 1.5 mL) was added via syringe and the resulting solution was stirred at reflux (90 ^{o}C) for 19 hours and subsequently cooled to room temperature. The solution was then basified to pH 10 via addition of aqueous sodium hydroxide (2% NaOH by mass) resulting in the formation of a white precipitate. The solid was collected by vacuum filtration and then dissolved in dichloromethane. Water was added, and the organic layer was extracted 3x with dichloromethane. The organic phase was dried over anhydrous magnesium sulfate and concentrated to yield **2.5a** as a white solid in 82% crude yield (2.42 g, 10.8 mmol). The crude product was brought on to the next step without further purification. R_f = 0.6 in 3:1 hexanes-ethyl acetate; ^{1}H NMR (600 MHz, $CDCl_3$): δ 8.26 (s, 1H), 7.62 (d, *J* = 7.3 Hz, 1H), 7.43 (d, *J* = 7.5 Hz, 1H), 7.36 (dd, *J* = 7.9, 5.2 Hz, 1H), 7.27 (m, *J* = 8.0 Hz, 1H), 7.22–7.12 (m, 2H), 7.04 (t, *J* = 8.7 Hz, 1H), 3.73 (s, 2H); ^{13}C NMR (151 MHz, $CDCl_3$): δ 161.2 (d, *J* = 243.6 Hz), 150.1 (d, *J* = 8.4 Hz), 142.4 (s), 140.5 (s), 131.2 (s), 124.8 (s), 121.7 (s), 121.4 (s), 120.4 (s), 118.8 (s), 117.5 (d, *J* = 8.8 Hz), 113.5 (d, *J* = 23.3 Hz), 113.2 (d, *J* = 23.0 Hz), 112.0 (s), 30.6 (s); ^{19}F NMR (376 MHz, $CDCl_3$): δ –117.00 (m). HRMS (ESI) calcd for $C_{15}H_{11}FN$ $[M+H]^+$: 224.0870; found: 224.0869.

2-fluoro-5-methyl-5,10-dihydroindeno[1,2-*b*]indole (2.5b). To a solution of indole **2.5a**, (2.38 g, 10.6 mmol, 1.00 equiv.) in benzene (26 mL) was added aqueous sodium hydroxide (50% NaOH by mass, 8 mL), tetrabutylammonium iodide (471 mg, 1.27 mmol, 0.120 equiv.), and iodomethane (5.3 mL, 85 mmol, 8.0 equiv.). The reaction mixture was stirred vigorously at 40 ^{o}C for 21 hours and subsequently cooled to room temperature. The solution was then diluted with 20 mL benzene and 30 mL water, and

the aqueous layer was extracted 2x with 30 mL ethyl acetate. The organic layers were combined, dried over anhydrous magnesium sulfate and concentrated *in vacuo* to yield a red solid. Crude product was purified by flash column chromatography (20:1 hexanes-ethyl acetate). The product was isolated in 81% yield (2.05 g, 8.64 mmol). R_f = 0.8 in 3:1 hexanes-ethyl acetate; ^{1}H NMR (600 MHz, $CDCl_3$): δ 7.61 (d, *J* = 7.8 Hz, 1H), 7.47 (dd, *J* = 8.0, 5.1 Hz, 1H), 7.35 (d, *J* = 8.2 Hz, 1H), 7.23 (ddd, *J* = 20.0, 15.0, 7.3 Hz, 3H), 7.06 (t, *J* = 8.7 Hz, 1H), 3.89 (s, 3H), 3.58 (s, 2H); ^{13}C NMR (151 MHz, $CDCl_3$): δ 160.9 (d, *J* = 243.6 Hz), 150.4 (d, *J* = 8.2 Hz), 143.6 (s), 141.5 (s), 131.5 (d, *J* = 2.4 Hz), 123.9 (s), 121.0 (s), 119.6 (d, *J* = 3.1 Hz), 119.5 (s), 118.7 (s), 117.6 (d, *J* = 8.7 Hz), 113.4 (d, *J* = 23.1 Hz), 112.9 (d, *J* = 22.8 Hz), 109.6 (s), 30.7 (s), 30.1 (d, *J* = 2.2 Hz); ^{19}F NMR (376 MHz, $CDCl_3$): δ –117.14 (td, *J* = 9.0, 5.2 Hz); HRMS (EI+) calcd for $C_{16}H_{12}FN$ $[M]^+$: 237.0954; found: 237.0952.

2-fluoro-5-methyl-10-(trimethylsilyl)-5,10-dihydroindeno[1,2-*b*]indole (2.5c). Methylated indole **2.5b** (1.14 g, 4.79 mmol, 1.00 equiv.) was dried by azeotrope (2x with 5mL toluene) and then dried for an additional 1 hr under vacuum. After drying, **2.5b** was dissolved in anhydrous ether (31 mL) and the reaction mixture was immersed in a room temperature water bath. *n*-BuLi (1.70 M in hexanes, 2.83 mL, 4.79 mmol, 1.00 equiv.) was added dropwise via syringe pump over one hour and then cooled to –78 °C. Some precipitate formed upon cooling, so the reaction mixture was slowly warmed to room temperature. Once most of the precipitate had re-dissolved in the ether, TMSCl (1.2 mL, 9.6 mmol, 1.9 equiv.) was added rapidly via syringe and the resulting mixture was warmed to room temperature over 2 hr. Upon warming, the reaction was diluted with ether, filtered, and concentrated *in vacuo* to yield a brown oil. ^{1}H NMR of the crude product indicated ~8% disilylated product. This mixture was purified by flash column chromatography (20:1 → 5:1 hexanes-ethyl acetate) to give **2.5c** in 25% yield (370 mg, 1.20 mmol) as a mixture with ~2% disilylated byproduct. Due to the similar R_f values of the desired product and the disilylated byproduct, an additional 945 mg of product was isolated as a mixture with byproduct present in ~13%. Only fractions with 2% impurity were brought on to the next step. R_f = 0.8 in 3:1 hexanes:ethyl acetate; ^{1}H NMR (600 MHz, $CDCl_3$): δ 7.69 (d, *J* = 7.9 Hz, 1H), 7.65 (dd, *J* = 8.1, 5.2 Hz, 1H), 7.42 (d, *J* = 8.2 Hz, 1H), 7.32– 7.26 (m, 2H), 7.20 (t, *J* = 7.5 Hz, 1H), 7.09 (t, *J* = 8.6 Hz, 1H), 4.05 (s, 3H), 3.76 (s, 1H), 0.04 (s, 9H); ^{13}C NMR (151 MHz, $CDCl_3$): δ 160.5 (d, *J* = 243.1 Hz), 152.4 (d, *J* = 7.6 Hz), 142.6 (s), 141.9 (s), 130.0 (d, *J* = 3.0 Hz), 123.7 (s), 122.9 (d, *J* = 3.0 Hz), 121.1 (s), 120.1 (s), 119.3 (s), 118.0 (d, *J* = 9.1 Hz), 112.3 (d, *J* = 7.6 Hz), 112.1 (d, *J* = 6.0 Hz), 109.7 (s), 37.5 (d, *J* = 3.0 Hz), 31.2 (s), –2.2 (s); ^{19}F NMR (376 MHz, $CDCl_3$): δ –117.57 (td, *J* = 9.3, 5.2 Hz); HRMS (EI+) calcd for $C_{19}H_{20}FNSi$ $[M]^+$: 309.1349; found: 309.1355.

Fluoro-BARAC (2.5). To a solution of **2.5c** as a mixture with 2% disilylated byproduct (168 mg mixture, 0.54 mmol mixture; 163 mg **2.5c**, 0.527 mmol **2.5c**) in dichloromethane (18 mL) and saturated aqueous $NaHCO_3$ (5 mL) at 0 °C was added *m*-CPBA (77%, 444 mg, 1.98 mmol, 3.67 equiv.) portionwise over 2 minutes. The mixture was stirred at 0 °C for 30 minutes and then warmed to room temperature over 30 minutes. The reaction was quenched via addition of 1N NaOH (30 mL) and the resulting aqueous

layer was extracted 2x with 20 mL dichloromethane and 1x with 20 mL ethyl acetate. The organic layers were combined and washed 1x with 50 mL brine, dried over anhydrous magnesium sulfate, and concentrated *in vacuo* to yield a white solid (**2.5d**), which was immediately brought on to the next step in crude form.

To a solution of **2.5d** (0.53 mmol assuming 100% yield from the previous step) in anhydrous THF (6.5 mL) at –78 ^{o}C was added potassium hexamethyldisilazide (0.5 M in toluene, 1.2 µL, 0.60 mmol, 1.1 equiv.) dropwise via syringe to give an orange solution, which was stirred an additional 20 minutes at –78 ^{o}C. Triflic anhydride (110 µL, 0.65 mmol, 1.2 equiv.) was then added and the solution immediately turned yellow. The solution was stirred for 10 minutes at –78 ^{o}C prior to dilution with 18 mL anhydrous ether and subsequent warming to room temperature. After warming for 30 minutes, the reaction was quenched via addition of saturated aqueous $NaHCO_3$ (10 mL). The aqueous layer was then immediately extracted 2x with 10 mL ethyl acetate and the organic layer was dried over anhydrous magnesium sulfate and concentrated to yield **2.5e** as yellow oil. Compound **2.5e** was purified by flash column chromatography (10:1hexanes-ethyl acetate) to give pure **2.5e** as a yellow oil in 43% yield (110 mg, 0.23 mmol).

Compound **2.5e** (62 mg, 0.10 mmol, 1.0 equiv.) was subsequently dissolved in acetonitrile and cesium fluoride (260 mg, 1.69 mmol, 16.9 equiv.) was added. The reaction was stirred at room temperature for 30 minutes, then filtered and concentrated *in vacuo* to give a brown solid. Crude product was purified by flash column chromatography to give **2.5** in 70% yield (18 mg, 0.072 mmol). For the purposes of characterization and kinetic analysis, **2.5** was further purified by HPLC. The compound was injected onto a C18 preparatory column in a 1:2 water(A):acetonitrile(B) solution and eluted at 20 mL/min using a gradient of 35% B to 75% B over 35 minutes. The product was collected at 19 minutes. Elution was monitored at 210 and 254 nM. ^{1}H NMR (600 MHz, $CDCl_3$): δ 7.62 (dd, J = 7.8, 0.9 Hz, 1H), 7.57 (dd, J = 8.4, 5.4 Hz, 1H), 7.49 (td, J = 7.6, 1.7 Hz, 1H), 7.44 (dd, J = 7.7, 1.6 Hz, 1H), 7.41–7.37 (m, 1H), 7.15 (td, J = 8.5, 2.5 Hz, 1H), 7.07 (dd, J = 8.8, 2.5 Hz, 1H), 2.73 (s, 3H); ^{13}C NMR (151 MHz, $CDCl_3$): δ 175.8 (s), 162.8 (d, J = 249.3 Hz), 156.8 (s), 145.3 (s), 130.2 (s), 129.4 (s), 128.1 (s), 127.6 (s), 127.1 (d, J = 9.3 Hz), 124.3 (d, J = 10.4 Hz), 121.8 (s), 115.8 (d, J = 22.4 Hz), 113.8 (d, J = 24.1 Hz), 110.0 (s), 107.9 (d, J = 3.9 Hz), 38.6; ^{19}F NMR (376 MHz, $CDCl_3$): δ –109.89 (td, J = 8.8, 5.4 Hz); HRMS (ESI) calcd for $C_{16}H_{11}ONF$ $[M+H]^+$: 252.0819; found: 252.0817.

2,8-difluoro-5,10-dihydroindeno[1,2-*b*]indole (2.6a). To a 100 mL cyclindrical, heavy wall, high pressure vessel was added 4-fluorophenylhydrazine hydrochloride (1.00 g, 6.15 mmol, 1.00 equiv.), 5-fluoro-1-indanone (822 mg, 6.22 mmol, 1.01equiv.), isopropanol (27 mL), and sulfuric acid (0.7 mL). The reaction vessel was sealed and heated to 125 ^{o}C. Upon heating, starting material dissolved and the reaction mixture acquired a dark red color. The reaction was stirred at 125 ^{o}C for 4 days and then cooled to room temperature. The resulting mixture was basified to pH 10 with aqueous sodium hydroxide (2% by mass). The aqueous layer was subsequently extracted 3x with ethyl acetate. Organics were combined, concentrated to a red solid, and re-dissolved in ethyl acetate. The solution was then dried over anhydrous magnesium sulfate and concentrated

to a red solid (1.33 g, 5.50 mmol, 89% crude yield). Crude product was brought on to the next step without purification. R_f= 0.5 in 3:1 hexanes:ethyl acetate; ^{1}H NMR (600 MHz, $CDCl_3$): δ 8.24 (s, 1H), 7.36 (dd, *J* = 8.2, 5.0 Hz, 1H), 7.31 (dt, *J* = 20.0, 10.0 Hz, 1H), 7.29–7.21 (m, 2H), 7.09–7.01 (m, 1H), 6.92 (td, *J* = 9.1, 2.4 Hz, 1H), 3.69 (s, 2H); ^{13}C NMR (151 MHz, $CDCl_3$): δ 161.4 (d, *J* = 244.3 Hz), 158.2 (d, *J* = 235.2 Hz), 150.1 (d, *J* = 8.4 Hz), 144.2 (s), 136.9 (s), 130.8 (d, *J* = 2.4 Hz), 125.0 (d, *J* = 10.4 Hz), 121.2 (d, *J* = 3.1 Hz), 117.9 (d, *J* = 8.8 Hz), 113.5 (d, *J* = 50 Hz), 113.5 (d, *J* = 3.0 Hz), 112.4 (d, *J* = 9.8 Hz), 109.7 (d, *J* = 26.3 Hz), 103.9 (d, *J* = 23.8 Hz), 30.5 (d, *J* = 2.3 Hz); ^{19}F NMR (376 MHz, $CDCl_3$): δ –116.27 (td, *J* = 9.0, 5.1 Hz), –122.82 (td, *J* = 9.3, 4.3 Hz); HRMS (ESI) calcd for $C_{15}H_9F_2N$ $[M]^+$: 241.0703; found: 241.0696.

2,8-difluoro-5-methyl-5,10-dihydroindeno[1,2-*b*]indole (2.6b). To a solution of indole **2.6a**, (1.22 g, 5.06 mmol, 1.00 equiv.) in benzene (31 mL) was added aqueous sodium hydroxide (50% NaOH by mass, 10 mL), tetrabutylammonium iodide (427 mg, 1.16 mmol, 0.229 equiv.), and iodomethane (2.50 mL, 40.5 mmol, 8.00 equiv.). The reaction mixture was stirred vigorously at 40 °C for 17 hours and subsequently cooled to room temperature. The solution was then diluted with benzene and water, and the aqueous layer was extracted 2x with 25 mL ethyl acetate and washed 1x with 50mL water. Organic layers were combined, dried over anhydrous magnesium sulfate and concentrated *in vacuo* to yield a red solid. The crude product was purified by flash column chromatography (20:1 to 10:1 hexanes-ethyl acetate). Mixed fractions were purified in a second round of column chromatography using the same eluent system. The product was isolated in 56 % yield (729 mg, 2.86 mmol). R_f = 0.6 in 3:1 hexanes:ethyl acetate; ^{1}H NMR (600 MHz, $CDCl_3$): δ 7.51 (dd, *J* = 8.3, 5.0 Hz, 1H), 7.25–7.18 (m, 3H), 7.09– 7.00 (m, 1H), 6.94 (td, *J* = 9.1, 2.3 Hz, 1H), 3.97 (d, *J* = 11.9 Hz, 3H), 3.61 (s, 2H); ^{13}C NMR (151 MHz, $CDCl_3$): δ 161.2 (d, *J* = 244.5 Hz), 158.0 (d, *J* = 234.6 Hz), 150.5 (d, *J* = 8.3 Hz), 145.4 (s), 138.2 (s), 131.2 (s), 124.0 (d, *J* = 10.3 Hz), 119.3 (s), 118.0 (d, *J* = 8.7 Hz), 113.6 (d, *J* = 23.2 Hz), 113.2 (d, *J* = 22.9 Hz), 110.2 (d, *J* = 9.9 Hz), 109.1 (d, *J* = 26.4 Hz), 103.7 (d, *J* = 23.7 Hz), 31.1 (s), 30.1 (d, *J* = 2.2 Hz); ^{19}F NMR (376 MHz, $CDCl_3$): δ fds –116.40 (td, *J* = 9.0, 5.1 Hz), –123.79 (td, *J* = 9.4, 4.2 Hz); HRMS (EI) calcd for $C_{16}H_{11}F_2N$ $[M]^+$: 255.0860; found: 255.0853.

2,8-difluoro-5-methyl-10-(trimethylsilyl)-5,10-dihydroindeno[1,2-*b*]indole (2.6c). Methylated indole **2.6b** (209 mg, 0.819 mmol, 1.00 equiv.) was dried by azeotrope (1x with 4 mL toluene) and then dried for an additional 2 hours under vacuum. After drying, **2.6b** was dissolved in anhydrous ether (5.5 mL) and the reaction mixture was immersed in a room temperature water bath. *n*-BuLi (1.70 M in hexanes, 480 µL, 0.82 mmol, 1.0 equiv.) was added dropwise over fifteen minutes and the reaction mixture immediately acquired a dark red color. After stirring for an additional 20 minutes at room temperature, the reaction was cooled to –78 °C. TMSCl (208 µL, 1.64 mmol, 2.00 equiv.) was added rapidly via syringe and the resulting mixture was warmed to room temperature over 50 minutes. Upon warming, the reaction was diluted with ether, filtered, and concentrated *in vacuo* to yield a brown oil. The crude product was purified by flash column chromatography (20:1 hexanes-ethyl acetate) to give **2.6c** in 82% yield (219 mg, 0.669 mmol). R_f = 0.7 in 3:1 hexanes:ethyl acetate; ^{1}H NMR (600 MHz, $CDCl_3$): δ 7.61 (dd, *J* = 8.3, 5.1 Hz, 1H), 7.31–7.20 (m, 3H), 7.06 (td, *J* = 8.9, 2.0 Hz, 1H), 6.98 (td, *J* = 9.0, 2.2

Hz, 1H), 3.99 (s, 3H), 3.66 (s, 1H), 0.00 (s, 9H); ^{13}C NMR (151 MHz, $CDCl_3$): δ 160.5 (d, J = 242.9 Hz), 157.6 (d, J = 233.9 Hz), 152.3 (d, J = 8.3 Hz), 143.9 (s), 138.3 (s), 129.4 (s), 123.4 (d, J = 10.2 Hz), 122.3 (s), 118.1 (d, J = 9.0 Hz), 112.2 (d, J = 10.3 Hz), 112.0 (d, J = 10.4 Hz), 109.9 (d, J = 10.0 Hz), 108.8 (d, J = 26.3 Hz), 104.8 (d, J = 23.9 Hz), 37.1 (d, J = 2.3 Hz), 31.1 (s), –2.5 (s); ^{19}F NMR (400 MHz, $CDCl_3$): δ –107.05 (td, J = 9.2, 5.3 Hz), –113.94 (td, J = 9.5, 4.3 Hz); HRMS (EI) calcd for $C_{19}H_{19}F_2NSi$ $[M]^+$: 327.1255; found: 327.1252.

Difluoro-BARAC (2.6). To a solution of **2.6c** (106 mg, 0.324 mmol, 1.00 equiv.) in dichloromethane (10 mL) and saturated aqueous $NaHCO_3$ (3 mL) at 0 °C was added *m*-CPBA (77%, 256 mg, 1.14 mmol, 3.53 equiv.) portionwise over 2 minutes. The mixture was stirred at 0 °C for 10 minutes and then warmed to room temperature over 20 minutes. The reaction was quenched via addition of 1N NaOH (30 mL) and the resulting aqueous layer was extracted 2x with 20 mL dichloromethane and 1x with 20 mL ethyl acetate. The organic layers were combined and washed 1x with 50 mL brine, dried over anhydrous magnesium sulfate, and concentrated *in vacuo* to yield a yellow oil that crystallized upon sitting (**2.6d**). Crude product was immediately brought on to the next step without purification.
To a solution of **2.6d** (0.32 mmol assuming 100% yield from the previous step) in anhydrous THF (4.0 mL) at –78 °C was added potassium hexamethyldisilazide (0.5 M in toluene, 710 μL, 0.36 mmol, 1.1 equiv.) dropwise via syringe to give an orange solution which was stirred for an additional 30 minutes at –78 °C. Triflic anhydride (65 μL, 0.39 mmol, 1.2 equiv.) was then added and the solution immediately turned yellow. The solution was stirred for 30 additional minutes at –78 °C prior to dilution with 20 mL anhydrous ether and subsequent warming to room temperature. After warming for 30 minutes, the reaction was quenched via addition of saturated aqueous $NaHCO_3$ (20 mL). The aqueous layer was subsequently extracted 3x with 20 mL ethyl acetate and the organic layer was dried over anhydrous magnesium sulfate and concentrated to give **6e** as a yield a yellow oil. Compound **2.6e** was purified by flash column chromatography (10:1 to 5:1 hexanes-ethyl acetate) to give **2.6e** in 28% yield over two steps (44 mg, 0.090 mmol).

Compound **2.6e** (25 mg, 0.051 mmol, 1.0 eq) was subsequently dissolved in acetonitrile (5 mL) and cesium fluoride (141 mg, 0.928 mmol, 18.2 equiv.) was added. The reaction was stirred at room temperature for 10 minutes, and an additional 106 mg cesium fluoride (0.698 mmol, 13.7 eq) was added. Following addition, the reaction was stirred 30 minutes at room temperature, then filtered and concentrated *in vacuuo* to give a brown solid. The crude product was purified by flash column chromatography (10:1 hexanes-ethyl acetate) to give **2.6** in 71% yield (10 mg, 0.037 mmol). For the purposes of characterization and kinetics analysis, **2.6** was further purified by HPLC. The compound was injected onto a C18 preparatory column in a 1:2.5 water(A):acetonitrile(B) solution and eluted at 20 mL/min using a gradient of 35% B to 75% B over 35 minutes. The product was collected at 20 minutes. Elution was monitored at 210 and 254 nM. R_f = 0.3 in 3:1 hexanes:ethyl acetate; ^{1}H NMR (600 MHz, $CDCl_3$): δ 7.64–7.51 (m, 2H), 7.18 (td, J = 8.4, 2.5 Hz, 2H), 7.13 (dd, J = 8.3, 2.9 Hz, 1H), 7.09 (dd, J = 8.7, 2.4 Hz, 1H), 2.70 (s, 3H); ^{13}C NMR (151 MHz, $CDCl_3$): δ 175.7 (s), 162.9 (d, J = 200.8 Hz), 161.3 (d, J = 199.4 Hz), 152.6 (s),

145.6 (s), 130.6 (d, J = 9.3 Hz), 127.2 (d, J = 9.3 Hz), 123.8 (d, J = 10.3 Hz), 123.5 (d, J = 11.0 Hz), 116.9 (d, J = 22.8 Hz), 116.2 (d, J = 22.4 Hz), 114.8 (d, J = 25.0 Hz), 114.0 (d, J = 24.1 Hz), 109.1 (d, J = 3.8 Hz), 108.6 (s), 38.7 (s); ^{19}F NMR (376 MHz, $CDCl_3$): δ – 108.76 (dd, J = 14.0, 8.5 Hz), –111.01 (dd, J = 13.3, 8.2 Hz); HRMS (ESI) calcd for $C_{16}H_{10}F_2NO$ $[M+H]^+$: 270.0725; found: 270.0722.

7-methoxy-5-methyl-5,10-dihydroindeno[1,2-*b*]indole (2.7b). To a solution of 3-methoxyphenylhydrazine hydrochloride (1.93 g, 11.1 mmol, 1.00 equiv.) and 1-indanone (1.46 g, 11.1 mmol, 1.00 equiv.) in ethanol (7.0 mL) was added glacial acetic acid (3 drops). The solution was stirred at reflux (85 ^{o}C) for 20 minutes and cooled to room temperature. EtOH was removed *in vaccuo* and the remaining orange solid was dissolved in isopropanol (20 mL). Sulfuric acid (36 N, 1.3 mL) was added via syringe, and the resulting solution was stirred at reflux (90 ^{o}C) for 18 hours. Upon cooling to room temperature, the solution was basified to pH 10 with aqueous sodium hydroxide (2% NaOH by mass) resulting in the formation of precipitate. The solid was collected by vacuum filtration to yield **2.7a** as a mixture with **2.7a'** and the corresponding hydrazone intermediate (1.65 g). This mixture was brought on to the next step in crude form. To a solution of the mixture of **2.7a**, **2.7a'**, and hydrazone acquired in the previous step (1.65g) in benzene (22 mL) was added aqueous sodium hydroxide (50% NaOH by mass, 8 mL), tetrabutylammonium iodide (425 mg), and iodomethane (3.48 mL, 7.94 g). The reaction mixture was stirred vigorously at 50 ^{o}C for 16 hours and then at 55 ^{o}C for 2 additional hours. Upon cooling to room temperature, the mixture was diluted with benzene and H_2O, and the aqueous layer was extracted 3x with ethyl acetate. The organic layers were combined, dried over anhydrous magnesium sulfate and concentrated to yield a brown solid. Compound **2.7b** was purified from its regioisomer by flash column chromatography (10:1 to 5:1 hexanes: ethyl acetate) to give **2.7b** in 4% yield over two steps (117 mg, 0.469 mmol). Regiochemistry was confirmed by 2D NOESY. R_f = 0.6 in 2:1 hexanes:ethyl acetate; ^{1}H NMR (600 MHz, $CDCl_3$): δ 7.60 (d, J = 7.5 Hz, 1H), 7.50 (m, 2H), 7.32 (t, J = 7.5 Hz, 1H), 7.17 (t, J = 7.4 Hz, 1H), 6.85 (s, 1H), 6.82 (d, J = 8.7 Hz, 1H), 4.01 (s, 3H), 3.91 (s, 3H), 3.67 (s, 2H). ^{13}C NMR (151 MHz, $CDCl_3$): δ 156.0, 147.6, 143.8, 142.7, 135.7, 126.4, 125.4, 123.9, 120.3, 119.6, 118.7, 116.9, 108.9, 93.8, 55.7, 31.1, 30.1; EI-HRMS: Calcd. for $C_{17}H_{15}NO^+$ $[M]^+$: 249.1154, found 249.1158.

7-methoxy-5-methyl-10-(trimethylsilyl)-5,10-dihydroindeno[1,2-*b*]indole (2.7c). Compound **2.7b** (116 mg, 0.465 mmol, 1.00 equiv.) was dissolved in anhydrous ether (4 mL) and the reaction mixture was immersed in a room temperature water bath. *n*-BuLi (1.61M in hexanes, 290 μL, 0.47 mmol, 1.0 equiv) was added dropwise over 10 min. Following addition of base, the reaction mixture was stirred for one hour at room temperature and then was cooled to –78 ^{o}C. TMSCl (237 μL, 1.87 mmol, 4.00 equiv.) was added rapidly via syringe and the resulting mixture was immediately warmed to room temperature for 40 min. The reaction mixture was diluted with ether, filtered, and concentrated *in vacuo* to yield a brown solid which was subsequently purified by flash column chromatography (40:1 to 10:1 hexanes-ethyl acetate) to give **2.7c** as a tan solid in 55% yield (82 mg, 0.26 mmol). R_f = 0.8 in 2:1 hexanes:ethyl acetate ^{1}H NMR (600 MHz, $CDCl_3$): δ 7.69 (t, J = 19.2 Hz, 1H), 7.56 (dd, J = 17.9, 7.9 Hz, 2H), 7.34 (t, J = 7.0Hz, 1H), 7.21 (t, J = 7.1 Hz, 1H), 6.89 (s, 1H), 6.86 (d, J = 8.3 Hz, 1H), 4.04 (s, 3H), 3.95 (s,

3H), 3.75 (s, 1H), 0.02 (s, 9H); ^{13}C NMR (151 MHz, $CDCl_3$): δ 155.8, 149.3, 142.8, 142.4, 133.8, 124.9, 124.5, 123.2, 122.9, 120.7, 118.2, 116.9, 108.3, 93.6, 55.6, 36.8, 31.2, –2.4; EI-HRMS: Calcd. for $C_{20}H_{23}NOSi^+$ $[M]^+$: 321.1549, found 321.1546.

Methoxy-BARAC (2.7). To a solution of **2.7c** (78 mg, 0.24 mmol, 1.0 equiv.) in dichloromethane (6.7 mL) and saturated aqueous $NaHCO_3$ (1.8 mL) at 0 °C was added *m*-CPBA (77%, 215 mg, 0.959 mmol, 4.00 equiv). portionwise over 2 minutes. The mixture was stirred at 0 °C for 15 minutes and then warmed to room temperature. The reaction was quenched via addition of 1N NaOH (30 mL) and the resulting aqueous layer was extracted 2x with 25 mL dichloromethane and 1x with 25 mL ethyl acetate. The organic layers were combined and washed 1x with brine, dried over anhydrous magnesium sulfate, and concentrated *in vacuo* to yield **2.7d** as a yellow oil, which was immediately brought on to the next step in crude form.

To a solution of **2.7d** (0.24 mmol assuming 100% yield from the previous step) in anhydrous THF at –78 °C was added potassium hexamethyldisilazide (0.5 M in toluene, 530 μL, 0.27 mmol, 1.1 equiv.) dropwise via syringe. The resulting solution was stirred an additional 35 minutes at –78 °C. Triflic anhydride (71 μL, 0.42 mmol, 1.8 equiv.) was added, and the solution was stirred for 35 minutes at –78 °C prior to dilution with anhydrous ether and addition of tetrabutyl ammonium fluoride (1M in THF, 3.0 mL, 3.0 mmol, 12 equiv.). The reaction mixture was warmed to room temperature then quenched with saturated aqueous $NaHCO_3$. The aqueous layer was subsequently extracted 2x with ethyl acetate and the organic layer was dried over anhydrous magnesium sulfate and concentrated. The compound was purified by flash column chromatography (10:1, 5:1, 2:1 hexanes – ethyl acetate) to give **2.7** in 36% yield (23 mg, 0.087 mmol). For the purposes of characterization and kinetic analysis, the compound was purified by HPLC. A 23 mg sample of **2.7** was dissolved in a 2 mL solution of water (A) and acetonitrile (B) (1:3 A:B). The compound was injected onto a C18 column and eluted at 20 mL/min using a gradient of 35% B to 75% B over 35 minutes. The product was collected at 19 minutes. Elution was monitored at 210 and 254 nM. R_f = 0.2 in 3:1 hexanes:ethyl acetate. ^{1}H NMR (600 MHz, $CDCl_3$): δ 7.58 (d, J = 7.0 Hz, 1H), 7.47–7.38 (m, 2H), 7.34 (m, 2H), 7.21 (d, J = 1.6 Hz, 1H), 6.94–6.88 (m, 1H), 3.87 (s, 3H), 2.73 (s, 3H); ^{13}C NMR (151 MHz, $CDCl_3$): δ 176.8, 160.9, 158.1, 148.9, 129.3, 128.2, 128.1, 126.0, 125.4, 122.6, 115.9, 113.8, 113.5, 108.9, 108.2, 55.6, 38.7; ESI-HRMS: Calcd. for $C_{17}H_{14}O_2N^+$ $[M+H]^+$: 264.1019, found 264.1021.

3-methoxy-5,10-dihydroindeno[1,2-*b*]indole (2.8a). To a solution of phenyl hydrazine (1.21 mL, 1.33 g, 12.3 mmol, 1.00 equiv.) and 6-methoxy-1-indanone (2.01 g, 12.4 mmol, 1.00 equiv.) in ethanol (20 mL) was added glacial acetic acid (4 drops). The solution was stirred at reflux (85 °C) for 15 minutes and cooled to room temperature. Upon cooling, pale yellow crystals precipitated out of solution. Crystals were collected via vacuum filtration and dissolved in isopropanol (41 mL). Sulfuric acid (36 N, 1.4 mL) was added via syringe and the resulting solution was stirred at reflux (90 °C) for 18 hours – some precipitate formed over the course of the reaction. Upon cooling to room temperature, the solution was basified to pH 10 with aqueous sodium hydroxide (2% NaOH by mass) resulting in the formation of additional precipitate. The solid was

collected by vacuum filtration to yield a brown solid which was subsequently dissolved in dichloromethane. H_2O was added, and the aqueous layer was extracted 1x with dichloromethane. The organic layers were combined, dried over anhydrous magnesium sulfate and concentrated to yield a brown solid in 61% crude yield (1.76 g, 7.50 mmol). The crude product was brought on to the next step without further purification. For purposes of characterization, the product was purified by flash column chromatography (20:1 hexanes – ethyl acetate). R_f = 0.6 in 3:1 hexanes:ethyl acetate; ^{1}H NMR (400 MHz, $CDCl_3$): δ 8.20 (s, 1H), 7.60–7.48 (m, 1H), 7.34 (dd, *J* = 11.7, 5.1 Hz, 2H), 7.13–7.02 (m, 2H), 6.95 (d, *J* = 2.4Hz, 1H), 6.67 (dd, *J* = 8.2, 2.4 Hz, 1H), 3.79 (s, 3H), 3.59 (s, 2H); ^{13}C NMR (151 MHz, $CDCl_3$): δ 159.0, 143.0, 140.6, 139.8, 136.1, 125.7, 124.7, 123.2, 121.8, 120.2, 119.0, 112.0, 109.9, 103.8, 55.5, 29.5; ESI-HRMS: Calcd. for $C_{16}H_{14}ON^+$ $[M+H]^+$: 236.1070, found 263.1071.

3-methoxy-5-methyl-5,10-dihydroindeno[1,2-*b*]indole (2.8b). To a solution of **2.8a** (592 mg, 2.52 mmol, 1.00 equiv.) in benzene (8 mL) was added aqueous sodium hydroxide (50% NaOH by mass, 4 mL), tetrabutylammonium iodide (83 mg, 0.22mmol, 0.09 equiv.), and iodomethane (1.25 mL, 20.1 mmol, 8.00 equiv.). The reaction mixture was stirred vigorously at 40 °C for 16 hours and then at 55 °C for 2 additional hours. Upon cooling to room temperature, the mixture was diluted with benzene (20 mL) and H_2O (20 mL), and the aqueous layer was extracted 2x with 15 mL ethyl acetate. The organic layers were combined, washed 1x with 25 mL H_2O, dried over anhydrous magnesium sulfate and concentrated to yield a brown solid. The crude product was purified by flash column chromatography (20:1 to 10:1 hexanes-ethyl acetate) to give a tan brown solid in 87% yield (545 mg, 2.19 mmol). ^{1}H NMR (600 MHz, $CDCl_3$): δ 7.65 (d, *J* = 7.8 Hz, 1H), 7.43 (d, *J* = 8.2 Hz, 1H), 7.38 (d, *J* = 8.2 Hz, 1H), 7.26 (t, *J* = 7.6 Hz, 1H), 7.20 (dd, *J* = 13.0, 4.8 Hz, 2H), 6.78 (dd, *J* = 8.2, 2.3 Hz, 1H), 4.00 (s, 3H), 3.92 (s, 3H), 3.63 (s, 2H); ^{13}C NMR (151 MHz, $CDCl_3$): δ 158.7, 144.2, 141.8, 140.1, 136.5, 125.6, 124.0, 121.5, 121.2, 119.5, 119.0, 109.6, 109.0, 104.6, 55.5, 30.8, 29.2; ESI-HRMS: Calcd. for $C_{17}H_{15}ON^+$ $[M]^+$: 249.1148, found 249.1149.

3-methoxy-5-methyl-10-(trimethylsilyl)-5,10-dihydroindeno[1,2-*b*]indole (2.8c). A round bottom flask containing **2.8b** (982 mg, 3.94 mmol, 1.00 equiv.) in dry ether (24 mL) was immersed in a room temperature water bath. *n*-BuLi (1.5 M in THF, 3.05 mL, 4.57 mmol, 1.16 equiv.) was added via syringe pump over one hour, generating an orange solution. Following addition of base, the reaction mixture was stirred at room temperature for an additional 45 minutes and then cooled to –78 °C. TMSCl (1.05 mL, 899 mg, 8.27 mmol, 2.10 equiv.) was added rapidly via syringe, and the reaction mixture was stirred an additional 4 minutes at –78 °C, then warmed to room temperature over 1.5 hours. The reaction was subsequently diluted with ether, filtered, and concentrated *in vacuo*. The crude product was purified by flash column chromatography (15:1 to 6:1 hexanes – ethyl acetate) to yield an inseparable mixture of **2.8c** and its corresponding di-silylated indole (3:1 **2.8c**:side product) in 59% yield (1.04 g mixture, 3.06 mmol mixture; 2.33 mmol **2.8c**, 59% yield **2.8c**). **2.8c** was brought on to the next step as the mixture. R_f = 0.8 in 3:1 hexanes:ethyl acetate; ^{1}H NMR (600 MHz, $CDCl_3$): δ 7.79 (d, *J* = 7.9 Hz, 1H), 7.52 (d, *J* = 8.3 Hz, 1H), 7.47 (d, *J* = 8.2 Hz, 1H), 7.39 (d, *J* = 2.4 Hz, 1H), 7.38–7.33 (m, 1H), 7.30–7.26 (m, 1H), 6.91 (dd, *J* = 8.3, 2.4 Hz, 1H), 4.09 (s, 3H), 3.99 (s, 3H), 3.77–3.73

(m, 1H), 0.12 (s, 9H); ^{13}C NMR (151 MHz, $CDCl_3$): δ 157.7, 142.9, 142.2, 141.9, 134.5, 124.7, 124.3, 123.5, 121.2, 120.1, 118.9, 109.4, 109.1, 103.7, 55.4, 35.6, 30.8, –2.4; EI-HRMS: Calcd. for $C_{20}H_{23}NOSi^+$ $[M]^+$: 321.1549, found 321.1548.

Methoxy-BARAC (2.8). To a solution of **2.8c** as a mixture with 10% disilylated compound (145 mg mixture, 0.44 mmol total; 0.40 mmol **2.8c**, 1.0 equiv.) in dichloromethane (13.5 mL) and saturated aqueous $NaHCO_3$ (2.0 mL) at 0 °C was added *m*-CPBA (77%, 303 mg, 1.35 mmol, 3.38 equiv.) portionwise over 3 minutes. The reaction mixture was stirred at 0 °C for 20 minutes and slowly warmed to room temperature over 1 hour 20 minutes. The reaction was subsequently quenched via addition of 1N NaOH (10 mL) and the resulting aqueous layer was extracted 2x with 15 mL dichloromethane and 1x with 15 mL ethyl acetate. The organic layers were combined and washed 1x with 40 mL brine, dried over anhydrous magnesium sulfate, and concentrated *in vacuo* to yield a tan solid (**2.8d**) which solidified under high vacuum. Crude product was immediately brought on to the next step without further purification.

To a solution of **2.8d** (0.40 mmol assuming 100% yield from the previous step, 1.0 equiv.) in anhydrous THF (5.5 mL) at –78 °C was added potassium hexamethyldisilazide (0.5 M in toluene, 990 μL, 0.50 mmol, 1.3 equiv.) dropwise via syringe to give an orange solution which was stirred for an additional 30 minutes at –78 °C. Triflic anhydride (91 μL, 0.54 mmol, 1.4 equiv.) was added, and the solution was stirred for 15 minutes at –78 °C prior to dilution with 22 mL anhydrous ether and addition of tetrabutyl ammonium fluoride (1M in THF, 4.5 mL, 4.5 mmol, 11 equiv.). The reaction mixture was warmed to room temperature over 45 minutes and then quenched with saturated aqueous $NaHCO_3$ (20 mL). The aqueous layer was subsequently extracted 2x with 30 mL ethyl acetate and the organic layer was dried over anhydrous magnesium sulfate and concentrated to yield an orange oil. The product was purified by flash column chromatography (10:1 to 5:1 hexanes – ethyl acetate) to yield an orange solid in 75% yield (78 mg, 0.30 mmol). For the purposes of characterization and kinetic analysis, the compound was purified by HPLC. A 25 mg sample of **2.8** was dissolved in a 4 mL solution of water (A) and acetonitrile (B) (1:3 A:B). The compound was injected (2mL x 2 runs) onto a C18 column and eluted at 20 mL/min using a gradient of 35% B to 75% B over 35 minutes. The product was collected at 19 minutes. Elution was monitored at 210 and 254 nM. ^{1}H NMR (600 MHz, $CDCl_3$): δ 7.59 (d, J = 7.7 Hz, 1H), 7.42 (dd, J = 10.5, 4.3 Hz, 1H), 7.40–7.32 (m, 2H), 7.29 (d, J = 8.5 Hz, 1H), 7.17 (d, J = 2.3 Hz, 1H), 6.96 (dd, J = 8.5, 2.4 Hz, 1H), 3.88 (s, 3H), 2.74 (s, 3H); ^{13}C NMR (151 MHz, $CDCl_3$): δ 176.2, 160.0, 156.0, 150.9, 129.3, 129.2, 128.0, 127.6, 127.1, 122.6, 114.8, 113.9, 111.8, 109.5, 107.4, 55.6, 38.7; ESI-HRMS: Calcd. for $C_{17}H_{14}O_2N^+$ $[M+H]^+$: 264.1019, found 264.1022.

2-fluoro-7,9-dimethyl-5,10-dihydroindeno[1,2-*b*]indole (2.10a). To a solution of 3,5-dimethylphenylhydrazine hydrochloride (2.54 g, 14.7 mmol, 1.00 equiv.) and 5-fluoro-1-indanone (2.21 g, 14.7 mmol, 1.00 equiv.) in ethanol (24 mL) was added glacial acetic acid (3 drops). The solution was stirred at reflux (85 °C) for 15 minutes and cooled to room temperature. Ethanol was removed *in vacuo* and the resulting orange solid was dissolved in isopropanol (24 mL). Sulfuric acid (36N, 1.65 mL) was added via syringe and the mixture was stirred at reflux (90 °C) for 17 hours and subsequently cooled to

room temperature. The solution was basified to pH 10 via addition of aqueous sodium hydroxide (2% NaOH by mass) resulting in the formation of a precipitate. The solid was collected by vacuum filtration to yield **2.10a** in 76% crude yield (2.80 g, 11.2 mmol). Crude product was brought on to the next step without further purification. R_f= 0.7 in 3:1 hexanes:ethyl acetate; ^{1}H NMR (500 MHz, $CDCl_3$): δ 8.11 (s, 1H), 7.33 (dd, *J* = 8.2, 5.0 Hz, 1H), 7.25 (d, *J* = 8.4 Hz, 1H), 7.11–6.95 (m, 2H), 6.79 (s, 1H), 3.83 (s, 2H), 2.62 (s, 3H), 2.44 (s, 3H); ^{13}C NMR (101 MHz, $CDCl_3$): δ 160.7 (d, *J* = 242.8 Hz), 150.0 (d, *J* = 8.3 Hz), 140.9 (s), 140.6 (s), 131.8 (s), 131.2 (s), 128.9 (s), 122.6 (s), 122.3 (s), 121.2 (d, *J* = 3.2 Hz), 117.0 (d, *J* = 8.7 Hz), 113.1 (d, *J* = 40.4 Hz), 113.1 (d, *J* = 5.8 Hz), 109.4 (s), 31.5 (d, *J* = 2.1 Hz), 21.6 (s), 19.1 (s); ^{19}F NMR (376 MHz, $CDCl_3$): δ –117.87 (dd, *J* = 14.1, 9.1 Hz); ESI-HRMS: Calcd. for $C_{17}H_{14}FN^+$ $[M]^+$: 251.1105, found 251.1106.

2-fluoro-5,7,9-trimethyl-5,10-dihydroindeno[1,2-*b*]indole (210b). To a solution of **2.10a** (2.74 g, 10.9 mmol, 1.00 equiv.) in benzene (59 mL) was added aqueous sodium hydroxide (50% NaOH by mass, 5.0 mL), tetrabutylammonium iodide (289 mg, 0.782 mmol, 0.072 equiv.) and iodomethane (5.42 mL, 87.1 mmol, 8.00 equiv.). The reaction mixture was stirred vigorously at 40 °C for 16 hours and then cooled to room temperature. The mixture was diluted with benzene (20 mL) and H_2O (20 mL), and the aqueous layer was extracted 2x with 20 mL ethyl acetate. Organic layers were combined, washed 1x with 25 mL H_2O, dried over anhydrous magnesium sulfate and concentrated to yield a brown solid. The crude product was purified by flash column chromatography (15:1 hexanes - ethyl acetate followed by a second column 40:1 to 26:1 hexanes - ethyl acetate) to give **2.10b** in 39% yield (1.12 g, 4.24 mmol). R_f = 0.8 in 3:1 hexanes:ethyl acetate; ^{1}H NMR (400 MHz, $CDCl_3$): δ 7.48 (dd, *J* = 8.3, 5.0 Hz, 1H), 7.23 (dd, *J* = 8.9, 2.3 Hz, 1H), 7.04 (td, *J* = 9.1, 2.4 Hz, 1H), 6.98 (s, 1H), 6.79 (s, 1H), 3.93 (s, 3H), 3.74 (s, 2H), 2.61 (s, 3H), 2.50 (s, 3H); ^{13}C NMR (101 MHz, $CDCl_3$): δ 160.47 (d, *J* = 242.9 Hz), 150.37 (d, *J* = 8.1 Hz), 142.41 (s), 141.71 (s), 131.63 (d, *J* = 2.3 Hz), 131.26 (s), 128.97 (s), 121.85 (s), 121.62 (s), 119.50 (d, *J* = 3.1 Hz), 117.12 (d, *J* = 8.6 Hz), 113.0 (d, *J* = 62.6 Hz), 113.01 (d, *J* = 17.3 Hz), 107.13 (s), 31.21 (d, *J* = 2.1 Hz), 30.84 (s), 21.76 (s), 18.98 (s); ^{19}F NMR (376 MHz, $CDCl_3$): δ –117.99 (dd, *J* = 14.0, 9.0 Hz); ESI-HRMS: Calcd. for $C_{18}H_{16}FN^+$ $[M]^+$: 265.1261, found 265.1261.

2-fluoro-5,7,9-trimethyl-10-(trimethylsilyl)-5,10-dihydroindeno[1,2-*b*]indole (2.10c). A round bottom flask containing **2.10b** (1.11g, 4.17 mmol, 1.00 equiv.) in dry ether (27 mL) was immersed in a room temperature water bath. *n*-BuLi (1.5 M in THF, 3.33 mL, 5.00 mmol, 1.20 equiv.) was added via syringe pump over one hour, generating a brown solution. Following addition of base, the reaction mixture was stirred at room temperature for an additional 30 minutes and then cooled to –78 °C. TMSCl (1.11 mL, 8.76 mmol, 2.10 eq) was added rapidly via syringe and the solution was subsequently warmed to room temperature. The reaction was diluted with ether, filtered, and concentrated *in vacuo*. The crude product was purified by flash column chromatography (20:1 hexanes - ethyl acetate followed by a second column 40:1 to 26:1 hexanes - ethyl acetate) to yield **2.10c** as an orange solid in 78% yield (1.09 g, 3.24 mmol). R_f = 0.8 in 3:1 hexanes:ethyl acetate; ^{1}H NMR (400 MHz, $CDCl_3$): δ 7.58 (dd, *J* = 8.4, 5.1 Hz, 1H), 7.20 (dd, *J* = 9.5, 2.3 Hz, 1H), 7.02 (dt, *J* = 8.5, 3.3 Hz, 2H), 6.78 (s, 1H), 4.01 (s, 3H), 3.97 (s, 1H), 2.61 (s, 3H), 2.49 (s, 3H), -0.16 (d, *J* = 3.2 Hz, 9H); ^{13}C NMR (126 MHz, $CDCl_3$): δ 159.7 (d,

J = 242.0 Hz), 152.2 (d, *J* = 8.4 Hz), 142.1 (s), 141.2 (s), 131.2 (s), 129.4 (s), 129.0 (s), 122.7 (s), 121.9 (s), 121.7 (s), 117.2 (d, *J* = 8.9 Hz), 111.6 (d, *J* = 39.4 Hz); 111.7 (s), 107.0 (s), 38.2 (s), 31.0 (s), 21.8 (s), 20.1 (s), –2.2 (s); ^{19}F NMR (376 MHz, $CDCl_3$): δ –119.30 (dd, *J* = 14.2, 9.2 Hz). EI-HRMS: Calcd. for $C_{21}H_{24}FNSi^+$ $[M]^+$: 337.1662, found 337.1664.

Dimethylfluoro-BARAC (2.10). To a solution of **2.10c** (177 mg, 0.524 mmol, 1.00 equiv.) in dichloromethane (11 mL) and saturated aqueous $NaHCO_3$ (3.0 mL) at 0 °C was added *m*-CPBA (77%, 459 mg, 2.05 mmol, 3.91 equiv.) portionwise over 3 minutes. The reaction mixture was stirred at 0 °C for 1 h and then warmed to room temperature over 1 h. The reaction was subsequently quenched via addition of 1N NaOH (15 mL) and the resulting aqueous layer was extracted 2x with 15 mL dichloromethane and 1x with 15 mL ethyl acetate. Organic layers were combined, dried over anhydrous magnesium sulfate, and concentrated *in vacuo* to yield an orange oil (**2.10d**). The crude product was immediately brought on to the next step without further purification.

To a solution of **2.10d** (0.52 mmol assuming 100% yield from the previous step, 1.00 equiv.) in anhydrous THF (6.2 mL) at –78 °C was added potassium hexamethyldisilazide (0.5 M in toluene, 1.2 mL, 0.58 mmol, 1.1 equiv.) dropwise via syringe. The reaction was stirred an additional 30 min at –78 °C and then triflic anhydride (110 μL, 0.63 mmol, 1.2 equiv.) was added. The solution was stirred for 47 min at –78 °C prior to dilution with 20 mL anhydrous ether and addition of tetrabutyl ammonium fluoride (1M in THF, 6.0 mL, 6.0 mmol, 12 equiv.). The reaction mixture was warmed to room temperature and subsequently quenched with saturated aqueous $NaHCO_3$ (35 mL). The aqueous layer was extracted 2x with 20 mL ethyl acetate and the organic layer was dried over anhydrous magnesium sulfate and concentrated to yield a brown oil. The product was purified by flash column chromatography (20:1 to 10:1 hexanes – ethyl acetate) to yield **2.10** as a white solid in 36% yield (52 mg, 0.19 mmol). For the purposes of characterization and kinetics analysis, compound **2.10** was purified by HPLC. The compound was injected onto a C18 preparatory column and eluted at 20 mL/min using a gradient of 35% B to 75% B over 35 minutes. Elution was monitored at 210 and 254 nM, and the product was collected at 27 minutes. R_f = 0.4 in 3:1 hexanes:ethyl acetate; ^{1}H NMR (600 MHz, $CDCl_3$): δ 7.55 (dd, *J* = 8.4, 5.4 Hz, 1H), 7.27 (s, 1H), 7.12 (td, *J* = 8.5, 2.5 Hz, 1H), 7.04 (dd, *J* = 9.1, 2.5 Hz, 2H), 2.71 (s, 3H), 2.42 (s, 3H), 2.39 (s, 3H); ^{13}C NMR (151 MHz, $CDCl_3$): δ 176.1 (s), 162.7 (d, *J* = 249.0 Hz), 156.7 (s), 145.0 (s), 140.5 (s), 137.7 (s), 129.9 (s), 127.4 (s), 127.0 (d, *J* = 9.2 Hz), 124.8 (d, *J* = 10.2 Hz), 118.8 (s), 115.3 (d, *J* = 22.4 Hz), 113.5 (d, *J* = 24.0 Hz), 110.3 (s), 108.8 (d, *J* = 3.9 Hz), 38.6 (s), 21.5 (s), 21.3 (s); ^{19}F NMR (376 MHz, $CDCl_3$): δ –109.42 (dd, *J* = 14.2, 8.7 Hz); ESI-HRMS: Calcd. for $C_{18}H_{14}FNO^+$ $[M+H]^+$: 280.1132, found 280.1133.

7,9-dimethyl-5,10-dihydroindeno[1,2-*b*]indole (2.11a). To a solution of 3,5-dimethylphenylhydrazine hydrochloride (3.01 g, 17.4 mmol, 1.00 equiv.) and 1- indanone (2.30 g, 17.4 mmol, 1.00 equiv.) in ethanol (16 mL) was added glacial acetic acid (3 drops). The solution was stirred at reflux (85 °C) for 15 minutes. Upon heating, the reaction mixture acquired a dark red color, and some precipitate formed. An additional 6 mL ethanol was added. After 15 minutes at 85 °C, the reaction mixture was cooled to

room temperature and the resulting precipitate was collected by vacuum filtration to give an off-white solid. The solid was combined with isopropanol (30 mL) and sulfuric acid (36N, 2 mL) was added via syringe. The resulting solution was stirred at reflux (90 ^{o}C) for 21 hours and was subsequently cooled to room temperature. The solution was then basified to pH 10 via addition of aqueous sodium hydroxide (2% NaOH by mass) resulting in the formation of precipitate. The solid was collected by vacuum filtration to give **2.11a** as a brown solid in 49% crude yield (2.00 g, 8.59 mmol). The crude product was brought on to the next step without further purification. For the purposes of purification, the solid was purified by flash column chromatography (20:1 hexanes-ethyl acetate). R_f = 0.7 in 3:1 hexanes:ethyl acetate; ^{1}H NMR (600 MHz, $CDCl_3$): δ 8.13 (s, 1H), 7.53 (d, *J* = 7.4 Hz, 1H), 7.43 (d, *J* = 7.5 Hz, 1H), 7.36– 7.30 (m, 1H), 7.20 (t, *J* = 7.4 Hz, 1H), 7.03 (d, *J* = 11.8 Hz, 1H), 6.80 (s, 1H), 3.83 (s, 2H), 2.64 (s, 3H), 2.45 (s, 3H); ^{13}C NMR (151 MHz, $CDCl_3$): δ 147.8, 141.9, 140.9, 135.1, 131.9, 129.2, 126.5, 125.3, 124.1, 122.7, 122.3, 121.7, 116.9, 109.5, 31.4, 21.7, 19.2; HRMS (ESI) calcd for $C_{17}H_{15}N$ $[M]^+$: 233.1199; found: 233.1199.

5,7,9-trimethyl-5,10-dihydroindeno[1,2-*b*]indole (2.11b). To a solution of indole **2.11a**, (1.93 g, 8.27 mmol, 1.00 equiv.) in benzene (15 mL) was added aqueous sodium hydroxide (50% NaOH by mass, 15 mL), tetrabutylammonium iodide (161 mg, 0.436 mmol, 0.053 equiv.), and iodomethane (4.1 mL, 66 mmol, 8.0 equiv.). The reaction mixture was stirred vigorously at 44 ^{o}C for 16 hours and subsequently cooled to room temperature. The solution was then diluted with 30 mL benzene and 27 mL water, and the aqueous layer was extracted 2x with 30 mL ethyl acetate. The organic layers were combined, dried over anhydrous magnesium sulfate and concentrated *in vacuo* to yield a brown solid. The crude product was purified by flash column chromatography (20:1 to 5:1 hexanes-ethyl acetate). Mixed fractions were combined and purified in a second column using the same eluent. Compound **2.11b** was collected in 41% yield (844 mg, 3.41 mmol). R_f = 0.8 in 3:1 hexanes:ethyl acetate; ^{1}H NMR (600 MHz, $CDCl_3$): δ 7.64 (d, *J* = 7.5 Hz, 1H), 7.55 (d, *J* = 7.4 Hz, 1H), 7.37 (t, *J* = 7.5 Hz, 1H), 7.22 (td, *J* = 7.4, 0.8 Hz, 1H), 7.02 (s, 1H), 6.82 (s, 1H), 3.98 (s, 3H), 3.80 (s, 2H), 2.66 (s, 3H), 2.53 (s, 3H); ^{13}C NMR (151 MHz, $CDCl_3$): δ 148.2, 143.4, 142.0, 135.6, 131.4, 129.3, 126.3, 125.3, 123.9, 122.0, 121.6, 120.1, 117.1, 107.2, 31.2, 31.0, 21.9, 19.1; HRMS (ESI) calcd for $C_{18}H_{17}N$ $[M]^+$: 247.1356; found: 247.1355.

5,7,9-trimethyl-10-(trimethylsilyl)-5,10-dihydroindeno[1,2-*b*]indole (2.11c). Methylated indole **2.11b** (573 mg, 2.32 mmol, 1.00 equiv.) was combined with anhydrous ether (15 mL) and the reaction mixture was immersed in a room temperature water bath. *n*-BuLi (1.68 M in hexanes, 1.38 mL, 2.32 mmol, 1.00 equiv.) was added dropwise via syringe pump over one hour and the reaction mixture was then stirred at room temperature for an additional 45 minutes then cooled to –78 ^{o}C. Some precipitate formed upon cooling, so the reaction mixture was slowly warmed to room temperature. Once most of the precipitate had re-dissolved in the ether, TMSCl (740 µL, 5.8 mmol, 2.5 equiv.) was added rapidly via syringe and the resulting mixture was warmed to room temperature. Upon warming, the reaction was diluted with ether, filtered, and concentrated *in vacuo* to yield a brown solid. Crude product was purified by flash column chromatography (20:1 hexanes-ethyl acetate) to give **2.11c** in 83% yield (612 mg, 1.92

mmol). R_f = 0.9 in 3:1 hexanes:ethyl acetate; ^{1}H NMR (600 MHz, $CDCl_3$): δ 7.72 (d, *J* = 7.6 Hz, 1H), 7.53 (d, *J* = 7.6 Hz, 1H), 7.33 (t, *J* = 7.5 Hz, 1H), 7.20 (t, *J* = 7.5 Hz, 1H), 7.05 (s, 1H), 6.82 (s, 1H), 4.06 (s, 3H), 4.01 (s, 1H), 2.67 (s, 3H), 2.53 (s, 3H), –0.12 (s, 9H); ^{13}C NMR (151 MHz, $CDCl_3$): δ 150.1, 142.4, 142.2, 133.2, 131.3, 129.3, 124.9, 124.2, 123.2, 122.8, 121.9, 121.8, 117.1, 107.0, 37.8, 31.2, 21.8, 20.2, –2.0; HRMS (ESI) calcd for $C_{21}H_{25}NSi$ $[M]^+$: 319.1751; found: 319.1751.

Dimethyl-BARAC (2.11). To a solution of silylated indole **2.11c** (545 mg, 1.71 mmol, 1.00 equiv.) in dichloromethane (57 mL) and saturated aqueous $NaHCO_3$ (12 mL) at 0 °C was added *m*-CPBA (77%, 1.26 g, 5.62 mmol, 3.29 equiv.) portionwise over 4 minutes. The reaction mixture was stirred at 0 °C for 30 minutes and then warmed to room temperature. Upon warming, the reaction was quenched via addition of 1N NaOH (30 mL) and the resulting aqueous layer was extracted 2x with 30 mL dichloromethane and 1x with 30 mL ethyl acetate. The organic layers were combined and washed 1x with 40 mL brine, dried over anhydrous magnesium sulfate, and concentrated *in vacuo* to yield an orange oil (**2.11d**) which was immediately brought on to the next step in crude form.

Compound **2.11d** (1.71 mmol assuming 100% yield from the previous step) was dried on a schlenck line for ~15 minutes and then transferred via syringe to a flame dried round bottom flask as a solution in dry THF (20 mL). The solution was cooled to –78 °C, and potassium hexamethyldisilazide (0.5 M in toluene, 3.8 mL, 1.9 mmol, 1.1 equiv.) was added dropwise. The solution was stirred an additional 30 minutes at –78 °C, and then triflic anhydride (345 μL, 2.05 mmol, 1.20 eq) was added. The solution was stirred for 25 minutes at –78 °C prior to dilution with 20 mL anhydrous ether and addition of tetrabutyl ammonium fluoride (1M in THF, 17mL, 17 mmol, 10 eq). The reaction mixture was then warmed to room temperature and quenched with saturated aqueous $NaHCO_3$ (40 mL). The aqueous layer was subsequently extracted 2x with ethyl acetate and the organic layer was dried over anhydrous magnesium sulfate and concentrated to yield a brown oil. The crude product was purified by flash column chromatography (10:1 to 2:1 hexanes-ethyl acetate) to yield **2.11** in 21% yield (93 mg, 0.35 mmol). For the purposes of characterization and kinetic analysis, **2.11** was further purified by HPLC. The compound was injected onto a C18 preparatory column in a 3:5 water(A):acetonitrile(B) solution and eluted at 20 mL/min using a gradient of 35% B to 75% B over 35 minutes. The product was collected at 25 minutes. Elution was monitored at 210 and 254 nM. R_f = 0.4 in 3:1 hexanes:ethyl acetate ^{1}H NMR (500 MHz, $CDCl_3$): δ 7.61–7.56 (m, 1H), 7.46–7.39 (m, 2H), 7.35 (dt, *J* = 6.4, 3.6 Hz, 1H), 7.27 (s, 1H), 7.05 (s, 1H), 2.71 (s, 3H), 2.42 (s, 3H), 2.39 (s, 3H); ^{13}C NMR (151 MHz, $CDCl_3$): δ 176.9, 156.5, 149.0, 140.0, 137.4, 129.8, 129.3, 128.3, 127.4, 126.2, 125.4, 122.8, 119.3, 110.3, 108.9, 38.6, 21.5, 21.3; HRMS (ESI) calcd for $C_{18}H_{16}NO$ $[M+H]^+$: 262.1226; found: 262.1224.

2D NOESY Analysis of Triazole Adducts of 2.10 and 2.11

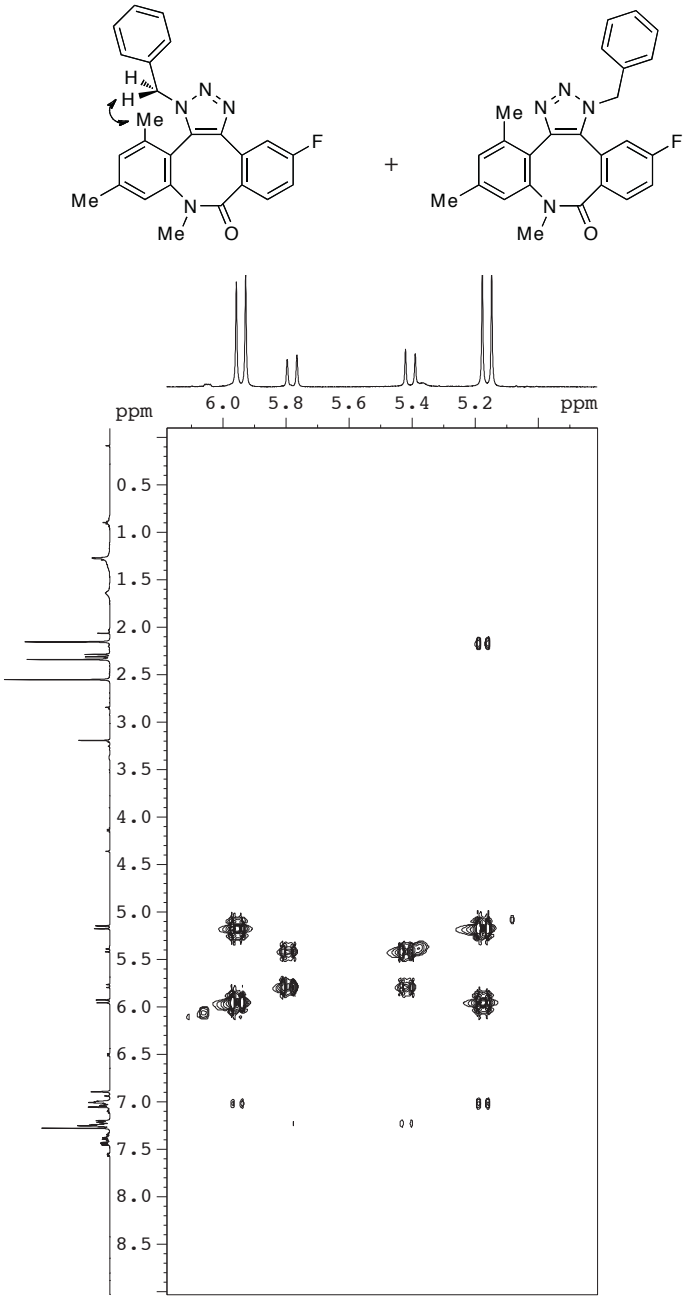


Figure S2.1. The triazole adducts of BARAC analog **2.10** were characterized by 2D NOESY experiments.

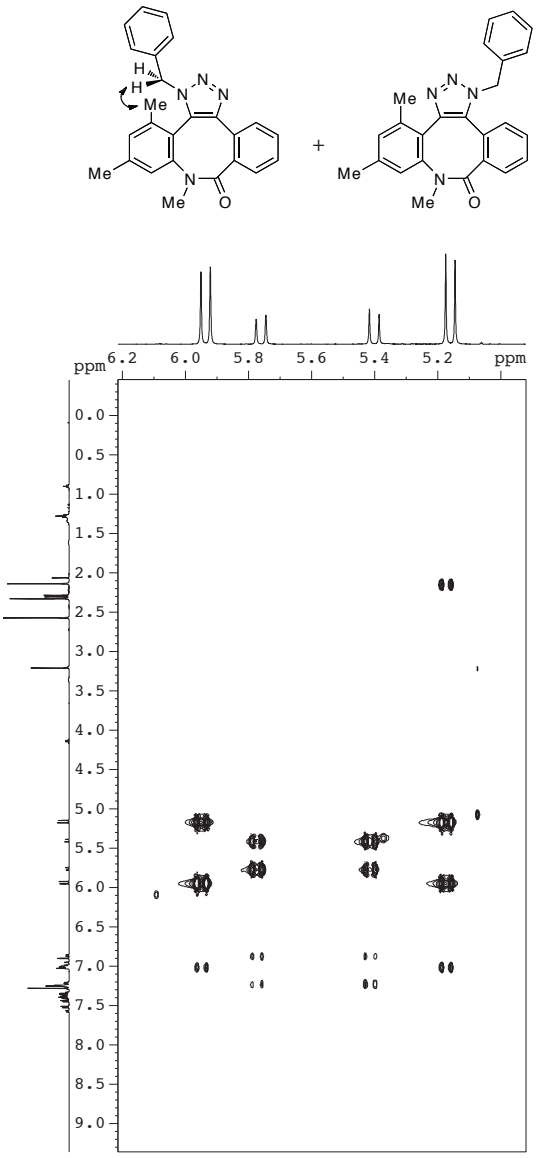


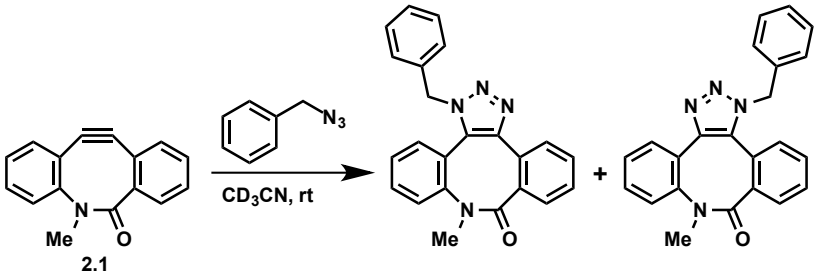
Figure S2.2. The triazole adducts of BARAC analog **2.11** were characterized by 2D NOESY experiments.

NMR Kinetic Analysis

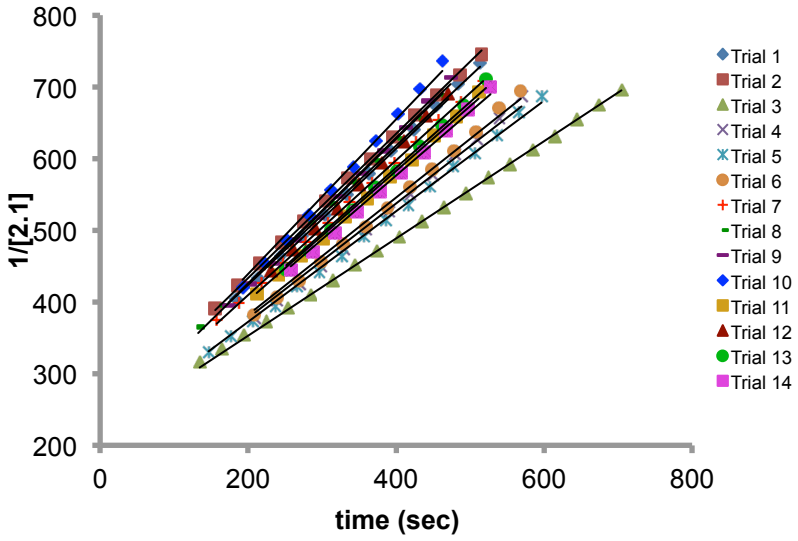
General Procedures. Kinetic data for the reactions between cyclooctynes **2.1-2.11** and benzyl azide were acquired by ^{1}H NMR at room temperature using a Bruker AV-500 spectrometer equipped with a TBI probe. A 5 mM solution of cyclooctyne and a 50 mM solution of benzyl azide were each prepared in deuterated acetonitrile (CD_3CN) containing ~2mM hexamethyldisilane (HMDS) as an internal standard. Proton integration relative to the internal standard was utilized to ensure the proper relative concentrations of each solution. For each experiment, three or four separate NMR tubes were prepared, each containing 500 μL of the 5mM cyclooctyne solution. Benzyl azide (50 mM in CD_3CN/HMDS) was added to one of the prepared NMR tubes such that the resulting solution contained cyclooctyne and benzyl azide in a 1:1 ratio, and the proper ratio was confirmed by proton integration. The reaction solution was scanned once every 30 seconds over 30 minutes unless otherwise noted. This procedure was repeated for each of the remaining prepared NMR tubes.

For each of the cyclooctynes tested, proton spectra showed formation of the expected triazoles without any side products unless otherwise noted. The disappearance of cyclooctyne was monitored by integration of the methyl amide peak for all compounds except **2.7**, which was monitored by disappearance of the methoxy methyl peak. Prior to analysis, all spectra were subjected to baseline correction using the Whittaker smoother algorithm. Phasing was corrected manually. Second order rate constants were calculated by plotting 1/[cyclooctyne] as a function of time. The y-intercept of each plot was set to 1/[starting cyclooctyne concentration]. Plots show data collected to ~70% conversion to triazole with the exception of plots shown in Figures S2.12b and S2.13b, which show data to ~ 80% conversion.

a.



b.



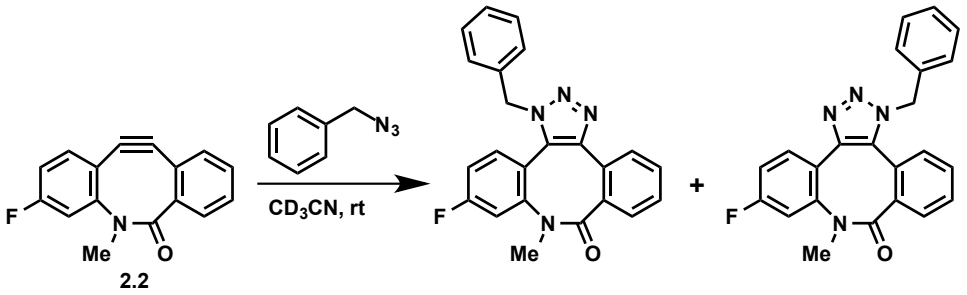
c.

Trial	Rate ($M^{-1}s^{-1}$)
1	0.970
2	1.007
3	0.679
4	0.799
5	0.771
6	0.818
7	0.940
8	1.013
9	1.016
10	1.079
11	0.904
12	0.982
13	0.916
14	0.889

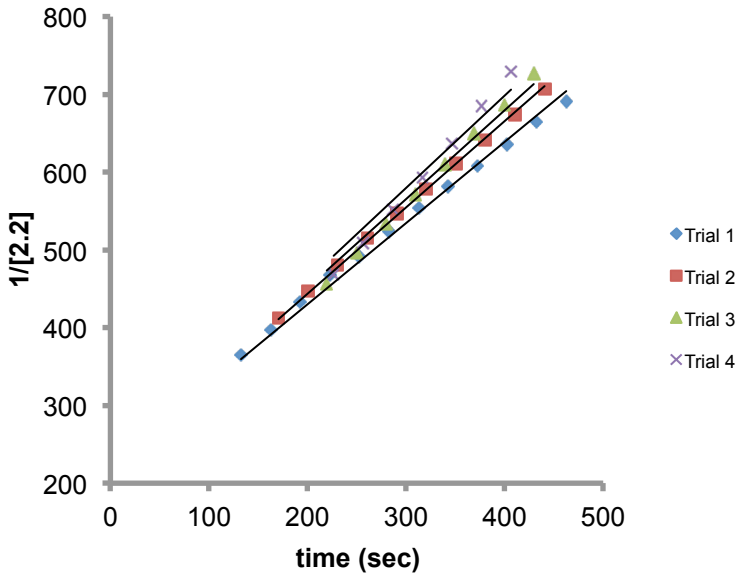
Average second order rate constant: 0.9 ± 0.1 $M^{-1}s^{-1}$

Figure S2.3. a. The reaction between fully unsubstituted BARAC (**2.1**) and benzyl azide was monitored at ~5mM concentrations in CD_3CN by ^1H NMR at room temperature. **b.** The second-order rate constant was calculated by plotting 1/[**2.1**] and a function of time. The slope of the resulting line is the rate constant. Data are plotted to within 67% and 69% conversion to the triazole. **c.** Calculated second-order rate constants for each trial; average $k = 0.9 \pm 0.1$ $M^{-1}s^{-1}$.

a.



b.



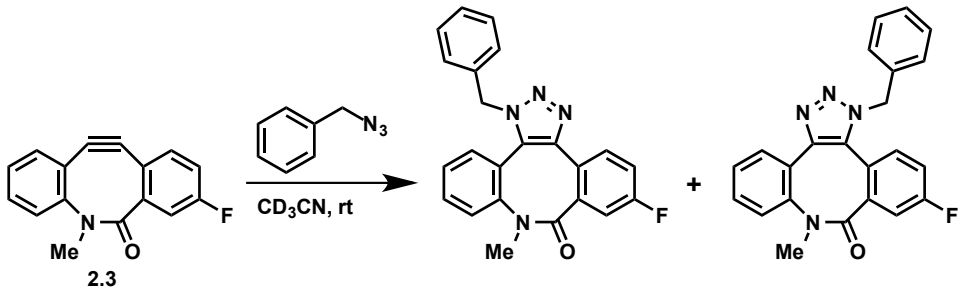
c.

Trial	k ($M^{-1}s^{-1}$)
1	1.044
2	1.110
3	1.142
4	1.187

Average second order rate constant: 1.1 ± 0.1 $M^{-1}s^{-1}$

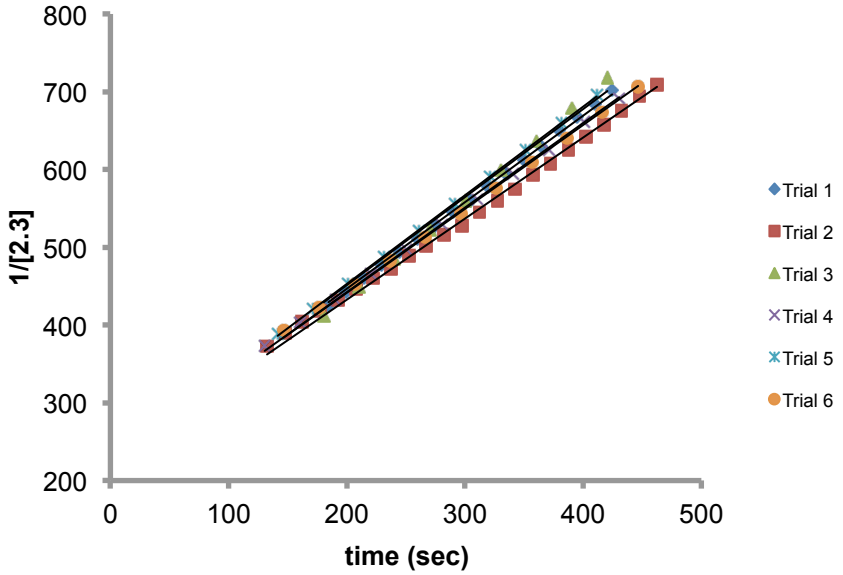
Figure S2.4. a. The reaction between fully fluorinated BARAC (**2.2**) and benzyl azide was monitored at ~5mM concentrations in CD_3CN by ^1H NMR at room temperature. **b.** The second-order rate constant was calculated by plotting 1/[**2.2**] and a function of time. The slope of the resulting line is the rate constant. Data are plotted to within 68% and 70% conversion to the triazole. **c.** Calculated second-order rate constants for each trial; average k = 1.1 ± 0.1 $M^{-1}s^{-1}$.

a.



2.3

b.



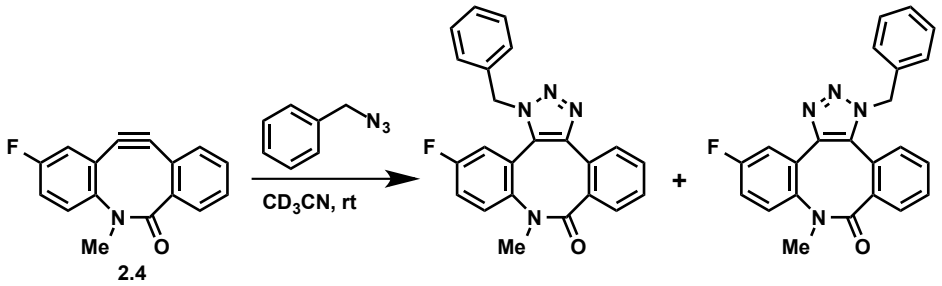
c.

Trial	k ($M^{-1}s^{-1}$)
1	1.113
2	1.043
3	1.132
4	1.087
5	1.14
6	1.079

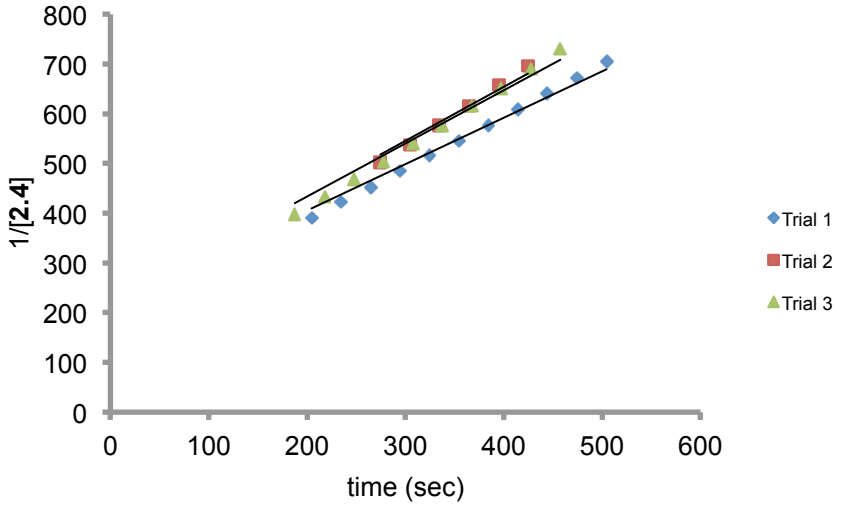
Average second order rate constant: 1.1 ± 0.04 $M^{-1}s^{-1}$

Figure S2.5. a. The reaction between fluorinated BARAC (**2.3**) and benzyl azide was monitored at ~5mM concentrations in CD_3CN by ^1H NMR at room temperature. **b.** The second-order rate constant was calculated by plotting 1/[**2.3**] and a function of time. The slope of the resulting line is the rate constant. Data are plotted to within 67% and 69% conversion to the triazole. **c.** Calculated second-order rate constants for each trial; average k = 1.1 ± 0.04 $M^{-1}s^{-1}$.

a.



b.



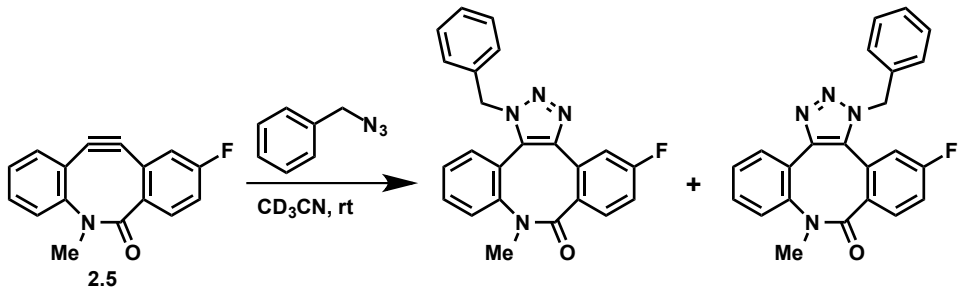
c.

Trial	k ($M^{-1}s^{-1}$)
1	0.933
2	1.085
3	1.068

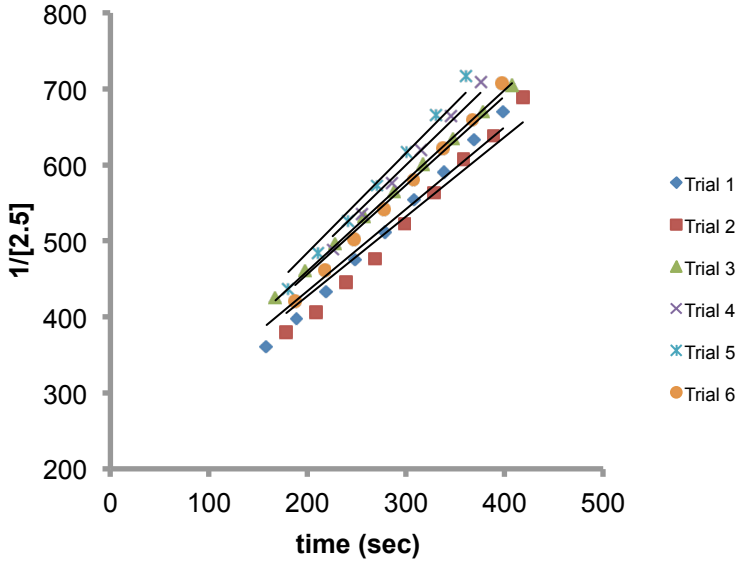
Average second order rate constant: 1.0 ± 0.1 $M^{-1}s^{-1}$

Figure S2.6. a. The reaction between fluorinated BARAC (**2.4**) and benzyl azide was monitored at ~5mM concentrations in CD_3CN by ^1H NMR at room temperature. **b.** The second-order rate constant was calculated by plotting 1/[**2.4**] and a function of time. The slope of the resulting line is the rate constant. Data are plotted to within 68% and 70% conversion to the triazole. **c.** Calculated second-order rate constants for each trial; average k = 1.0 ± 0.1 $M^{-1}s^{-1}$.

a.



b.



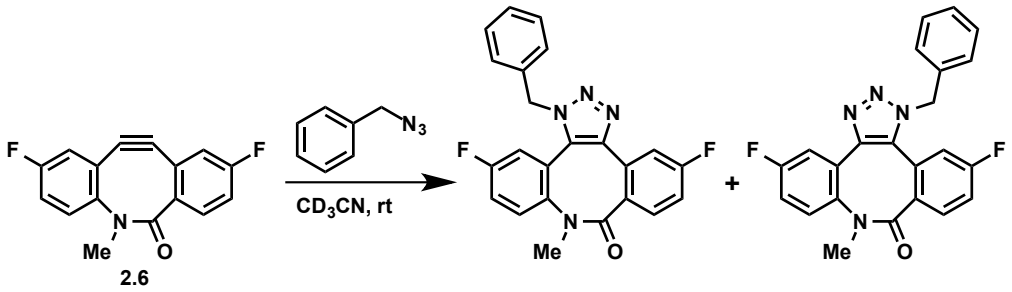
c.

Trial	k ($M^{-1}s^{-1}$)
1	1.0783
2	1.0458
3	1.1909
4	1.2583
5	1.3108
6	1.1703

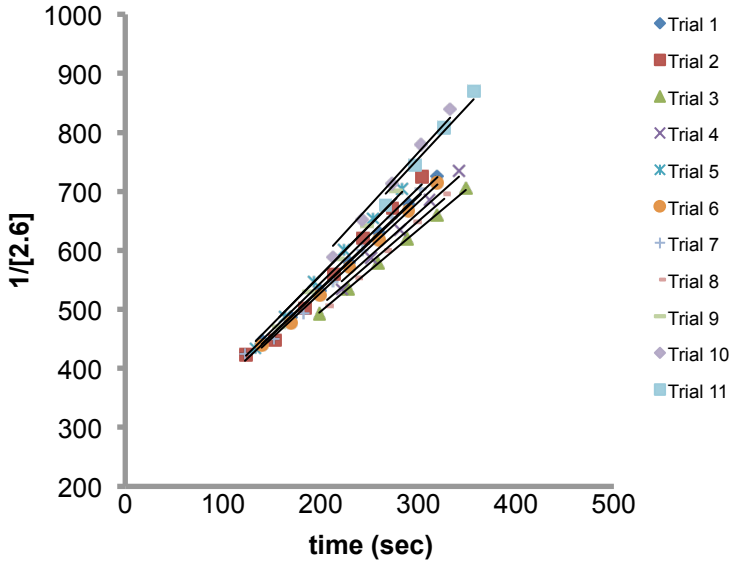
Average second order rate constant: 1.2 ± 0.1 $M^{-1}s^{-1}$

Figure S2.7. a. The reaction between fluorinated BARAC (**2.5**) and benzyl azide was monitored at ~5mM concentrations in CD_3CN by ^1H NMR at room temperature. **b.** The second-order rate constant was calculated by plotting 1/[**2.5**] and a function of time. The slope of the resulting line is the rate constant. Data are plotted to within 67% and 69% conversion to the triazole. **c.** Calculated second-order rate constants for each trial; average k = 1.2 ± 0.1 $M^{-1}s^{-1}$.

a.



b.



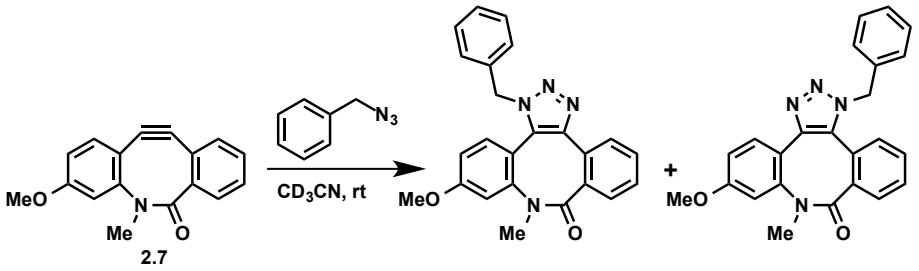
c.

Trial	k ($M^{-1}s^{-1}$)
1	1.573
2	1.613
3	1.387
4	1.479
5	1.688
6	1.537
7	1.568
8	1.429
9	1.681
10	1.811
11	1.778

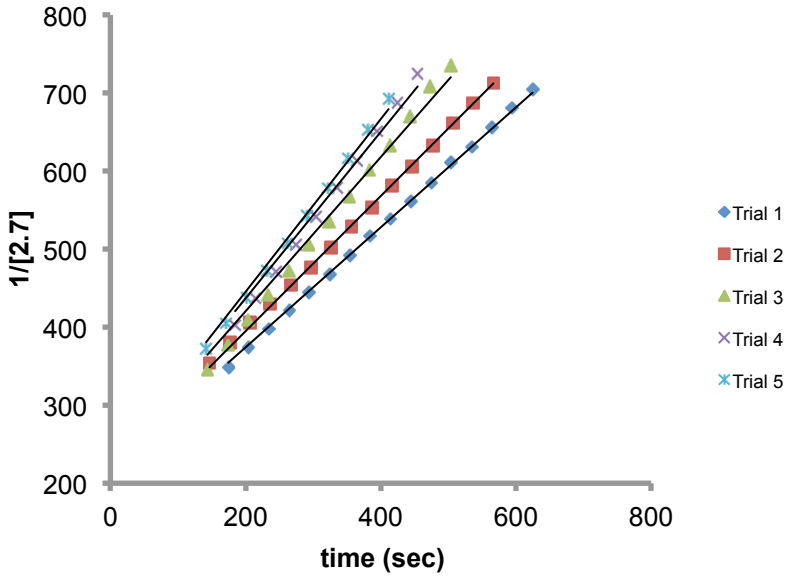
Average second order rate constant: 1.6 ± 0.1 $M^{-1}s^{-1}$

Figure S2.8. a. The reaction between difluorinated BARAC (**2.6**) and benzyl azide was monitored at ~5mM concentrations in CD_3CN by ^1H NMR at room temperature. **b.** The second-order rate constant was calculated by plotting 1/[**2.6**] and a function of time. The slope of the resulting line is the rate constant. Data are plotted to within 68% and 75% conversion to the triazole. **c.** Calculated second-order rate constants for each trial; average k = 1.6 ± 0.1 $M^{-1}s^{-1}$.

a.



b.



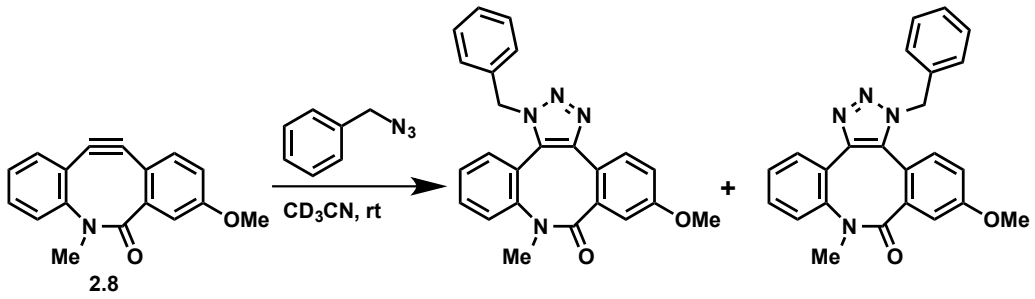
c.

Trial	k ($M^{-1}s^{-1}$)
1	0.7686
2	0.866
3	0.9878
4	1.0665
5	1.1064

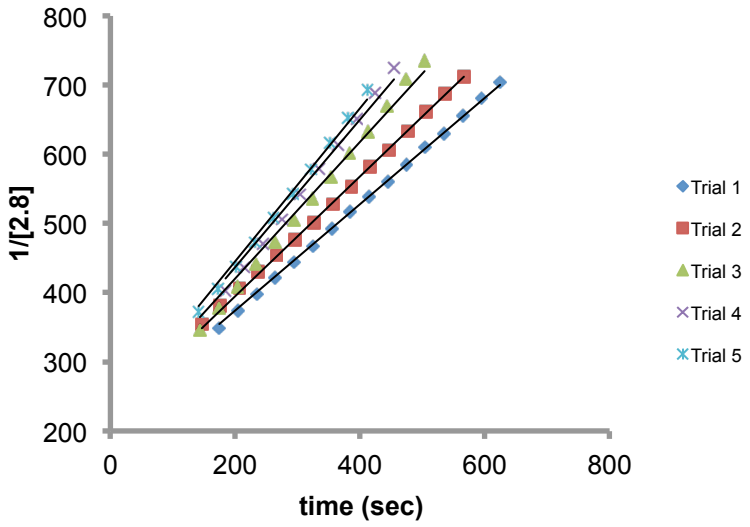
Average second order rate constant: 1.0 ± 0.1 $M^{-1}s^{-1}$

Figure S2.9. a. The reaction between **2.7** and benzyl azide was monitored at ~5mM concentrations in CD_3CN by ^1H NMR at room temperature. **b.** The second-order rate constant was calculated by plotting 1/[**2.7**] and a function of time. The slope of the resulting line is the rate constant. Data are plotted to within 68% and 70% conversion to the triazole. **c.** Calculated second-order rate constants for each trial; average k = 1.0 ± 0.1 $M^{-1}s^{-1}$.

a.



b.



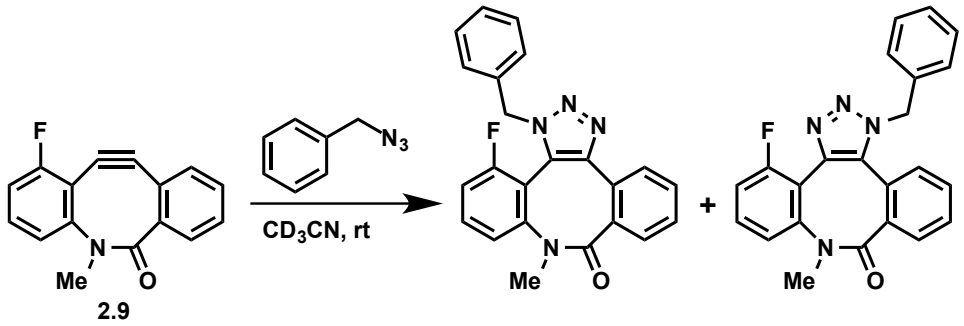
c.

Trial	k ($M^{-1}s^{-1}$)
1	1.0225
2	1.1135
3	1.2156
4	0.9832
5	1.097

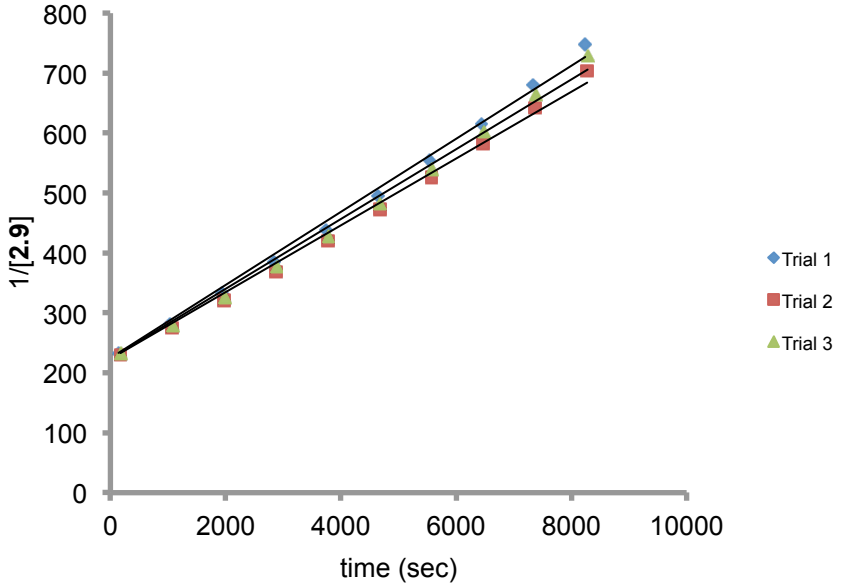
Average second order rate constant: 1.1 ± 0.1 $M^{-1}s^{-1}$

Figure S2.10. a. The reaction between **2.8** and benzyl azide was monitored at ~5mM concentrations in CD_3CN by ^1H NMR at room temperature. **b.** The second-order rate constant was calculated by plotting 1/[**2.8**] and a function of time. The slope of the resulting line is the rate constant. Data is plotted to within 68% and 69% conversion to the triazole. **c.** Calculated second-order rate constants for each trial; average k = 1.1 ± 0.1 $M^{-1}s^{-1}$.

a.



b.



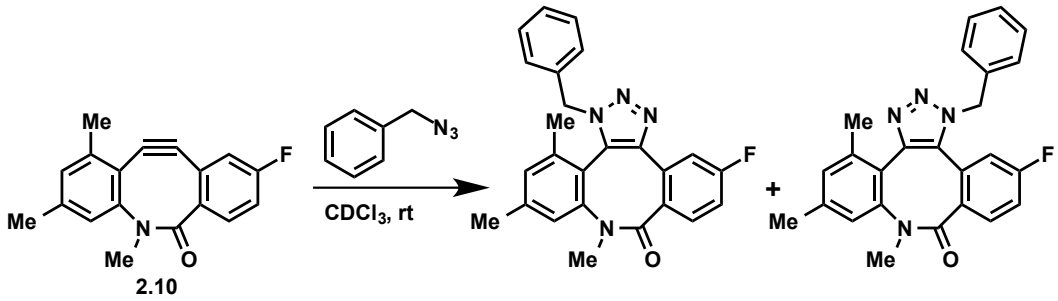
c.

Trial	k ($M^{-1}s^{-1}$)
1	0.061
2	0.056
3	0.058

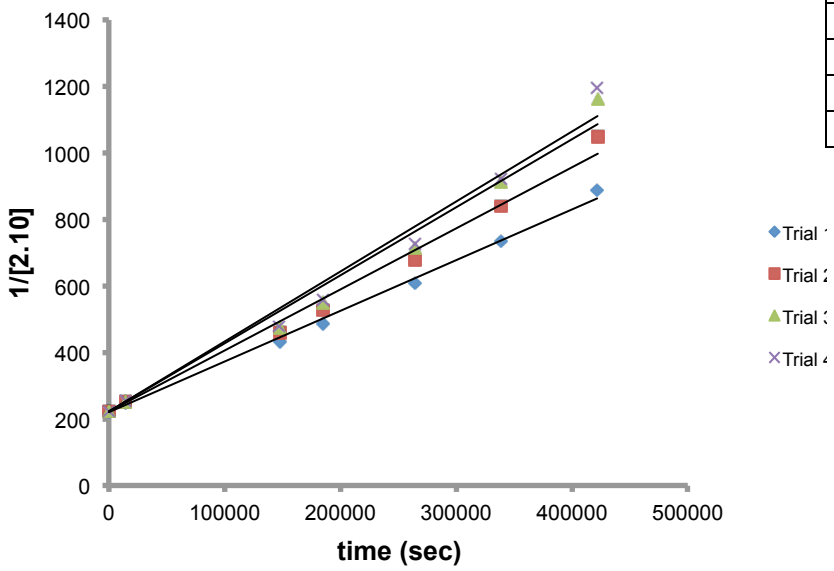
Average second order rate constant: 0.06 ± 0.003 $M^{-1}s^{-1}$

Figure S2.11. a. The reaction between **2.9** and benzyl azide was monitored at ~5mM concentrations in $CDCl_3$ by ^1H NMR at room temperature. **b.** The second-order rate constant was calculated by plotting 1/[**2.9**] and a function of time. The slope of the resulting line is the rate constant. Data are plotted to within 68% and 70% conversion to the triazole. **c.** Calculated second-order rate constants for each trial; average k = 0.06 ± 0.003 $M^{-1}s^{-1}$.

a.



b.



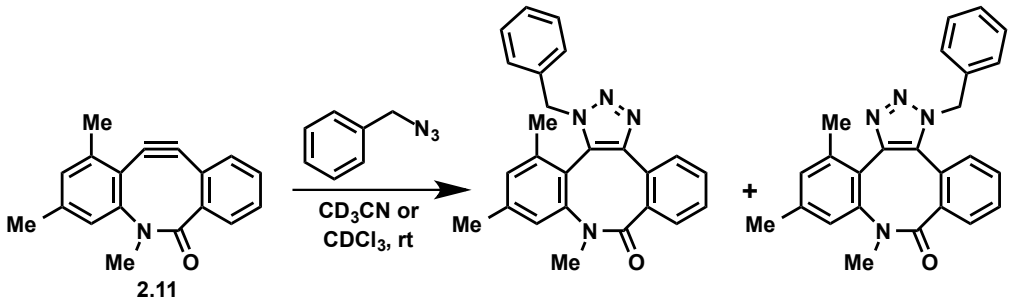
c.

Trial	k ($M^{-1}s^{-1}$)
1	0.0015
2	0.0018
3	0.002
4	0.0021

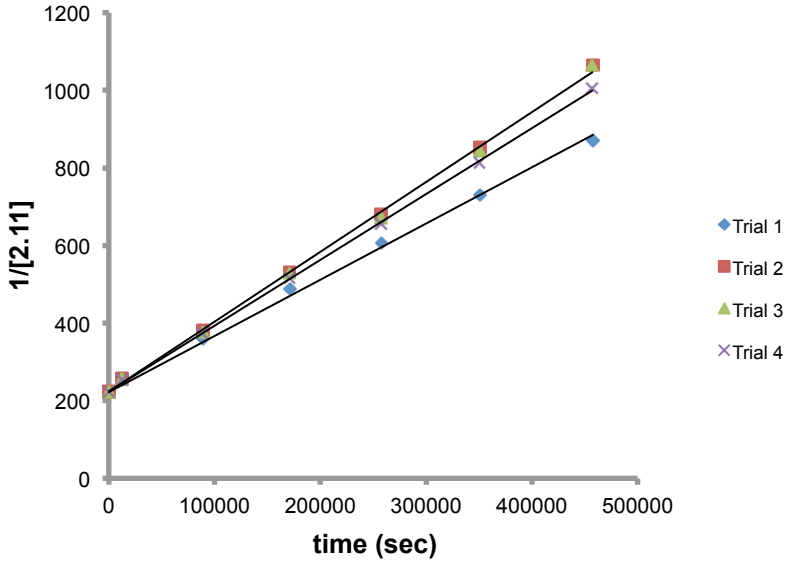
Average second order rate constant: $2.0 \times 10^{-3} \pm 0.3 \times 10^{-3}$ $M^{-1}s^{-1}$

Figure S2.12. a. The reaction between **2.10** and benzyl azide was monitored at ~5mM concentrations in $CDCl_3$ by ^1H NMR at room temperature. $CDCl_3$ was used as the solvent due to the limited solubility of **2.10** in CD_3CN. **b.** The second-order rate constant was calculated by plotting 1/[**2.10**] and a function of time. The slope of the resulting line is the rate constant. Data are plotted to within 75% and 81% conversion to the triazole. **c.** Calculated second-order rate constants for each trial; average $k = 2.0 \times 10^{-3} \pm 0.3 \times 10^{-3}$ $M^{-1}s^{-1}$.

a.



b.

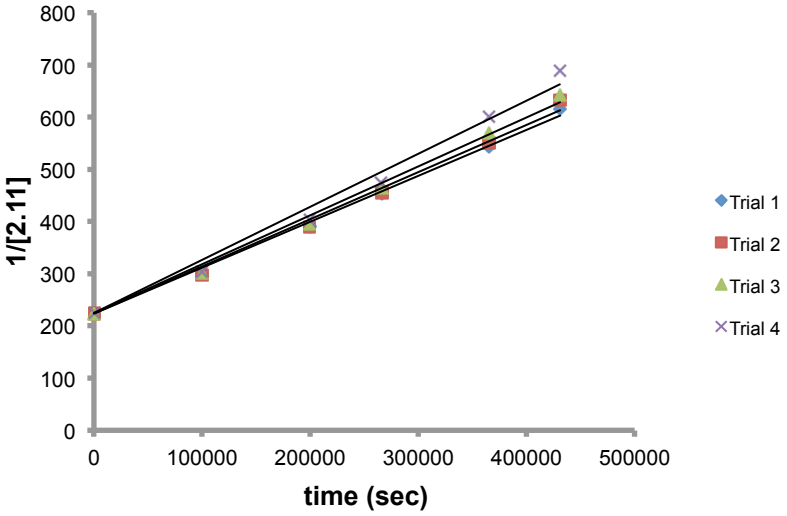


c.

Trial	k ($M^{-1}s^{-1}$)
1	0.0014
2	0.0018
3	0.0018
4	0.0017

Average second order rate constant: $2.0 \times 10^{-3} \pm 0.2 \times 10^{-3}$ $M^{-1}s^{-1}$

d.



e.

Trial	k ($M^{-1}s^{-1}$)
1	0.0009
2	0.0009
3	0.0009
4	0.001

Average second order rate constant: $1.0 \times 10^{-3} \pm 0.1 \times 10^{-3}$ $M^{-1}s^{-1}$

Figure S2.13. a. The reaction between **2.11** and benzyl azide was monitored at ~5mM concentrations in CD_3CN or $CDCl_3$ by ^1H NMR at room temperature. Both solvents were used to enable comparison of **2.11** to **2.10** as well as all of the other cyclooctynes tested. **b.** Results for the reaction of **2.11** with benzyl azide in CD_3CN. The second-order rate constant was calculated by plotting 1/[**2.11**] and a function of time. The slope of the resulting line is the rate constant. Data are plotted to within 75% and 79% conversion to the triazole. **c.** Calculated second-order rate constants for each trial in CD_3CN; average $k = 2.0 \times 10^{-3} \pm 0.2 \times 10^{-3}$ $M^{-1}s^{-1}$. **d.** Results for the reaction of **2.11** with benzyl azide in $CDCl_3$. The second-order rate constant was calculated by plotting 1/[**2.11**] and a function of time. The slope of the resulting line is the rate constant. Data are plotted to within 64% and 67% conversion to the triazole. **e.** Calculated second-order rate constants for each trial in $CDCl_3$; average $k = 1.0 \times 10^{-3} \pm 0.1 \times 10^{-3}$ $M^{-1}s^{-1}$.

Computational Methods

All computations were performed by J. L. Mackey and K. N. Houk

All geometry optimizations were performed with Gaussian 09[1]using the B3LYP density functional with the 6-31G(d) basis set. A fine grid density was used for numerical integration. Harmonic vibrational frequencies were computed for all optimized structures to verify that they were either minima (zero imaginary frequencies) or transition states (a single imaginary frequency). Unscaled zero-point energies are included in all Gibbs free energies. The effects of solvation on the reaction energetics were evaluated using a conductor-like polarizable continuum solvation model (CPCM).[2] The solute surface was defined by UAHF radii in each case.[3]

1) Gaussian 09, Revision A.02,
M. J. Frisch, G. W. Trucks, H. B. Schlegel, G. E. Scuseria, M. A. Robb, J. R. Cheeseman, G. Scalmani, V. Barone, B. Mennucci, G. A. Petersson, H. Nakatsuji, M. Caricato, X. Li,H. P. Hratchian, A. F. Izmaylov, J. Bloino, G. Zheng, J. L. Sonnenberg, M. Hada, M., Ehara, K. Toyota, R. Fukuda, J. Hasegawa, M. Ishida, T. Nakajima, Y. Honda, O. Kitao, H. Nakai, T. Vreven, J. A. Montgomery, Jr., J. E. Peralta, F. Ogliaro, M. Bearpark, J. J. Heyd, E. Brothers, K. N. Kudin, V. N. Staroverov, R. Kobayashi, J. Normand, K., Raghavachari, A. Rendell, J. C. Burant, S. S. Iyengar, J. Tomasi, M. Cossi, N. Rega, J., M. Millam, M. Klene, J. E. Knox, J. B. Cross, V. Bakken, C. Adamo, J. Jaramillo, R., Gomperts, R. E. Stratmann, O. Yazyev, A. J. Austin, R. Cammi, C. Pomelli, J. W., Ochterski, R. L. Martin, K. Morokuma, V. G. Zakrzewski, G. A. Voth, P. Salvador, J. J., Dannenberg, S. Dapprich, A. D. Daniels, O. Farkas, J. B., Foresman, J. V. Ortiz, J., Cioslowski, and D. J. Fox, Gaussian, Inc., Wallingford CT, 2009.
2) (a) Barone, V.; Cossi, M. *J. Phys. Chem. A* **1998**, *102*, 1995–2001.
(b) Cossi, M.; Rega, N.; Scalmani, G.; Barone, V. *J. Comput. Chem.* **2003**, *24*, 669–681.
3) Takano, Y.; Houk, K. N. *J. Chem. Theory Comput.* **2005**, *1*, 70–77.

Table S2.1. Complete list of angles for *trans* compounds 2.1–2.11.

Alkyne	syn angle°	anti angle°
Compound 2.1	152.7°	153.0°
Compound 2.2	152.4°	153.1°
Compound 2.3	153.0°	152.7°
Compound 2.4	152.3°	153.4°
Compound 2.5	153.0°	152.7°
Compound 2.6	152.5°	153.1°
Compound 2.7	152.6°	152.8°
Compound 2.8	152.5°	153.0°
Compound 2.9	151.1°	153.7°
Compound 2.10	153.6°	152.1°
Compound 2.11	153.0°	152.7°

Table S2.2. Comparison of *trans* vs *cis* cycloaddition pathways

Data in kcal/mol

	Trans		Cis	
	$\Delta G^{\ddagger}$solv anti	$\Delta G^{\ddagger}$solv syn	$\Delta G^{\ddagger}$solv anti	$\Delta G^{\ddagger}$solv syn
Compound 2.1	24.1	24.0	27.3	27.6
Compound 2.2	24.0	24.1	27.0	27.9
Compound 2.3	24.0	23.8	27.5	27.7
Compound 2.4	23.7	23.7	27.2	27.7
Compound 2.5	23.9	23.7	27.2	27.4
Compound 2.6	23.6	23.5	27.0	27.4
Compound 2.7	24.0	23.9	27.6	27.8
Compound 2.8	23.9	23.8	27.7	28.3
Compound 2.9	26.0	24.7	27.1	27.2
Compound 2.10	30.1	28.2	28.7	28.8
Compound 2.11	30.2	28.3	28.8	28.8

Table S2.3. Energy difference between *trans* and *cis* lactam

Energy is in kcal/mol and represents the favored *trans* lactam by the indicated amount.

	ΔG_{MeCN} SCF
Compound 2.1	9.4
Compound 2.2	9.4
Compound 2.3	9.5
Compound 2.4	9.4
Compound 2.5	9.1
Compound 2.6	9.2
Compound 2.7	9.5
Compound 2.8	9.7
Compound 2.9	9.5
Compound 2.10	9.3
Compound 2.11	9.6

Table S2.4. Comparison of MeN_3 and BnN_3

Values are calculated for the the *syn* TS in both cases. There appears to be no difference except an extra kcal in the free energy of the BnN_3 but it appears to be in both cases suggesting that it will not influence any relative rates and energies calculated.

	cis			*trans*		
	E	H	G	E	H	G
BARAC w/ MeN_3	5.1	5.5	17.2	8.3	8.8	21.4
BARAC w/ BnN_3	5.1	5.5	18.1	8.4	8.9	22.3

Table S2.5. Comparison of B3LYP functional with M06-2X functional

A side by side comparison of B3LYP and M06-2X. The conclusions are the same except that with M06-2X, all reactants go through the trans isomer.

		Trans			**Cis**		
	Energies in kcal/mol	**B3LYP**	**M06-2X**	**Differ-ence**	**B3LYP**	**M06-2X**	**Difference**
Compound 2.1 Anti	$\Delta G^{\ddagger}$	21.3	17.3	4.0	16.6	15.3	1.3
	$\Delta G^{\ddagger}_{Solv\ (MeCN)}$	24.1	20.3	3.8	18.0	16.1	1.8
Compound 2.1 Syn	$\Delta G^{\ddagger}$	21.4	17.6	3.7	17.2	15.3	1.9
	$\Delta G^{\ddagger}_{Solv\ (MeCN)}$	24.0	20.3	3.7	18.2	16.0	2.3
Compound 2.9 Anti	$\Delta G^{\ddagger}$	23.7	18.8	4.9	17.4	15.4	2.0
	$\Delta G^{\ddagger}_{Solv\ (MeCN)}$	26.0	21.4	4.6	18.1	15.8	2.3
Compound 2.9 Syn	$\Delta G^{\ddagger}$	21.8	18.8	3.0	16.4	14.6	1.8
	$\Delta G^{\ddagger}_{Solv\ (MeCN)}$	24.7	21.1	3.6	18.2	16.4	1.8
Compound 2.10 Anti	$\Delta G^{\ddagger}$	27.2	22.9	4.3	17.9	16.0	2.0
	$\Delta G^{\ddagger}_{Solv\ (MeCN)}$	30.1	25.8	4.3	19.4	17.0	2.4
Compound 2.10 Syn	$\Delta G^{\ddagger}$	25.1	21.2	3.9	18.0	14.3	3.7
	$\Delta G^{\ddagger}_{Solv\ (MeCN)}$	28.2	24.0	4.2	19.5	15.8	3.7
Compound 2.11 Anti	$\Delta G^{\ddagger}$	27.4	23.5	3.9	17.9	16.9	1.0
	$\Delta G^{\ddagger}_{Solv\ (MeCN)}$	30.2	26.4	3.8	19.3	17.9	1.4
Compound 2.11 Syn	$\Delta G^{\ddagger}$	25.2	21.5	3.7	17.7	15.8	1.9
	$\Delta G^{\ddagger}_{Solv\ (MeCN)}$	28.3	24.3	4.0	19.2	17.3	1.9

Isomerization

	Energies in kcal/mol	B3LYP	M06-2X	Difference
Compound 2.1	$\Delta G^{\ddagger}$	14.5	16.3	-1.8
	$\Delta G^{\ddagger}_{Solv\ (MeCN)}$	15.9	18.2	-2.3
Compound 2.10	$\Delta G^{\ddagger}$	15.2	16.3	-1.1
	$\Delta G^{\ddagger}_{Solv\ (MeCN)}$	16.2	18.2	-2.0
Compound 2.11	$\Delta G^{\ddagger}$	15.1	16.4	-1.3
	$\Delta G^{\ddagger}_{Solv\ (MeCN)}$	16.2	18.4	-2.1

$\Delta\Delta G$ ***Trans* vs. *Cis***

	Energies in kcal/mol	B3LYP	M06-2X	Difference
Compound 2.1	$\Delta\Delta G$	7.2	9.3	-2.1
	$\Delta\Delta G_{Solv\ (MeCN)}$	9.4	11.2	-1.9
Compound 2.10	$\Delta\Delta G$	7.2	9.4	-2.2
	$\Delta\Delta G_{Solv\ (MeCN)}$	9.3	11.5	-2.2
Compound 2.11	$\Delta\Delta G$	7.6	8.5	-1.0
	$\Delta\Delta G_{Solv\ (MeCN)}$	9.6	10.6	-1.0

References

1. Johnson, J. A.; Baskin, J. M.; Bertozzi, C. R.; Koberstein, J. T.; Turro, N. J. Copper-free click chemistry for the in situ crosslinking of photodegradable star polymers. *Chem. Commun.* **2008**, 3064-3066.
2. Sumerlin, B. S.; Vogt, A. P. Macromolecular engineering through click chemistry and other efficient transformations. *Macromolecules* **2010***, 43*, 1-13.
3. Zheng, J.; Liu, K.; Reneker, D. H.; Becker, M. L. Post-assembly derivatization of electrospun nanofibers via strain-promoted azide alkyne cycloaddition. *J. Am. Chem. Soc.* **2012***, 134*, 17274-17277.
4. Agard, N. J.; Baskin, J. M.; Prescher, J. A.; Lo, A.; Bertozzi, C. R. A comparative study of bioorthogonal reactions with azides. *ACS Chem. Biol.* **2006***, 1*, 644-648.
5. Agard, N. J.; Prescher, J. A.; Bertozzi, C. R. A strain-promoted [3 + 2] azide-alkyne cycloaddition for covalent modification of biomolecules in living systems. *J. Am. Chem. Soc.* **2004***, 126*, 15046-15047.
6. Baskin, J. M.; Prescher, J. A.; Laughlin, S. T.; Agard, N. J.; Chang, P. V.; Miller, I. A.; Lo, A.; Codelli, J. A.; Bertozzi, C. R. Copper-free click chemistry for dynamic in vivo imaging. *Proc. Natl. Acad. Sci. USA* **2007***, 104*, 16793-16797.

7. Ning, X.; Guo, J.; Wolfert, M.; Boons, G. Visualizing metabolically labeled glycoconjugates of living cells by copper-free and fast huisgen cycloadditions. *Angew Chem* **2008**, *120*, 2285-2287.
8. Mbua, N. E.; Guo, J.; Wolfert, M. A.; Steet, R.; Boons, G. Strain-promoted alkyne-azide cycloadditions (SPAAC) reveal new features of glycoconjugate biosynthesis. *ChemBioChem* **2011**, *12*, 1912-1921.
9. Debets, M. F.; van Berkel, S. S.; Schoffelen, S.; Rutjes, F. P. J. T.; van Hest, Jan C. M.; van Delft, F. L. Aza-dibenzocyclooctynes for fast and efficient enzyme PEGylation via copper-free (3+2) cycloaddition. *Chem. Commun.* **2010**, *46*, 97-99.
10. Jewett, J. C.; Sletten, E. M.; Bertozzi, C. R. Rapid cu-free click chemistry with readily synthesized biarylazacyclooctynones. *J. Am. Chem. Soc.* **2010**, *132*, 3688-3690.
11. Dommerholt, J.; Schmidt, S.; Temming, R.; Hendriks, L. J. A.; Rutjes, F. P. J. T.; van Hest, J. C. M.; Lefeber, D. J.; Friedl, P.; van Delft, F. L. Readily accessible bicyclononynes for bioorthogonal labeling and three-dimensional imaging of living cells. *Angew. Chem. Int. Ed.* **2010**, *49*, 9422-9425.
12. Sletten, E. M.; Bertozzi, C. R. A hydrophilic azacyclooctyne for cu-free click chemistry. *Org. Lett.* **2008**, *10*, 3097-3099.
13. Chenoweth, K.; Chenoweth, D.; Goddard III, W. A. Cyclooctyne-based reagents for uncatalyzed click chemistry: A computational survey. *Org. Biomol. Chem.* **2009**, *7*, 5255-5258.
14. Ess, D. H.; Jones, G. O.; Houk, K. N. Transition states of strain-promoted metal-free click chemistry: 1,3-dipolar cycloadditions of phenyl azide and cyclooctynes. *Org. Lett.* **2008**, *10*, 1633-1636.
15. Schoenebeck, F.; Ess, D. H.; Jones, G. O.; Houk, K. N. Reactivity and regioselectivity in 1,3-dipolar cycloadditions of azides to strained alkynes and alkenes: A computational study. *J. Am. Chem. Soc.* **2009**, *131*, 8121-8133.
16. Gold, B.; Shevchenko, N. E.; Bonus, N.; Dudley, G. B.; Alabugin, I. V. Selective transition state stabilization via hyperconjugative and conjugative assistance: Stereoelectronic concept for copper-free click chemistry. *J. Org. Chem.* **2012**, *77*, 75-89.
17. Anslyn, E. V.; Dougherty, D. A. *Modern Physical Organic Chemistry;* University Science Books: Mill Valley, CA, **2006**.
18. Carey, F., A.; Sundberg, R., J. *Advanced Organic Chemistry, Part A: Structure and Mecahnisms, Fourth Edition;* Springer: New York, New York, **2006**.
19. Tadross, P. M.; Stoltz, B. M. A comprehensive history of arynes in natural product total synthesis. *Chem. Rev.* **2012**, *112*, 3550-3577.
20. Atanes, N.; Escudero, S.; Perez, D.; Guitian, E.; Castedo, L. Generation of cyclohexyne and its diels-alder reaction with alpha-pyrones. *Tetrahedron Lett.* **1998**, *39*, 3039-3040.
21. Himeshima, Y.; Sonoda, T.; Kobayashi, H. Fluoride-induced 1,2-elimination of o-trimethylsilylphenyl triflate to benzyne under mild conditions. *Chem. Lett.* **1983**, *8*, 1211-1214.
22. Sato, S.; Matsuda, I.; Izumi, Y. A regiodefined synthesis of alpha-trimethylsilyl ketones catalyzed by rhodium(I) hydride complex. *J. Organomet. Chem.* **1988**, *344*, 71-88.
23. Stork, G.; Hudrlik, P. F. Isolation of ketone enolates as trialkylsilyl ethers. *J. Am. Chem. Soc.* **1968**, *90*, 4462-4464.
24. Letcher, R. M.; Ng, K.; Cheung, K. Reactions of an indeno1,2-b]indole and novel rearrangements of a dioxodibenzb,f]azocine to derivatives of 5,12-diaza- and 5-oxa-12-aza-chrysene. *J. Chem. Soc. , Chem. Commun.* **1987**, 1602-1603.
25. Hughes, D. L. Progress in the fischer indole reaction, A review. *Org. Prep. Proced. Int.* **1993**, *25*, 607-632.

26. Lan, Y.; Zou, L.; Cao, Y.; Houk, K. N. Computational methods to calculate accurate activation and reaction energies of 1,3-dipolar cycloadditions of 24 1,3-dipoles. *J. Phys. Chem. A* **2011***, 115*, 13906-13920.
27. Ess, D. H.; Houk, K. N. Activation energies of pericyclic reactions:Â€‰ performance of DFT, MP2, and CBS-QB3 methods for the prediction of activation barriers and reaction energetics of 1,3-dipolar cycloadditions, and revised activation enthalpies for a standard set of hydrocarbon pericyclic reactions. *J. Phys. Chem. A* **2005***, 109*, 9542-9553.
28. de Graaff, Rudolf A. G.; Gorter, S.; Romers, C.; Wong, H. N. C.; Sondheimer, F. Crystal structure of 5,6-didehydrodibenzoa,e]cyclo-octene. *J. Chem. Soc. , Perkin Trans. 2* **1981**, 478-480.
29. Cheong, P. H. -.; Paton, R. S.; Bronner, S. M.; Im, G.; Garg, N. K.; Houk, K. N. Indolyne and aryne distortions and nucleophilic regioselectivites. *J. Am. Chem. Soc.* **2010***, 132*, 1267-1269.
30. Im, G.; Bronner, S. M.; Goetz, A. E.; Paton, R. S.; Cheong, P. H. -.; Houk, K. N.; Garg, N. K. Indolyne experimental and computational studies: Synthetic applications and origins of selectivities of nucleophilic additions. *J. Am. Chem. Soc.* **2010***, 132*, 17933-17944.
31. Codelli, J. A.; Baskin, J. M.; Agard, N. J.; Bertozzi, C. R. Second-generation difluorinated cyclooctynes for copper-free click chemistry. *J. Am. Chem. Soc.* **2008***, 130*, 11486-11493.
32. Kornmayer, S. C.; Rominger, F.; Gleiter, R. Synthesis of 11,12-didehydrodibenzo[*a,e*]cycloocten-5(6*H*)-one: A strained eight-membered alkyne. *Synthesis* **2009***, 15*, 2547-2552.
33. Destro, R.; Pilati, T.; Simonetta, M. Crystal structure of 5,6,11,12-tetradehydrodibenzoa,e]cyclooctene (sym-dibenzo-1,5-cyclooctadiene-3,7-diyne). *J. Am. Chem. Soc.* **1975***, 97*, 658-659.
34. Kii, I.; Shiraishi, A.; Hiramatsu, T.; Matsushita, T.; Uekusa, H.; Yoshida, S.; Yamamoto, M.; Kudo, A.; Hagiwara, M.; Hosoya, T. Strain-promoted double-click reaction for chemical modification of azido-biomolecules. *Org. Biomol. Chem.* **2010***, 8*, 4051-4055.
35. Meier, H.; Hanold, N.; Molz, T.; Bissinger, H. J.; Kolshorn, H.; Zountsas, J. Strained cycloalkenynes. *Tetrahedron* **1986***, 42*, 1711-1719.
36. Yoshida, S.; Shiraishi, A.; Kanno, K.; Matsushita, T.; Johmoto, K.; Uekusa, H.; Hosoya, T. Enhanced clickability of doubly sterically-hindered aryl azides. *Scientific Reports* **2011***, 1*, 82.
37. Furman, J. L.; Kang, M.; Choi, S.; Cao, Y.; Wold, E. D.; Sun, S. B.; Smider, V. V.; Schultz, P. G.; Kim, C. H. A genetically encoded aza-michael acceptor for covalent cross-linking of protein-receptor complexes. *J. Am. Chem. Soc.* **2014***, 136*, 8411-8417.
38. Xiang, Z.; Ren, H.; Hu, Y. S.; Coin, I.; Wei, J.; Cang, H.; Wang, L. Adding an unnatural covalent bond to proteins through proximity-enhanced bioreactivity. *Nat. Methods* **2013***, 10*, 885-888.
39. Cravatt, B. F.; Wright, A. T.; Kozarich, J. W. Activity-based protein profiling: From enzyme chemistry to proteomic chemistry. *Annu. Rev. Biochem.* **2008***, 77*, 383-414.
40. Xiang, Z.; Lacey, V. K.; Ren, H.; Xu, J.; Burban, D. J.; Jennings, P. A.; Wang, L. Proximity-enabled protein crosslinking through genetically encoding haloalkane unnatural amino acids. *Angew. Chem.* **2014***, 126*, 2222-2225.
41. Koshi, Y.; Nakata, E.; Miyagawa, M.; Tsukiji, S.; Ogawa, T.; Hamachi, I. Target-specific chemical acylation of lectins by ligand-tethered DMAP catalysts. *J. Am. Chem. Soc.* **2008***, 130*, 245-251.
42. Wang, H.; Koshi, Y.; Minato, D.; Nonaka, H.; Kiyonaka, S.; Mori, Y.; Tsukiji, S.; Hamachi, I. Chemical cell-surface receptor engineering using affinity-guided, multivalent organocatalysts. *J. Am. Chem. Soc.* **2011***, 133*, 12220-12228.
43. Pangborn, A. B.; Giardello, M. A.; Grubbs, R. H.; Rosen, R. K.; Timmers, F. J. Safe and convenient procedure for solvent purification. *Organometallics* **1996***, 15*, 1518-1520.

44. Still, W. C.; Kahn, M.; Mitra, A. Rapid chromatographic technique for preparative separations with moderate resolution. *J. Org. Chem.* **1978***, 43*, 2923-2925.

Chapter 3:
The Quadricyclane (QC) Ligation: Protein Labeling via Site-Specific Incorporation of a QC Amino Acid

Introduction

The scope of the current bioorthogonal toolbox does not compare to the immense repertoire of synthetic chemical reactions. This is in part because the field is so new, established only fifteen years ago. It is also because the constraints placed upon a bioorthogonal reaction are considerably more formidable than those placed on traditional organic reactions. The solvent is limited to water at physiological pH. Temperature is usually set at 37 ºC or lower. Cross-reactivity between bioorthogonal reagents and biological functionalities is not tolerated, and the ligation has to be rapid enough to proceed on the timescale of the biological process of interest. One of the reagents must be small and capable of incorporation into a target biomolecule via the organism's own biosynthetic machinery. Together, these requirements are a tall order, making the design of new bioorthogonal reactions a formidable challenge.

The four most developed and widely used bioorthogonal reactions — the Staudinger ligation, copper-click chemistry, copper-free click chemistry, and the tetrazine ligation — have proven valuable in their ability to generate covalent bonds under physiological conditions. However, there is a strong need for new bioorthogonal chemistries. This need is driven by the demands of multiplexed imaging experiments as well as the lack of chemical manipulations accessible via the current bioorthogonal repertoire.

Multiplexed imaging is any technique by which multiple components of a system are labeled and imaged simultaneously. In the context of a bioorthogonal reaction, this means using two or more bioorthogonal reactions at the same time to image two or more biomolecules in a living organism. In order for this approach to be successful, the selected bioorthogonal reactions have to be mutually orthogonal, meaning the chemical functionalities unique to each ligation do not react with each other. For the four most developed bioorthogonal reactions, this requirement is a challenge due to inherent cross-reactivity between reagents.

Figure 3.1 highlights this cross-reactivity. The Staudinger ligation, copper-click chemistry, and copper-free click chemistry all employ the azide as a bioorthogonal handle, and thus, cannot be used simultaneously. As well, the azide is known to react with strained alkenes to generate triazolines, which are considerably less stable than the triazole and can undergo various cleavage or rearrangement reactions.[1] Likewise, some cyclooctynes are known to react with tetrazines to form the adduct shown.[2,3] These cross-reactions preclude simultaneous use of multiple reactions.

Despite this lack of mutual orthogonality, there are certain conditions under which cross-reactivity can be minimized. For example, although strained alkenes and azides react with each other, the reactivity between azides and cyclopropene is minimal under conditions

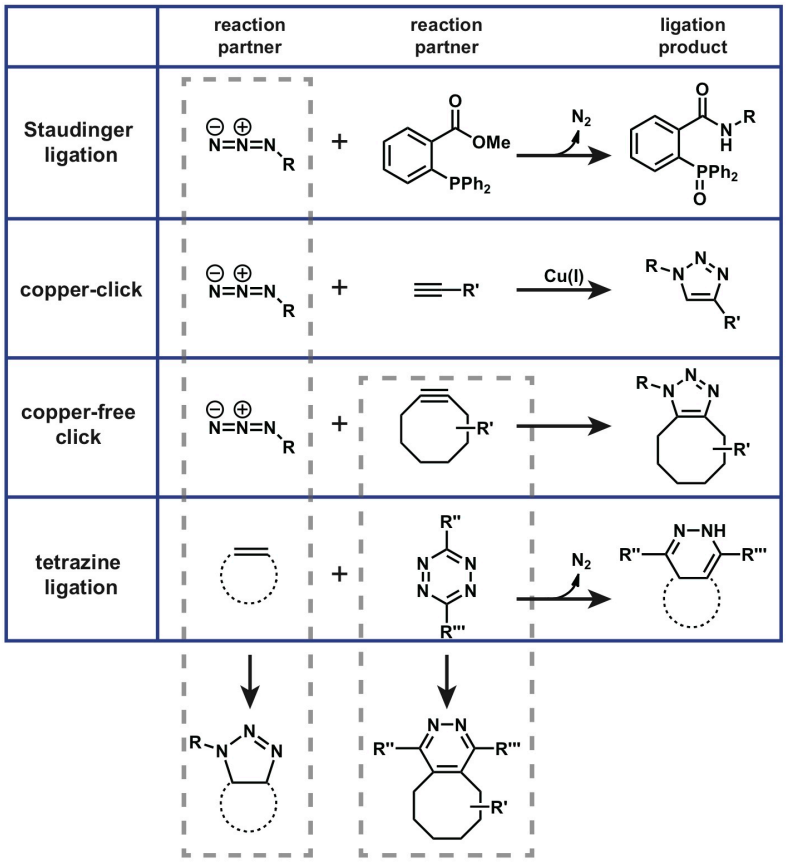


Figure 3.1. Cross-reactivity of bioorthogonal ligations. Gray dotted line surrounds components of cross-reactions.

used for bioorthogonal labeling. This has enabled simultaneous use of the tetrazine /cyclopropene reaction and copper-click chemistry.[4]

It is also possible to engineer mutual orthogonality across reactions through careful tuning of electronics or sterics (Figure 3.2). For example, Hilderbrand and co-workers used electronic modulation to engineer mutually orthogonal variants of the tetrazine ligation and copper-free click chemistry.[5] In the inverse-electron-demand Diels—Alder cycloaddition between tetrazines and dienophiles, electron poor tetrazines react faster than electron rich tetrazines.[6] Hilderbrand showed that the reaction between tetrazine **3.1** and DIBAC **3.2** proceeds with a second order rate constant of $k = 0.06 \pm 0.1$ M^{-1} s^{-1} in PBS (pH = 7.4) at 37 ºC. However, the analogous reaction with the more electron rich tetrazine **3.3** does not proceed to any appreciable extent after 48 hours under the same conditions. Hilderbrand also found that *trans*-cyclooctene (TCO) reacts rapidly with tetrazine **3.3** and roughly five orders of magnitude more slowly with the azide. Combined, these kinetic analyses enabled simultaneous use of the tetrazine ligation (**3.3** plus TCO) and copper-free click chemistry (DIBAC **3.2** plus azide) on cells with no observable cross reactivity.[5] Chin and co-workers used a similar approach to engineer orthogonality between two tetrazine ligations, each employing a unique tetrazine/dienophile pair.[7]

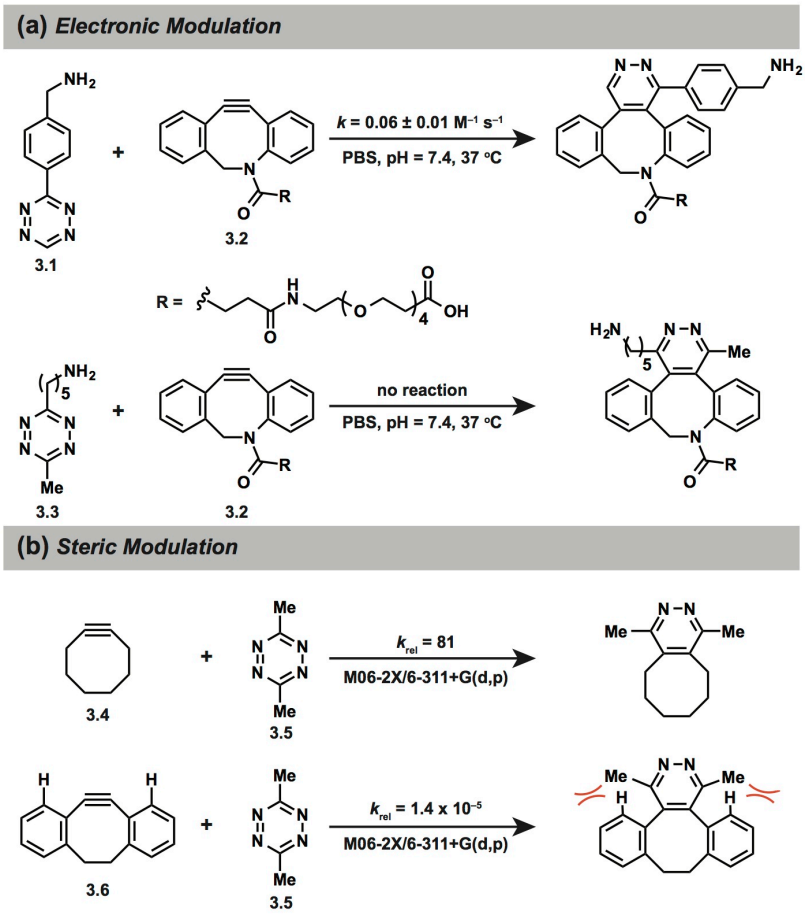


Figure 3.2. Modulating reactivity between two bioorthogonal reagents via (a) electronic or (b) steric modulation.

Steric tuning can also be used to engineer mutual orthogonality between reactions. Houk and co-workers have studied the importance of sterics in the cyclooctyne/tetrazine reaction.[3] Whereas they calculate a k_{rel} of 81 for the reaction between cyclooctyne **3.4** (Figure 3.2b) and tetrazine **3.5**, the reaction between cyclooctyne **3.6** and tetrazine **3.5** is orders of magnitude slower with a k_{rel} of 1.4 x 10^{-5}. Houk attributes this reactivity difference to the steric effects of **3.6**'s flagpole hydrogen atoms, which impede access of the bulky tetrazine to the strained alkyne as shown in Figure 3.2b. These results suggest a method for blocking reactivity between tetrazines and cyclooctynes, enabling simultaneous use of the tetrazine and copper-free click ligations. Along the same lines, Prescher and Houk used sterics to engineer various cyclopropenes with a range of reactivities toward tetrazines. In this way, they were able to use the cyclopropene/tetrazine reaction and a cyclopropene/nitrile imine reaction in the same system (though more work is required to optimize this system for use of both reactions simultaneously).[8]

From these examples, it is clear that while it is possible to engineer existing bioorthogonal reactions to achieve mutual orthogonality, this process is not trivial, and also limits the types of reagents available for use. A simpler approach would be to design

reactions that are inherently orthogonal, without the need for careful steric and electronic tuning. The need for reactions that meet the demands of this approach drive the development of new bioorthogonal reactions.

New function is the second driver of bioorthogonal reaction development. The majority of bioorthogonal reactions developed to date succeed in producing a stable, covalent bond between two entities under physiological conditions. However, among the vast functionality represented by the totality of synthetic chemical transformations, covalent bond formation represents only a fraction. For example, chemists have invented synthetic organic reactions that are reversible, stereoselective, or regioselective. They have also engineered polymerizations that afford high degrees of control over polymer structure and size. And they have developed reactions that are triggered by environmental cues (i.e. photochemistries, pH sensitive reactions, etc.). The field of bioorthgoonal chemistry has just begun to branch into these areas of new chemical functionality, and innovations in the design of unique ligations will drive this growth.

The Quadricyclane Ligation

In 2011, Sletten *et al.* proposed a new bioorthogonal reaction — the quadricyclane ligation.[9] The reaction is unique because it exploits a chemical space previously unexplored through the lens of bioorthogonality. It is a formal [2σ + 2σ + 2π] cycloaddition, proceeding between the strained hydrocarbon quadricyclane (QC, **3.7**) and nickel bis(dithiolene) (**3.8**) to form adduct **3.9** (Figure 3.3).

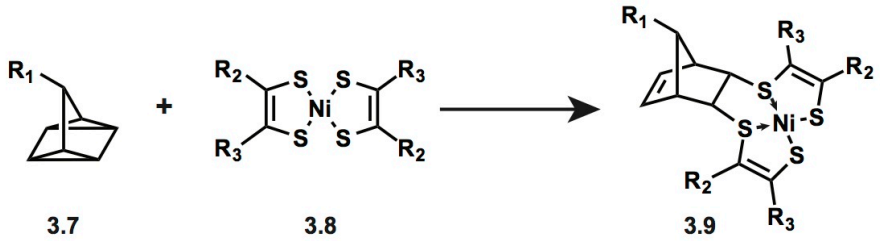


Figure 3.3. The quadricyclane (QC) ligation.

Importantly, both QC and nickel bis(dithiolene) fulfill the requirements of a bioorthogonal reagent. Quadricyclane is abiotic, and its strained, all-carbon core is unlikely to react to any appreciable extent with biological functionalities.[10,11] Sletten found that compound **3.7** (where R_1 = OAc, referred to as QCOAc throughout the rest of this chapter) is stable in PBS buffer (pH = 7.4) at room temperature for more than two months, is stable in tissue culture media, and is unreactive towards sugars, oxidants, and amino acids including cysteine.[9]

Aside from its bioorthogonality, QC also possesses a high degree of molecular strain, which is only released under the proper conditions. This "spring-loaded" energy profile fits Sharpless' original description of the ideal click chemistry reagent.[12] Empirical measurements and calculations place QC's strain energy between 79–96 kcal/mol.[13–15] Using norbornadiene, an isomer of QC, as a proxy for the product of QC's ligation with

an appropriate reagent (via [2σ + 2σ + 2π] cycloaddition), we estimate that the average strain energy released upon reaction of QC is between 21 and 24 kcal/mol, the value of $\Delta H_{isomerization}$ of QC to NBD.[13,15] This compares favorably with the magnitude of strain energy driving the reactions of cyclooctynes with 1,3-dipoles, which Krebs and Wilke have estimated at 13 kcal/mol.[16***]

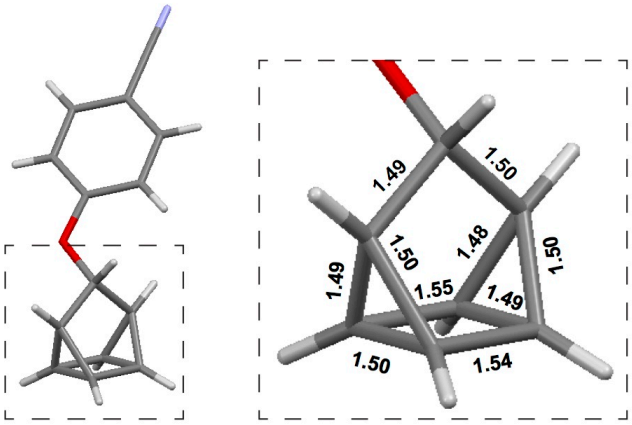


Figure 3.4. Crystal structure of QC. All bond lengths in Å.[17]

QC is also an ideal bioorthogonal reagent because it is small in size, a parameter that opens opportunities for incorporation of QC into target biomolecules as a bioorthogonal handle. Methods of installing reactive handles onto biomolecules include metabolic glycan engineering and non-natural amino acid incorporation.[18,19] The success of an incorporation technique is often a function of the size and physical properties of the reactive functional group being installed.[20–23]As well, a goal of bioorthogonal chemistry is to achieve the lowest magnitude structural perturbation to the target biomolecule as possible, thus strongly favoring small reactive handles. A crystal structure of QC is shown in Figure 3.4.[17] Its size is within the same range as that of the azide[24] and cyclooctyne,[25–27] two widely used biorthogonal reagents that have been successfully incorporated into biomolecules via various methods.

Sletten identified nickel bis(dithiolene) as an ideal reaction partner for QC after a large screen of potential reagents.[9] Metal dithiolenes are an interesting class of organometallic compound because their dithiolene ligands display a property known as redox non-innocence.[28] This means that the molecular orbitals responsible for redox reactions on the metal and ligand are similar in energy, enabling the ligand to participate in these reactions. In the case of the QC ligation, the dithiolene ligands in the nickel bis(dithiolene) complex react with QC to form a covalent bond as shown in Figure 3.3.

*** Krebs and Wilke used "angle strain" as a measure of the overall molecular strain resulting from deformation of the alkyne bond in cyclooctyne. They defined angle strain by the following equation [Angle strain = ($\Delta H_{hydrogenation\ cyclooctyne} - \Delta H_{hydrogenation\ cyclooctene}$) − ($\Delta H_{hydrogenation\ octyne} - \Delta H_{hydrogenation\ octene}$)] where $\Delta H_{hydrogenation\ cyclooctyne}$ is the heat of hydrogenation of cyclooctyne to *cis*-cyclooctene, $\Delta H_{hydrogenation\ cyclooctene}$ is the heat of hydrogenation of *cis*- cyclooctene to cyclooctane, $\Delta H_{hydrogenation\ octyne}$ is the heat of hydrogenation of a correspondingly substituted linear octyne to linear *cis*-octene, and $\Delta H_{hydrogenation\ octene}$ is the heat of hydrogenation of the linear *cis*-octene to octane. Using this equation, they calculated the angle strain of unsubstituted cyclooctyne to be ~13 kcal/mol. See reference 16.

Often, it is challenging to assign an oxidation state to a metal that is bound to non-innocent ligands, as is the case for nickel bis(dithiolene).[28] Figure 3.5 shows the compound's various resonance structures and corresponding metal oxidation states.[29]

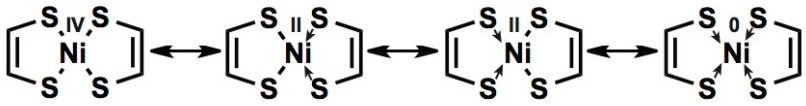


Figure 3.5. The redox non-innocence of nickel bis(dithiolene) ligands.

In addition to its unique, ligand based reactivity toward QC, nickel bis(dithiolene) possesses many of the qualities of a bioorthogonal reagent. Sletten identified compound **3.10** (Figure 3.6) as the ideal incarnation of the reagent after testing many ligand variants.[9]

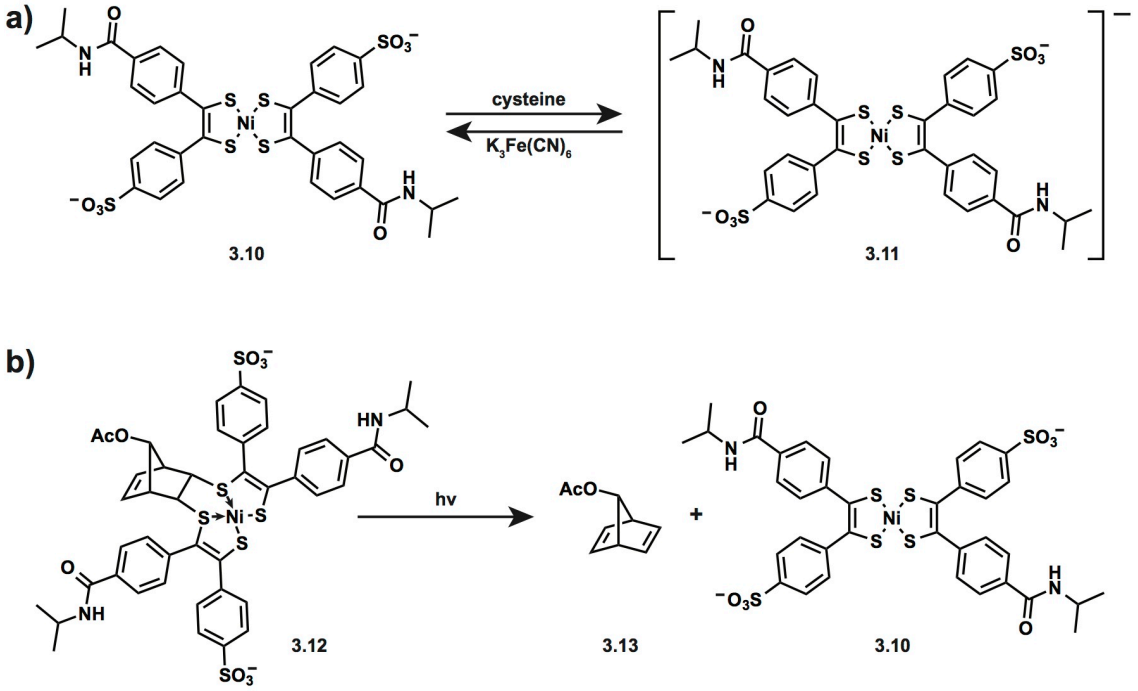


Figure 3.6. Stability of nickel bis(dithiolene) and its adduct with QC. (a) Nickel bis(dithiolene) **3.10** is reduced to anion **3.11** in the presence of cysteine. **3.11** is oxidized to **3.10** with $K_3Fe(CN)_6$. (b) Adduct **3.12** cleaves to form norbornadiene **3.13** and nickel bis(dithiolene) **3.10** in ambient light.

3.10's sulfonated ligands enhance its aqueous solubility, and its amide groups provide convenient handles for appending affinity probes or fluorophores. **3.10** reacts with QCOAc with a second order rate constant of $k = 0.25 \pm 0.05$ M^{-1} s^{-1} in 1:1 PBS:EtOH at room temperature – on par with rates of widely used cyclootyne/azide bioorthogonal reactions. As for **3.10**'s amenability to biological environments, it persists in PBS for up to 20 hours and is stable to amino acids with the exception of cysteine, which causes immediate reduction of the neutral nickel bis(dithiolene) complex to its anion **3.11**.[9,30] **3.11** is not reactive toward QC, making reduction of **3.10** in the presence of free sulfhydryl groups a serious liability. To overcome this challenge, Sletten used

$K_3Fe(CN)_6$, capable of oxidizing **3.11** to **3.10** in aqueous solution, as an additive in biological labeling experiments.[31,32†††]

The product of the reaction between nickel bis(dithiolene) and QCOAc (**3.12**) is photosensitive, cleaving to form **3.10** and norbornadiene **3.13** (Figure 3.6b) with a half life of ~35 hours in ambient light.[9] Sodium diethyldithiocarbamate (Na-DEDTC) is added to QC ligation treated biological samples following the reaction to prevent photoreversion.[‡‡‡9] The mechanism through which photoreversion is inhibited by Na-DEDTC has not been elucidated.

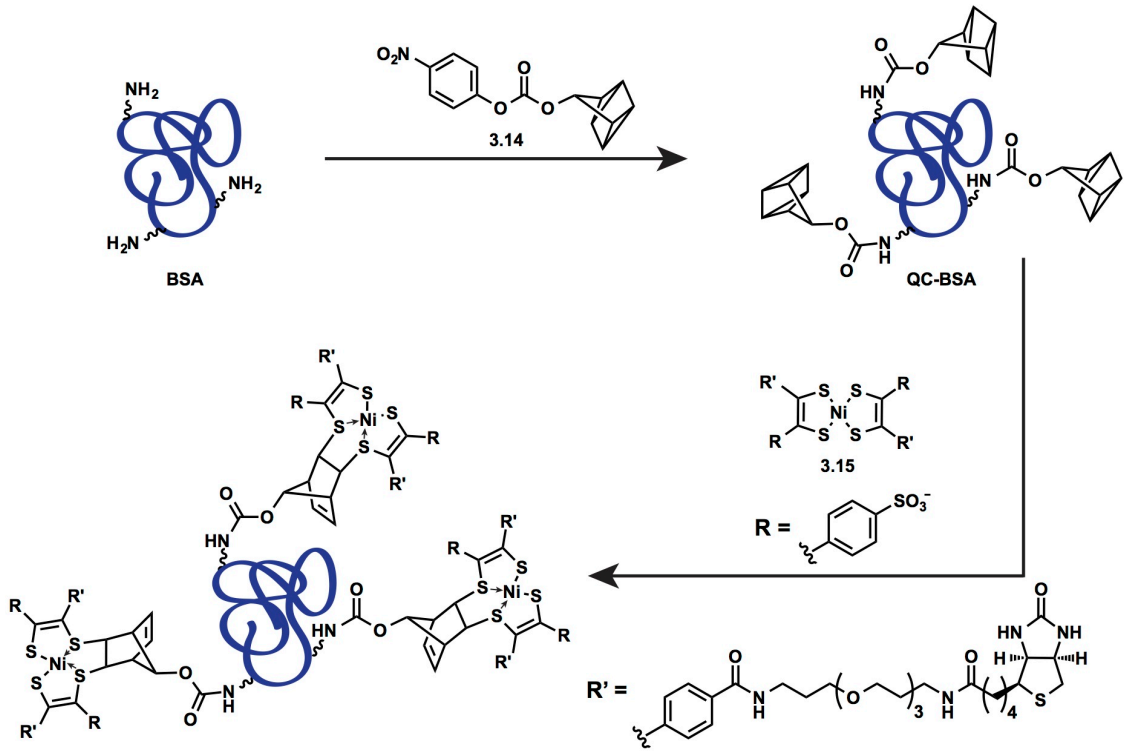


Figure 3.7. Model QC labeling experiments on Bovine Serum Albumin (BSA). Lysines on BSA were capped with *p*-nitrophenyl carbonate QC **3.14** to form QC-BSA. QC-BSA was subsequently combined with Ni bis(dithiolene) **3.15** to generate biotin-labeled BSA.

††† The known toxicity of $K_3Fe(CN)_6$ to biological systems is a challenge of this approach. Lai and co-workers reported less than 40% cell survival after CHO cells were incubated for 30 min with 100 mM $K_3Fe(CN)_6$ at 37 ºC. Similarly, Dowden and co-workers found that the median tolerance limit (the concentration of a chemical that is lethal to 50% of test animals) of $K_3Fe(CN)_6$ to *Daphnia magna* is ~2.8 mM over the course of 24 hours. Although we use $K_3Fe(CN)_6$ at lower concentrations and for less time (1 mM in PBS for ~1 h), we have not yet conducted a thorough study of its toxicity under QC-ligation labeling conditions. However, preliminary experiments in which the QC ligation was performed on Jurkat cells in the presence of 125 or 500 μM $K_3Fe(CN)_6$ for 1 h followed by washing 3x with 3.8 mM Na-DEDTC in PBS supplemented with 1% FBS showed ~90% cell survival at the end of the experiment. Cell survival was determined by 7-aminoactinomycin D staining and flow cytometry analysis (data not shown). See references 31 and 32.

‡‡‡ Similar to the $K_3Fe(CN)_6$ additive, Na-DEDTC may reduce the bioorthogonality of the QC ligation. We have not performed a thorough analysis of Na-DEDTC toxicity, however, preliminary studies in which the QC ligation was performed on Jurkat cells followed by washing 3x with 3.8 mM Na-DEDTC in PBS supplemented with 1% FBS resulted in 79–92% cell survival at the end of the experiment.

Sletten has shown that the QC ligation is capable of labeling a model QC-containing protein under physiological conditions.[9] QC-conjugated bovine serum albumin (BSA) was prepared by capping BSA lysines with *p*-nitrophenyl carbonate **3.14** (Figure 3.7). The resulting QC-BSA underwent selective ligation with nickel bis(dithiolene) biotin **3.15**, and the adduct was detected by Western blot with only minimal labeling of the minus QC control. Sletten also showed that the QC ligation fulfills one of the key motivations of bioorthogonal ligation development — mutual orthogonality to aldehyde/aminooxy chemistry and the copper-free click reaction — by using both reactions simultaneously with the QC ligation to label proteins.[9]

Site-Selective Incorporation of QC Into a Protein

The properties of the QC ligation make it an ideal bioorthogonal reaction. Sletten's development of this chemistry via optimization on a model protein set the stage for its future use in biological systems. However, installing QC onto proteins via global capping of lysines is an inherently non-specific approach. In more complex systems, the technique affords no target-selectivity and will tag all available lysine-containing substrates with the QC handle. This precludes use of the chemistry for visualization of a target protein in a living system. At the level of a single protein, the lysine-capping technique is not site-selective, generating a heterogeneous population of proteins with varying degrees of QC modification. Such heterogeneity is a challenge for many applications of bioconjugation chemistries such as development of antibody drug conjugates.[33]

To overcome this challenge, we worked to develop a system capable of site-selectively installing a QC-modified non-natural amino acid into a target protein. Non-natural amino acid (nnaa) incorporation is a commonly used method of installing a bioorthogonal handle into a protein of interest. The method is valuable because rather than relying on global modification of lysine or cysteine residues, it enables more control over the location and number of modifications.

There are two approaches to achieving incorporation of a nnaa into a protein of interest. One method, referred to as the residue-specific approach, relies on the ability of various aminoacyl tRNA synthetases, the enzymes that charge tRNAs with corresponding amino acids, to accept minor structural perturbations to their naturally occurring substrates.[34] By using bacterial strains that are auxotrophic for a given amino acid and supplementing cultures with a nnaa analog, one can achieve global replacement of the natural substrate with the nnaa. However, one major disadvantage of the residue-specific method is its lack of protein- and site-specificity.

An alternative site-specific method hijacks the amber stop codon, reengineering it to code for a nnaa in a target protein. Early versions of the site-specific approach relied on synthetic acylation of a suppressor tRNA (anticodon complementary to the amber stop codon) with the nnaa followed by protein expression *in vitro*[35,36] or in xenopus oocytes.[37] Later advancements enabled *in vivo* expression of nnaa modified proteins. In 2001, Schultz and co-workers engineered bacteria to express a mutant synthetase that recognizes a target nnaa and its complementary suppressor tRNA.[38] Specifically, the

tyrosyl tRNA/synthetase pair from the archaea *Methanococcus jannaschii* was engineered to selectively charge a suppressor tRNA with a non-natural amino acid in *E. coli*.[38] The charged tRNA then installs the nnaa into a growing peptide chain in response to an in-frame amber stop codon. The selectivity of the engineered synthetase for the nnaa and suppressor tRNA was achieved by synthetase evolution through numerous rounds of positive and negative selection The technique has since been used to develop tRNA/synthetase pairs for use in yeast[39] and mammalian cells.[40] Though more challenging to engineer than the residue-specific method, the site-specific method of nnaa incorporation provides more control over product structure, introducing only one amino acid analog into a specific protein of interest at a predetermined site.

An important requirement of the site-selective method is that both the synthetase and suppressor tRNA used in the experiment need to be orthogonal to the system under study.[19] An orthogonal synthetase only recognizes the target nnaa and does not recognize any of the proteinogenic amino acids. Additionally, the synthetase is only capable of charging the suppressor tRNA, and not any of the naturally occurring tRNAs. An orthogonal suppressor tRNA is not recognized by any of the naturally occurring synthetases in the system, and possesses a unique anti-codon selective for a blank codon such as the amber stop. The orthogonality of the tRNA/synthetase pair ensures that the nnaa, and no other amino acid, is incorporated at the amber codon. As well, orthogonality guarantees that the non-natural amino acid will not be installed in response to any of the sense codons, enabling exquisite homogeneity in expression products.

Orthogonality is a tall order and often requires use of a tRNA/sythetase pair that is heterologous to the organism under study. Across organisms, the structure and specificity of tRNAs and synthetases vary, thus providing a basis for orthogonality in a heterologous host.[19] Subsequent evolution of an imported synthetase enables specificity for the target nnaa. This heterologous approach formed the basis of Schultz's design of the tyrosyl synthetase/tRNA pair from *Methanococcus* for use in *E. coli*,[38] and design of the *E. coli* tyrosyl synthetase/tRNA pair for use in eukaryotic cells.[39]

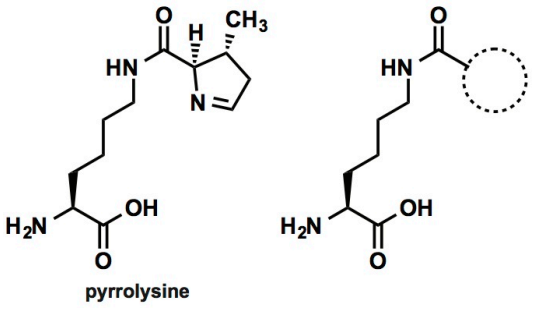


Figure 3.8. Pyrrolysine and analogs. Pyrrolysine synthetase (PylRS) accepts structural analogs of the natural pyrrolysine substrate.

Despite the success of this approach to accessing orthogonality, it does have some liabilities. For example, protein evolution in mammalian cells is inherently challenging. [41] Thus, to engineer an orthogonal synthetase for nnaa incorporation in mammalian cells,

protein evolution of a bacterial tRNA/synthetase pair must be performed in yeast.[38,41] As well, the heterologous approach precludes use of the same optimized tRNA/synthetase pair in both eukaryotes and bacteria because pairs that are evolved to be orthogonal in one type of organism are often not orthogonal in the other.[19]

To overcome these challenges one can start with a tRNA/synthetase pair that is unique to both prokaryotes and eukaryotes. The pyrrolysine synthetase/tRNA pair fulfills this need. Pyrrolysine (Figure 3.8) is the 22nd proteinogenic amino acid. It was first identified by Krzycki and co-workers in *Methanosarchina barkeri*, a species of methanogen within the archaea domain.[42] In 1998, Krzycki noticed a single in-frame amber stop codon in an *M. barkeri* gene encoding a monomethylamine methytransferase enzyme,[42] and later confirmed that it is translated as a sense codon. [43] X-ray crystallography revealed the structure of the amber-encoded amino acid as pyrrolysine (Figure 3.8),[44] and later studies identified a unique pyrrolysine tRNA with an anticodon complementary to the amber stop codon ($tRNA_{CUA}$)[45] as well as a dedicated pyrrolysine aminoacyl tRNA synthetase (PylRS) endogenous to the archaea.[46,47]

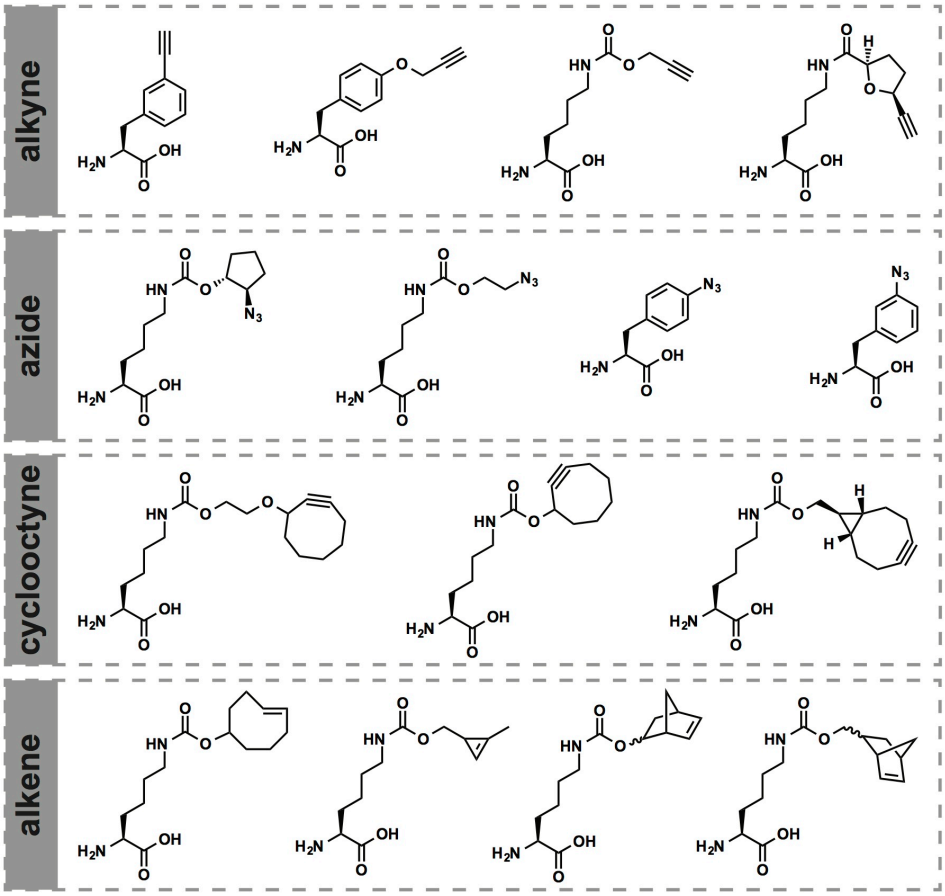


Figure 3.9. Selected non-natural amino acids incorporated into proteins via the pyrrolysine synthetase/$tRNA_{CUA}$ system. The PylRS/$tRNA_{CUA}$ system has been used to incorporate terminal alkynes, azides, cyclooctynes, and strained alkenes into proteins site-specifically.[4,25,27,48–56]

In many ways, the system is ideal for use as a method of non-natural amino acid incorporation. The pyrrolysine synthetase uniquely recognizes an amber suppressor tRNA and an amino acid that is not found in most organisms.

It was later shown that the PylRS/$tRNA_{CUA}$ pair is orthogonal[57] in both *E. coli*[47] and mammalian cells,[58,59] meaning that the same synthetase/tRNA pair can be used across organisms.[19] Most importantly, PylRS is known to accept structural variants of the pyrrolysine substrate (Figure 3.8), enabling ready incorporation of non-natural amino acids.[21]

Since its discovery, the PylRS/$tRNA_{CUA}$ system has been used to incorporate myriad bioorthgonal handles into *E. coli*,[19,50,54] yeast,[60] mammalian cells,[19,54] *Caenorhabditis elegans*,[61] and *Drosophila melanogaster*.[62] Figure 3.9 shows the structures of select nnaas used in these experiments. Some were installed via the wildtype PylRS, whereas others were installed via a mutated form of the synthetase.

In 2012, Chin and co-workers showed that a norbornadiene-functionalized amino acid can be incorporated into a protein using the PylRS/$tRNA_{CUA}$ system without any active site modification to the wildtype synthetase.[54] Given the structural similarity between norbornadiene and QC, we hypothesized that the same system could be used to site-specifically install a QC-functionalized amino acid into a protein of interest.

Components of a QC Amino Acid Incorporation Experiment

There are a number of inputs required to achieve incorporation of a nnaa into a protein of interest. These inputs, highlighted in Figure 3.10, include plasmids encoding PylRS, $tRNA_{CUA}$, and a protein of interest with an in-frame amber stop codon at an appropriate modification site. Also required is a nnaa containing a bioorthogonal handle.

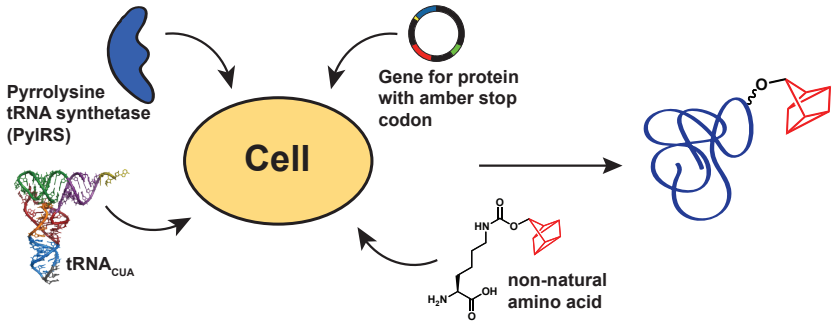


Figure 3.10. Components of a non-natural amino acid incorporation experiment.

We obtained all of the required genes via a collaboration with the Chin lab at the Medical Research Council in Cambridge UK. They provided plasmid *psfGFP150TAGHis$_6$PylT* with a gene encoding a C-terminal His_6-tagged superfolder GFP (sfGFP) with an in-frame amber stop codon at position 150 as well as a gene encoding $tRNA_{CUA}$ (Figure 3.11). In *psfGFP150TAGHis$_6$PylT*, sfGFP expression is regulated by the arabinose operon (AraC), $tRNA_{CUA}$ (PylT) expression is initiated by the LPP promoter, and

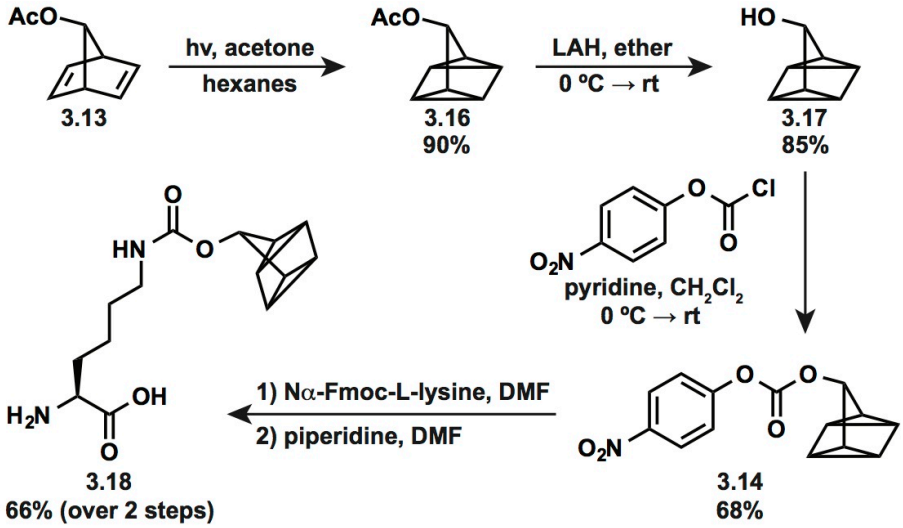
selection of transformed bacteria is achieved by a tetracycline resistance gene (TetR). Chin and co-workers also provided plasmid *pBKPylT*, which encodes the pyrrolysine synthetase PylRS from *Methanosarcina barkeri* as well as a kanamycin resistance gene.



Figure 3.11. Plasmid *psfGFP150TAGHis$_6$PylT*.

With the required genes in hand, we moved on to synthesize a QC-modified amino acid. We designed target QC amino acid (QCaa, **3.18**, Scheme 3.1) based on its accessibility from known intermediate **3.14** and its structural similarity to the norbornene amino acid successfully incorporated by Chin and co-workers using the same PylRS/tRNA$_{CUA}$ system. Intermediate *para*-nitrophenyl carbonate **3.14** was synthesized as reported by Sletten *et al.*[9] In contrast to accepted strategies of cyclooctyne construction in which strain is installed at a late stage, the strained QC moiety in intermediate **3.14** is formed early in its synthesis, underscoring QC's stability toward a wide variety of conditions. Norbornadiene acetate **3.13**, formed from commercially available *tert*-butoxy norbornadiene, underwent a photo [2+2] reaction to generate QCOAc **3.16**. Reduction of **3.16** to form the corresponding alcohol was followed by careful removal of reaction solvent and ethanol byproduct through fractional distillation on a kugelrohr.

Scheme 3.1. Synthesis of QCaa 3.18.



Alcohol **3.17** was then activated by reaction with *para*-nitrophenyl chloroformate to form *p*-nitrophenyl QC carbonate **3.14**. Removal of all excess ethanol in the previous reduction step was essential to avoid formation of inseparable by-product *p*-nitrophenyl ethyl carbonate. Upon isolation, **3.14** was conjugated to Nα-Fmoc-L-lysine to form Fmoc-QCaa. Piperidine deprotection followed by trituration afforded pure QCaa **3.18**.

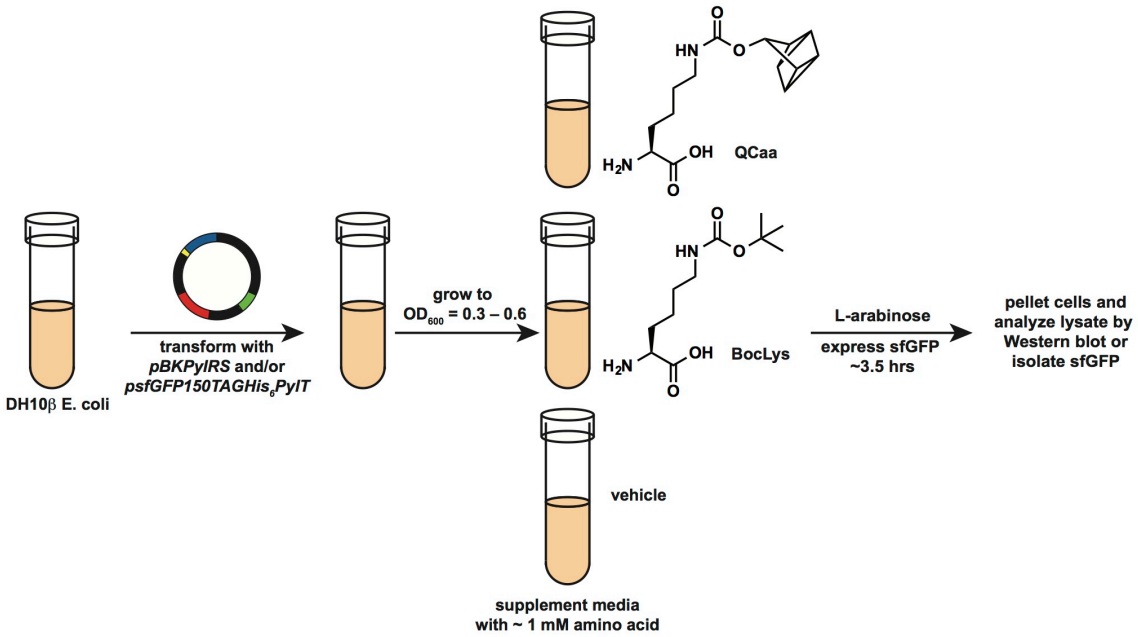
With all components of the nnaa incorporation experiment in hand, we set out to express QCaa-containing sfGFP (QC-sfGFP) in *E. coli.*

QC-sfGFP Expression

Scheme 3.2 shows the experimental procedure of our QCaa incorporation experiments. DH10β *E. coli* were transformed with *pBKPylRS* and *psfGFP150TAGHis$_6$PylT* (+RS+T) or with *pBKPylRS* only (+RS–T). Cells were grown to OD_{600} 0.3-0.6 at which point cultures were supplemented with approximately 1 mM QCaa, 1 mM Nε-Boc-L-lysine (BocLys, Scheme 3.2), or vehicle (for these experiments, vehicle is the solvent in which nnaas are dissolved for subsequent addition to *E. coli* cultures). BocLys is a known substrate of wildtype PylRS, and served as a positive control in this study. *E. coli* were incubated with the amino acids for 30 minutes at which point protein expression was induced via addition of L-arabinose. Protein was expressed for 3.5 hours, cells were pelleted, resuspended in SDS loading buffer with 2.5% β-mercaptoethanol and subjected to sodium dodecyl sulfate polyacrylamide gel electrophoresis (SDS-PAGE). Proteins were then transferred to nitrocellulose and analyzed via Western blot for the presence of full-length sfGFP-His_6 with an α-GFP antibody.

We expected to see production of full-length sfGFP-His_6 only in samples treated with QCaa or BocLys and transformed with the gene encoding PylRS. Without addition of QCaa or BocLys, PylRS is not able to charge $tRNA_{CUA}$ with an amino acid (assuming PylRS orthogonality), and translation of sfGFP-His_6 terminates at the amber stop codon.

Scheme 3.2. Incorporation of QCaa into sfGFP in DH10β *E. coli*.



Likewise, because $tRNA_{CUA}$ cannot be charged by endogenous synthetases (assuming $tRNA_{CUA}$ orthogonality), translation cannot proceed past the amber codon if the gene for PylRS is not introduced.

Results are shown in Figure 3.12. For bacteria transformed with both plasmids (+RS+T), a dark band is visible at ~28 kDa in the + QCaa (Q) and + Boc-lys (B) lanes whereas only a faint band is apparent in the minus amino acid (–) lane. This band represents full-length sfGFP-His_6, and its presence in the QCaa and BocLys lanes suggests that an amino acid has been incorporated at the amber site in both of these samples. The comparative faintness of the ~28 kDa band in the +RS+T, minus amino acid lane is evidence that the majority of full-length sfGFP in the Q and B lanes is a result of incorporation of QCaa and BocLys at the amber site. Taken together, these results suggest that QCaa is accepted by wild type PylRS and incorporated site-specifically into proteins via the PylRS/$tRNA_{CUA}$ system. Full-length sfGFP production in the minus amino acid samples may be caused by mis-acylation of $tRNA_{CUA}$ with endogenous amino acids by either PylRS or endogenous synthetases.

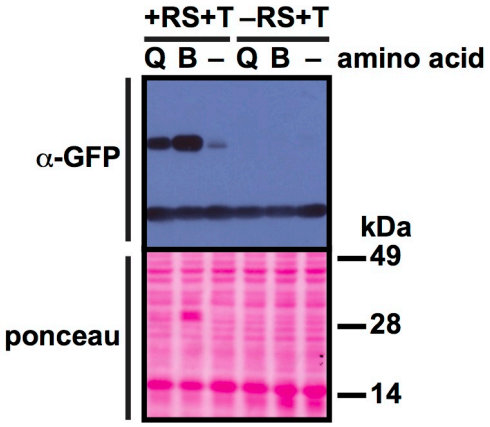


Figure 3.12. QC-sfGFP-His_6 expression. DH10β *E. coli* were transformed with *pBKPylRS* and *pfsGFP150TAGHis$_6$PylT* (+RS+T) or with just *pfsGFP150TAG His$_6$PylT* (–RS+T) and cultures were supplemented with QCaa[§§§] in 0.1 M NaOH ddH_2O to ~1 mM (Q), Boc-lysine in 0.1 M NaOH ddH_2O to ~1 mM (B), or vehicle (0.1 M NaOH ddH_2O, –) and sfGFP was expressed for 3.5 hours. Protein expression was analyzed by Western blot with an α-GFP antibody.

As expected, *E. coli* that were not transformed with the gene for PylRS (–RS+T) did not generate full length sfGFP-His_6, suggesting that PylRS is necessary for read-through of the amber stop codon. The absence of full length sfGFP in the minus amino acid, –RS+T lane is evidence that PylRS is necessary for the low level incorporation of endogenous amino acid observed in the minus amino acid, +RS+T lane.

[§§§] The solubility of QCaa is limited in most solvents. After rigorous screens of solvent conditions, we identified 0.1 mM NaOH in ddH_2O as the optimal solvent. However, even under these conditions, solubility of QCaa in the stock solution was not complete. Thus, it is likely that the 1 mM concentration reported here is slightly higher than the true concentration of QCaa in solution.

The lower band at ~14 kDa present in all samples represents amber termination product. This is a common byproduct of non-natural amino acid incorporation experiments as the amber codon still acts as a stop codon and is recognized by release factors such as RF1 in *E. coli*, causing termination of translation.[63] A number of solutions to this challenge are under development in other labs, including design of orthogonal ribosomes and global deletion of RF1.[64]

We further characterized full length QC-sfGFP-His_6 and Boc-sfGFP-His_6 and also confirmed the identity of the amber termination product via high-resolution mass spectrometry (Figure 3.13).[****]

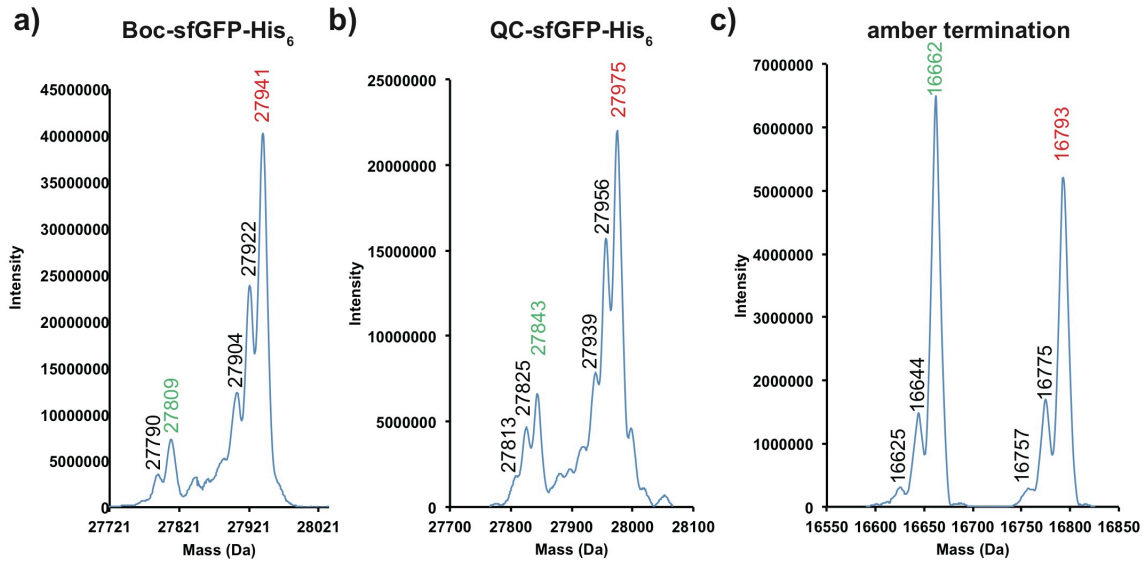


Figure 3.13. High-resolution mass spectrometry analysis of non-natural amino acid incorporation products. Red numbers represent the mass of full-length protein and green numbers represent the mass of full-length protein minus methionine. (a) Purified Boc-sfGFP-His_6: calculated mass: 27941.5 Daltons. (b) Purified QC-sfGFP-His_6: calculated mass: 27975.5 Daltons. (c) Purified amber termination product isolated from bacteria expressing QC-sfGFP-His_6: calculated mass: 16794.04 Daltons.

Labeling QC-sfGFP-His_6 via the Quadricyclane Ligation

After confirming the presence of QCaa in sfGFP-His_6, we sought to label the QC handle with nickel bis(dithiolene) biotin **3.19**. As shown in Figure 3.14, our first labeling experiment was performed on purified protein. QC-sfGFP-His_6 or Boc-sfGFP-His_6 was incubated for 1 h with 200 μM **3.19** in 1mM $K_3Fe(CN)_6$ in PBS or with vehicle (1 mM $K_3Fe(CN)_6$ in PBS). Samples were kept in the dark for the duration of labeling to avoid the photocleavage reaction shown in Figure 3.6b. After 1 h, the reaction was quenched

[****] The HRMS data do not enable us to distinguish norbornadiene from QC. Therefore, we cannot exclude the possibility that QC on the QCaa has undergone isomerization over the course of its metabolic incorporation into the sfGFP via PylRS and $tRNA_{CUA}$.

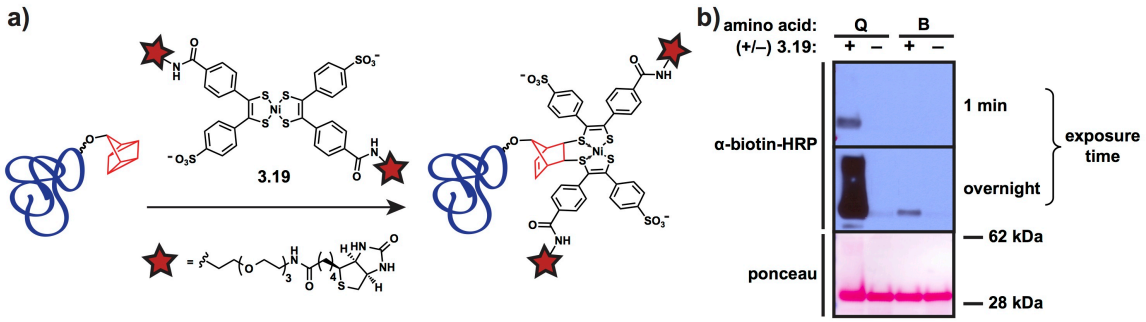


Figure 3.14. Labeling QC-sfGFP-His$_6$ via the quadricyclane ligation. (a) Schematic of labeling experiment. (b) Purified QC-sfGFP-His$_6$ (Q) or purified Boc-sfGFP-His$_6$ (B) was incubated with 200 μM **3.19** in PBS with 1 mM $K_3Fe(CN)_6$ (+ **3.19**) or with 1 mM $K_3Fe(CN)_6$ in PBS (– **3.19**) for 1 h at rt in the dark. The reaction was quenched with 100 equiv. QCOAc (relative to **3.19**) followed by 100 equiv. Na-DEDTC. Protein was analyzed by Western blot with an α-biotin-HRP antibody. The top image represents a 1 min exposure of film to the blot, the middle image represents an overnight exposure, and the bottom image is the ponceau stained blot to show equal protein loading.

with QCOAc followed by addition of Na-DEDTC. Ligation product was analyzed by Western blot with an α-biotin-horseradish peroxidase (HRP) antibody.

Results indicate robust labeling of QC-sfGFP-His$_6$ in the presence of **3.19**, with minimal labeling of the Boc-sfGFP-His$_6$ negative control. Even after overnight exposure of the Western blot, minimal signal is seen in the **3.19**-treated Boc-sfGFP-His$_6$ lane. These data suggest selective reaction of the QCaa in sfGFP with **3.19** and minimal side reactivity of **3.19** with other amino acids in sfGFP.

We next sought to achieve selective labeling of QC-sfGFP-His$_6$ in the more complex environment of bacterial lysate. For this experiment, we doped varying amounts of QC-sfGFP-His$_6$ or Boc-sfGFP-His$_6$ into 10 μg samples of bacterial lysate (Figure 3.15). Each sample was then incubated with 200 μM Ni bis(dithiolene) biotin **3.19** in 1mM $K_3Fe(CN)_6$ in PBS for 1 h 15 min at rt. Again, samples were kept in the dark for the duration of labeling. After 1 h, the reaction was quenched with QCOAc and Na-DEDTC. Samples were analyzed by Western blot and the presence of biotin was probed with an α-biotin-HRP antibody.

Results are shown in Figure 3.15, where the top blot was exposed to film for 5 seconds and the center blot was exposed for 30 seconds. In the top blot, it is clear that QC-sfGFP-His$_6$ is selectively labeled in the presence of complex cell lysate when present at high concentrations (5.0 or 2.0 μg added to 10.0 μg lysate or 33% and 13% of total protein). However, at lower concentrations of QC-sfGFP-His$_6$, labeling is less evident. As well, Boc-sfGFP-His$_6$ samples show minor labeling at the highest concentrations (5.0 or 2.0 μg), suggesting occurrence of background labeling on sfGFP-His$_6$. In a 30 second exposure of Western blot to film (center blot), background labeling on lysate protein is evident. Thus, while it is clear that we have achieved labeling of QC-sfGFP-His$_6$ in the presence of bacterial lysate, it is also clear that background reactivity, both on Boc-GFP-His$_6$ as well as on lysate, is a liability of the QC ligation.

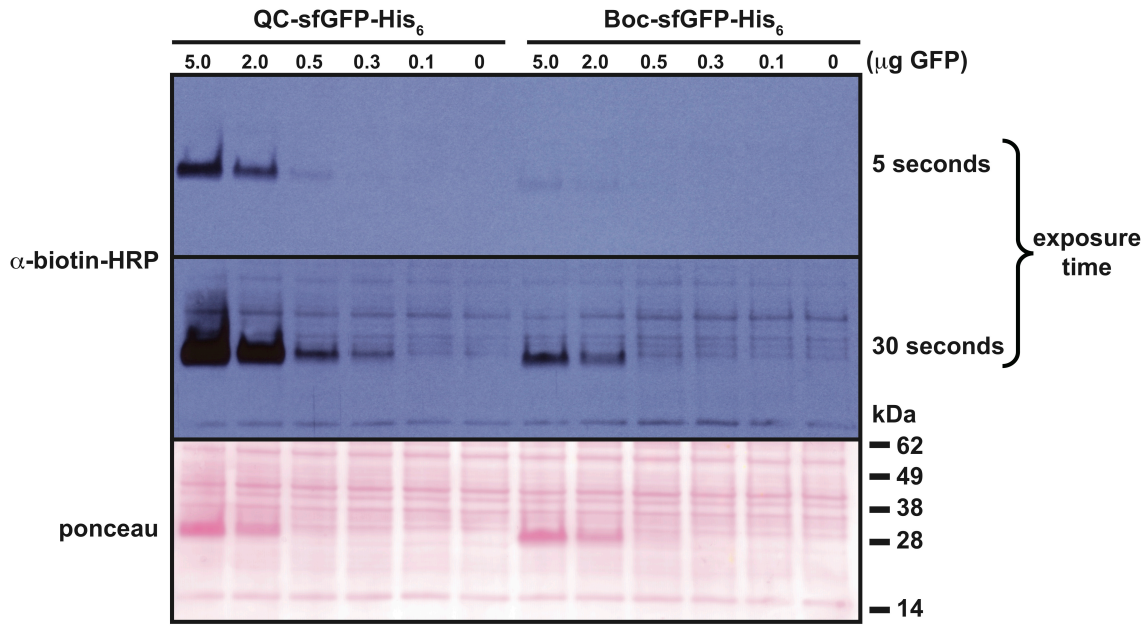


Figure 3.15. Labeling QC-sfGFP-His$_6$ in *E. coli* lysate via the QC ligation. Various quantities of purified QC-sfGFP-His$_6$ or Boc-sfGFP-His$_6$ (5.0, 2.0, 0.5, 0.3, 0.1, or 0 μg) were added to 10.0 μg bacterial lysate. The mixture was incubated with 200 μM **3.19** in 1 mM $K_3Fe(CN)_6$ in PBS for 1 h 15 min at rt an quenched via addition of 100 equiv. QCOAc (relative to **3.19**) and 100 equiv. Na-DEDTC. 87% of each reaction mixture was loaded onto an SDS-PAGE gel, proteins were separated by electrophoresis, and the gels were further analyzed via Western blot with an α-biotin-HRP antibody. Top blot represents a 5 second exposure time, middle blot is a 30 second exposure time, and bottom blot is ponceau stained to show equal loading.

Eliminating the His$_6$ Tag

In addressing the background reactivity of **3.19** with Boc-sfGFP-His$_6$, we hypothesized that the protein's hexahistidine purification handle may be interfering with the reactivity of nickel bis(dithiolene) **3.19**. Hexahistidine is a six amino acid tag designed to bind Ni-NTA, and is commonly used as a purification handle.[65,66] Given His$_6$'s propensity to bind Ni^{+2} species, it is possible that it is also capable of binding the nickel bis(dithiolene) reagent, and/or displacing the dithiolene ligands. His$_6$-nickel bis(dithiolene) binding would create background signal in any His$_6$-labeled protein, whereas ligand displacement could lead to subsequent reaction of the free dithiolate with biological functionalities.

To test this hypothesis, we designed and constructed plasmid *psfGFP150TAGFLAGPylT* (see Materials and Methods section) in which the His$_6$ tag on sfGFP is converted to a FLAG tag. FLAG is an eight amino acid peptide tag (DYKDDDDK) that tightly binds the α-FLAG antibody. Similar to His$_6$, it is used for protein purification with α-FLAG functionalized resins. However, unlike His$_6$, it is not known to bind nickel species.

QC-sfGFP-FLAG was expressed via the procedure shown in Scheme 3.2 and cell lysate was analyzed by Western blot with an α-GFP and α-FLAG antibody (Figure 3.16a). Similar to the His$_6$-tagged variant, results suggest PylRS- and nnaa-dependent production

of full-length sfGFP-FLAG. The presence of QCaa in QC-sfGFP-FLAG was confirmed by HRMS (Figure 3.16b).

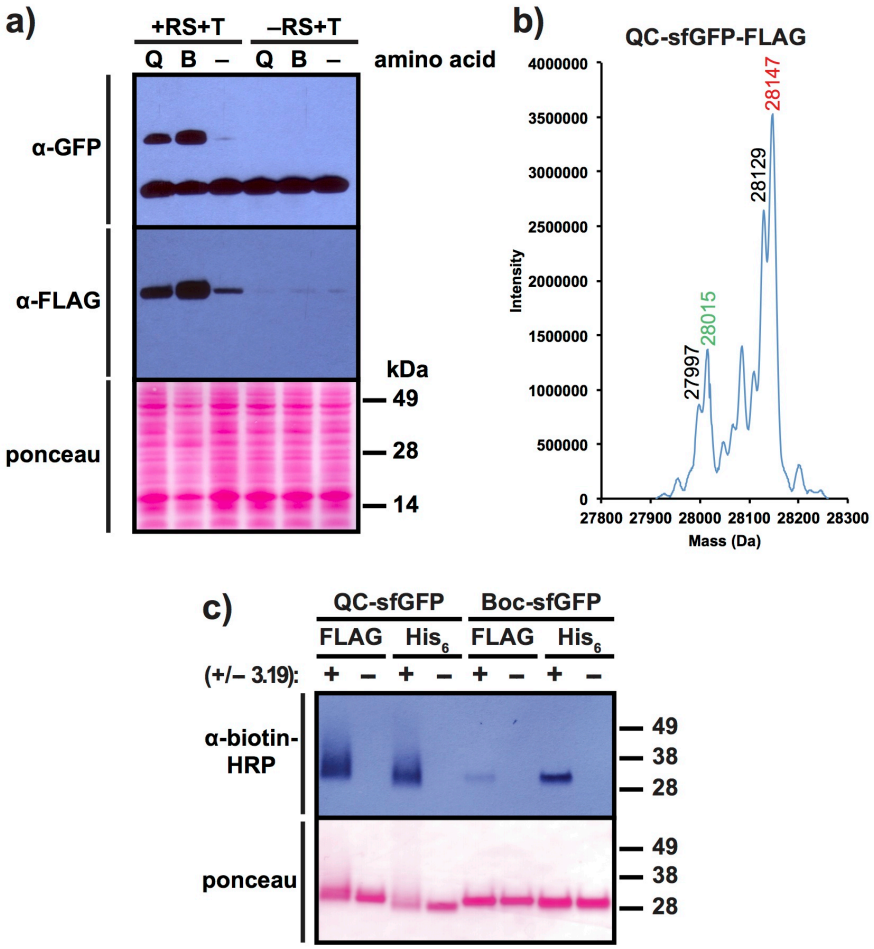


Figure 3.16. FLAG versus His_6 tag on sfGFP. (a) Expression of full-length sfGFP-FLAG in the presence of QCaa or BocLys. *E. coli* were transformed with *pBKPylRS* and *pfsGFP150TAGFLAGPylT*(+RS+T) or with just *pfsGFP150TAGFLAGPylT* (–RS+T) and cultures were supplemented with 1 mM QCaa†††† (Q), Boc-lysine (B), or vehicle. Protein was expressed for 3.5 hours after which, lysate was analyzed by Western blot probing with α-GFP and α-FLAG antibodies. (b) High-resolution mass spectrometry analysis of purified QC-sfGFP-FLAG. Red number represents the full-length mass of the protein and the green number represents the full-length mass minus methionine. QC-sfGFP-FLAG calculated mass: 28147.61 Daltons. (c) Comparison of labeling efficiency and background reactivity on FLAG- vs. His_6-tagged sfGFP. Purified QC-sfGFP-FLAG, QC-sfGFP-His_6, Boc-sfGFP-FLAG, or Boc-sfGFP-His_6 was incubated with 200 μM **3.19** in 1 mM $K_3Fe(CN)_6$ in PBS (+ **3.19**) or 1 mM $K_3Fe(CN)_6$ in PBS (– **3.19**) for 1 h 45 min at which point reactions were quenched via addition of 100 equiv. QCOAc (relative to **3.19**) and 100 equiv. Na-DEDTC. Samples were analyzed by Western blot with an α-biotin-HRP antibody.

Upon characterizing QC-sfGFP-FLAG, we sought to confirm reactivity of the QC functionality in QC-sfGFP-FLAG with **3.19**, and also sought to compare background

†††† Due to the limited solubility of QCaa, the actual concentration of QCaa in solution may be lower than 1 mM.

reactivity of **3.19** on Boc-sfGFP-FLAG versus Boc-sfGFP-His_6. For this experiment, purified QC-sfGFP-FLAG, QC-sfGFP-His_6, Boc-sfGFP-FLAG, and Boc-sfGFPHis_6 were each combined with 200 μM **3.19** in 1 mM $K_3Fe(CN)_6$ in PBS or vehicle (in 1 mM $K_3Fe(CN)_6$ in PBS) for 1 h 45 min at rt in the dark. The reaction was quenched with QCOAc followed by addition of Na-DEDTC, and ligation product was analyzed by Western blot with an α-biotin antibody. Results are shown in Figure 3.16c. Both the FLAG and His_6 tagged QC-sfGFP proteins are labeled via reaction with **3.19**, however, more background signal is observed on Boc-sfGFP-His_6 than on Boc-sfGFP-FLAG as determined via densitometry analysis. As a result, future experiments are being performed exclusively on FLAG-tagged sfGFP.

Conclusion

We have shown for the first time that a QC-functionalized amino acid can be installed site-selectively into a protein using the wildtype pyrrolysine synthetase/$tRNA_{CUA}$ pair from *M. barkeri*. As well, the incorporated QC handle reacts selectively with nickel bis(dithiolene) biotin **3.19** when the tagged protein is in purified form or in complex cell lysate. These results expand the potential applications of the QC ligation, opening the doors for its use in generation of homogeneously modified antibody drug conjugates, selective tagging of proteins of interest *in vivo*, and multiplexed imaging of target biomolecules.

Materials and Methods

Synthesis of quadricyclane amino acid (QCaa) 3.18 and Ni bis(dithiolene) biotin 3.19

General Procedures. Reagents and solvents were obtained commercially and used without further purification with the exception of anhydrous solvents which were prepared by the method developed by Pangborn *et al.*[67] Anhydrous dimethylformamide was obtained from Sigma Aldrich in a Sure/Seal™ container. Flash column chromatography was performed according to the method described by Still *et al.* using Silicycle Silica Flash P60 silica (40-63 mm, 230-400 mesh).[68] All high pressure liquid chromatography purifications were performed on a Varian ProStar HPLC equipped with UV/vis detector using a 100 Å C18 column (250 x 21.4 mm) at a flow rate of 20 mL/min.

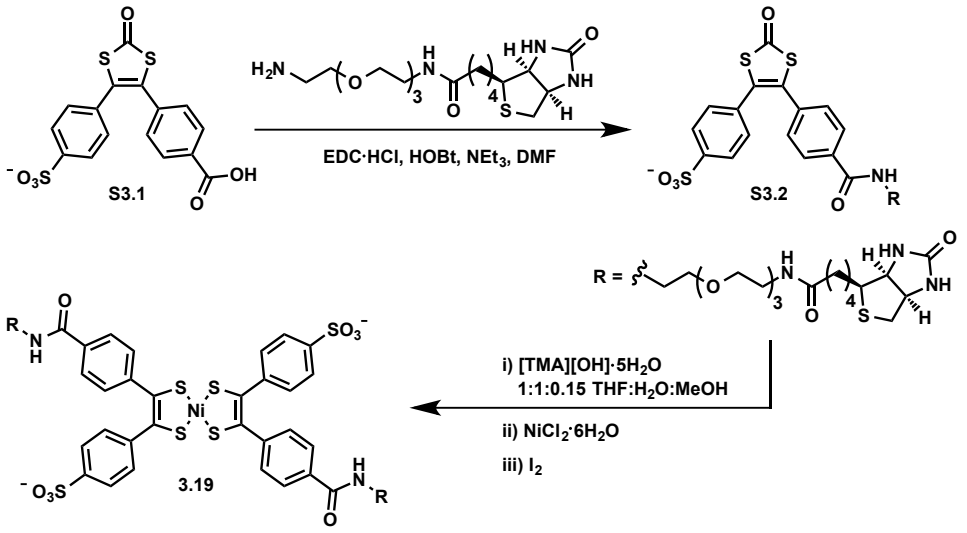
Reaction progress was monitored by TLC with Silicycle glass backed extra hard layer TLC plates (60 Å, 250 μm) visualized with ultraviolet light or with potassium permanganate or *p*-anisaldehyde staining followed by brief heating on a hot plate. Unless otherwise noted, anhydrous magnesium sulfate was used to dry organic extracts and solutions were concentrated using a Buchi Rotovapor-114 equipped with a Welch 2026 self-cleaning dry vacuum system. Compounds were dried under reduced pressure on a Schlenk line equipped with an Edwards high vacuum. Lyophilization was performed using a Labconco FreeZone Plus 4.5 Liter benchtop lyophilizer equipped with a Labconco vacuum (Model 117).

All ^{1}H and ^{13}C spectra were obtained with a Bruker AV-600, AV-500, AVB-400, or AVQ-400 spectrometer. Peaks are reported in ppm and referenced to the solvent. Data are presented as follows: chemical shift in ppm, multiplicity (s = singlet, d = doublet, t = triplet, q = quartet, quin = quintet, m = multiplet), coupling constant in Hz, and integration value. High-resolution electrospray ionization (ESI) mass spectrometry data were obtained through the UC Berkeley Mass Spectrometry Facility on a Linear trap quadrupole fourier transform ion cyclotron resonance (LTQ-FT-ICR) mass spectrometer from Thermo Fisher. High-resolution electron ionization (EI) mass spectrometry data were obtained through the UC Berkeley Mass Spectrometry Facility on an AutoSpec mass spectrometer from Waters.

Fmoc-protected QCaa. To a flame dried round bottom flask was added 30 mL dry dimethylformamide followed by Nα-Fmoc-L-lysine (455 mg, 1.23 mmol, 1.00 equiv.). *P*-nitrophenyl carbonate 3.14 (508 mg, 1.86 mmol, 1.50 equiv.), prepared via the method published by Sletten *et al*.[9] was added, and the reaction mixture immediately turned yellow. The solution was stirred at room temperature overnight, and the following day was concentrated to a yellow oil. Crude product was purified by flash column chromatography on silica gel that was pre-treated with 0.1% acetic acid in hexanes followed by washing with ~4 column volumes of hexanes. Product was eluted with hexanes:EtOAc:MeOH (10:1:0, 2:1:0, 0:1:0, 0:95:5, 0:9:1) to give the product in 85% yield (526 mg as a mixture with 140 mg DMF as determined by ^{1}H NMR). R_f = 0.54 in 100% EtOAc; ^{1}H NMR (600 MHz, MeOD) δ 7.78 (d, *J* = 7.5 Hz, 2H), 7.67 (dd, *J* = 11.3, 7.5 Hz, 2H), 7.38 (t, *J* = 7.5 Hz, 2H), 7.30 (t, *J* = 7.5 Hz, 2H), 5.53–5.46 (m, 1H), 4.34 (qd, *J* = 10.6, 7.1 Hz, 2H), 4.21 (t, *J* = 7.0 Hz, 1H), 4.14 (dd, *J* = 9.5, 4.6 Hz, 1H), 3.16–3.06 (m, 2H), 1.87–1.84 (m, 1H), 1.81–1.65 (m, 3H), 1.62–1.36 (m, 8H); ^{13}C NMR (151 MHz, MeOD) δ 176.0, 159.6, 158.7, 145.3, 145.1, 142.6, 142.5, 128.8, 128.8, 128.2, 128.1, 126.3, 126.2, 120.9, 120.9, 83.7, 67.9, 55.3, 48.4, 41.4, 32.3, 30.5, 26.8, 26.8, 24.2, 16.8, 15.3; HRMS (ESI) calcd for $C_{29}H_{30}O_6N_2Na$ $[M+Na]^+$: 525.1996; found: 525.1993.

Compound 3.18 (QCaa). Fmoc-protected QCaa (598 mg, 1.19 mmol, 1.00 equiv.) was dissolved in anhydrous dimethylformamide (10 mL) in a round bottom flask. Piperidine (400 μl, 4.05 mmol, 3.40 equiv.) was added, causing an immediate color change to yellow followed by cloudiness in the reaction mixture. The reaction mixture was stirred at room temperature for 2 hours at which point it was concentrated to an off white solid. The solid was triturated with cold EtOAc and filtered. The remaining white solid was washed with cold EtOAc to yield pure **3.18** (263 mg, 78% yield). R_f = 0.44 in 3:1 MeOH:EtOAC; ^{1}H NMR (600 MHz, D_2O) δ 5.50 (s, 1H), 3.70 (s, 1H), 3.14 (t, *J* = 6.9 Hz, 2H), 1.85–1.80 (m, 4H), 1.63 (s, 2H), 1.57–1.46 (m, 4H), 1.42–1.32 (m, 2H); ^{13}C NMR (151 MHz, DMSO) δ 169.5, 156.5, 81.0, 54.1, 40.1, 30.8, 29.2, 25.5, 22.5, 15.6, 13.9; HRMS (ESI) calcd for $C_{14}H_{20}O_4N_2Na$ $[M+Na]^+$: 303.1315; found: 303.131

Scheme S3.1. Synthesis of Ni bis(dithiolene) biotin 3.19.[‡‡‡‡]



Dithiocarbonate ligand S3.2. Dithiocarbonate **S3.1** was synthesized according to the route developed by Sletten *et al.* [9] EZ-link amine-PEG_3-biotin from Thermo Scientific (53 mg) was transferred to a round bottom flask as a solution in water, concentrated to a solid on a rotary evaporator, and azeotroped from toluene (2 x 2 ml). The amine-PEG_3-biotin was then dissolved in 1 ml dry dimethylformamide under an atmosphere of nitrogen. In a separate flask **S3.1** (24.2 mg, 0.06 mmol, 1.00 equiv.) was dissolved in 1 ml dry dimethylformamide. 500 μl of the amine-PEG_3-biotin solution (26.5 mg, 0.07 mmol, 1.17 equiv.) was added to the solution of **S3.1** followed by addition of EDC•HCl (22.6 mg, 0.12 mmol, 2.00 equiv.), HOBt hydrate (13.0 mg) and triethylamine (20 μl, 0.14 mmol, 2.33 equiv.). The reaction mixture was stirred at room temperature for 3 days, then concentrated to a yellow oil. Crude product was dissolved in 1:2 MeOH:H_2O, filtered through a 0.2 micron filter, and purified by HPLC on a C18 prep column, 30 to 95% MeOH in H_2O over 30 min, 20 ml/min flow rate. The product eluted as a broad peak between 8 and 12 min, yielding **S3.2** as a yellow oil (28 mg, 0.035 mmol, 58% yield). ^{1}H NMR (600 MHz, MeOD) d 7.76 (t, J = 8.5 Hz, 4H), 7.34 (dd, J = 11.2, 8.1 Hz, 4H), 4.49–4.46 (m, 1H), 4.30–4.28 (m, 1H), 3.65–3.61 (m, 10H), 3.57–3.53 (m, 5H), 3.50–3.48(m, 2H), 3.21–3.17 (m, 2H), 3.15–3.11 (m, 1H), 2.92–2.87 (m, 2H), 2.70–2.68 (m, 1H), 2.49–2.48 (m, 1H), 2.20 (t, J = 7.5 Hz, 2H), 1.75–1.69 (m, 1H), 1.66–1.54 (m, 3H), 1.44–1.39 (m, 2H); ^{13}C NMR (151 MHz, MeOD) δ 190.7, 176.1, 169.1, 166.0, 147.2, 136.2, 135.8, 134.4, 130.9, 130.7, 130.2, 129.8, 129.0, 127.7, 71.5, 71.5, 71.3, 71.2, 70.6, 70.5, 63.4, 61.6, 57.0, 49.9, 43.4, 41.1, 41.0, 40.4, 40.3, 40.3, 37.2, 36.7, 35.9, 32.3, 29.7, 29.5, 27.0, 26.8, 19.3, 15.7. HRMS (ESI) calcd for $C_{34}H_{41}O_{10}N_4S_4$ $[M–H]^-$: 793.1711; found: 793.1698

Nickel bis(dithiolene) biotin 3.19. Dithiocarbonate **S3.1** (17.3 mg, 0.02 mmol, 1.00 equiv.) was dissolved in 400 μl THF and 400 μl H_2O. Tetramethylammonnium hydroxide

[‡‡‡‡] Nickel bis(dithiolene) **3.19** was synthesized according to the route developed by Sletten *et al.* [9] However, a linker with two fewer methylene groups than that used by Sletten was employed.

pentahydrate (8.4 mg, 0.05 mmol, 2.5 equiv.) was added to the reaction mixture as a solution in 60 μl MeOH and the mixture quickly became a dark yellow/orange color. After stirring the resulting mixture at room temperature for 30 minutes, nickel(II) chloride hexahydrate (2.8 mg, 0.01 mmol, 0.5 equiv.) was added. The solution immediately became dark red, and was stirred at room temperature overnight. The following morning, iodine (3.2 mg, 0.01 mmol, 0.5 equiv.) was added and the reaction mixture immediately became dark green. After stirring at room temperature for 3 hrs, the reaction mixture was concentrated to a green solid on a rotary evaporator. The crude product was purified by flash column chromatography and eluted with acetonitrile:H_2O (10:1, 5:1, 3:1, 2:1). Fractions containing product were pooled, acetonitrile was evaporated on a rotary evaporator, and the remaining aqueous solution was lyophilized overnight to yield **3.19** as a dark green, fluffy solid (7.2 mg, 0.005 mmol, 21% yield). Rf = 0.64 in 5:1 acetonitrile:H_2O; UV/vis/NIR 225–900 nm (water): 859 nm (1.3 au), 311 nm (3.9 au), 282 nm (4.1 au), 232 nm (44.3 au); HRMS (ESI) calcd for $C_{66}H_{82}O_{18}N_8NiS_8$ $[M–2H]^{2–}$: 794.1439; found: 794.1417.

Non-natural amino acid incorporation and QC ligation labeling experiments

Materials and Equipment. Nε-Boc-L-lysine (Boc-lysine) was purchased from Chem-Impex and used without further purification. QCaa was synthesized and purified as described above. Phosphate-buffered saline 1X, –calcium –magnesium (PBS) was obtained from Corning Cellgro. All protein expression experiments were performed using DH10β cells from Invitrogen (MAX efficiency, chemically competent). A New Brunswick Scientific C25 incubator shaker was used to incubate *E. coli* liquid cultures at 37 ºC with shaking at 225 rpm. A Lab-line Imperial II incubator was used to incubate LB agar plates at 37 ºC. LB agar plates were prepared using Luria Broth Base (Miller's LB Broth Base, Invitrogen) and agar (granulated, Fisher Scientific). LB liquid media and LB agar plates were supplemented with kanamycin to 50 μg/ml and/or tetracycline to 25 μg/ml depending on the combination of plasmids used. Sample centrifugation was performed in a Thermo Scientific Sorvall RC 6+ centrifuge, Sorvall RC 5C Plus centrifuge, a Sorvall Legent RT centrifuge, or an Eppendorf centrifuge 5417C.

Gel electrophoresis was performed using BioRad Criterion gel electrophoresis chambers equipped with a BioRad Power Pac 200. All gels (Biorad Criterion XT pre-cast) were run in MES buffer. Western blot transfers were performed using BioRad Criterion blotter transfer boxes equipped with a BioRad Power Pac 200. Gels were transferred to nitrocellulose (BioRad 0.45 μm) in tris-glycine buffer (20% MeOH). See Blue Plus 2 pre-stained protein ladder from Life Technologies was used for all gels and Western blots. α-GFP (4B10) Mouse mAb (#2955), α-Mouse IgG horseradish-peroxidase-linked (HRP) antibody (#7076), and α-FLAG®-HRP rabbit polyclonal antibody (DYKDDDDK Tag antibody HRP conjugate, #2044) were obtained from Cell Signaling Technologies. Mouse α-biotin-HRP was obtained from Southern Biotech. Protein loading was assessed via staining with Ponceau (5% acetic acid, 0.1% (w/v) ponceau). Blots were visualized on Premium X-ray film (blue) from Phenix Research Products. Densitometry analyses were performed using ImageJ 1.48v (National Institutes of Health). Fast protein liquid chromatography (FPLC) was performed on a Pharmacia Biotech Akta explorer 10. High

resolution mass spectrometry data were obtained on a Linear Trap Quadrupole LTQ-Orbitrap-XL mass spectrometer (Thermo Scientific) equipped with an electrospray ionization (ESI) source.

General Procedure for Transformation of *E. coli* with plasmids *psfGFP150TAGHis$_6$PylT* or *psfGFP150TAGFLAGPylT* and/or *pBKPylRS*

DH10β *E. coli* were transformed with *psfGFP150TAGHis$_6$PylT* and *pBKPylRS* (+RS+T) or with *psfGFP150TAGHis$_6$PylT* and sterile ddH_2O (–RS+T) by heat shock (30 sec, 42 ºC, 2 min, wet ice) and recovered in 250 μL super optimal broth with 20 mM glucose (S.O.C. medium) for 35 min at 37 ºC and 225 rpm. Cells were then plated on kanamycin/tetracycline (+RS+T *E. coli*) or tetracycline (–RS+T *E. coli*) LB agar plates and incubated at 37 ºC overnight. The following day, 5 ml liquid cultures of LB media supplemented with kanamycin/tetracycline (+RS+T *E. coli*) or tetracycline (–RS+T *E. coli*) were inoculated with one colony from +RS+T and one colony from –RS+T respectively. Cultures were incubated at 37 ºC and 225 rpm overnight. The following morning, glycerol stocks were prepared (375 μl culture and 125 μl sterile 80% glycerol in ddH_2O) and frozen to –80 ºC for future use. The same method was used for transformation of DH10β cells with *psfGFP150TAGFLAGPylT* and *pBKPylRS* (+RS+T) or with *psfGFP150TAGFLAGPylT* and sterile ddH_2O (–RS+T).

Expression of QC- and Boc-sfGFP-His$_6$ or QC- and Boc-sfGFP-FLAG

DH10β cells were transformed with the relevant plasmids (+RS+T or –RS+T) as described above and the resulting 5 ml overnight cultures were used immediately. Alternatively, glycerol stabs of transformed DH10β cells stored at –80 ºC were used to streak fresh LB agar plates (supplemented with the requisite antibiotics). The plates were grown overnight at 37 ºC, and 5 ml liquid media cultures (supplemented with the requisite antibiotics) were inoculated with single colonies from each plate. These 5 ml cultures were then incubated overnight at 37 ºC and 225 rpm and used the next day to inoculate larger cultures for protein expression. All protein expression protocols begin with a 5 ml overnight culture. The following section describes the various expression procedures used in experiments discussed in this chapter, and is organized according to figure.

Expression of QC-sfGFP-His$_6$ and Boc-sfGFP-His$_6$ for use in the experiment shown in Figure 3.12.

+RS+T DH10β and –RS+T DH10β 5 ml overnight cultures were prepared as described using *pBKPylRS* and *psfGFP150FLAGHis$_6$PylT* plasmids. The following morning, 1 ml from each culture was used to inoculate 50 mL liquid media cultures (supplemented with the requisite antibiotic), which were subsequently grown to OD_{600} ~0.4–0.5 at which point 4 ml aliquots were removed and added to each of three 15 ml culture tubes. Each

tube was supplemented with amino acid (from a 50 mM[§§§§] amino acid stock solution in sterile 0.1 M NaOH ddH_2O) to ~1 mM or was supplemented with the same volume of vehicle (0.1 M NaOH) and incubated at 37 ºC and 225 rpm for 30 min. Protein expression was induced via addition of sterile 20% L-arabinose in ddH_2O to 0.2%. After 3.5 hrs of induction, cells were pelleted (3500 rpm, 10 min, 4 ºC), the supernatant was aspirated, and pellets were washed to remove excess nnaa by resuspension in PBS followed by pelleting via centrifugation (9700 rpm, 5 min) and aspiration of supernatant. The wash procedure was repeated two additional times. Pellets from each culture were split into thirds and two of the resulting pellets were stored at –80 ºC. The third pellet from each sample was resuspended in 100 µl 1X sodium dodecyl sulfate (SDS) loading buffer supplemented with 2.5% β-mercaptoethanol and centrifuged at 14,000 rpm for 15 min. Samples were stored at –20 ºC.

Samples in SDS loading buffer were thawed, loaded onto a 26-well 4–12% bis-tris Criterion XT precast polyacrylamide gel (8 µl sample/per well), and treated as described in the General Western Blotting Procedure section with α-GFP Mouse mAb and α-Mouse-HRP.

Large-scale expression and purification of QC- and Boc-sfGFP-His_6 for use in the experiments shown in Figures 3.13, 3.14, 3.15, and 3.16b,c.

+RS+T DH10β and –RS+T DH10β *E. coli* 5 ml overnight cultures were prepared as described above using *pBKPylRS* and *psfGFP15TLAGHis$_6$PylT* plasmids. The following morning, 2 ml from each culture was used to inoculate 100 mL LB media (supplemented with the requisite antibiotics). Cultures were grown to OD_{600} = 0.3–0.5 and supplemented with Boc-Lys or QCaa (from 50 mM[*****] amino acid stock solution in 0.1 M NaOH ddH_2O) to ~1 mM. Flasks were incubated for an additional 30 min at 37 ºC and 225 rpm after which protein expression was induced via addition of 20% L-arabinose in sterile ddH_2O to 0.2%. Protein was expressed for 3.5 hours and then each culture was separated into two 50 ml falcon tubes and pelleted at 3,500 rpm for 10 min at 4 ºC. The supernatant was aspirated and pellets from each culture were combined and washed 3x by resuspension in 20 ml LB media, pelleting at 3,500 rpm for 10 min at 4 ºC, and aspiration of supernatant. Pellets were stored at –20 ºC until lysis, at which point they were resuspended in 3 ml lysis buffer (tris-HCl (10 mM), NaCl (200 mM), imidazole (20 mM), pH = 8, Roche protease inhibitor) and, lysed via sonication (Misonix Sonicator 3000, power level 2, 4 min on total: 10 sec on, 10 sec off). The resulting lysate was clarified by centrifugation (20 min, 21,000 x g, 4 ºC).

Qiagen Ni^{2+}-NTA beads (500 µl) were washed 3x via suspension in binding buffer (imidazole (5 mM), tris-HCl (10 mM), NaCl (200 mM), pH = 8) followed by centrifugation and aspiration of supernatant. Beads were then added to clarified lysate as

[§§§§] Due to limited solubility of QCaa, the actual concentration of QCaa in solution may be lower than 50 mM.

[*****] Due to limited solubility of QCaa, the actual concentration of QCaa in solution may be lower than 50 mM.

a suspension in 500 µl binding buffer, and the mixture was incubated with agitation for 1–1.25 h at 4 ºC, after which beads were transferred to a fritted column. At 4 ºC, the beads were washed 3 x 3 ml wash buffer (tris-HCl (10 mM), imidazole (20 mM), NaCl (200 mM), pH = 8) followed by elution with 6 x 1 ml wash buffer supplemented with imidazole to 200 mM. Elutions were pooled and concentrated to ~500 µl using an Amicon Ultra 4 ml, 10 kDa molecular weight cutoff centrifugal filter. Protein was further purified by fast protein liquid chromatography (FPLC) at 4 ºC on a Superdex 75 10/300 GL (GE Healthcare Life Science) column using FPLC buffer (tris-HCl (20 mM), NaCl (100 mM), pH = 7.4) at a flow rate of 0.5–0.6 ml/min Fractions (0.5 ml each) were analyzed by polyacrylamide gel electrophoresis followed by protein visualization with coomassie stain (0.25% (w/v) coomassie, 40% methanol, 10% acetic acid). Following FPLC purification, protein was transferred to PBS via solvent exchange using Amicon Ultra 10 kDa molecular weight cutoff filters.

The same procedure was used to express QC-sfGFP-FLAG and Boc-sfGFP-FLAG from *E. coli* transformed with *pBKPylRS* and *psfGFP150TAGFLAGPylT* plasmids except expression was performed on the 200 ml scale rather than 100 ml scale and pellets were lysed in 6 ml lysis buffer rather than 3 ml. FLAG-tagged protein was then purified via affinity column at room temperature using ANTI-FLAG® M2 Affinity Gel from Sigma Aldrich. The gel was equilibrated with 5 column volumes of TBS buffer (150 mM NaCl, 50 mM tris-HCl, pH = 7.4), lysate was loaded via three passes through the column, and unbound protein was washed off the column with 20 column volumes of TBS buffer. Bound protein was eluted with five column volumes 100 µg/ml 3XFLAG peptide (Sigma Aldrich) in TBS. Protein was further purified by FPLC and transferred to PBS as described for His_6-tagged proteins.

Expression of QC-sfGFP-FLAG and Boc-sfGFP-FLAG for use in the experiment shown in Figure 3.16a.

DH10β *E. coli* were transformed with *pBKPylRS* and/or *psfGFP150TAGFLAGPylT* and 5 ml overnight cultures were prepared as described in previous experiments. The following morning, 2 ml from each culture was used to inoculate 50 mL LB media cultures (supplemented with the requisite antibiotics). Each culture was incubated at 37 ºC and 225 rpm to OD_{600} ~0.4 at which point the cultures were divided into three separate 15 ml polystyrene tubes (5 ml/tube) and supplemented with QCaa or BocLys (from 22 mM[†††††] stock solution of amino acid in sterile 0.1 M NaOH ddH_2O) to ~1 mM or supplemented with the same volume of vehicle (0.1 M NaOH) and incubated at 37 ºC and 225 rpm for 30 min. Protein expression was induced via addition of 20% L-arabinose in sterile ddH_2O to 0.2% and expressed for 3.5 hours. Following expression, cultures were transferred to 15 ml falcon tubes and pelleted at 3500 rom and 4 ºC for 10 min. Pellets were washed 3x via resuspension in LB media followed by pelleting at 9,700 rpm for 5 min and aspiration of the supernatant. Washed pellets were stored at –80 ºC until further use.

[†††††] Due to limited solubility of QCaa, the actual concentration of QCaa in solution may have been slightly lower than 22 mM.

Samples were thawed on ice, then warmed to rt. 1/6 of each pellet was isolated and resuspended in 40 μl 1X SDS loading buffer supplemented with 2.5% β-mercaptoethanol. The suspension was centrifuged at 14,000 rpm for 15 min, and samples were loaded onto two, 18-well 4–12% bis-tris Criterion XT precast polyacrylamide gels (15 μl sample/per well). Gels were treated as described in the General Western Blotting Procedure section with α-GFP Mouse mAb and α-Mouse-HRP or with α-FLAG-HRP rabbit polyclonal antibody.

General QC ligation procedure

Purified QC- or Boc-sfGFP in the presence or absence of *E. coli* lysate was combined with 200 μM **3.19** and 1 mM $K_3Fe(CN)_6$ in PBS and incubated in the dark at room temperature for various amounts of time (see Table S3.1). Reactions were quenched via addition of 100 equiv. QCOAc (200 mM solution in DMSO) relative to **3.19**. Samples were then combined with 100 equiv. Na-DEDTC (100 mM solution in PBS).

Table S3.1. QC ligation setup* for experiments shown in Figures 3.14, 3.15, and 3.16c.

Figure	Concentration of QC-sfGFP or Boc-sfGFP	Concentration of lysate	Concentration of 3.19	Concentration of $K_3Fe(CN)_6$	Reaction time
3.14	0.25 mg/ml	0 mg/ml	200 μM	1 mM	1 h
3.15	0 – 0.17 mg/ml	0.33 mg/ml	200 μM	1 mM	1 h 15 min
3.16c	0.20 mg/ml	0 mg/ml	200 μM	1 mM	1 h 45 min

*The solvent for all reactions is PBS.

General Western Blotting Procedure

All samples were combined with 4X sodium dodecyl sulfate (SDS) loading buffer (supplemented with 10% β-mercaptoethanol) to a final loading buffer concentration of 1X for separation via sodium dodecyl sulfate polyacrylamide gel electrophoresis (SDS-PAGE). All SDS-PAGE was performed using 4–12% bis-tris Criterion XT precast polyacrylamide gels. Gels were run at 175 V for 40 min and then were transferred to nitrocellulose at 75 V for 90 min. The blots were treated with Ponceau stain to visualize proteins.

Blots to be analyzed with α-biotin-HRP were blocked with 5% bovine serum albumin (BSA) in PBST at 4 ºC in the dark overnight. All other blots were blocked with 5% milk in PBST at 4 ºC in the dark overnight. After blocking, α-biotin-HRP blots were incubated in a 1:50,000 (Figure 3.14) or 1:30,000 (Figures 3.15 and 3.16c) dilution of α-biotin-HRP in 5% BSA, PBST for 1 h at room temperature in the dark and then washed 3 x 10 min with PBST. α-FLAG blots were incubated in a 1:3,000 dilution of α-FLAG-HRP in 5% milk PBST followed by washing 3 x 10 min PBST. α-GFP blots were incubated in a 1:3,000 (Figure 3.12) or a 1:5,000 (Figure 3.16a) dilution of α-GFP Mouse mAb in 5% milk, PBST for 1 h at room temperature followed by washing 3 x 10 min with PBST.

After washing, blots were incubated in a 1:10,000 dilution of α-mouse-HRP in 5% milk, PBST for 1 h at room temperature followed by washing 3 x 10 min with PBST.

For all gels, detection was performed by chemiluminescence using SuperSignal West Pico Chemiluminescent Substrate (Thermo Scientific). Blots were developed on a Kodak X-OMAT 500RA processor.

Cloning to exchange His_6 tag for FLAG tag

The sfGFP gene from *psfGFP150TAGHis$_6$PylT* (sequence below, plasmid obtained from Jason Chin Lab, Medical Research Council, Cambridge, UK) was amplified using forward primer and reverse primer 1 purchased from Elim Biopharma (see Table S3.5) according to the conditions in Tables S3.2 and S3.3. The PCR reaction was purified by agarose gel electrophoresis, and the band corresponding to the PCR product was excised from the gel and purified using a Zymoclean Gel DNA Recovery Kit (Zymo Research) to give gene sfGFP150TAGFLAG1. Gene sfGFP150TAGFLAG1 was further amplified with forward primer and reverse primer 2 (see Table S3.8) according to the conditions in Tables S3.3 and S3.4 to form full-length insert sfGFP150TAGFLAG2. The insert was isolated by agarose gel electrophoresis as described above, and the gene ends were digested for 1 h 45 min at 37 ºC with XhoI and NcoI-HF (both from New England Biolabs) according to Table S3.5 and purified using a Zymo DNA Clean & Concentrator Kit (Zymo Research). Vector *psfGFP150TAGHis$_6$PylT* was linearized with XhoI and NcoI-HF (both from New England Biolabs) at 37 ºC for 1 h 40 min according to Table S3.5, and linearized vector was isolated by agarose gel electrophoresis and treated with Antarctic phosphatase (New England Biolabs) at 37 ºC for 1 h according to the conditions in Table S3.6 followed by purification with a Zymo DNA Clean & Concentrator Kit. The full-length sfGFP150TAGFLAG insert was ligated to linearized vector with T4 DNA ligase (New England Biolabs) at rt for 50 min according to the conditions in Table S3.7 to form *psfGFP150TAGFLAGPylT*.

One Shot, chemically competent DH5α *E. coli* (Life Technologies) were transformed with 2 μl ligation reaction containing the full plasmid *psfGFP150TAGFLAGPylT*. *E.* coli were transformed by heat shock (30 sec, 42 ºC, 2 min, wet ice) and recovered in 250 μL super optimal broth with 20 mM glucose (S.O.C. medium) for 35 min at 37 ºC and 225 rpm. Cells were then plated on tetracycline LB agar plates (~100–200 μl S.O.C. culture per plate) and incubated at 37 ºC overnight. Single colonies were selected for inoculation of 5 ml liquid LB media cultures (supplemented with tetracycline) and cultures were incubated overnight at 37 ºC and 225 rpm. The resulting cultures were used to prepare *psfGFP150TAGFLAGPylT* plasmid DNA using a Qiagen Miniprep kit. The sfGFP150TAGFLAG portion of the plasmid was sequenced using forward primer and reverse primer 2 by Elim Bioharma.

Table S3.2. PCR reaction components for amplification of gene sfGFP150TAGFLAG1.

Volume	Reagent
36 μl	Sterile ddH_2O
1.5 μl	DMSO
5 μl	10x Pfu Ultra II buffer (Agilent Technologies)
0.5 μl	20 μM forward primer
0.5 μl	20 μM reverse primer 1
5 μl	10 mM dNTPs
0.5 μl	25 ng *psfGFPTAGHis$_6$PylT*
1 μl	Pfu ultra II HotStart DNA polymerase (Agilent Technologies)

Table S3.3. PCR reaction conditions for amplification of gene sfGFP150TAGFLAG1 and sfGFP150TAGFLAG2.

Temperature (ºC)	Duration	# Cycles
95 ºC	2 min	1
95 ºC	20 sec	30
53 ºC	20 sec	
72 ºC	30 sec	
72 ºC	3 min	1
4 ºC	forever	1

Table S3.4. PCR reaction components for amplification of gene sfGFP150TAGFLAG2.

Volume	Reagent
35.9 μl	Sterile ddH_2O
1.5 μl	DMSO
5 μl	10x Pfu Ultra II buffer (Agilent Technologies)
0.5 μl	20 μM forward primer
0.5 μl	20 μM reverse primer 2
5 μl	10 mM dNTPs
0.6 μl	25 ng sfGFP150TAGFLAG1
1 μl	Pfu ultra II HotStart DNA polymerase (Agilent Technologies)

Table S3.5. Restriction enzyme digest conditions for digestion of sfGFP150TAGFLAG2 insert and *psfGFPTAGHis$_6$PylT vector*.

Volume	Reagent
33 μl	sterile ddH_2O
5 μl	10x New England Biolabs Cutsmart Buffer
10 μl	2.5 μg sfGFP150TAGFLAG2 insert or 2.5 μg *psfGFPTAGHis$_6$PylT* vector
1 μl	XhoI
1 μl	NcoI-HF

Table S3.6. Phosphatase reaction conditions.

Volume	Reagent
8.6 µl	sterile ddH_2O
9 µl	linearized *psfGFPTAGHis$_6$PylT* vector
2 µl	10X phosphatase buffer
0.4 µl	Antarctic phosphatase

Table S3.7. sfGFP150TAGFLAG2 insert + linearized *psfGFPTAGHis$_6$PylT* vector ligation conditions.

Volume	Reagent
7.71 µl	sterile ddH_2O
1 µl	10X T4 DNA ligase buffer
0.38 µl	25 ng linearized *psfGFPTAGHis$_6$PylT* vector
0.41 µl	11.3 ng sfGFP150TAGFLAG2 insert
0.5 µl	T4 DNA ligase

Plasmid map legend:
Tet repressor gene; Pyrrolysine tRNACUA gene; LPP promoter; AraC; sfGFP150TAG; His_6; FLAG; NcoI restriction site; XhoI restriction site

psfGFP150TAGHis$_6$PylT

GAGAGAAGATTTTCAGCCTGATACAGATTAAATCAGAACGCAGAAGCGGTCT
GATAAAACAGAATTTGCCTGGCGGCAGTAGCGCGGTGGTCCCACCTGACCCC
ATGCCGAACTCAGAAGTGAAACGCCGTAGCGCCGATGGTAGTGTGGGGTCTC
CCCATGCGAGAGTAGGGAACTGCCAGGCATCAAATAAAACGAAAGGCTCAG
TCGAAAGACTGGGCCTTTCGTTTTATCTGTTGTTTGTCGGTGAACGCTCTCCTG
AGTAGGACAAATCCGCCGGGAGCTGTCCCTCCTGTTCAGCTACTGACGGGGT
GGTGCGTAACGGCAAAAGCACCGCCGGACATCAGCGCTAGCGGAGTGTATA
CTGGCTTACTATGTTGGCACTGATGAGGGTGTCAGTGAAGTGCTTCATGTGGC
AGGAGAAAAAAGGCTGCACCGGTGCGTCAGCAGAATATGTGATACAGGATA
TATTCCGCTTCCTCGCTCACTGACTCGCTACGCTCGGTCGTTCGACTGCGGCG
AGCGGAAATGGCTTACGAACGGGGCGGAGATTTCCTGGAAGATGCCAGGAA
GATACTTAACAGGGAAGTGAGAGGGCCGCGGCAAAGCCGTTTTTCCATAGGC
TCCGCCCCCCTGACAAGCATCACGAAATCTGACGCTCAAATCAGTGGTGGCG
AAACCCGACAGGACTATAAAGATACCAGGCGTTTCCCCCTGGCGGCTCCCTC
GTGCGCTCTCCTGTTCCTGCCTTTCGGTTTACCGGTGTCATTCCGCTGTTATGG
CCGCGTTTGTCTCATTCCACGCCTGACACTCAGTTCCGGGTAGGCAGTTCGCT
CCAAGCTGGACTGTATGCACGAACCCCCCGTTCAGTCCGACCGCTGCGCCTT
ATCCGGTAACTATCGTCTTGAGTCCAACCCGGAAAGACATGCAAAAGCACCA
CTGGCAGCAGCCACTGGTAATTGATTTAGAGGAGTTAGTCTTGAAGTCATGC
GCCGGTTAAGGCTAAACTGAAAGGACAAGTTTTGGTGACTGCGCTCCTCCAA
GCCAGTTACCTCGGTTCAAAGAGTTGGTAGCTCAGAGAACCTTCGAAAAACC
GCCCTGCAAGGCGGTTTTTTCGTTTTCAGAGCAAGAGATTACGCGCAGACCA

AAACGATCTCAAGAAGATCATCTTATTAATCAGATAAAATATTTCTAGATTTC
AGTGCAATTTATCTCTTCAAATGTAGCACCTGAAGTCAGCCCCATACGATATA
AGTTGTAATTCTCATGTTTGACAGCTTATCATCGATAAGCTTTAATGCGGTAG
TTTATCACAGTTAAATTGCTAACGCAGTCAGGCACCGTGTATGAAATCTAACA
ATGCGCTCATCGTCATCCTCGGCACCGTCACCCTGGATGCTGTAGGCATAGGC
TTGGTTATGCCGGTACTGCCGGGCCTCTTGCGGGATATCGTCCATTCCGACAG
CATCGCCAGTCACTATGGCGTGCTGCTAGCGCTATATGCGTTGATGCAATTTC
TATGCGCACCCGTTCTCGGAGCACTGTCCGACCGCTTTGGCCGCCGCCCAGTC
CTGCTCGCTTCGCTACTTGGAGCCACTATCGACTACGCGATCATGGCGACCAC
ACCCGTCCTGTGGATCCTCTACGCCGGACGCATCGTGGCCGGCATCACCGGC
GCCACAGGTGCGGTTGCTGGCGCCTATATCGCCGACATCACCGATGGGGAAG
ATCGGGCTCGCCACTTCGGGCTCATGAGCGCTTGTTTCGGCGTGGGTATGGTG
GCAGGCCCCGTGGCCGGGGGACTGTTGGGCGCCATCTCCTTGCATGCACCAT
TCCTTGCGGCGGCGGTGCTCAACGGCCTCAACCTACTACTGGGCTGCTTCCTA
ATGCAGGAGTCGCATAAGGGAGAGCGTCGACCGATGCCCTTGAGAGCCTTCA
ACCCAGTCAGCTCCTTCCGGTGGGCGCGGGGCATGACTATCGTCGCCGCACT
TATGACTGTCTTCTTTATCATGCAACTCGTAGGACAGGTGCCGGCAGCGCTCT
GGGTCATTTTCGGCGAGGACCGCTTTCGCTGGAGCGCGACGATGATCGGCCT
GTCGCTTGCGGTATTCGGAATCTTGCACGCCCTCGCTCAAGCCTTCGTCACTG
GTCCCGCCACCAAACGTTTCGGCGAGAAGCAGGCCATTATCGCCGGCATGGC
GGCCGACGCGCTGGGCTACGTCTTGCTGGCGTTCGCGACGCGAGGCTGGATG
GCCTTCCCCATTATGATTCTTCTCGCTTCCGGCGGCATCGGGATGCCCGCGTT
GCAGGCCATGCTGTCCAGGCAGGTAGATGACGACCATCAGGGACAGCTTCAA
GGATCGCTCGCGGCTCTTACCAGCCTAACTTCGATCATTGGACCGCTGATCGT
CACGGCGATTTATGCCGCCTCGGCGAGCACATGGAACGGGTTGGCATGGATT
GTAGGCGCCGCCCTATACCTTGTCTGCCTCCCCGCGTTGCGTCGCGGTGCATG
GAGCCGGGCCACCTCGACCTGAATGGAAGCCGGCGGCACCTCGCTAACGGAT
TCACCACTCCAAGAATTGGAGCCAATCAATTCTTGCGGAGAACTGTGAATGC
GCAAACCAACCCTTGGCAGAACATATCCATCGCGTCCGCCATCTCCAGCAGC
CGCACGCGGCGCATCTCGGGCTCCTTGCATGCACCATTCCTTGCGGCGGCGGT
GCTCAACGGCCTCAACCTACTACTGGGCTGCTTCCTAATGCAGGAGTCGCAT
AAGGGAGAGCGTCTGGCGAAAGGGGGATGTGCTGCAAGGCGATTAAGTTGG
GTAACGCCAGGGTTTTCCCAGTCACGACGTTGTAAAACGACGGCCAGTGCCA
AGCTTAAAAAAAATCCTTAGCTTTCGCTAAGATCTGCAGtggcggaaaccccgggaatct
aacccggctgaacggatttagagtccattcgatctacatgatcaggttcccGCGGCCGCGAATTCAGCGTTA
CAAGTATTACACAAAGTTTTTTATGTTGAGAATATTTTTTTGATGGGGCGCCA
CTTATTTTTGATCGTTCGCTCAAAGAAGCGGCGCCAGGGTTGTTTTTCTTTTCA
CCAGTGAGACGGGCAACAGAACGCCATGAGCGGCCTCATTTCTTATTCTGAG
TTACAACAGTCCGCACCGCTGCCGGTAGCTCCTTCCGGTGGGCGCGGGGCAT
GACTATCGTCGCCGCACTTATGACTGTCTTCTTTATCATGCAACTCGTAGGAC
AGGTGCCGGCAGCGCCCAACAGTCCCCCGGCCACGGGGCCTGCCACCATACC
CACGCCGAAACAAGCGCCCTGCACCATTATGTTCCGGATCTGCATCGCAGGA
TGCTGCTGGCTACCCTGTGGAACACCTACGGTACCGCTATCGCTACGTGACTG
GGTCATGGCTGCGCCCCGACACCCGCCAACACCCGCTGACGCGCCCTGACGG
GCTTGTCTGCTCCCGGCATCCGCTTACAGACAAGCTGTGACCGTCTCCGGGAG
CTGCATGTGTCAGAGGTTTTCACCGTCATCACCGAAACGCGCGAGGCAGCAG

ATCAATTCGCGCGCGAAGGCGAAGCGGCATGCATAATGTGCCTGTCAAATGG
ACGAAGCAGGGATTCTGCAAACCCTATGCTACTCCGTCAAGCCGTCAATTGT
CTGATTCGTTACCAATTATGACAACTTGACGGCTACATCATTCACTTTTTCTTC
ACAACCGGCACGGAACTCGCTCGGGCTGGCCCCGGTGCATTTTTTAAATACC
CGCGAGAAATAGAGTTGATCGTCAAAACCAACATTGCGACCGACGGTGGCGA
TAGGCATCCGGGTGGTGCTCAAAAGCAGCTTCGCCTGGCTGATACGTTGGTC
CTCGCGCCAGCTTAAGACGCTAATCCCTAACTGCTGGCGGAAAAGATGTGAC
AGACGCGACGGCGACAAGCAAACATGCTGTGCGACGCTGGCGATATCAAAA
TTGCTGTCTGCCAGGTGATCGCTGATGTACTGACAAGCCTCGCGTACCCGATT
ATCCATCGGTGGATGGAGCGACTCGTTAATCGCTTCCATGCGCCGCAGTAAC
AATTGCTCAAGCAGATTTATCGCCAGCAGCTCCGAATAGCGCCCTTCCCCTTG
CCCGGCGTTAATGATTTGCCCAAACAGGTCGCTGAAATGCGGCTGGTGCGCT
TCATCCGGGCGAAAGAACCCCGTATTGGCAAATATTGACGGCCAGTTAAGCC
ATTCATGCCAGTAGGCGCGCGGACGAAAGTAAACCCACTGGTGATACCATTC
GCGAGCCTCCGGATGACGACCGTAGTGATGAATCTCTCCTGGCGGGAACAGC
AAAATATCACCCGGTCGGCAAACAAATTCTCGTCCCTGATTTTTCACCACCCC
CTGACCGCGAATGGTGAGATTGAGAATATAACCTTTCATTCCCAGCGGTCGG
TCGATAAAAAAATCGAGATAACCGTTGGCCTCAATCGGCGTTAAACCCGCCA
CCAGATGGGCATTAAACGAGTATCCCGGCAGCAGGGGATCATTTTGCGCTTC
AGCCATACTTTTCATACTCCCGCCATTCAGAGAAGAAACCAATTGTCCATATT
GCATCAGACATTGCCGTCACTGCGTCTTTTACTGGCTCTTCTCGCTAACCAAA
CCGGTAACCCCGCTTATTAAAAGCATTCTGTAACAAAGCGGGACCAAAGCCA
TGACAAAAACGCGTAACAAAAGTGTCTATAATCACGGCAGAAAAGTCCACAT
TGATTATTTGCACGGCGTCACACTTTGCTATGCCATAGCATTTTTATCCATAA
GATTAGCGGATCCTACCTGACGCTTTTTATCGCAACTCTCTACTGTTTCTCCAT
ACCCGTTTTTTGGGCTAACAGGAGGAATTAACCATGGTTAGCAAAGGTGAAG
AACTGTTTACCGGCGTTGTGCCGATTCTGGTGGAACTGGATGGTGATGTGAAT
GGCCATAAATTTAGCGTTCGTGGCGAAGGCGAAGGTGATGCGACCAACGGTA
AACTGACCCTGAAATTTATTTGCACCACCGGTAAACTGCCGGTTCCGTGGCCG
ACCCTGGTGACCACCCTGACCTATGGCGTTCAGTGCTTTAGCCGCTATCCGGA
TCATATGAAACGCCATGATTTCTTTAAAAGCGCGATGCCGGAAGGCTATGTG
CAGGAACGTACCATTAGCTTCAAAGATGATGGCACCTATAAAACCCGTGCGG
AAGTTAAATTTGAAGGCGATACCCTGGTGAACCGCATTGAACTGAAAGGTAT
TGATTTTAAAGAAGATGGCAACATTCTGGGTCATAAACTGGAATATAATTTC
AACAGCCATTAGGTGTATATTACCGCCGATAAACAGAAAAATGGCATCAAAG
CGAACTTTAAAATCCGTCACAACGTGGAAGATGGTAGCGTGCAGCTGGCGGA
TCATTATCAGCAGAATACCCCGATTGGTGATGGCCCGGTGCTGCTGCCGGAT
AATCATTATCTGAGCACCCAGAGCGTTCTGAGCAAAGATCCGAATGAAAAAC
GTGATCATATGGTGCTGCTGGAATTTGTTACCGCCGCGGGCATTACCCACGGT
ATGGATGAACTGTATAAAGGCAGCCACCATCATCATCACCATTAAAGCTCGA
GCGAAGCTTGNGCCCGAACAAAAACTCATCTCANAAGAGGATCTGANTAG

Table S3.8. Primers used in this study.

Primer name	Sequence
Forward primer	5'- CAGGAGGAATTAACCATGGTTAGCAAAG-3'
Reverse primer 1	5'-ATCGTCGTCCTTGTAGTCGCTGCCTTTATACAGTTCATCCATACC-3'
Reverse primer 2	5'-TTCGCTCGAGCTTTACTTGTCATCGTCGTCCTTGTAGTCGCTG-3'

***sfGFP150TAGFLAG* sequence from *psfGFP150TAGFLAGPylT* plasmid:**

ATACCCGTTTTTTGGGCTAACAGGAGGAATTAACCATGGTTAGCAAAGGTGA
AGAACTGTTTACCGGCGTTGTGCCGATTCTGGTGGAACTGGATGGTGATGTG
AATGGCCATAAATTTAGCGTTCGTGGCGAAGGCGAAGGTGATGCGACCAACG
GTAAACTGACCCTGAAATTTATTTGCACCACCGGTAAACTGCCGGTTCCGTGG
CCGACCCTGGTGACCACCCTGACCTATGGCGTTCAGTGCTTTAGCCGCTATCC
GGATCATATGAAACGCCATGATTTCTTTAAAAGCGCGATGCCGGAAGGCTAT
GTGCAGGAACGTACCATTAGCTTCAAAGATGATGGCACCTATAAAACCCGTG
CGGAAGTTAAATTTGAAGGCGATACCCTGGTGAACCGCATTGAACTGAAAGG
TATTGATTTTAAAGAAGATGGCAACATTCTGGGTCATAAACTGGAATATAATT
TCAACAGCCATTAGGTGTATATTACCGCCGATAAACAGAAAAATGGCATCAA
AGCGAACTTTAAAATCCGTCACAACGTGGAAGATGGTAGCGTGCAGCTGGCG
GATCATTATCAGCAGAATACCCCGATTGGTGATGGCCCGGTGCTGCTGCCGG
ATAATCATTATCTGAGCACCCAGAGCGTTCTGAGCAAAGATCCGAATGAAAA
ACGTGATCATATGGTGCTGCTGGAATTTGTTACCGCCGCGGGCATTACCCACG
GTATGGATGAACTGTATAAAGGCAGCGACTACAAGGACGACGATGACAAGT
AAAGCTCGAGCGAAGCTTGGGCCCGAACAAAAACTCATCTCAGAAGAGGAT
CTGAATAGCGCCGTCGACCATCATCATCATCATCATTGAGTTTAAACGGT

References

1. Padwa, A., Ed.; In *1,3-Dipolar Cycloaddition Chemistry;* Wiley-Interscience Publication: New York, 1984; Vol. 1.
2. Chen, W.; Wang, D.; Dai, C.; Hamelberg, D.; Wang, B. Clicking 1,2,4,5-tetrazine and cyclooctynes with tunable reaction rates. *Chem. Commun.* **2012**, *48*, 1736-1738.
3. Liang, Y.; Mackey, J. L.; Lopez, S. A.; Liu, F.; Houk, K. N. Control and design of mutual orthogonality in bioorthogonal cycloadditions. *J. Am. Chem. Soc.* **2012**, *134*, 17904-17907.
4. Sachdeva, A.; Wang, K.; Elliott, T.; Chin, J. W. Concerted, rapid, quantitative, and site-specific dual labeling of proteins. *J. Am. Chem. Soc.* **2014**, *136*, 7785-7788.
5. Karver, M. R.; Weissleder, R.; Hilderbrand, S. A. Bioorthogonal reaction pairs enable simultaneous, selective, multi-target imaging. *Angew. Chem. Int. Ed.* **2012**, *51*, 920-922.
6. Karver, M. R.; Weissleder, R.; Hilderbrand, S. A. Synthesis and evaluation of a series of 1,2,4,5-tetrazines for bioorthogonal conjugation. *Bioconjugate Chem.* **2011**, *22*, 2263-2270.
7. Wang, K.; Sachdeva, A.; Cox, D. J.; Wilf, N. W.; Lang, K.; Wallace, S.; Mehl, R. A.; Chin, J. W. Optimized orthogonal translation of unnatural amino acids enables spontaneous protein double-labelling and FRET. *Nature Chem.* **2014**, *6*, 393-403.
8. Kamber, D. N.; Nazarova, L. A.; Liang, Y.; Lopez, S. A.; Patterson, D. M.; Shih, H.; Houk, K. N.; Prescher, J. A. Isomeric cyclopropenes exhibit unique bioorthogonal reactivities. *J. Am. Chem. Soc.* **2013**, *135*, 13680-13683.

9. Sletten, E. M.; Bertozzi, C. R. A bioorthogonal quadricyclane ligation. *J. Am. Chem. Soc.* **2011**, *133*, 17570-17573.
10. Hill, W. E.; Szechi, J.; Hofstee, C.; Dane, J. H. Fate of a highly strained hydrocarbon in aqueous soil environment. *Environ. Sci. Technol.* **1997**, *31*, 651-655.
11. Jin, S.; Swoboda-Colberg, N.; Colberg, P. J. S. Microbial degradation of quadricyclane-derived tricyclo[2.2.1.$0^{2,6}$]heptan-3-ol in soil. *Can. J. Microbiol.* **1997**, *43*, 300-303.
12. Kolb, H. C.; Finn, M. G.; Sharpless, K. B. Click chemistry: Diverse chemical function from a few good reactions. *Angew. Chem. Int. Ed.* **2001**, *40*, 2004-2021.
13. Kabakoff, D. S.; Buenzli, J. C. G.; Oth, J. F. M.; Hammond, W. B.; Berson, J. A. Enthalpy and kinetics of isomerization of quadricyclane to norbornadiene. strain energy of quadricyclane. *J. Am. Chem. Soc.* **1975**, *97*, 1510-1512.
14. Hall, H. K.; Smith, C. D.; Baldt, J. H. Enthalpies of formation of nortricyclene, norbornene, norbornadiene, and quadricyclane. *J. Am. Chem. Soc.* **1973**, *95*, 3197-3201.
15. Turner, R. B.; Goebel, P.; Mallon, B. J.; Doering, W.; Coburn, J. F.; Pomerantz, M. Heats of hydrogenation. VIII. compounds with three-and four-membered rings. *J. Am. Chem. Soc.* **1968**, *90*, 4315-4322.
16. Krebs, A.; Wilke, J. Angle strained cycloalkynes. *Top. Curr. Chem.* **1983**, *109*, 189-233.
17. Watson, W. H.; Tavanaiepour, I.; Marchand, A. P.; Dave, P. R. 3-(*p*-cyanophenoxy)quadricyclane and a redetermination of the structure of a hexachloroquadricyclane dicarboxylate. *Acta Crystallogr. , Sect. C: Cryst. Struct. Commun.* **1987**, *C43*, 1356-1359.
18. Dube, D. H.; Bertozzi, C. R. Metabolic oligosaccharide engineering as a tool for glycobiology. *Curr. Opin. Chem. Biol.* **2003**, *7*, 616-625.
19. Lang, K.; Chin, J. W. Cellular incorporation of unnatural amino acids and bioorthogonal labeling of proteins. *Chem. Rev.* **2014**, *114*, 4764-4806.
20. Jacobs, C. L.; Goon, S.; Yarema, K. J.; Hinderlich, S.; Hang, H. C.; Chai, D. H.; Bertozzi, C. R. Substrate specificity of the sialic acid biosynthetic pathway. *Biochemistry* **2001**, *40*, 12864-12874.
21. Polycarpo, C. R.; Herring, S.; Bérubé, A.; Wood, J. L.; Söll, D.; Ambrogelly, A. Pyrrolysine analogues as substrates for pyrrolysyl-tRNA synthetase. *FEBS Lett.* **2006**, *580*, 6695-6700.
22. Li, W.; Mahapatra, A.; Longstaff, D. G.; Bechtel, J.; Zhao, G.; Kang, P. T.; Chan, M. K.; Krzycki, J. A. Specificity of pyrrolysyl-tRNA synthetase for pyrrolysine and pyrrolysine analogs. *J. Mol. Biol.* **2009**, *385*, 1156-1164.
23. Fekner, T.; Li, X.; Chan, M. K. Pyrrolysine analogs for translational incorporation into proteins. *Eur. J. Org. Chem.* **2010**, *2010*, 4171-4179.
24. Debets, M. F.; van der Doelen, C. W. J.; Rutjes, F. P. J. T.; van Delft, F. L. Azide: A unique dipole for metal-free bioorthogonal ligations. *ChemBioChem* **2010**, *11*, 1168-1184.
25. Plass, T.; Milles, S.; Koehler, C.; Szymanski, J.; Mueller, R.; Wießler, M.; Schultz, C.; Lemke, E. A. Amino acids for diels-alder reactions in living cells. *Angew. Chem. Int. Ed.* **2012**, *51*, 4166-4170.
26. Shieh, P.; Siegrist, M. S.; Cullen, A. J.; Bertozzi, C. R. Imaging bacterial peptidoglycan with near-infrared fluorogenic azide probes. *Proc. Natl. Acad. Sci. USA* **2014**, *111*, 5456-5461.
27. Borrmann, A.; Milles, S.; Plass, T.; Dommerholt, J.; Verkade, J. M. M.; Wießler, M.; Schultz, C.; van Hest, J. C. M.; van Delft, F. L.; Lemke, E. A. Genetic encoding of a bicyclo[6.1.0]nonyne-charged amino acid enables fast cellular protein imaging by metal-free ligation. *ChemBioChem* **2012**, *13*, 2094-2099.
28. Ward, M. D.; McCleverty, J. A. Non-innocent behaviour in mononuclear and polynuclear complexes: Consequences for redox and electronic spectroscopic properties. *J. Chem. Soc. Dalton Trans.* **2002**, 275-288.
29. Beswick, C., L.; Schulman, J., M; Stiefel, E., I. In *Structures and Structural Trends in Homoleptic Dithiolene Complexes;* Karlin, K. D., Stiefel, E. I., Eds.; Dithiolene Chemistry:

Synthesis, Properties, and Applications. Progress in Inorganic Chemistry. 2004; Vol. 52, pp 55-110.
30. Sletten, E. M. Bioorthogonal Chemistries for Labeling Living Systems. Ph.D. dissertation. University of California, Berkeley, Berkeley, CA, 2011.
31. Lai, C. S.; Froncisz, W.; Hopwood, L. E. An evaluation of paramagnetic broadening agents for spin probe studies of intact mammalian cells. *Biophys. J.* **1987**, *52*, 625-628.
32. Dowden, B. F.; Bennett, H. J. Toxicity of selected chemicals to certain animals. *Journal (Water Pollution Control Federation)* **1965**, *37*, 1308-1316.
33. Agarwal, P.; Bertozzi, C. R. Site-specific Antibody–Drug conjugates: The nexus of bioorthogonal chemistry, protein engineering, and drug development. *Bioconjugate Chem.* **2015**, *26*, 176-192.
34. Link, A. J.; Mock, M. L.; Tirrell, D. A. Non-canonical amino acids in protein engineering. *Curr. Opin. Biotechnol.* **2003**, *14*, 603-609.
35. Bain, J. D.; Diala, E. S.; Glabe, C. G.; Dix, T. A.; Chamberlin, A. R. Biosynthetic site-specific incorporation of a non-natural amino acid into a polypeptide. *J. Am. Chem. Soc.* **1989**, *111*, 8013-8014.
36. Noren, C.; Anthony-Cahill, S.; Griffith, M.; Schultz, P. A general method for site-specific incorporation of unnatural amino acids into proteins. *Science* **1989**, *244*, 182-188.
37. Nowak, M.; Kearney, P.; Sampson; Saks, M.; Labarca, C.; Silverman, S.; Zhong, W.; Thorson, J.; Abelson, J.; Davidson, N.; et, a. Nicotinic receptor binding site probed with unnatural amino acid incorporation in intact cells. *Science* **1995**, *268*, 439-442.
38. Wang, L.; Brock, A.; Herberich, B.; Schultz, P. G. Expanding the genetic code of escherichia coli. *Science* **2001**, *292*, 498-500.
39. Chin, J. W.; Cropp, T. A.; Anderson, J. C.; Mukherji, M.; Zhang, Z.; Schultz, P. G. An expanded eukaryotic genetic code. *Science* **2003**, *301*, 964-967.
40. Liu, W.; Brock, A.; Chen, S.; Chen, S.; Schultz, P. G. Genetic incorporation of unnatural amino acids into proteins in mammalian cells. *Nat. Methods* **2007**, *4*, 239-244.
41. Liu, C. C.; Schultz, P. G. Adding new chemistries to the genetic code. *Annu. Rev. Biochem.* **2010**, *79*, 413-444.
42. Burke, S. A.; Lo, S. L.; Krzycki, J. A. Clustered genes encoding the methyltransferases of methanogenesis from monomethylamine. *J. Bacteriol.* **1998**, *180*, 3432-3440.
43. James, C. M.; Ferguson, T. K.; Leykam, J. F.; Krzycki, J. A. The amber codon in the gene encoding the monomethylamine methyltransferase isolated from methanosarcina barkeri is translated as a sense codon. *J. Biol. Chem.* **2001**, *276*, 34252-34258.
44. Hao, B.; Gong, W.; Ferguson, T. K.; James, C. M.; Krzycki, J. A.; Chan, M. K. A new UAG-encoded residue in the structure of a methanogen methyltransferase. *Science* **2002**, *296*, 1462-1466.
45. Srinivasan, G.; James, C. M.; Krzycki, J. A. Pyrrolysine encoded by UAG in archaea: Charging of a UAG-decoding specialized tRNA. *Science* **2002**, *296*, 1459-1462.
46. Polycarpo, C.; Ambrogelly, A.; Bérubé, A.; Winbush, S. M.; McCloskey, J. A.; Crain, P. F.; Wood, J. L.; Söll, D. An aminoacyl-tRNA synthetase that specifically activates pyrrolysine. *Proc. Natl. Acad. Sci. USA* **2004**, *101*, 12450-12454.
47. Blight, S. K.; Larue, R. C.; Mahapatra, A.; Longstaff, D. G.; Chang, E.; Zhao, G.; Kang, P. T.; Green-Church, K.; Chan, M. K.; Krzycki, J. A. Direct charging of tRNACUA with pyrrolysine in vitro and in vivo. *Nature* **2004**, *431*, 333-335.
48. Wang, Y.; Fang, X.; Chen, H.; Wu, B.; Wang, Z. U.; Hilty, C.; Liu, W. R. Genetic incorporation of twelve meta-substituted phenylalanine derivatives using a single pyrrolysyl-tRNA synthetase mutant. *ACS Chem. Biol.* **2013**, *8*, 405-415.
49. Wang, Y.; Fang, X.; Wallace, A. L.; Wu, B.; Liu, W. R. A rationally designed pyrrolysyl-tRNA synthetase mutant with a broad substrate spectrum. *J. Am. Chem. Soc.* **2012**, *134*, 2950-2953.

50. Nguyen, D. P.; Lusic, H.; Neumann, H.; Kapadnis, P. B.; Deiters, A.; Chin, J. W. Genetic encoding and labeling of aliphatic azides and alkynes in recombinant proteins via a pyrrolysyl-tRNA synthetase/tRNACUA pair and click chemistry. *J. Am. Chem. Soc.* **2009**, *131*, 8720-8721.
51. Fekner, T.; Li, X.; Lee, M. M.; Chan, M. K. A pyrrolysine analogue for protein click chemistry. *Angew. Chem.* **2009**, *121*, 1661-1663.
52. Hao, Z.; Song, Y.; Lin, S.; Yang, M.; Liang, Y.; Wang, J.; Chen, P. R. A readily synthesized cyclic pyrrolysine analogue for site-specific protein "click" labeling. *Chem. Commun.* **2011**, *47*, 4502-4504.
53. Yanagisawa, T.; Ishii, R.; Fukunaga, R.; Kobayashi, T.; Sakamoto, K.; Yokoyama, S. Multistep engineering of pyrrolysyl-tRNA synthetase to genetically encode N(epsilon)-(o-azidobenzyloxycarbonyl) lysine for site-specific protein modification. *Chem. Biol.* **2008**, *15*, 1187-1197.
54. Lang, K.; Davis, L.; Torres-Kolbus, J.; Chou, C.; Deiters, A.; Chin, J. W. Genetically encoded norbornene directs site-specific cellular protein labelling via a rapid bioorthogonal reaction. *Nature Chem.* **2012**, *4*, 298-304.
55. Plass, T.; Milles, S.; Koehler, C.; Schultz, C.; Lemke, E. A. Genetically encoded copper-free click chemistry. *Angew. Chem. Int. Ed.* **2011**, *50*, 3878-3881.
56. Lang, K.; Davis, L.; Wallace, S.; Mahesh, M.; Cox, D. J.; Blackman, M. L.; Fox, J. M.; Chin, J. W. Genetic encoding of bicyclononynes and trans-cyclooctenes for site-specific protein labeling in vitro and in live mammalian cells via rapid fluorogenic diels-alder reactions. *J. Am. Chem. Soc.* **2012**, *134*, 10317-10320.
57. Nozawa, K.; O'Donoghue, P.; Gundllapalli, S.; Araiso, Y.; Ishitani, R.; Umehara, T.; Soll, D.; Nureki, O. Pyrrolysyl-tRNA synthetase-tRNAPyl structure reveals the molecular basis of orthogonality. *Nature* **2009**, *457*, 1163-1167.
58. Chen, P. R.; Groff, D.; Guo, J.; Ou, W.; Cellitti, S.; Geierstanger, B. H.; Schultz, P. G. A facile system for encoding unnatural amino acids in mammalian cells. *Angew. Chem. Int. Ed.* **2009**, *48*, 4052-4055.
59. Mukai, T.; Kobayashi, T.; Hino, N.; Yanagisawa, T.; Sakamoto, K.; Yokoyama, S. Adding l-lysine derivatives to the genetic code of mammalian cells with engineered pyrrolysyl-tRNA synthetases. *Biochem. Biophys. Res. Commun.* **2008**, *371*, 818-822.
60. Hancock, S. M.; Uprety, R.; Deiters, A.; Chin, J. W. Expanding the genetic code of yeast for incorporation of diverse unnatural amino acids via a pyrrolysyl-tRNA synthetase/tRNA pair. *J. Am. Chem. Soc.* **2010**, *132*, 14819-14824.
61. Greiss, S.; Chin, J. W. Expanding the genetic code of an animal. *J. Am. Chem. Soc.* **2011**, *133*, 14196-14199.
62. Bianco, A.; Townsley, F. M.; Greiss, S.; Lang, K.; Chin, J. W. Expanding the genetic code of drosophila melanogaster. *Nat. Chem. Biol.* **2012**, *8*, 748-750.
63. Wang, K.; Neumann, H.; Peak-Chew, S.; Chin, J. W. Evolved orthogonal ribosomes enhance the efficiency of synthetic genetic code expansion. *Nat. Biotechnol.* **2007**, *25*, 770-777.
64. Chin, J. W. Expanding and reprogramming the genetic code of cells and animals. *Annu. Rev. Biochem.* **2014**, *83*, 379-408.
65. Hochuli, E.; Döbeli, H.; Schacher, A. New metal chelate adsorbent selective for proteins and peptides containing neighbouring histidine residues. *J. Chromatogr. A* **1987**, *411*, 177-184.
66. Hochuli, E.; Bannwarth, W.; Dobeli, H.; Gentz, R.; Stuber, D. Genetic approach to facilitate purification of recombinant proteins with a novel metal chelate adsorbent. *Nat. Biotechnol.* **1988**, *6*, 1321-1325.
67. Pangborn, A. B.; Giardello, M. A.; Grubbs, R. H.; Rosen, R. K.; Timmers, F. J. Safe and convenient procedure for solvent purification. *Organometallics* **1996**, *15*, 1518-1520.

68. Still, W. C.; Kahn, M.; Mitra, A. Rapid chromatographic technique for preparative separations with moderate resolution. *J. Org. Chem.* **1978**, *43*, 2923-2925.

Chapter 4:
A "Click-Unclick" Quadricyclane Ligation

Introduction

As the field of bioorthogonal chemistry develops, researchers are working to expand the repertoire of chemical transformations available for use *in vivo*. Whereas the first bioorthogonal ligations were optimized to selectively form covalent bonds in living systems, there is now growing interest in the development of biocompatible reactions that parallel the vast library of organic transformations. For example, one can imagine polymerizations, isomerization chemistries, stereoselective reactions, or reversible transformations that are designed for use *in vivo*. Ligations that proceed in response to cues such as pH or temperature would also be valuable additions to the bioorthogonal toolkit. Indeed, researchers have begun to engineer bioconjugations that achieve new function. At the forefront of these developments are new reversible bioconjugations and ligations that are responsive to environmental cues.

Reversible Bioconjugations

There is considerable interest in the development of reversible bioconjugations for use in design of cleavable linkers capable of releasing cargoes from antibody-drug conjugates[1] and as methods of mimicking transient post-translational modifications.[2]

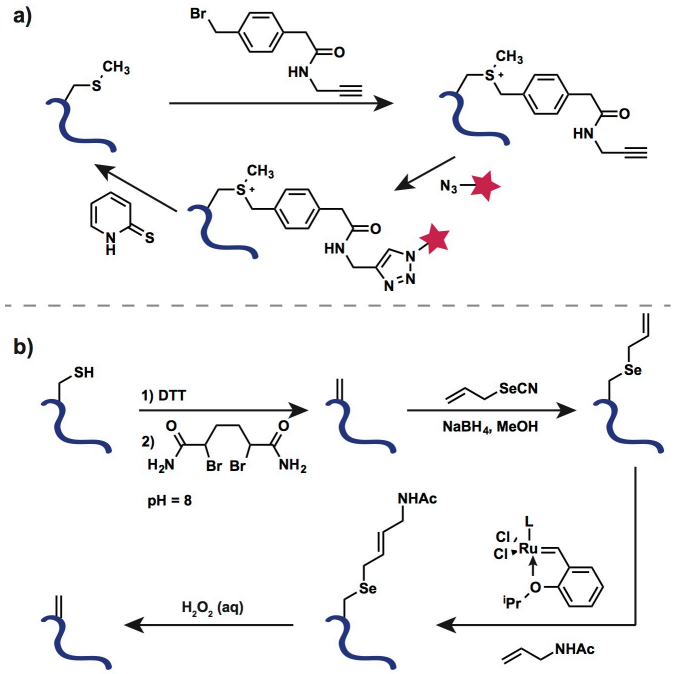


Figure 4.1. Examples of reversible conjugation chemistries for modification of proteins and peptides. (a) Reversible modification of methionine residues via a "tag-modify-release" strategy and (b) a "read-write-erase" strategy for reversible modification of dehydroalanine residues, accessed via modification of cysteine.

As well, chemical functionalities that partake in reversible reactions are valuable purification handles for protein isolation and enrichment.[3]

In 2013, Deming and co-workers introduced a "tag-modify-release" strategy (Figure 4.1a) based on the reversible alkylation of methionine (Met) residues.[4] They identified optimal conditions for selective alkylation of Met followed by facile de-alkylation using appropriate nucleophiles such as 2-mercaptopyridine. By this method, Deming was able to append bioorthogonal functional groups such as azides and alkynes to Met residues in peptides, functionalize these groups with fluorophores by copper-click chemistry, and cleave off the modification via addition of an appropriate nucleophile.

A similar "read-write-erase" technique was introduced by Davis and co-workers for selective modification of cysteine residues in proteins (Figure 4.1b).[2] By their method, cysteine is converted to dehydroalanine via bis-alkylative elimination with dibromohexanediamide. Dehydroalanine is then converted to allyl selenocysteine via nucleophilic addition of allyl selonolate. The resulting allyl selenocysteine is known to undergo ruthenium catalyzed cross metathesis (CM) under biological conditions.[5] Davis elected to install an N-acyl moiety via CM to generate a model for lysine acetylation in histones. To recapitulate the reversibility of histone acetylation, the CM-installed acyl group can be cleaved via a Cope-type elimination with hydrogen peroxide to re-form the starting dehydroalanine. In this way, the strategy serves as a "read-write-erase" approach.

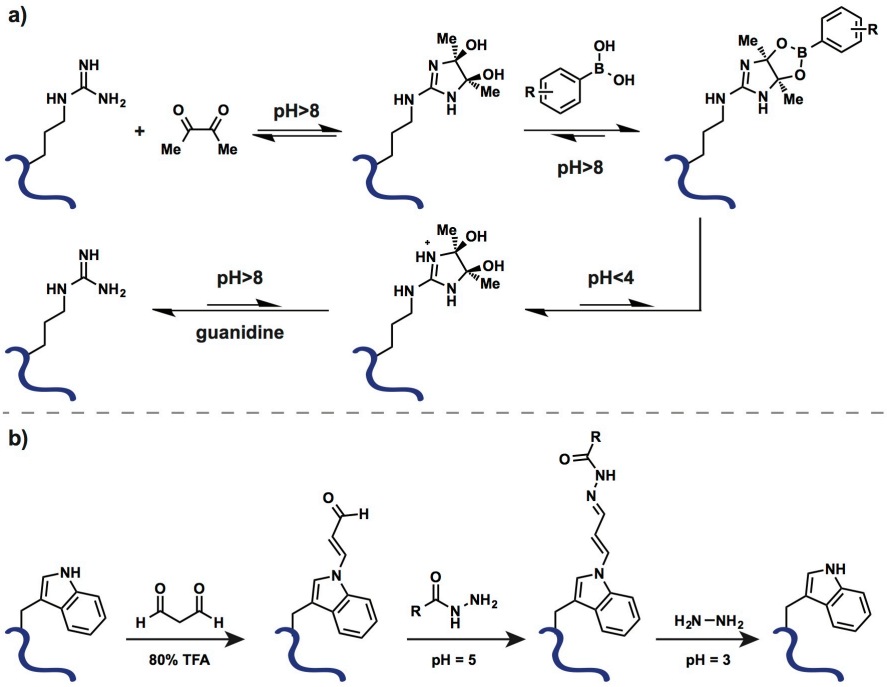


Figure 4.2. Reversible bioconjugation chemistries for amino-acid dependent peptide enrichment. (a) Functionalization of arginine residues via installation of a vicinal diol followed by modification with reversible boronic acid chemistry. (b) Reversible functionalization of tryptophan residues via installation of an α,β-unsaturated aldehyde followed by hydrazone formation and subsequent cleavage with excess hydrazine under acidic conditions.

Other examples of reversible bioconjugations include the pH-dependent reaction between boronic acids and 1,2- or 1,3-diols to form boronic esters. This reaction has been widely used for isolation and enrichment of nucleosides, sugar-containing molecules, and biomolecules containing synthetically installed diol moieties.[3,6,7] An example in which this chemistry is used for enrichment of arginine-containing peptides is shown in Figure 4.2a.[6] Here, arginine residues are converted to a 1,2-diol via reaction with 2,3-butanedione. The resulting diol then reversibly reacts with phenylboronic acid-modified beads, enabling enrichment of arginine-containing peptides.

Hydrazone formation between ketones and hydrazines has also been employed as a reversible reaction for enrichment of biomolecules that have been synthetically modified with carbonyl groups. The hydrazone can be cleaved by introducing an excess of hydrazine at low pH.[3,8,9] An example of reversible hydrazone chemistry is shown in Figure 4.2b, where tryptophan residues are modified via condensation with malondialdehyde and subsequently pulled down with hydrazide-conjugated beads.[8,9] In addition to hydrazone and boronic ester chemistries, the reversible formation of disulfide bonds has been widely exploited for enrichment of cysteine-containing proteins.[3]

Despite the utility of these reactions as methods of enrichment and *ex-vivo* protein modification, they all rely on native biological functionalities as a reaction partner. Thus, these conjugations are inherently non-selective. To date, a reversible bioconjugation employing all non-native functionalities has not been reported. A truly bioorthogonal and reversible reaction would be valuable to achieve high levels of selectivity for protein purifications and enrichments, as a controlled method of cleaving cargoes from protein carriers, and as a method of achieving transient and selective protein modifications *in vitro* or *in vivo*.

Bioconjugations that are responsive to environmental cues

Researchers are also working toward the development of bioorthogonal reactions that proceed in response to environmental cues. These reactions afford high levels of spatial and temporal control over target labeling.

To this end, Lin and co-workers have developed a new class of reactions termed "photo-click" chemistries.[10–12] The reactions rely on the photolytic conversion of tetrazole to nitrile imine, and the subsequent 1,3-dipolar cycloaddition between nitrile imines and alkenes to form pyrazolines (Figure 4.3a). This cycloaddition is particularly attractive because it is fluorogenic, meaning the pyrazoline product is fluorescent whereas the starting materials are not. This technique has been used to achieve selective labeling of individual cells in culture via two-photon irradiation.[13] Similar studies have been performed for spatially controlled imaging of microtubules in mammalian cells.[14,15] A related reaction employs the photochemical conversion of azirines to nitrile ylides for subsequent cycloaddition with alkenes (Figure 4.3b).[16]

In another example of photo-click chemistry, Boons, Popik and co-workers have developed a cyclopropenone-masked cyclooctyne, which cleaves to reveal the strained

alkyne upon irradiation (Figure 4.3c).[17] The resulting chemistry has been used to label azides on cells and also to generate patterned surfaces via photolithography.[18,19]

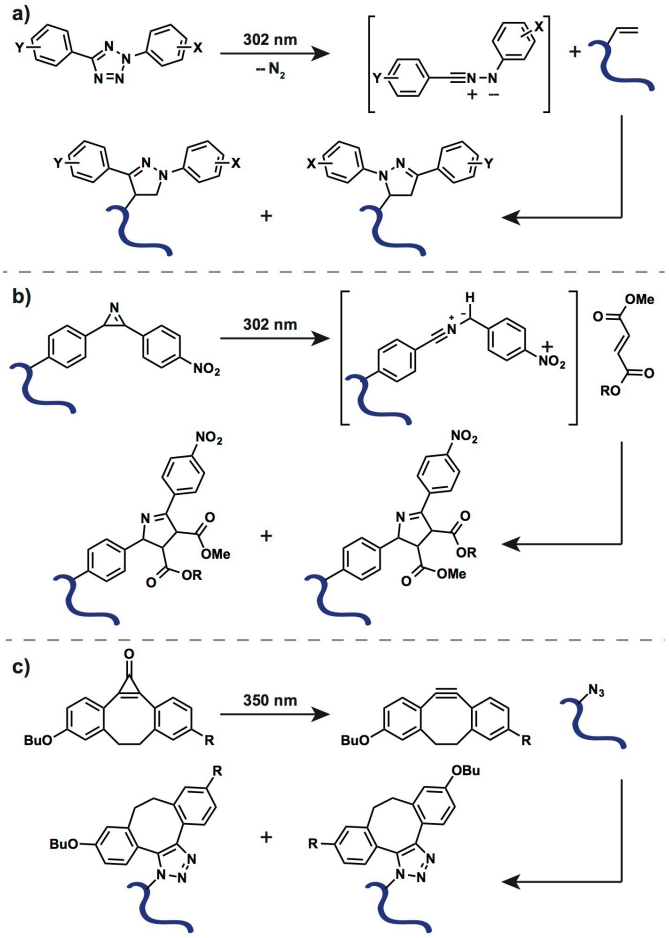


Figure 4.3. "Photo-click" chemistries. (a) Irradiation of tetrazole at 302 nm generates nitrile imine, which reacts with alkenes to form the pyrazoline shown. (b) Azirine cleaves to form a nitrile ylide upon irradiation at 302 nm, which subsequently reacts with alkenes to form the indicated pyrroline. (c) Cyclopropenone is cleaved via irradiation at 350 nm to unmask the cyclooctyne moiety, which then undergoes copper-free click chemistry with the azide to form triazoles.

Van Delft and co-workers recently reported another example of a bioconjugation that responds to environmental cues.[20] This reaction takes advantage of the Diels—Alder cycloaddition between cyclooctynes and 1,2-quinones to form the adduct shown in Figure 4.4. The cycloaddition is rendered environment-dependent by using the reduced form of the quinone, the catechol, as the tagging agent. Then, only upon introduction of an appropriate oxidizing agent does the reaction proceed. Van Delft demonstrated the use of this reaction to label purified proteins but has yet to apply the chemistry to more complex mixtures, likely because of the rapid reactivity between quinones and biological nucleophiles such as cysteines and lysines.

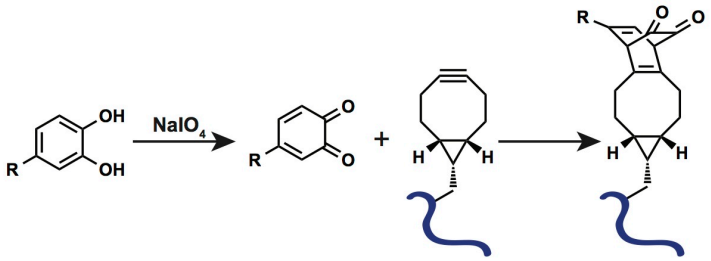


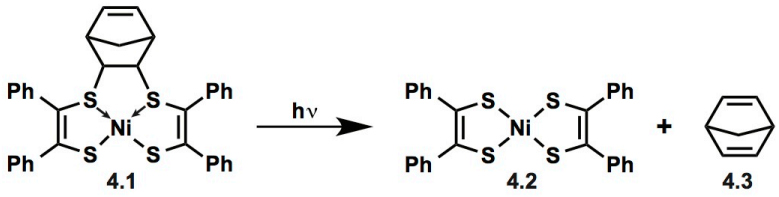
Figure 4.4. Oxidation-controlled click chemistry. Oxidation of a catechol with sodium periodate to form the quinone followed by Diels—Alder cycloaddition with bicyclononyne.

Overall, these reactions pave the way for expanding the utility of bioorthogonal tools *in vitro* and *in vivo*. Inspired by this work, we endeavored to explore additional biocompatible transformations accessible through the quadricyclane ligation.

A "Click-Unclick" Quadricyclane Ligation

Background

Early reports of the photolability of the QC/metal bis(dithiolene) adduct piqued our interest. This photolability was first discussed by Schrauzer and Mayweg in 1965 when they noticed that the adduct decomposes when exposed to daylight.[21] Later studies by Wing and Sugimori describe the photolysis reaction to be that shown in Figure 4.5, where adduct **4.1** is cleaved to form the starting nickel bis(dithiolene) **4.2** and norbornadiene **4.3**, an isomer of QC.[22–24] Sugimori analyzed the quantum yield of photolysis at varying wavelengths, and results are shown in Figure 4.5.[23]



wavelength (nm)	Φ
254	0.083
313	0.068
365	0.14
436	0.13

Figure 4.5. Photodissociation of the QC/nickel bis(dithiolene) adduct. Wavelengths and associated quantum yields measured by Sugimori and co-workers are listed. [23]

We envisioned taking advantage of the photolability of adduct **4.1** to render the QC ligation reversible. However, the success of the photocleavage in the presence of myriad biological functionalities would depend on an absence of long-lived reactive

intermediates produced as a by-product of photolysis. Sugimori published a thorough mechanistic analysis of the photolysis of various nickel bis(dithiolene) adducts, beginning with the S,S'-dibenzyl–nickel bis(dithiolene) adduct shown in Figure 4.6a.[25] The proposed mechanism is based on ESR and UV-vis studies. Sugimori found that upon irradiation of the adduct, a long-lived benzyl/nickel bis(dithiolene) radical pair is formed in solution and persists with a lifetime of approximately 1,000 seconds prior to cleavage of the second benzyl group to form the free nickel bis(dithiolene). Sugimori was able to trap the benzyl radical with TEMPO as further evidence of its long lifetime in solution. Similarly, the bridged nickel bis(dithiolene) adduct shown in Figure 4.6b was found to generate two long-lived radicals with lifetimes of 100 and 500 seconds respectively. Such long-lived radical species would be a liability for biological experiments, as many biological functionalities are susceptible to damage via radical pathways.

Sugimori also performed ESR studies on the photolysis of the adducts of QC and norbornene with nickel bis(dithiolene) (compound **4.1**) and, unlike the dibenzyl and bridged butanediyl adducts, found no evidence of long-lived radical species.[25] This result suggests that photolysis of adduct **4.1** proceeds via a concerted process or a rapid two-step mechanism. The absence of long-lived radical species is evidence that the cleavage may proceed cleanly in biological environments.

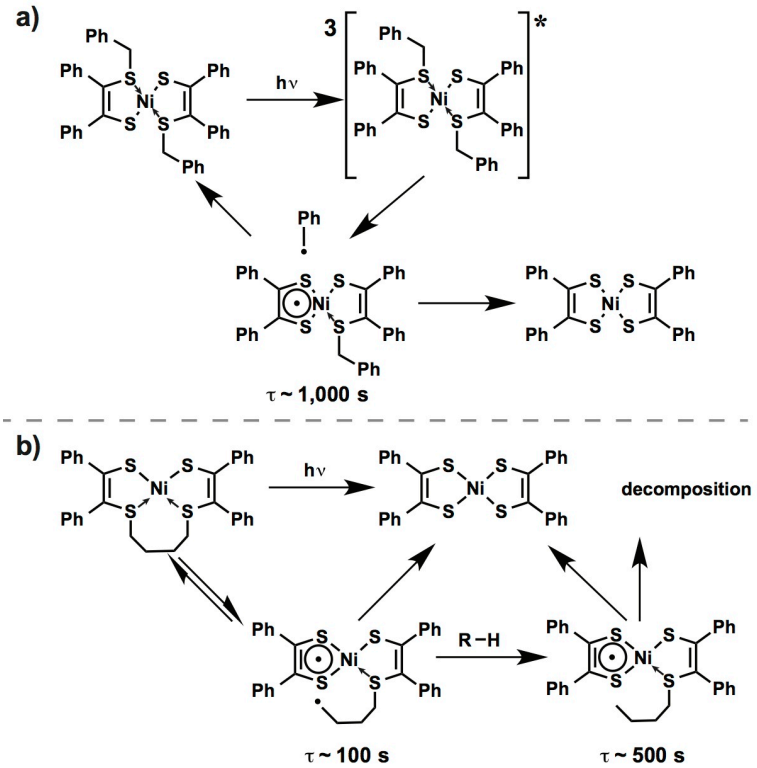


Figure 4.6. Mechanistic analysis of photolytic cleavage of nickel bis(dithiolene) adducts. (a) Sugimori's proposed mechanism for the photolytic cleavage of the S,S'-dibenzyl-nickel bis(ditholene) adduct and (b) proposed mechanism for photocleavage of the bridged butanediyl adduct.

^{1}H NMR Analysis of Photolysis

We began by analyzing the efficiency of the photocleavage reaction in a flask, aiming to determine its half-life upon irradiation with a handheld UV lamp. We chose to analyze the photocleavage at 365 nm because of the relatively high quantum yield associated with this wavelength (Figure 4.5). Adduct **4.4** (Figure 4.7) was synthesized from commercially available nickel bis(dithiolene) **4.2** and quadricyclane acetate **3.16** (hereafter referred to as QCOAc) via the route published by Sletten *et al.*[26] Upon purification, **4.4** was dissolved in $CDCl_3$ to 8.2 mM, and 700 μL of the solution was aliquoted into each of two quartz NMR tubes. One tube was maintained in ambient light at room temperature for 90 min, while the other was irradiated with a 365 nm handheld UV lamp for 90 min. ^{1}H NMR spectra were taken of the solutions at various timepoints over the course of the 90 min irradiation. We observed clean conversion of the adduct to the corresponding norbornadiene acetate **3.13** and nickel bis(dithiolene) **4.2**. Figure 4.7 shows the ^{1}H NMR spectra of samples exposed to 365 nm light or ambient light for 90 min.‡‡‡‡‡ We observed no photolysis of the starting material in ambient light and roughly 90% photolysis upon irradiation at 365 nm. The reaction reached ~50% conversion between 10 and 20 min irradiation with 365 nm (see Materials and Methods section). As further evidence of the progression of the photolysis, the reaction mixture underwent a remarkable color change from orange to dark green upon irradiation at 365 nm, consistent with the production of nickel bis(dithiolene) **4.2** which has a characteristic absorption band at ~850 nm.[23] Given the rapid photolysis of adduct **4.4** at room temperature using a handheld lamp, we decided to move forward to test this approach on proteins labeled via the QC ligation.

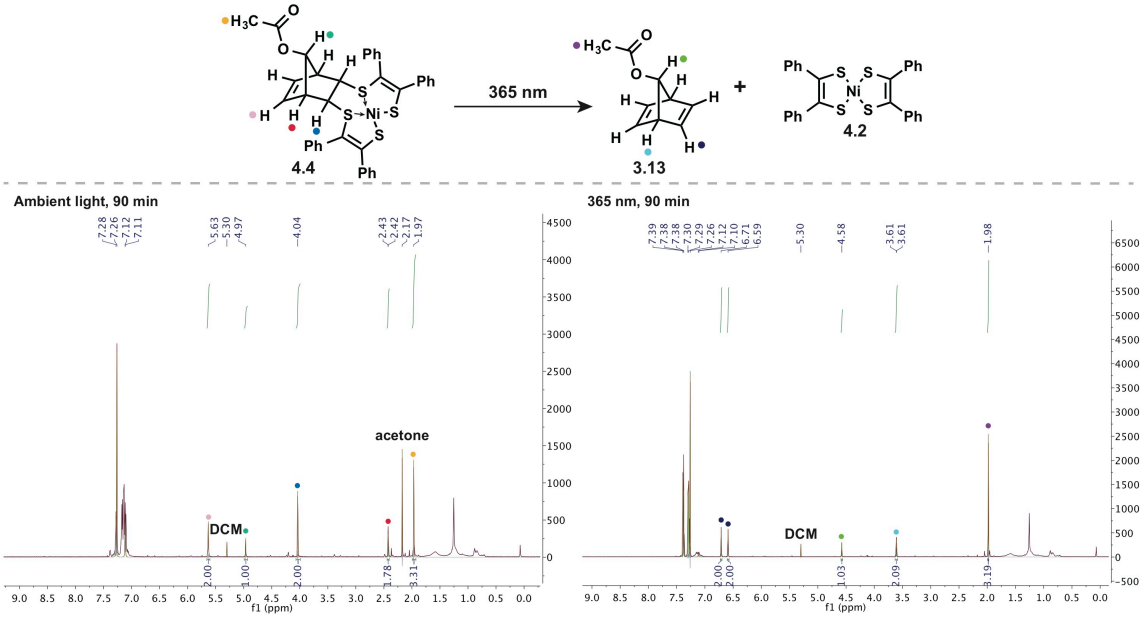


Figure 4.7. ^{1}H NMR analysis of the photolytic cleavage of QC/nickel bis(dithiolene) adduct 4.4 to norbornadiene 3.13 and nickel bis(dithiolene) 4.2.

‡‡‡‡‡ Spectral data are consistent with those reported by Kajitani *et al.* for a similar compound. See reference 23.

Proof-of-Concept Photolysis on a Model Protein

We labeled bovine serum albumin (BSA) with *p*-nitrophenyl quadricyclane carbonate **3.14** via the route developed by Sletten *et al.*[26] to give QC-BSA (Figure 4.8a), our model protein for optimization of the photocleavage reaction. QC-BSA was then labeled via QC ligation with nickel bis(dithiolene) biotin **3.19** to yield biotin-labeled BSA **4.5** (Figure 4.8a). As a negative control, BSA that was not labeled with QC was exposed to the same reaction conditions with **3.19** (hereafter referred to as **3.19**-treated BSA). The reactions were quenched with free QCOAc and then underwent two rounds of solvent exchange into fresh PBS with a centrifugal filter to remove excess **3.19** or adduct between **3.19** and QCOAc. Next, samples were aliquoted into borosilicate glass tubes and tubes were irradiated for various amounts of time (0, 30, 60, and 90 min) with a 365 nm handheld UV lamp or with ambient light (Figure 4.8b). After irradiation, centrifugal filters were again used to remove any ejected **3.19**, and samples were analyzed by Western blot for the presence of biotin with an α-biotin antibody.

We expected to see a decrease in α-biotin signal on **4.5** irradiated with 365 nm light relative to sample exposed only to ambient light. Results, shown in Figure 4.8c, confirm this hypothesis. After 30 min irradiation, there appears to be a noticeable decrease in signal in samples of **4.5** that were treated with UV light. However, this signal does not continue to decrease after the 30 min timepoint, and is never completely abolished. Interestingly, we also observed a slight decrease in signal for samples of **4.5** that were exposed to ambient light, not unexpected considering the quantum yields of the photocleavage at higher wavelengths (Figure 4.5) and Sletten's report that an adduct similar to **4.5** has a half life of ~35 hours in ambient light for the photocleavage.

We were surprised, however, to observe an increase in signal in the **3.19**-treated BSA lanes for samples that were irradiated at 365 nm. Despite our attempts to wash away excess **3.19** following the QC ligation step, it is clear that some amount of **3.19** or other biotin-containing derivative remained even after the washes.

The failure of biotin signal to be completely abolished in the UV-treated QC-BSA lanes could be caused by reaction between the norbornadiene product of photolysis (NBD-BSA, Figure 4.8b) and ejected **3.19**. Norbornadiene is known to react with nickel bis(dithiolenes), albeit 1–4 orders of magnitude more slowly than QC depending on the reagents and solvents used.[23,27] For example, Sletten measured the second order rate constant for the reaction of norbornadiene acetate (**3.13**) and nickel bis(dithiolene) (**3.10**) to be 0.007 M^{-1} s^{-1} in 1:1 PBS:EtOH, as compared to the reaction between QCOAc and **3.10**, which has a second order rate constant of 0.25 M^{-1} s^{-1} in 1:1 PBS:EtOH.[26,27] We hypothesized that addition of excess QCOAc to scavenge ejected **3.19**, combined with decreasing the overall concentration of the photolysis reaction, would reduce the rate of the reaction between **3.19** and NBD-BSA, thereby increasing cleavage efficiency.

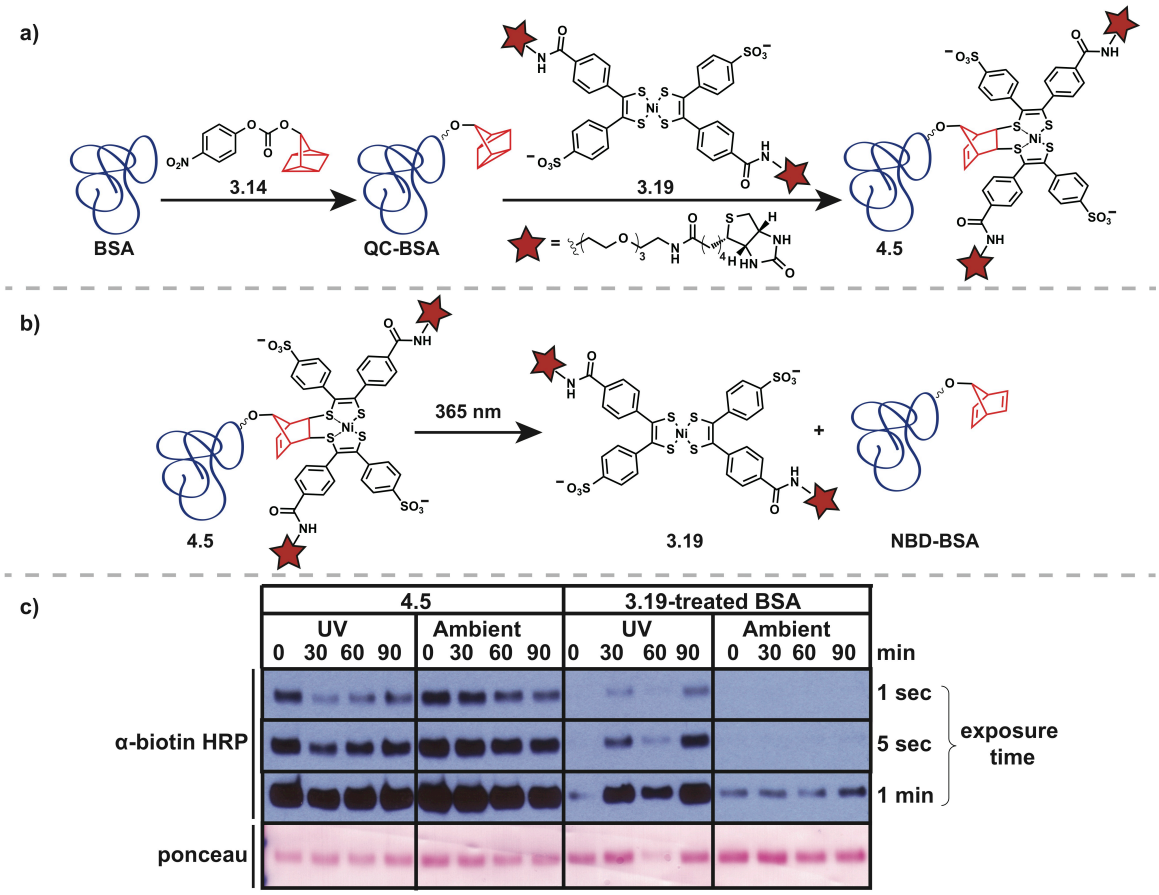


Figure 4.8. Photodissociation of the QC adduct on a protein. (a) Lysines on bovine serum albumin (BSA) were capped via reaction with *p*-nitrophenyl quadricyclane carbonate **3.14**. The resulting QC-BSA and untreated BSA (negative control) were treated with nickel bis(dithiolene) biotin **3.19** at 50 μM in PBS for 30 min to form adduct **4.5** or **3.19**-treated BSA. The reactions were quenched with QCOAc and protein was purified from excess small molecule (QCOAc, free **3.19**, and adduct between **3.19** and QCOAc) via centrifugal filtration with a 10 kDa molecular weight cutoff filter. (b) **4.5** and **3.19**-treated BSA in PBS were then irradiated with a 365 nm handheld UV lamp or with ambient light for 0, 30, 60, or 90 min to cleave the adduct. Protein products were separated from free **3.19** via centrifugal filtration. (c) Protein was analyzed via Western blot with an α-biotin-HRP antibody.

However, the increase in signal in the UV-treated BSA lanes is evidence that a QC-independent reaction between BSA and **3.19** is also occurring upon UV irradiation. While we have not yet characterized this reaction, we hypothesize that it may be a radical-mediated process occurring between BSA's sulfhydryl and disulfide groups (1 free sulfhydryl group and 17 disulfides per BSA)[28,29] and **3.19**. This background reaction is likely a contributor to the increasing signal observed in the **4.5** UV-treated samples at the 60 and 90 min timepoints. We hypothesized that decreasing the overall concentration of protein in the photolysis reaction would reduce the rate of this (likely bimolecular) background reaction.

Figure 4.9a shows the results of attempts to scavenge ejected **3.19** via addition of QCOAc. QC-BSA and BSA samples were prepared as in Figure 4.8a and treated with **3.19**. After centrifugal filtration to remove excess small molecule (QCOAc, free **3.19**,

and adduct between **3.19** and QCOAc), 50 µl samples were aliquoted into borosilicate glass tubes and supplemented with 1.2 µl 200 mM QCOAc in DMSO to a total QCOAc concentration of 4.8 mM[§§§§§] (QCOAc lanes), 1.2 µl DMSO (DMSO lanes) or 1.2 µl PBS (PBS lanes). All samples were irradiated at 365 nm with a handheld UV lamp for 60 min or left in ambient light for 60 min. After subsequent removal of released **3.19** by

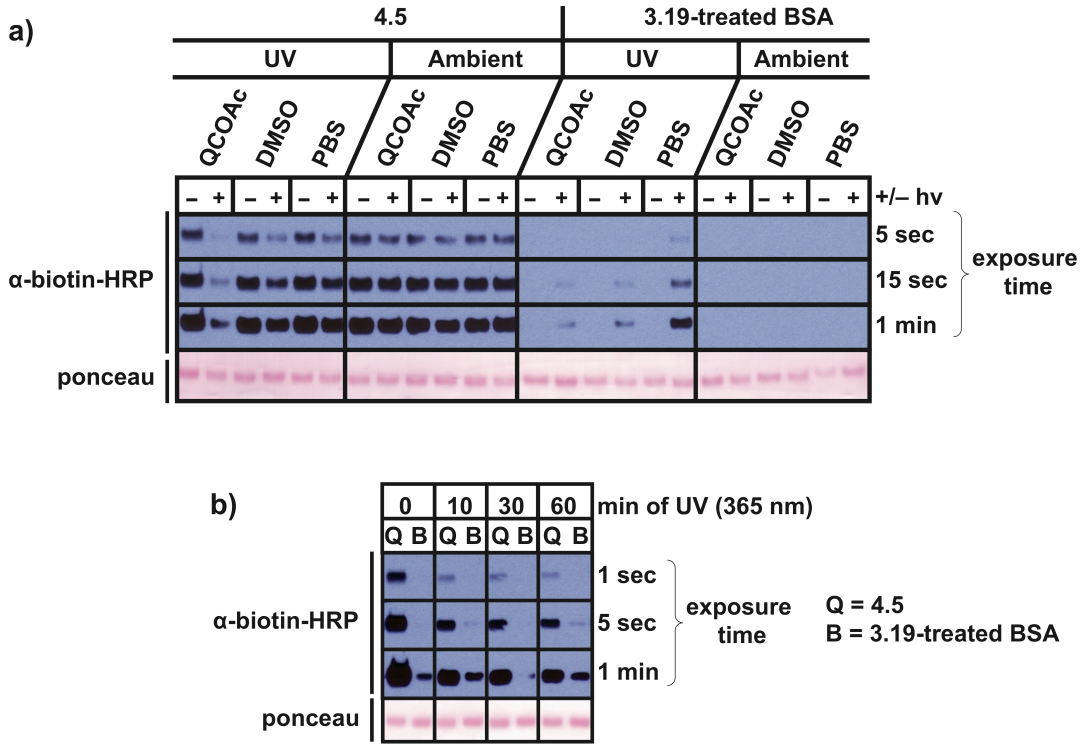


Figure 4.9. Optimization of the photodissociation reaction. (a) Addition of excess QCOAc to the reaction mixture to scavenge free nickel bis(dithiolene)biotin (**3.19**). **4.5** and **3.19**-treated BSA were aliquoted into borosilicate glass tubes as solutions in PBS and supplemented with 200 mM QCOAc in DMSO to a final concentration of 4.8 mM QCOAc and 2% DMSO (QCOAc lanes),[******] or were supplemented with DMSO to 2% (DMSO lanes), or an equivalent volume of PBS (PBS lanes). Samples were exposed to 365 nm UV light or ambient light for 60 min (+hv lanes) or were kept in the dark for 60 min (–hv lanes) at which point excess small molecule (QCOAc, free **3.19**, and adduct between **3.19** and QCOAc) was removed via centrifugal filtration. Samples were analyzed by Western blot with an α-biotin-HRP antibody.[††††††] (b) Combined effects of added QCOAc scavenger and reduced protein concentrations on the outcome of the photocleavage reaction. **4.5** and **3.19**-treated BSA were aliquoted as solutions in PBS into borosilicate glass tubes. Protein concentration was ~10-fold lower than that used in (a) of this figure and in Figure 4.8c. Samples were supplemented with QCOAc to 5 mM and irradiated at 365 nm with a handheld UV lamp for 0, 10, 30 and 60 min. Excess small molecule (QCOAc, free **3.19**, and adduct between **3.19** and QCOAc) was removed via centrifugal filtration. Protein was analyzed via Western blot with an α-biotin-HRP antibody.

[§§§§§] QCOAc is minimally soluble in PBS at this concentration and solutions were cloudy.
[******] QCOAc is minimally soluble in PBS at this concentration and solutions were cloudy.
[††††††] Prior to Western blot analysis, samples were exposed to 50 uM TAMRA-tetrazine for 15 min to probe the reactivity of NBD-BSA with tetrazine (see next section). Results of this treatment are not shown. As all samples were treated equally, it is unlikely that tetrazine exposure altered the results of the photodissociation experiment.

centrifugal filtration, samples were analyzed for the presence of biotin via Western blot with an α-biotin-HRP antibody.

We observed a dramatic decrease in biotin signal upon irradiation of the QCOAc-supplemented samples of **4.5** and a lesser decrease in biotin signal for those samples not supplemented with excess QCOAc (DMSO and PBS lanes). That the UV irradiated DMSO- and PBS- treated samples of **4.5** display similar levels of biotin signal suggests that DMSO (vehicle for QCOAc addition) does not significantly affect the photodissociation. We were also pleased to observe that the **3.19**-treated BSA lanes showed a lesser increase in signal upon UV irradiation when supplemented with QCOAc than when supplemented with PBS. However, the **3.19**-treated BSA samples supplemented with DMSO also displayed less signal after UV irradiation when compared to the PBS-supplemented **3.19**-treated BSA lanes, so we cannot definitively say that the reduced background signal in UV irradiated, QCOAc-supplemented **3.19**-treated BSA samples is a result of QCOAc and not the DMSO solvent. Regardless, these results suggest that QCOAc supplementation of the reaction enhances the efficiency of photocleavage of **4.5** and may minimize background reactivity.

We also investigated the effects of lower protein concentrations during photolysis on background reactivity and cleavage efficiency. Figure 4.9b shows the combined effects of QCOAc supplementation and decreased protein concentrations (~10 fold lower concentration of **4.5** that that used in Figures 4.9a and 4.8c). Overall, we observed a successful decrease in biotin signal on irradiated samples and diminished background reactivity (Figure 4.9b).

Overall, our results suggest that the adduct between QC and nickel bis(dithiolene) biotin on a model protein can be cleaved via photolysis. In future studies, we aim to analyze the efficiency of photolysis on a model protein containing fewer cysteines. As well, we plan to utilize this reaction on a protein that has been site-selectively labeled with QC amino acid.

Towards a Click-Unclick-Click Quadricyclane Ligation

We realized that the norbornadiene product of the photolysis reaction has the potential to serve as a secondary bioorthogonal handle, rendering the QC ligation a "click-unclick-

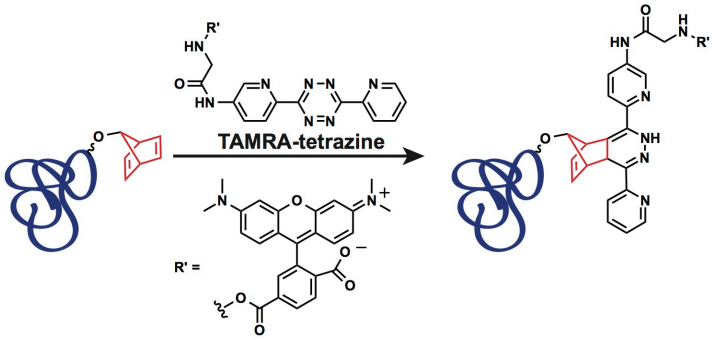


Figure 4.10. Proposed bioorthogonal reaction of norbornadiene with tetrazine.

click" reaction. Thus, in work that is currently ongoing, we endeavor to identify a bioorthogonal reaction partner for norbornadiene.

We first considered tetrazine as a ligation partner for norbornadiene. Tetrazine is known to react rapidly with norbornene with a second order rate constant between 1 and 9 $M^{-1} s^{-1}$.[30] We hypothesized that norbornadiene would react similarly, as shown in Figure 4.10. To test this hypothesis, we prepared norbornadiene-labeled BSA (NBD-BSA), norbornene-labeled BSA (NB-BSA), QC-BSA, and BSA as shown in Figure 4.11a. We then incubated these proteins with 50 μM carboxytetramethyl rhodamine (TAMRA) tetrazine‡‡‡‡‡‡ (Figure 4.10) for 10 min at room temperature and analyzed samples for the presence of TAMRA via SDS-PAGE.

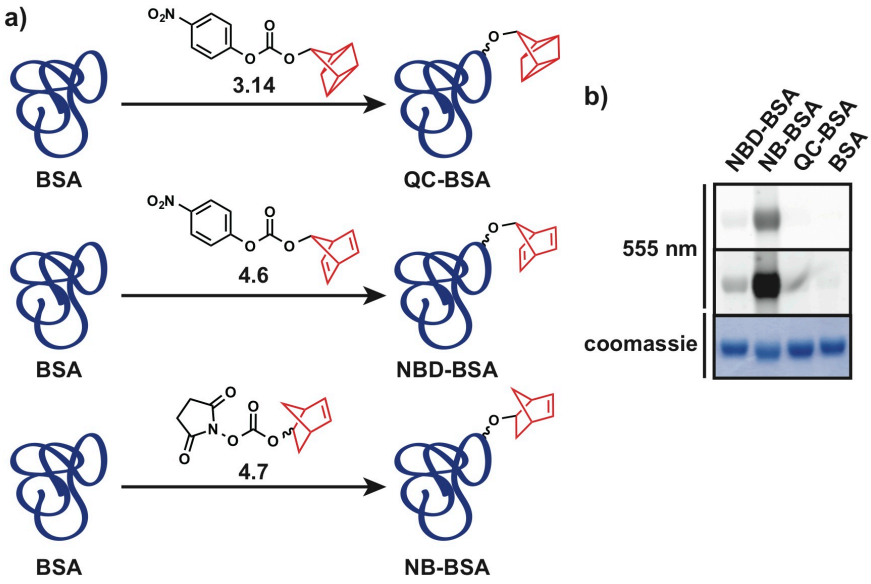


Figure 4.11. Analysis of the reaction of tetrazine with norbornadiene on a model protein. (a) Lysines on BSA were capped with *p*-nitrophenyl quadricyclane carbonate (**3.14**) to form QC-BSA, *p*-nitrophenyl norbornadiene carbonate (**4.6**) to form NBD-BSA, and with norbornene NHS-ester (**4.7**) to form NB-BSA. b) NBD-BSA, NB-BSA, QC-BSA and unlabeled BSA were combined with 50 μM TAMRA-tetrazine (10% DMSO in PBS) and incubated at room temperature for 10 min. After 10 min, excess tetrazine was removed via centrifugal filtration and analyzed by SDS-PAGE followed by fluorescence visualization on a typhoon imager (532 excitation/555 emission).

Results, shown in Figure 4.10b, reveal robust labeling of our NB-BSA positive control but comparatively minimal labeling of NBD-BSA. On explanation for this labeling difference is that there may be on average more NB moieties per NB-BSA than there are NBD moieties per NBD-BSA. This difference in the number of functional groups per protein could result from the different chemistries used to install the NB and NBD moieties (activated carbonate versus NHS-ester). However, upon reviewing the literature for precedent on the reaction between NBD and tetrazine, we found that the NBD/tetrazine adduct is known to undergo a rapid retro-Diels-Alder reaction at

‡‡‡‡‡‡ TAMRA-tetrazine was synthesized by Dr. Justin Kim according to the route published by Lang *et al.* See reference 30.

temperatures above –10 ºC to form cyclopentadiene and the pyridazine shown in Figure 4.12. This retro-Diels—Alder reaction may be the cause of the comparatively low signal observed for tetrazine treated NBD-BSA samples.

Tetrazine is known to react with cyclopentadiene to form a stable adduct (albeit 10-fold more slowly than the reaction between tetrazine and norbornene),[31] and this reaction may in part generate the weak signal observed in the NBD-BSA lanes. In addition, should two tetrazines react with norbornadiene (one per double bond) prior to retro-Diels—Alder elimination of cyclopentadiene, a stable adduct would result. This double click reaction may also contribute to the minimal signal observed in the NBD-BSA lane (Figure 4.11b).

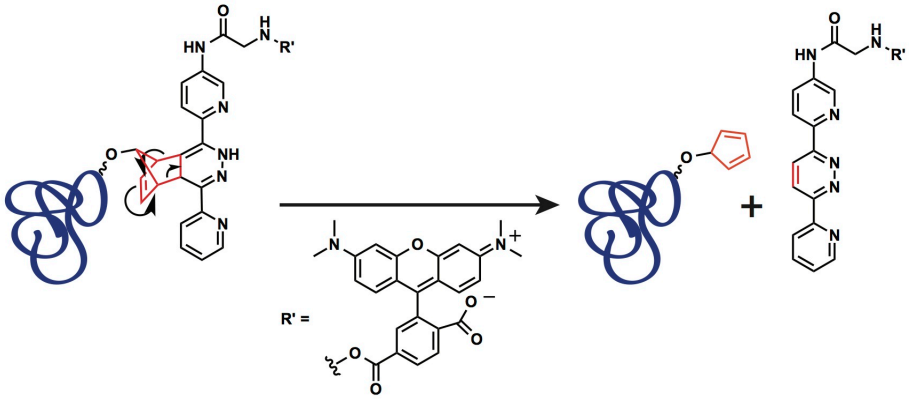


Figure 4.12. Retro-Diels—Alder reaction of norbornadiene-tetrazine adduct.

Given evidence to suggest the rapid retro-Diels—Alder elimination of the TAMRA probe from the NBD-tetrazine adduct, we decided to investigate alternative chemistries that produce a more robust ligation product. Nitrile imines, which are readily produced via photolysis of tetrazoles (Figure 4.3a) are known to react with alkenes. The reaction between norbornadiene and nitrile imine has been investigated. Reports from Mitsuhashi and co-workers find that the *exo*-isomer of the reaction product is stable at room temperature, whereas the *endo*-isomer undergoes the retro-Diels—Alder reaction readily at room temperature to form the corresponding pyrazole and cyclopentadiene (Figure 4.13).[32] For the cycloaddition with unsubstituted norbornadiene, the *exo* product is favored. Substitution at the bridgehead position of our norbornadiene-linked BSA may alter this regioselectivity preference, but we hypothesized that the amount of *exo*-product

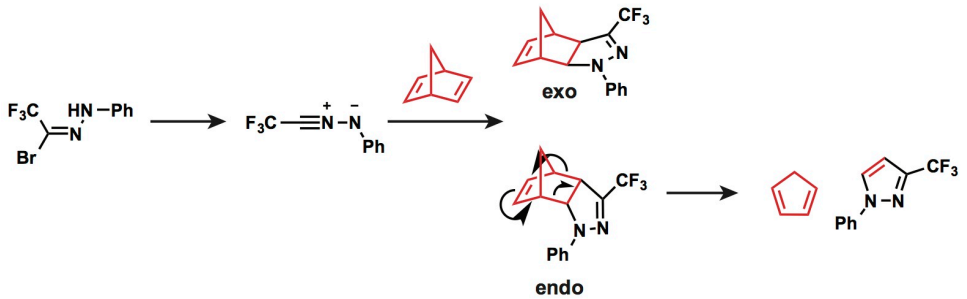


Figure 4.13. 1,3-dipolar cycloaddition between norbornadiene and nitrile imine. Reports from Mitsuhashi and co-workers find that the *exo* product of the above cycloaddition is isolable, but the *endo* product undergoes the retro-Diels—Alder reaction to form cyclopentadiene and the pyrazole shown. [32]

formed would be sufficient to enable detection of this regioisomer on protein samples. Thus, we decided to test the ability of the nitrile-imine photochemistry to label NBD-BSA.

Tetrazole **4.8** (Figure 4.14) was selected for our studies because it is one of the fastest reacting diphenyl tetrazoles known, reacting with norbornene with a second order rate constant of $k = 32 \pm 12$ M^{-1} s^{-1}.[33,34] Thus we hypothesized that **4.8** would react with NBD-modified proteins as shown in Figure 4.14a to produce at least one stable regioisomer. **4.8** was synthesized via the route of Kondo and co-workers.[35] We incubated NBD-BSA, NB-BSA, QC-BSA, and BSA, with 500 μM tetrazole and irradiated at 302 nm with a handheld lamp or irradiated with ambient light for 10 min. Excess tetrazole was then removed from the samples via centrifugal filtration, and proteins were analyzed via sodium dodecyl sulfate polyacrylamide gel electrophoresis (SDS-PAGE). The nitrile-imine/alkene adduct is fluorescent with maximum absorption at 360 nm and emission between 450 and 600 nm.[33] Thus, we elected to image our gels using an Ultra-violet Products (UVP) gel imager equipped with a 302 nm UVP transilluminator and a 570–640 nm filter.

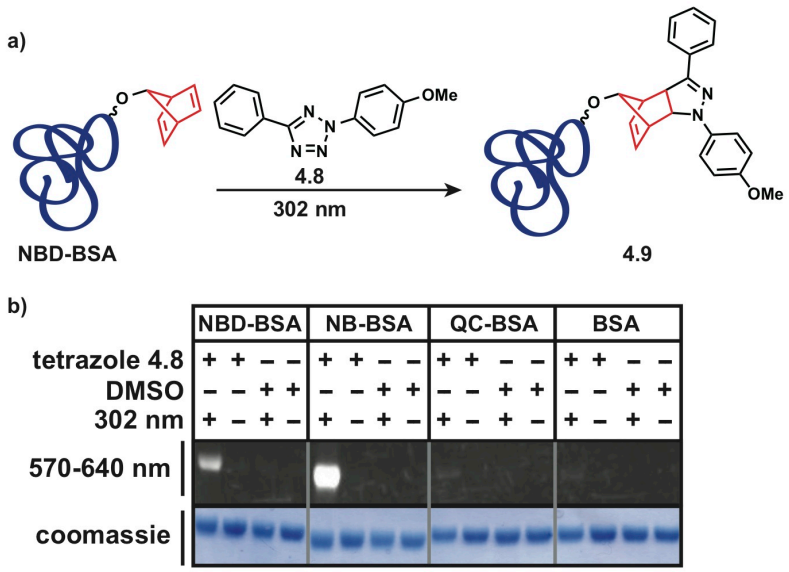


Figure 4.14. Photo-click chemistry on a model norbornadiene-tagged protein. (a) Proposed reaction between norbornadiene and nitrile imine formed via photolysis of tetrazole **4.8**. (b) Solutions of NBD-BSA, NB-BSA, QC-BSA, and BSA in PBS were supplemented with tetrazole **4.8** to a final concentration of 500 μM tetrazole and 10% DMSO (+ tetrazole) or 10% DMSO (+ DMSO). Solutions were irradiated with a 302 nm handheld UV lamp for 10 min (+ 302 nm) or were exposed to ambient light for 10 min (– 302 nm). Excess tetrazole was removed via centrifugal filtration. Protein was analyzed by SDS-PAGE followed by visualization on a UVP gel imager system (302 nm excitation/570–640 nm emission).

Results are shown in Figure 4.14b. We were pleased to observe labeling of tetrazole and UV-treated NBD-BSA sample and no signal in our –302 nm and –tetrazole control samples. As expected, NB-BSA displayed higher signal upon reaction with tetrazole than did NBD-BSA, likely a result of the retro-Diels—Alder reaction of the NBD/nitrile imine *endo* adduct. However, we cannot discount the possibility that the difference in signal is a result of more NB moieties than NBD moieties per protein.

We are now working to further characterize adduct **4.9**, and endeavor to apply this reaction for labeling of "unclicked" QC moieties on proteins.

Conclusion

We have shown that the adduct between QC and nickel bis(dithiolene) **3.19** undergoes photolysis on a model QC-labeled BSA protein. In combination with our method for site-selective incorporation of a QC amino acid, this "click-unclick" strategy has the potential to serve as an improved method of protein purification. Current methods of purification involve the genetic fusion of a peptide tag such as the FLAG tag or the His_6 tag to the C- or N-terminus of a protein of interest. These tags are bulky compared to the QC amino acid: 8 and 6 amino acids in length respectively.[36,37] As well, further genetic modification is often required if these tags are to be cleaved off of the protein target following purification.[36] With the QC ligation "click-unclick" method, we envision purification of proteins using a single QCaa handle installed at any solvent exposed site on the target protein (assuming it does not affect protein folding and function). QC-containing biomolecules can be pulled down using nickel bis(dithiolene) conjugated beads or resin, and subsequently cleaved from the resin via photolysis. Upon further development of a secondary reaction to derivatize the resulting norbornadiene moiety, a method of functionalizing the purified protein with a cargo would be available. Thus, the "click-unclick-click" approach, once optimized, would enable purification and derivatization of a target biomolecule using a single non-natural amino acid. Currently, no method exists to achieve such chemical diversity from a single amino acid site.

As mentioned, this research is ongoing. We are working to optimize the photolysis chemistry for pull-down purifications of QC-tagged proteins and also aim to improve the norbornadiene labeling chemistry. Once optimized, this chemistry will have immediate applications in protein purification but may also have utility in other areas including biomolecule tracking, photolithography, and the development of antibody-drug conjugates.

Our transformation of the QC ligation to a new "click-unclick-click" reaction highlights trends in the field of bioorthogonal chemistry toward reactions capable of expanded function.

Materials and Methods

Compound Synthesis

General Procedures. Reagents and solvents were obtained commercially and used without further purification with the exception of anhydrous solvents, which were prepared by the method developed by Pangborn *et al.*[38] Flash column chromatography was performed according to the method described by Still *et al.*[39] using Silicycle Silica Flash P60 silica (40-63 mm, 230-400 mesh). Reactions were monitored by TLC with Silicycle glass backed extra hard layer TLC plates (60 Å, 250 μm) and visualized with

ultraviolet light or with potassium permanganate or *p*-anisaldehyde staining followed by brief heating on a hot plate. Solutions were concentrated using a Buchi Rotovapor-114 equipped with a Welch 2026 self-cleaning dry vacuum system. Compounds were dried under reduced pressure on a Schlenk line equipped with an Edwards high vacuum.

All ^{1}H and ^{13}C spectra were obtained with a Bruker AV-600, AV-500, AVB-400, or AVQ-400 spectrometer. Peaks are reported in ppm and referenced to the solvent. Data are presented as follows: chemical shift in ppm, multiplicity (s = singlet, d = doublet, t = triplet, q = quartet, quin = quintet, m =multiplet), coupling constant in Hz, and integration value. High-resolution electrospray ionization (ESI) mass spectrometry data were obtained through the UC Berkeley Mass Spectrometry Facility on a Linear trap quadrupole fourier transform ion cyclotron resonance (LTQ-FT-ICR) mass spectrometer from Thermo Fisher. High-resolution electron ionization (EI) mass spectrometry data were obtained through the UC Berkeley Mass Spectrometry Facility on an AutoSpec mass spectrometer from Waters.

***P*-nitrophenyl norbornadiene carbonate (4.6).** *P*-nitrophenyl quadricyclane carbonate **3.14** was synthesized via the route published by Sletten *et al.*[26] and 14.5 mg (0.05 mmol, 1.00 equiv.) of this compound was dissolved in dichloromethane (1 ml). Iodine (2.4 mg, 0.01 mmol, 0.20 equiv.) was added and the reaction mixture was stirred at room temperature for 10 min. After 10 min, the reaction mixture was concentrated to a brown film and purified by column chromatography eluting with 100% hexanes to remove excess iodine and then with 15:1 hexanes:ether. The product was isolated in quantitative yield (13.8 mg, 0.05 mmol). Rf = 0.7 in 2:1 hexanes:ethyl acetate; ^{1}H NMR (600 MHz, $CDCl_3$) δ 8.26 (d, J = 8.9 Hz, 2H), 7.36 (d, J = 9.0 Hz, 2H), 6.75 (s, 2H), 6.67 (s, 2H), 4.64 (s, 1H), 3.74 (s, 2H); ^{13}C NMR (151 MHz, $CDCl_3$) δ 155.6, 152.0, 145.5, 140.2, 137.7, 125.4, 121.9, 101.1, 52.3; HRMS (EI) calcd for $C_{14}H_{11}NO_5$ [M]: 273.0637; found: 273.0635.

Norbornene NHS-ester (4.7). 5-norbornen-2-ol (obtained as a mixture of *endo* and *exo* isomers from Sigma Aldrich; 1.50 g, 13.6 mmol, 1.00 equiv.) was combined with anhydrous acetonitrile (42 ml). Note that 5-norbornen-2-ol is not fully soluble in acetonitrile. Triethylamine was added to the reaction (5.7 ml, 41 mmol, 3.0 equiv.) causing a slight color change to yellow. Disuccinimde carbonate (6.30 g, 24.6 mmol, 1.81 equiv.) was subsequently added and the reaction mixture was stirred under an atmosphere of nitrogen. After ~5 min, all starting material went into solution and the reaction mixture acquired an orange brown color. The mixture was stirred at room temperature overnight. The following day, the solution was concentrated to a brown sludge on a rotary evaporator and the product was purified by two rounds of column chromatography (column one: elute with 9:1, 1:0 dichloromethane:ether, pooled fractions containing product; column two: elute with 4:1 dichloromethane:ether). **4.7** was isolated as a mixture of diasteriomers in a 1:3 ratio and 64% yield (2.19 g, 8.71 mmol). Rf = 0.3 in 100% dichloromethane; ^{1}H NMR (600 MHz, $CDCl_3$) δ 6.38–6.34 (m, 1H), 6.29–6.25 (m, 0.3H), 6.02–5.96 (m, 1H), 5.95–5.90(m, 0.3H), 5.35–5.29 (m, 1H), 4.70 (d, J = 6.7 Hz, 0.3H), 3.23 (s, 1H), 3.04 (s, 0.3H), 2.87 (s, 1.6H), 2.80 (s, 1.6H), 2.78 (s, 4H), 2.16 (ddd, J = 12.8, 8.0, 3.7 Hz, 1H), 1.79–1.73 (m, 0.3H), 1.69 (d, J = 8.8 Hz, 0.3H), 1.63 (d, J =

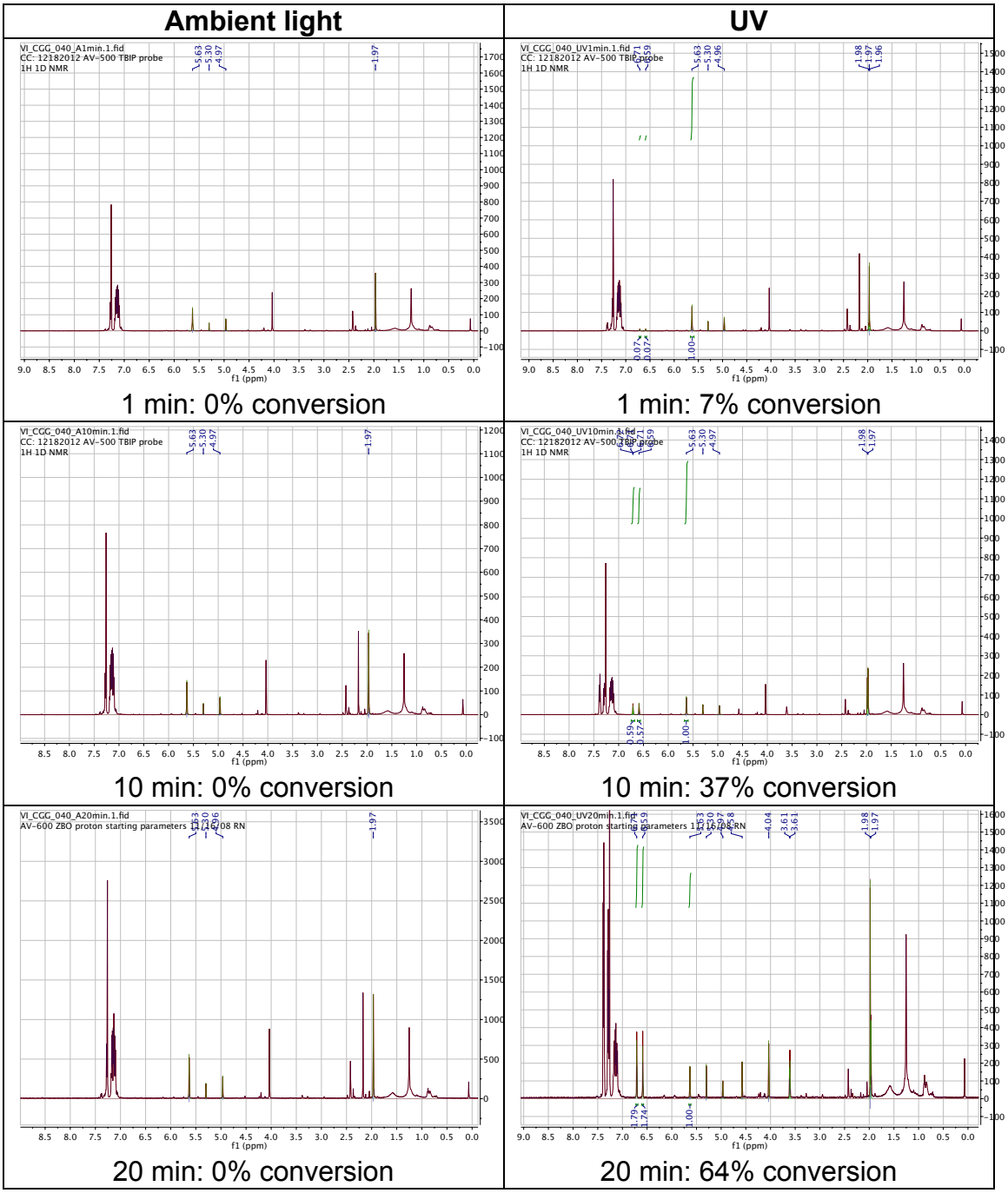
9.1 Hz, 0.3H), 1.60 –1.55 (m, 0.3H), 1.52 –1.47 (m, 1H), 1.31 (d, J = 9.2 Hz, 1H), 1.10 (dd, J = 13.1,1H); ^{13}C NMR (151 MHz, $CDCl_3$) δ 168.9, 168.8, 151.3, 151.3, 142.2, 139.2, 131.8, 131.0, 83.3, 82.8, 47.7, 47.31, 46.3, 45.8, 42.2, 40.6, 34.5, 34.4, 25.5, 25.5. HRMS (EI) calcd for $C_{12}H_{13}NO_5$ [M]: 251.0794; found: 251.0793.

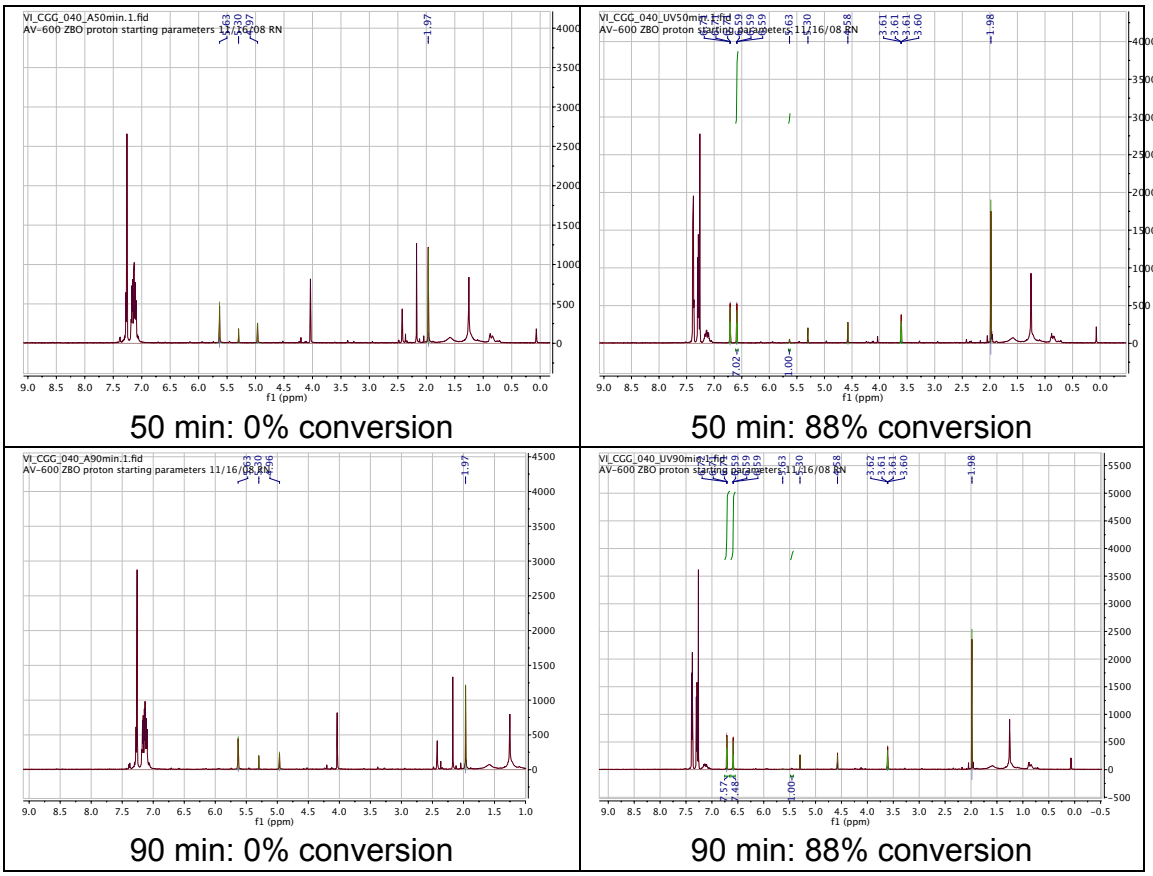
Photolysis Experiments and Norbornadiene Model Reactions

General Procedures. Bovine Serum Albumin (BSA) was obtained from Sigma Aldrich as a lyophilized power. Protein concentrations were assessed via BCA assay (Pierce, Thermo Scientific). Gel electrophoresis was performed using BioRad Criterion gel electrophoresis chambers equipped with a BioRad Power Pac 200. All gels (Biorad Criterion XT pre-cast) were run in MES buffer. Western blot transfers were performed using BioRad Criterion blotter transfer boxes equipped with a BioRad Power Pac 200. Gels were transferred to nitrocellulose (BioRad 0.45 μm) in tris-glycine buffer (20% MeOH). See Blue Plus 2 pre-stained protein ladder from Life Technologies was used for all gels and Western blots. Mouse α-biotin-HRP was obtained from Southern Biotech. Protein loading was assessed via staining with Ponceau (5% acetic acid, 0.1% (w/v) ponceau) or coomassie blue (10% acetic acid, 40% MeOH, 2.5% (w/v) coomassie blue). Blots were visualized on Premium X-ray film (blue) from Phenix Research Products. Gels were imaged for fluorescence on a UVP VisiDoc-It Imaging system (570-640 nm emission filter) equipped with a UVP transilluminator (302 nm, model M-26) or were imaged on a Typhoon imager.

All QC-BSA was prepared via the method published by Sletten *et al.*[26] Photolysis reactions (in flask and on protein) were performed via irradiation with a 365 nm handheld lamp (Spectroline model ENF-260c, 254/365 nm) or a 302 nm handheld lamp (UVP, 6W; 302nm; 115V 60Hz; Intensity: 1500μw/cm^2). On-protein samples were aliquoted into borosilicate glass tubes (Kimble Chase 6 x 50 mm or larger tubes from Fisher Brand) or 96-well plates (black wall, clear bottom) for all irradiation experiments. For photolysis reactions, lamp and sample were surrounded by a layer of aluminum foil. All centrifugal filters used were 10 kDa molecular weight cutoff Amicon Ultra filters.

Figure 4.7. ^{1}H NMR Analysis of the Photolysis of Adduct 4.4





Adduct **4.4** was prepared as described by Sletten *et al.* [26] and was then dissolved in $CDCl_3$ to 8.3 mM (18.2 mg **4.4**, 0.026 mmol **4.4** into 3.15 ml $CDCl_3$). 700 µl of this solution was transferred to each of four quartz NMR tubes. Tube 1 was irradiated at 365 nm with a handheld UV lamp for one min. The tube and lamp were surrounded in foil for the duration of irradiation to increase the amount of UV light the sample was exposed to. Tube 2 was exposed to ambient light for 1 min. Tubes 1 and 2 were then placed in foil for transportation to the NMR facility and ^{1}H NMR spectra were acquired for each sample (1 min timepoint). All spectra were acquired with a Bruker AV-500 spectrometer equipped with a TBI probe.

Tube 3 was exposed to 365 nm light via handheld UV lamp for 10 min and tube 4 was exposed to ambient light for 10 min. Tubes 3 and 4 were then covered in foil for transportation to the NMR facility and ^{1}H NMR spectra were obtained (10 min timepoint). Tubes 3 and 4 were then re-exposed to UV or ambient light for an additional 10 min to provide the 20 min timepoint, covered with foil, and ^{1}H NMR spectra were acquired. This procedure was repeated with tubes 3 and 4 undergoing UV or ambient exposure for an additional 30 min (50 min timepoint) and then 40 min (90 min timepoint). ^{1}H NMR spectra for each timepoint are shown above.

Figure 4.8c. Photodissociation of adduct 4.5

*QC Ligation to generate **4.5** or **3.19**-treated BSA*
65 μl of a QC-BSA or BSA solution (770 μg/ml in PBS) was combined with 65 μl of a nickel bis(dithiolene) biotin **3.19** solution (100 μM in PBS) to a final concentration of 50 μM **3.19**. Reactions were incubated in the dark at room temperature for 30 min, then quenched via addition of 3.3 μL of a 200 mM solution of QCOAc in DMSO (100 equiv QCOAc relative to **3.19**). To remove excess small molecule (QCOAc, free **3.19**, and adduct between **3.19** and QCOAc) from the protein samples, each reaction was diluted with 350 μl PBS and then transferred to a 0.5 ml Amicon Ultra centrifugal filter and centrifuged at 14,000 x g for 5 min. Concentrated reactions were diluted with 200 μl PBS followed by centrifugation in a centrifugal filter at 14,000 x g for 5 min as a second wash. This wash procedure was repeated one additional time to give the resulting proteins as solutions in ~70 μl PBS.

Photodissociation
50 μl of each sample was then transferred to a fresh 1.5 mL eppendorf tube and diluted with 480 μl PBS. The resulting solutions were aliquoted into borosilicate glass tubes (50 μl /tube). Tubes were irradiated with 365 nm light via handheld UV lamp (surrounded by a foil encasement) or with ambient light for 0, 30, 60, or 90 min. Samples were kept in the dark when not undergoing UV or ambient light exposure. To remove free **3.19** from the reactions following irradiation, the samples were diluted with 100 μl PBS, transferred to 0.5 ml Amicon Ultra centrifugal filters, and centrifuged at 14,000 x g for 5 min. Concentrated protein solutions were then re-dissolved in 200 μl additional PBS and centrifuged in a centrifugal filter at 14,000 x g for 5 min as a second wash. This wash procedure was repeated two additional times.

Western blot
15 μl each sample was combined with 5 μl 4x SDS loading buffer (supplemented with 10% β-mercaptoethanol) and loaded onto a 26-well 4–12% bis-tris Criterion pre-cast gel (15 μl sample/well). Western blotting was performed according to the general Western blot procedure using an α-biotin HRP antibody.

Figure 4.9a Optimization of the photodissociation reaction via addition of excess QCOAc to scavenge released 3.19

*QC Ligation to generate **4.5** or **3.19**-treated BSA*
98 μl of a QC-BSA or BSA solution (1.2 mg/ml in PBS) was combined with 98 μl of a 114 μM solution of nickel bis(dithiolene) biotin **3.19** (57 μM final concentration of **3.19**). Reactions were incubated in the dark at room temperature for 30 min, then quenched via addition of 5 μL of a 200 mM solution of QCOAc in DMSO (100 equiv QCOAc relative to **3.19**). To remove excess small molecule (QCOAc, free **3.19**, and adduct between **3.19** and QCOAc) from the protein samples, each reaction was diluted with 300 μl PBS, then transferred to an Amicon Ultra centrifugal filter and centrifuged at 14,000 x g for 5 min. Concentrated reactions were diluted with 200 μl PBS followed by centrifugation in a

centrifugal filter at 14,000 x g for 5 min as a second wash. This wash procedure was repeated one additional time to give the resulting proteins as solutions in ~50–70 μl PBS.

Photodissociation
50 μl of each sample was then transferred to a fresh 1.5 mL eppendorf tube and diluted with 720 μl PBS. The resulting solutions were aliquoted into borosilicate glass tubes (50 μl protein solution/tube). Samples were supplemented with 1.2 μl of a 200 mM solution of QCOAc in DMSO to a final QCOAc concentration of 4.8 mM (solution was cloudy due to minimal solubility of QCOAc in PBS at this concentration) or were supplemented with 1.2 μl DMSO or 1.2 μl PBS.

Tubes were then irradiated with 365 nm light via handheld UV lamp (surrounded by a foil encasement) or with ambient light for 0, or 60 min. Samples were kept in the dark when not undergoing UV exposure and 0 min samples were kept in the dark for the duration of the experiment. To remove (QCOAc, free **3.19**, and adduct between **3.19** and QCOAc) from the reactions following irradiation, 40 μl of each sample was diluted with 400 μl PBS, transferred to 0.5 ml Amicon Ultra centrifugal filters (10 kDa molecular weight cutoff), and centrifuged at 14,000 x g for 5 min. Concentrated protein solutions were then re-dissolved in 200 μl additional PBS and centrifuged at 14,000 x g for 5 min as a second wash. This wash procedure was repeated one additional time. Samples were stored at 4 ºC until further use.

Western blot
20 μl of each sample was combined with 0.2 μl 5 mM TAMRA-tetrazine in DMSO (50 μM TAMRA-tetrazine final concentration) for 15 min.[§§§§§§] Samples were then combined with 6.7 μl 4x SDS (supplemented with 10% β-mercaptoethanol) and loaded onto a 26-well 4–12% bis-tris Criterion pre-cast gel (15 μl sample/well). Western blotting was performed according to the general Western blot procedure using an α-biotin HRP antibody.

Figure 4.9b. Optimization of the photodissociation reaction via 1) addition of excess QCOAc to scavenge released 3.19 and 2) reduced protein concentration

*QC Ligation to generate **4.5** or **3.19**-treated BSA*
80 μl of a solution of QC-BSA or BSA (1 mg/ml in PBS as determined by BCA assay) was combined with 80 μl of a 100 μM solution of nickel bis(dithiolene) biotin **3.19** (50 μM final concentration **3.19**). Reactions were incubated in the dark at room temperature for 30 min, then quenched via addition of 4 μL of a 200 mM solution of QCOAc in DMSO (100 equiv QCOAc relative to **3.19**). To remove excess small molecule (QCOAc, free **3.19**, and adduct between **3.19** and QCOAc) from the protein samples, each reaction was diluted with 300 μl PBS, then transferred to an Amicon Ultra centrifugal filter and

[§§§§§§] Samples were combined with TAMRA-tetrazine for analysis of reactivity of the norbornadiene product of photodissociation. We did not observe significant TAMRA-tetrazine labeling of photodissociated products (data not shown). As all samples underwent the same TAMRA-tetrazine treatment, we do not expect this additional step to affect the results of the α-biotin-HRP Western blot.

centrifuged at 14,000 x g for 5 min. Concentrated reactions were diluted with 350 μl PBS followed by centrifugation in a centrifugal filter at 14,000 x g for 5 min as a second wash. This wash procedure was repeated one additional time to give the resulting proteins as solutions in ~50 μl PBS.

Photodissociation
50 μl of each sample was then transferred to a fresh 1.5 mL eppendorf tube and diluted with 380 μl PBS. The resulting solutions were aliquoted into borosilicate glass tubes (50 μl protein solution/tube). The protein in each tube was then diluted with an additional 550 μl PBS and 15 μl 200 mM QCOAc in DMSO to a final QCOAc concentration of 5 mM (solution is cloudy due to minimal solubility of QCOAc in PBS at this concentration). Tubes were irradiated at 365 nm with a handheld UV lamp or were irradiated with ambient light for 0, 10, 30, or 60 min (0 min samples were kept in the dark for the duration of the experiment).

To remove small molecule (QCOAc, free **3.19**, and adduct between **3.19** and QCOAc) from the reactions following irradiation, 400 μl of each sample was transferred to a 0.5 ml Amicon Ultra centrifugal filter and centrifuged at 14,000 x g for 5 min. The remaining sample (~200 μl) was then added to each filter and centrifuged at 14,000 x g for 5 min. Concentrated protein solutions were then re-dissolved in 350 μl additional PBS and centrifuged in a centrifugal filter at 14,000 x g for 5 min as a second wash. This wash process was repeated one additional time.

Western blot
12 μl each sample was combined with 4 μl 4x SDS (supplemented with 10% β-mercaptoethanol) and loaded onto a 26-well 4–12% bis-tris Criterion pre-cast gel (15 μl sample/well). Western blotting was performed according to the general Western blot procedure using an α-biotin HRP antibody.

General Western blotting procedure
All gels were run for 40 min at 175 V, then transferred to nitrocellulose for 90 min at 75 V. The resulting Western blots were stained with ponceau, then blocked in 5% BSA in PBST in the dark at 4 ºC for 0.5–2.5 days. Blots were then incubated in a 1:200,000 dilution of α-biotin-HRP in 5% BSA PBST at room temperature in the dark for 15–30 min, washed 3 x PBST, and developed via chemiluminescence using SuperSignal West Pico Chemiluminescent Substrate (Thermo Scientific).

Click-unclick-click experiments with tetrazine and tetrazole

Figure 4.11. Analysis of the reaction of tetrazine with norbornadienene on a model protein

Preparation of NBD-BSA
BSA (103.1 mg) was dissolved in 10 ml PBS. *Para*-nitrophenyl norbornadiene carbonate **4.6** (4.6 mg) was dissolved in 277.4 μl DMSO plus 55.6 μl DMF. 500 μl of the BSA

solution was combined with 100 μl of the **4.6** solution and 200 μl DMSO in a 1.5 ml eppendorf tube. The reaction was incubated for 3 hr 50 min on a shaker at room temperature. 350 μl of the reaction mixture was then loaded onto each of two NAP5 columns (GE Healthcare Life Sciences, pre-equilibrated with 10 ml PBS). Four 500 μl fractions were collected from each column. Fraction one from one of the columns was used for future experiments with NBD-BSA.

Preparation of NB-BSA
BSA (50 mg) was dissolved in 2.5 ml PBS. Norbornene NHS-ester **4.7** (5.3 mg) was dissolved in 300 μl DMSO and 60 μl DMF. 500 μl of the BSA solution was combined with 100 μl of the **4.7** solution plus 200 μl DMSO. The reaction was incubated for 2 hr 55 min at room temperature on a shaker. After 2 hr 55 min, 350 μl of the reaction was loaded onto a NAP5 column (GE Healthcare Life Sciences, pre-equilibrated with 10 ml PBS) and eluted with PBS. Six 500 μl fractions were collected. The second fraction was used for future experiments.

Tetrazine labeling
300 μg/ml solutions of QC-BSA, NB-BSA, NBD-BSA, and BSA were prepared in PBS. 100 μl each sample was pipetted into a well of a 96-well plate (clear bottom, black walls) and combined with 11.25 μl 0.5 mM TAMRA tetrazine (Figure 4.10)[*******] in DMSO to 50 μM final concentration. Reactions were incubated at room temperature for 10 min, at which point reactions were diluted with 100 μl PBS, transferred to 0.5 ml Amicon Ultra centrifugal filters, further diluted with 200 μl PBS, and centrifuged at 14,000 x g for 5 min. Concentrated samples were then diluted with 200 μl PBS and centrifuged at 14,000 x g for 5 min.

SDS-PAGE analysis
9 μl each sample was combined with 3 μl 4x SDS loading buffer (supplemented with 10% β-mercaptoethanol) and loaded onto a 26-well 4–12% bis-tris Criterion pre-cast gel (9 μl sample/well). The gel was run for 40 min at 175 V, then analyzed for TAMRA-tetrazine signal with a typhoon imager (532 ex/555 em). Following imaging, the gel was stained with coomassie blue stain to assess protein loading.

Figure 4.14. Photo-click chemistry on a model norbornadiene-tagged protein

Tetrazole labeling
300 μg/ml solutions of QC-BSA, NB-BSA, NBD-BSA, and BSA were prepared in PBS. 100 μl aliquots of each sample were pipetted into wells (2 wells/sample/plate) of two 96-well plates (clear bottom, black walls) and combined with 11.25 μl of a 5 mM solution of tetrazole **4.8** in DMSO to a final concentration of 500 μm or were combined with 11.25 μl DMSO. The plate was irradiated with a 302 nm handheld UV lamp for 10 min. A second, identical plate was prepared and exposed to ambient light for 10 min. Samples

[*******] TAMRA-tetrazine was synthesized by Dr. Justin Kim via the route published by Lang *et al*. See reference 30.

were diluted with 100 μl PBS, transferred to 0.5 ml Amicon Ultra centrifugal filters, further diluted with 200 μl PBS, and centrifuged at 14,000 x g for 5 min. Concentrated samples were then diluted with 200 μl PBS and centrifuged at 14,000 x g for 5 min in centrifugal filters.

SDS-PAGE analysis

9 μl each sample was combined with 3 μl 4x SDS loading buffer (supplemented with 10% β-mercaptoethanol) and loaded onto a 26-well 4–12% bis-tris Criterion pre-cast gel (9 μl sample/well). The gel was run for 40 min at 175 V, then analyzed for the presence of the tetrazole adduct via imaging on a UVP gel imager (302 nm excitation and 570–640 nm emission filter). Following imaging, the gel was stained with coomassie blue stain to assess protein loading.

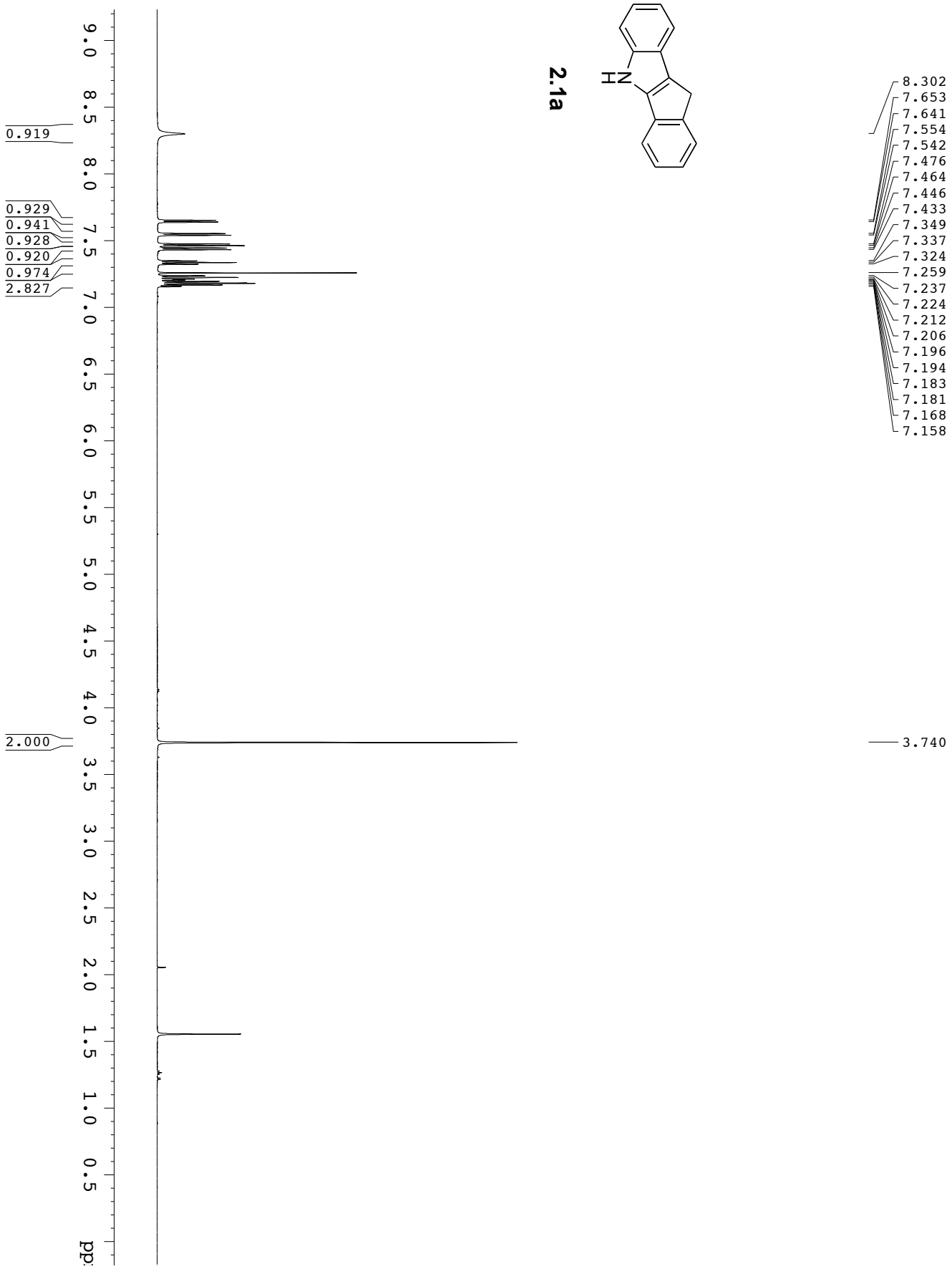
References

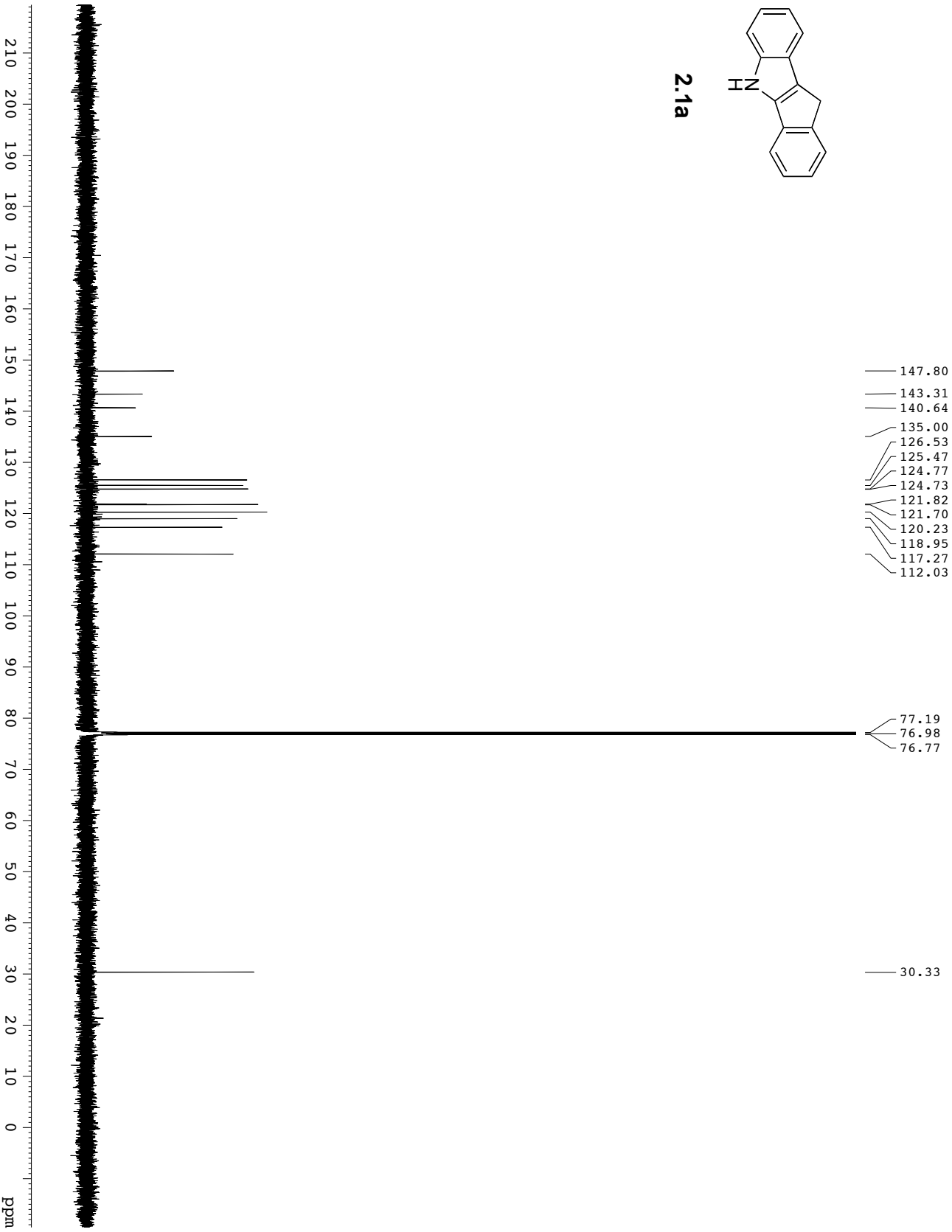
1. West, K., R.; Otto, S. Reversible covalent chemistry in drug delivery. *Curr. Drug Discovery Technol.* **2005***, 2*, 123-160.
2. Lin, Y. A.; Boutureira, O.; Lercher, L.; Bhushan, B.; Paton, R. S.; Davis, B. G. Rapid cross-metathesis for reversible protein modifications via chemical access to se-allyl-selenocysteine in proteins. *J. Am. Chem. Soc.* **2013***, 135*, 12156-12159.
3. Siegel, D. Applications of reversible covalent chemistry in analytical sample preparation. *Analyst* **2012***, 137*, 5457-5482.
4. Kramer, J. R.; Deming, T. J. Reversible chemoselective tagging and functionalization of methionine containing peptides. *Chem. Commun.* **2013***, 49*, 5144-5146.
5. Lin, Y. A.; Chalker, J. M.; Floyd, N.; Bernardes, G. J. L.; Davis, B. G. Allyl sulfides are privileged substrates in aqueous cross-metathesis: Application to site-selective protein modification. *J. Am. Chem. Soc.* **2008***, 130*, 9642-9643.
6. Foettinger, A.; Leitner, A.; Lindner, W. Solid-phase capture and release of arginine peptides by selective tagging and boronate affinity chromatography. *J. Chromatogr. A* **2005***, 1079*, 187-196.
7. Egawa, Y.; Seki, T.; Takahashi, S.; Anzai, J. Electrochemical and optical sugar sensors based on phenylboronic acid and its derivatives. *Mater. Sci. Eng. , C* **2011***, 31*, 1257-1264.
8. Foettinger, A.; Leitner, A.; Lindner, W. Selective enrichment of tryptophan-containing peptides from protein digests employing a reversible derivatization with malondialdehyde and solid-phase capture on hydrazide beads. *J. Proteome Res.* **2007***, 6*, 3827-3834.
9. Foettinger, A.; Melmer, M.; Leitner, A.; Lindner, W. Reaction of the indole group with malondialdehyde: Application for the derivatization of tryptophan residues in peptides. *Bioconjugate Chem.* **2007***, 18*, 1678-1683.
10. Song, W.; Wang, Y.; Qu, J.; Madden, M. M.; Lin, Q. A photoinducible 1,3-dipolar cycloaddition reaction for rapid, selective modification of tetrazole-containing proteins. *Angew. Chem. Int. Ed.* **2008***, 47*, 2832-2835.
11. Song, W.; Wang, Y.; Qu, J.; Lin, Q. Selective functionalization of a genetically encoded alkene-containing protein via "photoclick chemistry" in bacterial cells. *J. Am. Chem. Soc.* **2008***, 130*, 9654-9655.
12. Ramil, C. P.; Lin, Q. Photoclick chemistry: A fluorogenic light-triggered in vivo ligation reaction. *Curr. Opin. Chem. Biol.* **2014***, 21*, 89-95.
13. Song, W.; Wang, Y.; Yu, Z.; Vera, C. I. R.; Qu, J.; Lin, Q. A metabolic alkene reporter for spatiotemporally controlled imaging of newly synthesized proteins in mammalian cells. *ACS Chem. Biol.* **2010***, 5*, 875-885.

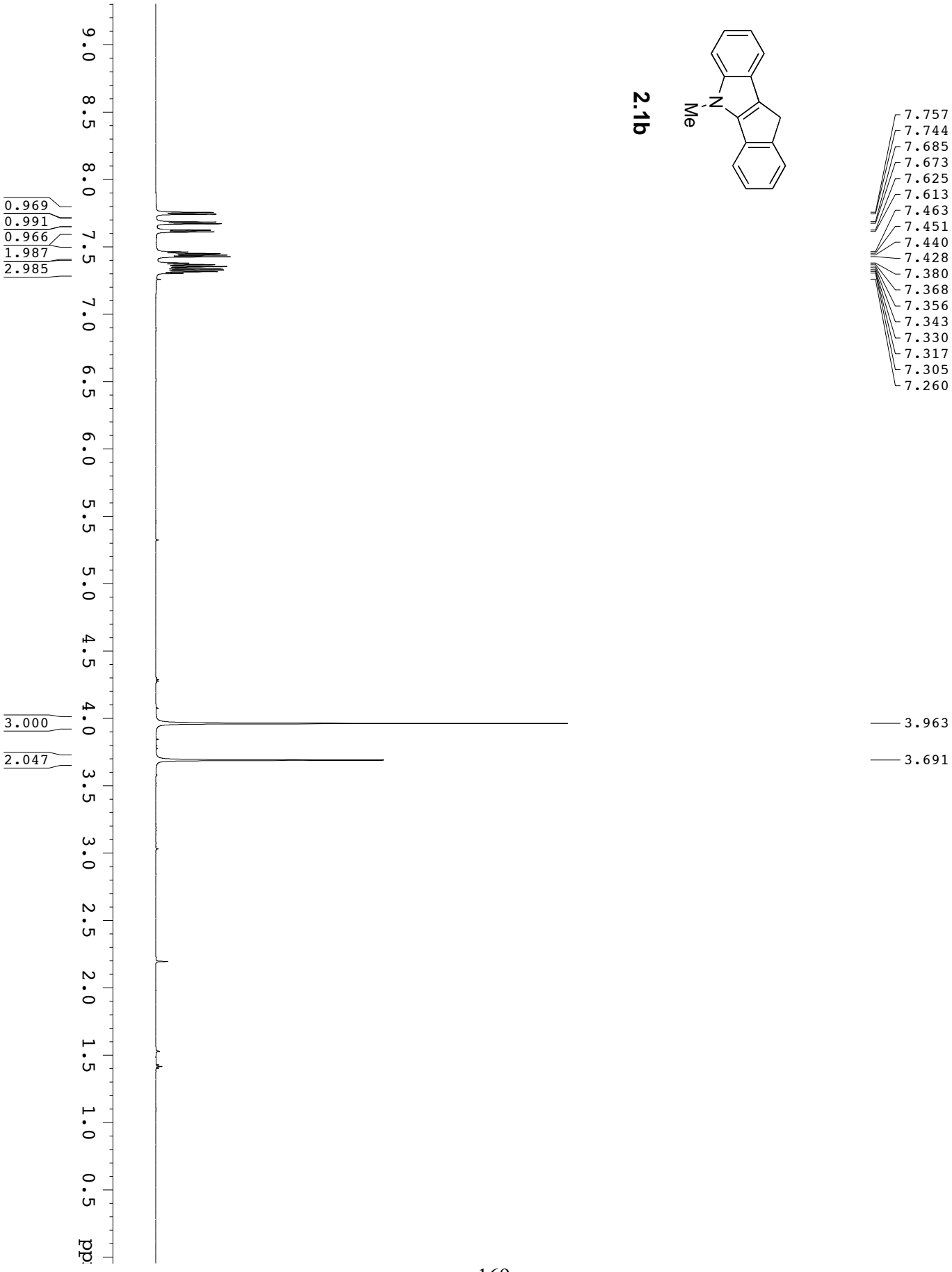
14. An, P.; Yu, Z.; Lin, Q. Design of oligothiophene-based tetrazoles for laser-triggered photoclick chemistry in living cells. *Chem. Commun.* **2013**, *49*, 9920-9922.
15. Yu, Z.; Ohulchanskyy, T. Y.; An, P.; Prasad, P. N.; Lin, Q. Fluorogenic, two-photon-triggered photoclick chemistry in live mammalian cells. *J. Am. Chem. Soc.* **2013**, *135*, 16766-16769.
16. Lim, R. K. V.; Lin, Q. Azirine ligation: Fast and selective protein conjugation via photoinduced azirine-alkene cycloaddition. *Chem. Commun.* **2010**, *46*, 7993-7995.
17. Arumugam, S.; Orski, S., V.; Mbua, N., E.; McNitt, C.; Boons, G.; Locklin, J.; Popik, V., C. Photo-click chemistry strategies for spatiotemporal control of metal-free ligation, labeling, and surface derivatization. *Pure Appl. Chem.* **2013**, *85*, 1499-1513.
18. Poloukhtine, A. A.; Mbua, N. E.; Wolfert, M. A.; Boons, G.; Popik, V. V. Selective labeling of living cells by a photo-triggered click reaction. *J. Am. Chem. Soc.* **2009**, *131*, 15769-15776.
19. Orski, S. V.; Poloukhtine, A. A.; Arumugam, S.; Mao, L.; Popik, V. V.; Locklin, J. High density orthogonal surface immobilization via photoactivated copper-free click chemistry. *J. Am. Chem. Soc.* **2010**, *132*, 11024-11026.
20. Borrmann, A.; Fatunsin, O.; Dommerholt, J.; Jonker, A. M.; Lowik, Dennis W. P. M.; van Hest, Jan C. M.; van Delft, F. L. Strain-promoted oxidation-controlled cyclooctyne-1,2-quinone cycloaddition (SPOCQ) for fast and activatable protein conjugation. *Bioconjugate Chem.* **2014**, *ASAP*.
21. Schrauzer, G. N.; Mayweg, V. P. Preparation, reactions, and structure of bisdithio-alpha-diketone complexes of nickel, palladium, and platinum. *J. Am. Chem. Soc.* **1965**, *87*, 1483-1489.
22. Baker, J. R.; Hermann, A.; Wing, R. M. Mechanism of oxidative cycloaddition of olefins to metal dithiolenes. *J. Am. Chem. Soc.* **1971**, *93*, 6486-6489.
23. Kajitani, M.; Kohara, M.; Kitayama, T.; Akiyama, T.; Sugimori, A. Formation of 1:1 adducts between bis(1,2-diaryl-1,2-ethylenedithiolato)metal(0) (metal = NI, PD, and PT) and quadricyclane and their photodissociation. *J. Phys. Org. Chem.* **1989**, *2*, 131-145.
24. Kajitani, M.; Kohara, M.; Kitayama, T.; Asano, Y.; Sugimori, A. Photosensitive 1:1 adduct between bis(1,2-diphenyl-1,2-ethylenedithiolato)nickel(0) and quadricyclane. *Chem. Lett.* **1986**, *15*, 2109-2112.
25. Sugimori, A. Long-lived metal-complex-radicals in photoreactions of S,S'-dialkyl and S,S'-alkanediyl derivatives of bis(1,2-ethenedithiolato)metal complexes. *Coord. Chem. Rev.* **1997**, *159*, 397-406.
26. Sletten, E. M.; Bertozzi, C. R. A bioorthogonal quadricyclane ligation. *J. Am. Chem. Soc.* **2011**, *133*, 17570-17573.
27. Sletten, E. M. Bioorthogonal Chemistries for Labeling Living Systems. Ph.D. dissertation. University of California, Berkeley, Berkeley, CA, 2011.
28. Bujacz, A. Structures of bovine, equine and leporine serum albumin. *Acta Crystallogr. , Sect. D: Biol. Crystallogr.* **2012**, *68*, 1278-1289.
29. Kang, Y. N.; Kim, H.; Shin, W. S.; Woo, G.; Moon, T. W. Effect of disulfide bond reduction on bovine serum albumin-stabilized emulsion gel formed by microbial transglutaminase. *J. Food Sci.* **2003**, *68*, 2215-2220.
30. Lang, K.; Davis, L.; Torres-Kolbus, J.; Chou, C.; Deiters, A.; Chin, J. W. Genetically encoded norbornene directs site-specific cellular protein labelling via a rapid bioorthogonal reaction. *Nature Chem.* **2012**, *4*, 298-304.
31. Thalhammer, F.; Wallfahrer, U.; Sauer, J. Reaktivität einfacher offenkettiger und cyclischer dienophile bei diels-alder-reaktionen mit inversem elektronenbedarf. *Tetrahedron Lett.* **1990**, *31*, 6851-6854.

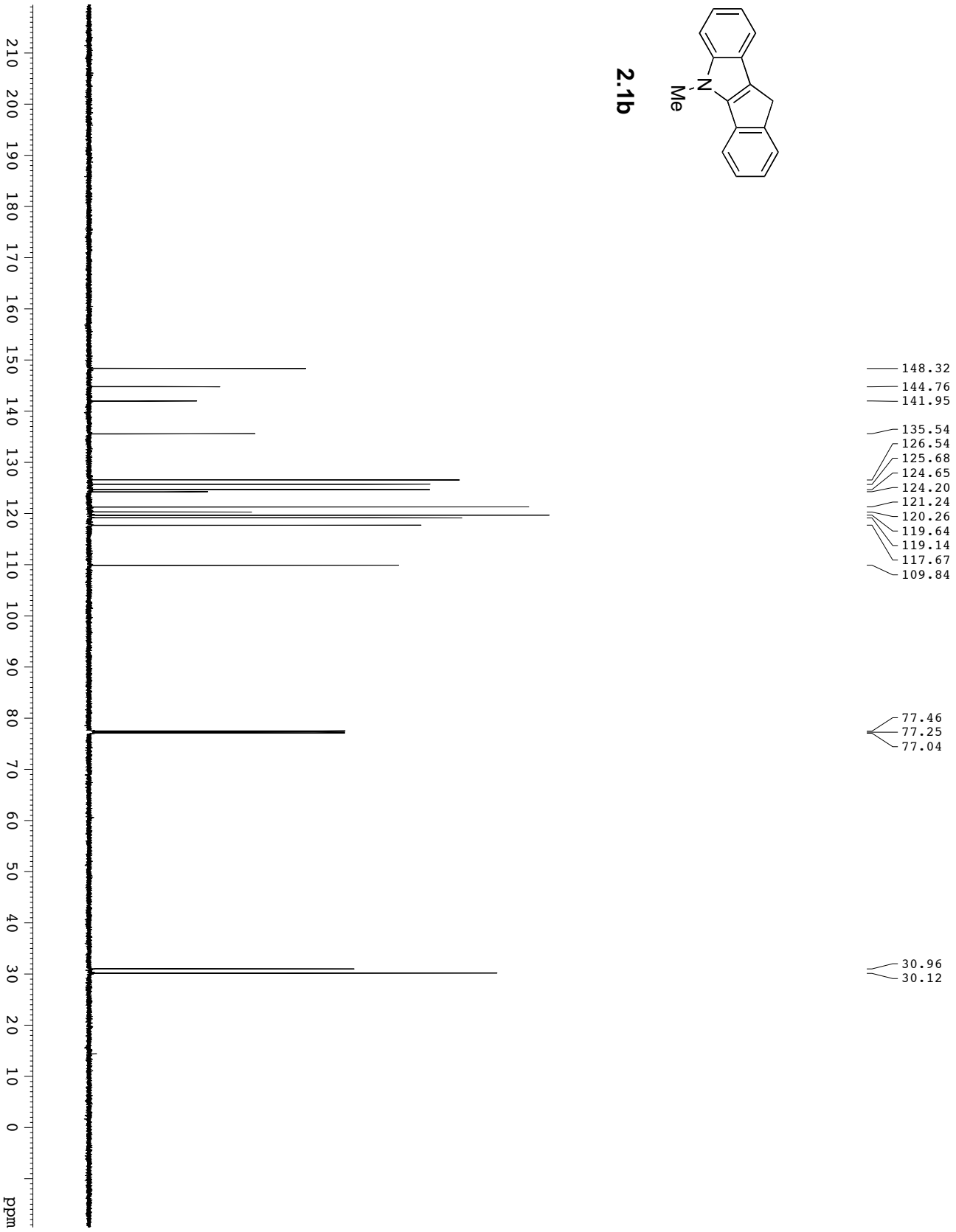
32. Tanaka, K.; Masuda, H.; Mitsuhashi, K. Exo/endo stereoselectivity in 1,3-dipolar cycloaddition of trifluoroacetonitrile oxide and -nitrilimine with bicyclic olefins. *Bull. Chem. Soc. Jpn.* **1986***, 59*, 3901-3904.
33. Wang, Y.; Song, W.; Hu, W. J.; Lin, Q. Fast alkene functionalization in vivo by photoclick chemistry: HOMO lifting of nitrile imine dipoles. *Angew. Chem. Int. Ed.* **2009***, 48*, 5330-5333.
34. Yu, Z.; Pan, Y.; Wang, Z.; Wang, J.; Lin, Q. Genetically encoded cyclopropene directs rapid, photoclick-chemistry-mediated protein labeling in mammalian cells. *Angew. Chem. Int. Ed.* **2012***, 51*, 10600-10604.
35. Ito, S.; Tanaka, Y.; Kakehi, A.; Kondo, K. A facile synthesis of 2,5-disubstituted tetrazoles by the reaction of phenylsulfonylhydrazones with arenediazonium salts. *Bull. Chem. Soc. Jpn.* **1976***, 49*, 1920-1923.
36. Einhauer, A.; Jungbauer, A. The FLAG™ peptide, a versatile fusion tag for the purification of recombinant proteins. *J. Biochem. Biophys. Methods* **2001***, 49*, 455-465.
37. Hochuli, E.; Döbeli, H.; Schacher, A. New metal chelate adsorbent selective for proteins and peptides containing neighbouring histidine residues. *J. Chromatogr. A* **1987***, 411*, 177-184.
38. Pangborn, A. B.; Giardello, M. A.; Grubbs, R. H.; Rosen, R. K.; Timmers, F. J. Safe and convenient procedure for solvent purification. *Organometallics* **1996***, 15*, 1518-1520.
39. Still, W. C.; Kahn, M.; Mitra, A. Rapid chromatographic technique for preparative separations with moderate resolution. *J. Org. Chem.* **1978***, 43*, 2923-2925.

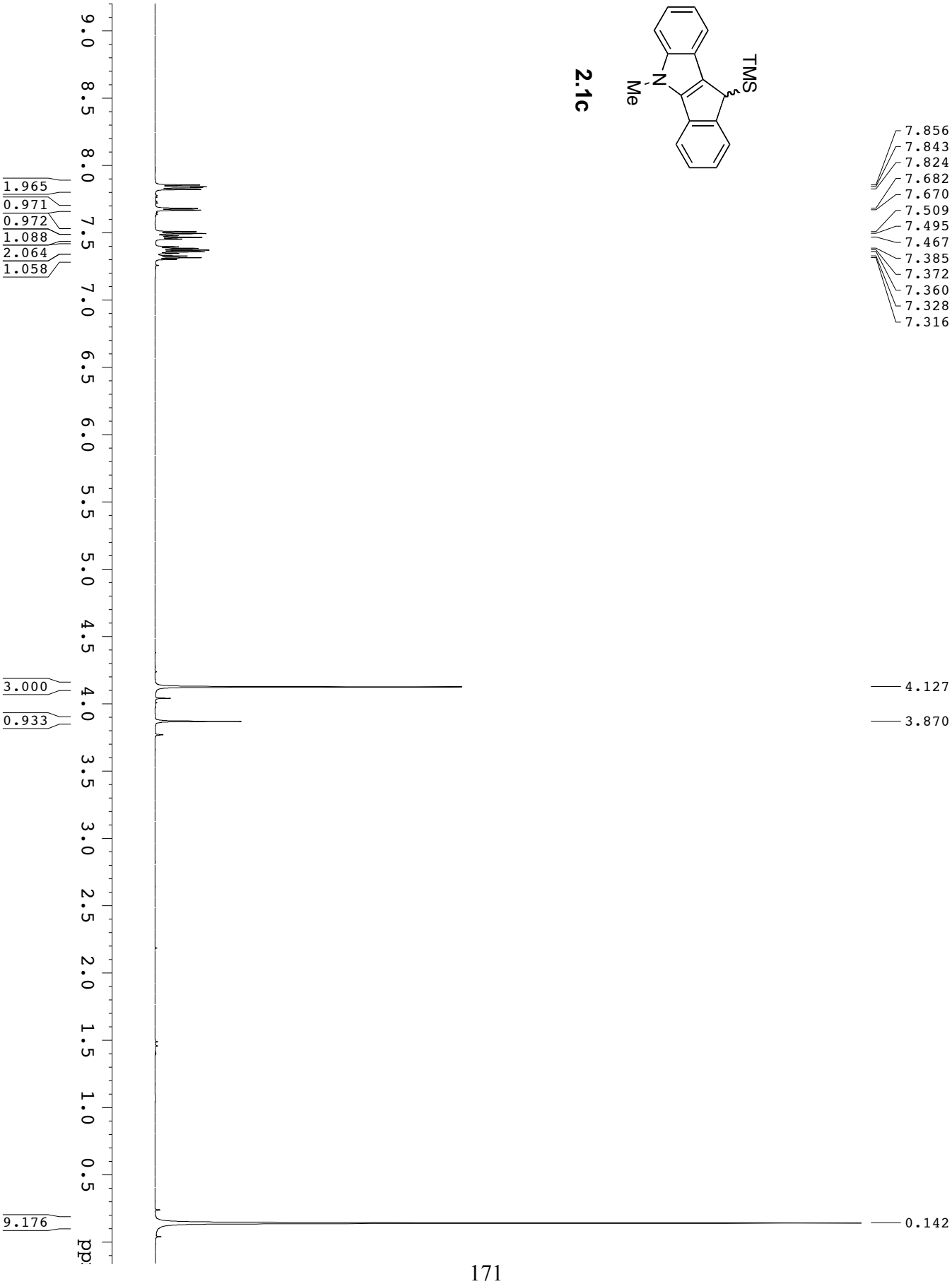
Appendix A:
^{1}H and ^{13}C NMR Spectra

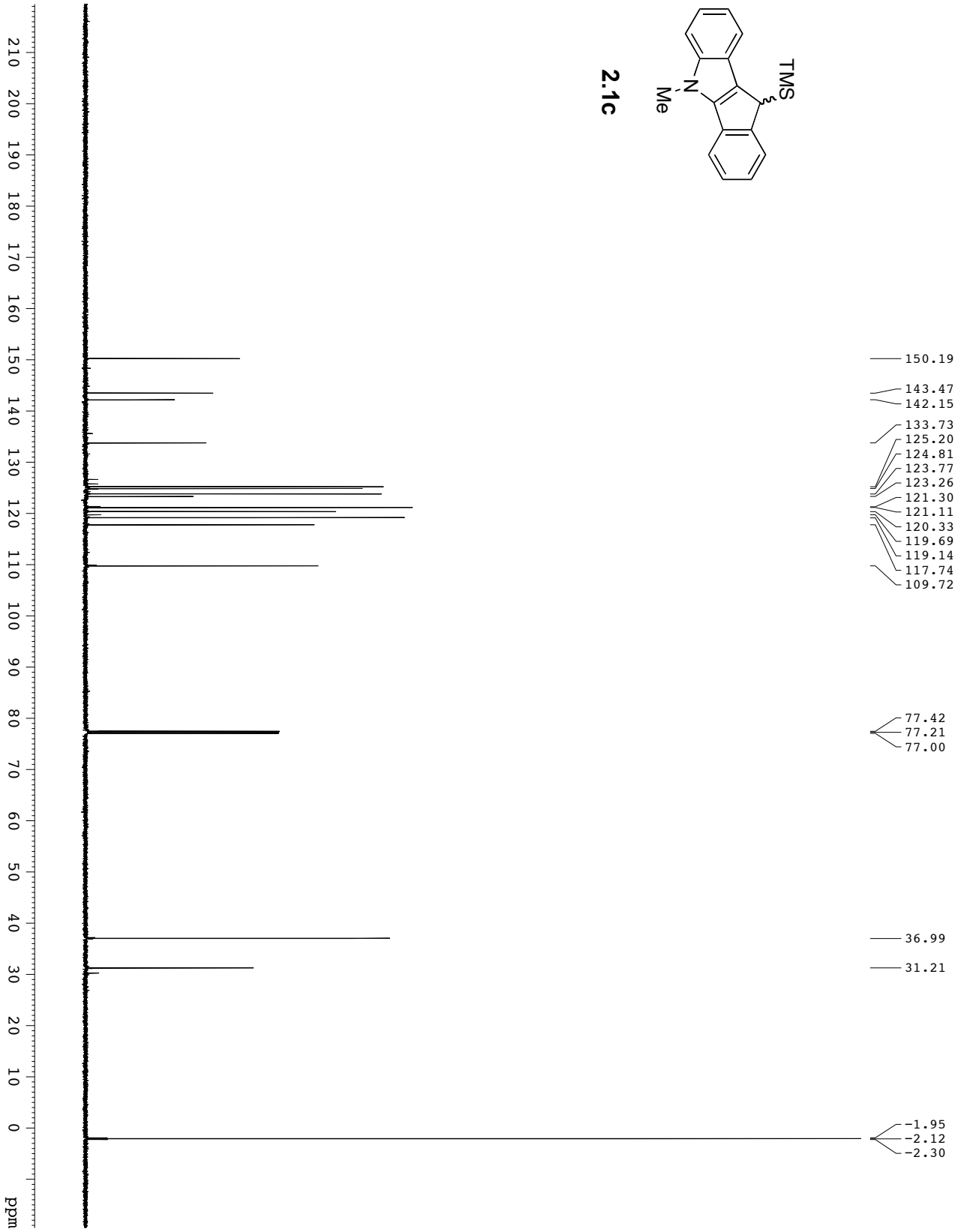

2.1a
8.302
7.653
7.641
7.554
7.542
7.476
7.464
7.446
7.433
7.349
7.337
7.324
7.259
7.237
7.224
7.212
7.206
7.196
7.194
7.183
7.181
7.168
7.158
3.740
0.919
0.929
0.941
0.928
0.920
0.974
2.827
2.000
9.0
8.5
8.0
7.5
7.0
6.5
6.0
5.5
5.0
4.5
4.0
3.5
3.0
2.5
2.0
1.5
1.0
0.5
ppm

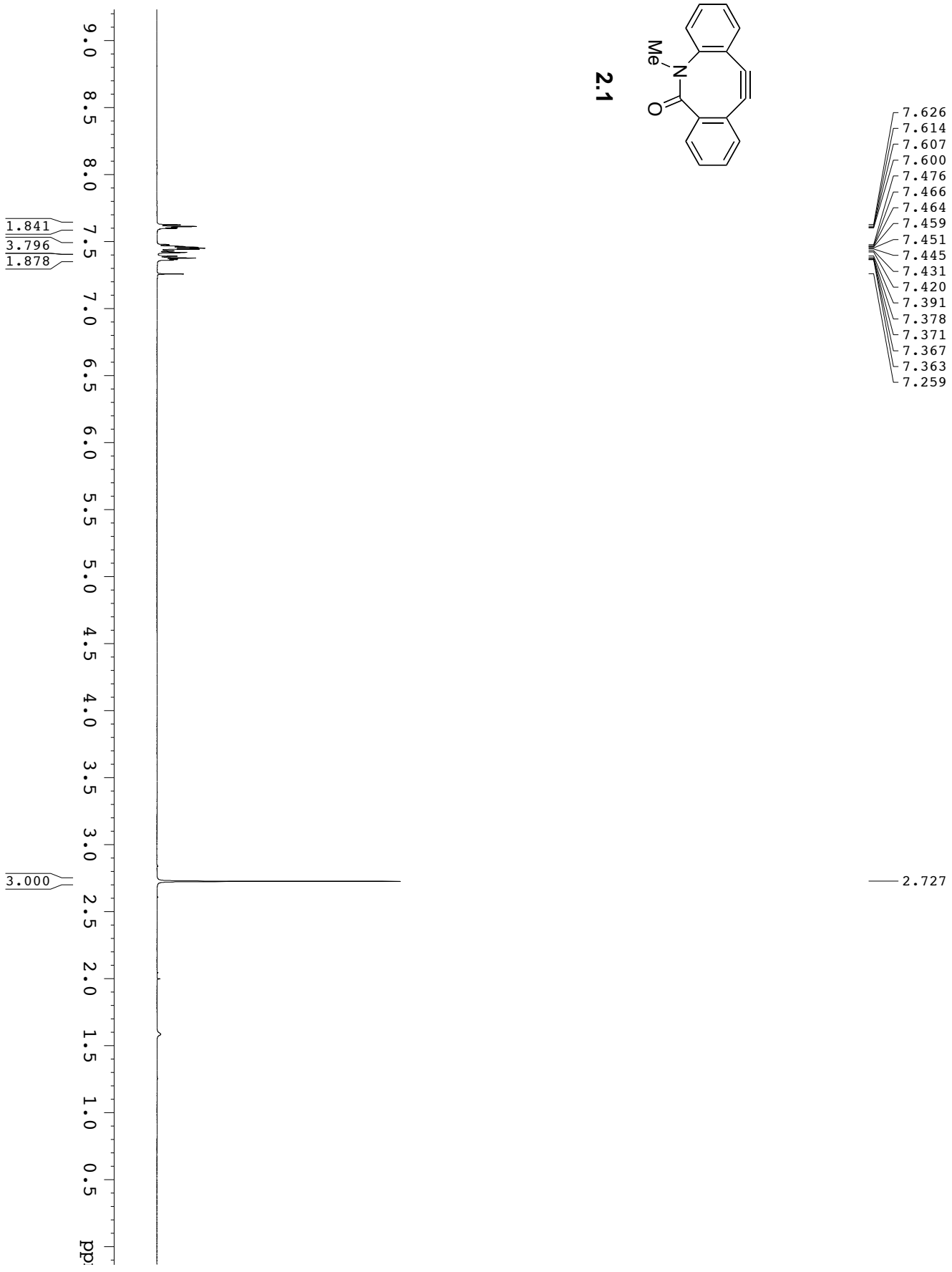

2.1a
147.80
143.31
140.64
135.00
126.53
125.47
124.77
124.73
121.82
121.70
120.23
118.95
117.27
112.03
77.19
76.98
76.77
30.33
ppm

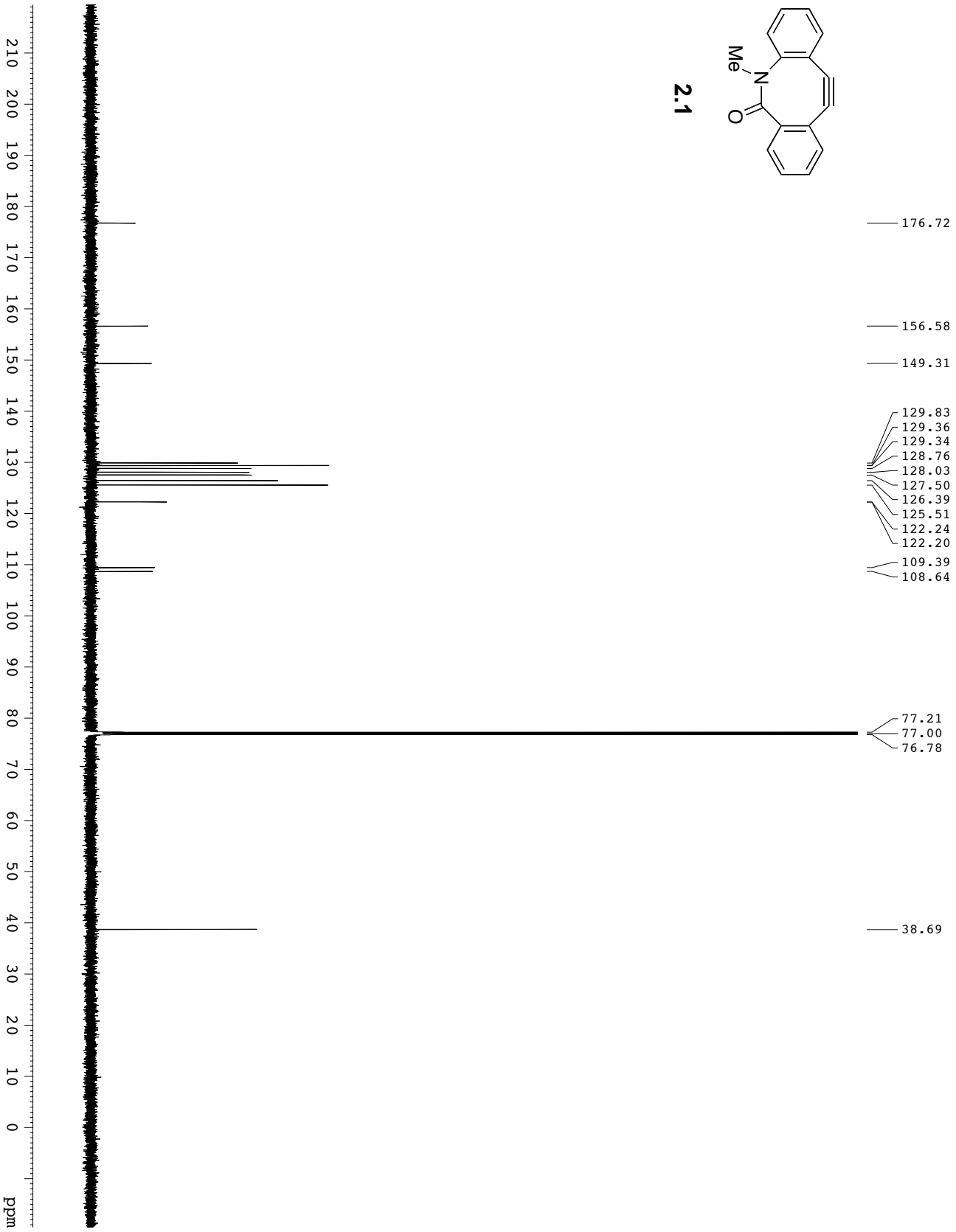

2.1b
N
Me
7.757
7.744
7.685
7.673
7.625
7.613
7.463
7.451
7.440
7.428
7.380
7.368
7.356
7.343
7.330
7.317
7.305
7.260
3.963
3.691
0.969
0.991
0.966
1.987
2.985
3.000
2.047
9.0
8.5
8.0
7.5
7.0
6.5
6.0
5.5
5.0
4.5
4.0
3.5
3.0
2.5
2.0
1.5
1.0
0.5
ppm

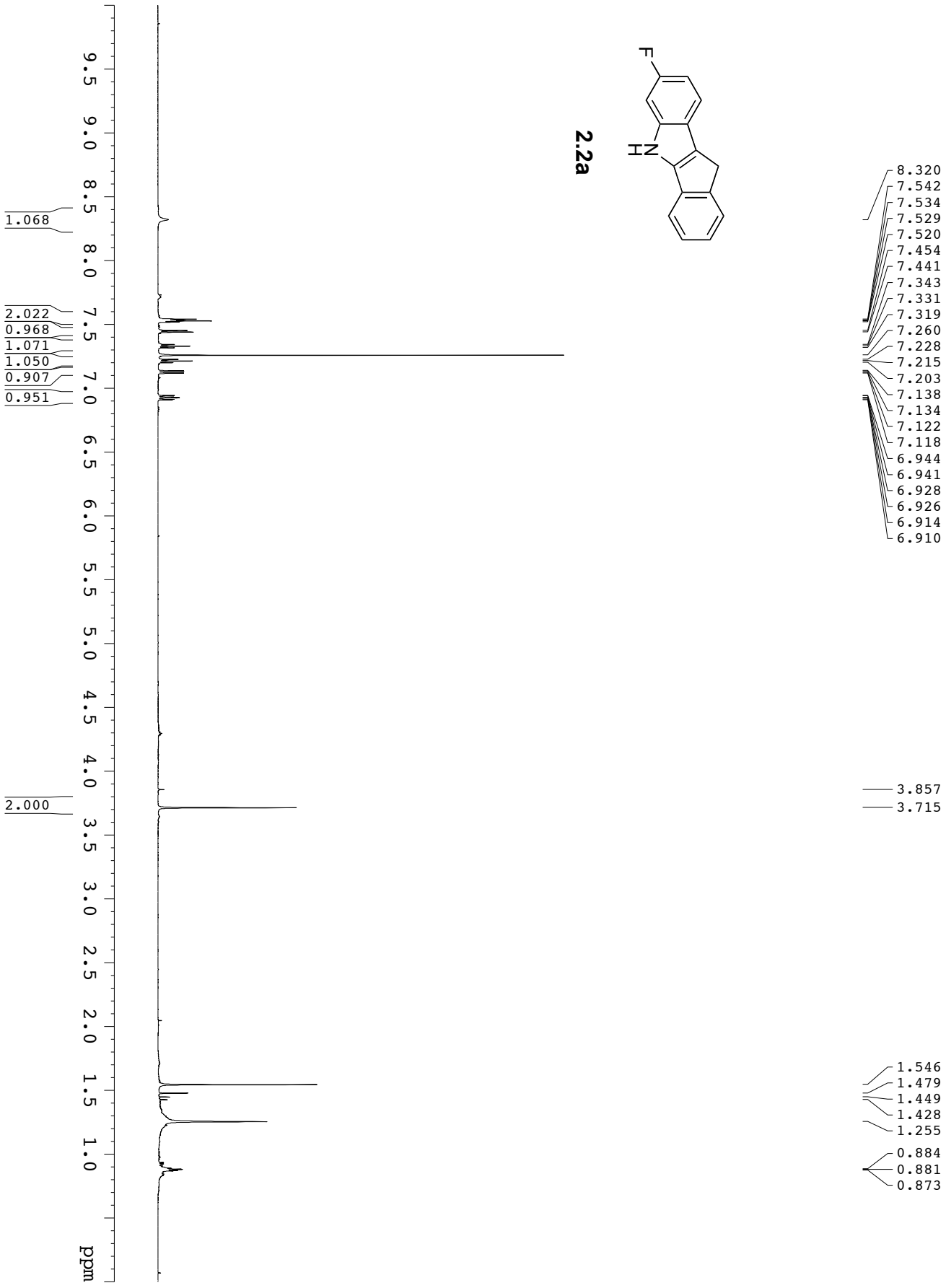

2.1b
N
Me
148.32
144.76
141.95
135.54
126.54
125.68
124.65
124.20
121.24
120.26
119.64
119.14
117.67
109.84
77.46
77.25
77.04
30.96
30.12
210
200
190
180
170
160
150
140
130
120
110
100
90
80
70
60
50
40
30
20
10
0
ppm

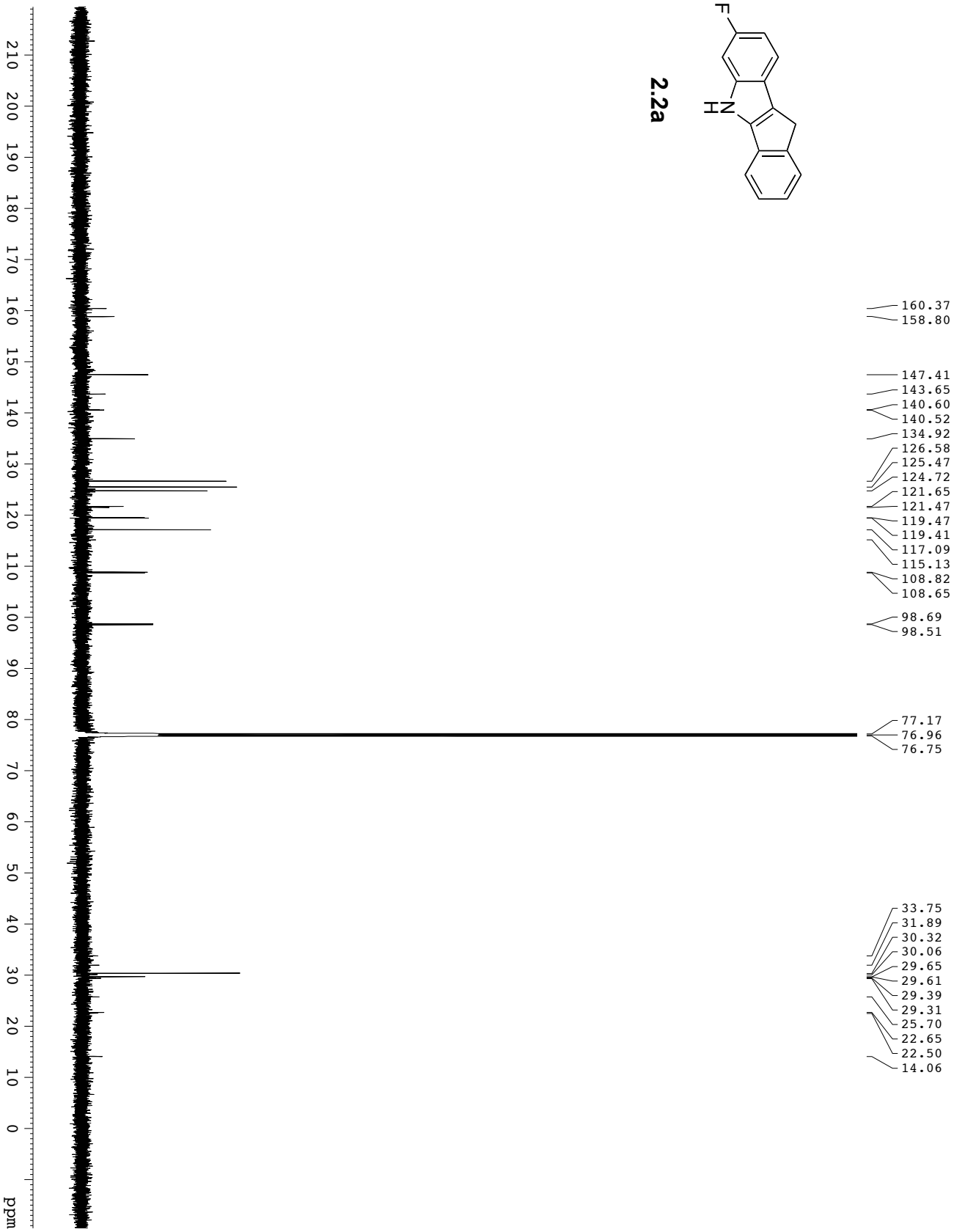

2.1c
TMS
N
Me
7.856
7.843
7.824
7.682
7.670
7.509
7.495
7.467
7.385
7.372
7.360
7.328
7.316
4.127
3.870
0.142
1.965
0.971
0.972
1.088
2.064
1.058
3.000
0.933
9.176
9.0
8.5
8.0
7.5
7.0
6.5
6.0
5.5
5.0
4.5
4.0
3.5
3.0
2.5
2.0
1.5
1.0
0.5
ppm

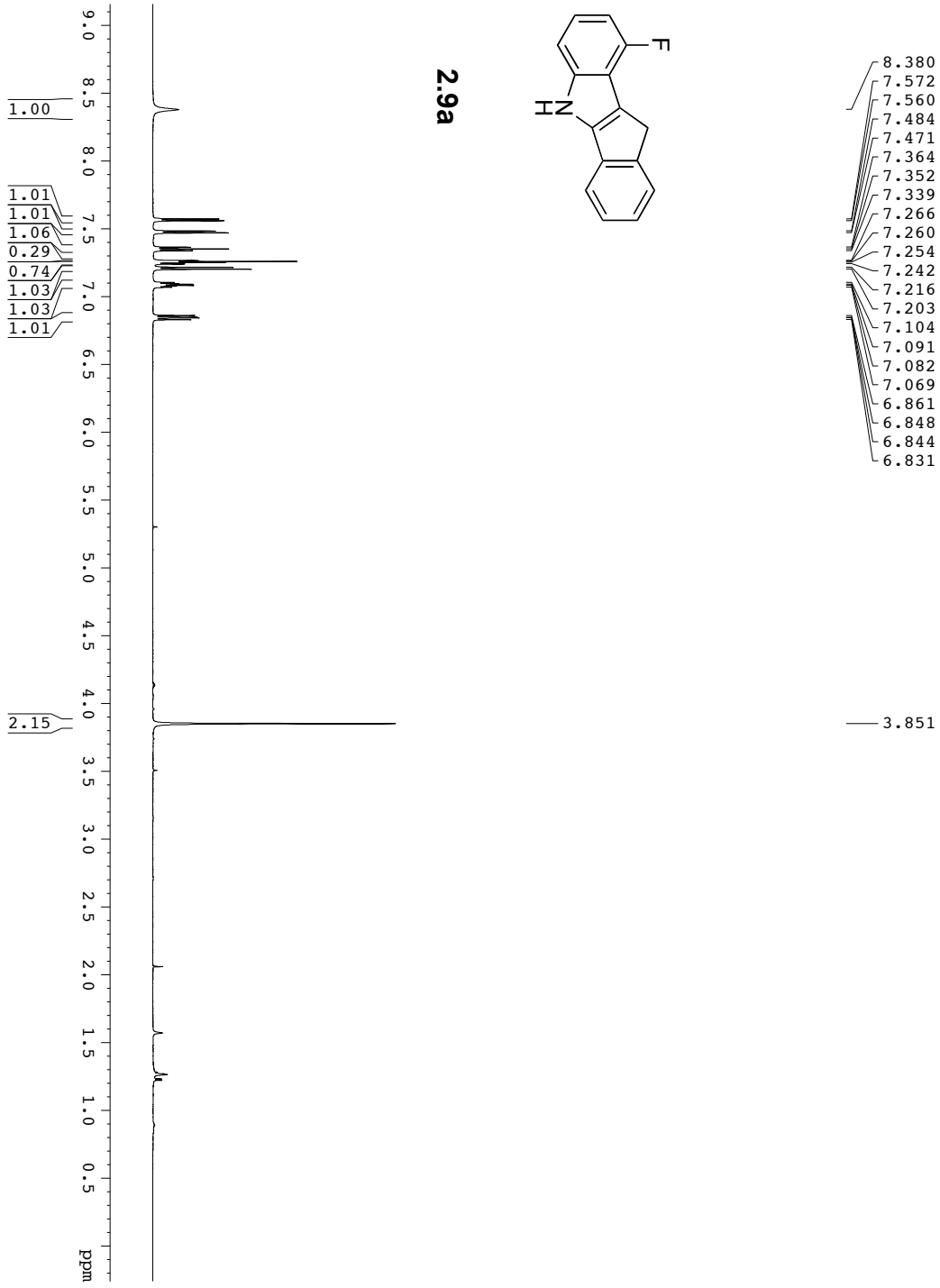

2.1c
TMS
N
Me
150.19
143.47
142.15
133.73
125.20
124.81
123.77
123.26
121.30
121.11
120.33
119.69
119.14
117.74
109.72
77.42
77.21
77.00
36.99
31.21
-1.95
-2.12
-2.30
ppm

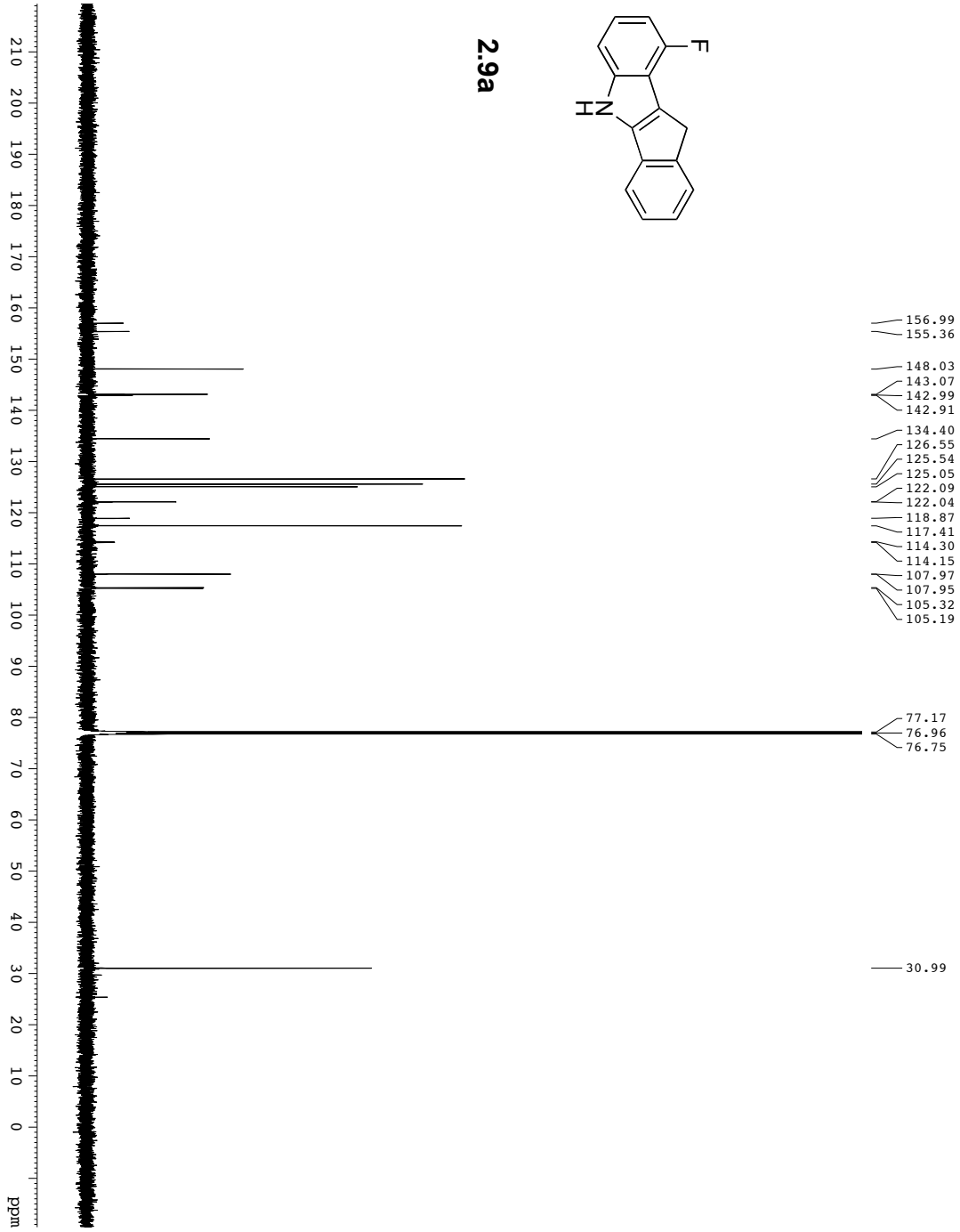

2.1
Me
N
O
7.626
7.614
7.607
7.600
7.476
7.466
7.464
7.459
7.451
7.445
7.431
7.420
7.391
7.378
7.371
7.367
7.363
7.259
2.727
1.841
3.796
1.878
3.000
9.0
8.5
8.0
7.5
7.0
6.5
6.0
5.5
5.0
4.5
4.0
3.5
3.0
2.5
2.0
1.5
1.0
0.5
ppm

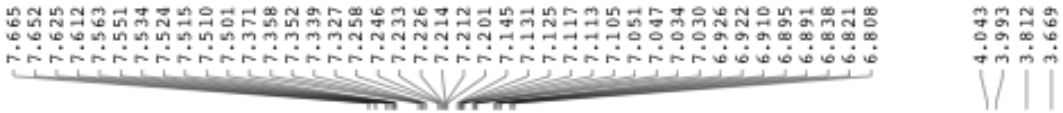

2.1
Me
N
O
176.72
156.58
149.31
129.83
129.36
129.34
128.76
128.03
127.50
126.39
125.51
122.24
122.20
109.39
108.64
77.21
77.00
76.78
38.69
210 200 190 180 170 160 150 140 130 120 110 100 90 80 70 60 50 40 30 20 10 0
ppm

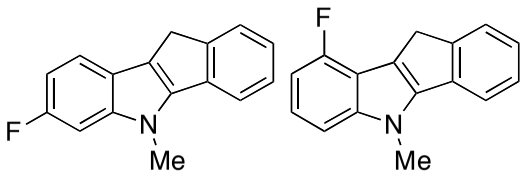

2.2a
F
N
H
8.320
7.542
7.534
7.529
7.520
7.454
7.441
7.343
7.331
7.319
7.260
7.228
7.215
7.203
7.138
7.134
7.122
7.118
6.944
6.941
6.928
6.926
6.914
6.910
3.857
3.715
1.546
1.479
1.449
1.428
1.255
0.884
0.881
0.873
1.068
2.022
0.968
1.071
1.050
0.907
0.951
2.000
9.5
9.0
8.5
8.0
7.5
7.0
6.5
6.0
5.5
5.0
4.5
4.0
3.5
3.0
2.5
2.0
1.5
1.0
ppm


2.2a
F
N
H
160.37
158.80
147.41
143.65
140.60
140.52
134.92
126.58
125.47
124.72
121.65
121.47
119.47
119.41
117.09
115.13
108.82
108.65
98.69
98.51
77.17
76.96
76.75
33.75
31.89
30.32
30.06
29.65
29.61
29.39
29.31
25.70
22.65
22.50
14.06
210 200 190 180 170 160 150 140 130 120 110 100 90 80 70 60 50 40 30 20 10 0
ppm

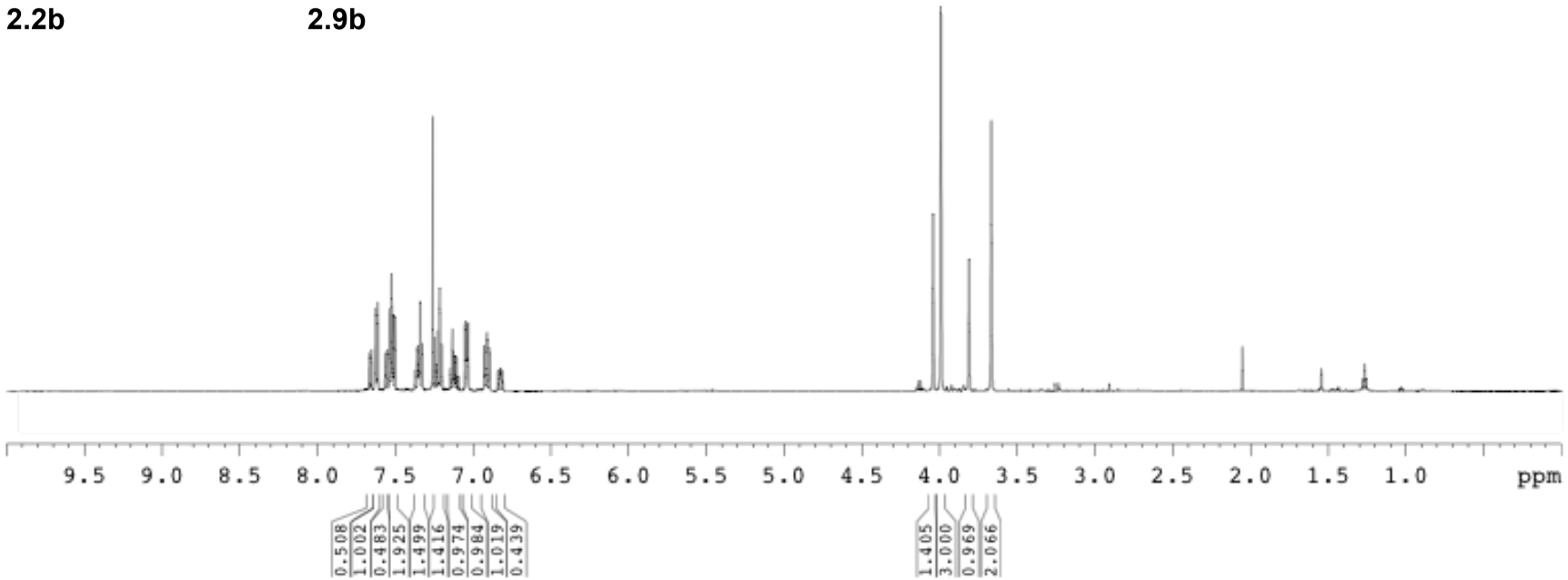

2.9a
F
N
H
8.380
7.572
7.560
7.484
7.471
7.364
7.352
7.339
7.266
7.260
7.254
7.242
7.216
7.203
7.104
7.091
7.082
7.069
6.861
6.848
6.844
6.831
3.851
1.00
1.01
1.01
1.06
0.29
0.74
1.03
1.03
1.01
2.15
9.0
8.5
8.0
7.5
7.0
6.5
6.0
5.5
5.0
4.5
4.0
3.5
3.0
2.5
2.0
1.5
1.0
0.5
ppm

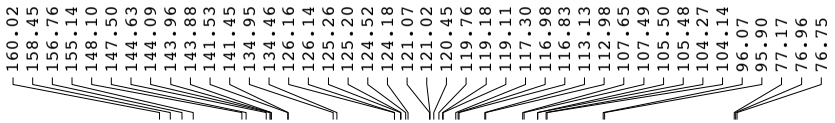

2.9a
F
N
H
156.99
155.36
148.03
143.07
142.99
142.91
134.40
126.55
125.54
125.05
122.09
122.04
118.87
117.41
114.30
114.15
107.97
107.95
105.32
105.19
77.17
76.96
76.75
30.99
ppm

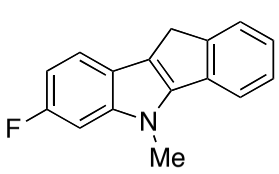

7.665
7.652
7.625
7.612
7.563
7.551
7.534
7.524
7.515
7.510
7.501
7.371
7.358
7.352
7.339
7.327
7.258
7.246
7.233
7.226
7.214
7.212
7.201
7.145
7.131
7.125
7.117
7.113
7.105
7.051
7.047
7.034
7.030
6.926
6.922
6.910
6.895
6.891
6.838
6.821
6.808
4.043
3.993
3.812
3.669


F
N
Me
F
N
Me

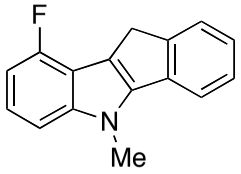
2.2b **2.9b**


9.5
9.0
8.5
8.0
7.5
7.0
6.5
6.0
5.5
5.0
4.5
4.0
3.5
3.0
2.5
2.0
1.5
1.0
ppm
0.508
1.002
0.483
1.925
1.499
1.416
0.974
0.984
1.019
0.439
1.405
3.000
0.969
2.066

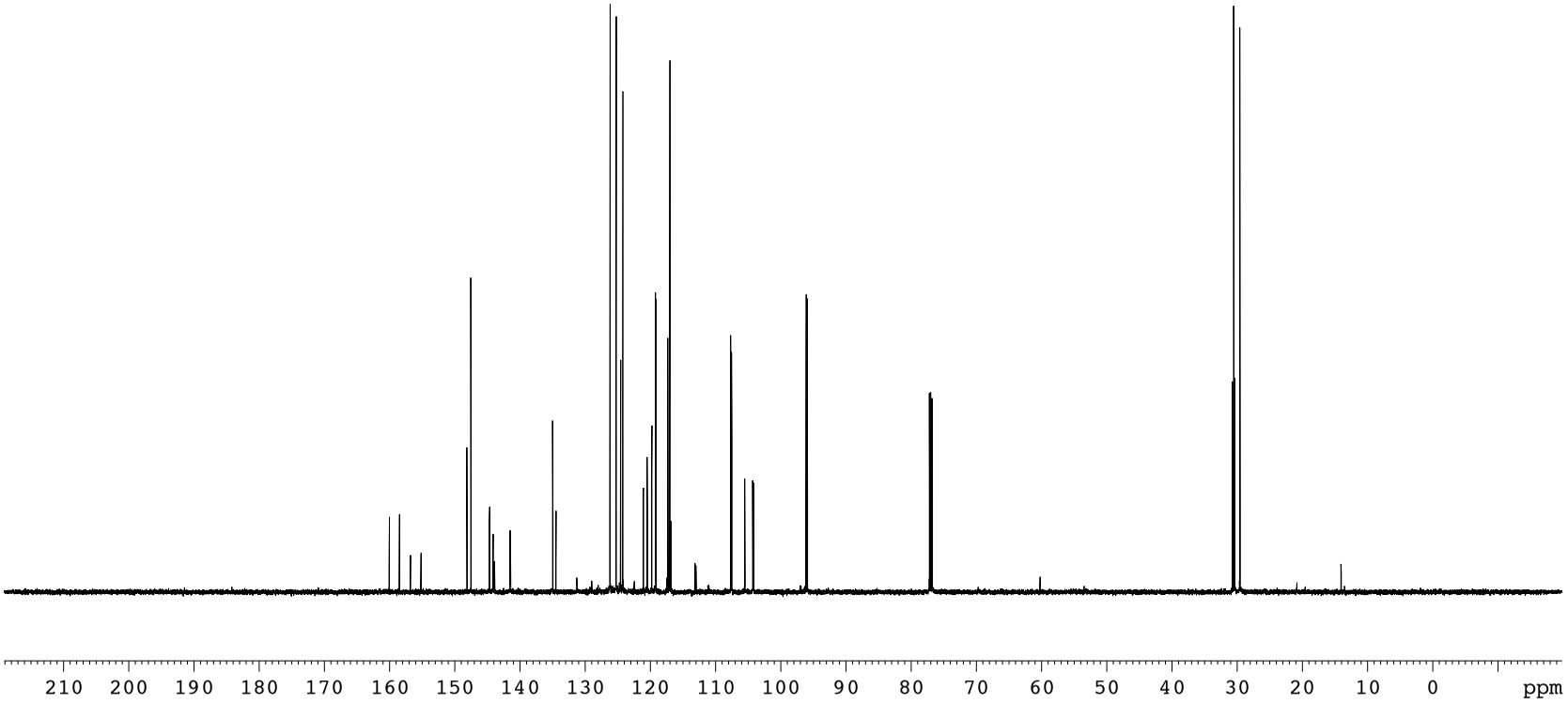

160.02
158.45
156.76
155.14
148.10
147.50
144.63
144.09
143.96
143.88
141.53
141.45
134.95
134.46
126.16
126.14
125.26
125.20
124.52
124.18
121.07
121.02
120.45
119.76
119.18
119.11
117.30
116.98
116.83
113.13
112.98
107.65
107.49
105.50
105.48
104.27
104.14
96.07
95.90
77.17
76.96
76.75
30.71
30.50
30.32
29.54
14.02

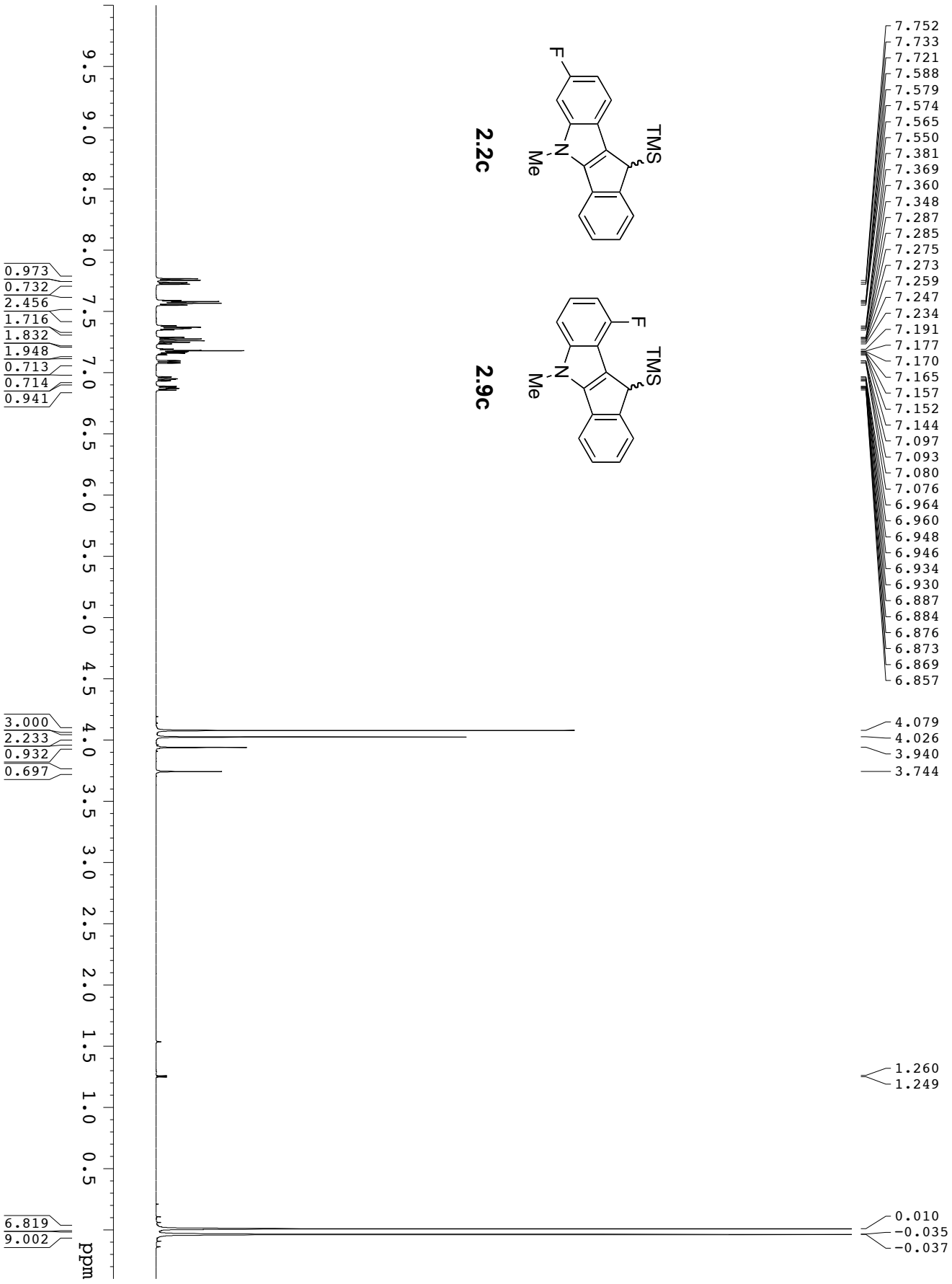

F
N
Me

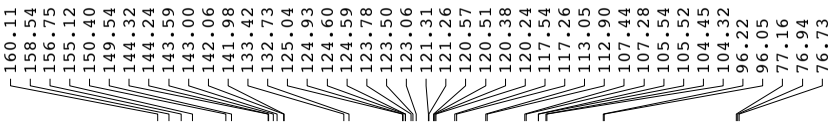
2.2b

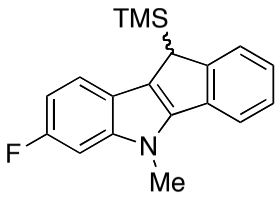

F
N
Me

2.9b

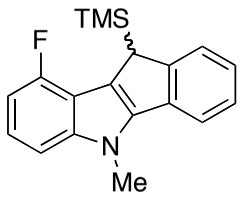

210
200
190
180
170
160
150
140
130
120
110
100
90
80
70
60
50
40
30
20
10
0
ppm


F
TMS
N
Me
2.2c
F
TMS
N
Me
2.9c
7.752
7.733
7.721
7.588
7.579
7.574
7.565
7.550
7.381
7.369
7.360
7.348
7.287
7.285
7.275
7.273
7.259
7.247
7.234
7.191
7.177
7.170
7.165
7.157
7.152
7.144
7.097
7.093
7.080
7.076
6.964
6.960
6.948
6.946
6.934
6.930
6.887
6.884
6.876
6.873
6.869
6.857
4.079
4.026
3.940
3.744
1.260
1.249
0.010
-0.035
-0.037
0.973
0.732
2.456
1.716
1.832
1.948
0.713
0.714
0.941
3.000
2.233
0.932
0.697
6.819
9.002
ppm

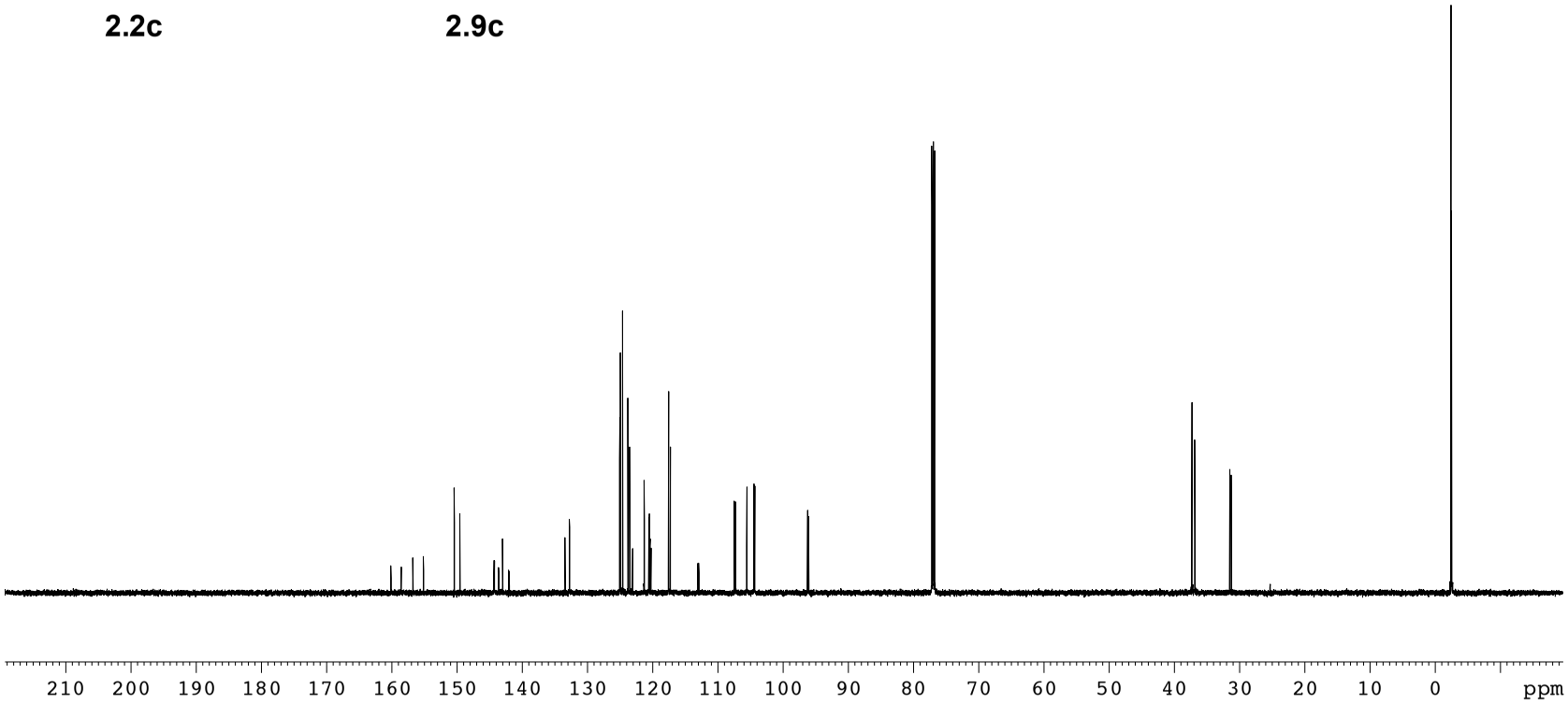

160.11
158.54
156.75
155.12
150.40
149.54
144.32
144.24
143.59
143.00
142.06
141.98
133.42
132.73
125.04
124.93
124.60
124.59
123.78
123.50
123.06
121.31
121.26
120.57
120.51
120.38
120.24
117.54
117.26
113.05
112.90
107.44
107.28
105.54
105.52
104.45
104.32
96.22
96.05
77.16
76.94
76.73
37.27
36.83
31.46
31.24
2.43
2.52
2.54


TMS
F
N
Me

2.2c


TMS
F
N
Me

2.9c


210
200
190
180
170
160
150
140
130
120
110
100
90
80
70
60
50
40
30
20
10
0
ppm

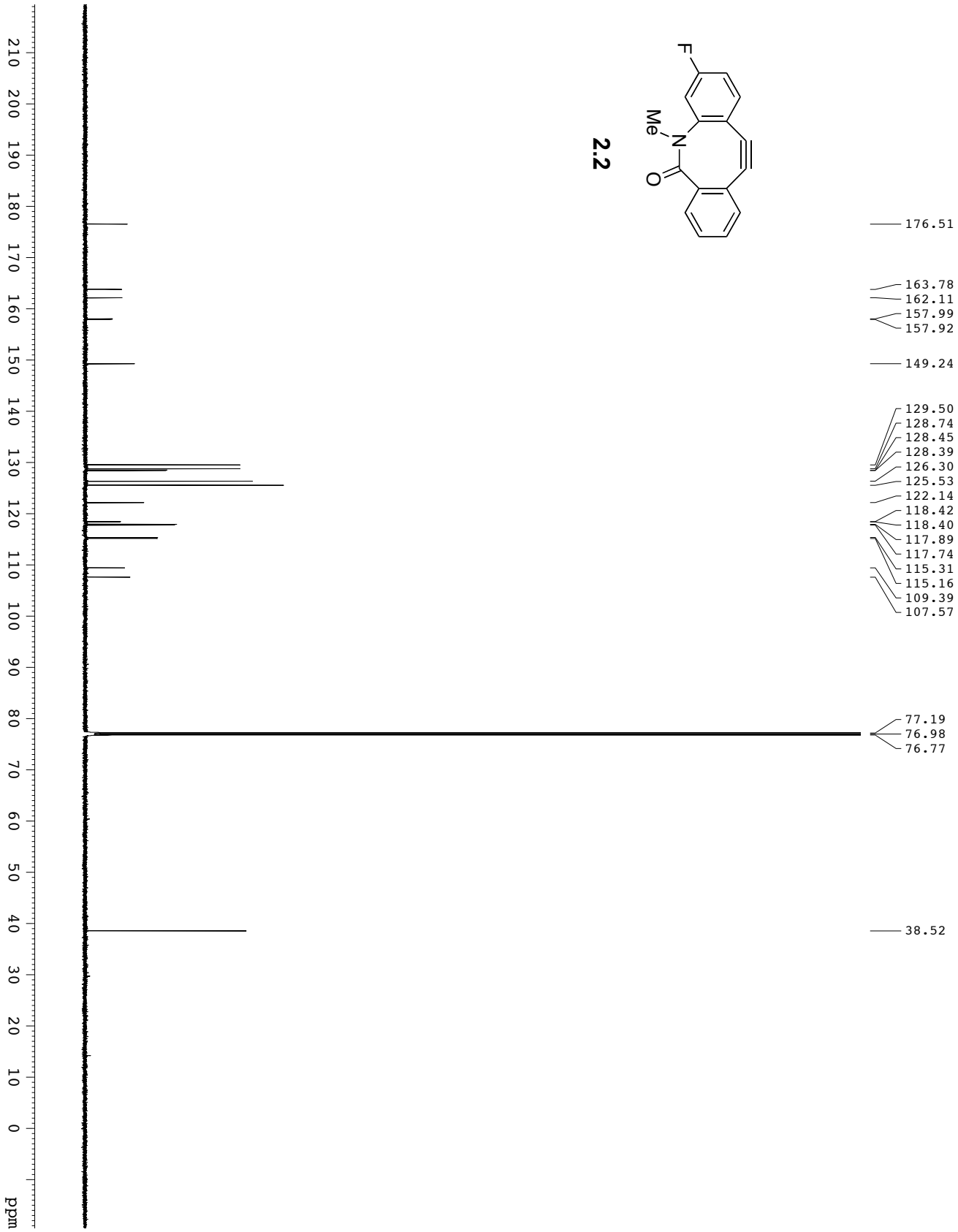
2.2

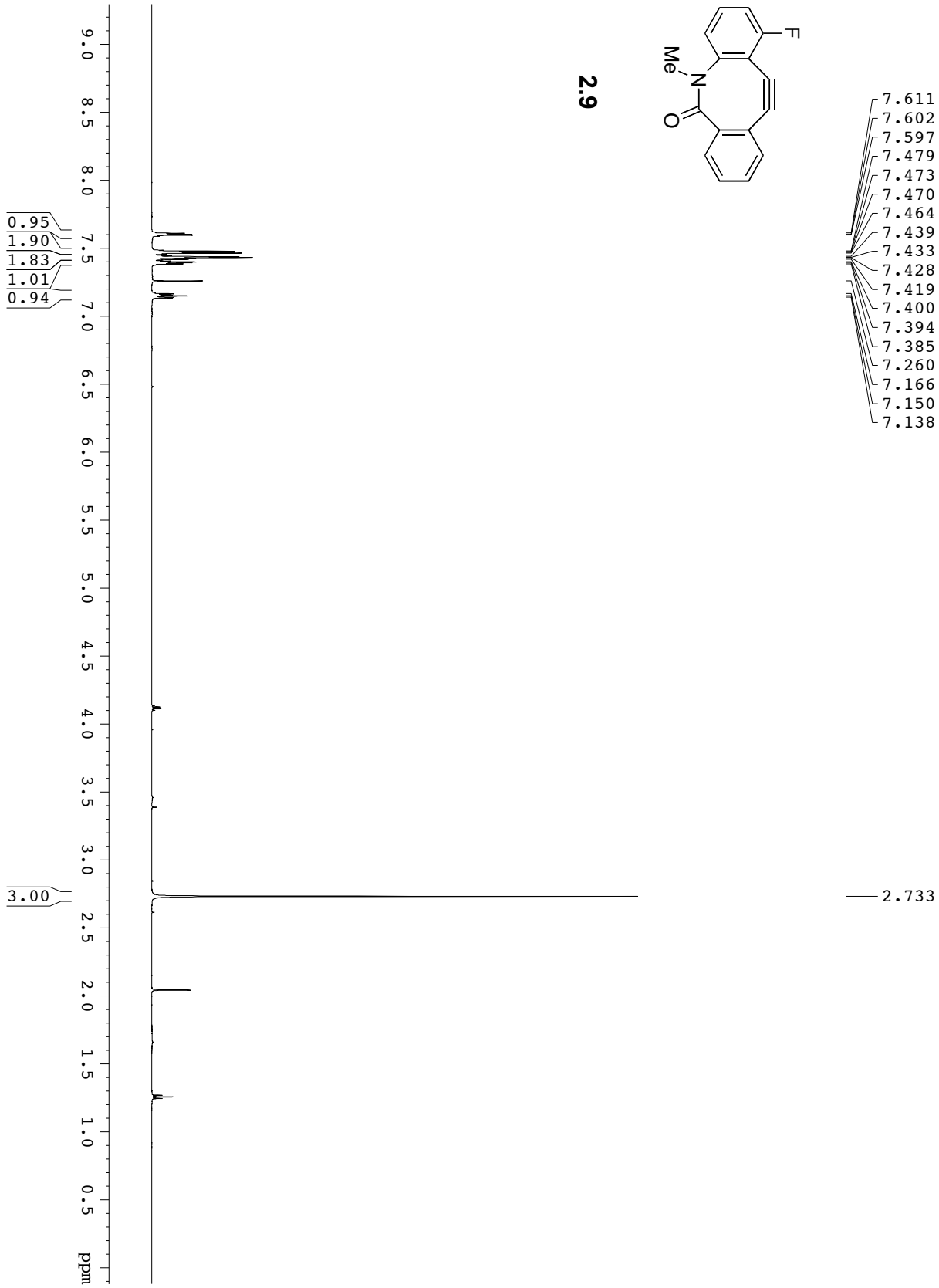
7.607
7.594
7.464
7.458
7.452
7.408
7.394
7.383
7.369
7.262
7.121
7.107
7.097

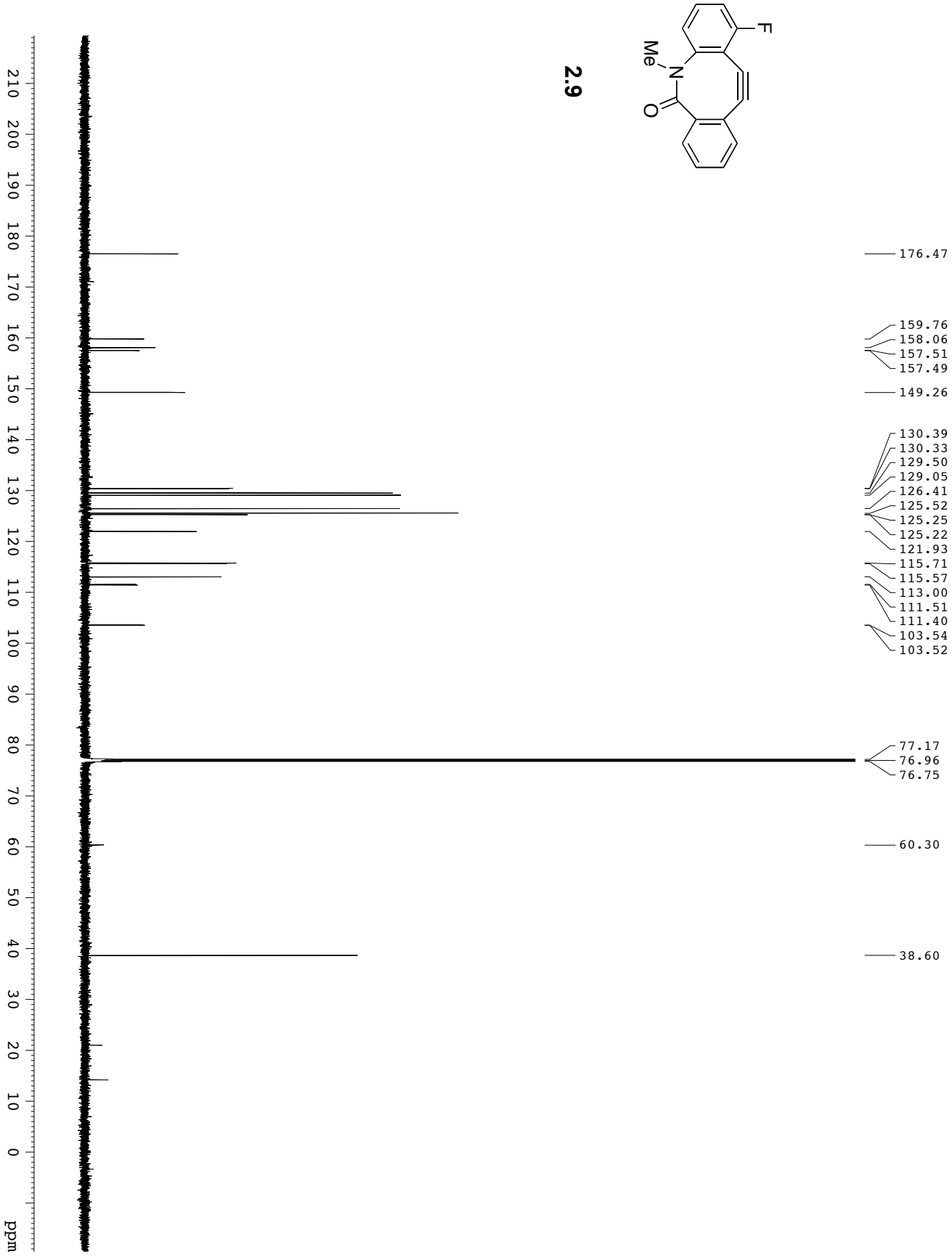
2.728

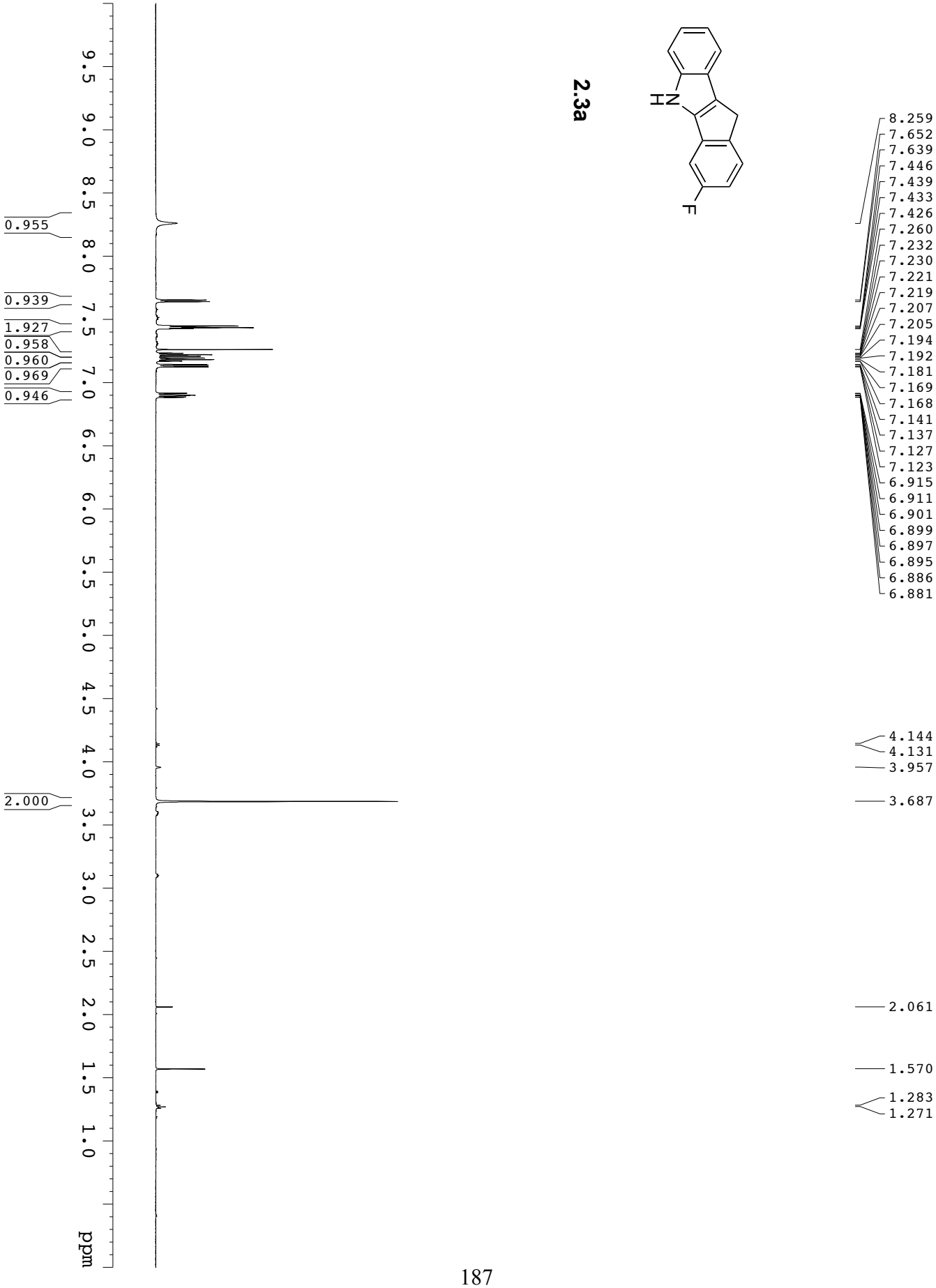
0.923
1.922
2.679
0.934
3.000

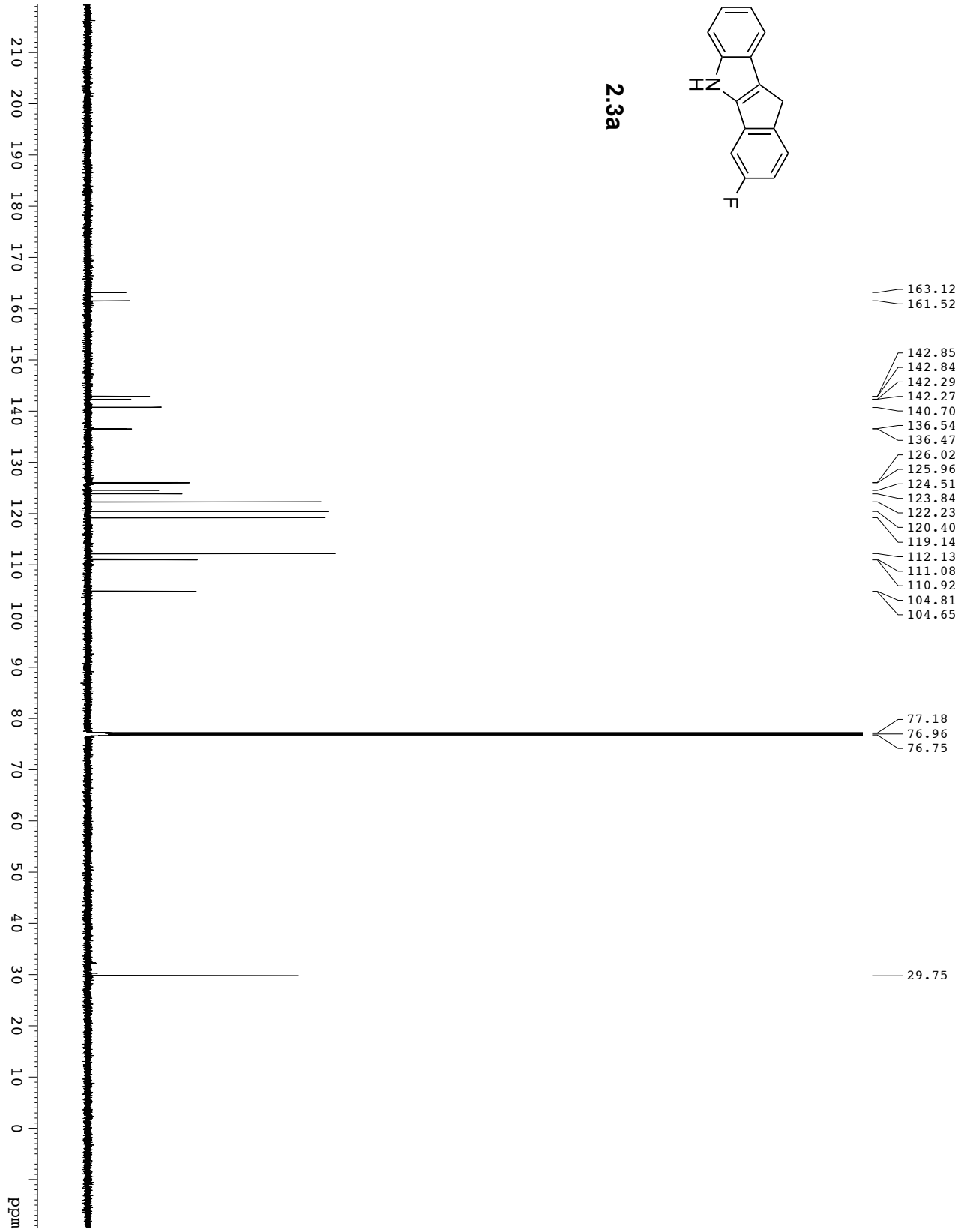
9.0 8.5 8.0 7.5 7.0 6.5 6.0 5.5 5.0 4.5 4.0 3.5 3.0 2.5 2.0 1.5 1.0 0.5 pp

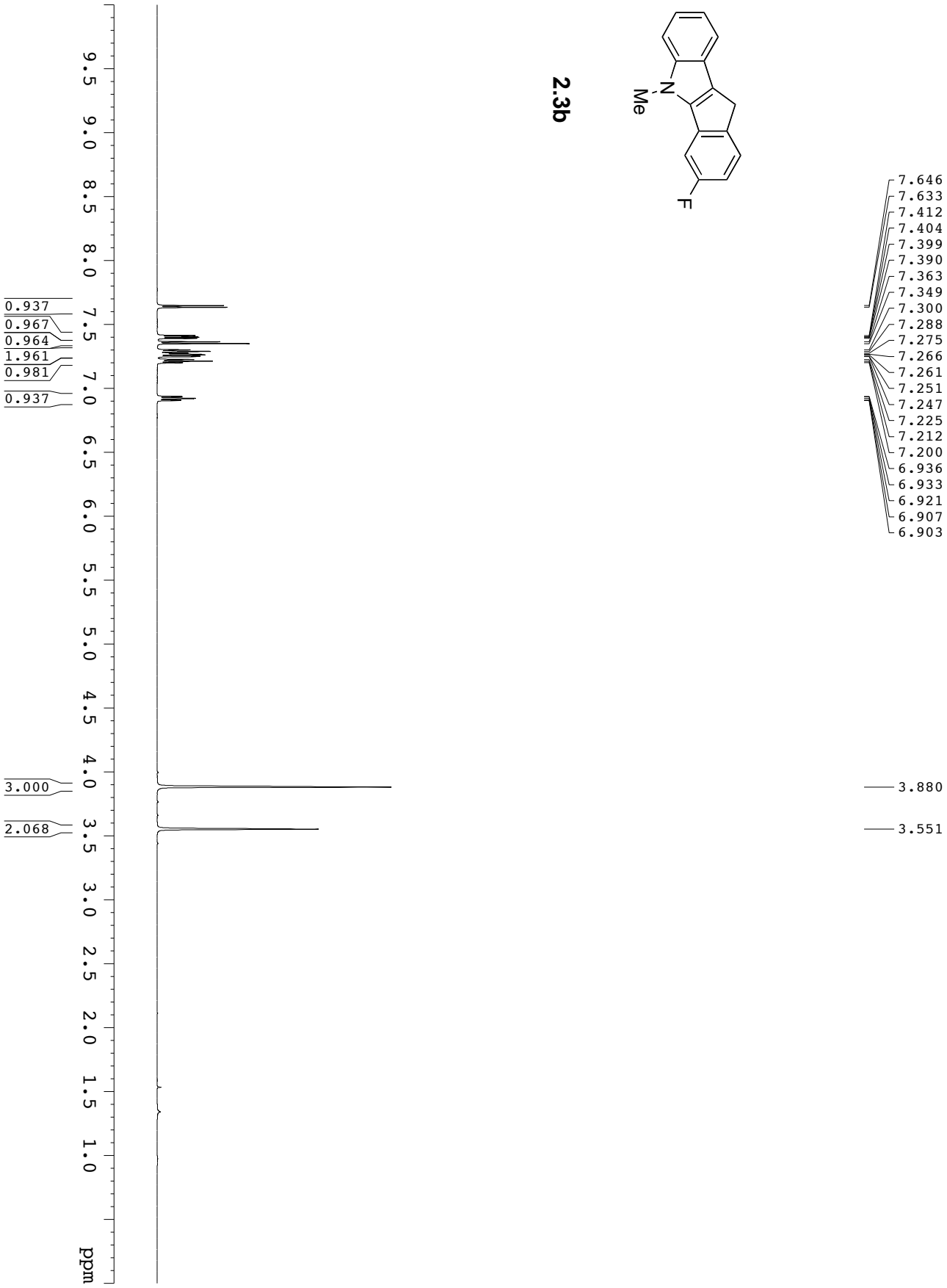

2.2
F
Me
N
O
176.51
163.78
162.11
157.99
157.92
149.24
129.50
128.74
128.45
128.39
126.30
125.53
122.14
118.42
118.40
117.89
117.74
115.31
115.16
109.39
107.57
77.19
76.98
76.77
38.52
210
200
190
180
170
160
150
140
130
120
110
100
90
80
70
60
50
40
30
20
10
0
ppm

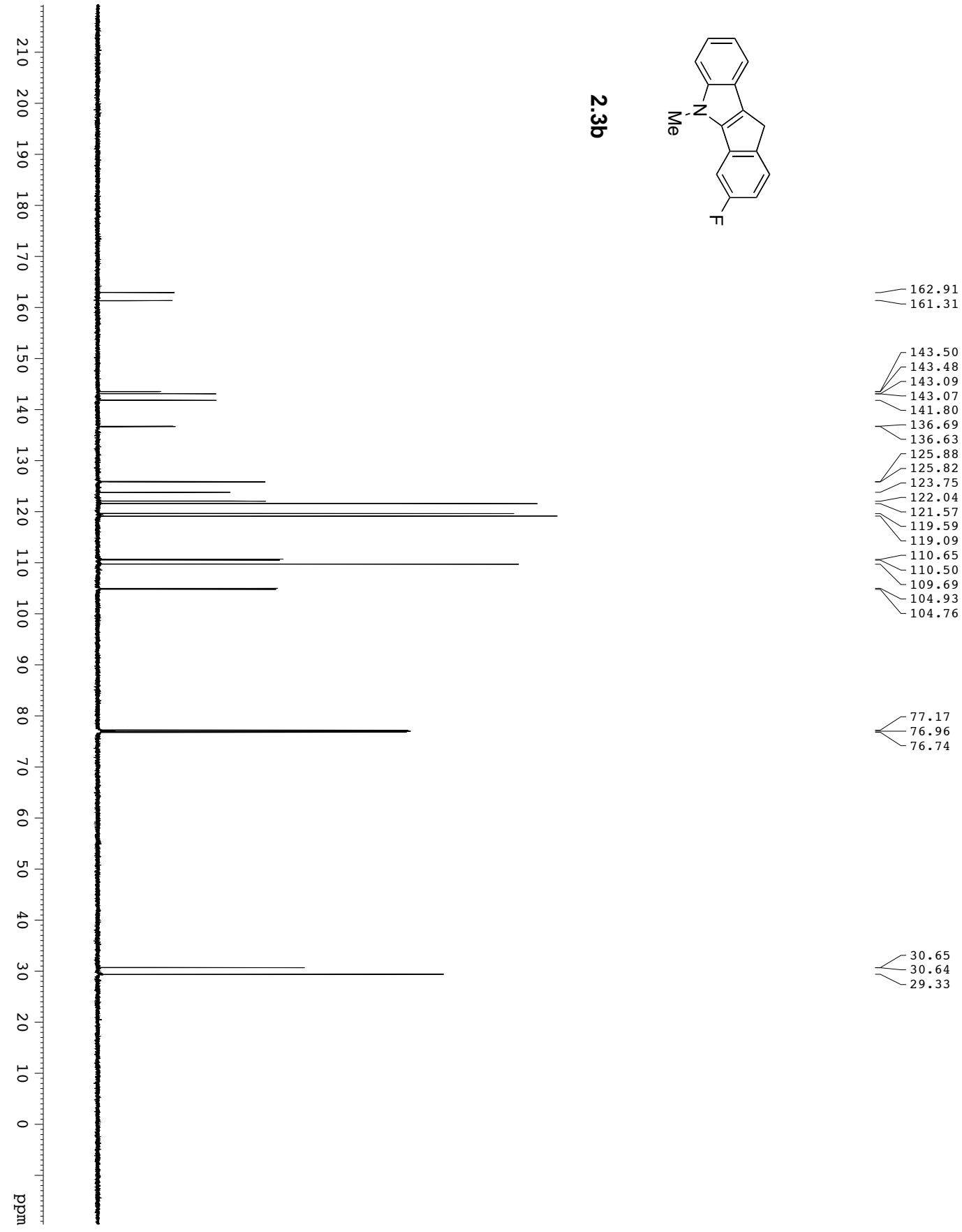

2.9
F
Me
N
O
7.611
7.602
7.597
7.479
7.473
7.470
7.464
7.439
7.433
7.428
7.419
7.400
7.394
7.385
7.260
7.166
7.150
7.138
2.733
0.95
1.90
1.83
1.01
0.94
3.00
9.0
8.5
8.0
7.5
7.0
6.5
6.0
5.5
5.0
4.5
4.0
3.5
3.0
2.5
2.0
1.5
1.0
0.5
ppm

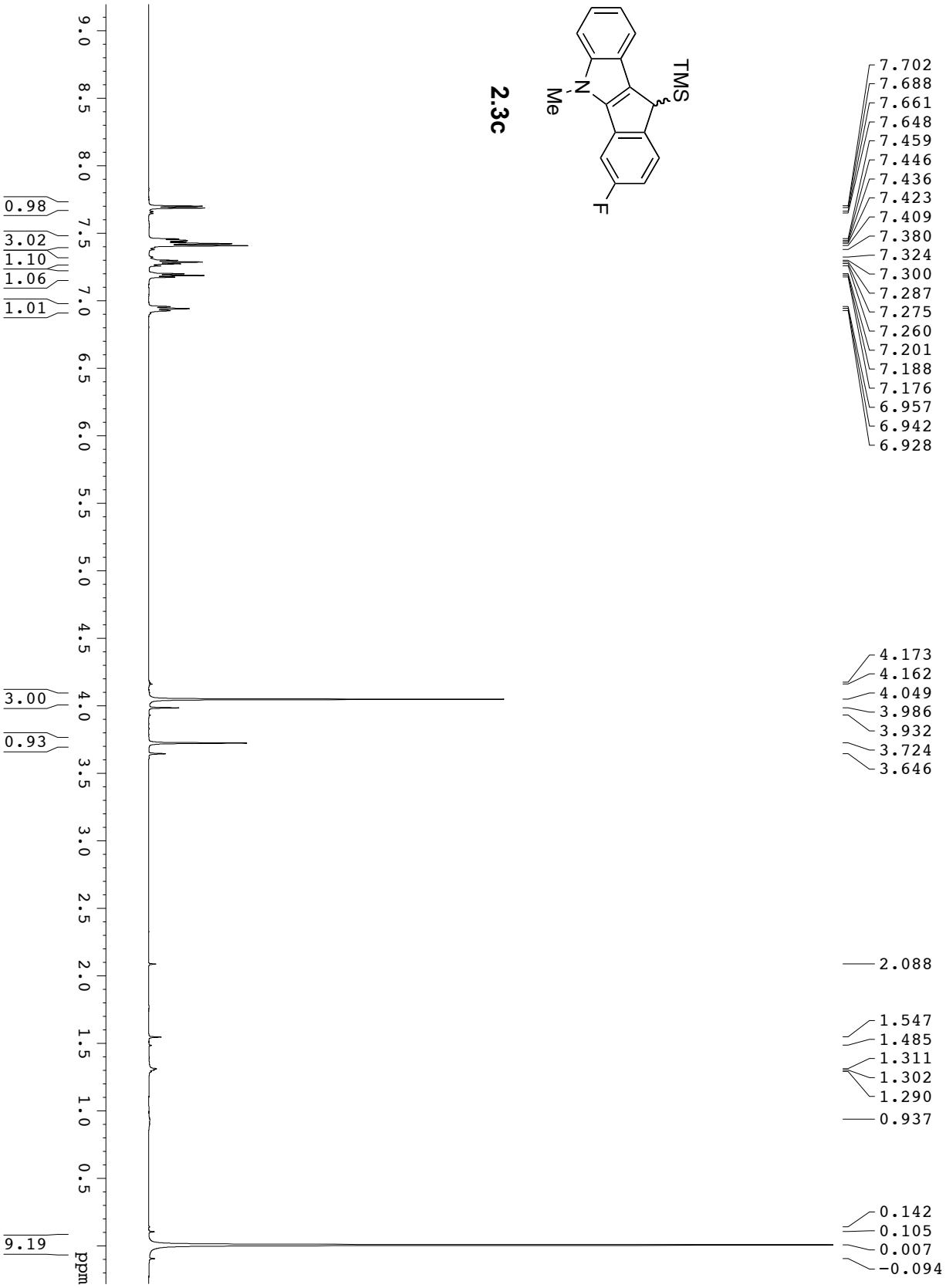

2.9
F
Me
N
O
176.47
159.76
158.06
157.51
157.49
149.26
130.39
130.33
129.50
129.05
126.41
125.52
125.25
125.22
121.93
115.71
115.57
113.00
111.51
111.40
103.54
103.52
77.17
76.96
76.75
60.30
38.60
210 200 190 180 170 160 150 140 130 120 110 100 90 80 70 60 50 40 30 20 10 0
ppm

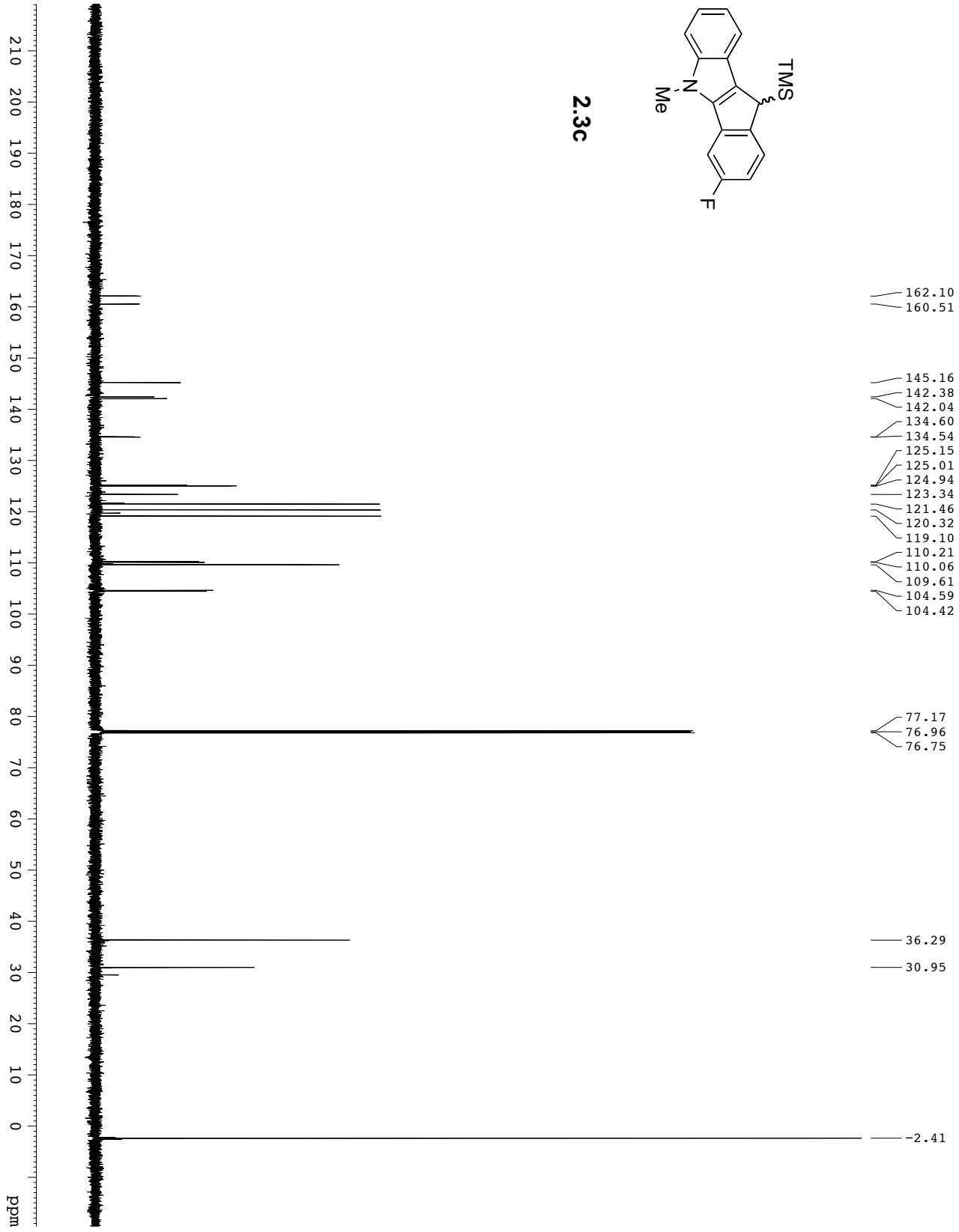

2.3a
F
8.259
7.652
7.639
7.446
7.439
7.433
7.426
7.260
7.232
7.230
7.221
7.219
7.207
7.205
7.194
7.192
7.181
7.169
7.168
7.141
7.137
7.127
7.123
6.915
6.911
6.901
6.899
6.897
6.895
6.886
6.881
4.144
4.131
3.957
3.687
2.061
1.570
1.283
1.271
0.955
0.939
1.927
0.958
0.960
0.969
0.946
2.000
ppm

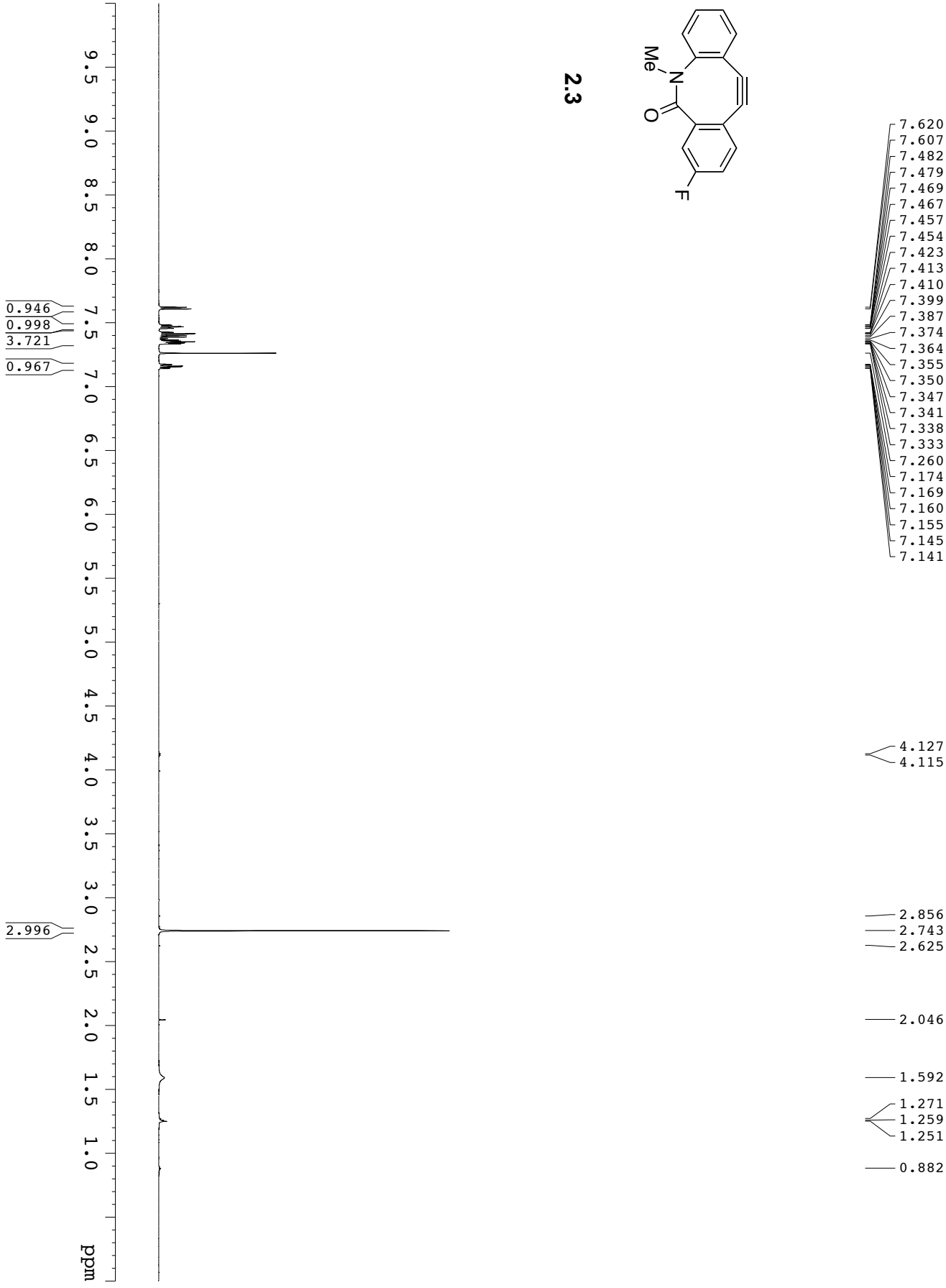

2.3a
H
N
F
163.12
161.52
142.85
142.84
142.29
142.27
140.70
136.54
136.47
126.02
125.96
124.51
123.84
122.23
120.40
119.14
112.13
111.08
110.92
104.81
104.65
77.18
76.96
76.75
29.75
210 200 190 180 170 160 150 140 130 120 110 100 90 80 70 60 50 40 30 20 10 0
ppm

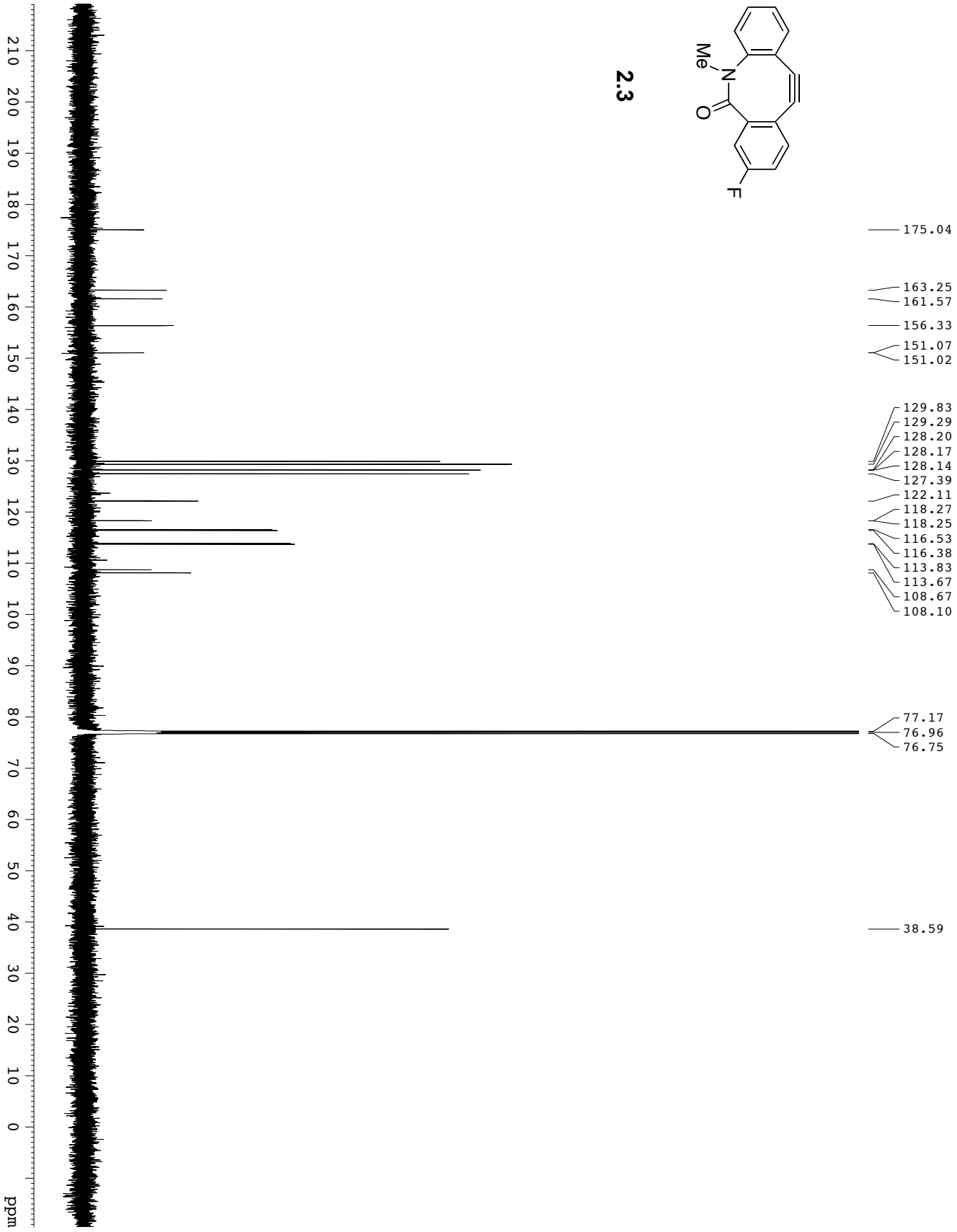

2.3b
N
Me
F
7.646
7.633
7.412
7.404
7.399
7.390
7.363
7.349
7.300
7.288
7.275
7.266
7.261
7.251
7.247
7.225
7.212
7.200
6.936
6.933
6.921
6.907
6.903
3.880
3.551
0.937
0.967
0.964
1.961
0.981
0.937
3.000
2.068
9.5
9.0
8.5
8.0
7.5
7.0
6.5
6.0
5.5
5.0
4.5
4.0
3.5
3.0
2.5
2.0
1.5
1.0
ppm

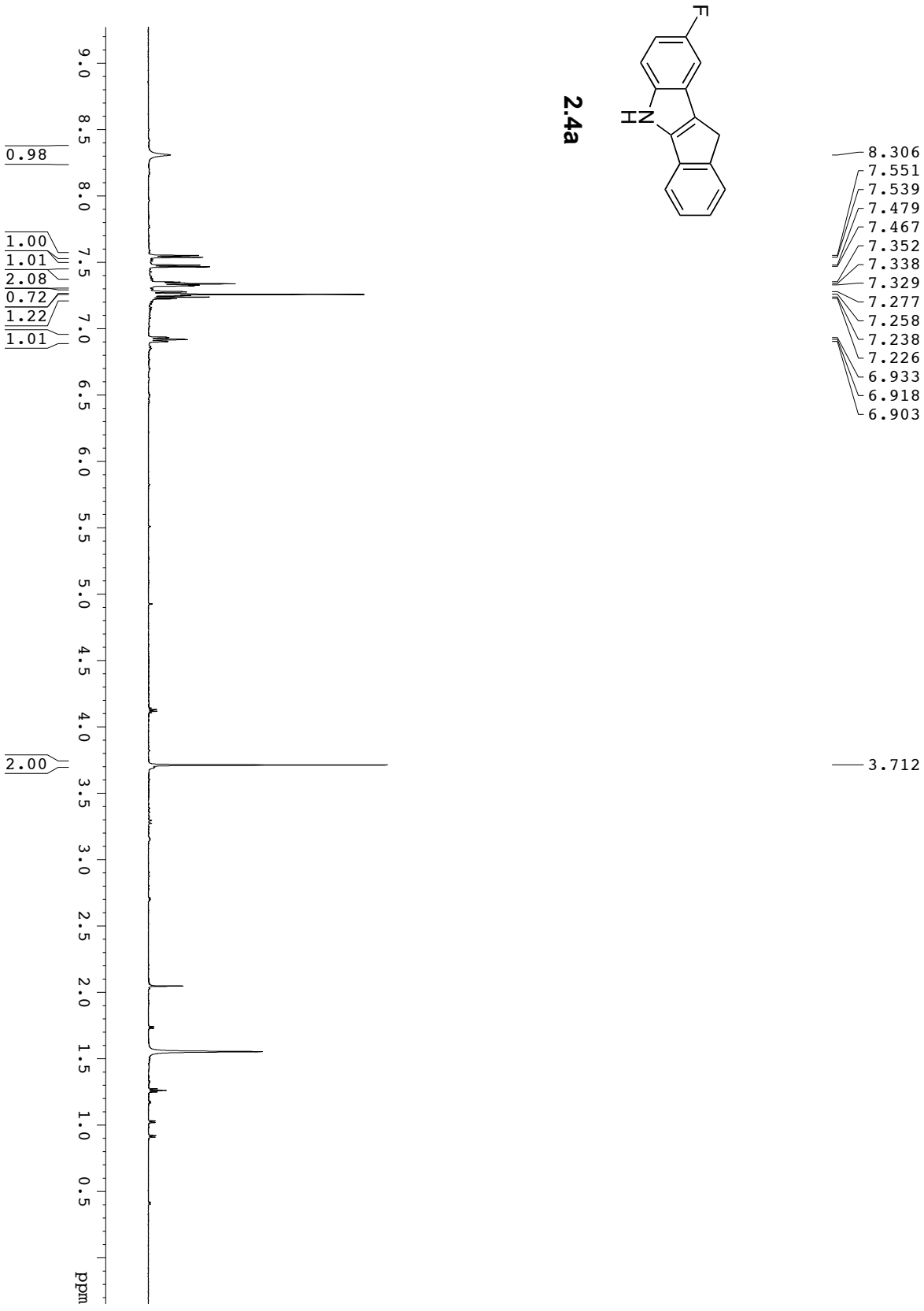

2.3b
N
Me
F
162.91
161.31
143.50
143.48
143.09
143.07
141.80
136.69
136.63
125.88
125.82
123.75
122.04
121.57
119.59
119.09
110.65
110.50
109.69
104.93
104.76
77.17
76.96
76.74
30.65
30.64
29.33
210
200
190
180
170
160
150
140
130
120
110
100
90
80
70
60
50
40
30
20
10
0
ppm

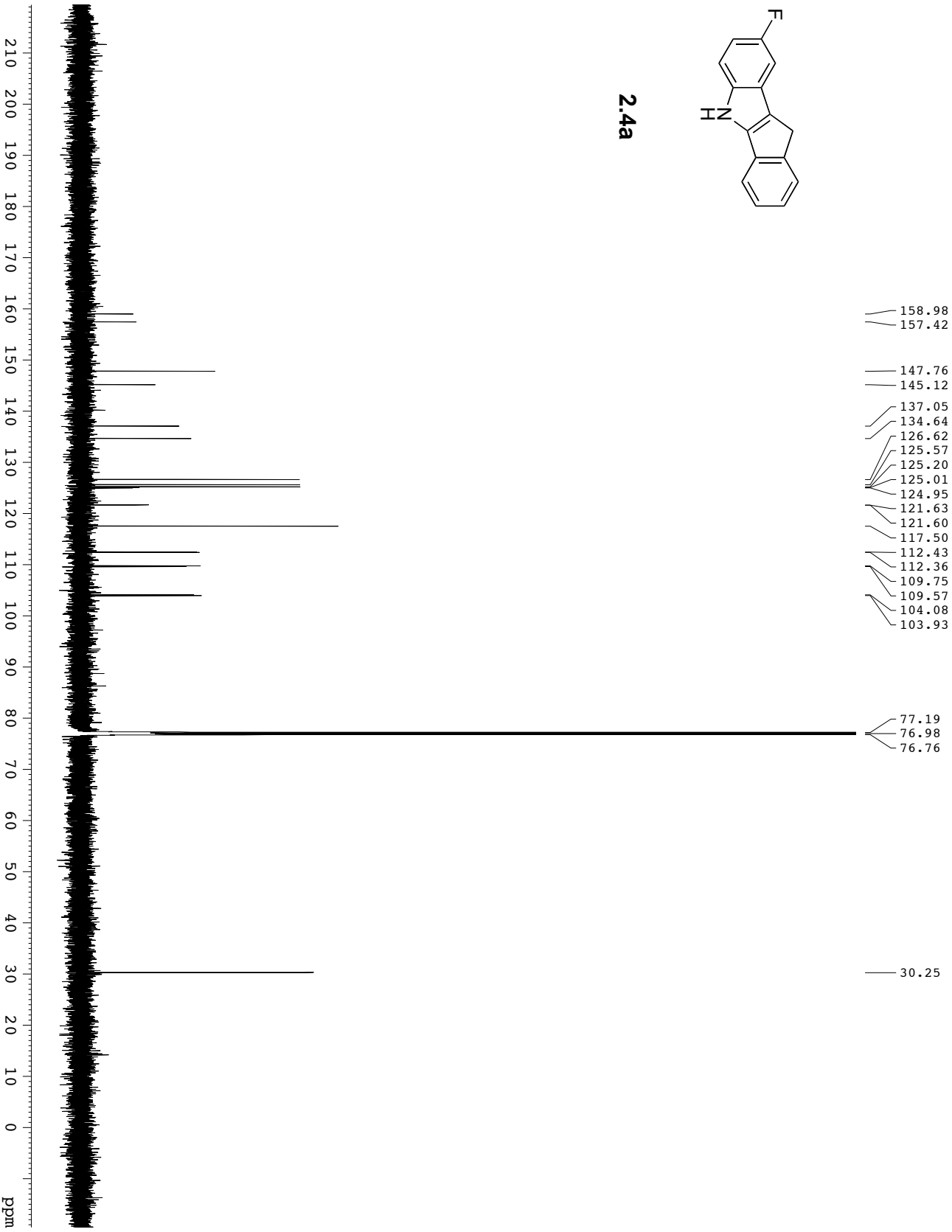

2.3c
TMS
N
Me
F
7.702
7.688
7.661
7.648
7.459
7.446
7.436
7.423
7.409
7.380
7.324
7.300
7.287
7.275
7.260
7.201
7.188
7.176
6.957
6.942
6.928
4.173
4.162
4.049
3.986
3.932
3.724
3.646
2.088
1.547
1.485
1.311
1.302
1.290
0.937
0.142
0.105
0.007
-0.094
0.98
3.02
1.10
1.06
1.01
3.00
0.93
9.19
ppm

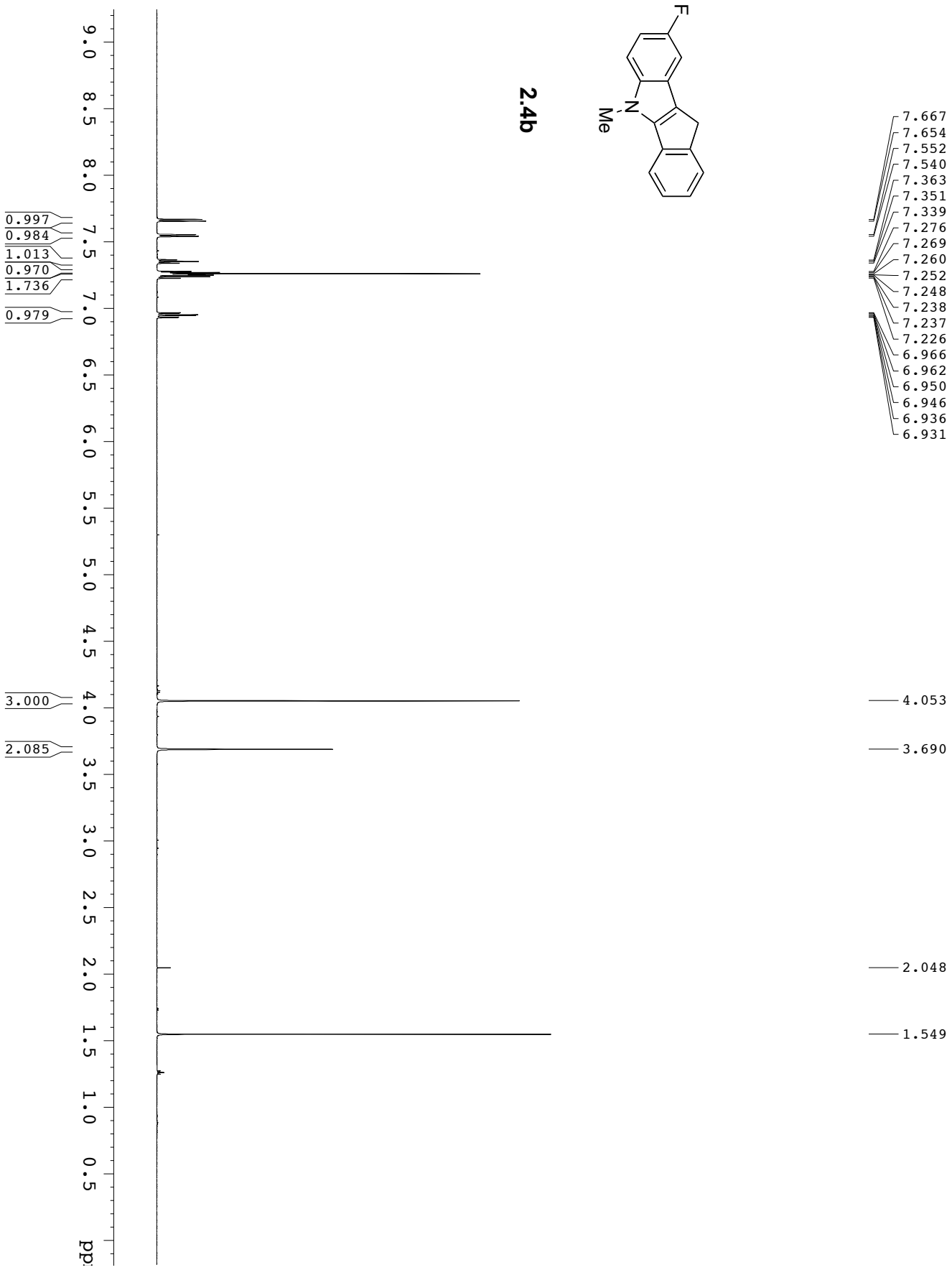

2.3c
TMS
N
Me
F
162.10
160.51
145.16
142.38
142.04
134.60
134.54
125.15
125.01
124.94
123.34
121.46
120.32
119.10
110.21
110.06
109.61
104.59
104.42
77.17
76.96
76.75
36.29
30.95
-2.41
ppm

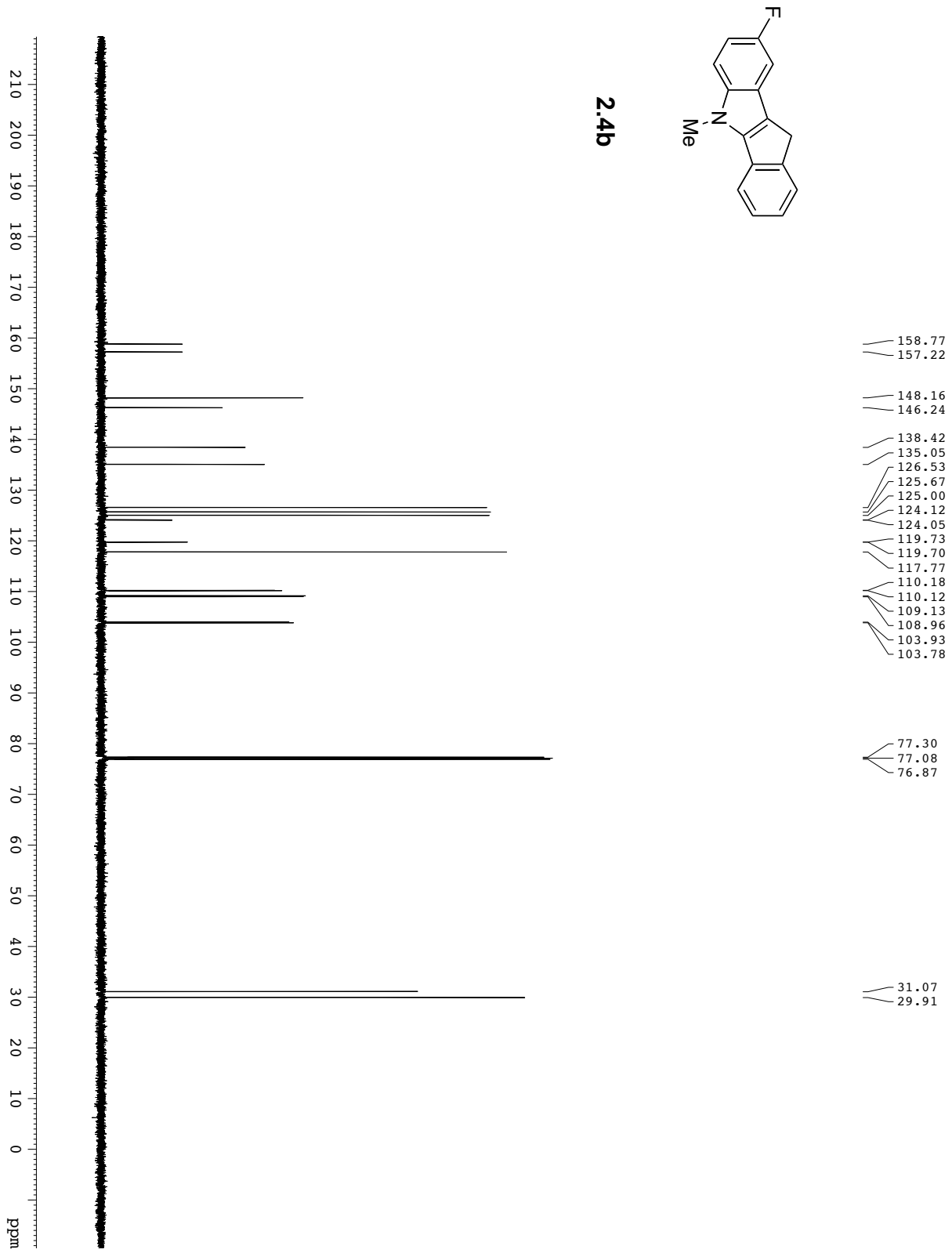

2.3
Me
N
O
F
7.620
7.607
7.482
7.479
7.469
7.467
7.457
7.454
7.423
7.413
7.410
7.399
7.387
7.374
7.364
7.355
7.350
7.347
7.341
7.338
7.333
7.260
7.174
7.169
7.160
7.155
7.145
7.141
4.127
4.115
2.856
2.743
2.625
2.046
1.592
1.271
1.259
1.251
0.882
0.946
0.998
3.721
0.967
2.996
9.5
9.0
8.5
8.0
7.5
7.0
6.5
6.0
5.5
5.0
4.5
4.0
3.5
3.0
2.5
2.0
1.5
1.0
ppm

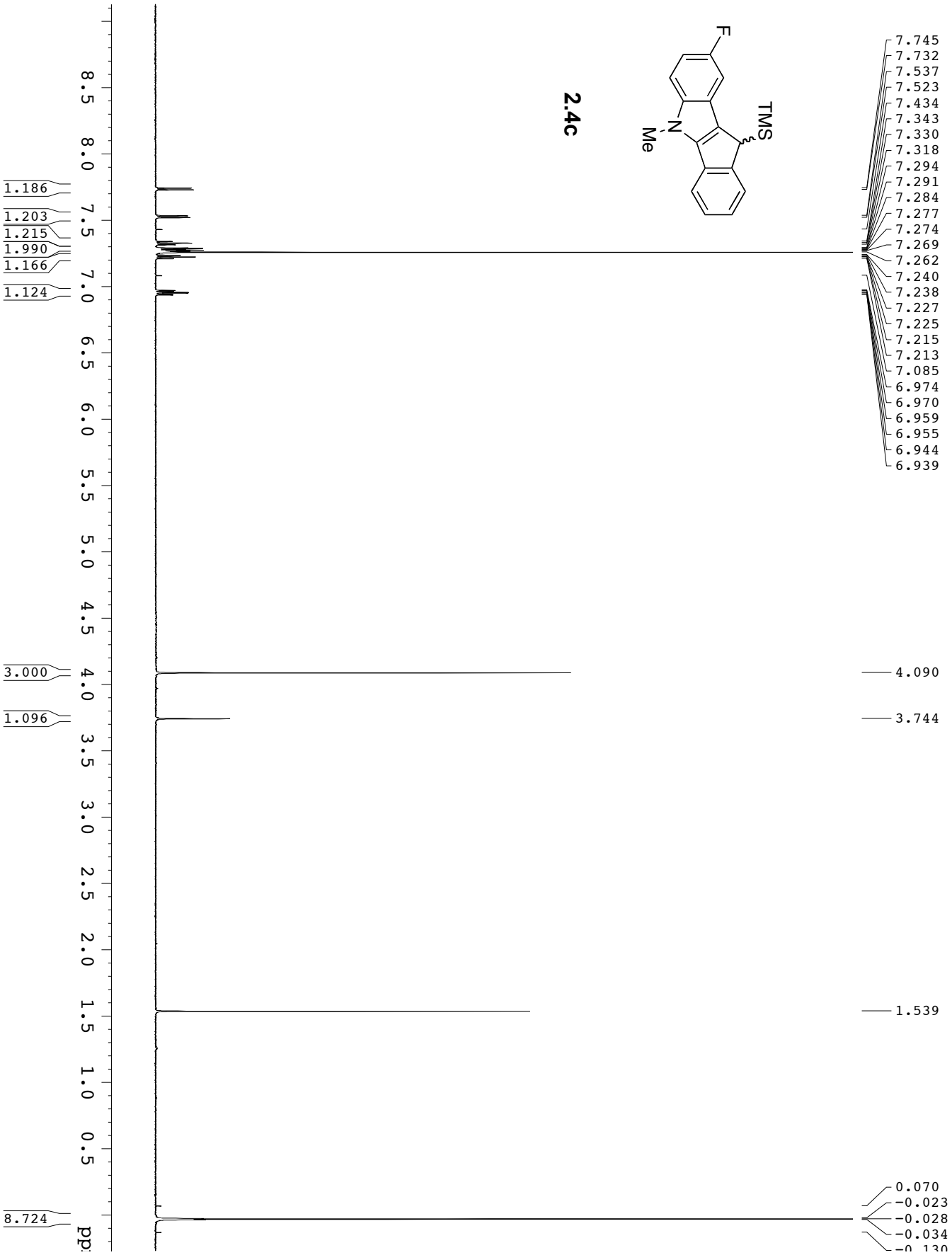

2.3
Me
N
O
F
175.04
163.25
161.57
156.33
151.07
151.02
129.83
129.29
128.20
128.17
128.14
127.39
122.11
118.27
118.25
116.53
116.38
113.83
113.67
108.67
108.10
77.17
76.96
76.75
38.59
210 200 190 180 170 160 150 140 130 120 110 100 90 80 70 60 50 40 30 20 10 0
ppm

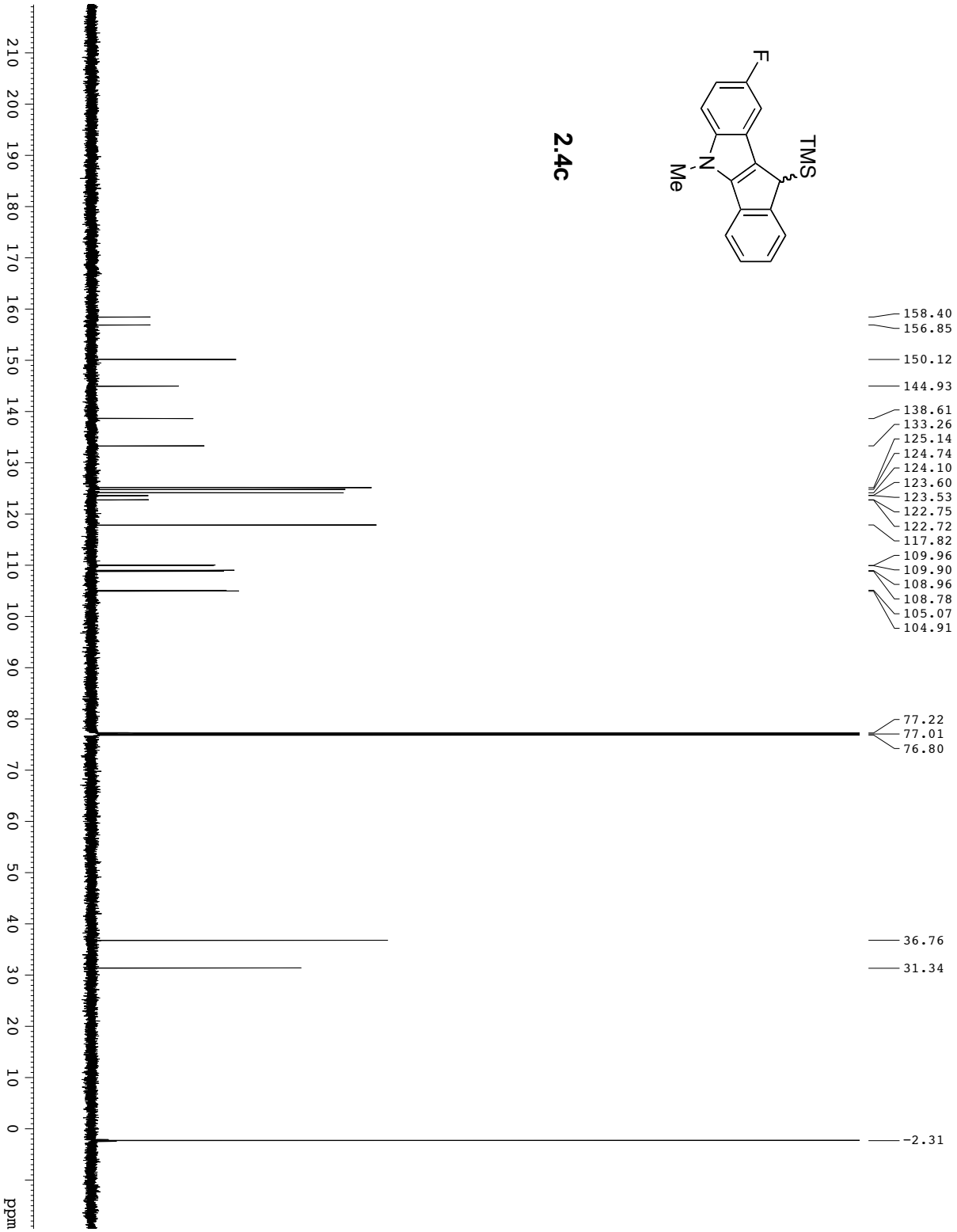

F
N
H
2.4a
8.306
7.551
7.539
7.479
7.467
7.352
7.338
7.329
7.277
7.258
7.238
7.226
6.933
6.918
6.903
3.712
0.98
1.00
1.01
2.08
0.72
1.22
1.01
2.00
9.0
8.5
8.0
7.5
7.0
6.5
6.0
5.5
5.0
4.5
4.0
3.5
3.0
2.5
2.0
1.5
1.0
0.5
ppm

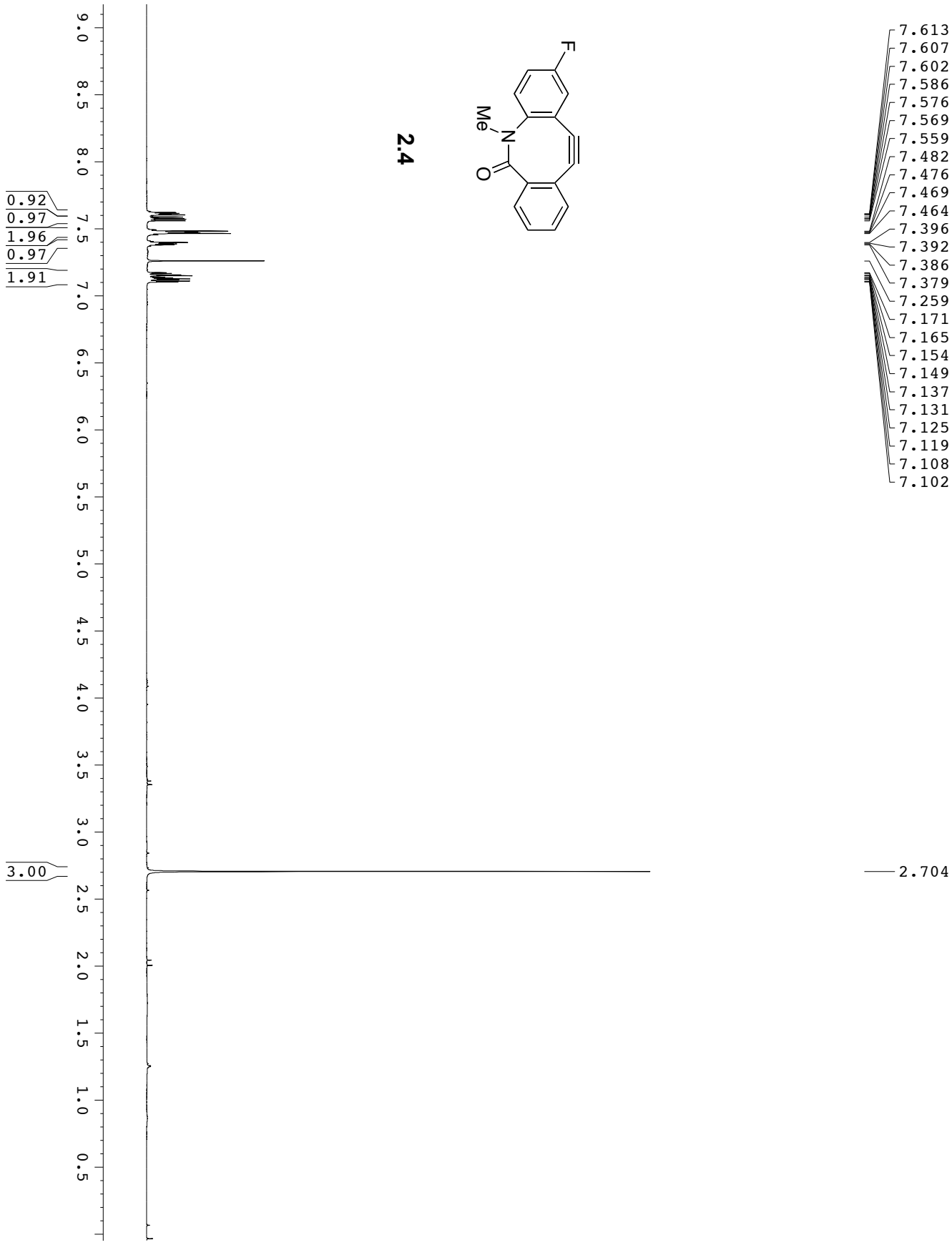

2.4a
F
N
H
158.98
157.42
147.76
145.12
137.05
134.64
126.62
125.57
125.20
125.01
124.95
121.63
121.60
117.50
112.43
112.36
109.75
109.57
104.08
103.93
77.19
76.98
76.76
30.25
210 200 190 180 170 160 150 140 130 120 110 100 90 80 70 60 50 40 30 20 10 0
ppm

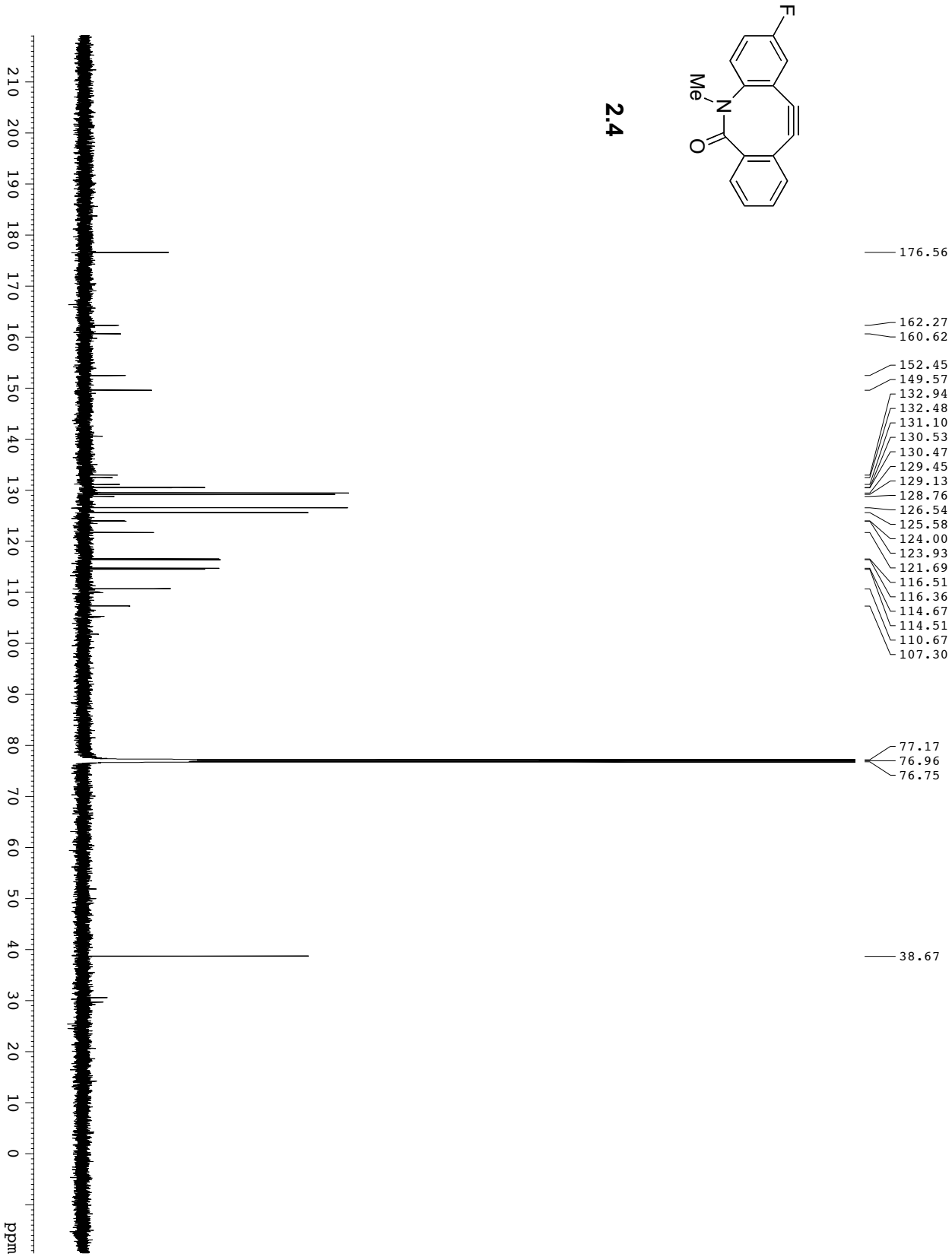

2.4b
F
N
Me
7.667
7.654
7.552
7.540
7.363
7.351
7.339
7.276
7.269
7.260
7.252
7.248
7.238
7.237
7.226
6.966
6.962
6.950
6.946
6.936
6.931
0.997
0.984
1.013
0.970
1.736
0.979
3.000
2.085
4.053
3.690
2.048
1.549
9.0
8.5
8.0
7.5
7.0
6.5
6.0
5.5
5.0
4.5
4.0
3.5
3.0
2.5
2.0
1.5
1.0
0.5
ppm

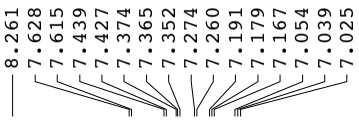

2.4b
F
N
Me
158.77
157.22
148.16
146.24
138.42
135.05
126.53
125.67
125.00
124.12
124.05
119.73
119.70
117.77
110.18
110.12
109.13
108.96
103.93
103.78
77.30
77.08
76.87
31.07
29.91
210 200 190 180 170 160 150 140 130 120 110 100 90 80 70 60 50 40 30 20 10 0
ppm

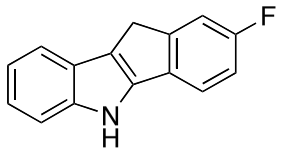

2.4c
F
N
Me
TMS
7.745
7.732
7.537
7.523
7.434
7.343
7.330
7.318
7.294
7.291
7.284
7.277
7.274
7.269
7.262
7.240
7.238
7.227
7.225
7.215
7.213
7.085
6.974
6.970
6.959
6.955
6.944
6.939
4.090
3.744
1.539
0.070
-0.023
-0.028
-0.034
1.186
1.203
1.215
1.990
1.166
1.124
3.000
1.096
8.724
8.5
8.0
7.5
7.0
6.5
6.0
5.5
5.0
4.5
4.0
3.5
3.0
2.5
2.0
1.5
1.0
0.5
ppm


2.4c
F
TMS
N
Me
158.40
156.85
150.12
144.93
138.61
133.26
125.14
124.74
124.10
123.60
123.53
122.75
122.72
117.82
109.96
109.90
108.96
108.78
105.07
104.91
77.22
77.01
76.80
36.76
31.34
-2.31
ppm

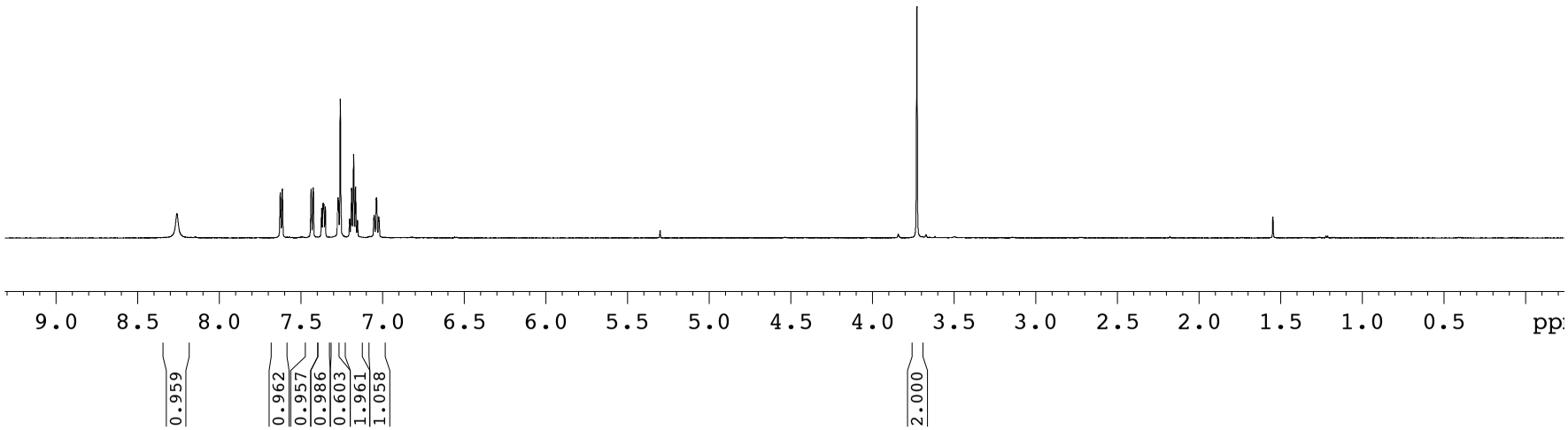

2.4
F
Me
N
O
7.613
7.607
7.602
7.586
7.576
7.569
7.559
7.482
7.476
7.469
7.464
7.396
7.392
7.386
7.379
7.259
7.171
7.165
7.154
7.149
7.137
7.131
7.125
7.119
7.108
7.102
2.704
0.92
0.97
1.96
0.97
1.91
3.00

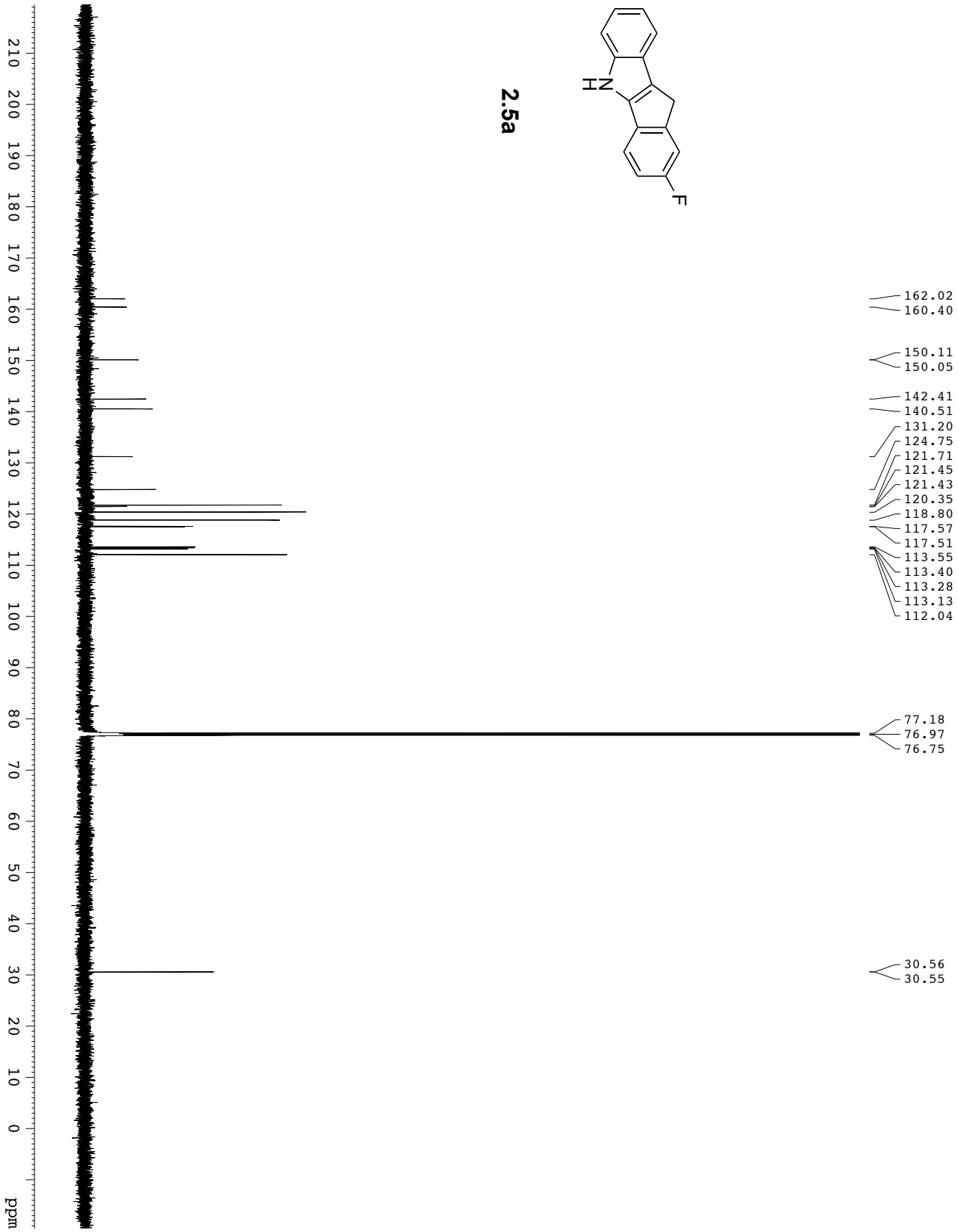

2.4
F
Me
N
O
176.56
162.27
160.62
152.45
149.57
132.94
132.48
131.10
130.53
130.47
129.45
129.13
128.76
126.54
125.58
124.00
123.93
121.69
116.51
116.36
114.67
114.51
110.67
107.30
77.17
76.96
76.75
38.67
210 200 190 180 170 160 150 140 130 120 110 100 90 80 70 60 50 40 30 20 10 0
ppm

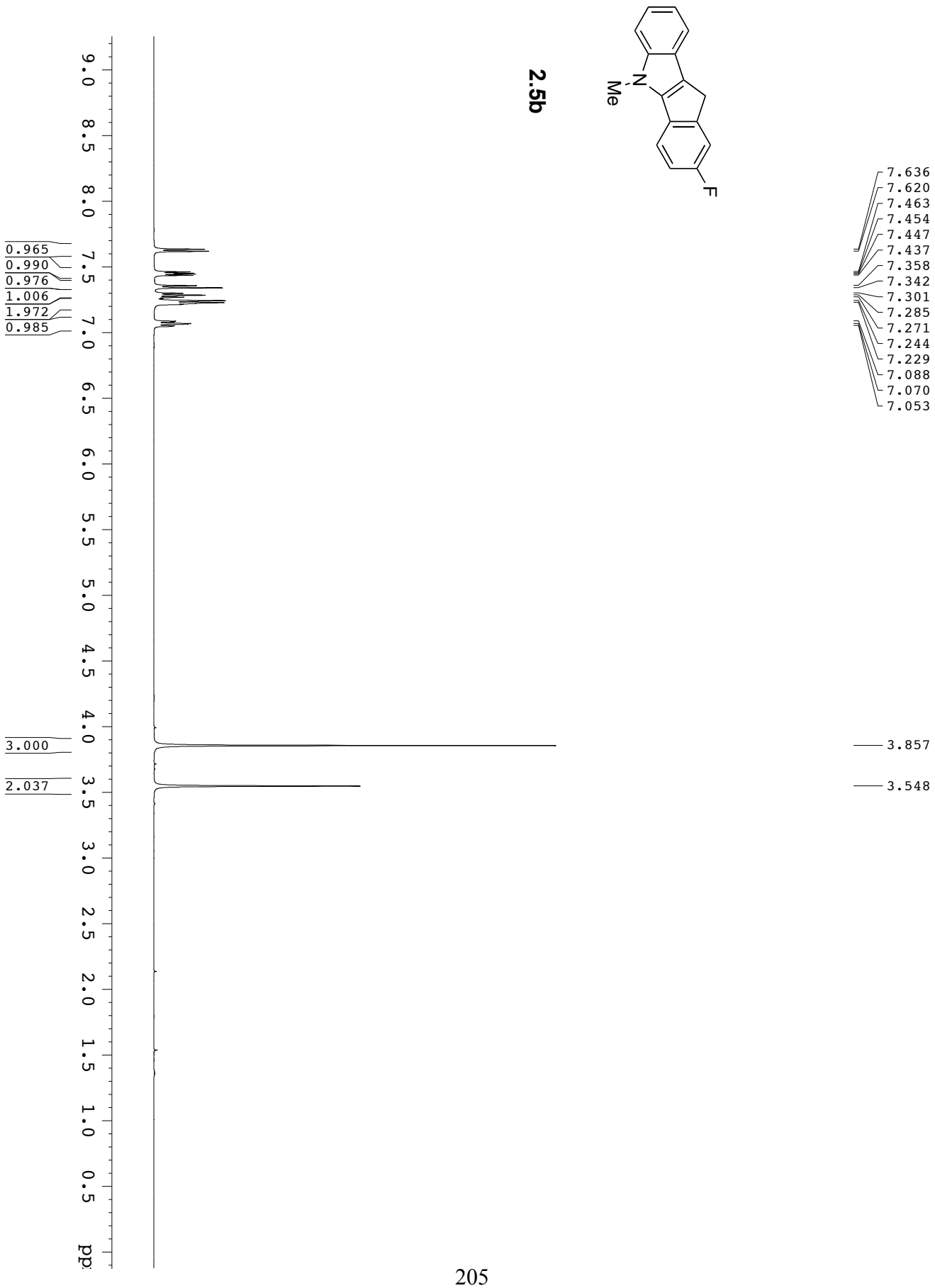

8.261
7.628
7.615
7.439
7.427
7.374
7.365
7.352
7.274
7.260
7.191
7.179
7.167
7.054
7.039
7.025
3.729

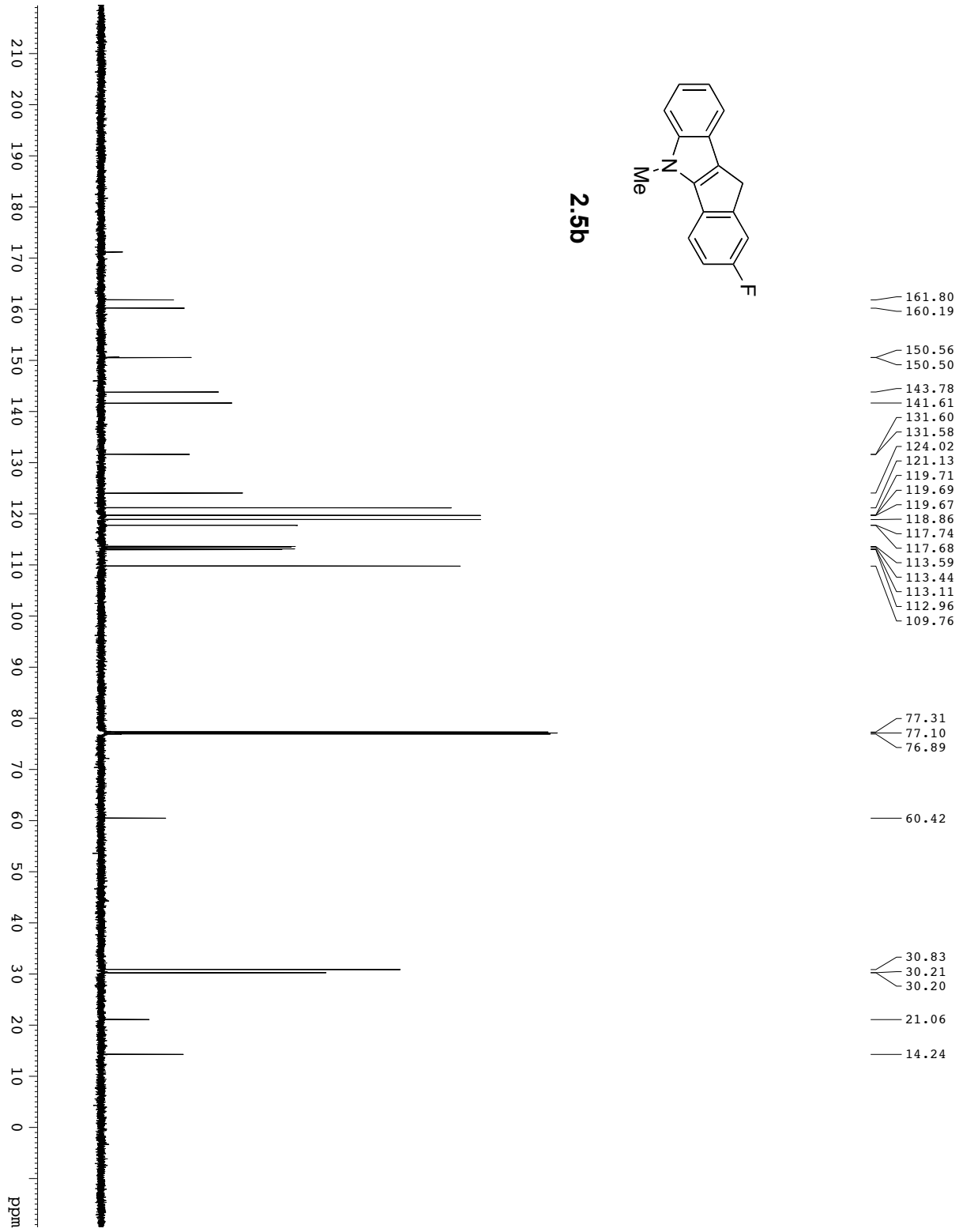

F
N
H

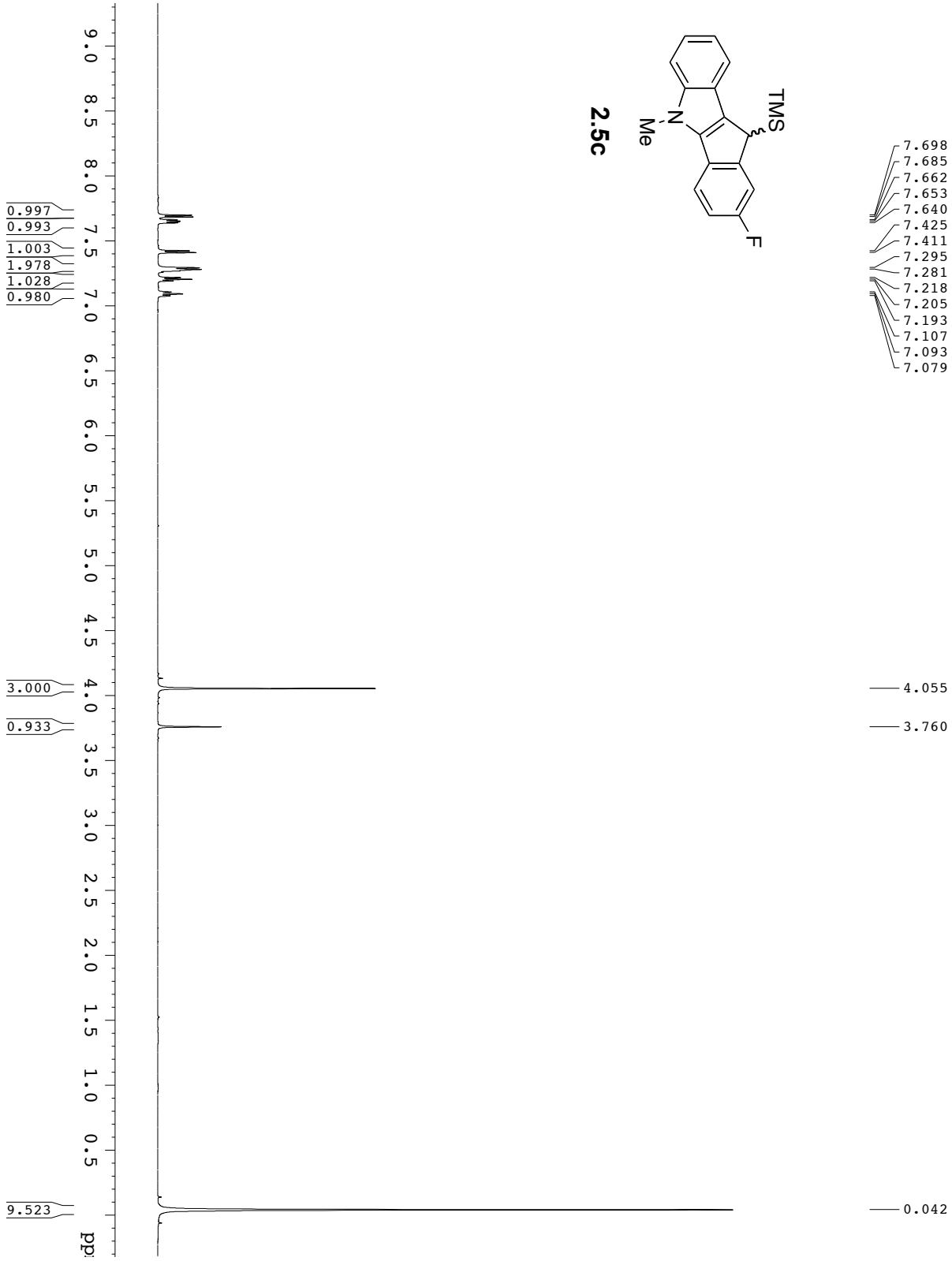
2.5a

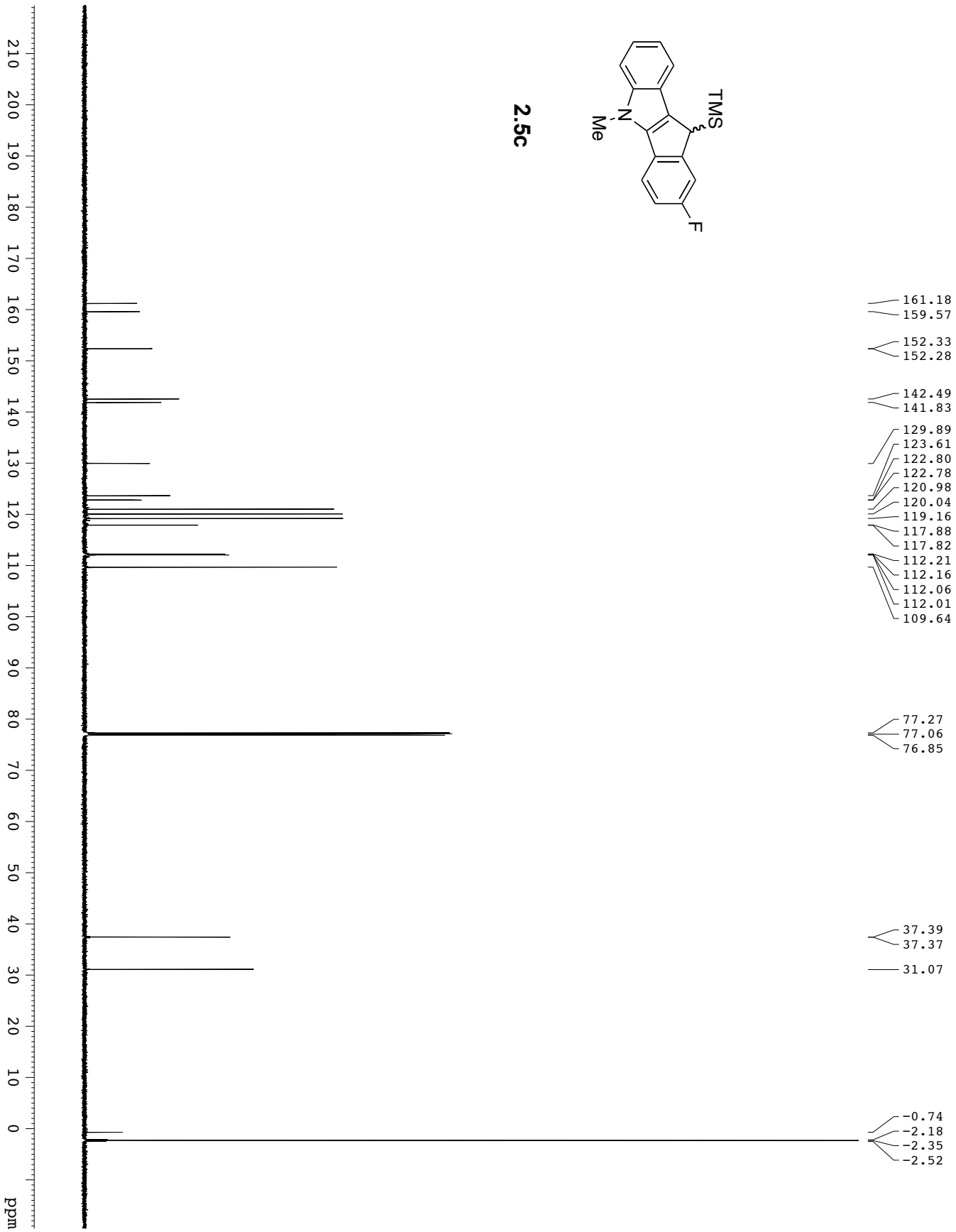

9.0
8.5
8.0
7.5
7.0
6.5
6.0
5.5
5.0
4.5
4.0
3.5
3.0
2.5
2.0
1.5
1.0
0.5
0.959
0.962
0.957
0.986
0.603
1.961
1.058
2.000

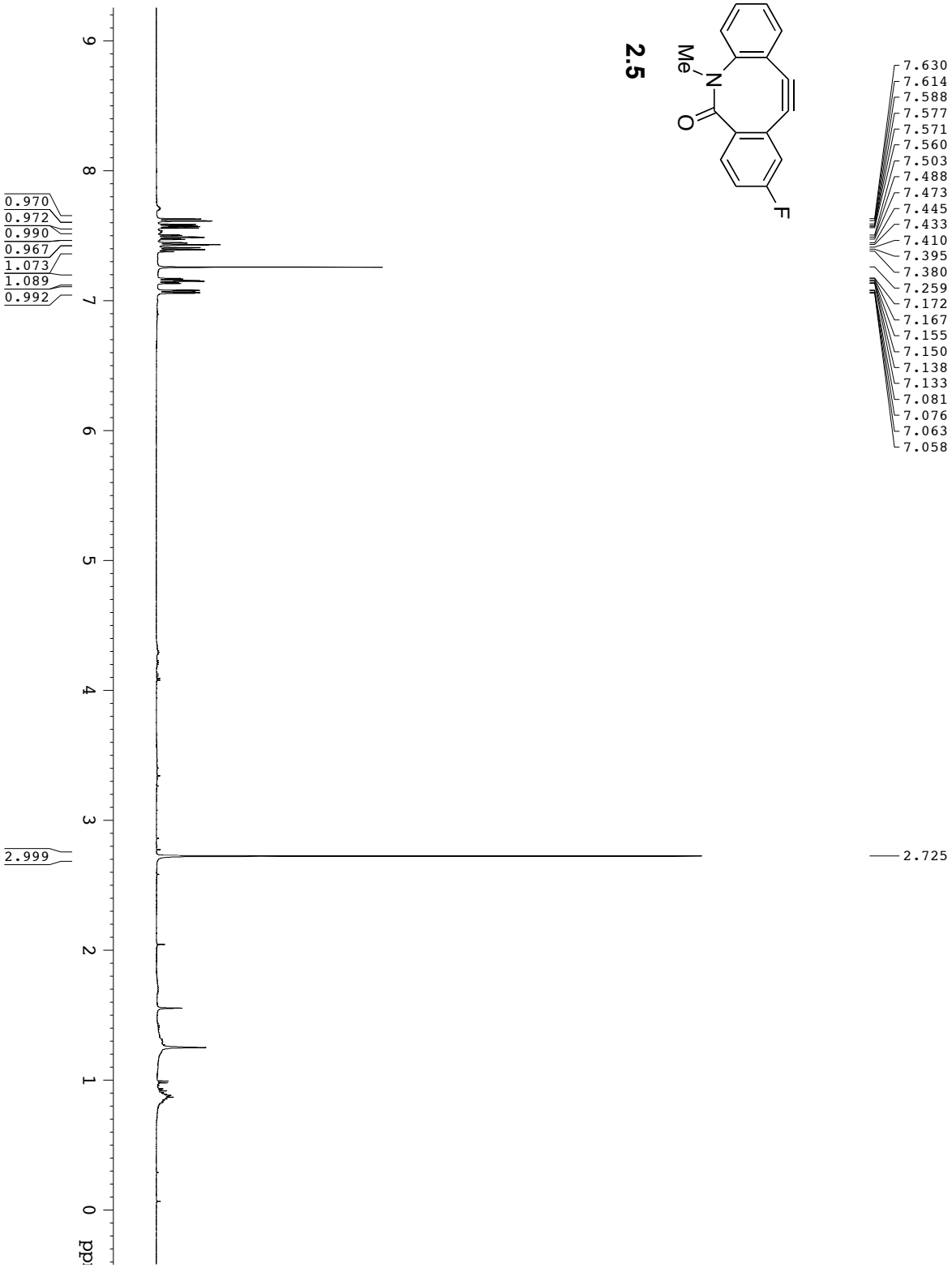

2.5a
F
162.02
160.40
150.11
150.05
142.41
140.51
131.20
124.75
121.71
121.45
121.43
120.35
118.80
117.57
117.51
113.55
113.40
113.28
113.13
112.04
77.18
76.97
76.75
30.56
30.55
ppm

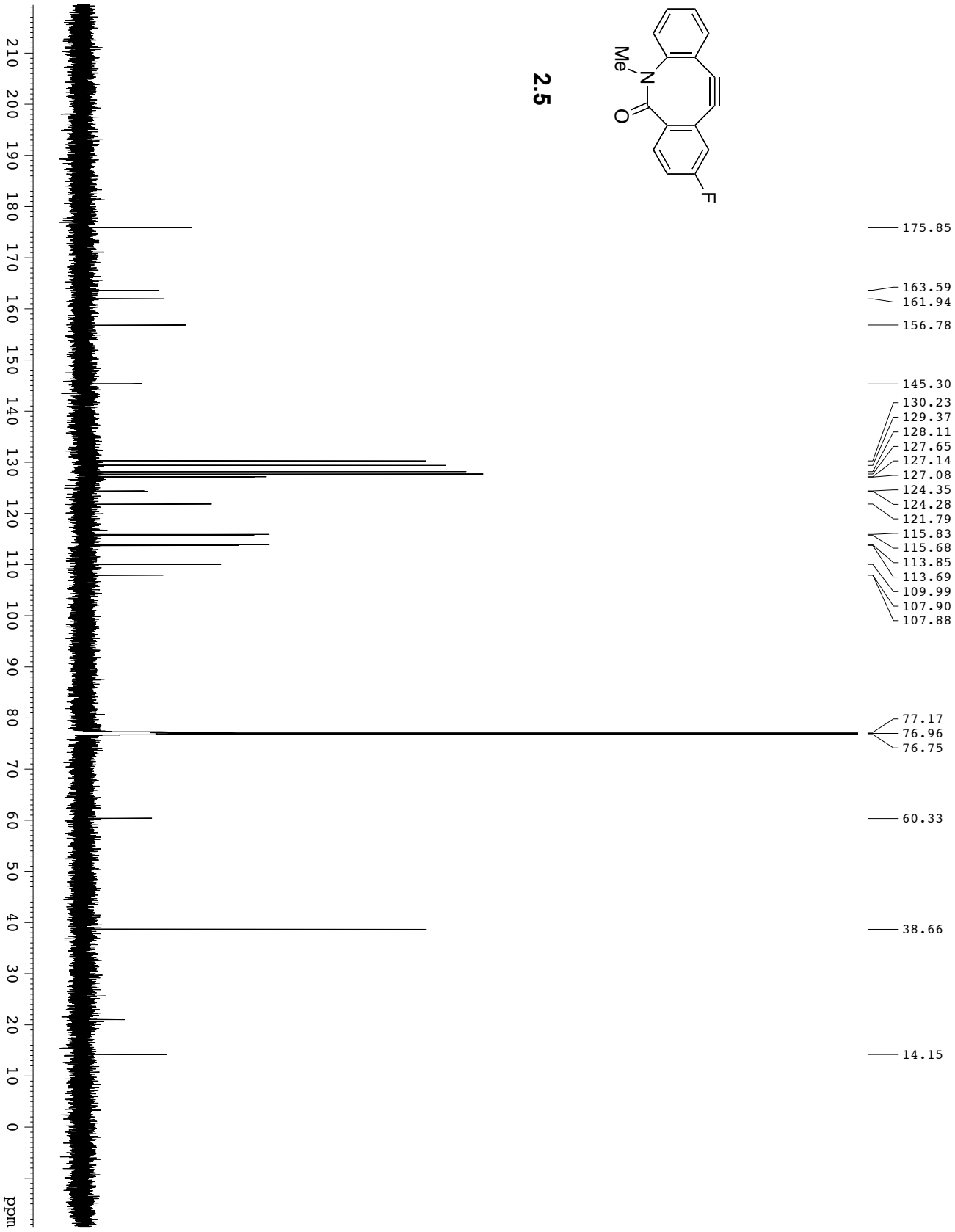

2.5b
N
Me
F
7.636
7.620
7.463
7.454
7.447
7.437
7.358
7.342
7.301
7.285
7.271
7.244
7.229
7.088
7.070
7.053
3.857
3.548
0.965
0.990
0.976
1.006
1.972
0.985
3.000
2.037
9.0
8.5
8.0
7.5
7.0
6.5
6.0
5.5
5.0
4.5
4.0
3.5
3.0
2.5
2.0
1.5
1.0
0.5
pp

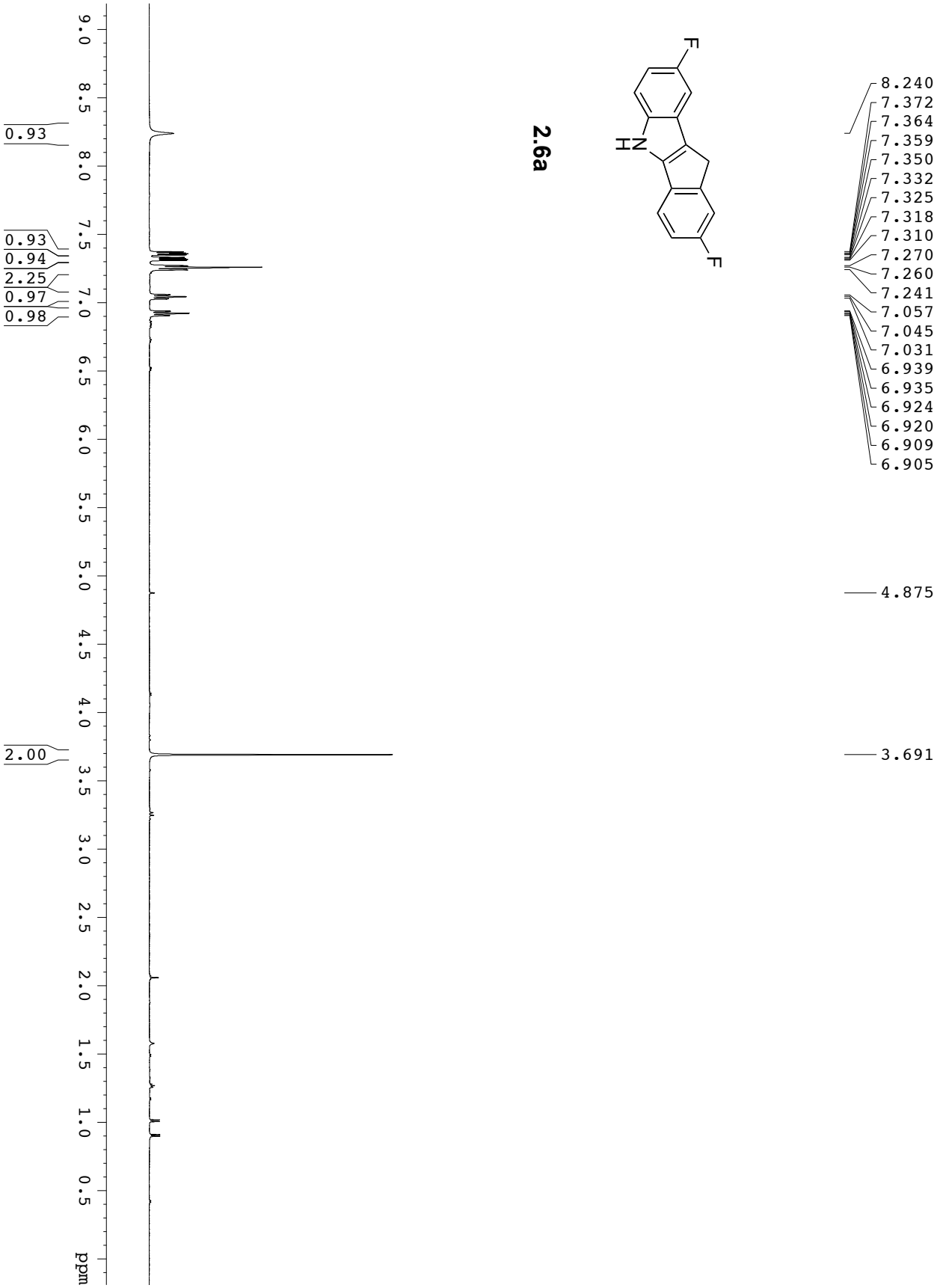

2.5b
N
Me
F
161.80
160.19
150.56
150.50
143.78
141.61
131.60
131.58
124.02
121.13
119.71
119.69
119.67
118.86
117.74
117.68
113.59
113.44
113.11
112.96
109.76
77.31
77.10
76.89
60.42
30.83
30.21
30.20
21.06
14.24
ppm

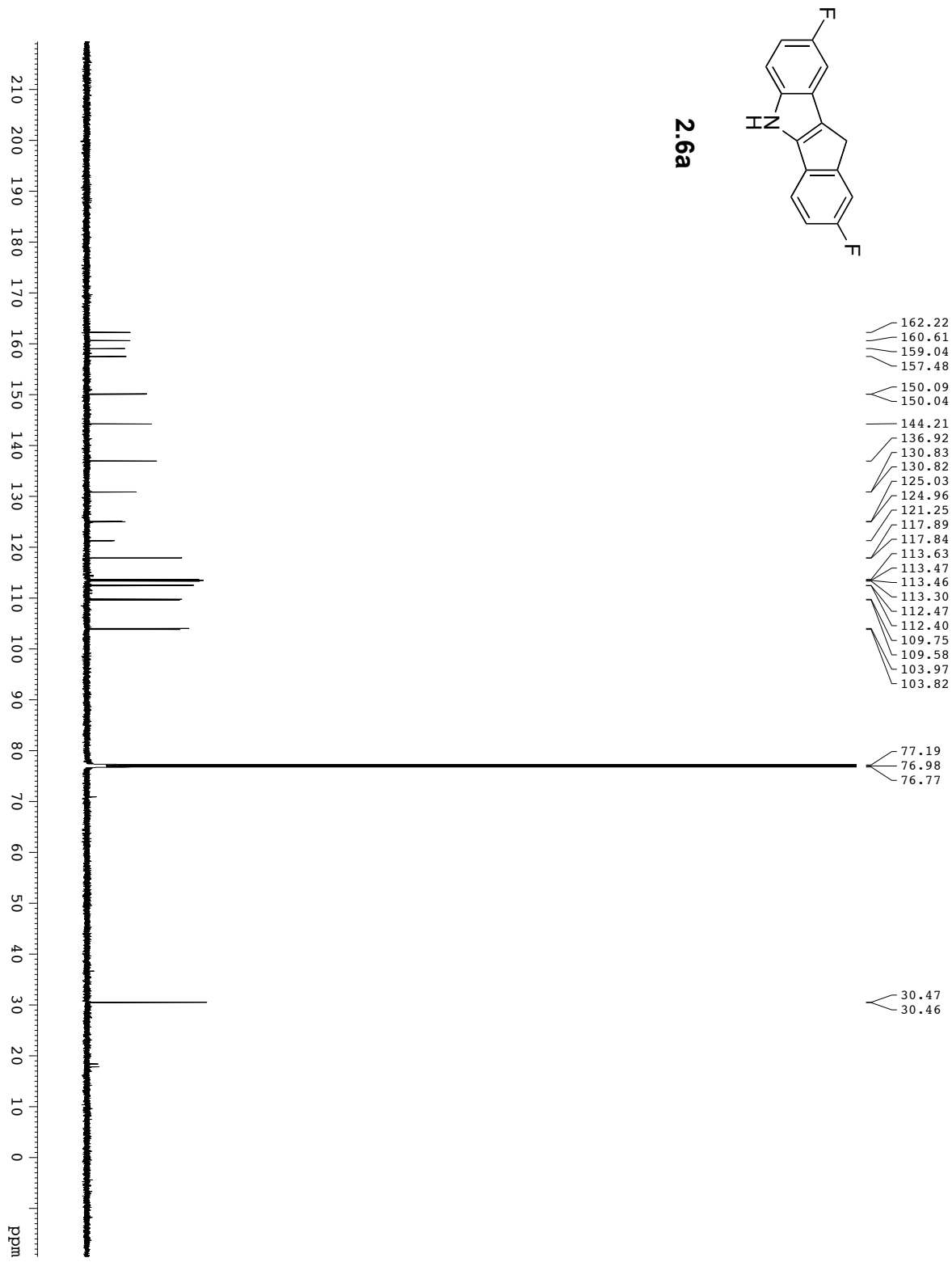

2.5c
TMS
N
Me
F
7.698
7.685
7.662
7.653
7.640
7.425
7.411
7.295
7.281
7.218
7.205
7.193
7.107
7.093
7.079
4.055
3.760
0.042
0.997
0.993
1.003
1.978
1.028
0.980
3.000
0.933
9.523
9.0
8.5
8.0
7.5
7.0
6.5
6.0
5.5
5.0
4.5
4.0
3.5
3.0
2.5
2.0
1.5
1.0
0.5
ppm

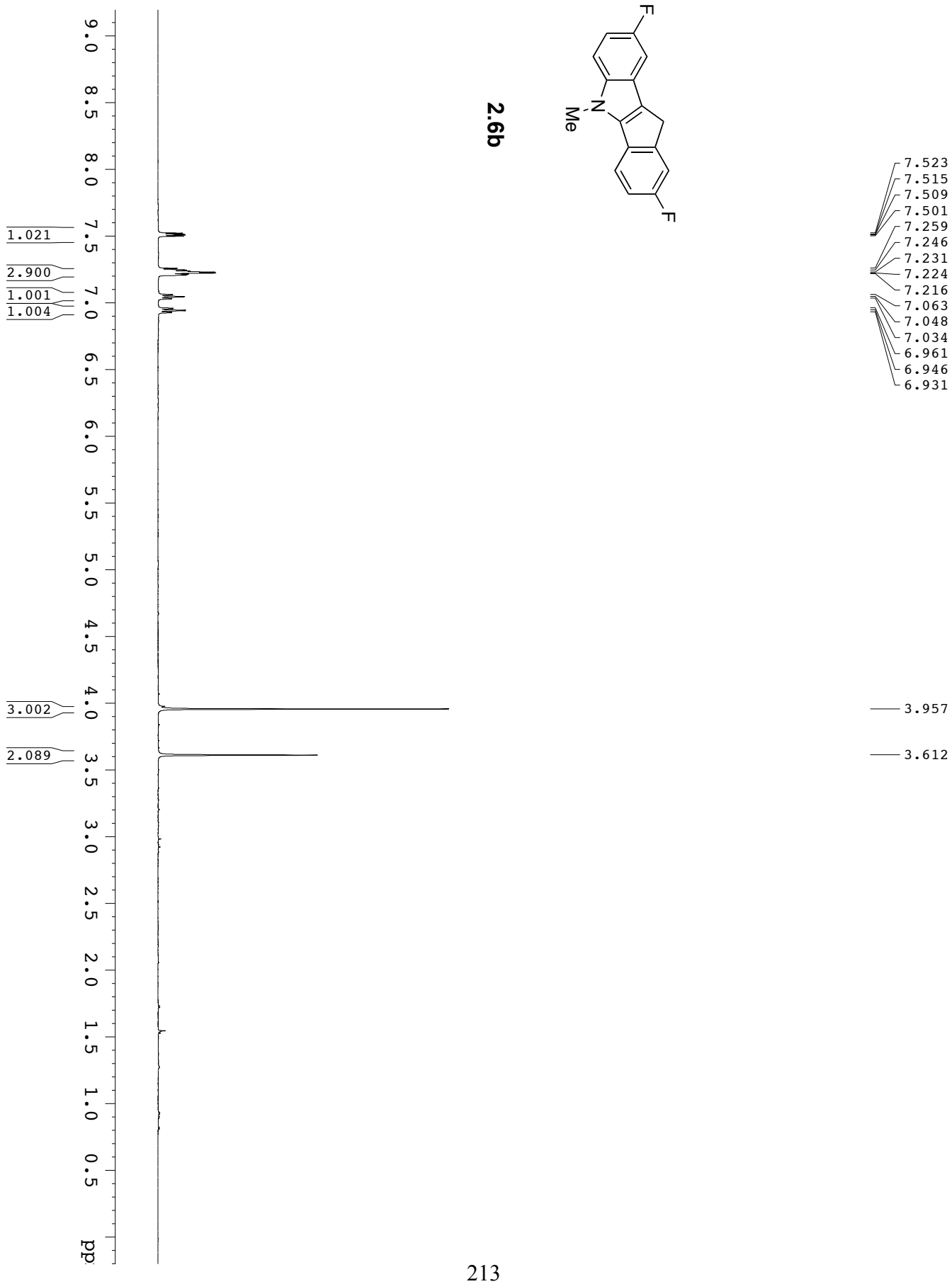

2.5c
TMS
N
Me
F
161.18
159.57
152.33
152.28
142.49
141.83
129.89
123.61
122.80
122.78
120.98
120.04
119.16
117.88
117.82
112.21
112.16
112.06
112.01
109.64
77.27
77.06
76.85
37.39
37.37
31.07
-0.74
-2.18
-2.35
-2.52
ppm

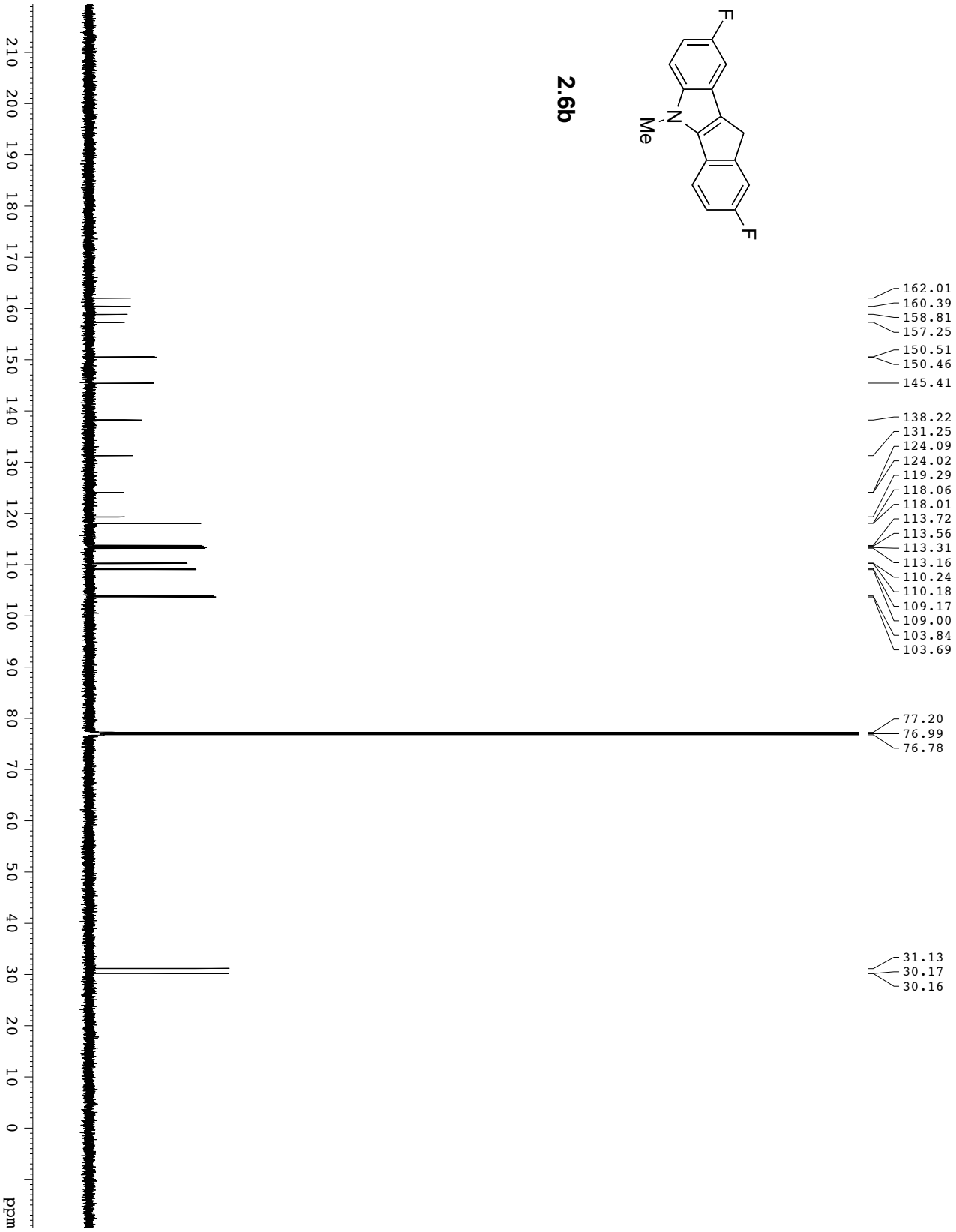

2.5
Me
N
O
F
7.630
7.614
7.588
7.577
7.571
7.560
7.503
7.488
7.473
7.445
7.433
7.410
7.395
7.380
7.259
7.172
7.167
7.155
7.150
7.138
7.133
7.081
7.076
7.063
7.058
2.725
0.970
0.972
0.990
0.967
1.073
1.089
0.992
2.999
9
8
7
6
5
4
3
2
1
0
ppm

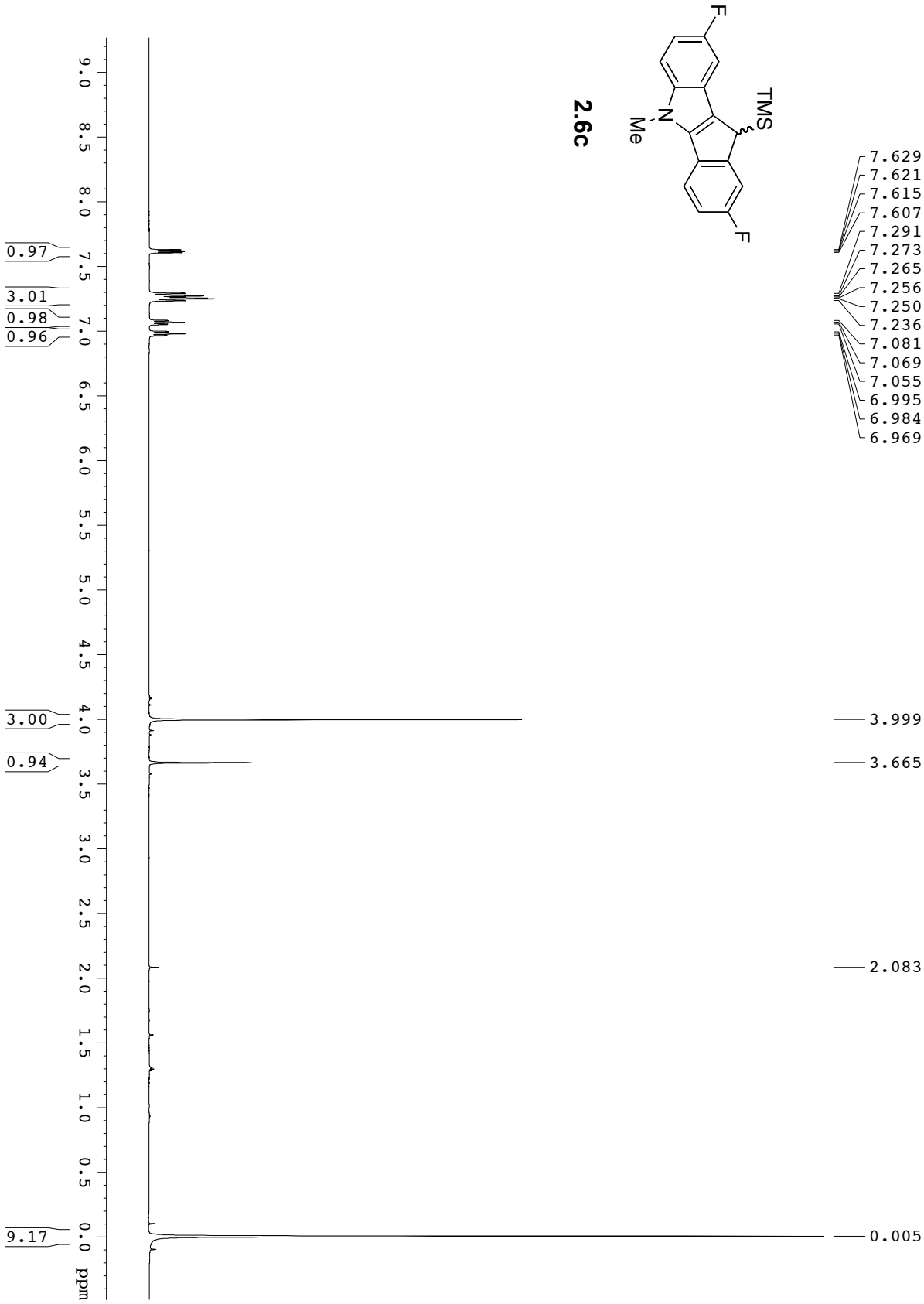

2.5
Me
N
O
F
175.85
163.59
161.94
156.78
145.30
130.23
129.37
128.11
127.65
127.14
127.08
124.35
124.28
121.79
115.83
115.68
113.85
113.69
109.99
107.90
107.88
77.17
76.96
76.75
60.33
38.66
14.15
210 200 190 180 170 160 150 140 130 120 110 100 90 80 70 60 50 40 30 20 10 0
ppm

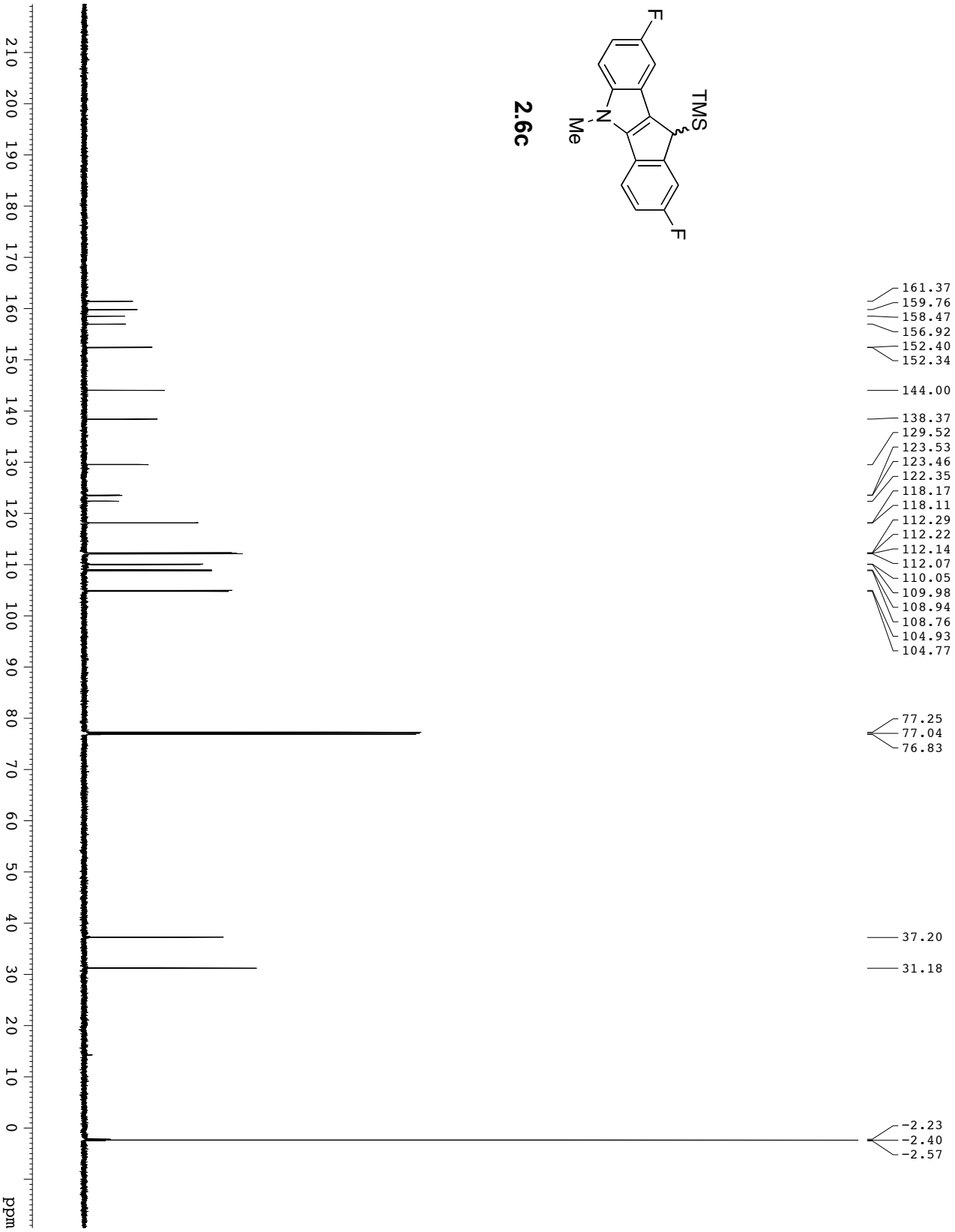

2.6a
F
N
H
F
8.240
7.372
7.364
7.359
7.350
7.332
7.325
7.318
7.310
7.270
7.260
7.241
7.057
7.045
7.031
6.939
6.935
6.924
6.920
6.909
6.905
4.875
3.691
0.93
0.93
0.94
2.25
0.97
0.98
2.00
9.0
8.5
8.0
7.5
7.0
6.5
6.0
5.5
5.0
4.5
4.0
3.5
3.0
2.5
2.0
1.5
1.0
0.5
ppm

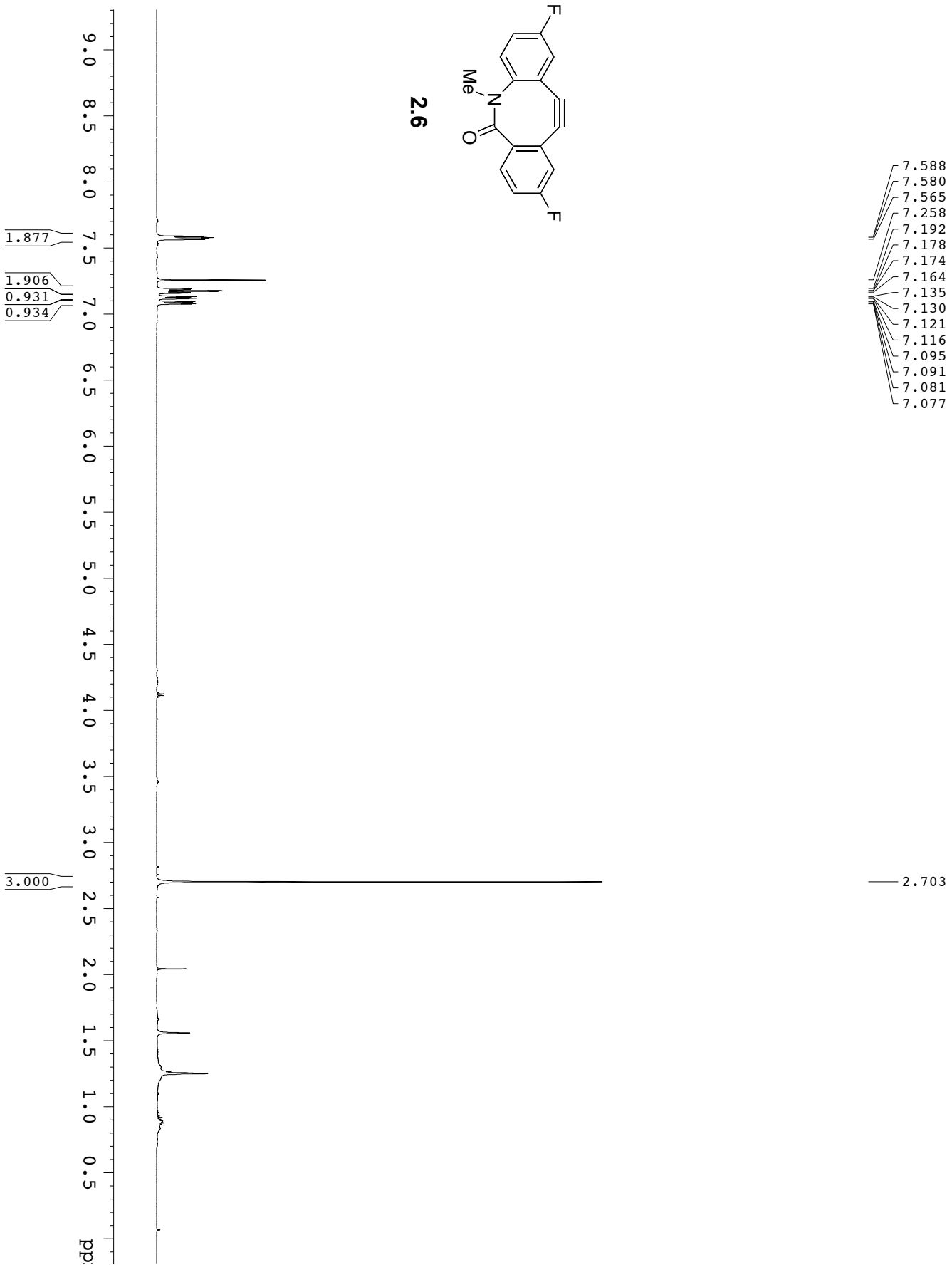

F
N
H
F
2.6a
162.22
160.61
159.04
157.48
150.09
150.04
144.21
136.92
130.83
130.82
125.03
124.96
121.25
117.89
117.84
113.63
113.47
113.46
113.30
112.47
112.40
109.75
109.58
103.97
103.82
77.19
76.98
76.77
30.47
30.46
210 200 190 180 170 160 150 140 130 120 110 100 90 80 70 60 50 40 30 20 10 0
ppm

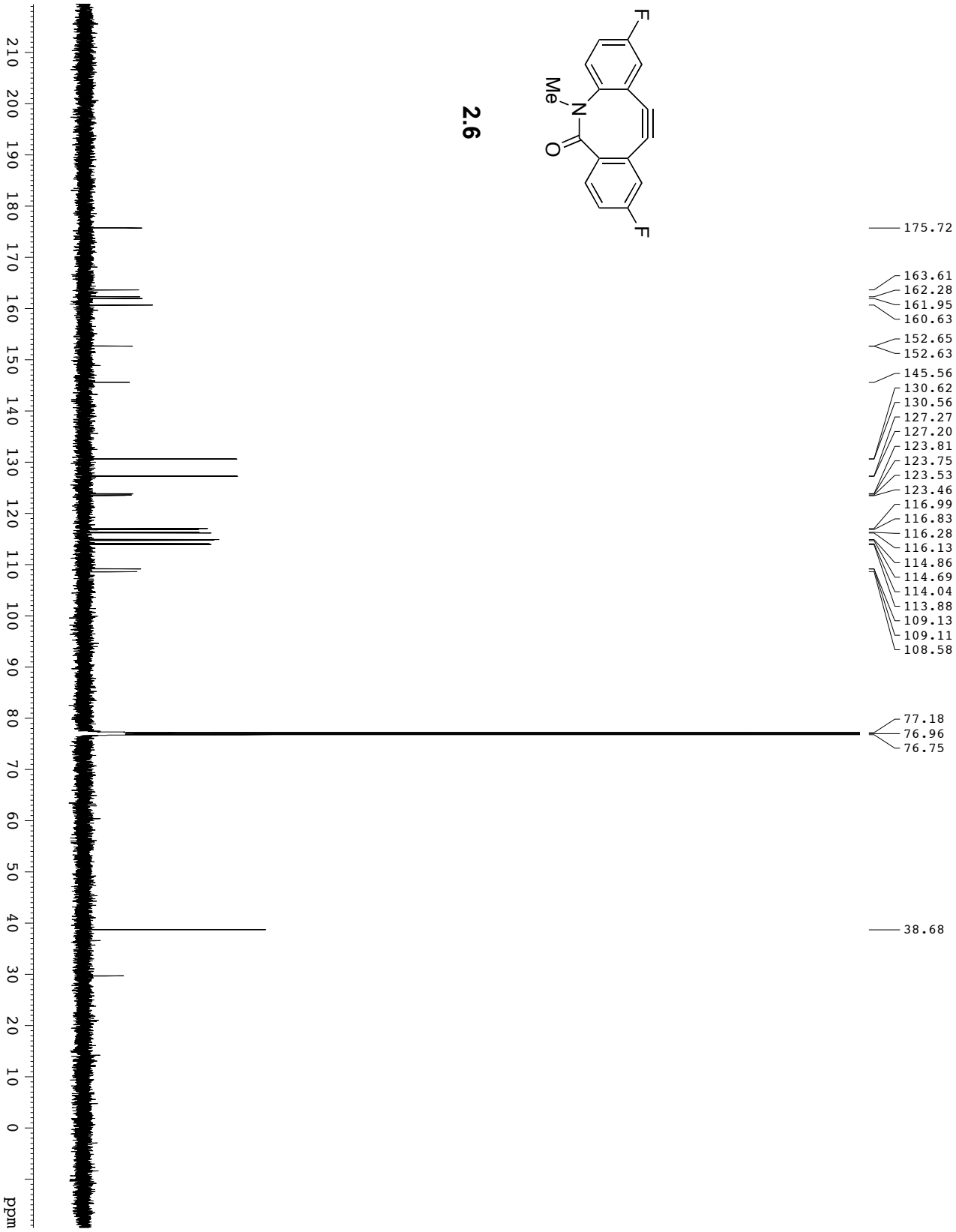

2.6b
F
N
Me
F
7.523
7.515
7.509
7.501
7.259
7.246
7.231
7.224
7.216
7.063
7.048
7.034
6.961
6.946
6.931
3.957
3.612
1.021
2.900
1.001
1.004
3.002
2.089
9.0
8.5
8.0
7.5
7.0
6.5
6.0
5.5
5.0
4.5
4.0
3.5
3.0
2.5
2.0
1.5
1.0
0.5
pp

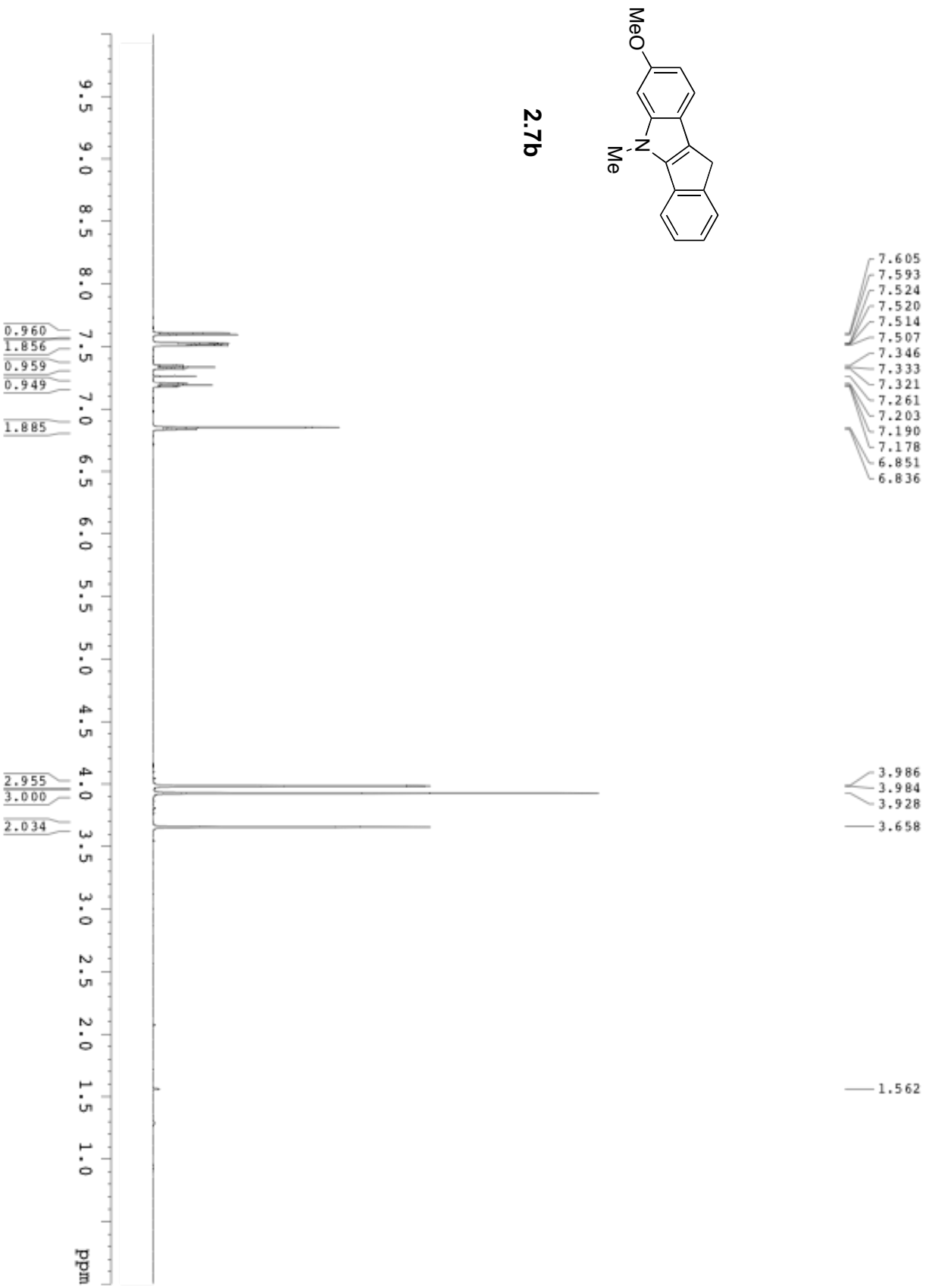

2.6b
F
N
Me
F
162.01
160.39
158.81
157.25
150.51
150.46
145.41
138.22
131.25
124.09
124.02
119.29
118.06
118.01
113.72
113.56
113.31
113.16
110.24
110.18
109.17
109.00
103.84
103.69
77.20
76.99
76.78
31.13
30.17
30.16
210
200
190
180
170
160
150
140
130
120
110
100
90
80
70
60
50
40
30
20
10
0
ppm


2.6c
F
TMS
N
Me
F
7.629
7.621
7.615
7.607
7.291
7.273
7.265
7.256
7.250
7.236
7.081
7.069
7.055
6.995
6.984
6.969
3.999
3.665
2.083
0.005
0.97
3.01
0.98
0.96
3.00
0.94
9.17
ppm

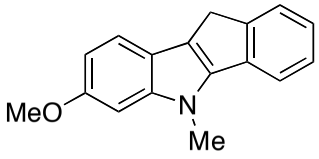

F
TMS
N
Me
F
2.6c
161.37
159.76
158.47
156.92
152.40
152.34
144.00
138.37
129.52
123.53
123.46
122.35
118.17
118.11
112.29
112.22
112.14
112.07
110.05
109.98
108.94
108.76
104.93
104.77
77.25
77.04
76.83
37.20
31.18
-2.23
-2.40
-2.57
210 200 190 180 170 160 150 140 130 120 110 100 90 80 70 60 50 40 30 20 10 0
ppm


F
Me
N
O
F
2.6
7.588
7.580
7.565
7.258
7.192
7.178
7.174
7.164
7.135
7.130
7.121
7.116
7.095
7.091
7.081
7.077
1.877
1.906
0.931
0.934
3.000
2.703
9.0
8.5
8.0
7.5
7.0
6.5
6.0
5.5
5.0
4.5
4.0
3.5
3.0
2.5
2.0
1.5
1.0
0.5
ppm

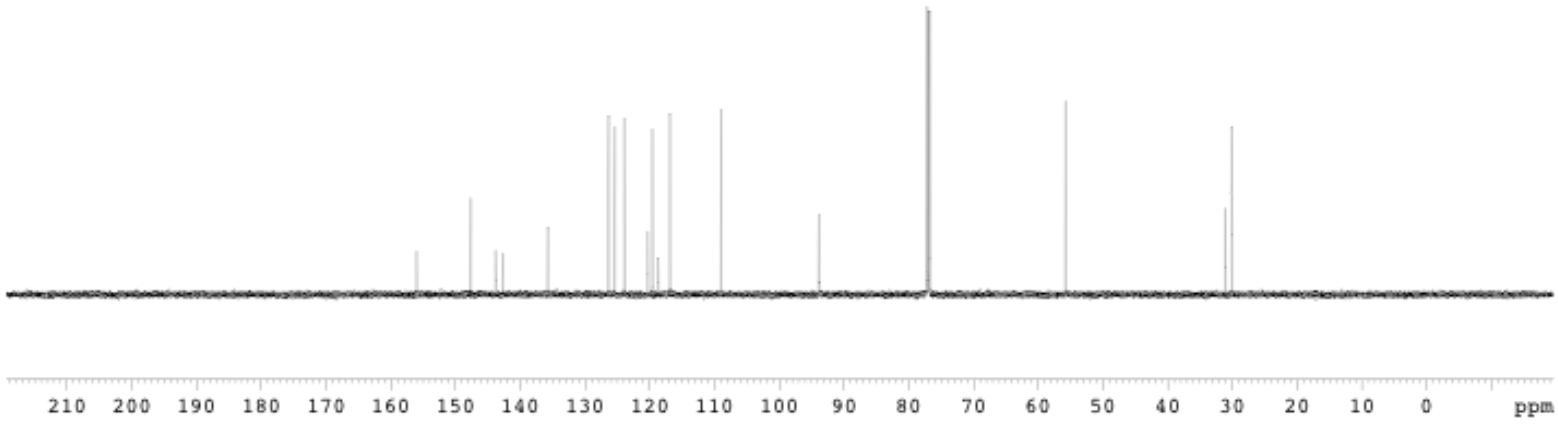

2.6
F
Me
N
O
F
175.72
163.61
162.28
161.95
160.63
152.65
152.63
145.56
130.62
130.56
127.27
127.20
123.81
123.75
123.53
123.46
116.99
116.83
116.28
116.13
114.86
114.69
114.04
113.88
109.13
109.11
108.58
77.18
76.96
76.75
38.68
210 200 190 180 170 160 150 140 130 120 110 100 90 80 70 60 50 40 30 20 10 0
ppm

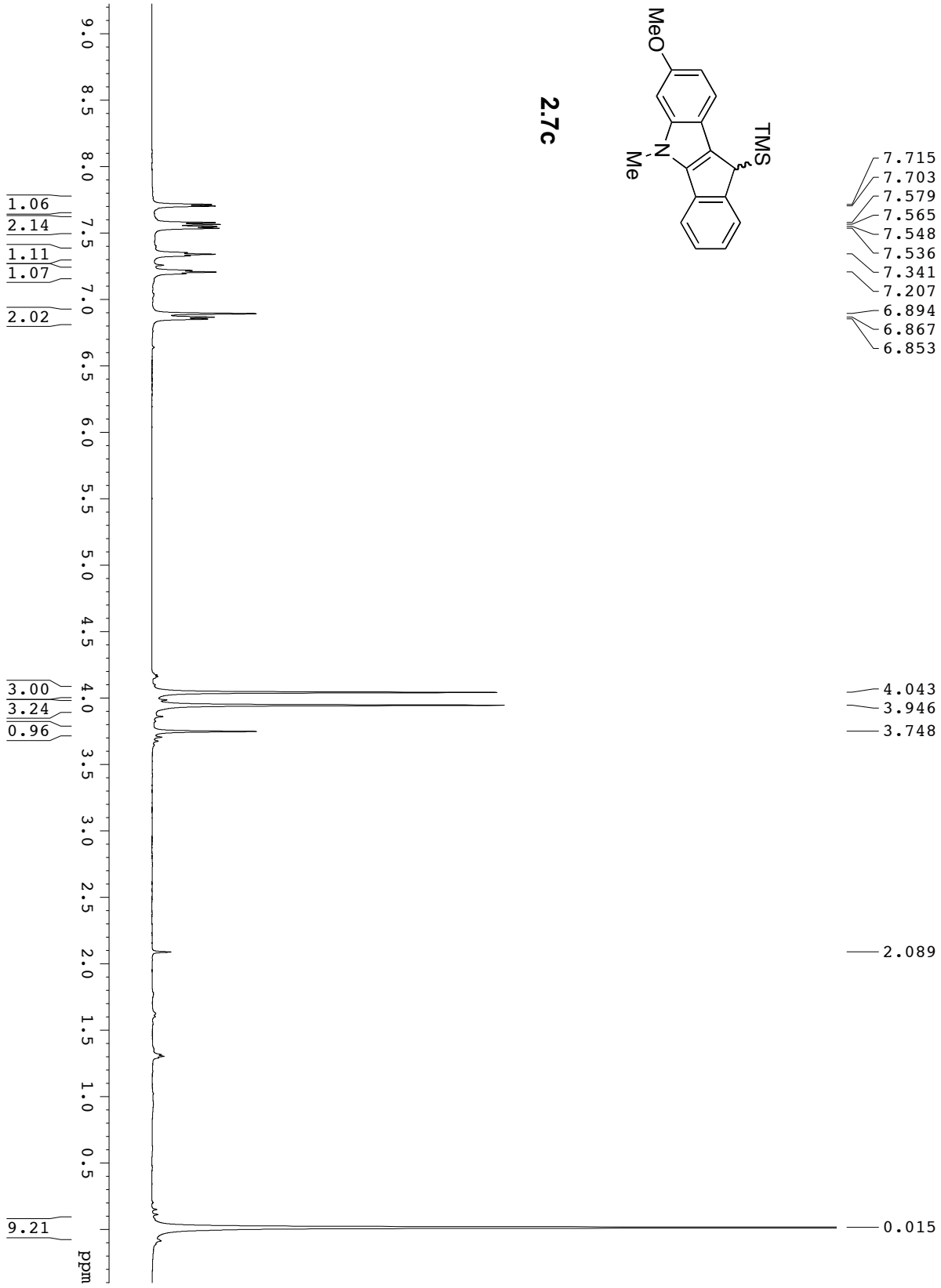

2.7b
MeO
N
Me
7.605
7.593
7.524
7.520
7.514
7.507
7.346
7.333
7.321
7.261
7.203
7.190
7.178
6.851
6.836
3.986
3.984
3.928
3.658
1.562
0.960
1.856
0.959
0.949
1.885
2.955
3.000
2.034
ppm

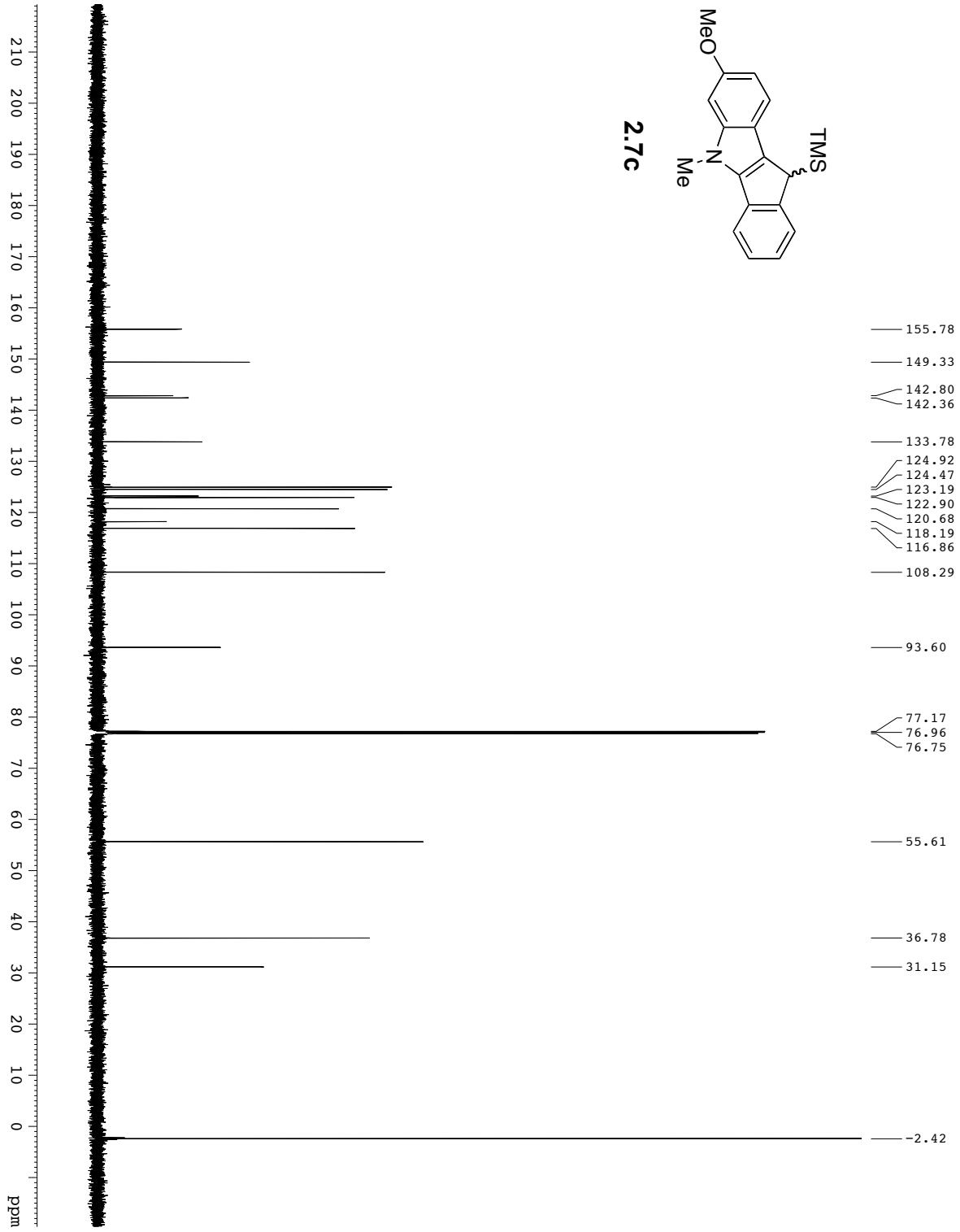
155.99
147.63
143.76
142.65
135.71
126.35
125.40
123.89
120.29
119.56
118.69
116.86
108.93
93.83
77.16
76.95
76.74
55.71
31.07
30.05

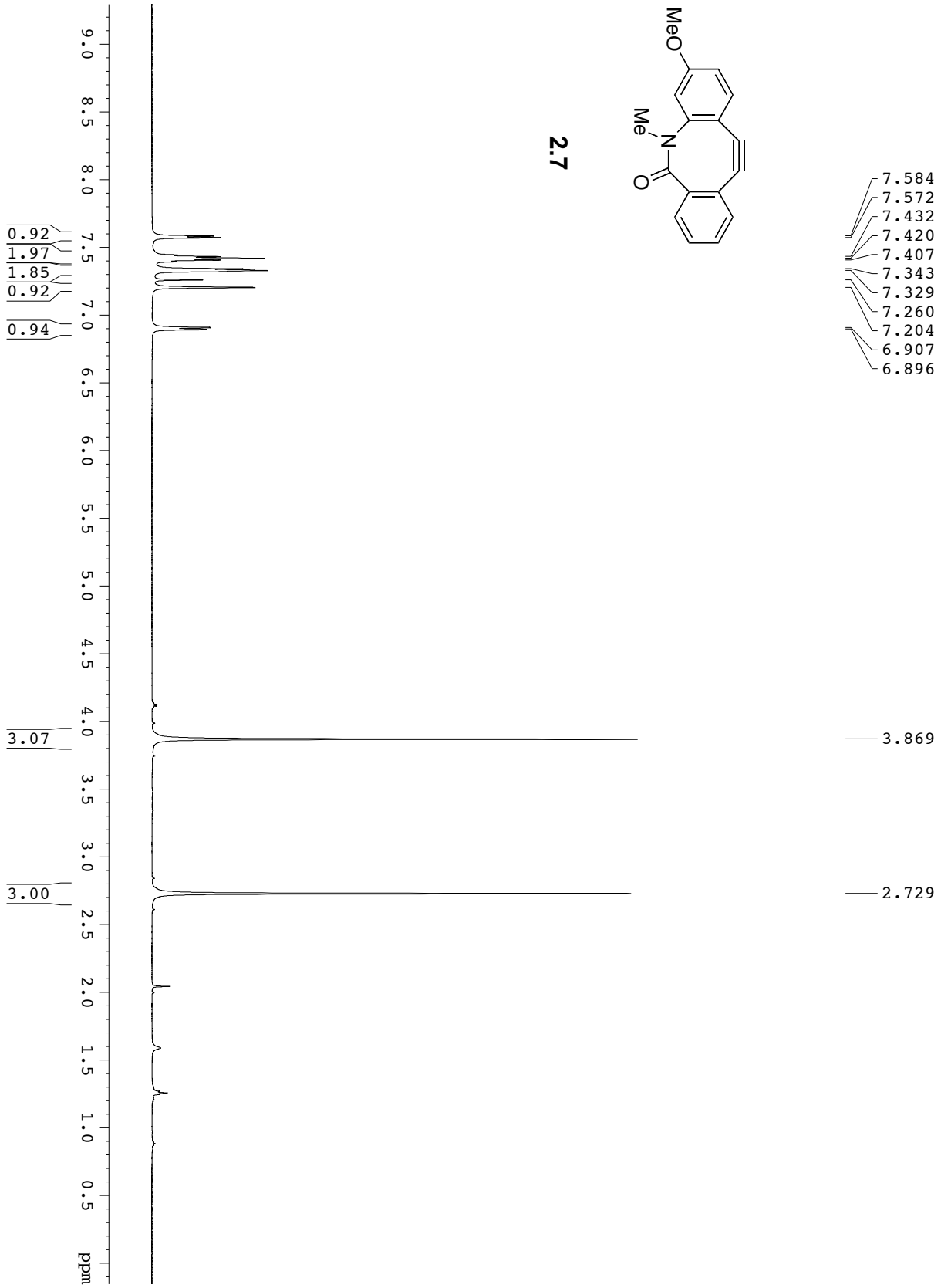


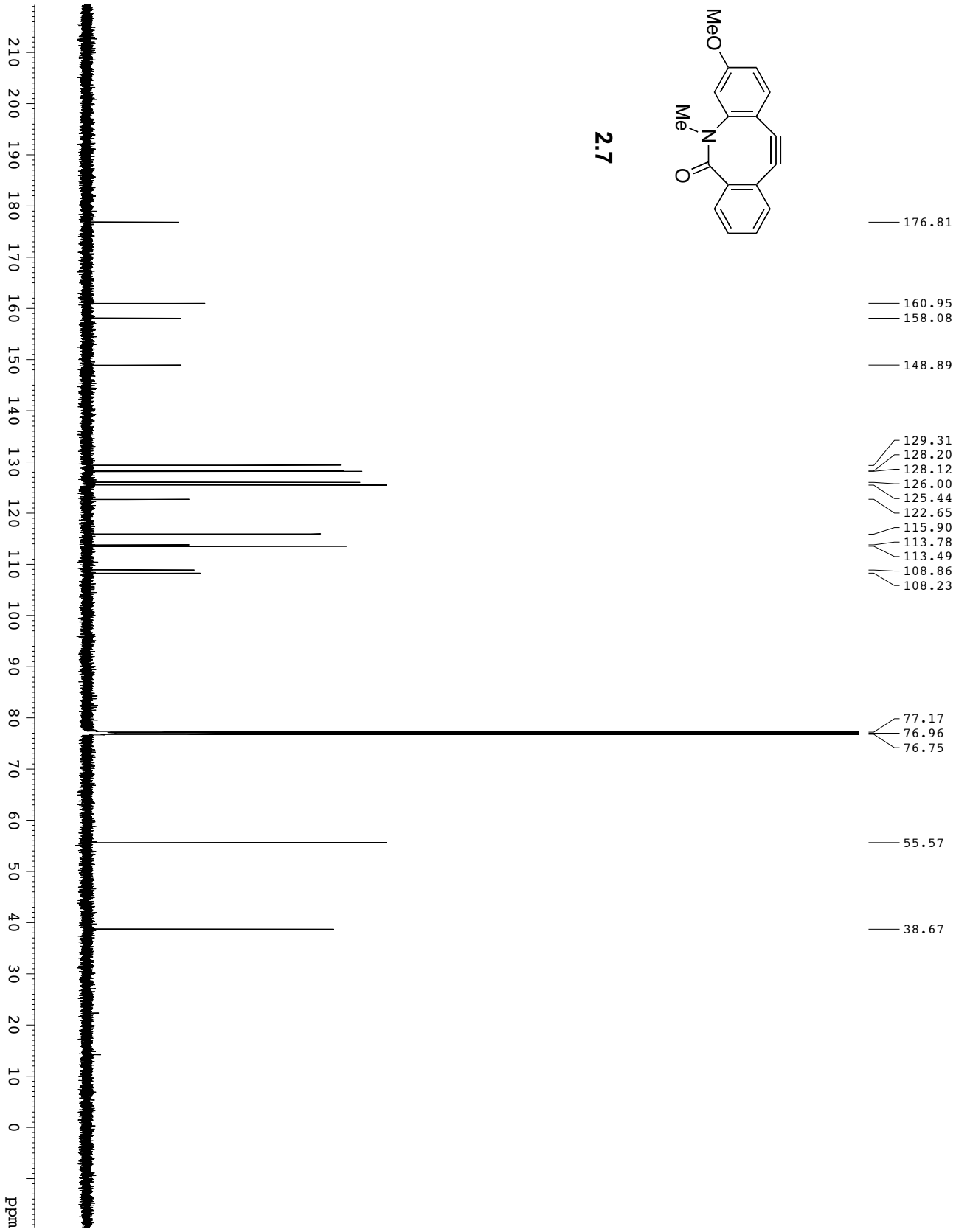
2.7b

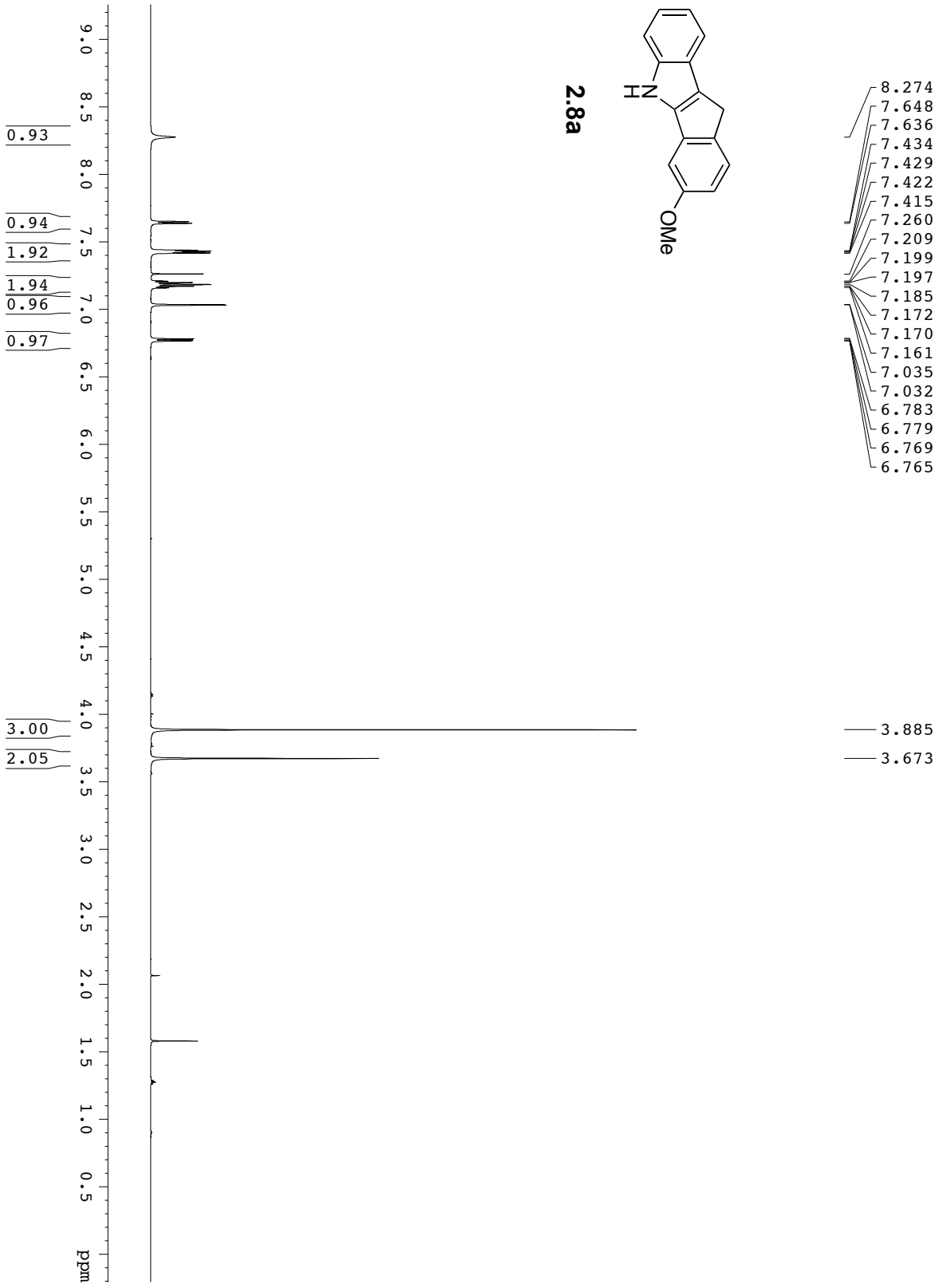


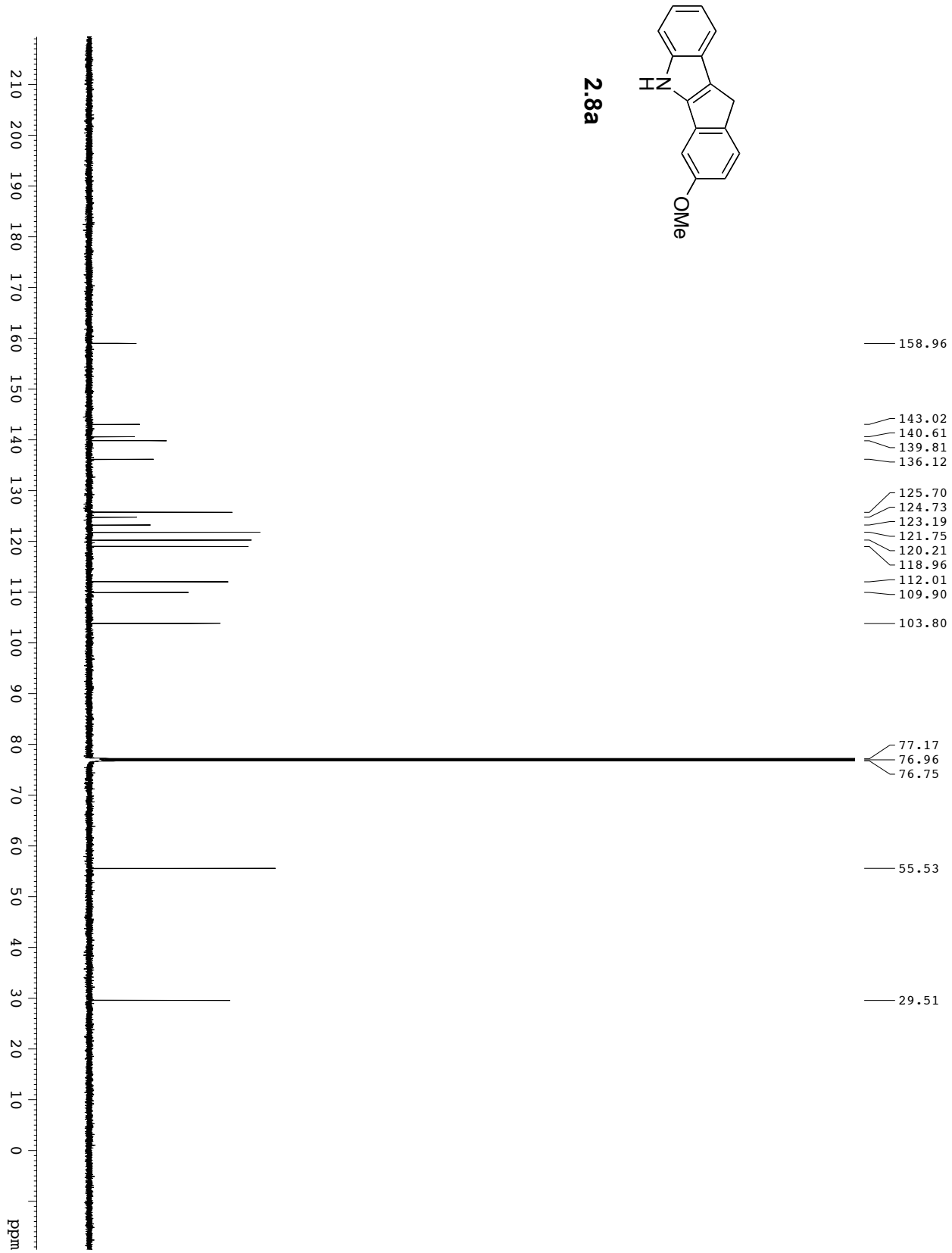

2.7c
MeO
N
Me
TMS
7.715
7.703
7.579
7.565
7.548
7.536
7.341
7.207
6.894
6.867
6.853
4.043
3.946
3.748
2.089
0.015
1.06
2.14
1.11
1.07
2.02
3.00
3.24
0.96
9.21
ppm

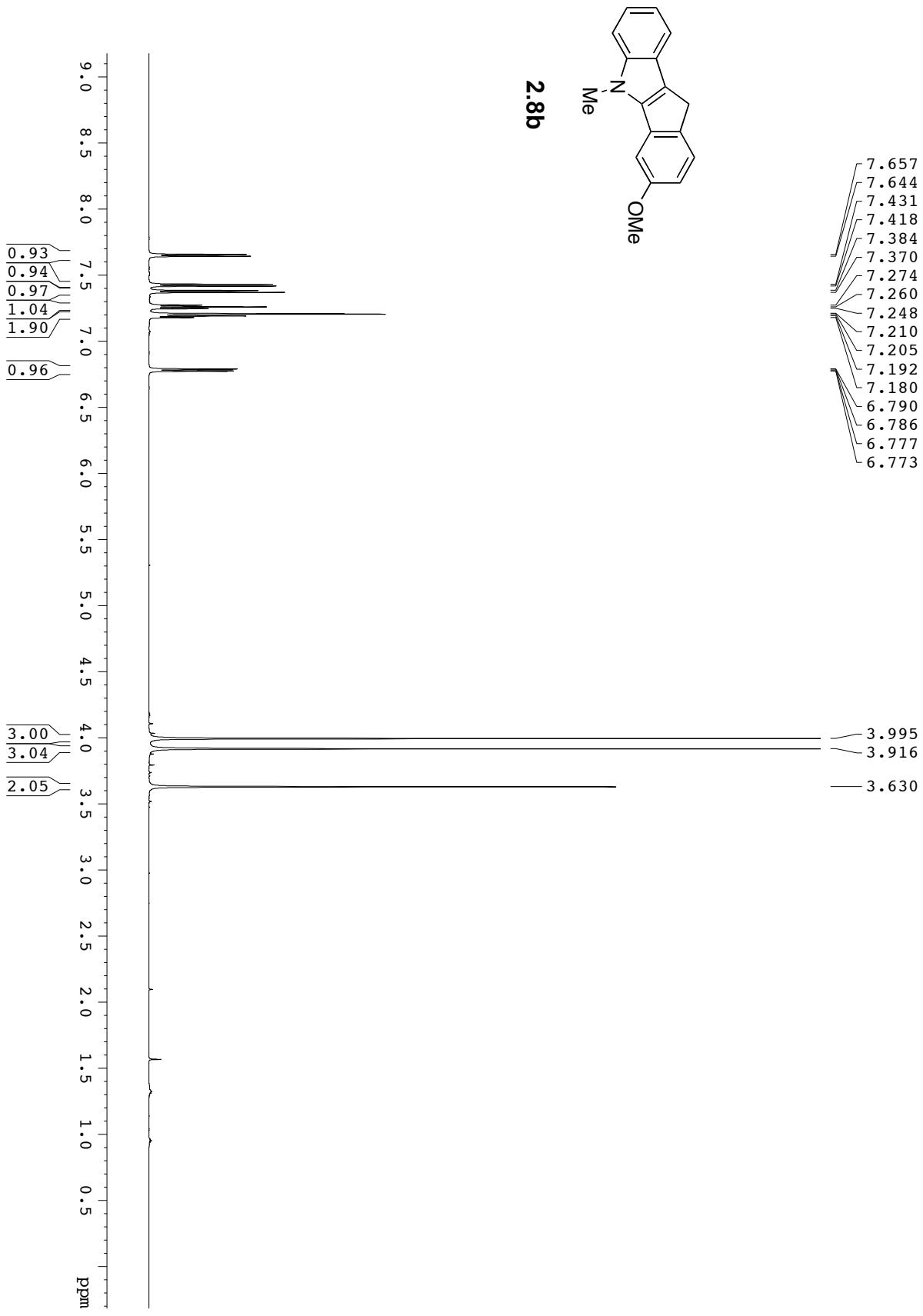

MeO
N
Me
TMS
2.7c
155.78
149.33
142.80
142.36
133.78
124.92
124.47
123.19
122.90
120.68
118.19
116.86
108.29
93.60
77.17
76.96
76.75
55.61
36.78
31.15
-2.42
ppm

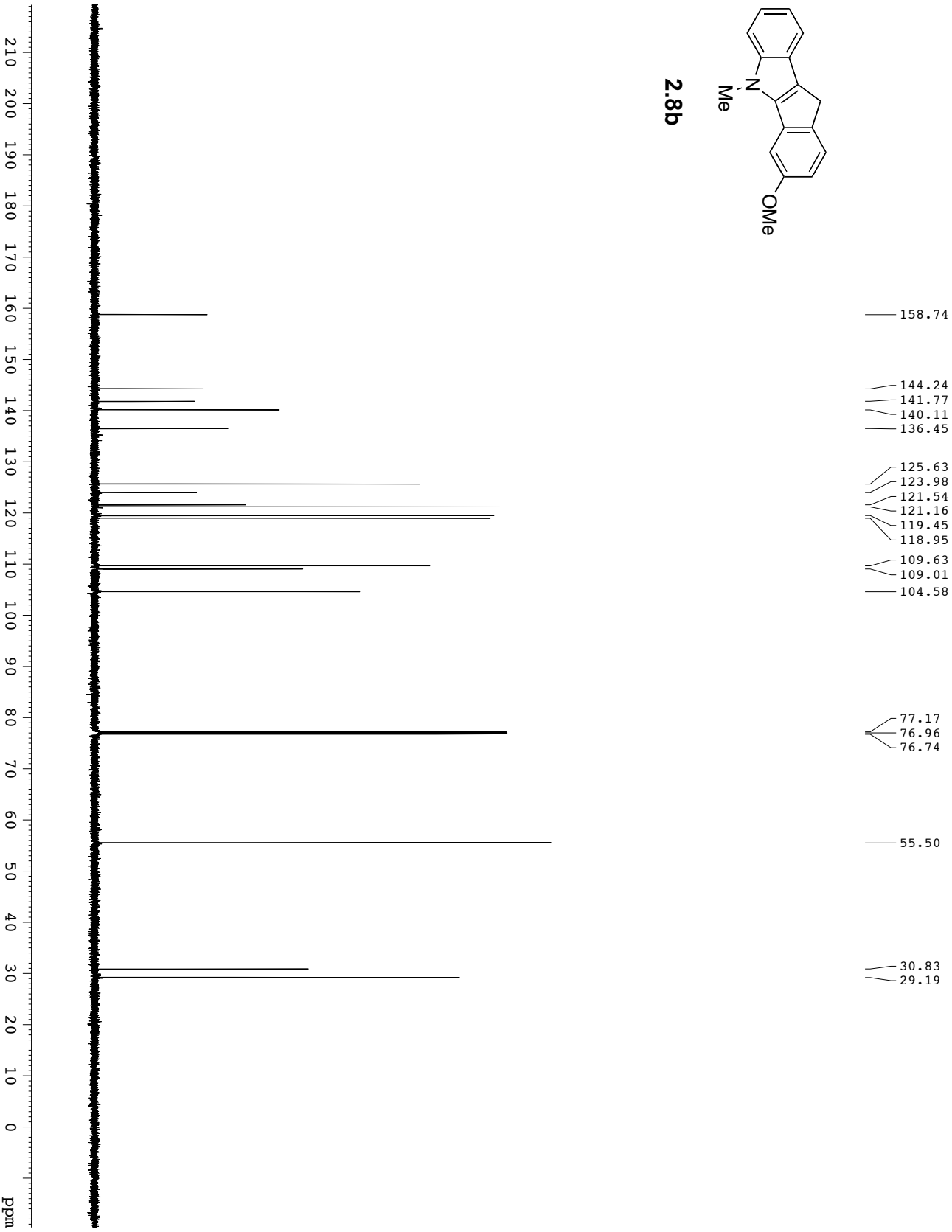

2.7
MeO
Me
N
O
7.584
7.572
7.432
7.420
7.407
7.343
7.329
7.260
7.204
6.907
6.896
3.869
2.729
0.92
1.97
1.85
0.92
0.94
3.07
3.00
9.0
8.5
8.0
7.5
7.0
6.5
6.0
5.5
5.0
4.5
4.0
3.5
3.0
2.5
2.0
1.5
1.0
0.5
ppm

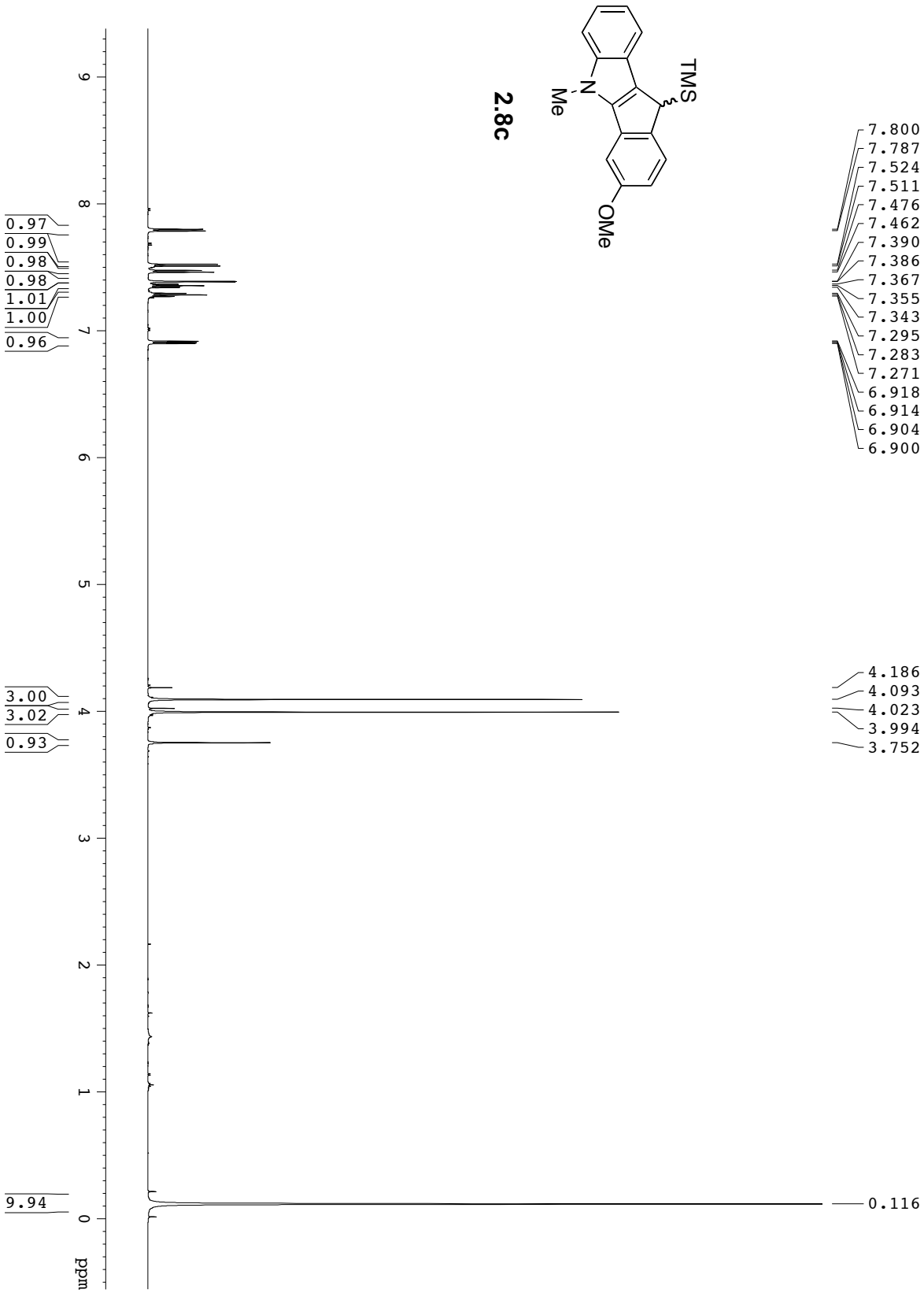

MeO
Me
N
O
2.7
176.81
160.95
158.08
148.89
129.31
128.20
128.12
126.00
125.44
122.65
115.90
113.78
113.49
108.86
108.23
77.17
76.96
76.75
55.57
38.67
210 200 190 180 170 160 150 140 130 120 110 100 90 80 70 60 50 40 30 20 10 0
ppm

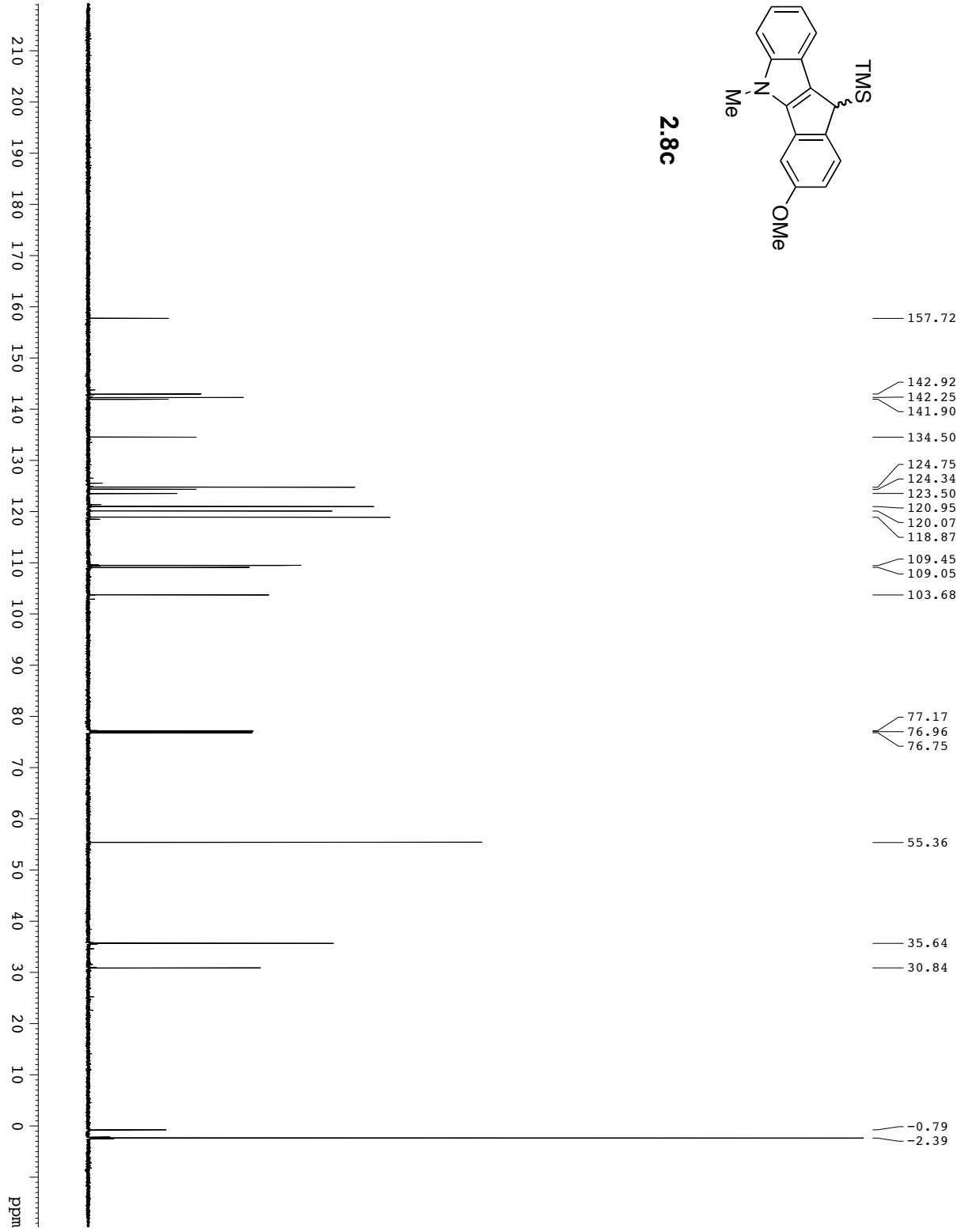

2.8a
OMe
N
H
8.274
7.648
7.636
7.434
7.429
7.422
7.415
7.260
7.209
7.199
7.197
7.185
7.172
7.170
7.161
7.035
7.032
6.783
6.779
6.769
6.765
3.885
3.673
0.93
0.94
1.92
1.94
0.96
0.97
3.00
2.05
ppm

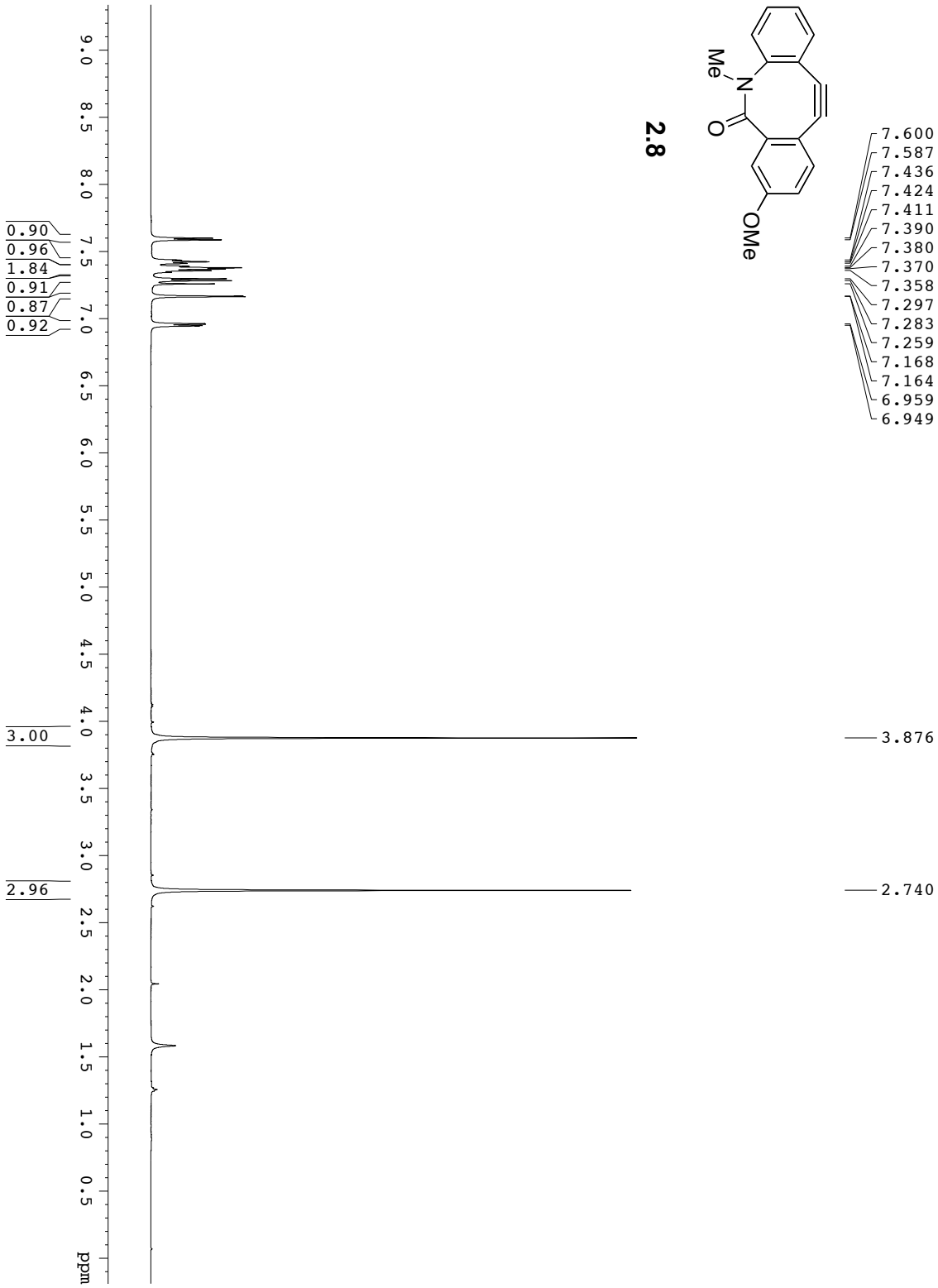

2.8a
N
H
OMe
158.96
143.02
140.61
139.81
136.12
125.70
124.73
123.19
121.75
120.21
118.96
112.01
109.90
103.80
77.17
76.96
76.75
55.53
29.51
210 200 190 180 170 160 150 140 130 120 110 100 90 80 70 60 50 40 30 20 10 0
ppm

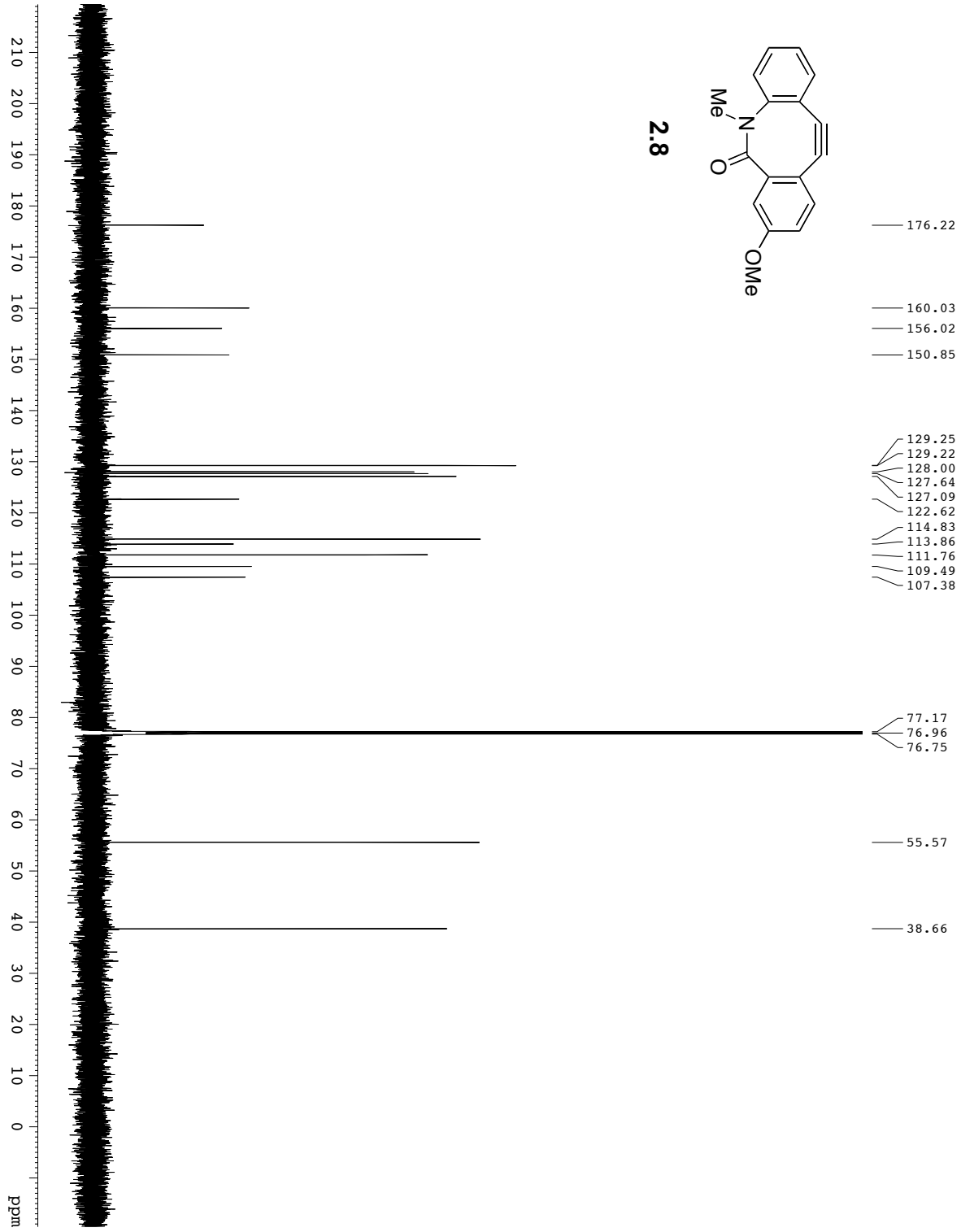

2.8b
N
Me
OMe
7.657
7.644
7.431
7.418
7.384
7.370
7.274
7.260
7.248
7.210
7.205
7.192
7.180
6.790
6.786
6.777
6.773
3.995
3.916
3.630
0.93
0.94
0.97
1.04
1.90
0.96
3.00
3.04
2.05
ppm

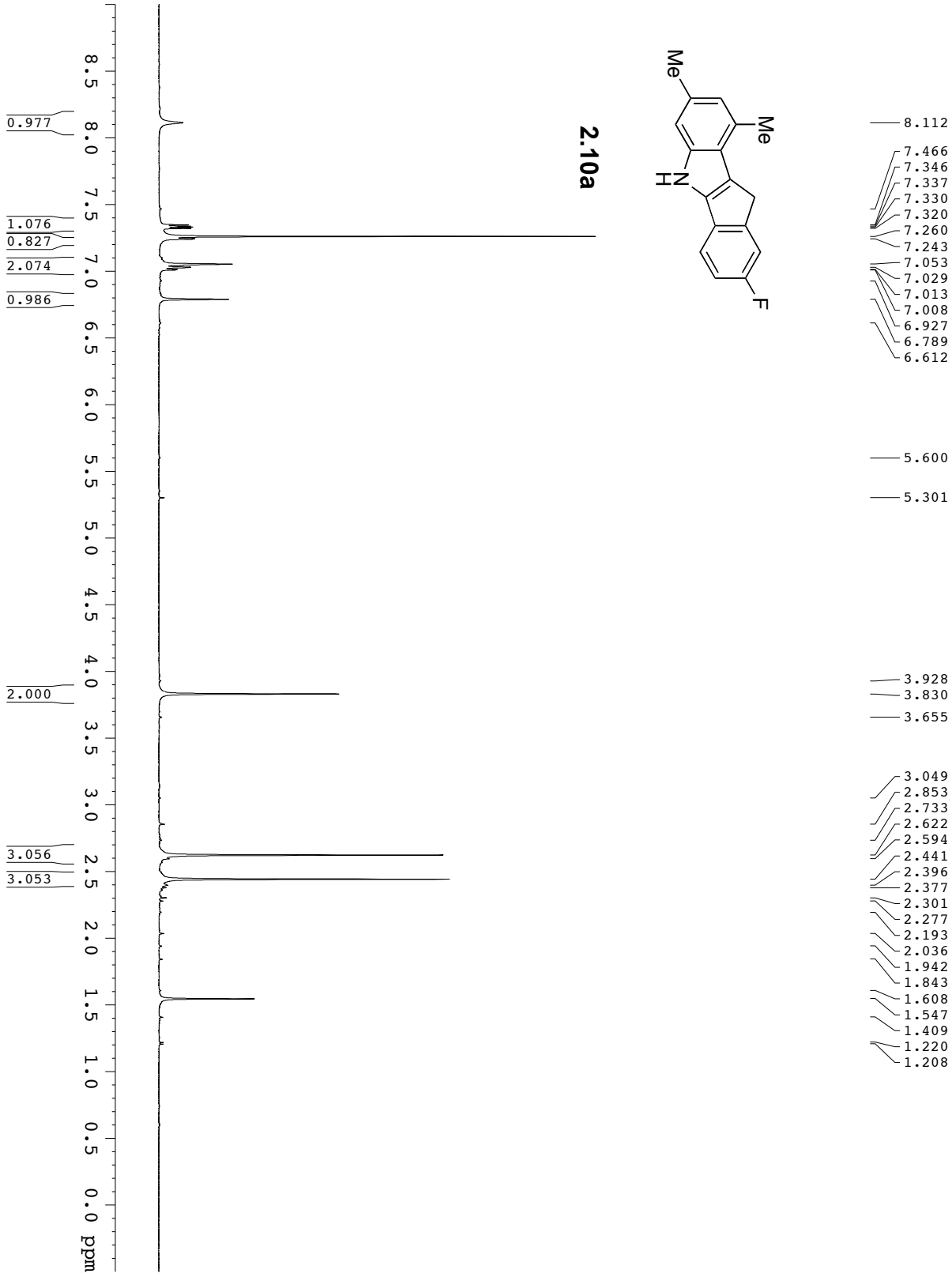

2.8b
N
Me
OMe
158.74
144.24
141.77
140.11
136.45
125.63
123.98
121.54
121.16
119.45
118.95
109.63
109.01
104.58
77.17
76.96
76.74
55.50
30.83
29.19
ppm

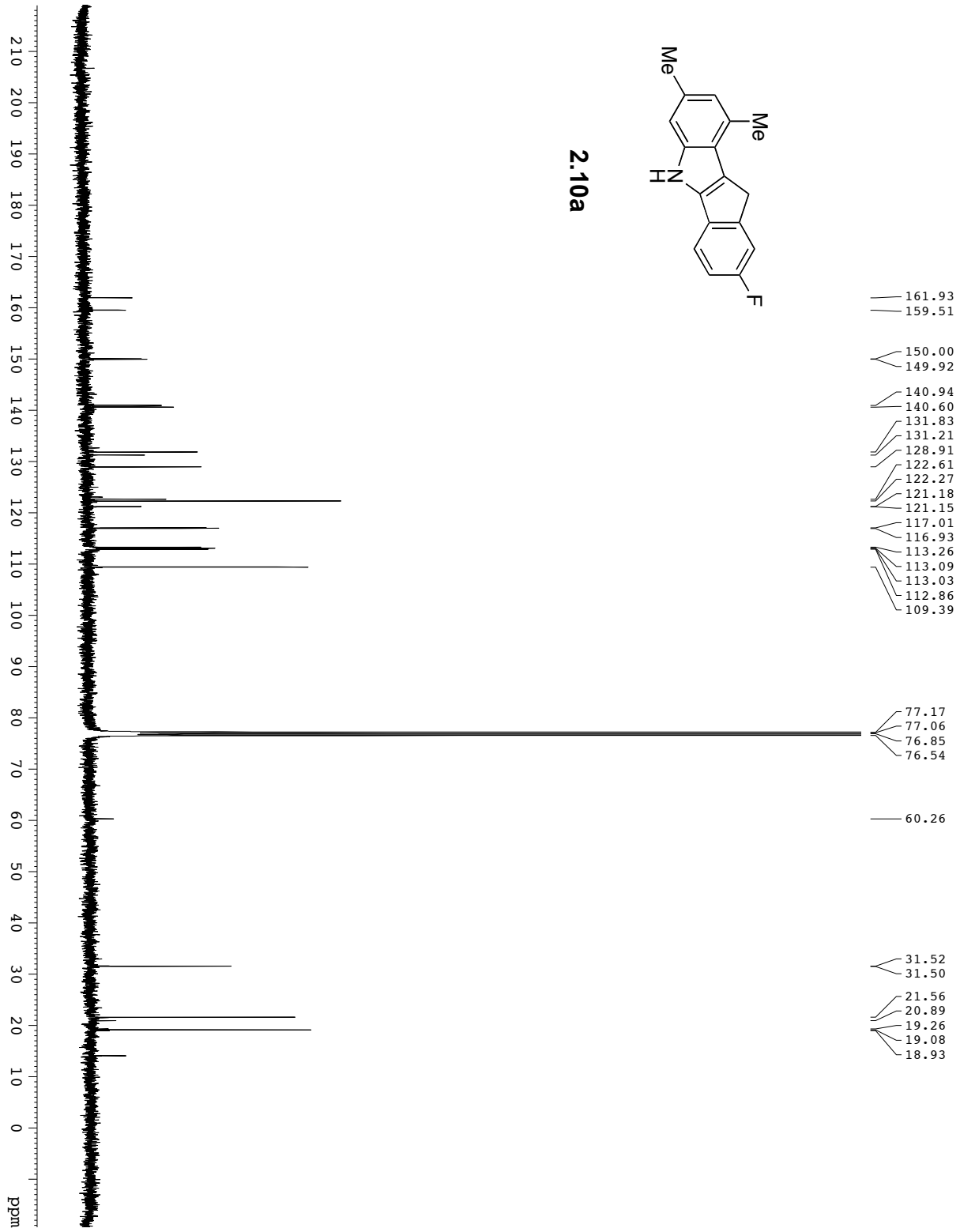

2.8c
TMS
N
Me
OMe
7.800
7.787
7.524
7.511
7.476
7.462
7.390
7.386
7.367
7.355
7.343
7.295
7.283
7.271
6.918
6.914
6.904
6.900
4.186
4.093
4.023
3.994
3.752
0.116
0.97
0.99
0.98
0.98
1.01
1.00
0.96
3.00
3.02
0.93
9.94
ppm

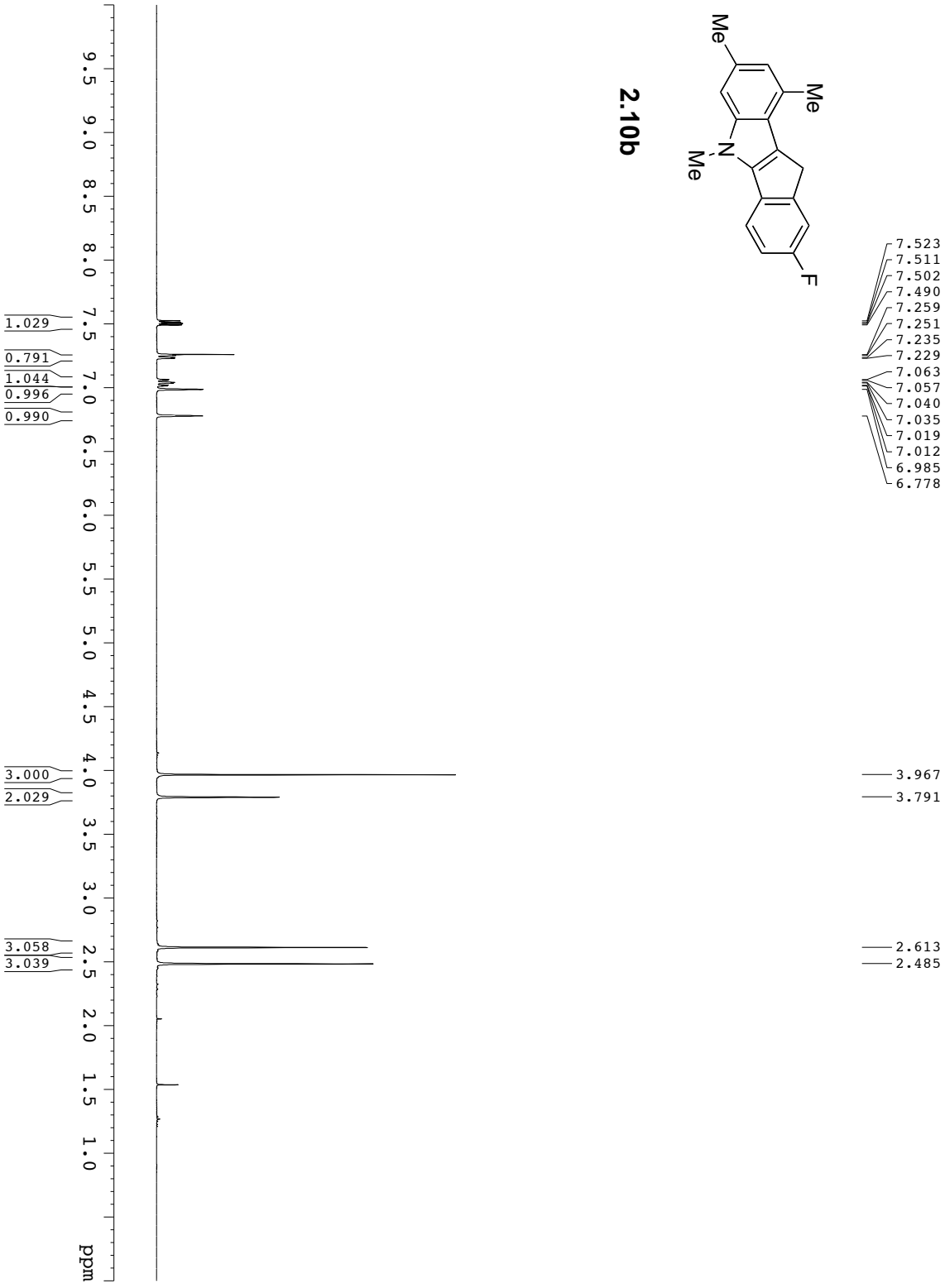

2.8c
TMS
N
Me
OMe
157.72
142.92
142.25
141.90
134.50
124.75
124.34
123.50
120.95
120.07
118.87
109.45
109.05
103.68
77.17
76.96
76.75
55.36
35.64
30.84
-0.79
-2.39
ppm

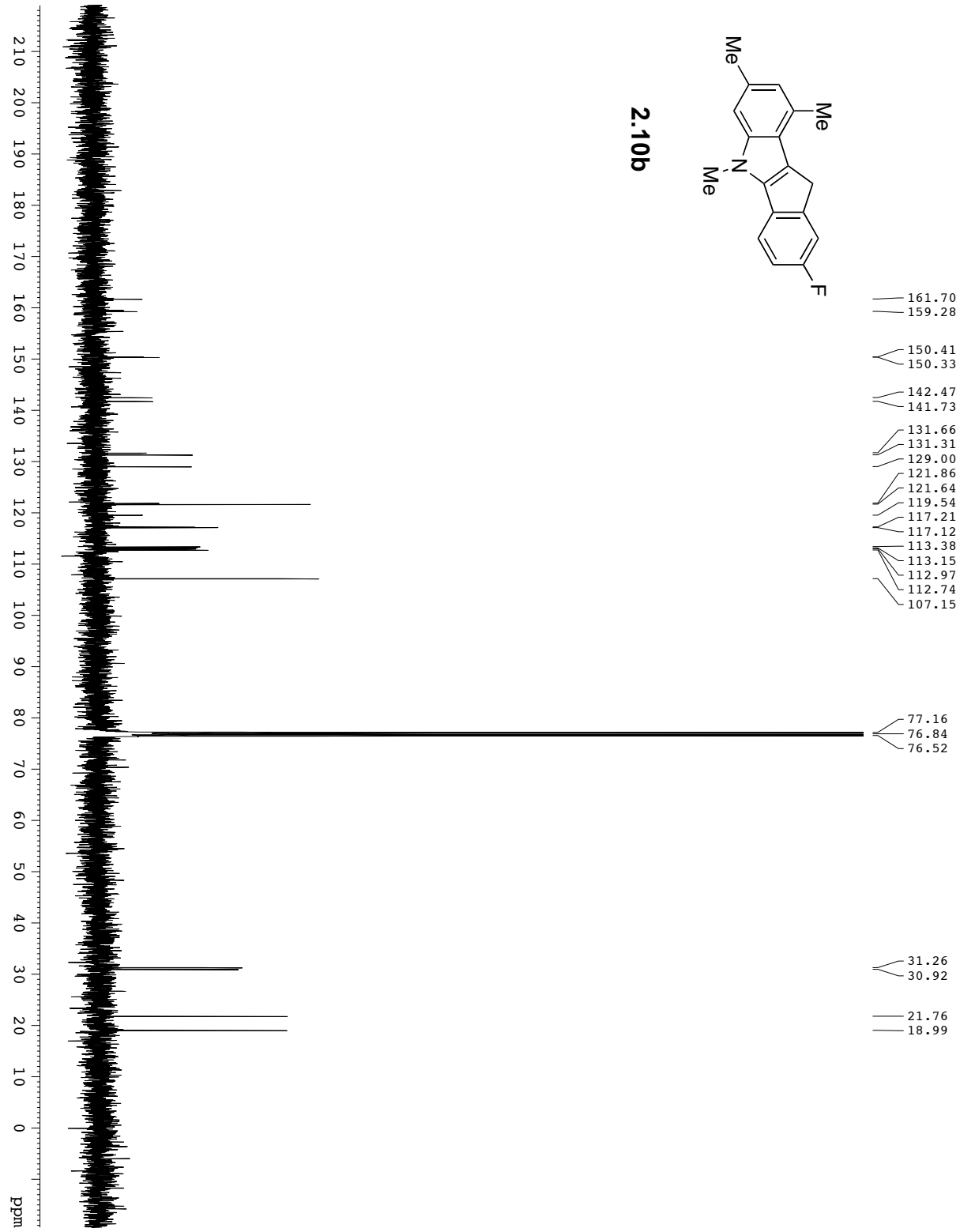

2.8
Me
N
O
OMe
7.600
7.587
7.436
7.424
7.411
7.390
7.380
7.370
7.358
7.297
7.283
7.259
7.168
7.164
6.959
6.949
3.876
2.740
0.90
0.96
1.84
0.91
0.87
0.92
3.00
2.96
9.0
8.5
8.0
7.5
7.0
6.5
6.0
5.5
5.0
4.5
4.0
3.5
3.0
2.5
2.0
1.5
1.0
0.5
ppm

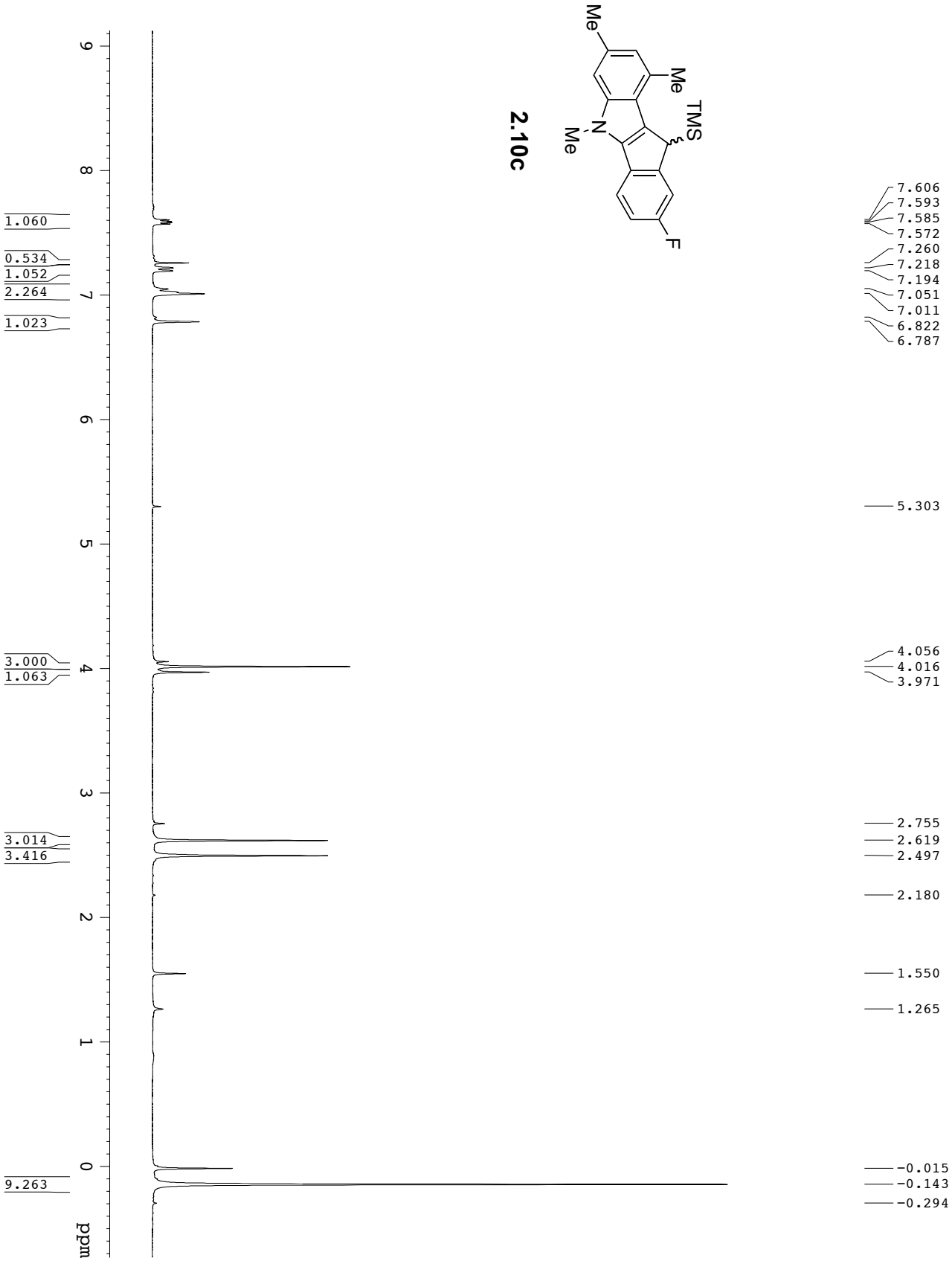

2.8
Me
N
O
OMe
176.22
160.03
156.02
150.85
129.25
129.22
128.00
127.64
127.09
122.62
114.83
113.86
111.76
109.49
107.38
77.17
76.96
76.75
55.57
38.66
210 200 190 180 170 160 150 140 130 120 110 100 90 80 70 60 50 40 30 20 10 0
ppm

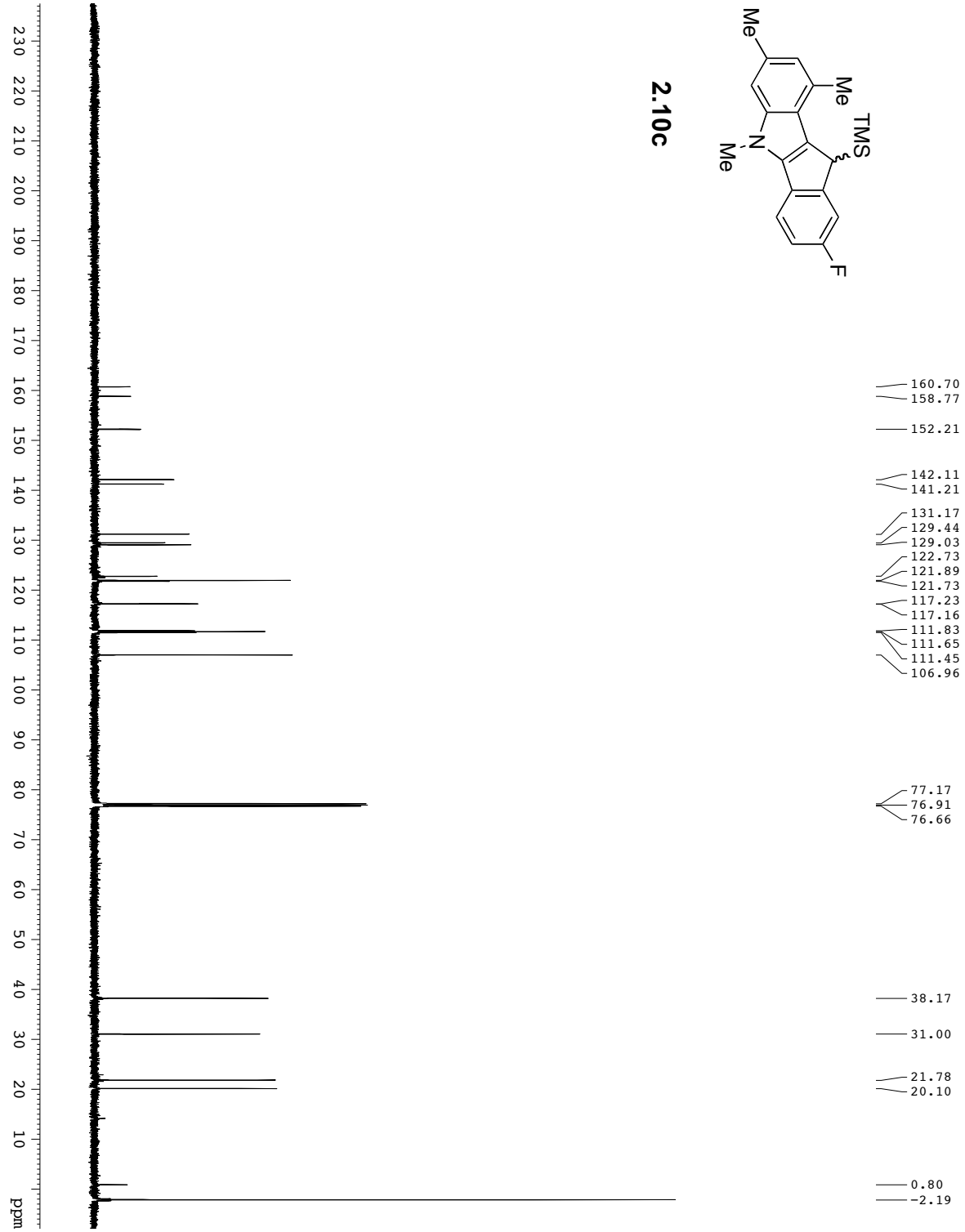

2.10a
Me
Me
N
H
F
0.977
1.076
0.827
2.074
0.986
2.000
3.056
3.053
8.112
7.466
7.346
7.337
7.330
7.320
7.260
7.243
7.053
7.029
7.013
7.008
6.927
6.789
6.612
5.600
5.301
3.928
3.830
3.655
3.049
2.853
2.733
2.622
2.594
2.441
2.396
2.377
2.301
2.277
2.193
2.036
1.942
1.843
1.608
1.547
1.409
1.220
1.208
8.5
8.0
7.5
7.0
6.5
6.0
5.5
5.0
4.5
4.0
3.5
3.0
2.5
2.0
1.5
1.0
0.5
0.0
ppm

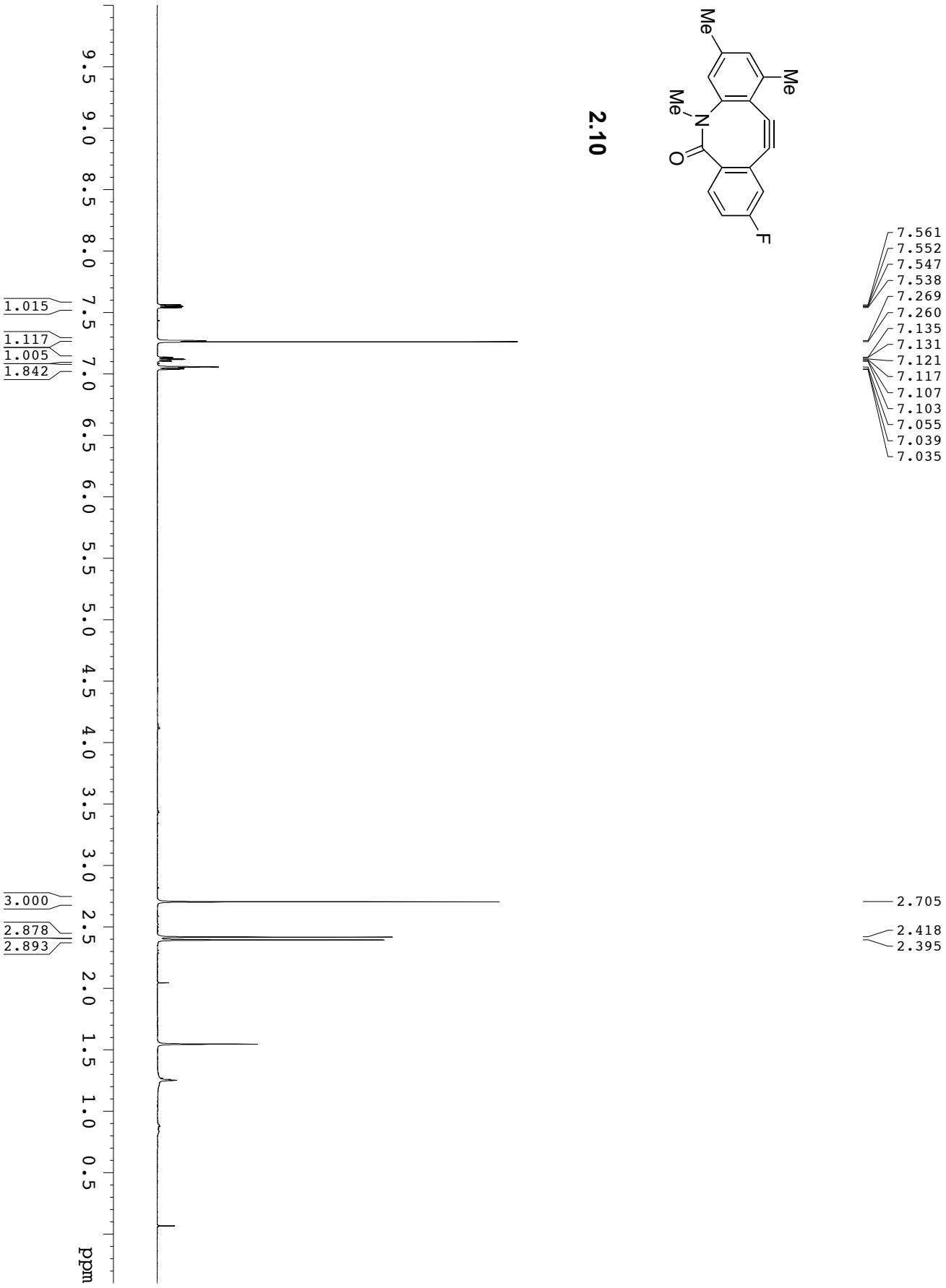

2.10a
Me
Me
N
H
F
161.93
159.51
150.00
149.92
140.94
140.60
131.83
131.21
128.91
122.61
122.27
121.18
121.15
117.01
116.93
113.26
113.09
113.03
112.86
109.39
77.17
77.06
76.85
76.54
60.26
31.52
31.50
21.56
20.89
19.26
19.08
18.93
210 200 190 180 170 160 150 140 130 120 110 100 90 80 70 60 50 40 30 20 10 0
ppm

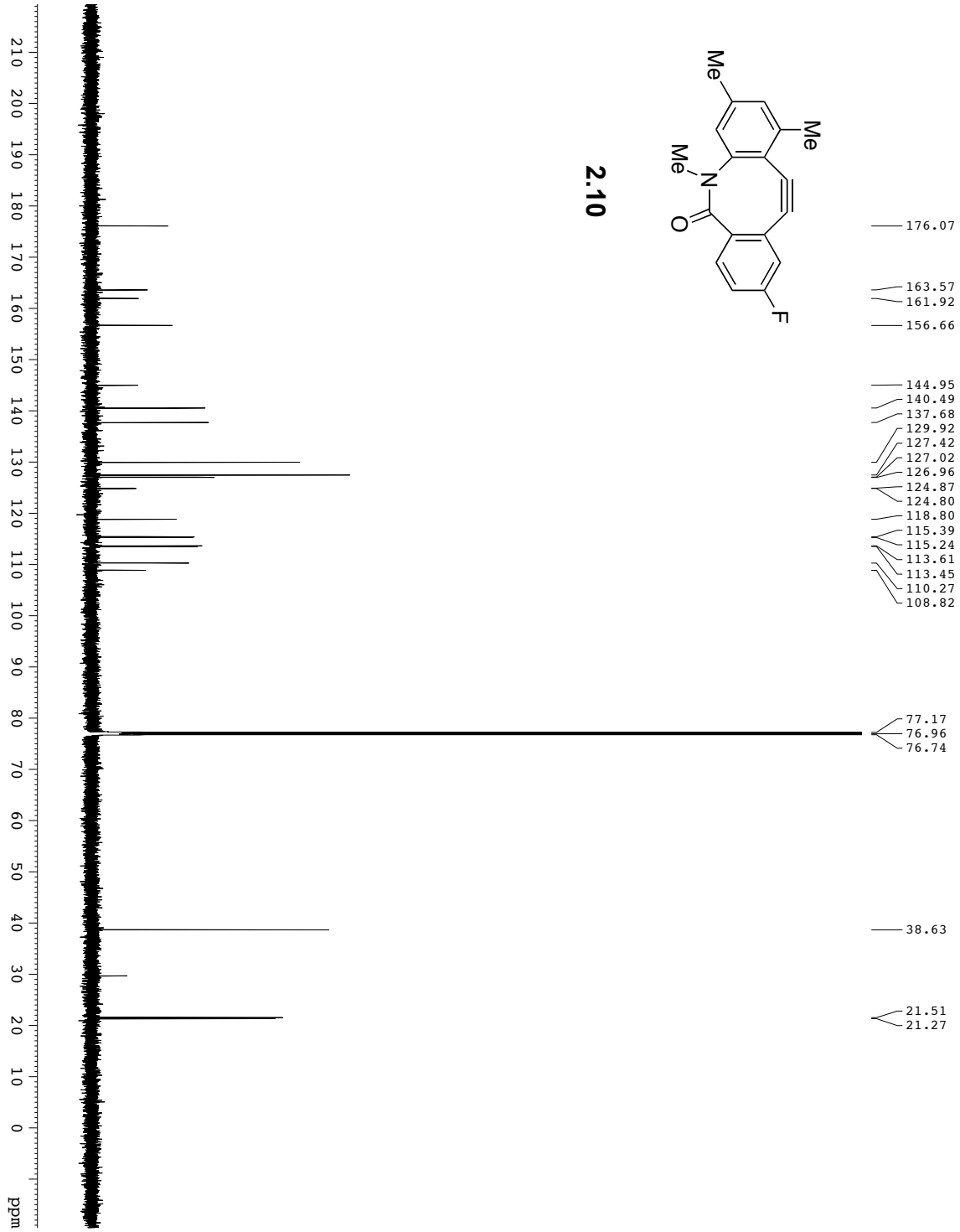

2.10b
Me
Me
N
Me
F
7.523
7.511
7.502
7.490
7.259
7.251
7.235
7.229
7.063
7.057
7.040
7.035
7.019
7.012
6.985
6.778
3.967
3.791
2.613
2.485
1.029
0.791
1.044
0.996
0.990
3.000
2.029
3.058
3.039
9.5
9.0
8.5
8.0
7.5
7.0
6.5
6.0
5.5
5.0
4.5
4.0
3.5
3.0
2.5
2.0
1.5
1.0
ppm

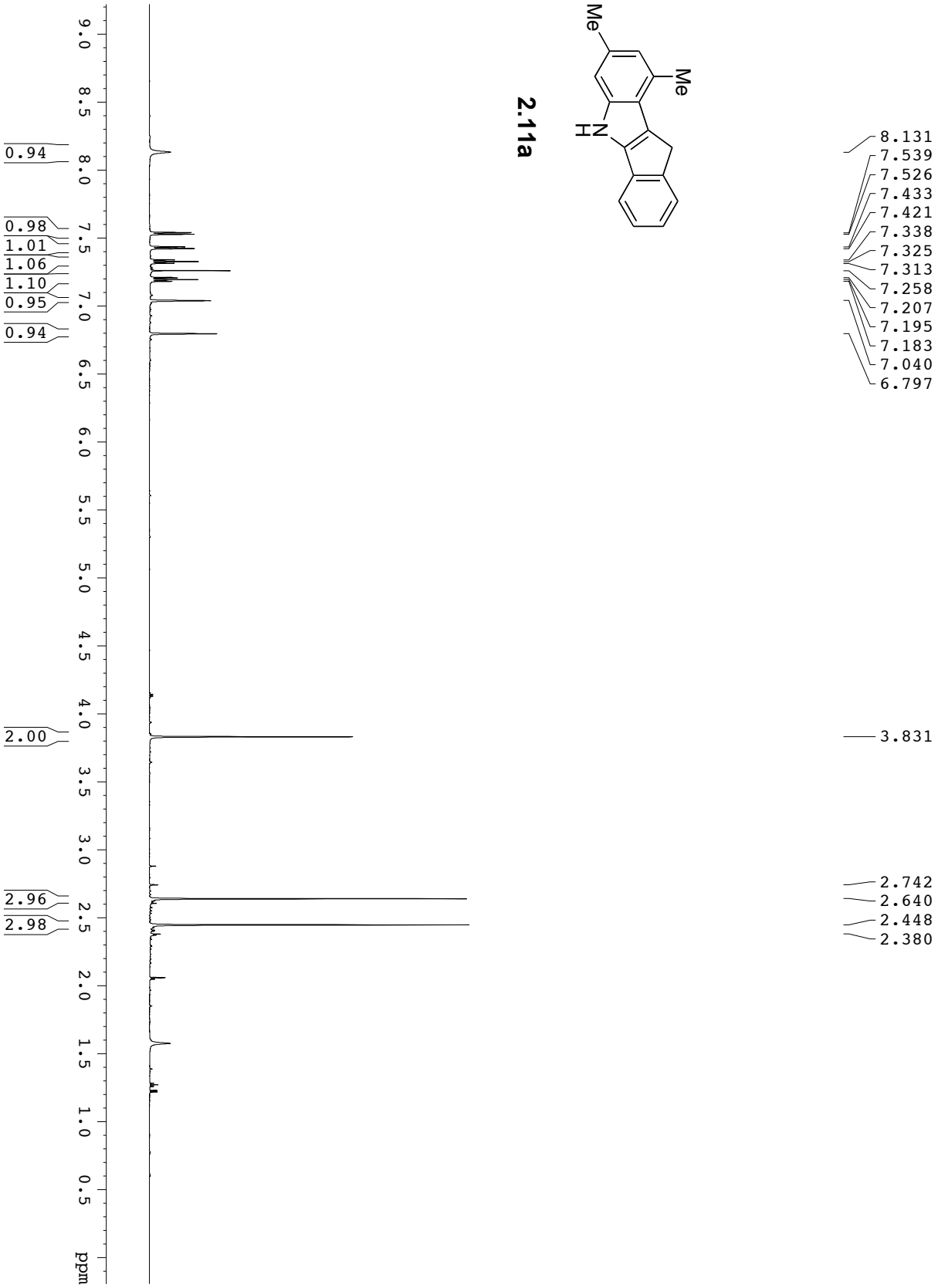

2.10b
Me
Me
N
Me
F
161.70
159.28
150.41
150.33
142.47
141.73
131.66
131.31
129.00
121.86
121.64
119.54
117.21
117.12
113.38
113.15
112.97
112.74
107.15
77.16
76.84
76.52
31.26
30.92
21.76
18.99
210 200 190 180 170 160 150 140 130 120 110 100 90 80 70 60 50 40 30 20 10 0
ppm

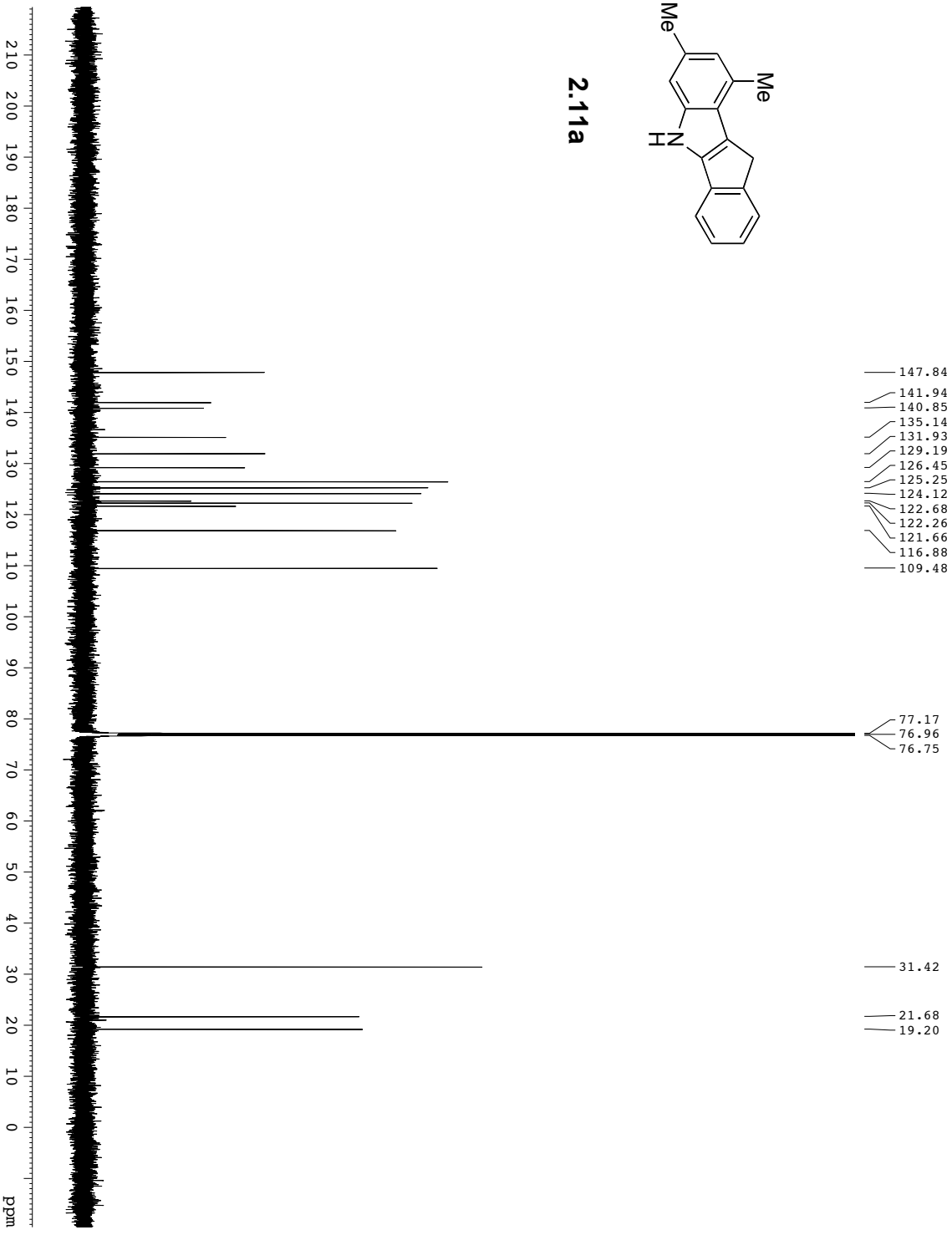

Me
Me
TMS
N
Me
F
2.10c
7.606
7.593
7.585
7.572
7.260
7.218
7.194
7.051
7.011
6.822
6.787
5.303
4.056
4.016
3.971
2.755
2.619
2.497
2.180
1.550
1.265
-0.015
-0.143
-0.294
1.060
0.534
1.052
2.264
1.023
3.000
1.063
3.014
3.416
9.263
ppm

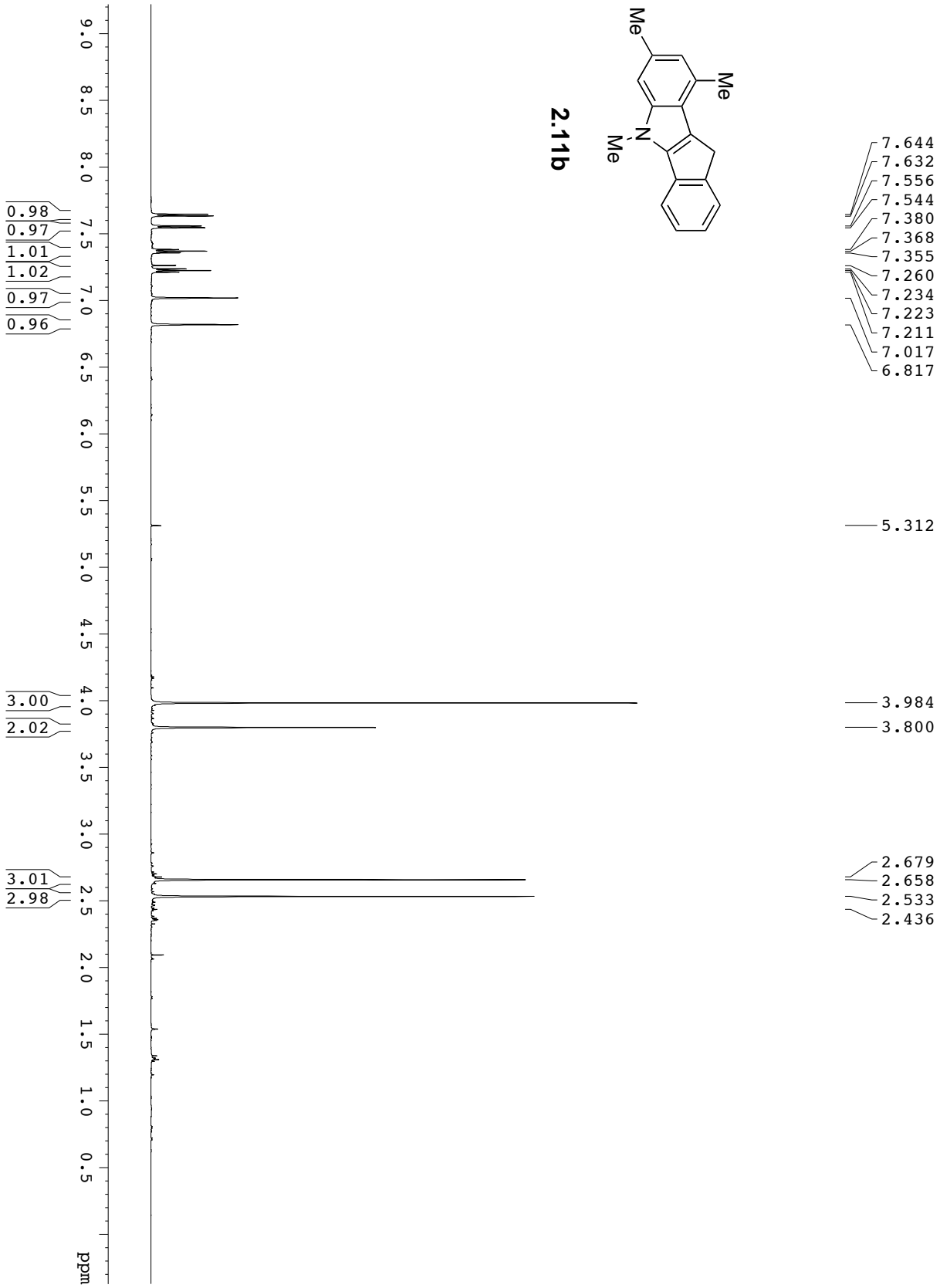

2.10c
Me
Me
TMS
N
Me
F
160.70
158.77
152.21
142.11
141.21
131.17
129.44
129.03
122.73
121.89
121.73
117.23
117.16
111.83
111.65
111.45
106.96
77.17
76.91
76.66
38.17
31.00
21.78
20.10
0.80
-2.19
230 220 210 200 190 180 170 160 150 140 130 120 110 100 90 80 70 60 50 40 30 20 10
ppm

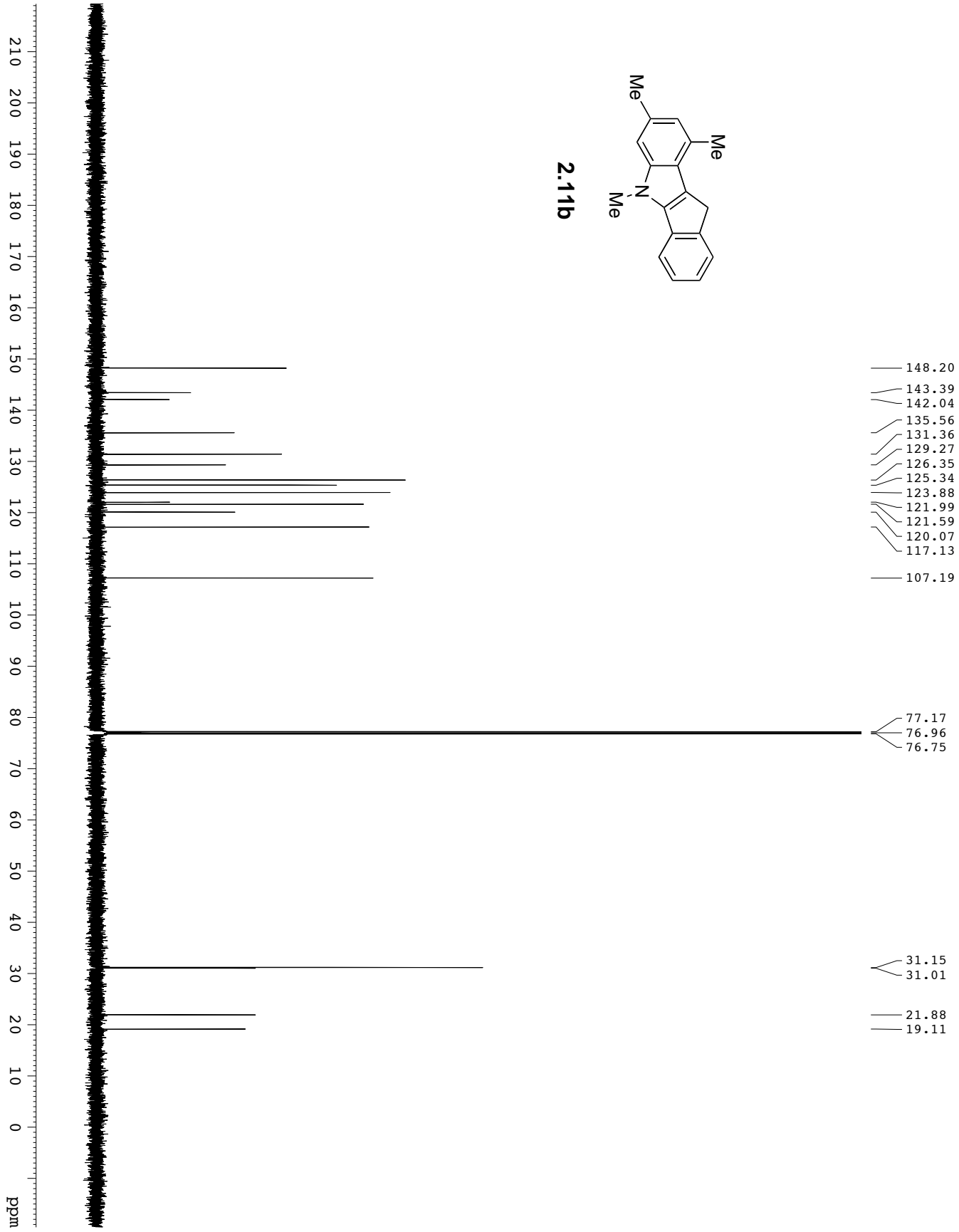

2.10
Me
Me
Me
N
O
F
7.561
7.552
7.547
7.538
7.269
7.260
7.135
7.131
7.121
7.117
7.107
7.103
7.055
7.039
7.035
2.705
2.418
2.395
1.015
1.117
1.005
1.842
3.000
2.878
2.893
9.5
9.0
8.5
8.0
7.5
7.0
6.5
6.0
5.5
5.0
4.5
4.0
3.5
3.0
2.5
2.0
1.5
1.0
0.5
ppm

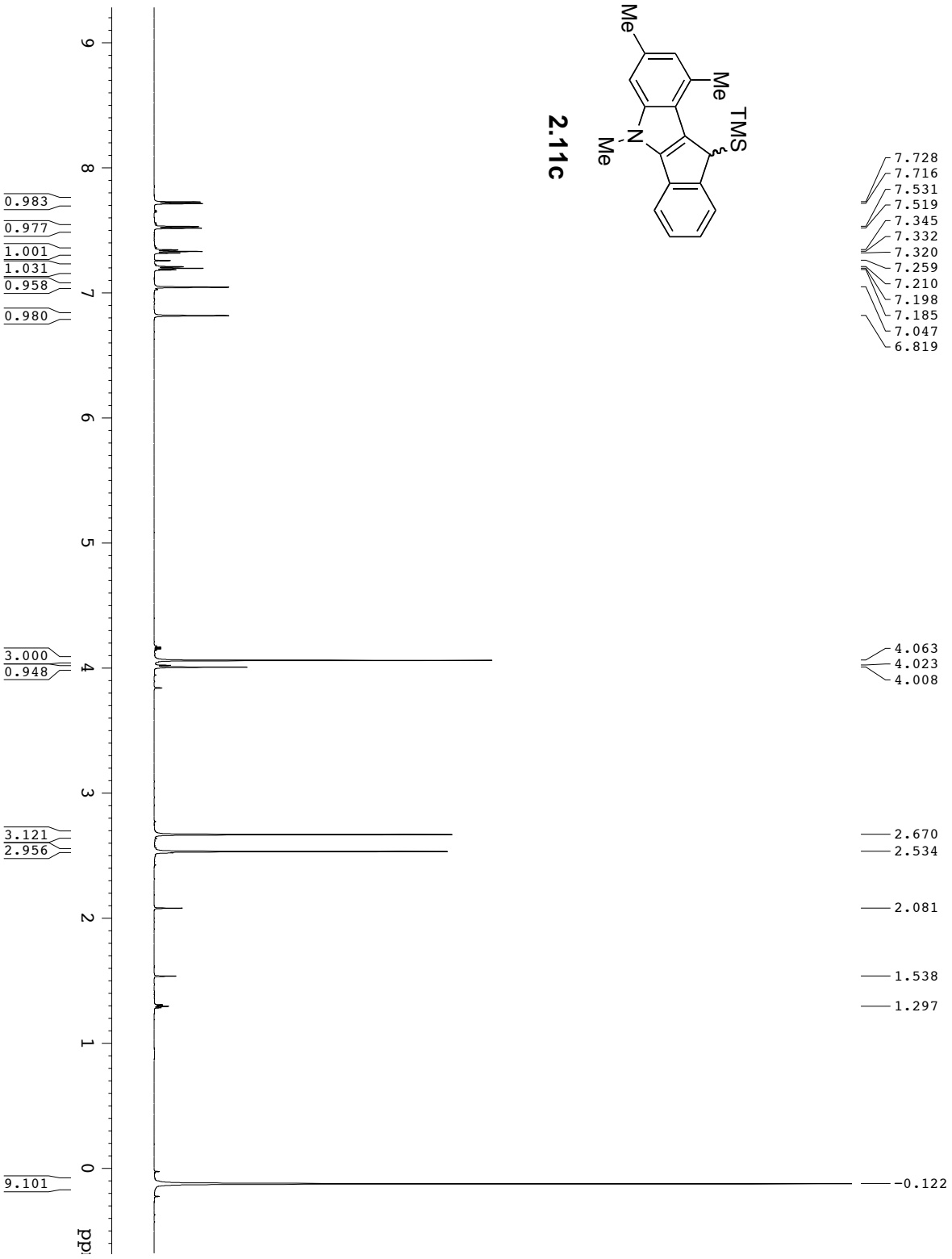

2.10
Me
Me
Me
N
O
F
176.07
163.57
161.92
156.66
144.95
140.49
137.68
129.92
127.42
127.02
126.96
124.87
124.80
118.80
115.39
115.24
113.61
113.45
110.27
108.82
77.17
76.96
76.74
38.63
21.51
21.27
210 200 190 180 170 160 150 140 130 120 110 100 90 80 70 60 50 40 30 20 10 0
ppm

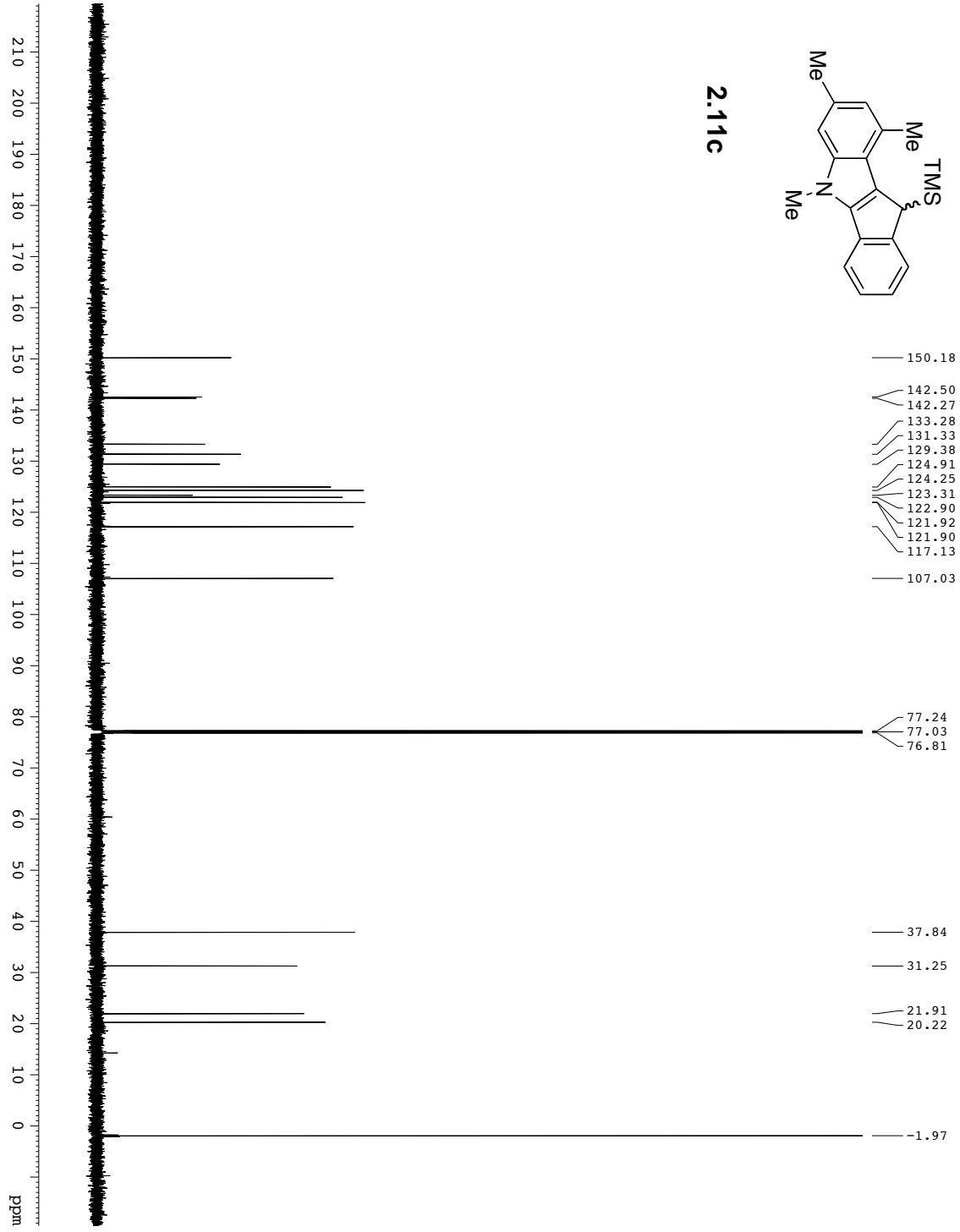

2.11a
Me
Me
N
H
8.131
7.539
7.526
7.433
7.421
7.338
7.325
7.313
7.258
7.207
7.195
7.183
7.040
6.797
3.831
2.742
2.640
2.448
2.380
0.94
0.98
1.01
1.06
1.10
0.95
0.94
2.00
2.96
2.98
9.0
8.5
8.0
7.5
7.0
6.5
6.0
5.5
5.0
4.5
4.0
3.5
3.0
2.5
2.0
1.5
1.0
0.5
ppm

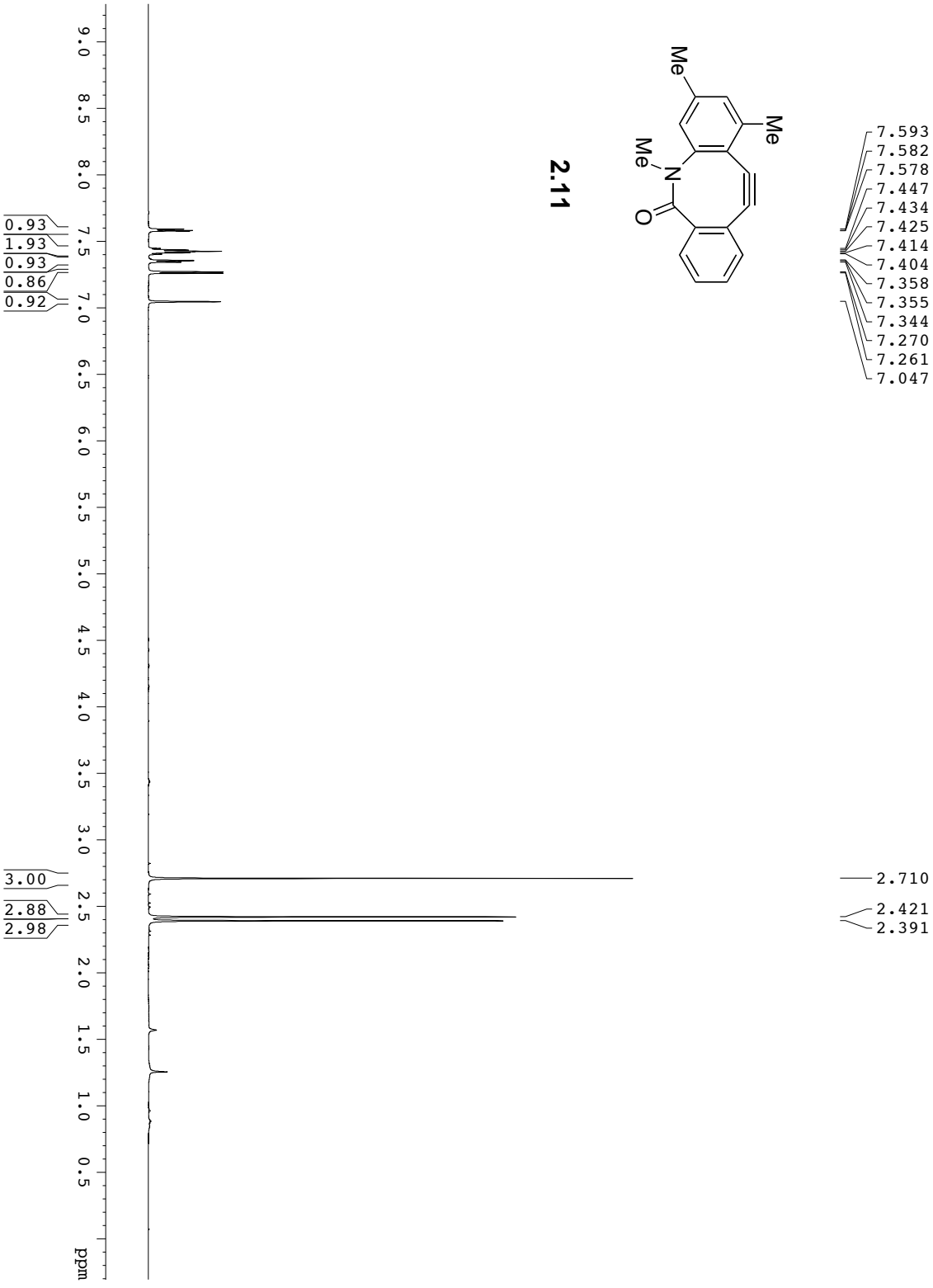

Me
Me
N
H
2.11a
147.84
141.94
140.85
135.14
131.93
129.19
126.45
125.25
124.12
122.68
122.26
121.66
116.88
109.48
77.17
76.96
76.75
31.42
21.68
19.20
210 200 190 180 170 160 150 140 130 120 110 100 90 80 70 60 50 40 30 20 10 0
ppm

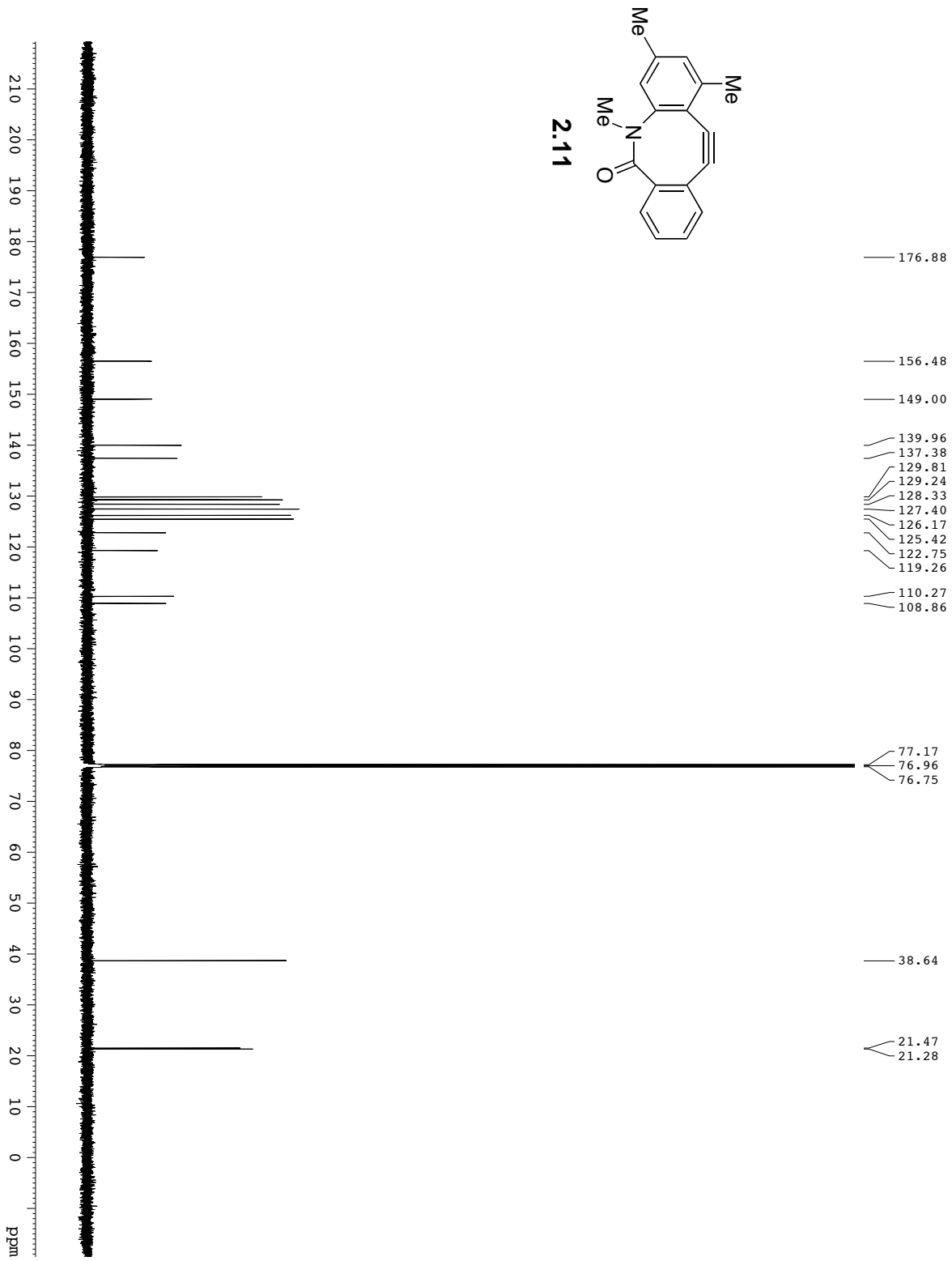

2.11b
Me
Me
N
Me
7.644
7.632
7.556
7.544
7.380
7.368
7.355
7.260
7.234
7.223
7.211
7.017
6.817
5.312
3.984
3.800
2.679
2.658
2.533
2.436
0.98
0.97
1.01
1.02
0.97
0.96
3.00
2.02
3.01
2.98
9.0
8.5
8.0
7.5
7.0
6.5
6.0
5.5
5.0
4.5
4.0
3.5
3.0
2.5
2.0
1.5
1.0
0.5
ppm

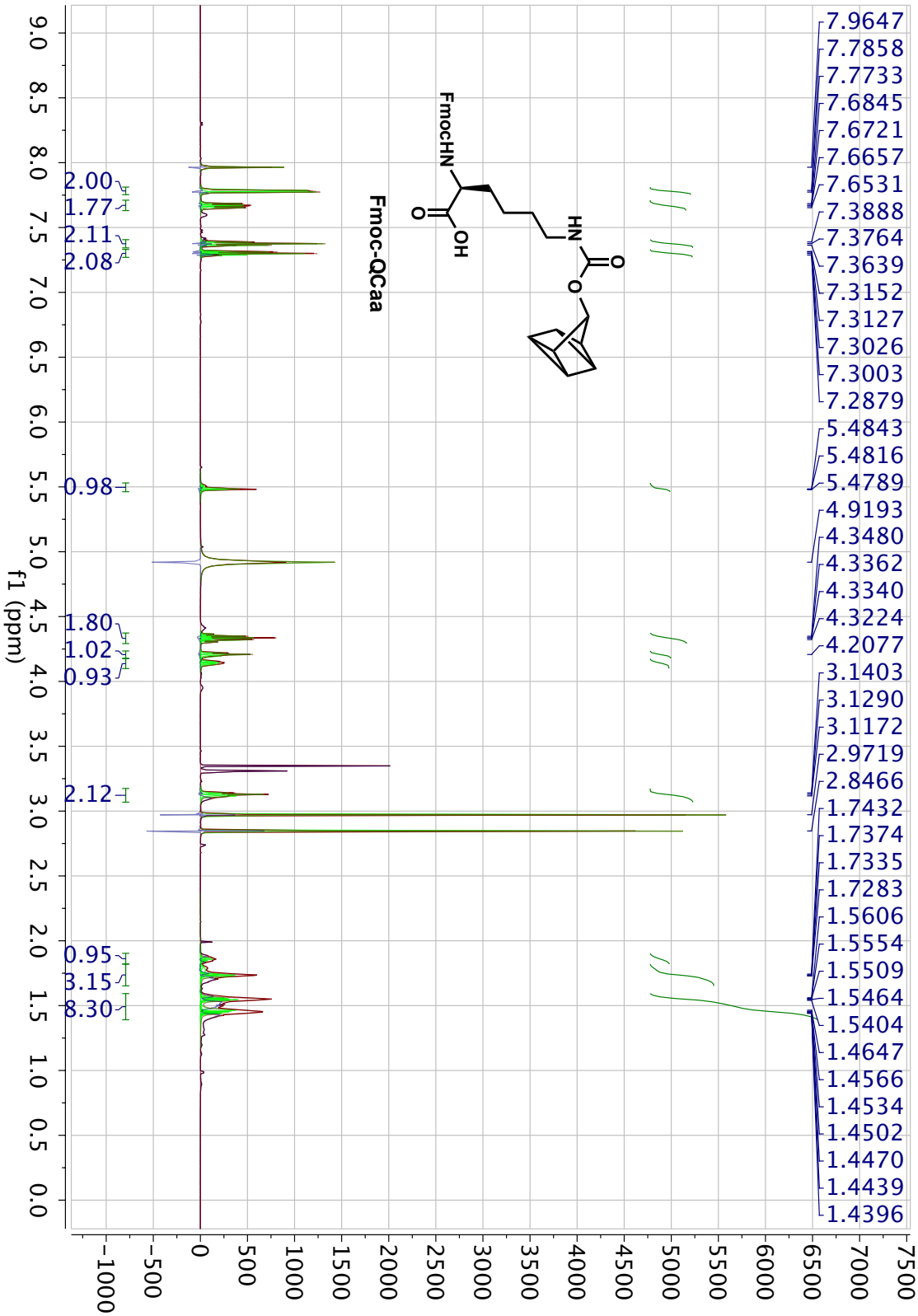

2.11b
Me
Me
N
Me
148.20
143.39
142.04
135.56
131.36
129.27
126.35
125.34
123.88
121.99
121.59
120.07
117.13
107.19
77.17
76.96
76.75
31.15
31.01
21.88
19.11
210 200 190 180 170 160 150 140 130 120 110 100 90 80 70 60 50 40 30 20 10 0
ppm

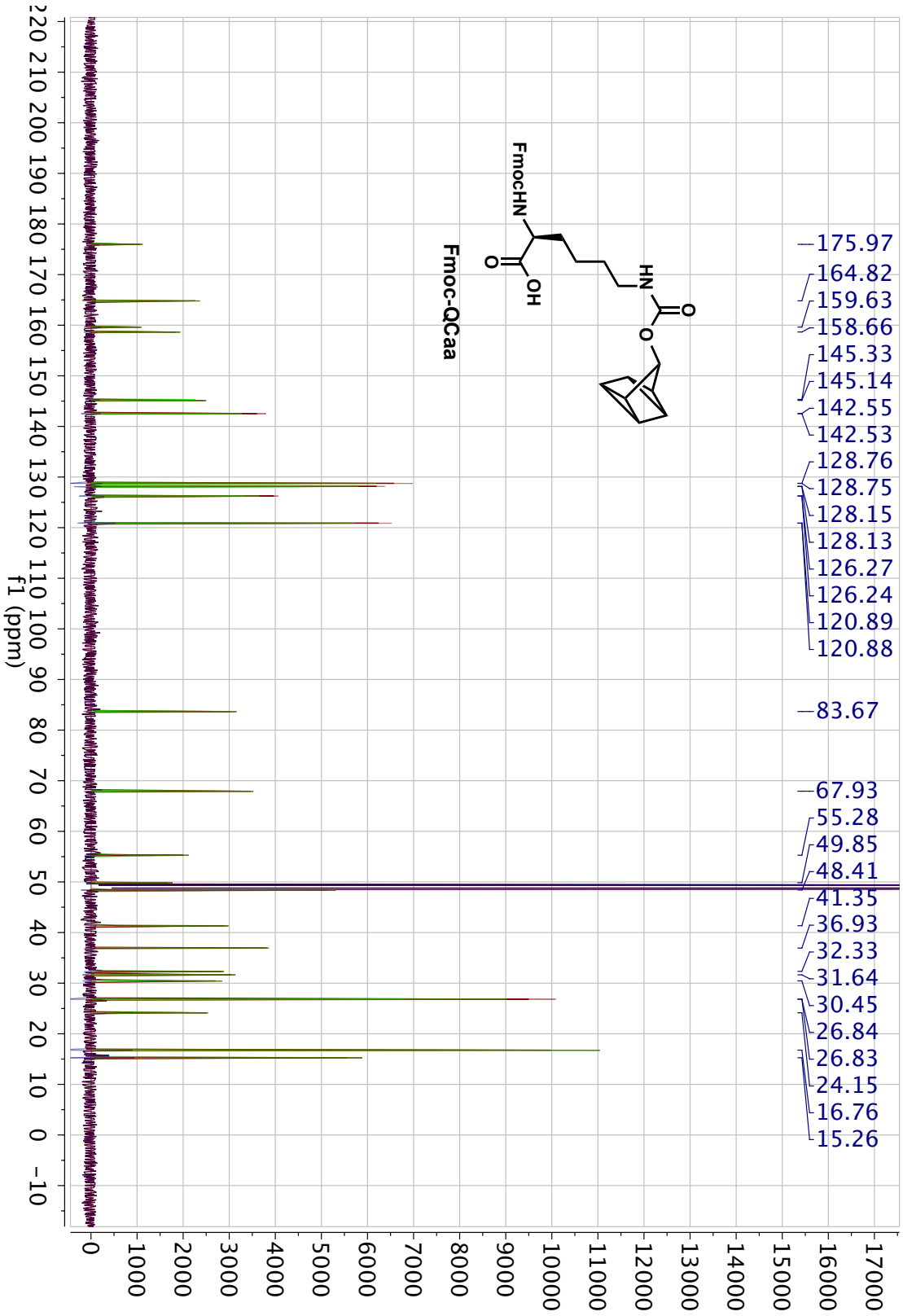

2.11c
Me
Me
TMS
N
Me
7.728
7.716
7.531
7.519
7.345
7.332
7.320
7.259
7.210
7.198
7.185
7.047
6.819
4.063
4.023
4.008
2.670
2.534
2.081
1.538
1.297
-0.122
0.983
0.977
1.001
1.031
0.958
0.980
3.000
0.948
3.121
2.956
9.101
ppm

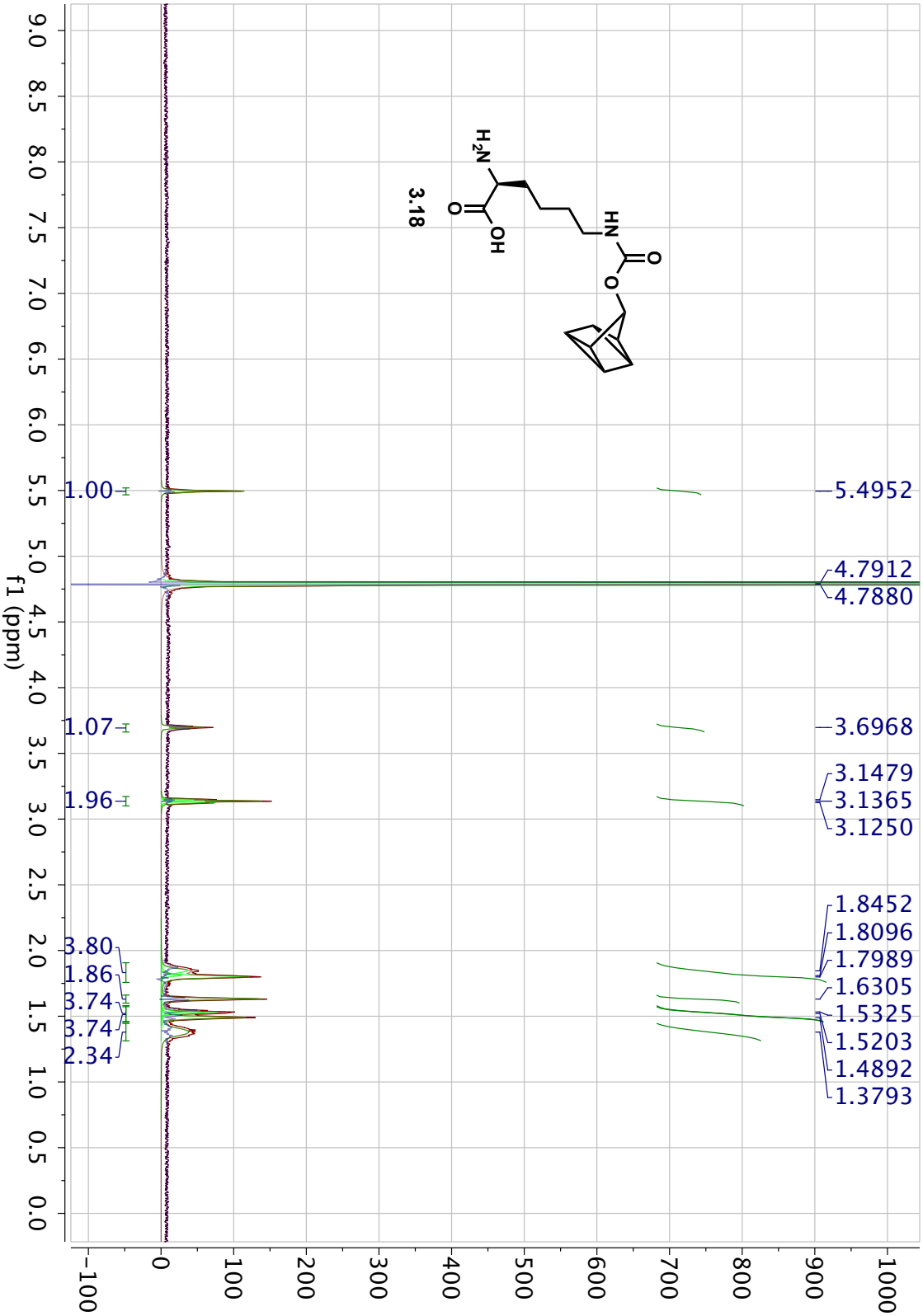

2.11c
Me
Me
TMS
N
Me
150.18
142.50
142.27
133.28
131.33
129.38
124.91
124.25
123.31
122.90
121.92
121.90
117.13
107.03
77.24
77.03
76.81
37.84
31.25
21.91
20.22
-1.97
ppm

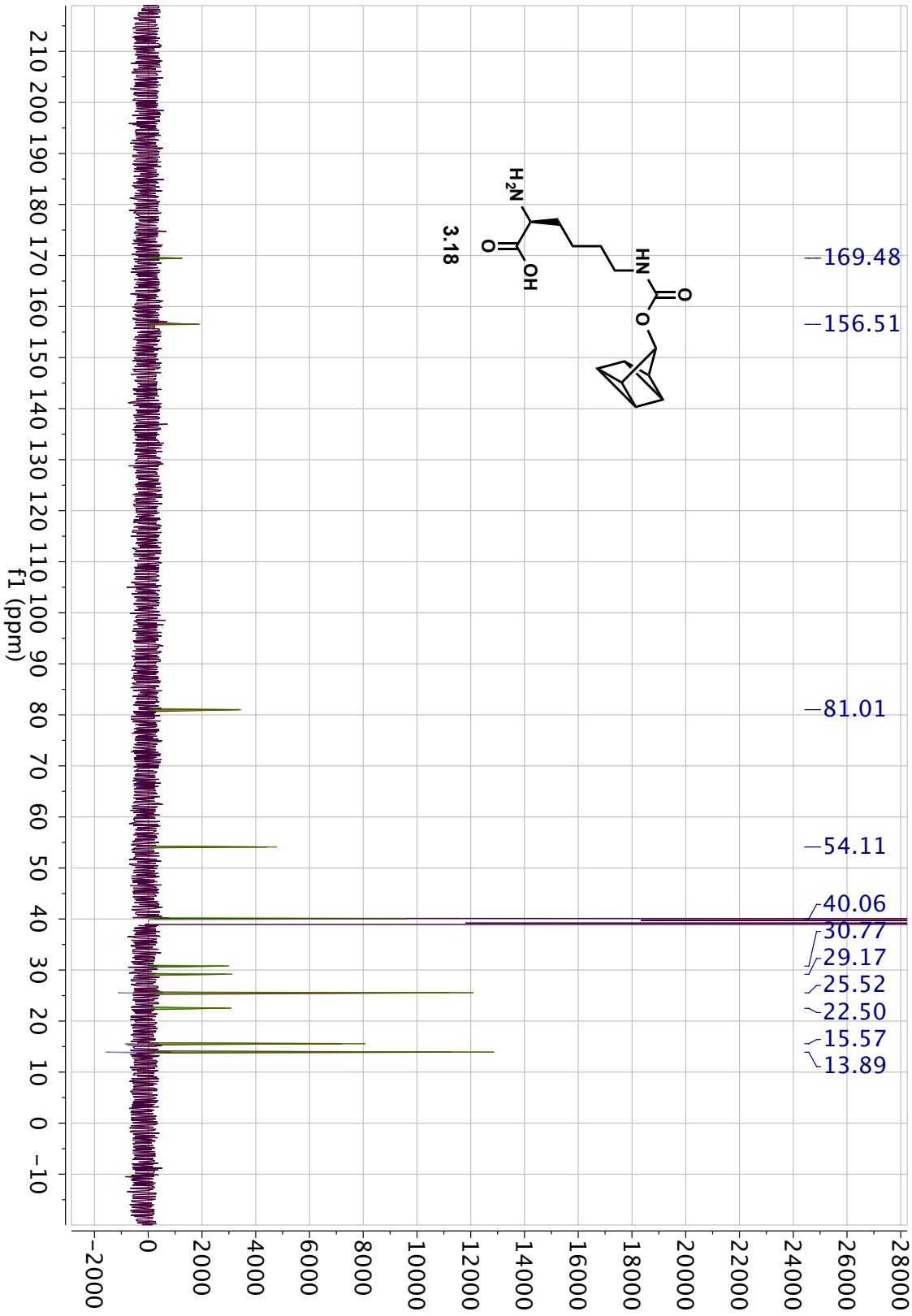

2.11
Me
Me
Me
N
O
7.593
7.582
7.578
7.447
7.434
7.425
7.414
7.404
7.358
7.355
7.344
7.270
7.261
7.047
2.710
2.421
2.391
0.93
1.93
0.93
0.86
0.92
3.00
2.88
2.98
9.0
8.5
8.0
7.5
7.0
6.5
6.0
5.5
5.0
4.5
4.0
3.5
3.0
2.5
2.0
1.5
1.0
0.5
ppm

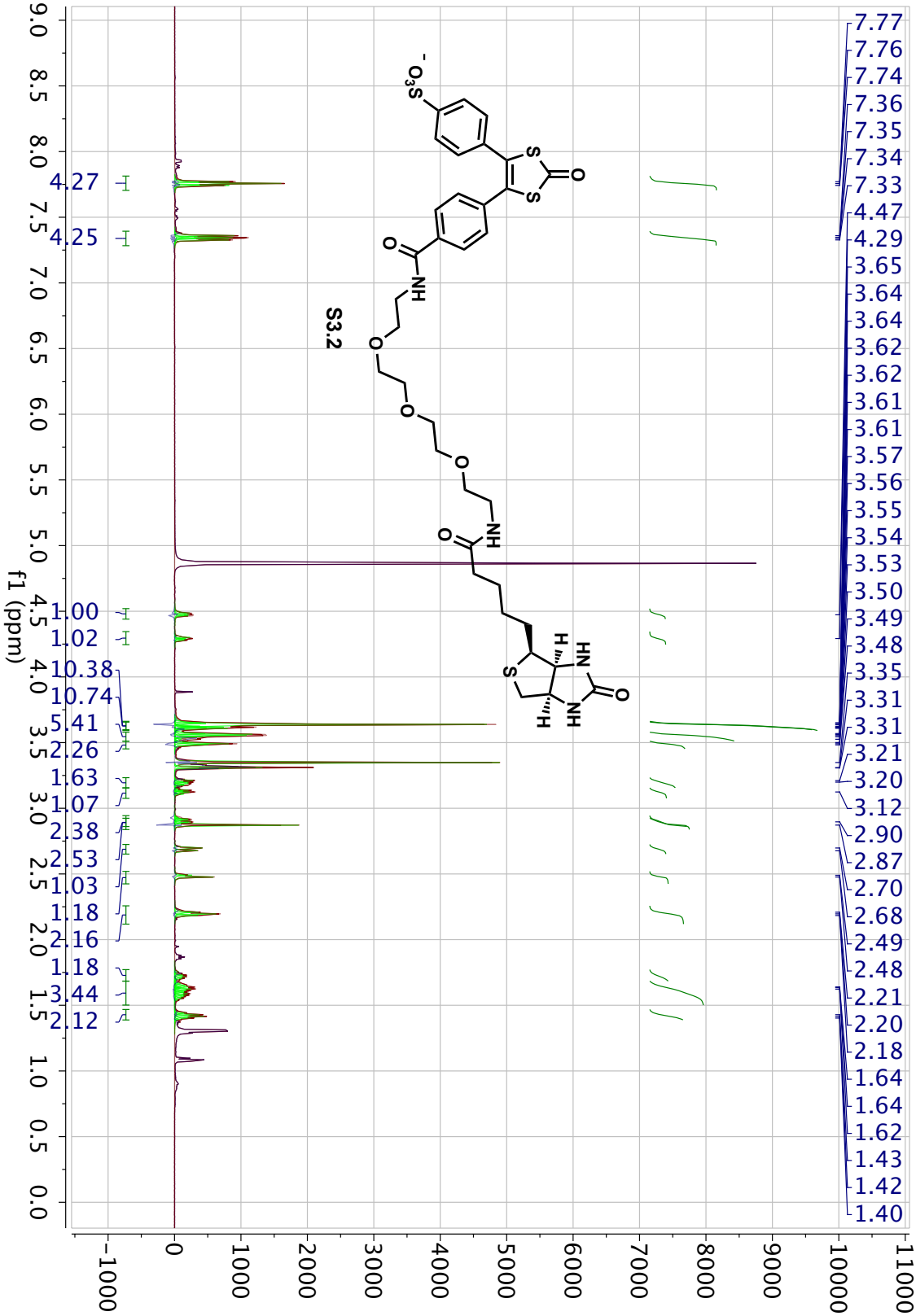

Me
Me
Me
N
O
2.11
176.88
156.48
149.00
139.96
137.38
129.81
129.24
128.33
127.40
126.17
125.42
122.75
119.26
110.27
108.86
77.17
76.96
76.75
38.64
21.47
21.28
210 200 190 180 170 160 150 140 130 120 110 100 90 80 70 60 50 40 30 20 10 0
ppm

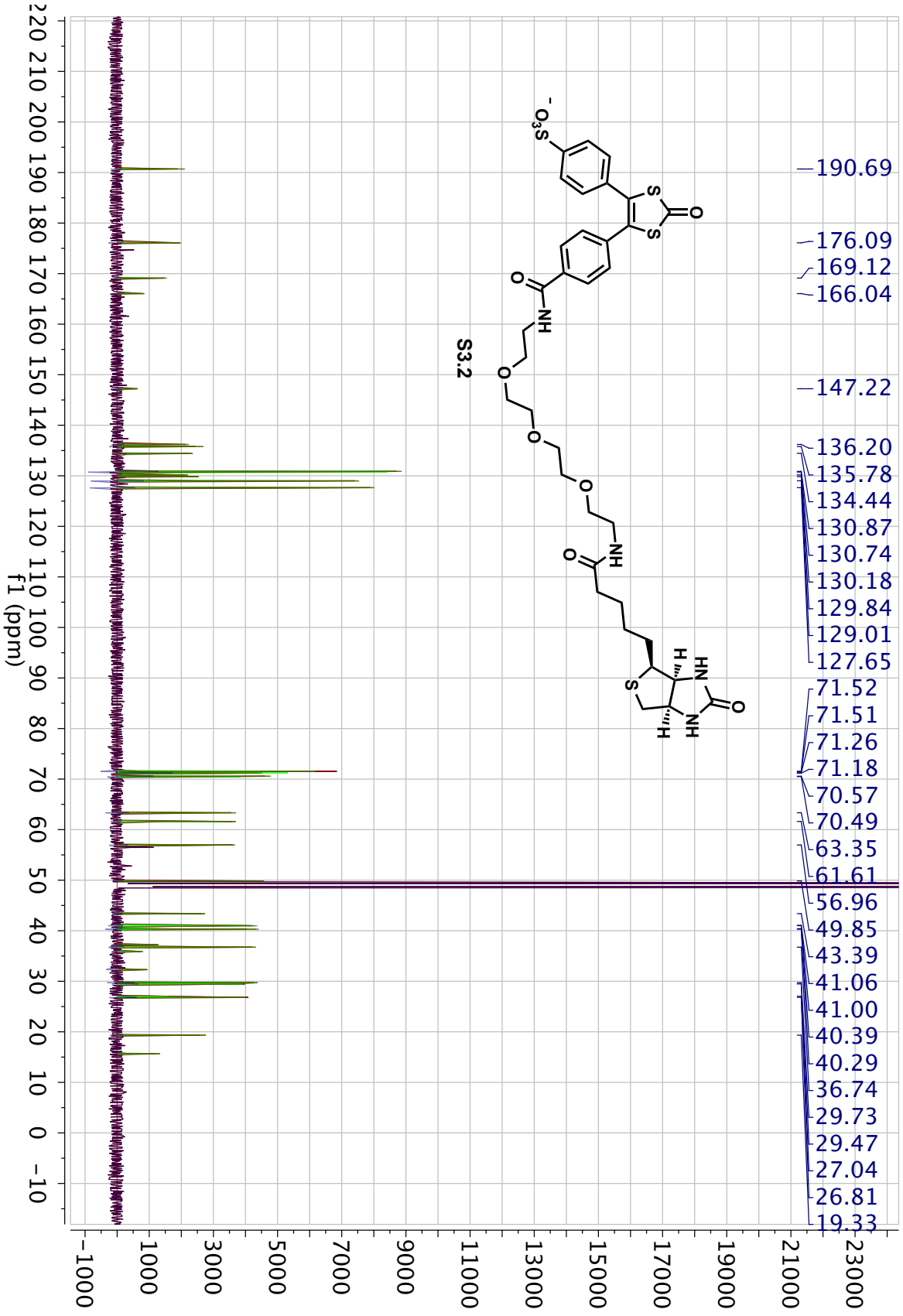

Fmoc-QCaa
FmocHN
OH
O
HN
O
O
O
f1 (ppm)
2.00
1.77
2.11
2.08
0.98
1.80
1.02
0.93
2.12
0.95
3.15
8.30
7.9647
7.7858
7.7733
7.6845
7.6721
7.6657
7.6531
7.3888
7.3764
7.3639
7.3152
7.3127
7.3026
7.3003
7.2879
5.4843
5.4816
5.4789
4.9193
4.3480
4.3362
4.3340
4.3224
4.2077
3.1403
3.1290
3.1172
2.9719
2.8466
1.7432
1.7374
1.7335
1.7283
1.5606
1.5554
1.5509
1.5464
1.5404
1.4647
1.4566
1.4534
1.4502
1.4470
1.4439
1.4396

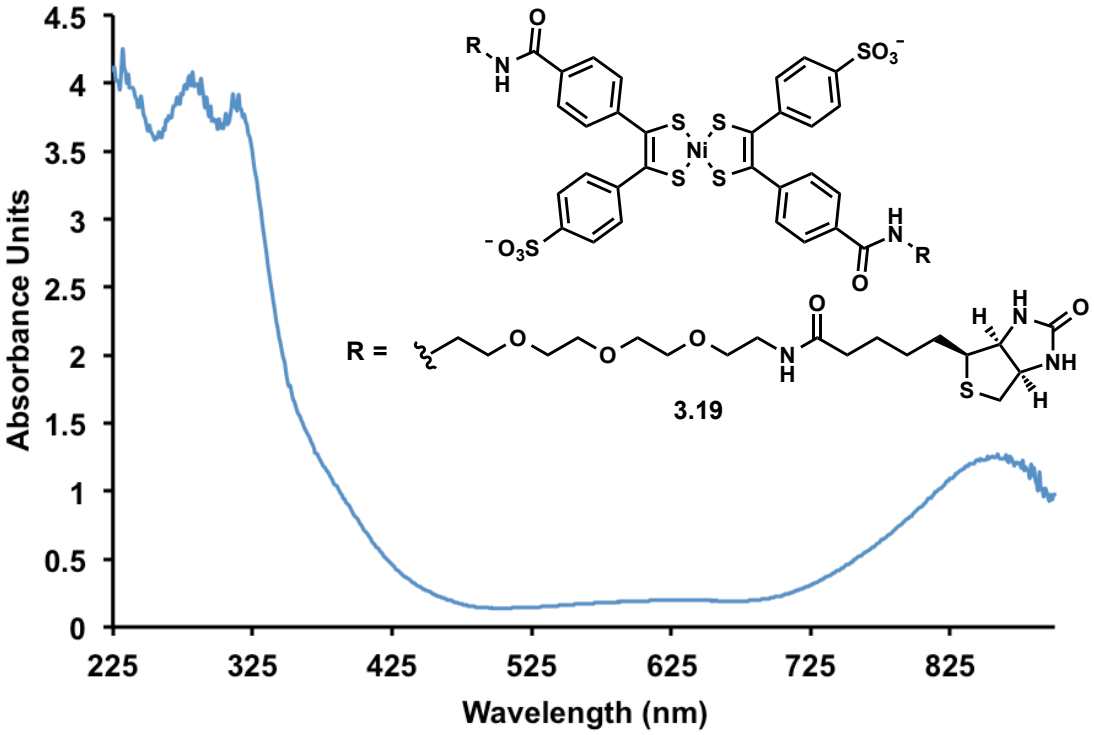

Fmoc-QCaa
FmocHN
OH
O
HN
O
O
175.97
164.82
159.63
158.66
145.33
145.14
142.55
142.53
128.76
128.75
128.15
128.13
126.27
126.24
120.89
120.88
83.67
67.93
55.28
49.85
48.41
41.35
36.93
32.33
31.64
30.45
26.84
26.83
24.15
16.76
15.26
f1 (ppm)

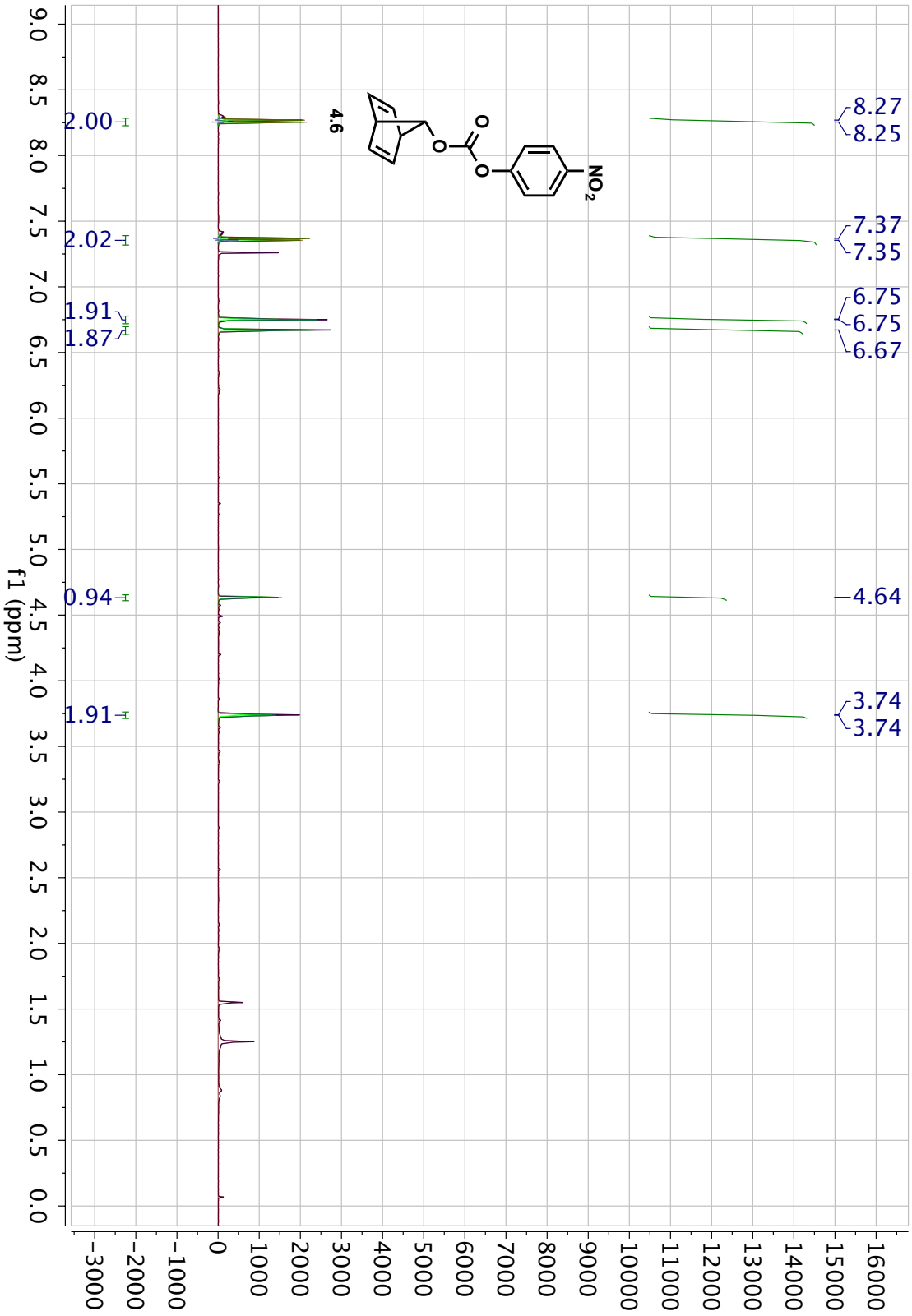

3.18
1.00
1.07
1.96
3.80
1.86
3.74
3.74
2.34
5.4952
4.7912
4.7880
3.6968
3.1479
3.1365
3.1250
1.8452
1.8096
1.7989
1.6305
1.5325
1.5203
1.4892
1.3793
f1 (ppm)

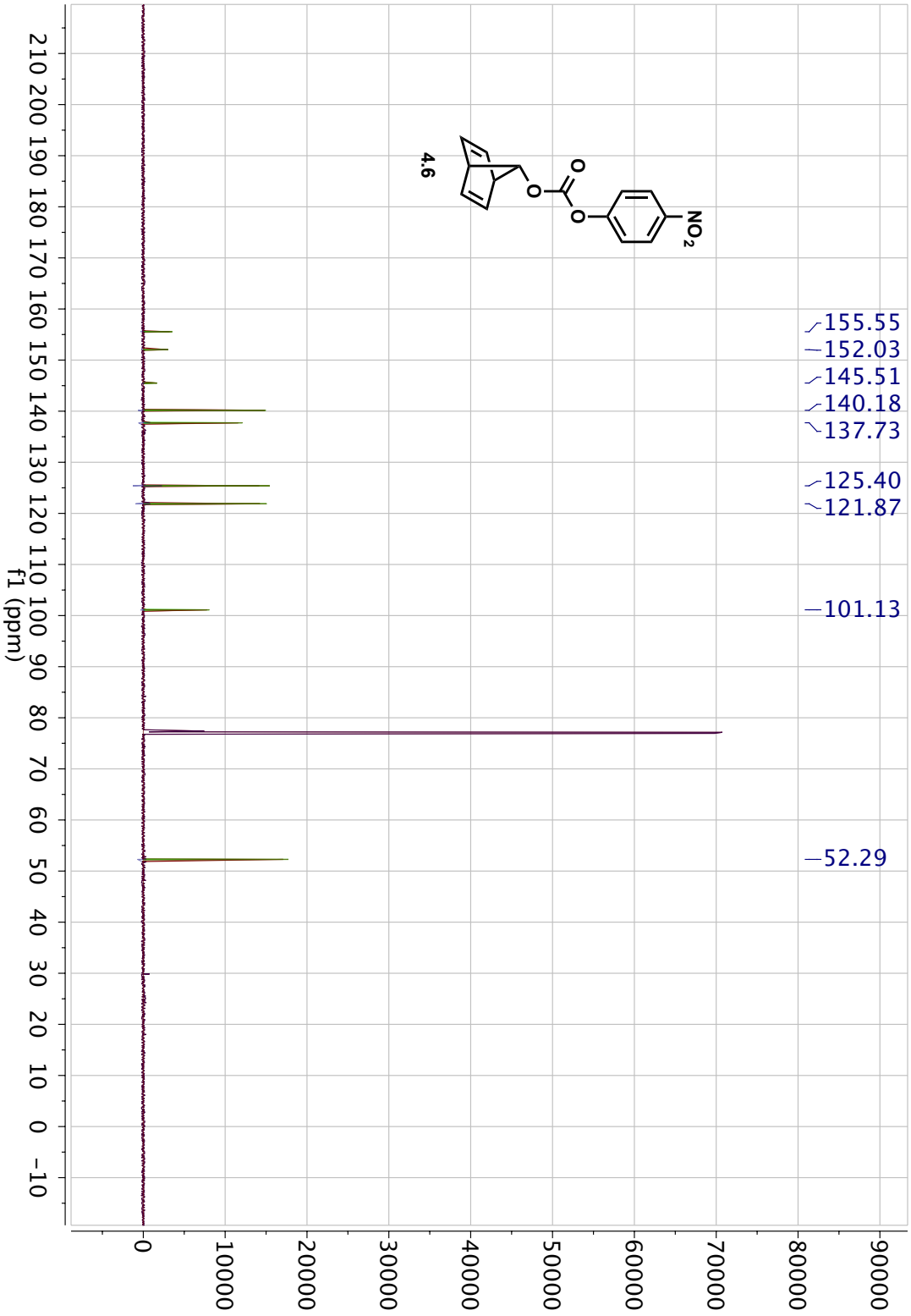

3.18
169.48
156.51
81.01
54.11
40.06
30.77
29.17
25.52
22.50
15.57
13.89
f1 (ppm)

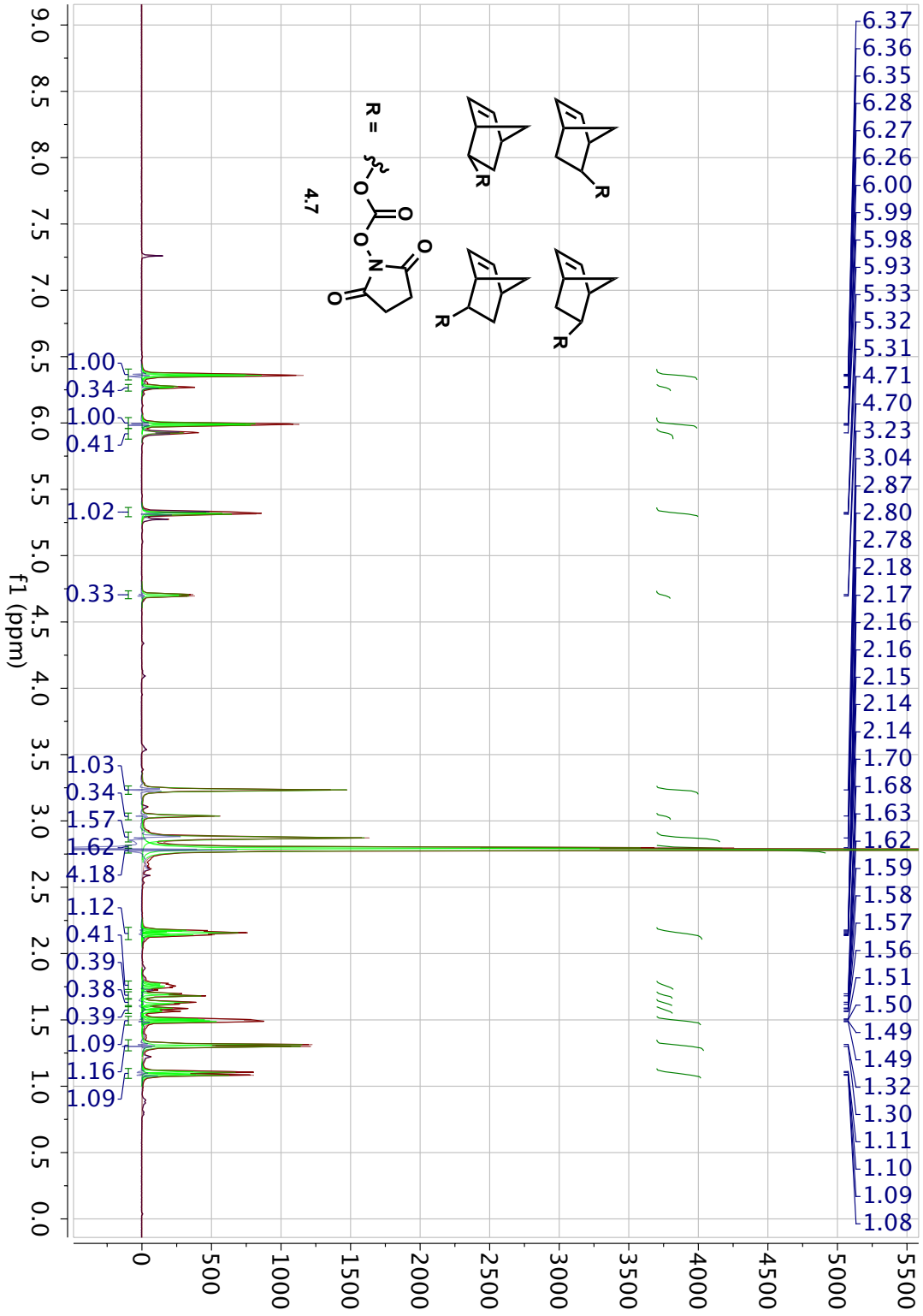

S3.2
f1 (ppm)

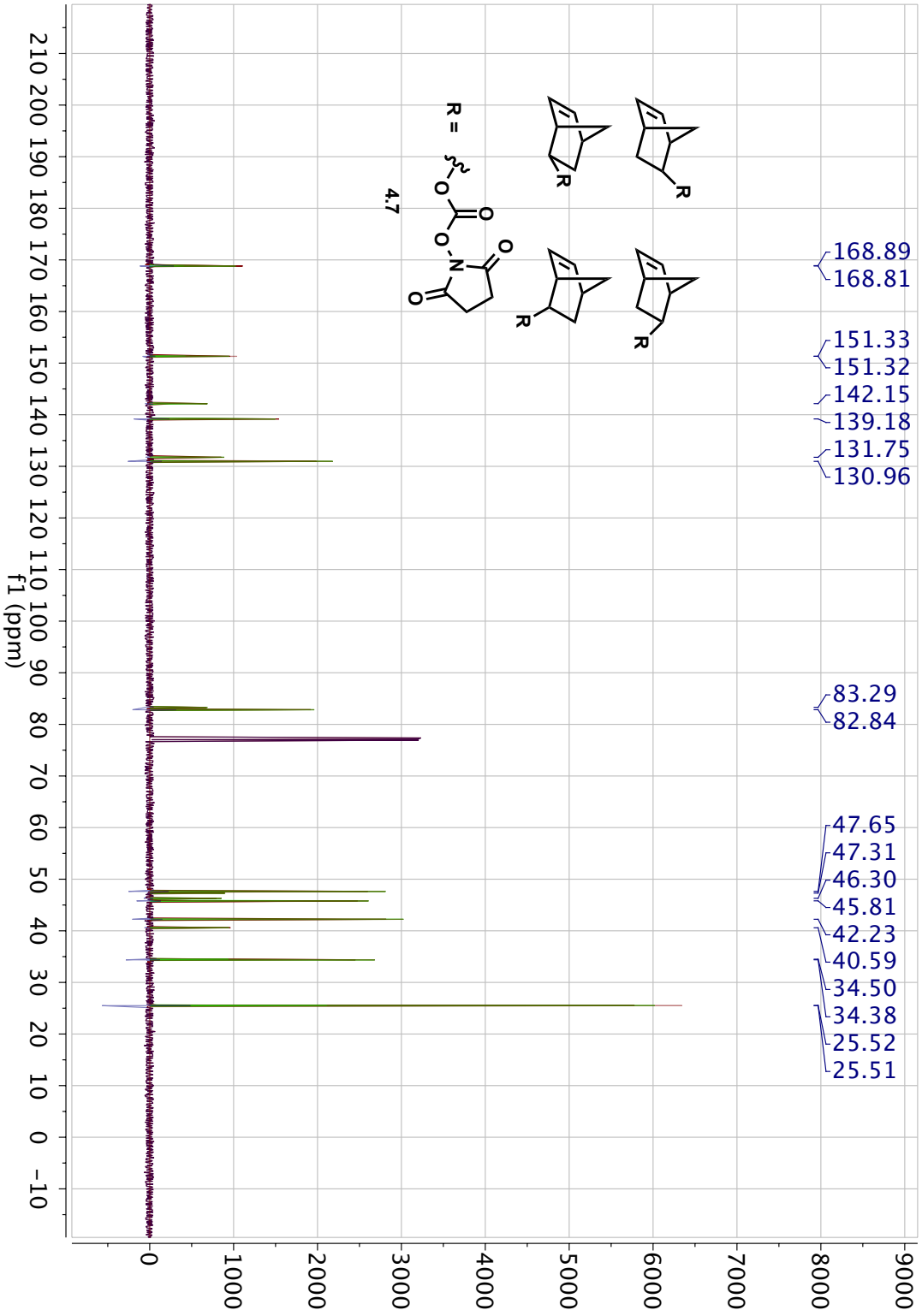

S3.2
190.69
176.09
169.12
166.04
147.22
136.20
135.78
134.44
130.87
130.74
130.18
129.84
129.01
127.65
71.52
71.51
71.26
71.18
70.57
70.49
63.35
61.61
56.96
49.85
43.39
41.06
41.00
40.39
40.29
36.74
29.73
29.47
27.04
26.81
19.33
f1 (ppm)


Absorbance Units
4.5
4
3.5
3
2.5
2
1.5
1
0.5
0
225
325
425
525
625
725
825
Wavelength (nm)
R =
3.19


4.6
NO2
2.00
2.02
1.91
1.87
0.94
1.91
8.27
8.25
7.37
7.35
6.75
6.75
6.67
4.64
3.74
3.74
f1 (ppm)


4.6
O
O
O
NO2
155.55
152.03
145.51
140.18
137.73
125.40
121.87
101.13
52.29
f1 (ppm)
210 200 190 180 170 160 150 140 130 120 110 100 90 80 70 60 50 40 30 20 10 0 -10
0 10000 20000 30000 40000 50000 60000 70000 80000 90000


f1 (ppm)
9.0 8.5 8.0 7.5 7.0 6.5 6.0 5.5 5.0 4.5 4.0 3.5 3.0 2.5 2.0 1.5 1.0 0.5 0.0
0 500 1000 1500 2000 2500 3000 3500 4000 4500 5000 5500
1.00 0.34 1.00 0.41 1.02 0.33 1.03 0.34 1.57 1.62 4.18 1.12 0.41 0.39 0.38 0.39 1.09 1.16 1.09
6.37 6.36 6.35 6.28 6.27 6.26 6.00 5.99 5.98 5.93 5.33 5.32 5.31 4.71 4.70 3.23 3.04 2.87 2.80 2.78 2.18 2.17 2.16 2.16 2.15 2.14 2.14 1.70 1.68 1.63 1.62 1.59 1.58 1.57 1.56 1.51 1.50 1.49 1.49 1.32 1.30 1.11 1.10 1.09 1.08
R =
4.7
R


168.89
168.81
151.33
151.32
142.15
139.18
131.75
130.96
83.29
82.84
47.65
47.31
46.30
45.81
42.23
40.59
34.50
34.38
25.52
25.51
R =
4.7
f1 (ppm)

Appendix B:
X-Ray Crystallography Data*

* All X-ray crystal structures were solved by Antonio DiPasquale at the UC Berkeley Small Molecule X-ray Crystallography Facility.

Monofluorinated cyclooctyne (MOFO, 2.21)

A colorless prism 0.12 x 0.10 x 0.05 mm in size was mounted on a Cryoloop with Paratone oil. Data were collected in a nitrogen gas stream at 100(2) K using phi and omega scans. Crystal-to-detector distance was 60 mm and exposure time was 5 seconds per frame using a scan width of 1.0°. Data collection was 98.3% complete to 67.00° in θ. A total of 19815 reflections were collected covering the indices, -5<=*h*<=8, -26<=*k*<=26, -10<=*l*<=10. 2449 reflections were found to be symmetry independent, with an R_{int} of 0.0202. Indexing and unit cell refinement indicated a primitive, monoclinic lattice. The space group was found to be P2(1)/n (No. 14). The data were integrated using the Bruker SAINT software program and scaled using the SADABS software program. Solution by direct methods (SIR-2008) produced a complete heavy-atom phasing model consistent with the proposed structure. All non-hydrogen atoms were refined anisotropically by full-matrix least-squares (SHELXL-97). All hydrogen atoms were placed using a riding model. Their positions were constrained relative to their parent atom using the appropriate HFIX command in SHELXL-97.

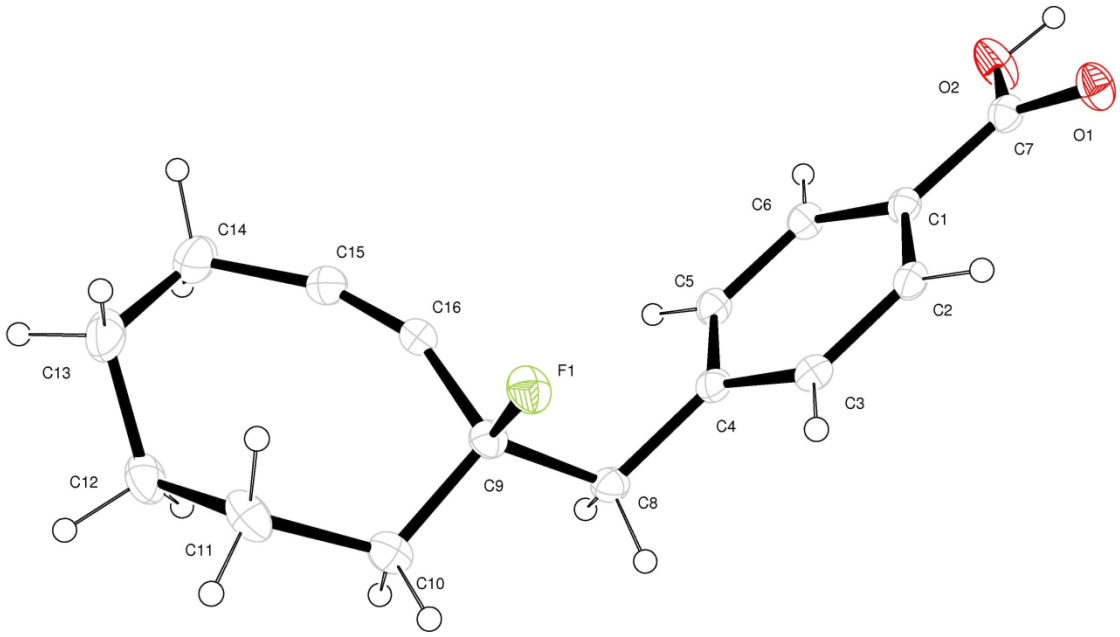


Figure B.1. X-ray crystal structure of monofluorinated cyclooctyne (MOFO, **2.21**).

Table B.1. Crystal data and structure refinement for MOFO (**2.21**).

Empirical formula	C16 H17 F O2
Formula weight	260.30
Temperature	100(2) K
Wavelength	1.54178 Å
Crystal system	Monoclinic
Space group	P2(1)/n
Unit cell dimensions	a = 7.3196(4) Å α= 90°.
	b = 22.0005(12) Å β= 98.230(2)°.
	c = 8.5948(5) Å γ = 90°.
Volume	1369.81(13) $Å^3$
Z	4
Density (calculated)	1.262 Mg/m^3
Absorption coefficient	0.746 mm^{-1}
F(000)	552
Crystal size	0.12 x 0.10 x 0.05 mm^3
Crystal color/habit	colorless prism
Theta range for data collection	4.02 to 68.10°.
Index ranges	-5<=h<=8, -26<=k<=26, -10<=l<=10
Reflections collected	19815
Independent reflections	2449 [R(int) = 0.0202]
Completeness to theta = 67.00°	98.3 %
Absorption correction	Semi-empirical from equivalents
Max. and min. transmission	0.9636 and 0.9158
Refinement method	Full-matrix least-squares on F^2
Data / restraints / parameters	2449 / 0 / 173
Goodness-of-fit on F^2	1.074
Final R indices [I>2sigma(I)]	R1 = 0.0428, wR2 = 0.1064
R indices (all data)	R1 = 0.0436, wR2 = 0.1071
Largest diff. peak and hole	0.413 and -0.180 $e.Å^{-3}$

Table B.2. Atomic coordinates (x 10^4) and equivalent isotropic displacement parameters ($Å^2$x 10^3) for MOFO (**2.21**). U(eq) is defined as one third of the trace of the orthogonalized U^{ij} tensor.

x	y	z	U(eq)	
C(1)	6793(2)	1026(1)	3472(2)	24(1)
C(2)	4927(2)	876(1)	3361(2)	25(1)
C(3)	3606(2)	1283(1)	2700(2)	26(1)
C(4)	4106(2)	1849(1)	2153(2)	25(1)
C(5)	5970(2)	1997(1)	2291(2)	27(1)
C(6)	7311(2)	1591(1)	2938(2)	26(1)
C(7)	8188(2)	580(1)	4156(2)	26(1)
C(8)	2644(2)	2287(1)	1429(2)	28(1)
C(9)	1949(2)	2715(1)	2609(2)	27(1)
C(10)	271(2)	3084(1)	1872(2)	33(1)
C(11)	-415(3)	3581(1)	2895(2)	40(1)
C(12)	430(3)	4229(1)	2850(2)	42(1)
C(13)	1762(3)	4449(1)	4277(2)	49(1)
C(14)	3793(3)	4275(1)	4288(3)	51(1)
C(15)	3825(2)	3634(1)	3866(2)	37(1)
C(16)	3298(2)	3149(1)	3371(2)	31(1)
O(1)	7769(2)	102(1)	4754(1)	33(1)
O(2)	9900(2)	731(1)	4069(2)	42(1)
F(1)	1354(1)	2345(1)	3800(1)	34(1)

Table B.3. Bond lengths [Å] and angles [°] for MOFO (**2.21**).

C(1)-C(2)	1.395(2)	C(9)-C(10)	1.532(2)
C(1)-C(6)	1.396(2)	C(10)-C(11)	1.532(2)
C(1)-C(7)	1.477(2)	C(10)-H(10A)	0.9900
C(2)-C(3)	1.380(2)	C(10)-H(10B)	0.9900
C(2)-H(2)	0.9500	C(11)-C(12)	1.557(3)
C(3)-C(4)	1.397(2)	C(11)-H(11A)	0.9900
C(3)-H(3)	0.9500	C(11)-H(11B)	0.9900
C(4)-C(5)	1.391(2)	C(12)-C(13)	1.532(3)
C(4)-C(8)	1.506(2)	C(12)-H(12A)	0.9900
C(5)-C(6)	1.384(2)	C(12)-H(12B)	0.9900
C(5)-H(5)	0.9500	C(13)-C(14)	1.534(3)
C(6)-H(6)	0.9500	C(13)-H(13A)	0.9900
C(7)-O(1)	1.2279(18)	C(13)-H(13B)	0.9900
C(7)-O(2)	1.309(2)	C(14)-C(15)	1.458(2)
C(8)-C(9)	1.524(2)	C(14)-H(14A)	0.9900
C(8)-H(8A)	0.9900	C(14)-H(14B)	0.9900
C(8)-H(8B)	0.9900	C(15)-C(16)	1.192(2)
C(9)-F(1)	1.4245(16)	O(2)-H(2A)	0.8400
C(9)-C(16)	1.459(2)		

C(2)-C(1)-C(6)	119.83(14)	C(4)-C(5)-H(5)	119.5
C(2)-C(1)-C(7)	119.01(13)	C(5)-C(6)-C(1)	119.74(14)
C(6)-C(1)-C(7)	121.15(14)	C(5)-C(6)-H(6)	120.1
C(3)-C(2)-C(1)	119.77(14)	C(1)-C(6)-H(6)	120.1
C(3)-C(2)-H(2)	120.1	O(1)-C(7)-O(2)	122.73(14)
C(1)-C(2)-H(2)	120.1	O(1)-C(7)-C(1)	122.37(14)
C(2)-C(3)-C(4)	121.00(14)	O(2)-C(7)-C(1)	114.90(13)
C(2)-C(3)-H(3)	119.5	C(4)-C(8)-C(9)	113.93(12)
C(4)-C(3)-H(3)	119.5	C(4)-C(8)-H(8A)	108.8
C(5)-C(4)-C(3)	118.71(14)	C(9)-C(8)-H(8A)	108.8
C(5)-C(4)-C(8)	121.02(13)	C(4)-C(8)-H(8B)	108.8
C(3)-C(4)-C(8)	120.27(14)	C(9)-C(8)-H(8B)	108.8
C(6)-C(5)-C(4)	120.93(14)	H(8A)-C(8)-H(8B)	107.7
C(6)-C(5)-H(5)	119.5	F(1)-C(9)-C(16)	107.99(12)

F(1)-C(9)-C(8)	106.87(12)	C(15)-C(16)-C(9)	155.33(17)
C(16)-C(9)-C(8)	115.70(13)	C(7)-O(2)-H(2A)	109.5
F(1)-C(9)-C(10)	106.88(12)		
C(16)-C(9)-C(10)	106.91(13)		
C(8)-C(9)-C(10)	112.10(13)		
C(9)-C(10)-C(11)	116.70(14)		
C(9)-C(10)-H(10A)	108.1		
C(11)-C(10)-H(10A)	108.1		
C(9)-C(10)-H(10B)	108.1		
C(11)-C(10)-H(10B)	108.1		
H(10A)-C(10)-H(10B)	107.3		
C(10)-C(11)-C(12)	118.40(15)		
C(10)-C(11)-H(11A)	107.7		
C(12)-C(11)-H(11A)	107.7		
C(10)-C(11)-H(11B)	107.7		
C(12)-C(11)-H(11B)	107.7		
H(11A)-C(11)-H(11B)	107.1		
C(13)-C(12)-C(11)	118.63(15)		
C(13)-C(12)-H(12A)	107.7		
C(11)-C(12)-H(12A)	107.7		
C(13)-C(12)-H(12B)	107.7		
C(11)-C(12)-H(12B)	107.7		
H(12A)-C(12)-H(12B)	107.1		
C(12)-C(13)-C(14)	115.52(16)		
C(12)-C(13)-H(13A)	108.4		
C(14)-C(13)-H(13A)	108.4		
C(12)-C(13)-H(13B)	108.4		
C(14)-C(13)-H(13B)	108.4		
H(13A)-C(13)-H(13B)	107.5		
C(15)-C(14)-C(13)	106.89(17)		
C(15)-C(14)-H(14A)	110.3		
C(13)-C(14)-H(14A)	110.3		
C(15)-C(14)-H(14B)	110.3		
C(13)-C(14)-H(14B)	110.3		
H(14A)-C(14)-H(14B)	108.6		
C(16)-C(15)-C(14)	159.9(2)		

Table B.4. Anisotropic displacement parameters ($Å^2 x\ 10^3$) for MOFO (**2.21**). The anisotropic displacement factor exponent takes the form: $-2\pi^2[\ h^2 a^{*2} U^{11} + ... + 2\ h\ k\ a^*\ b^*\ U^{12}\ ]$

U^{11}	U^{22}	U^{33}	U^{23}	U^{13}	U^{12}	
C(1)	29(1)	23(1)	21(1)	-2(1)	6(1)	-1(1)
C(2)	32(1)	21(1)	23(1)	-2(1)	6(1)	-4(1)
C(3)	26(1)	27(1)	24(1)	-3(1)	4(1)	-4(1)
C(4)	31(1)	24(1)	19(1)	-2(1)	3(1)	0(1)
C(5)	34(1)	23(1)	25(1)	2(1)	6(1)	-5(1)
C(6)	27(1)	26(1)	26(1)	0(1)	6(1)	-4(1)
C(7)	30(1)	25(1)	25(1)	-2(1)	7(1)	-2(1)
C(8)	32(1)	26(1)	24(1)	2(1)	0(1)	-3(1)
C(9)	31(1)	25(1)	25(1)	6(1)	4(1)	-2(1)
C(10)	29(1)	33(1)	35(1)	7(1)	4(1)	-1(1)
C(11)	38(1)	43(1)	41(1)	15(1)	11(1)	12(1)
C(12)	59(1)	34(1)	34(1)	10(1)	10(1)	16(1)
C(13)	82(2)	31(1)	35(1)	2(1)	8(1)	14(1)
C(14)	71(2)	30(1)	50(1)	-7(1)	-5(1)	-2(1)
C(15)	40(1)	33(1)	37(1)	-1(1)	-5(1)	1(1)
C(16)	32(1)	29(1)	31(1)	1(1)	-2(1)	5(1)
O(1)	30(1)	26(1)	45(1)	9(1)	8(1)	0(1)
O(2)	26(1)	37(1)	65(1)	22(1)	10(1)	3(1)
F(1)	42(1)	30(1)	31(1)	9(1)	10(1)	2(1)

Table B.5. Hydrogen coordinates (x 10^4) and isotropic displacement parameters ($Å^2$x 10^3) for MOFO (**2.21**).

x	y	z	U(eq)	
H(2)	4567	495	3740	30
H(3)	2337	1178	2615	31
H(5)	6327	2382	1935	32
H(6)	8580	1696	3019	31
H(8A)	1586	2052	888	33
H(8B)	3152	2532	625	33
H(10A)	-760	2797	1558	39
H(10B)	576	3276	900	39
H(11A)	-199	3438	3999	48
H(11B)	-1767	3617	2592	48
H(12A)	1087	4250	1922	51
H(12B)	-605	4522	2671	51
H(13A)	1347	4283	5239	59
H(13B)	1677	4898	4331	59
H(14A)	4348	4525	3519	62
H(14B)	4500	4342	5344	62
H(2A)	10610	456	4471	63

Biarylazacyclooctynone (BARAC, 2.1)

A colorless plate 0.12 x 0.10 x 0.02 mm in size was mounted on a Cryoloop with Paratone oil. Data were collected in a nitrogen gas stream at 100(2) K using phi and omega scans. Crystal-to-detector distance was 60 mm and exposure time was 5 seconds per frame using a scan width of 1.0°. Data collection was 99.5% complete to 67.00° in θ. A total of 14537 reflections were collected covering the indices, -8<=*h*<=8, -6<=*k*<=7, -29<=*l*<=29. 2034 reflections were found to be symmetry independent, with an R_{int} of 0.0343. Indexing and unit cell refinement indicated a primitive, monoclinic lattice. The space group was found to be P2(1)/c (No. 14). The data were integrated using the Bruker SAINT software program and scaled using the SADABS software program. Solution by direct methods (SHELXS-97) produced a complete heavy-atom phasing model consistent with the proposed structure. All non-hydrogen atoms were refined anisotropically by full-matrix least-squares (SHELXL-97). All hydrogen atoms were placed using a riding model. Their positions were constrained relative to their parent atom using the appropriate HFIX command in SHELXL-97.

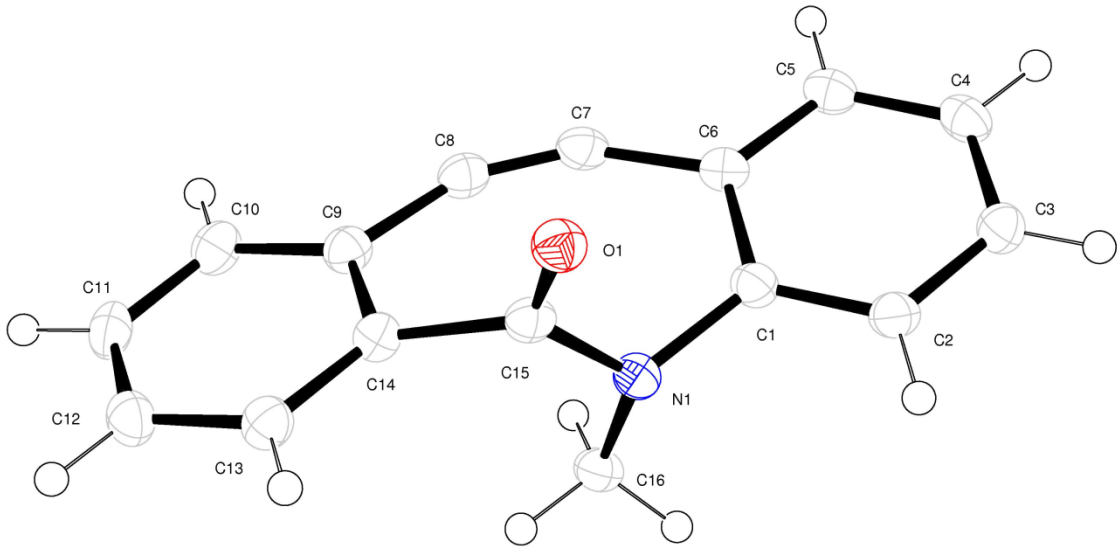


Figure B.2. X-ray crystal structure of biarylazacyclooctynone (BARAC, **2.1**).

Table B.6. Crystal data and structure refinement for BARAC (**2.1**).

Empirical formula	C16 H11 N O
Formula weight	233.26
Temperature	100(2) K
Wavelength	1.54178 Å
Crystal system	Monoclinic
Space group	P2(1)/c
Unit cell dimensions	a = 7.0936(4) Å α= 90°.
	b = 6.4862(3) Å β= 90.040(3)°.
	c = 24.4944(12) Å γ = 90°.
Volume	1127.00(10) $Å^3$
Z	4
Density (calculated)	1.375 Mg/m^3
Absorption coefficient	0.682 mm^{-1}
F(000)	488
Crystal size	0.12 x 0.10 x 0.02 mm^3
Crystal color/habit	colorless plate
Theta range for data collection	1.80 to 67.95°.
Index ranges	-8<=h<=8, -6<=k<=7, -29<=l<=29
Reflections collected	14537
Independent reflections	2034 [R(int) = 0.0343]
Completeness to theta = 67.00°	99.5 %
Absorption correction	Semi-empirical from equivalents
Max. and min. transmission	0.9865 and 0.9226
Refinement method	Full-matrix least-squares on F^2
Data / restraints / parameters	2034 / 0 / 165
Goodness-of-fit on F^2	1.060
Final R indices [I>2sigma(I)]	R1 = 0.0302, wR2 = 0.0761
R indices (all data)	R1 = 0.0335, wR2 = 0.0784
Largest diff. peak and hole	0.222 and -0.165 $e.Å^{-3}$

Table B.7. Bond lengths [Å] and angles [°] for BARAC (**2.1**).

C(1)-C(2)	1.379(2)	C(10)-C(11)	1.386(2)
C(1)-C(6)	1.421(2)	C(10)-H(10)	0.9500
C(1)-N(1)	1.4463(19)	C(11)-C(12)	1.385(3)
C(2)-C(3)	1.389(2)	C(11)-H(11)	0.9500
C(2)-H(2)	0.9500	C(12)-C(13)	1.392(2)
C(3)-C(4)	1.385(2)	C(12)-H(12)	0.9500
C(3)-H(3)	0.9500	C(13)-C(14)	1.383(2)
C(4)-C(5)	1.384(2)	C(13)-H(13)	0.9500
C(4)-H(4)	0.9500	C(14)-C(15)	1.519(2)
C(5)-C(6)	1.392(2)	C(15)-O(1)	1.218(2)
C(5)-H(5)	0.9500	C(15)-N(1)	1.379(2)
C(6)-C(7)	1.431(2)	C(16)-N(1)	1.473(2)
C(7)-C(8)	1.206(2)	C(16)-H(16A)	0.9800
C(8)-C(9)	1.435(2)	C(16)-H(16B)	0.9800
C(9)-C(10)	1.395(2)	C(16)-H(16C)	0.9800
C(9)-C(14)	1.422(2)		

C(2)-C(1)-C(6)	120.01(15)	C(5)-C(6)-C(7)	126.97(14)
C(2)-C(1)-N(1)	122.69(14)	C(1)-C(6)-C(7)	114.08(14)
C(6)-C(1)-N(1)	117.19(13)	C(8)-C(7)-C(6)	153.02(16)
C(1)-C(2)-C(3)	120.09(15)	C(7)-C(8)-C(9)	153.07(16)
C(1)-C(2)-H(2)	120.0	C(10)-C(9)-C(14)	119.52(15)
C(3)-C(2)-H(2)	120.0	C(10)-C(9)-C(8)	127.25(15)
C(4)-C(3)-C(2)	120.32(15)	C(14)-C(9)-C(8)	113.23(14)
C(4)-C(3)-H(3)	119.8	C(11)-C(10)-C(9)	119.43(16)
C(2)-C(3)-H(3)	119.8	C(11)-C(10)-H(10)	120.3
C(5)-C(4)-C(3)	120.24(15)	C(9)-C(10)-H(10)	120.3
C(5)-C(4)-H(4)	119.9	C(12)-C(11)-C(10)	120.82(15)
C(3)-C(4)-H(4)	119.9	C(12)-C(11)-H(11)	119.6
C(4)-C(5)-C(6)	120.37(15)	C(10)-C(11)-H(11)	119.6
C(4)-C(5)-H(5)	119.8	C(11)-C(12)-C(13)	120.62(15)
C(6)-C(5)-H(5)	119.8	C(11)-C(12)-H(12)	119.7
C(5)-C(6)-C(1)	118.93(14)	C(13)-C(12)-H(12)	119.7

C(14)-C(13)-C(12)	119.46(16)
C(14)-C(13)-H(13)	120.3
C(12)-C(13)-H(13)	120.3
C(13)-C(14)-C(9)	120.14(15)
C(13)-C(14)-C(15)	124.82(15)
C(9)-C(14)-C(15)	114.75(14)
O(1)-C(15)-N(1)	121.14(15)
O(1)-C(15)-C(14)	121.36(15)
N(1)-C(15)-C(14)	117.27(14)
N(1)-C(16)-H(16A)	109.5
N(1)-C(16)-H(16B)	109.5
H(16A)-C(16)-H(16B)	109.5
N(1)-C(16)-H(16C)	109.5
H(16A)-C(16)-H(16C)	109.5
H(16B)-C(16)-H(16C)	109.5
C(15)-N(1)-C(1)	116.42(13)
C(15)-N(1)-C(16)	119.79(13)
C(1)-N(1)-C(16)	114.72(13)

Table B.8. Anisotropic displacement parameters ($Å^2 x\ 10^3$) for BARAC (**2.1**). The anisotropic displacement factor exponent takes the form: $-2\pi^2[\ h^2 a^{*2} U^{11} + ... + 2\ h\ k\ a^*\ b^*\ U^{12}\ ]$

U^{11}	U^{22}	U^{33}	U^{23}	U^{13}	U^{12}	
C(1)	23(1)	21(1)	22(1)	2(1)	1(1)	1(1)
C(2)	26(1)	21(1)	24(1)	1(1)	3(1)	3(1)
C(3)	24(1)	29(1)	21(1)	1(1)	3(1)	3(1)
C(4)	24(1)	26(1)	27(1)	8(1)	3(1)	2(1)
C(5)	26(1)	20(1)	30(1)	3(1)	0(1)	0(1)
C(6)	21(1)	20(1)	26(1)	0(1)	0(1)	1(1)
C(7)	26(1)	16(1)	29(1)	-1(1)	-2(1)	0(1)
C(8)	24(1)	19(1)	27(1)	-5(1)	-2(1)	-1(1)
C(9)	22(1)	24(1)	24(1)	-2(1)	0(1)	1(1)
C(10)	25(1)	29(1)	24(1)	-5(1)	-1(1)	-3(1)
C(11)	25(1)	37(1)	17(1)	-2(1)	0(1)	2(1)
C(12)	25(1)	30(1)	23(1)	5(1)	3(1)	1(1)
C(13)	25(1)	24(1)	24(1)	-1(1)	2(1)	-2(1)
C(14)	25(1)	24(1)	21(1)	-1(1)	1(1)	2(1)
C(15)	27(1)	16(1)	24(1)	-2(1)	1(1)	-1(1)
C(16)	26(1)	23(1)	25(1)	3(1)	2(1)	6(1)
N(1)	29(1)	19(1)	21(1)	2(1)	2(1)	1(1)
O(1)	24(1)	24(1)	25(1)	-1(1)	-1(1)	1(1)

Table B.9. Hydrogen coordinates (x 10^4) and isotropic displacement parameters ($Å^2$x 10^3) for BARAC (**2.1**).

x	y	z	U(eq)	
H(2)	3239	9772	5157	29
H(3)	3359	7285	5847	30
H(4)	2762	3833	5646	31
H(5)	2193	2811	4748	30
H(10)	1239	5777	2267	31
H(11)	1669	8500	1656	32
H(12)	3064	11560	1941	31
H(13)	4027	11981	2848	29
H(16A)	562	10837	3667	37
H(16B)	-55	10400	4285	37
H(16C)	-124	8583	3843	37

Dimethoxyazacyclooctyne (DIMAC, 2.20)

A colorless prism 0.12 x 0.08 x 0.04 mm in size was mounted on a Cryoloop with Paratone oil. Data were collected in a nitrogen gas stream at 150(2) K using phi and omega scans. Crystal-to-detector distance was 60 mm and exposure time was 5 seconds per frame using a scan width of 2.0°. Data collection was 99.8% complete to 67.00° in θ. A total of 16229 reflections were collected covering the indices, -6<=*h*<=6, -9<=*k*<=9, -17<=*l*<=17. 2383 reflections were found to be symmetry independent, with an R_{int} of 0.0357. Indexing and unit cell refinement indicated a primitive, monoclinic lattice. The space group was found to be P2(1) (No. 4). The data were integrated using the Bruker SAINT software program and scaled using the SADABS software program. Solution by direct methods (SIR-2008) produced a complete heavy-atom phasing model consistent with the proposed structure. All non-hydrogen atoms were refined anisotropically by full-matrix least-squares (SHELXL-97). All hydrogen atoms were placed using a riding model. Their positions were constrained relative to their parent atom using the appropriate HFIX command in SHELXL-97. Absolute stereochemistry was unambiguously determined to be *S* at both C2 and C3, respectively.

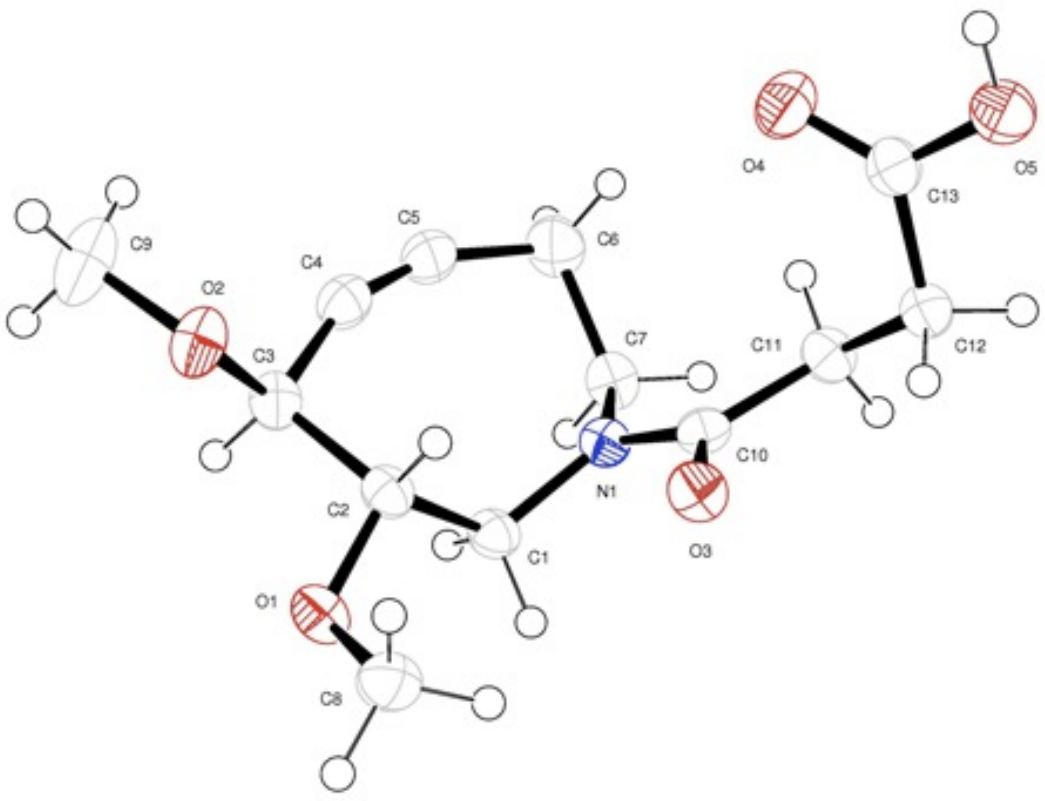


Figure B.3. X-ray crystal structure of dimethoxyazacyclooctyne (DIMAC, **2.20**).

Table B.10. Crystal data and structure refinement for **2.20**.

Empirical formula	C13 H19 N O5
Formula weight	269.29
Temperature	150(2) K
Wavelength	1.54178 Å
Crystal system	Monoclinic
Space group	P2(1)
Unit cell dimensions	a = 5.5553(2) Å α= 90°.
	b = 8.3543(3) Å β= 95.758(2)°.
	c = 14.6808(4) Å γ = 90°.
Volume	677.91(4) $Å^3$
Z	2
Density (calculated)	1.319 Mg/m^3
Absorption coefficient	0.848 mm^{-1}
F(000)	288
Crystal size	0.12 x 0.08 x 0.04 mm^3
Crystal color/habit	colorless prism
Theta range for data collection	3.03 to 68.08°.
Index ranges	-6<=h<=6, -9<=k<=9, -17<=l<=17
Reflections collected	16229
Independent reflections	2383 [R(int) = 0.0357]
Completeness to theta = 67.00°	99.8 %
Absorption correction	Semi-empirical from equivalents
Max. and min. transmission	0.9669 and 0.9051
Refinement method	Full-matrix least-squares on F^2
Data / restraints / parameters	2383 / 1 / 175
Goodness-of-fit on F^2	1.035
Final R indices [I>2sigma(I)]	R1 = 0.0317, wR2 = 0.0828
R indices (all data)	R1 = 0.0331, wR2 = 0.0841
Absolute structure parameter	-0.02(16)
Largest diff. peak and hole	0.168 and -0.122 $e.Å^{-3}$

Table B.11. Atomic coordinates (x 10^4) and equivalent isotropic displacement parameters ($Å^2$x 10^3) for **2.20**. U(eq) is defined as one third of the trace of the orthogonalized U^{ij} tensor.

x	y	z	U(eq)	
C(1)	8648(3)	10397(2)	2130(1)	28(1)
C(2)	11048(3)	10453(2)	1683(1)	27(1)
C(3)	11231(3)	9244(2)	906(1)	30(1)
C(4)	10346(3)	7704(2)	1235(1)	33(1)
C(5)	9337(3)	6820(2)	1703(1)	36(1)
C(6)	7987(4)	6339(2)	2468(1)	41(1)
C(7)	6780(3)	7889(2)	2767(1)	32(1)
C(8)	12407(3)	13124(2)	1910(1)	37(1)
C(9)	14068(4)	8197(3)	-29(1)	51(1)
C(10)	9797(3)	9560(2)	3690(1)	26(1)
C(11)	9370(3)	8545(2)	4517(1)	31(1)
C(12)	11367(3)	8691(2)	5307(1)	30(1)
C(13)	13372(3)	7505(2)	5253(1)	30(1)
N(1)	8505(2)	9242(2)	2887(1)	26(1)
O(1)	11274(2)	11993(1)	1290(1)	33(1)
O(2)	13677(2)	9206(2)	723(1)	35(1)
O(3)	11183(2)	10721(1)	3768(1)	32(1)
O(4)	13679(2)	6707(2)	4590(1)	41(1)
O(5)	14783(2)	7433(2)	6035(1)	42(1)

Table B.12. Bond lengths [Å] and angles [°] for **2.20**.

C(1)-N(1)	1.4801(19)	C(8)-H(8A)	0.9800
C(1)-C(2)	1.545(2)	C(8)-H(8B)	0.9800
C(1)-H(1A)	0.9900	C(8)-H(8C)	0.9800
C(1)-H(1B)	0.9900	C(9)-O(2)	1.422(2)
C(2)-O(1)	1.4211(19)	C(9)-H(9A)	0.9800
C(2)-C(3)	1.535(2)	C(9)-H(9B)	0.9800
C(2)-H(2)	1.0000	C(9)-H(9C)	0.9800
C(3)-O(2)	1.4118(19)	C(10)-O(3)	1.237(2)
C(3)-C(4)	1.476(2)	C(10)-N(1)	1.343(2)
C(3)-H(3)	1.0000	C(10)-C(11)	1.519(2)
C(4)-C(5)	1.187(2)	C(11)-C(12)	1.528(2)
C(5)-C(6)	1.468(3)	C(11)-H(11A)	0.9900
C(6)-C(7)	1.542(2)	C(11)-H(11B)	0.9900
C(6)-H(6A)	0.9900	C(12)-C(13)	1.499(2)
C(6)-H(6B)	0.9900	C(12)-H(12A)	0.9900
C(7)-N(1)	1.4805(19)	C(12)-H(12B)	0.9900
C(7)-H(7A)	0.9900	C(13)-O(4)	1.207(2)
C(7)-H(7B)	0.9900	C(13)-O(5)	1.3239(19)
C(8)-O(1)	1.415(2)	O(5)-H(5)	0.8400
N(1)-C(1)-C(2)	116.90(12)	C(4)-C(3)-C(2)	106.32(13)
N(1)-C(1)-H(1A)	108.1	O(2)-C(3)-H(3)	109.9
C(2)-C(1)-H(1A)	108.1	C(4)-C(3)-H(3)	109.9
N(1)-C(1)-H(1B)	108.1	C(2)-C(3)-H(3)	109.9
C(2)-C(1)-H(1B)	108.1	C(5)-C(4)-C(3)	157.53(16)
H(1A)-C(1)-H(1B)	107.3	C(4)-C(5)-C(6)	157.00(17)
O(1)-C(2)-C(3)	106.16(12)	C(5)-C(6)-C(7)	104.94(14)
O(1)-C(2)-C(1)	108.39(12)	C(5)-C(6)-H(6A)	110.8
C(3)-C(2)-C(1)	114.87(13)	C(7)-C(6)-H(6A)	110.8
O(1)-C(2)-H(2)	109.1	C(5)-C(6)-H(6B)	110.8
C(3)-C(2)-H(2)	109.1	C(7)-C(6)-H(6B)	110.8
C(1)-C(2)-H(2)	109.1	H(6A)-C(6)-H(6B)	108.8
O(2)-C(3)-C(4)	113.68(14)	N(1)-C(7)-C(6)	112.36(13)
O(2)-C(3)-C(2)	107.06(12)	N(1)-C(7)-H(7A)	109.1

C(6)-C(7)-H(7A)	109.1	C(1)-N(1)-C(7)	119.40(13)
N(1)-C(7)-H(7B)	109.1	C(8)-O(1)-C(2)	113.24(11)
C(6)-C(7)-H(7B)	109.1	C(3)-O(2)-C(9)	112.69(13)
H(7A)-C(7)-H(7B)	107.9	C(13)-O(5)-H(5)	109.5
O(1)-C(8)-H(8A)	109.5		
O(1)-C(8)-H(8B)	109.5		
H(8A)-C(8)-H(8B)	109.5		
O(1)-C(8)-H(8C)	109.5		
H(8A)-C(8)-H(8C)	109.5		
H(8B)-C(8)-H(8C)	109.5		
O(2)-C(9)-H(9A)	109.5		
O(2)-C(9)-H(9B)	109.5		
H(9A)-C(9)-H(9B)	109.5		
O(2)-C(9)-H(9C)	109.5		
H(9A)-C(9)-H(9C)	109.5		
H(9B)-C(9)-H(9C)	109.5		
O(3)-C(10)-N(1)	120.69(14)		
O(3)-C(10)-C(11)	120.58(13)		
N(1)-C(10)-C(11)	118.56(13)		
C(10)-C(11)-C(12)	113.78(13)		
C(10)-C(11)-H(11A)	108.8		
C(12)-C(11)-H(11A)	108.8		
C(10)-C(11)-H(11B)	108.8		
C(12)-C(11)-H(11B)	108.8		
H(11A)-C(11)-H(11B)	107.7		
C(13)-C(12)-C(11)	113.20(13)		
C(13)-C(12)-H(12A)	108.9		
C(11)-C(12)-H(12A)	108.9		
C(13)-C(12)-H(12B)	108.9		
C(11)-C(12)-H(12B)	108.9		
H(12A)-C(12)-H(12B)	107.8		
O(4)-C(13)-O(5)	123.71(16)		
O(4)-C(13)-C(12)	125.02(14)		
O(5)-C(13)-C(12)	111.27(13)		
C(10)-N(1)-C(1)	117.72(13)		
C(10)-N(1)-C(7)	122.58(13)		

Table B.13. Anisotropic displacement parameters ($Å^2 x\ 10^3$) for **2.20**. The anisotropic displacement factor exponent takes the form: $-2\pi^2[\ h^2 a^{*2} U^{11} + ... + 2\ h\ k\ a^*\ b^*\ U^{12}\ ]$

U^{11}	U^{22}	U^{33}	U^{23}	U^{13}	U^{12}	
C(1)	25(1)	30(1)	30(1)	3(1)	0(1)	4(1)
C(2)	23(1)	30(1)	28(1)	4(1)	0(1)	0(1)
C(3)	24(1)	38(1)	28(1)	1(1)	1(1)	0(1)
C(4)	33(1)	34(1)	32(1)	-6(1)	2(1)	2(1)
C(5)	44(1)	28(1)	36(1)	-5(1)	5(1)	-1(1)
C(6)	54(1)	30(1)	41(1)	-1(1)	7(1)	-12(1)
C(7)	28(1)	36(1)	32(1)	0(1)	0(1)	-7(1)
C(8)	42(1)	29(1)	41(1)	1(1)	7(1)	-1(1)
C(9)	34(1)	82(2)	38(1)	-21(1)	7(1)	-2(1)
C(10)	23(1)	25(1)	32(1)	-2(1)	3(1)	3(1)
C(11)	30(1)	32(1)	32(1)	2(1)	1(1)	-1(1)
C(12)	32(1)	29(1)	27(1)	1(1)	2(1)	1(1)
C(13)	29(1)	31(1)	30(1)	3(1)	5(1)	-4(1)
N(1)	22(1)	27(1)	28(1)	1(1)	2(1)	0(1)
O(1)	35(1)	31(1)	32(1)	6(1)	1(1)	-3(1)
O(2)	25(1)	50(1)	31(1)	-8(1)	3(1)	-2(1)
O(3)	32(1)	31(1)	33(1)	0(1)	0(1)	-6(1)
O(4)	40(1)	46(1)	37(1)	-7(1)	7(1)	4(1)
O(5)	38(1)	51(1)	36(1)	-1(1)	-3(1)	14(1)

Table B.14. Hydrogen coordinates (x 10^4) and isotropic displacement parameters ($Å^2$x 10^3) for **2.20**.

x	y	z	U(eq)	
H(1A)	8333	11480	2365	34
H(1B)	7328	10149	1647	34
H(2)	12426	10278	2166	33
H(3)	10188	9596	347	36
H(6A)	9091	5894	2977	50
H(6B)	6753	5523	2269	50
H(7A)	5440	8181	2301	39
H(7B)	6081	7694	3351	39
H(8A)	11491	13214	2445	56
H(8B)	12453	14168	1609	56
H(8C)	14061	12773	2108	56
H(9A)	13516	7111	93	77
H(9B)	15797	8175	-110	77
H(9C)	13161	8610	-586	77
H(11A)	9229	7410	4325	38
H(11B)	7812	8864	4737	38
H(12A)	12049	9786	5309	36
H(12B)	10652	8536	5892	36
H(5)	15935	6802	5978	63

Second generation difluorinated cyclooctyne (DIFO2, 2.22)

A colorless plate 0.12 x 0.10 x 0.06 mm in size was mounted on a Cryoloop with Paratone oil. Data were collected in a nitrogen gas stream at 100(2) K using phi and omega scans. Crystal-to-detector distance was 60 mm and exposure time was 5 seconds per frame using a scan width of 1.0°. Data collection was 97.7% complete to 67.00° in θ. A total of 20513 reflections were collected covering the indices, -9<=*h*<=9, -14<=*k*<=14, -15<=*l*<=17. 5166 reflections were found to be symmetry independent, with an R_{int} of 0.0163. Indexing and unit cell refinement indicated a primitive, triclinic lattice. The space group was found to be P-1 (No. 2). The data were integrated using the Bruker SAINT software program and scaled using the SADABS software program. Solution by direct methods (SIR-2008) produced a complete heavy-atom phasing model consistent with the proposed structure. All non-hydrogen atoms were refined anisotropically by full-matrix least-squares (SHELXL-97). All hydrogen atoms were placed using a riding model. Their positions were constrained relative to their parent atom using the appropriate HFIX command in SHELXL-97.

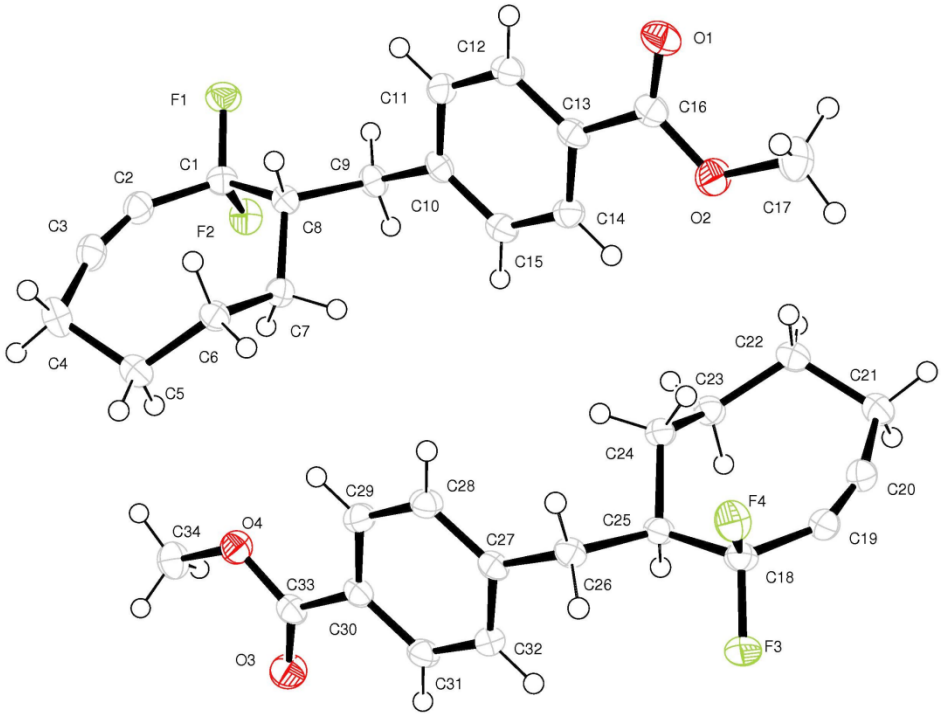


Figure B.4. X-ray crystal structure of second generation difluorinated cyclooctyne (DIFO2, **2.22**).

Table B.15. Crystal data and structure refinement for (DIFO2, **2.22**).

Empirical formula	C17 H18 F2 O2	
Formula weight	292.31	
Temperature	100(2) K	
Wavelength	1.54178 Å	
Crystal system	Triclinic	
Space group	P-1	
Unit cell dimensions	a = 8.2069(2) Å	α= 96.5440(10)°.
	b = 12.1823(4) Å	β= 95.0100(10)°.
	c = 14.7485(4) Å	γ = 93.4120(10)°.
Volume	1455.74(7) $Å^3$	
Z	4	
Density (calculated)	1.334 Mg/m^3	
Absorption coefficient	0.864 mm^{-1}	
F(000)	616	
Crystal size	0.12 x 0.10 x 0.06 mm^3	
Crystal color/habit	colorless plate	
Theta range for data collection	3.03 to 68.15°.	
Index ranges	-9<=h<=9, -14<=k<=14, -15<=l<=17	
Reflections collected	20513	
Independent reflections	5166 [R(int) = 0.0163]	
Completeness to theta = 67.00°	97.7 %	
Absorption correction	Semi-empirical from equivalents	
Max. and min. transmission	0.9500 and 0.9034	
Refinement method	Full-matrix least-squares on F^2	
Data / restraints / parameters	5166 / 0 / 381	
Goodness-of-fit on F^2	1.045	
Final R indices [I>2sigma(I)]	R1 = 0.0366, wR2 = 0.0979	
R indices (all data)	R1 = 0.0413, wR2 = 0.1025	
Largest diff. peak and hole	0.291 and -0.205 $e.Å^{-3}$	

Table B.16. Atomic coordinates (x 10^4) and equivalent isotropic displacement parameters ($Å^2$x 10^3) for (DIFO2, **2.22**). U(eq) is defined as one third of the trace of the orthogonalized U^{ij} tensor.

x	y	z	U(eq)	
C(1)	-1339(2)	-3007(1)	3718(1)	25(1)
C(2)	-2163(2)	-3768(1)	2966(1)	27(1)
C(3)	-2691(2)	-3972(1)	2180(1)	29(1)
C(4)	-3084(2)	-3879(1)	1208(1)	32(1)
C(5)	-2804(2)	-2638(1)	1108(1)	27(1)
C(6)	-1151(2)	-2102(1)	1581(1)	23(1)
C(7)	-1155(2)	-1557(1)	2585(1)	23(1)
C(8)	-266(2)	-2107(1)	3366(1)	22(1)
C(9)	388(2)	-1228(1)	4173(1)	25(1)
C(10)	1900(2)	-562(1)	3982(1)	23(1)
C(11)	3418(2)	-1029(1)	4002(1)	25(1)
C(12)	4834(2)	-418(1)	3868(1)	25(1)
C(13)	4762(2)	684(1)	3709(1)	22(1)
C(14)	3254(2)	1154(1)	3673(1)	24(1)
C(15)	1841(2)	534(1)	3804(1)	25(1)
C(16)	6315(2)	1341(1)	3626(1)	24(1)
C(17)	7529(2)	3090(1)	3447(1)	36(1)
C(18)	2086(2)	4947(1)	1435(1)	24(1)
C(19)	2820(2)	5705(1)	2216(1)	25(1)
C(20)	3255(2)	5911(1)	3012(1)	26(1)
C(21)	3528(2)	5829(1)	3993(1)	29(1)
C(22)	3193(2)	4592(1)	4105(1)	28(1)
C(23)	1636(2)	4022(1)	3540(1)	25(1)
C(24)	1804(2)	3491(1)	2545(1)	23(1)
C(25)	984(2)	4027(1)	1734(1)	22(1)
C(26)	462(2)	3146(1)	905(1)	23(1)
C(27)	-1109(2)	2479(1)	999(1)	22(1)
C(28)	-1114(2)	1376(1)	1160(1)	25(1)
C(29)	-2575(2)	769(1)	1230(1)	26(1)
C(30)	-4062(2)	1258(1)	1139(1)	23(1)
C(31)	-4066(2)	2364(1)	983(1)	26(1)

C(32)	-2610(2)	2962(1)	912(1)	26(1)
C(33)	-5664(2)	639(1)	1192(1)	25(1)
C(34)	-7004(2)	-1050(1)	1427(1)	32(1)
O(1)	7655(1)	983(1)	3660(1)	31(1)
O(2)	6068(1)	2401(1)	3522(1)	31(1)
O(3)	-6976(1)	1026(1)	1089(1)	36(1)
O(4)	-5491(1)	-405(1)	1366(1)	28(1)
F(1)	-396(1)	-3554(1)	4318(1)	31(1)
F(2)	-2484(1)	-2536(1)	4245(1)	30(1)
F(3)	1206(1)	5493(1)	810(1)	31(1)
F(4)	3307(1)	4493(1)	954(1)	29(1)

Table B.17. Bond lengths [Å] and angles [°] for (DIFO2, **2.22**).

C(1)-F(1)	1.3794(15)	C(16)-O(1)	1.2064(16)
C(1)-F(2)	1.3799(15)	C(16)-O(2)	1.3432(17)
C(1)-C(2)	1.452(2)	C(17)-O(2)	1.4417(17)
C(1)-C(8)	1.5304(18)	C(17)-H(17A)	0.9800
C(2)-C(3)	1.194(2)	C(17)-H(17B)	0.9800
C(3)-C(4)	1.461(2)	C(17)-H(17C)	0.9800
C(4)-C(5)	1.541(2)	C(18)-F(3)	1.3760(15)
C(4)-H(4A)	0.9900	C(18)-F(4)	1.3836(15)
C(4)-H(4B)	0.9900	C(18)-C(19)	1.453(2)
C(5)-C(6)	1.5424(18)	C(18)-C(25)	1.5268(18)
C(5)-H(5A)	0.9900	C(19)-C(20)	1.192(2)
C(5)-H(5B)	0.9900	C(20)-C(21)	1.459(2)
C(6)-C(7)	1.5535(18)	C(21)-C(22)	1.5463(19)
C(6)-H(6A)	0.9900	C(21)-H(21A)	0.9900
C(6)-H(6B)	0.9900	C(21)-H(21B)	0.9900
C(7)-C(8)	1.5474(17)	C(22)-C(23)	1.5451(19)
C(7)-H(7A)	0.9900	C(22)-H(22A)	0.9900
C(7)-H(7B)	0.9900	C(22)-H(22B)	0.9900
C(8)-C(9)	1.5432(18)	C(23)-C(24)	1.5556(18)
C(8)-H(8)	1.0000	C(23)-H(23A)	0.9900
C(9)-C(10)	1.5073(18)	C(23)-H(23B)	0.9900
C(9)-H(9A)	0.9900	C(24)-C(25)	1.5490(17)
C(9)-H(9B)	0.9900	C(24)-H(24A)	0.9900
C(10)-C(15)	1.3923(19)	C(24)-H(24B)	0.9900
C(10)-C(11)	1.3995(19)	C(25)-C(26)	1.5451(18)
C(11)-C(12)	1.3829(19)	C(25)-H(25)	1.0000
C(11)-H(11)	0.9500	C(26)-C(27)	1.5079(18)
C(12)-C(13)	1.3930(19)	C(26)-H(26A)	0.9900
C(12)-H(12)	0.9500	C(26)-H(26B)	0.9900
C(13)-C(14)	1.3929(18)	C(27)-C(28)	1.3910(19)
C(13)-C(16)	1.4860(18)	C(27)-C(32)	1.3983(19)
C(14)-C(15)	1.3855(19)	C(28)-C(29)	1.3887(19)
C(14)-H(14)	0.9500	C(28)-H(28)	0.9500
C(15)-H(15)	0.9500	C(29)-C(30)	1.3916(18)

C(29)-H(29)	0.9500	C(33)-O(3)	1.2047(17)
C(30)-C(31)	1.3929(19)	C(33)-O(4)	1.3392(17)
C(30)-C(33)	1.4890(18)	C(34)-O(4)	1.4450(16)
C(31)-C(32)	1.3803(19)	C(34)-H(34A)	0.9800
C(31)-H(31)	0.9500	C(34)-H(34B)	0.9800
C(32)-H(32)	0.9500	C(34)-H(34C)	0.9800

F(1)-C(1)-F(2)	104.11(10)	C(8)-C(7)-H(7B)	107.6
F(1)-C(1)-C(2)	111.52(11)	C(6)-C(7)-H(7B)	107.6
F(2)-C(1)-C(2)	109.76(11)	H(7A)-C(7)-H(7B)	107.0
F(1)-C(1)-C(8)	109.60(10)	C(1)-C(8)-C(9)	109.38(11)
F(2)-C(1)-C(8)	110.40(11)	C(1)-C(8)-C(7)	113.42(10)
C(2)-C(1)-C(8)	111.22(11)	C(9)-C(8)-C(7)	110.63(10)
C(3)-C(2)-C(1)	150.64(14)	C(1)-C(8)-H(8)	107.7
C(2)-C(3)-C(4)	161.96(14)	C(9)-C(8)-H(8)	107.7
C(3)-C(4)-C(5)	105.74(11)	C(7)-C(8)-H(8)	107.7
C(3)-C(4)-H(4A)	110.6	C(10)-C(9)-C(8)	112.81(11)
C(5)-C(4)-H(4A)	110.6	C(10)-C(9)-H(9A)	109.0
C(3)-C(4)-H(4B)	110.6	C(8)-C(9)-H(9A)	109.0
C(5)-C(4)-H(4B)	110.6	C(10)-C(9)-H(9B)	109.0
H(4A)-C(4)-H(4B)	108.7	C(8)-C(9)-H(9B)	109.0
C(4)-C(5)-C(6)	113.77(11)	H(9A)-C(9)-H(9B)	107.8
C(4)-C(5)-H(5A)	108.8	C(15)-C(10)-C(11)	118.22(12)
C(6)-C(5)-H(5A)	108.8	C(15)-C(10)-C(9)	121.48(12)
C(4)-C(5)-H(5B)	108.8	C(11)-C(10)-C(9)	120.27(12)
C(6)-C(5)-H(5B)	108.8	C(12)-C(11)-C(10)	121.30(12)
H(5A)-C(5)-H(5B)	107.7	C(12)-C(11)-H(11)	119.3
C(5)-C(6)-C(7)	116.54(11)	C(10)-C(11)-H(11)	119.3
C(5)-C(6)-H(6A)	108.2	C(11)-C(12)-C(13)	119.85(12)
C(7)-C(6)-H(6A)	108.2	C(11)-C(12)-H(12)	120.1
C(5)-C(6)-H(6B)	108.2	C(13)-C(12)-H(12)	120.1
C(7)-C(6)-H(6B)	108.2	C(12)-C(13)-C(14)	119.40(12)
H(6A)-C(6)-H(6B)	107.3	C(12)-C(13)-C(16)	118.72(12)
C(8)-C(7)-C(6)	118.85(11)	C(14)-C(13)-C(16)	121.82(12)
C(8)-C(7)-H(7A)	107.6	C(15)-C(14)-C(13)	120.36(12)
C(6)-C(7)-H(7A)	107.6	C(15)-C(14)-H(14)	119.8

C(13)-C(14)-H(14)	119.8	C(22)-C(23)-H(23B)	107.8
C(14)-C(15)-C(10)	120.85(12)	C(24)-C(23)-H(23B)	107.8
C(14)-C(15)-H(15)	119.6	H(23A)-C(23)-H(23B)	107.2
C(10)-C(15)-H(15)	119.6	C(25)-C(24)-C(23)	118.69(11)
O(1)-C(16)-O(2)	123.05(12)	C(25)-C(24)-H(24A)	107.6
O(1)-C(16)-C(13)	124.79(13)	C(23)-C(24)-H(24A)	107.6
O(2)-C(16)-C(13)	112.15(11)	C(25)-C(24)-H(24B)	107.6
O(2)-C(17)-H(17A)	109.5	C(23)-C(24)-H(24B)	107.6
O(2)-C(17)-H(17B)	109.5	H(24A)-C(24)-H(24B)	107.1
H(17A)-C(17)-H(17B)	109.5	C(18)-C(25)-C(26)	109.34(10)
O(2)-C(17)-H(17C)	109.5	C(18)-C(25)-C(24)	112.77(10)
H(17A)-C(17)-H(17C)	109.5	C(26)-C(25)-C(24)	110.85(10)
H(17B)-C(17)-H(17C)	109.5	C(18)-C(25)-H(25)	107.9
F(3)-C(18)-F(4)	104.27(10)	C(26)-C(25)-H(25)	107.9
F(3)-C(18)-C(19)	111.61(11)	C(24)-C(25)-H(25)	107.9
F(4)-C(18)-C(19)	109.64(11)	C(27)-C(26)-C(25)	113.28(11)
F(3)-C(18)-C(25)	109.67(10)	C(27)-C(26)-H(26A)	108.9
F(4)-C(18)-C(25)	109.94(10)	C(25)-C(26)-H(26A)	108.9
C(19)-C(18)-C(25)	111.47(11)	C(27)-C(26)-H(26B)	108.9
C(20)-C(19)-C(18)	151.17(14)	C(25)-C(26)-H(26B)	108.9
C(19)-C(20)-C(21)	162.32(14)	H(26A)-C(26)-H(26B)	107.7
C(20)-C(21)-C(22)	106.17(11)	C(28)-C(27)-C(32)	118.35(12)
C(20)-C(21)-H(21A)	110.5	C(28)-C(27)-C(26)	121.53(12)
C(22)-C(21)-H(21A)	110.5	C(32)-C(27)-C(26)	120.11(12)
C(20)-C(21)-H(21B)	110.5	C(29)-C(28)-C(27)	120.74(12)
C(22)-C(21)-H(21B)	110.5	C(29)-C(28)-H(28)	119.6
H(21A)-C(21)-H(21B)	108.7	C(27)-C(28)-H(28)	119.6
C(23)-C(22)-C(21)	114.80(11)	C(28)-C(29)-C(30)	120.37(12)
C(23)-C(22)-H(22A)	108.6	C(28)-C(29)-H(29)	119.8
C(21)-C(22)-H(22A)	108.6	C(30)-C(29)-H(29)	119.8
C(23)-C(22)-H(22B)	108.6	C(29)-C(30)-C(31)	119.24(12)
C(21)-C(22)-H(22B)	108.6	C(29)-C(30)-C(33)	122.50(12)
H(22A)-C(22)-H(22B)	107.5	C(31)-C(30)-C(33)	118.26(12)
C(22)-C(23)-C(24)	117.83(11)	C(32)-C(31)-C(30)	120.10(12)
C(22)-C(23)-H(23A)	107.8	C(32)-C(31)-H(31)	119.9
C(24)-C(23)-H(23A)	107.8	C(30)-C(31)-H(31)	119.9

C(31)-C(32)-C(27)	121.19(12)
C(31)-C(32)-H(32)	119.4
C(27)-C(32)-H(32)	119.4
O(3)-C(33)-O(4)	123.31(12)
O(3)-C(33)-C(30)	124.28(13)
O(4)-C(33)-C(30)	112.42(11)
O(4)-C(34)-H(34A)	109.5
O(4)-C(34)-H(34B)	109.5
H(34A)-C(34)-H(34B)	109.5
O(4)-C(34)-H(34C)	109.5
H(34A)-C(34)-H(34C)	109.5
H(34B)-C(34)-H(34C)	109.5
C(16)-O(2)-C(17)	115.07(11)
C(33)-O(4)-C(34)	115.13(11)

Table B.18. Anisotropic displacement parameters ($Å^2 x\ 10^3$) for (DIFO2, **2.22**). The anisotropic displacement factor exponent takes the form: $-2\pi^2[\ h^2a^{*2}U^{11} + ... + 2\ h\ k\ a^*\ b^*\ U^{12}\ ]$

U^{11}	U^{22}	U^{33}	U^{23}	U^{13}	U^{12}	
C(1)	24(1)	26(1)	25(1)	4(1)	3(1)	3(1)
C(2)	26(1)	24(1)	31(1)	5(1)	5(1)	-2(1)
C(3)	28(1)	24(1)	35(1)	2(1)	5(1)	-4(1)
C(4)	30(1)	34(1)	28(1)	-3(1)	0(1)	-7(1)
C(5)	23(1)	33(1)	24(1)	0(1)	1(1)	2(1)
C(6)	22(1)	25(1)	23(1)	3(1)	2(1)	2(1)
C(7)	24(1)	22(1)	24(1)	1(1)	1(1)	2(1)
C(8)	21(1)	24(1)	21(1)	1(1)	2(1)	1(1)
C(9)	25(1)	28(1)	20(1)	0(1)	2(1)	-1(1)
C(10)	24(1)	28(1)	15(1)	-2(1)	-1(1)	-1(1)
C(11)	28(1)	23(1)	24(1)	1(1)	0(1)	2(1)
C(12)	23(1)	28(1)	22(1)	0(1)	0(1)	6(1)
C(13)	21(1)	29(1)	16(1)	1(1)	0(1)	2(1)
C(14)	25(1)	25(1)	23(1)	4(1)	1(1)	3(1)
C(15)	21(1)	30(1)	23(1)	1(1)	0(1)	4(1)
C(16)	25(1)	29(1)	17(1)	1(1)	1(1)	2(1)
C(17)	31(1)	35(1)	41(1)	7(1)	9(1)	-7(1)
C(18)	24(1)	26(1)	22(1)	6(1)	0(1)	3(1)
C(19)	24(1)	23(1)	28(1)	7(1)	0(1)	-1(1)
C(20)	23(1)	23(1)	33(1)	5(1)	1(1)	0(1)
C(21)	28(1)	30(1)	26(1)	3(1)	-3(1)	-1(1)
C(22)	28(1)	31(1)	23(1)	4(1)	-4(1)	2(1)
C(23)	24(1)	26(1)	24(1)	6(1)	1(1)	0(1)
C(24)	22(1)	23(1)	24(1)	6(1)	0(1)	2(1)
C(25)	19(1)	23(1)	22(1)	4(1)	0(1)	2(1)
C(26)	23(1)	26(1)	20(1)	4(1)	1(1)	2(1)
C(27)	23(1)	26(1)	17(1)	1(1)	-1(1)	1(1)
C(28)	21(1)	27(1)	27(1)	4(1)	0(1)	5(1)
C(29)	24(1)	24(1)	30(1)	5(1)	1(1)	4(1)
C(30)	22(1)	26(1)	20(1)	0(1)	-1(1)	2(1)
C(31)	21(1)	28(1)	27(1)	1(1)	-3(1)	6(1)

C(32)	27(1)	22(1)	28(1)	4(1)	-2(1)	3(1)
C(33)	23(1)	29(1)	22(1)	-1(1)	0(1)	3(1)
C(34)	25(1)	34(1)	37(1)	4(1)	5(1)	-5(1)
O(1)	20(1)	39(1)	34(1)	6(1)	2(1)	3(1)
O(2)	25(1)	30(1)	39(1)	7(1)	6(1)	-1(1)
O(3)	20(1)	36(1)	53(1)	7(1)	2(1)	5(1)
O(4)	22(1)	28(1)	36(1)	5(1)	4(1)	0(1)
F(1)	33(1)	33(1)	29(1)	11(1)	-1(1)	2(1)
F(2)	27(1)	33(1)	31(1)	2(1)	10(1)	0(1)
F(3)	35(1)	30(1)	29(1)	12(1)	-7(1)	0(1)
F(4)	26(1)	33(1)	29(1)	2(1)	7(1)	-2(1)

Table B.19. Hydrogen coordinates (x 10^4) and isotropic displacement parameters ($Å^2$x 10^3) for (DIFO2, **2.22**).

x	y	z	U(eq)	
H(4A)	-4238	-4145	1011	38
H(4B)	-2360	-4321	831	38
H(5A)	-3703	-2239	1370	32
H(5B)	-2857	-2548	447	32
H(6A)	-754	-1531	1210	28
H(6B)	-348	-2678	1572	28
H(7A)	-666	-789	2619	28
H(7B)	-2313	-1507	2716	28
H(8)	698	-2461	3119	26
H(9A)	-480	-720	4307	30
H(9B)	646	-1602	4725	30
H(11)	3477	-1780	4111	30
H(12)	5853	-750	3885	30
H(14)	3195	1902	3558	29
H(15)	819	862	3773	30
H(17A)	8239	3152	4023	53
H(17B)	7226	3829	3324	53
H(17C)	8113	2759	2945	53
H(21A)	2774	6287	4334	34
H(21B)	4671	6087	4226	34
H(22A)	4150	4189	3926	33
H(22B)	3094	4526	4762	33
H(23A)	805	4577	3508	30
H(23B)	1195	3436	3883	30
H(24A)	2989	3477	2467	27
H(24B)	1355	2711	2489	27
H(25)	-27	4360	1938	26
H(26A)	323	3520	344	28
H(26B)	1349	2636	829	28
H(28)	-106	1034	1223	30

H(29)	-2560	17	1340	31
H(31)	-5073	2708	926	31
H(32)	-2628	3714	801	31
H(34A)	-7604	-682	1907	49
H(34B)	-6758	-1790	1578	49
H(34C)	-7676	-1118	838	49

Appendix C:
Cartesian Coordinates of B3LYP/6-31G(d) stationary points*

* All computations were performed by Joel L. Mackey and Kendall N. Houk

B3LYP/6-31G(d) and MeCN solvation energetics.

Reactants: ***Cis*** **lactam compounds**

Compound 2.1

E(B3LYP)	H(B3LYP)	G(B3LYP)
-746.209842488	-745.969591	-746.024989

6,0.000000,0.000000,0.000000
6,0.000000,0.000000,1.423528
6,1.229674,0.000000,2.087966
6,2.432225,0.046310,1.378476
6,2.423513,0.098758,-0.015804
6,1.211348,0.067039,-0.701267
1,1.243251,-0.019359,3.173652
1,3.373545,0.048669,1.920663
1,3.357286,0.146572,-0.568561
1,1.187688,0.066026,-1.786524
6,-1.269842,-0.285984,-0.571556
6,-2.298402,-0.916296,-0.404265
6,-3.050047,-1.857313,0.345989
6,-3.857289,-2.854403,-0.225227
6,-2.812172,-1.841599,1.749561
6,-4.388389,-3.866897,0.565865
1,-4.037515,-2.832687,-1.295394
6,-3.369716,-2.871569,2.519568
6,-4.126012,-3.886746,1.938275
1,-4.999822,-4.642651,0.113371
1,-3.221530,-2.846961,3.593343
1,-4.530143,-4.680151,2.560440
6,-2.245570,-0.677283,2.556106
7,-1.203483,0.185754,2.199980
8,-2.850093,-0.433665,3.599427
6,-1.140538,1.375092,3.076683
1,-0.765220,1.134532,4.077898
1,-0.486410,2.110595,2.606061
1,-2.143009,1.789608,3.190809

Compound 2.2

E(B3LYP)	H(B3LYP)	G(B3LYP)
-845.442238564	-845.209421	-845.267043

6,0.005108,-0.011808,-0.003155
6,0.001520,0.003086,1.421478
6,1.227195,0.022047,2.092920
6,2.412408,0.068863,1.365742
6,2.434407,0.104331,-0.022838
6,1.219396,0.053425,-0.700407

1,1.272300,0.019153,3.176314
1,3.381868,0.152064,-0.548344
1,1.200647,0.041144,-1.785218
6,-1.259543,-0.308792,-0.576491
6,-2.297131,-0.923019,-0.406456
6,-3.052757,-1.860612,0.343895
6,-3.866557,-2.852342,-0.226749
6,-2.813988,-1.846713,1.747255
6,-4.402899,-3.862136,0.564456
1,-4.047476,-2.829504,-1.296752
6,-3.376881,-2.873963,2.517344
6,-4.139695,-3.884524,1.936538
1,-5.019191,-4.633927,0.111791
1,-3.227295,-2.851267,3.590915
1,-4.547796,-4.675761,2.558758
6,-2.238838,-0.688743,2.555834
7,-1.201431,0.184607,2.194852
8,-2.828214,-0.452918,3.608396
6,-1.136947,1.366992,3.081977
1,-0.752239,1.120120,4.077967
1,-0.491710,2.110540,2.611795
1,-2.140842,1.774107,3.207034
9,3.578409,0.091516,2.041826

Compound 2.3

E(B3LYP)	H(B3LYP)	G(B3LYP)
-845.442265187	-845.209488	-845.267111

6,-0.001995,0.005291,0.000307
6,-0.000211,-0.001657,1.423511
6,1.228989,-0.007498,2.088123
6,2.431185,0.039546,1.377924
6,2.421147,0.099182,-0.016031
6,1.208723,0.073604,-0.701574
1,1.242736,-0.031822,3.173702
1,3.354728,0.147767,-0.569029
1,1.184986,0.078161,-1.786779
6,-1.274123,-0.276726,-0.568772
6,-2.295544,-0.919721,-0.406872
6,-3.047085,-1.857814,0.345174
6,-3.854113,-2.857485,-0.223739
6,-2.809183,-1.843041,1.749556
6,-4.391078,-3.870725,0.560757
1,-4.035594,-2.839847,-1.293382
6,-3.364905,-2.866457,2.526146
6,-4.115642,-3.865815,1.924825

1,-5.004229,-4.658608,0.136379
1,-3.240129,-2.860131,3.602125
6,-2.243214,-0.677046,2.558973
7,-1.204063,0.184621,2.201128
8,-2.851622,-0.436265,3.600243
6,-1.142640,1.377517,3.073802
1,-0.762118,1.140912,4.073889
1,-0.492788,2.113239,2.597849
1,-2.146160,1.788525,3.190492
9,-4.617887,-4.852248,2.694061
1,3.372895,0.037237,1.919215

Compound 2.4

E(B3LYP)	H(B3LYP)	G(B3LYP)
-845.442005543	-845.209225	-845.266812

6,1.989547,-1.134799,-0.511103
6,2.013465,0.177615,0.042340
6,3.020688,0.492737,0.959011
6,4.011143,-0.430105,1.301163
6,3.986365,-1.685341,0.706261
6,2.990462,-2.058069,-0.185432
1,3.041205,1.483574,1.402188
1,4.795195,-0.183590,2.008899
1,2.974947,-3.060903,-0.596656
6,0.784894,-1.443796,-1.200786
6,-0.414183,-1.230666,-1.185030
6,-1.557376,-0.642094,-0.586856
6,-2.803417,-1.280813,-0.477957
6,-1.326848,0.602627,0.064642
6,-3.808008,-0.729252,0.308903
1,-2.957684,-2.220667,-0.998551
6,-2.363451,1.135210,0.843162
6,-3.579348,0.470880,0.987495
1,-2.208076,2.099441,1.313991
1,-4.356897,0.901963,1.611539
6,-0.173273,1.562860,-0.207321
7,1.166070,1.239264,-0.446100
8,-0.500919,2.743361,-0.315328
6,1.931475,2.382427,-0.988082
1,2.132227,3.146037,-0.227838
1,2.874195,2.002508,-1.384895
1,1.356347,2.854144,-1.785864
9,4.945677,-2.578976,1.019845
1,-4.764489,-1.236432,0.399341

Compound 2.5

E(B3LYP)	H(B3LYP)	G(B3LYP)
-845.442948031	-845.210164	-845.267785

6,0.009159,-0.008867,-0.002468
6,0.004155,0.002515,1.420828
6,1.232398,0.017665,2.087892
6,2.435921,0.068381,1.380477
6,2.431028,0.108796,-0.014354
6,1.221054,0.060674,-0.702393
1,1.243703,0.006675,3.173546
1,3.375732,0.083033,1.925029
1,3.365897,0.159464,-0.564819
1,1.199782,0.049940,-1.787619
6,-1.256858,-0.309767,-0.572100
6,-2.294290,-0.925651,-0.408906
6,-3.046240,-1.862833,0.345179
6,-3.862098,-2.847169,-0.232622
6,-2.805494,-1.851013,1.749147
6,-4.391655,-3.839080,0.576516
1,-4.056738,-2.850500,-1.298883
6,-3.378245,-2.875804,2.517450
6,-4.147048,-3.884763,1.945643
1,-3.230259,-2.854971,3.590931
1,-4.574842,-4.682454,2.543246
6,-2.228728,-0.698466,2.562291
7,-1.203855,0.182137,2.191900
8,-2.808933,-0.474942,3.623587
6,-1.145549,1.369680,3.071830
1,-0.745901,1.134673,4.064898
1,-0.515019,2.118592,2.589954
1,-2.153141,1.764848,3.206418
9,-5.158922,-4.793575,0.016704

Compound 2.6

E(B3LYP)	H(B3LYP)	G(B3LYP)
-944.674905496	-944.449547	-944.509249

6,1.992287,-1.144008,-0.497796
6,2.019168,0.173709,0.042290
6,3.035760,0.497979,0.945501
6,4.030400,-0.421172,1.284911
6,4.001276,-1.682601,0.702970
6,2.995846,-2.064869,-0.173664
1,3.060317,1.492453,1.379879
1,4.821596,-0.167357,1.982088
1,2.975774,-3.071517,-0.575211
6,0.780758,-1.457606,-1.171030

6,-0.417040,-1.239855,-1.174704
6,-1.559177,-0.645496,-0.580466
6,-2.806234,-1.282286,-0.492234
6,-1.327863,0.596685,0.077492
6,-3.797982,-0.707798,0.285735
1,-2.987281,-2.221362,-1.002255
6,-2.374247,1.133002,0.842930
6,-3.597561,0.483699,0.976347
1,-2.220389,2.094802,1.318275
1,-4.397618,0.896350,1.581420
6,-0.171727,1.556200,-0.176246
7,1.162832,1.228436,-0.445900
8,-0.489815,2.741989,-0.246857
6,1.921618,2.376084,-0.988576
1,2.142445,3.129545,-0.223876
1,2.853893,1.997246,-1.410690
1,1.331487,2.859631,-1.767975
9,-4.988140,-1.328586,0.384282
9,4.964854,-2.571322,1.014865

Compound 2.7

E(B3LYP)	H(B3LYP)	G(B3LYP)
-860.732861567	-860.457275	-860.518801

6,-0.044820,-0.007970,-0.068539
6,-0.006135,-0.000148,1.357997
6,1.230938,0.016196,1.993261
6,2.426352,0.069593,1.257473
6,2.387083,0.113380,-0.140636
6,1.152503,0.062465,-0.786455
1,1.298155,0.010173,3.075813
1,3.296166,0.167022,-0.727626
1,1.112236,0.053736,-1.871152
6,-1.321274,-0.312694,-0.605995
6,-2.366800,-0.907609,-0.413310
6,-3.093394,-1.855118,0.354498
6,-3.926136,-2.842126,-0.197390
6,-2.810695,-1.854312,1.750030
6,-4.435619,-3.860147,0.601013
1,-4.142251,-2.809404,-1.260662
6,-3.348227,-2.889194,2.528145
6,-4.128427,-3.895645,1.963625
1,-5.065971,-4.628050,0.160935
1,-3.164277,-2.875438,3.596565
6,-2.212222,-0.702925,2.551345
7,-1.190444,0.176013,2.164583

8,-2.769590,-0.478083,3.624458
6,-1.104177,1.353883,3.054848
1,-0.680029,1.106038,4.034571
1,-0.482513,2.104905,2.565120
1,-2.106377,1.751110,3.219309
1,-4.515914,-4.692921,2.591398
8,3.565061,0.085964,2.004510
6,4.813496,0.139439,1.329542
1,5.574913,0.137638,2.111185
1,4.957149,-0.733751,0.680061
1,4.908800,1.055250,0.731825

Compound 2.8

E(B3LYP)	H(B3LYP)	G(B3LYP)
-860.733355923	-860.457726	-860.51925

6,0.028661,0.033634,-0.018109
6,0.034580,0.033927,1.405280
6,1.264313,0.027535,2.068203
6,2.466256,0.066735,1.356444
6,2.452829,0.121072,-0.037466
6,1.238827,0.097828,-0.721151
1,1.279037,0.009930,3.154064
1,3.385348,0.164976,-0.592908
1,1.213948,0.099590,-1.806401
6,-1.247505,-0.245212,-0.583640
6,-2.246001,-0.916629,-0.390240
6,-2.994842,-1.840883,0.376374
6,-3.797121,-2.859243,-0.172649
6,-2.765715,-1.807481,1.778176
6,-4.331973,-3.852393,0.627510
1,-3.976406,-2.864617,-1.243122
6,-3.321162,-2.819290,2.574172
6,-4.077720,-3.848361,2.009196
1,-4.941795,-4.647721,0.211144
1,-3.179218,-2.751471,3.644420
6,-2.193651,-0.634365,2.571644
7,-1.168469,0.231636,2.183637
8,-2.780769,-0.385780,3.624597
6,-1.105192,1.441047,3.031521
1,-0.706377,1.229378,4.030315
1,-0.469621,2.172964,2.530749
1,-2.110525,1.845715,3.155854
1,3.409000,0.064477,1.896093
8,-4.627406,-4.876299,2.712169
6,-4.429159,-4.915826,4.119241

1,-4.861392,-4.035344,4.611010
1,-4.942883,-5.814103,4.465772
1,-3.363509,-4.984928,4.372674

Compound 2.9

E(B3LYP)	H(B3LYP)	G(B3LYP)
-845.44116392	-845.208266	-845.265878

6,1.761087,-1.050633,-0.476901
6,1.679294,0.276549,0.029040
6,2.686130,0.732351,0.886167
6,3.772689,-0.082384,1.213445
6,3.880554,-1.371974,0.692864
6,2.869503,-1.832359,-0.137351
1,2.625348,1.738614,1.287525
1,4.544188,0.294601,1.878004
1,4.714219,-2.023409,0.931479
6,0.588101,-1.530627,-1.111270
6,-0.625302,-1.431262,-1.104092
6,-1.813787,-0.951185,-0.496880
6,-2.985465,-1.711655,-0.354012
6,-1.703824,0.324831,0.124762
6,-4.029272,-1.250284,0.440185
1,-3.049521,-2.673354,-0.853096
6,-2.777654,0.763731,0.911524
6,-3.915737,-0.019234,1.091418
1,-4.926370,-1.851787,0.557298
1,-2.715480,1.748427,1.360917
1,-4.723480,0.342574,1.721051
6,-0.662975,1.395970,-0.185317
7,0.701560,1.219314,-0.455522
8,-1.114396,2.534104,-0.295639
6,1.317933,2.437533,-1.025716
1,1.445355,3.228788,-0.278318
1,2.288774,2.164608,-1.441965
1,0.673445,2.828153,-1.813963
9,2.932240,-3.085554,-0.623727

Compound 2.10

E(B3LYP)	H(B3LYP)	G(B3LYP)
-924.080183877	-923.788499	-923.855094

6,0.003679,-0.006029,0.001962
6,0.005503,-0.000529,1.423073
6,1.231462,0.009220,2.090520
6,2.444545,0.060981,1.391938

6,2.411641,0.100276,-0.006779
6,1.211781,0.057922,-0.718305
1,1.240880,-0.007198,3.176905
1,3.348107,0.145620,-0.558364
6,-1.265535,-0.306770,-0.556933
6,-2.318394,-0.901354,-0.409628
6,-3.059925,-1.849692,0.342965
6,-3.883201,-2.826546,-0.237249
6,-2.805007,-1.856357,1.744743
6,-4.402433,-3.830006,0.564363
1,-4.090604,-2.816143,-1.301098
6,-3.369157,-2.891127,2.505823
6,-4.142731,-3.894242,1.929745
1,-3.210246,-2.883334,3.577956
1,-4.563230,-4.700078,2.521542
6,-2.223180,-0.712423,2.566486
7,-1.201795,0.172929,2.198879
8,-2.796659,-0.500523,3.634181
6,-1.141254,1.351917,3.089085
1,-0.741185,1.107876,4.079750
1,-0.510324,2.104213,2.613151
1,-2.148328,1.747217,3.228145
9,-5.175439,-4.777888,-0.000124
6,1.189875,0.038959,-2.226577
1,0.782713,-0.907670,-2.603100
1,0.556316,0.838646,-2.627831
1,2.195988,0.162690,-2.637887
6,3.756108,0.107711,2.139832
1,3.990316,1.129351,2.468016
1,3.728782,-0.520926,3.036541
1,4.586467,-0.231817,1.512572

Compound 2.11

E(B3LYP)	H(B3LYP)	G(B3LYP)
-824.846903484	-824.547808	-824.612088

6,-0.004873,0.006887,0.001598
6,-0.002255,-0.000942,1.422649
6,1.223056,-0.010101,2.091133
6,2.437185,0.035164,1.394248
6,2.404816,0.089480,-0.003846
6,1.204671,0.066757,-0.716310
1,1.230398,-0.036332,3.177438
1,3.342060,0.130582,-0.554735
6,-1.277634,-0.273308,-0.563445
6,-2.324081,-0.878893,-0.413634

6,-3.075256,-1.825735,0.331482
6,-3.897453,-2.806606,-0.246653
6,-2.826200,-1.833616,1.733321
6,-4.429475,-3.827504,0.533088
1,-4.087673,-2.766671,-1.314631
6,-3.385742,-2.870861,2.492117
6,-4.154940,-3.871510,1.902453
1,-3.228556,-2.863631,3.564910
1,-4.560002,-4.671200,2.515953
6,-2.247071,-0.685030,2.553610
7,-1.206843,0.181610,2.200596
8,-2.842043,-0.455528,3.605921
6,-1.139588,1.362088,3.088259
1,-0.754363,1.113881,4.083894
1,-0.491779,2.103862,2.618602
1,-2.142337,1.772100,3.215108
6,1.183997,0.058803,-2.224731
1,0.839363,-0.909621,-2.609063
1,0.499405,0.818192,-2.619499
1,2.180212,0.249531,-2.635002
6,3.749314,0.059664,2.142515
1,4.006585,1.078330,2.462816
1,3.708466,-0.561505,3.043855
1,4.572126,-0.302918,1.517972
1,-5.051578,-4.590812,0.073808

Reactants: *Trans* lactam compounds

Compound 2.1

E(B3LYP)	H(B3LYP)	G(B3LYP)
-746.22178527	-745.981672	-746.036445

6,0.362414,-0.373753,0.048518
6,0.515050,-0.506159,1.465281
6,1.553625,0.152596,2.112218
6,2.451783,0.936424,1.381535
6,2.310662,1.063983,-0.001802
6,1.270906,0.416619,-0.667641
1,1.648392,0.050628,3.188989
1,3.259420,1.449861,1.895467
1,3.009943,1.675799,-0.564654
1,1.152108,0.521981,-1.741550
6,-0.766914,-1.064880,-0.480243
6,-1.773819,-1.745524,-0.365621
6,-2.817130,-2.357818,0.395099
6,-3.832983,-3.191100,-0.090584
6,-2.764450,-2.046689,1.786670

6,-4.783061,-3.711647,0.787293
1,-3.873789,-3.421330,-1.150825
6,-3.737432,-2.554765,2.642915
6,-4.737412,-3.396937,2.147738
1,-5.567160,-4.360256,0.406845
1,-3.716586,-2.287071,3.695767
1,-5.487962,-3.797776,2.823137
6,-1.729010,-1.017210,2.201380
7,-0.377833,-1.390809,2.164931
6,0.020568,-2.800804,2.158653
1,0.126657,-3.206652,1.144378
1,0.978457,-2.899152,2.678813
1,-0.725034,-3.388701,2.698131
8,-2.067659,0.128258,2.443081

Compound 2.2

E(B3LYP)	H(B3LYP)	G(B3LYP)
-845.454373091	-845.221673	-845.278544

6,-0.001382,0.002512,-0.000724
6,-0.002074,-0.000699,1.431382
6,1.199529,-0.005057,2.128445
6,2.392310,-0.009247,1.409385
6,2.425981,-0.010088,0.019260
6,1.222871,-0.000154,-0.682907
1,1.212133,0.004349,3.212491
1,3.382479,-0.011834,-0.492251
6,-1.301093,0.046967,-0.582695
6,-2.518036,0.110587,-0.509768
6,-3.742598,0.344987,0.187974
6,-5.040091,0.213811,-0.323164
6,-3.555606,0.755993,1.541548
6,-6.138149,0.484198,0.492620
1,-5.179288,-0.093665,-1.355058
6,-4.663794,1.046700,2.332338
6,-5.953761,0.898428,1.814043
1,-4.518123,1.394651,3.351290
1,-6.814434,1.117860,2.439443
6,-2.123097,1.020664,1.965432
7,-1.264659,-0.080792,2.111564
6,-1.789132,-1.439053,2.280192
1,-1.915275,-1.965867,1.325718
1,-1.098737,-2.008922,2.909711
1,-2.754914,-1.390229,2.787220
8,-1.711164,2.163131,2.060412

1,1.227454,0.008863,-1.767933
1,-7.142662,0.378129,0.092883
9,3.555217,-0.014384,2.089814

Compound 2.3

E(B3LYP)	H(B3LYP)	G(B3LYP)
-845.454409709	-845.221702	-845.278539

6,-0.000092,0.000846,0.001356
6,0.000713,0.002073,1.432300
6,1.206496,0.000996,2.122643
6,2.416724,-0.009503,1.422253
6,2.421463,-0.016909,0.026026
6,1.221712,-0.008119,-0.684063
1,1.189231,0.013487,3.208164
1,3.364256,-0.023068,-0.513563
6,-1.301894,0.046750,-0.577708
6,-2.519062,0.113914,-0.513267
6,-3.742479,0.348871,0.185527
6,-5.041337,0.221995,-0.325546
6,-3.557284,0.753492,1.541767
6,-6.143978,0.486186,0.483992
1,-5.183378,-0.080544,-1.358134
6,-4.659412,1.039678,2.340428
6,-5.933447,0.887777,1.799478
1,-4.544227,1.383750,3.363087
6,-2.122943,1.020718,1.966526
7,-1.265828,-0.076759,2.111618
6,-1.791026,-1.434454,2.280246
1,-1.922017,-1.958335,1.324859
1,-1.096046,-2.005694,2.903196
1,-2.753483,-1.388956,2.794329
8,-1.720782,2.167231,2.054543
1,1.222176,-0.003304,-1.769575
1,-7.158283,0.391615,0.111283
9,-7.001679,1.148559,2.578180
1,3.354996,-0.008298,1.969462

Compound 2.4

E(B3LYP)	H(B3LYP)	G(B3LYP)
-845.454147587	-845.221454	-845.278214

6,-2.154471,1.006238,-0.049884
6,-2.168962,-0.405951,0.187126
6,-3.380450,-1.088287,0.198233
6,-4.583085,-0.408389,-0.010022

6,-4.546466,0.963806,-0.231879
6,-3.360315,1.685739,-0.260124
1,-3.377192,-2.160511,0.366386
1,-5.536800,-0.924988,-0.006598
1,-3.379255,2.753173,-0.448387
6,-0.848757,1.576168,-0.083158
6,0.368207,1.492398,-0.042018
6,1.600387,0.769234,-0.056739
6,2.887728,1.301594,0.089778
6,1.433093,-0.634816,-0.247447
6,3.996023,0.456576,0.050581
1,3.011118,2.371228,0.228750
6,2.553713,-1.458392,-0.310269
6,3.832183,-0.916731,-0.147792
1,2.426823,-2.521996,-0.492234
1,4.701748,-1.566584,-0.188355
6,0.022135,-1.104311,-0.551984
7,-0.923750,-1.059137,0.483348
6,-0.509219,-0.994425,1.887478
1,-0.405929,0.035720,2.251788
1,-1.255074,-1.511272,2.499234
1,0.446951,-1.508519,2.005711
8,-0.293001,-1.396158,-1.692114
9,-5.706244,1.621550,-0.432385
1,4.992710,0.872255,0.167975

Compound 2.5

E(B3LYP)	H(B3LYP)	G(B3LYP)
-845.454334281	-845.221641	-845.278528

6,-0.000817,-0.001191,0.000671
6,-0.000548,-0.002746,1.431680
6,1.206312,-0.001161,2.120543
6,2.415659,-0.004229,1.418678
6,2.420107,-0.007670,0.022305
6,1.219868,-0.002927,-0.686736
1,1.190153,0.008769,3.206057
1,3.354420,-0.000255,1.965186
1,3.362737,-0.007898,-0.517498
1,1.218965,0.004684,-1.772244
6,-1.303298,0.039546,-0.577016
6,-2.520340,0.104276,-0.511037
6,-3.742481,0.339481,0.189675
6,-5.035910,0.210685,-0.330733
6,-3.555844,0.749683,1.543948
6,-6.114313,0.491728,0.498159

1,-5.203979,-0.093162,-1.357808
6,-4.666859,1.049351,2.328759
6,-5.958718,0.908126,1.816600
1,-4.524979,1.400486,3.346746
1,-6.836450,1.127176,2.415112
6,-2.125136,1.014440,1.973968
7,-1.265706,-0.085416,2.110777
6,-1.788026,-1.444084,2.278877
1,-1.916979,-1.970636,1.324412
1,-1.093347,-2.013931,2.903733
1,-2.751563,-1.399313,2.790761
8,-1.719171,2.158253,2.082632
9,-7.360505,0.362106,0.000820

Compound 2.6

E(B3LYP)	H(B3LYP)	G(B3LYP)
-944.686498189	-944.46127	-944.520255

6,-2.153635,1.006930,-0.047537
6,-2.168116,-0.405024,0.190301
6,-3.379604,-1.087441,0.198016
6,-4.581112,-0.407256,-0.014950
6,-4.544260,0.965004,-0.237597
6,-3.358118,1.687116,-0.262313
1,-3.377052,-2.159540,0.366693
1,-5.534900,-0.923759,-0.014648
1,-3.376115,2.754352,-0.451633
6,-0.847137,1.575177,-0.077141
6,0.369774,1.494899,-0.034179
6,1.599879,0.769330,-0.050209
6,2.883710,1.309111,0.092845
6,1.432259,-0.634984,-0.242010
6,3.972553,0.448335,0.042447
1,3.037168,2.373194,0.232761
6,2.555564,-1.455335,-0.315029
6,3.836787,-0.922028,-0.157785
1,2.431930,-2.518261,-0.500787
1,4.723152,-1.545779,-0.201659
6,0.022905,-1.107953,-0.545302
7,-0.923228,-1.056739,0.489399
6,-0.512180,-0.995065,1.894685
1,-0.411556,0.034009,2.262869
1,-1.258544,-1.514884,2.503285
1,0.444326,-1.508272,2.013681
8,-0.291438,-1.409829,-1.682987
9,5.209021,0.964154,0.186518

9,-5.703058,1.622022,-0.442602

Compound 2.7

E(B3LYP)	H(B3LYP)	G(B3LYP)
-860.745206124	-860.469674	-860.530426

6,-0.032264,-0.002233,0.027467
6,-0.047425,-0.011209,1.453978
6,1.141743,-0.014987,2.175871
6,2.368413,-0.013472,1.495914
6,2.392404,-0.014053,0.091833
6,1.208646,-0.003873,-0.630153
1,1.086942,-0.007629,3.257464
1,3.355556,-0.012530,-0.407976
6,-1.322933,0.049346,-0.570956
6,-2.541428,0.113167,-0.517916
6,-3.772682,0.348822,0.166895
6,-5.064877,0.226240,-0.360796
6,-3.602817,0.748940,1.526195
6,-6.172541,0.494526,0.442534
1,-5.191973,-0.073375,-1.396595
6,-4.720451,1.037348,2.304679
6,-6.004424,0.897879,1.769493
1,-4.586101,1.377273,3.327990
6,-2.176804,1.006651,1.975854
7,-1.320068,-0.096334,2.120650
6,-1.851071,-1.455661,2.255139
1,-1.970731,-1.961843,1.288801
1,-1.167074,-2.041146,2.877482
1,-2.821000,-1.415232,2.755350
8,-1.768629,2.148302,2.099270
1,1.235137,0.008209,-1.715224
1,-7.172207,0.395057,0.028806
8,3.584398,-0.012353,2.106983
6,3.628953,0.032215,3.526342
1,3.157427,-0.853372,3.971986
1,4.687703,0.047929,3.790066
1,3.142752,0.936047,3.914706
1,-6.872317,1.115746,2.385481

Compound 2.8

E(B3LYP)	H(B3LYP)	G(B3LYP)
-860.745261113	-860.469726	-860.530441

6,0.029723,-0.010002,-0.025858
6,0.047458,-0.013229,1.405334

6,1.261006,-0.015834,2.082069
6,2.463808,-0.023517,1.368909
6,2.452424,-0.026568,-0.027268
6,1.244765,-0.016351,-0.723886
1,1.255216,-0.007200,3.167810
1,3.389130,-0.030514,-0.577594
6,-1.278132,0.038463,-0.590381
6,-2.494312,0.105232,-0.501550
6,-3.706118,0.342199,0.214326
6,-5.018686,0.221940,-0.270358
6,-3.506358,0.750148,1.562340
6,-6.099308,0.495969,0.554441
1,-5.183148,-0.083390,-1.299158
6,-4.593243,1.049477,2.380985
6,-5.896171,0.911514,1.881392
1,-4.411479,1.397836,3.391154
6,-2.068289,1.009020,1.976112
7,-1.210846,-0.093060,2.099620
6,-1.739712,-1.450363,2.258830
1,-1.877102,-1.966463,1.300197
1,-1.044128,-2.029199,2.874478
1,-2.700312,-1.405110,2.776425
8,-1.660736,2.152603,2.084090
1,1.233535,-0.008064,-1.809408
1,-7.118825,0.405013,0.193905
8,-7.025653,1.161845,2.598126
6,-6.891267,1.614074,3.938514
1,-6.351327,2.568092,3.988747
1,-7.908353,1.753674,4.308330
1,-6.376258,0.872572,4.563028
1,3.408170,-0.023835,1.905743

Compound 2.9

E(B3LYP)	H(B3LYP)	G(B3LYP)
-845.453405266	-845.220573	-845.277321

6,-1.640908,0.852430,0.051286
6,-1.643540,-0.571350,0.196298
6,-2.843462,-1.272289,0.181942
6,-4.052662,-0.585963,0.028141
6,-4.073014,0.802093,-0.112819
6,-2.870839,1.497027,-0.102118
1,-2.823295,-2.352328,0.283613
1,-5.000104,1.351589,-0.236448
6,-0.357209,1.463429,0.038020
6,0.860716,1.392086,0.069433

6,2.104887,0.694546,-0.001793
6,3.384251,1.238217,0.170414
6,1.960003,-0.696864,-0.282437
6,4.506207,0.416840,0.067651
1,3.490690,2.298431,0.378273
6,3.093597,-1.495179,-0.407049
6,4.364209,-0.943185,-0.218909
1,2.983119,-2.546693,-0.657312
1,5.244205,-1.573789,-0.308438
6,0.554890,-1.169375,-0.606911
7,-0.382485,-1.216489,0.437356
6,0.042077,-1.231515,1.840281
1,0.129378,-0.224225,2.267263
1,-0.688870,-1.800049,2.423335
1,1.008671,-1.733418,1.918218
8,0.232094,-1.388120,-1.760989
1,-4.987719,-1.137568,0.014785
1,5.496652,0.841379,0.204658
9,-2.881610,2.835632,-0.240469

Compound 2.10

E(B3LYP)	H(B3LYP)	G(B3LYP)
-924.091798918	-923.800226	-923.86653

6,-0.001665,-0.013666,0.000204
6,0.001800,-0.008303,1.429409
6,1.203206,-0.009375,2.122120
6,2.425063,-0.015991,1.432938
6,2.405211,-0.028047,0.032957
6,1.216775,-0.022416,-0.702770
1,1.180333,0.003380,3.208306
1,3.350417,-0.035153,-0.505663
6,-1.305922,0.028976,-0.572446
6,-2.524014,0.094773,-0.515208
6,-3.743315,0.339893,0.187322
6,-5.039010,0.214687,-0.328999
6,-3.552917,0.754971,1.539974
6,-6.114469,0.503629,0.501000
1,-5.210977,-0.093067,-1.354300
6,-4.660954,1.061266,2.326151
6,-5.954777,0.923596,1.817713
1,-4.515252,1.415460,3.342569
1,-6.830302,1.148146,2.417419
6,-2.120536,1.017083,1.966267
7,-1.265140,-0.084092,2.108986
6,-1.792401,-1.440064,2.280439

1,-1.927561,-1.966789,1.326978
1,-1.097173,-2.011946,2.902809
1,-2.753695,-1.390946,2.796276
8,-1.711292,2.160805,2.067551
9,-7.362558,0.377273,0.006368
6,1.223210,-0.021032,-2.211174
1,0.694789,-0.894014,-2.613332
1,0.716652,0.867427,-2.607236
1,2.244444,-0.032766,-2.603289
6,3.730523,0.013785,2.191562
1,4.576705,-0.234233,1.543340
1,3.918271,1.009336,2.614625
1,3.724463,-0.694416,3.028096

Compound 2.11

E(B3LYP)	H(B3LYP)	G(B3LYP)
-824.859117055	-824.560106	-824.624122

6,0.000442,0.004439,-0.000684
6,0.000497,0.006388,1.428464
6,1.200009,0.004217,2.124735
6,2.424036,-0.001178,1.439610
6,2.407946,-0.010156,0.039677
6,1.221416,-0.002558,-0.699244
1,1.173588,0.014155,3.210932
1,3.354671,-0.016647,-0.496408
6,-1.301772,0.047207,-0.578766
6,-2.520074,0.110816,-0.520720
6,-3.744475,0.346814,0.177681
6,-5.042141,0.215714,-0.333845
6,-3.559015,0.757162,1.531854
6,-6.141094,0.484828,0.481196
1,-5.180560,-0.091634,-1.365962
6,-4.668113,1.046000,2.322023
6,-5.957840,0.897376,1.803334
1,-4.522999,1.393275,3.341347
1,-6.819096,1.115366,2.428582
6,-2.126910,1.024503,1.958061
7,-1.267793,-0.073172,2.105646
6,-1.793292,-1.430751,2.269857
1,-1.926537,-1.952342,1.313309
1,-1.097918,-2.004670,2.890218
1,-2.755508,-1.385657,2.784432
8,-1.721462,2.170179,2.052887
6,1.232197,0.004346,-2.207674
1,0.673542,-0.847127,-2.614680

1,0.758725,0.912115,-2.601360
1,2.253469,-0.041901,-2.597322
6,3.727448,0.025127,2.202151
1,4.575717,-0.216771,1.554229
1,3.912921,1.017540,2.633508
1,3.720622,-0.689751,3.033053
1,-7.145395,0.378555,0.080628

Transition States: *Cis* lactam *syn* regioisomers

Compound 2.1

E(B3LYP)	H(B3LYP)	G(B3LYP)
-950.294970278	-949.998093	-950.066906

6,0.066952,0.052707,0.075666
6,0.074055,-0.003897,1.495320
6,1.301007,0.043744,2.165527
6,2.499880,0.178161,1.464354
6,2.488020,0.271807,0.071245
6,1.279524,0.202149,-0.615477
1,1.310315,-0.011864,3.250098
1,3.439426,0.214445,2.008446
1,3.418463,0.383891,-0.478201
1,1.258500,0.236748,-1.700275
6,-1.179192,-0.252636,-0.544079
6,-2.160741,-0.998201,-0.438567
6,-2.662297,-2.106157,0.314859
6,-3.270612,-3.214261,-0.298816
6,-2.412726,-2.123462,1.713701
6,-3.573511,-4.353890,0.437362
1,-3.482407,-3.164758,-1.361830
6,-2.751996,-3.276687,2.435535
6,-3.295974,-4.393140,1.806641
1,-4.027578,-5.210056,-0.054273
1,-2.603597,-3.272179,3.510046
1,-3.529575,-5.280509,2.388146
6,-2.081858,-0.911649,2.568093
7,-1.136420,0.066682,2.270556
8,-2.762563,-0.769272,3.582417
6,-1.198048,1.228145,3.178305
1,-0.812154,0.994154,4.177537
1,-0.612226,2.037347,2.739176
1,-2.237471,1.539657,3.290118
1,-1.557963,2.359112,-4.112213
6,-0.987951,1.612060,-3.547462
7,-1.758736,1.096114,-2.413930
1,-0.110056,2.101165,-3.122194

1,-0.660608,0.816602,-4.228626
7,-2.768735,0.397958,-2.639158
7,-3.507529,-0.416646,-2.275780

Compound 2.2

E(B3LYP)	H(B3LYP)	G(B3LYP)
-1049.52749768	-1049.237985	-1049.308587

6,0.001697,-0.004985,0.000766
6,-0.000976,0.005827,1.422656
6,1.220907,0.020209,2.103481
6,2.410071,0.052818,1.385399
6,2.437718,0.077436,-0.004210
6,1.225693,0.039822,-0.685724
1,1.255502,0.020633,3.187384
1,3.388192,0.109713,-0.525743
6,-1.255172,-0.263616,-0.615433
6,-2.289033,-0.929642,-0.481845
6,-2.860880,-1.974632,0.310556
6,-3.539198,-3.063321,-0.262799
6,-2.612553,-1.956346,1.709645
6,-3.913588,-4.153677,0.514126
1,-3.748009,-3.039607,-1.327263
6,-3.023784,-3.058761,2.472634
6,-3.638099,-4.160626,1.884267
1,-2.873820,-3.025212,3.546368
6,-2.204219,-0.739722,2.521447
7,-1.205351,0.176529,2.186755
8,-2.864133,-0.524431,3.535537
6,-1.195154,1.367001,3.059120
1,-0.810684,1.144028,4.061392
1,-0.573819,2.131181,2.589031
1,-2.215719,1.734849,3.170445
1,-1.468232,2.227517,-4.290537
6,-0.946444,1.465601,-3.699712
7,-1.743598,1.045978,-2.544708
1,-0.035268,1.910662,-3.296481
1,-0.677276,0.624900,-4.351355
7,-2.798931,0.408574,-2.739920
7,-3.589803,-0.337970,-2.341390
1,1.214150,0.023337,-1.770605
1,-4.421590,-4.996471,0.053139
9,3.574203,0.069698,2.065540
1,-3.926997,-5.009411,2.497588

Compound 2.3

E(B3LYP) H(B3LYP) G(B3LYP)
-1049.52774509 -1049.238282 -1049.3092

6,-0.004869,0.007437,0.002669
6,-0.000965,-0.000818,1.423283
6,1.225430,-0.008082,2.095574
6,2.430849,0.025748,1.393438
6,2.425074,0.072601,-0.002057
6,1.215169,0.056158,-0.689737
1,1.230076,-0.026631,3.181458
1,3.360940,0.106834,-0.552620
6,-1.267907,-0.242535,-0.607916
6,-2.288041,-0.930814,-0.482013
6,-2.856860,-1.973985,0.313121
6,-3.531140,-3.068126,-0.256894
6,-2.608567,-1.953403,1.712897
6,-3.905707,-4.160906,0.515062
1,-3.741329,-3.049945,-1.320851
6,-3.013382,-3.050043,2.484235
6,-3.619451,-4.138360,1.876627
1,-2.884268,-3.035984,3.559967
6,-2.209350,-0.728772,2.522642
7,-1.205464,0.174072,2.192636
8,-2.889296,-0.506652,3.522569
6,-1.199855,1.375576,3.049470
1,-0.833579,1.160568,4.060156
1,-0.562795,2.126943,2.580237
1,-2.218495,1.755188,3.140232
1,-1.469221,2.228274,-4.287475
6,-0.945368,1.474012,-3.688758
7,-1.752293,1.046155,-2.543608
1,-0.045220,1.930706,-3.274149
1,-0.657268,0.635437,-4.334927
7,-2.797850,0.396817,-2.749742
7,-3.585775,-0.357684,-2.360971
1,3.370585,0.021031,1.938276
1,1.197656,0.054237,-1.775128
1,-4.410303,-5.019111,0.083706
9,-3.971664,-5.196789,2.635747

Compound 2.4
E(B3LYP) H(B3LYP) G(B3LYP)
-1049.5275811 -1049.238085 -1049.308653

6,1.838054,-0.100948,-0.443648
6,1.522853,-1.448554,-0.118320

6,2.228987,-2.476747,-0.752156
6,3.248942,-2.206452,-1.664507
6,3.559466,-0.879145,-1.936817
6,2.870796,0.172640,-1.352567
1,1.983975,-3.507648,-0.515542
1,3.799731,-3.002239,-2.154199
1,3.112583,1.194107,-1.622592
6,0.922572,0.877404,0.040369
6,-0.288778,1.053966,0.220590
6,-1.571146,0.458223,0.004454
6,-2.659569,1.192498,-0.496409
6,-1.690856,-0.946527,0.185684
6,-3.832400,0.550398,-0.876537
1,-2.556334,2.268148,-0.594027
6,-2.894613,-1.563681,-0.183244
6,-3.943976,-0.835849,-0.737228
1,-3.002396,-2.627884,-0.003151
1,-4.857180,-1.344590,-1.032768
6,-0.755985,-1.814983,1.009736
7,0.635167,-1.785536,0.962233
8,-1.293934,-2.554690,1.831460
6,1.273579,-2.560262,2.042987
1,1.193289,-3.641911,1.881520
1,2.325828,-2.274674,2.092730
1,0.780455,-2.329677,2.988219
1,3.257578,4.484103,1.078963
6,2.972806,3.716913,0.349693
7,1.881131,2.880262,0.855068
1,3.824890,3.051342,0.202805
1,2.723979,4.198532,-0.604091
7,0.752091,3.389681,1.007842
7,-0.396749,3.253002,1.055399
9,4.549526,-0.603006,-2.810770
1,-4.659550,1.129047,-1.278778

Compound 2.5

E(B3LYP)	H(B3LYP)	G(B3LYP)
-1049.52858277	-1049.239063	-1049.309634

6,-0.001057,0.004667,-0.001371
6,-0.001575,0.004857,1.419164
6,1.224419,0.007944,2.092830
6,2.430656,0.043381,1.392167
6,2.428137,0.079972,-0.003658
6,1.219401,0.053367,-0.692849
1,1.228439,-0.003997,3.178749

1,3.369355,0.047025,1.938856
1,3.364938,0.114243,-0.552531
1,1.203310,0.043309,-1.778211
6,-1.261641,-0.252859,-0.613308
6,-2.290873,-0.926321,-0.481362
6,-2.854949,-1.973127,0.313108
6,-3.531182,-3.057038,-0.269136
6,-2.605378,-1.957504,1.713189
6,-3.897850,-4.130831,0.524354
1,-3.749834,-3.059366,-1.330405
6,-3.024757,-3.060092,2.473109
6,-3.640326,-4.163338,1.891697
1,-2.878304,-3.029060,3.547029
1,-3.945878,-5.022497,2.479087
6,-2.196493,-0.745404,2.529269
7,-1.208886,0.175097,2.183944
8,-2.847902,-0.539585,3.551888
6,-1.203394,1.372011,3.046546
1,-0.809560,1.161172,4.047795
1,-0.591574,2.137138,2.565514
1,-2.226206,1.732728,3.162713
1,-1.457157,2.210894,-4.293176
6,-0.940352,1.459017,-3.685509
7,-1.752677,1.050970,-2.536703
1,-0.036998,1.912629,-3.274557
1,-0.659011,0.610585,-4.321638
7,-2.802800,0.407629,-2.738489
7,-3.594408,-0.342069,-2.348706
9,-4.524081,-5.178782,-0.047261

Compound 2.6

E(B3LYP)	H(B3LYP)	G(B3LYP)
-1148.76092526	-1148.478826	-1148.551413

6,1.841811,-0.100276,-0.450616
6,1.526290,-1.446165,-0.119273
6,2.235442,-2.476337,-0.746615
6,3.257339,-2.208527,-1.657437
6,3.567604,-0.882301,-1.935545
6,2.875870,0.171336,-1.358352
1,1.991768,-3.506670,-0.506372
1,3.810413,-3.005980,-2.141843
1,3.116547,1.191950,-1.632451
6,0.922992,0.878621,0.026102
6,-0.286996,1.055485,0.213529
6,-1.568084,0.458297,-0.002018

6,-2.651294,1.201054,-0.498137
6,-1.690147,-0.947063,0.179740
6,-3.814152,0.542086,-0.859697
1,-2.572691,2.275955,-0.609963
6,-2.901776,-1.558033,-0.177752
6,-3.956399,-0.835964,-0.725651
1,-3.013871,-2.620999,0.004472
1,-4.884827,-1.314371,-1.018373
6,-0.756869,-1.821469,0.996041
7,0.635375,-1.778379,0.960382
8,-1.293796,-2.579248,1.801834
6,1.269961,-2.556835,2.041110
1,1.194627,-3.637847,1.873909
1,2.320702,-2.267357,2.099110
1,0.770119,-2.332706,2.984342
1,3.252869,4.480957,1.083034
6,2.966812,3.718174,0.349792
7,1.878123,2.876790,0.854823
1,3.819290,3.054881,0.195464
1,2.712692,4.205282,-0.599665
7,0.748446,3.382683,1.011461
7,-0.400152,3.246259,1.059442
9,-4.840612,1.259081,-1.357789
9,4.559501,-0.609602,-2.807759

Compound 2.7

E(B3LYP)	H(B3LYP)	G(B3LYP)
-1064.81792606	-1064.485683	-1064.560605

6,-0.035562,0.001875,0.029587
6,-0.051381,0.007684,1.445974
6,1.159235,0.017731,2.151566
6,2.380962,0.052428,1.470278
6,2.397094,0.085030,0.066863
6,1.203866,0.050469,-0.634230
1,1.127461,0.011258,3.234217
1,3.354316,0.119611,-0.442992
6,-1.281265,-0.266371,-0.601000
6,-2.325806,-0.919702,-0.486245
6,-2.898190,-1.971615,0.297652
6,-3.569923,-3.059572,-0.285429
6,-2.661067,-1.960624,1.699298
6,-3.946877,-4.155161,0.482775
1,-3.770851,-3.030825,-1.351303
6,-3.075672,-3.068130,2.453201

6,-3.682000,-4.169015,1.855041
1,-2.934926,-3.038999,3.528405
6,-2.264915,-0.746269,2.520553
7,-1.267614,0.173074,2.197284
8,-2.936707,-0.535661,3.528895
6,-1.281569,1.370941,3.057588
1,-0.916552,1.161101,4.070291
1,-0.655108,2.133840,2.592243
1,-2.306173,1.734577,3.145789
1,-1.436898,2.198067,-4.320760
6,-0.918924,1.444174,-3.716095
7,-1.729163,1.026187,-2.569991
1,-0.016560,1.898188,-3.303083
1,-0.633556,0.601121,-4.357945
7,-2.781710,0.387726,-2.778330
7,-3.582436,-0.351502,-2.385399
1,1.212630,0.039102,-1.719524
1,-4.448836,-4.996995,0.013279
8,3.600589,0.064421,2.076497
6,3.653596,0.023866,3.495166
1,4.713765,0.030760,3.753702
1,3.165829,0.900092,3.941901
1,3.189244,-0.889214,3.889607
1,-3.973392,-5.021821,2.461676

Compound 2.8

E(B3LYP)	H(B3LYP)	G(B3LYP)
-1064.81826635	-1064.485964	-1064.560505

6,0.022988,0.053383,-0.003872
6,0.033418,0.046634,1.416754
6,1.262184,0.041886,2.084258
6,2.465238,0.079429,1.377662
6,2.452895,0.127507,-0.017662
6,1.240268,0.107583,-0.700771
1,1.270756,0.024569,3.170262
1,3.386323,0.165392,-0.572339
6,-1.242866,-0.202583,-0.605389
6,-2.249049,-0.908241,-0.460334
6,-2.815420,-1.940345,0.348168
6,-3.493260,-3.044093,-0.205159
6,-2.569178,-1.913348,1.744574
6,-3.868495,-4.121024,0.577565
1,-3.705684,-3.039679,-1.269053
6,-2.977730,-3.001618,2.530487
6,-3.594489,-4.113212,1.954994

1,-2.835214,-2.931681,3.600958
6,-2.157190,-0.689089,2.547270
7,-1.169594,0.223041,2.189876
8,-2.810141,-0.468331,3.566643
6,-1.161442,1.432454,3.034569
1,-0.771403,1.233688,4.039898
1,-0.543545,2.186844,2.544641
1,-2.182500,1.800916,3.142706
1,-1.477928,2.168547,-4.349913
6,-0.945979,1.438396,-3.728634
7,-1.746443,1.037648,-2.569504
1,-0.049859,1.916727,-3.329883
1,-0.649914,0.583516,-4.349544
7,-2.785474,0.371081,-2.756333
7,-3.561047,-0.383844,-2.343408
1,1.218871,0.105399,-1.786135
1,-4.376722,-4.980163,0.151202
1,3.407287,0.077879,1.918577
8,-3.990597,-5.220911,2.643676
6,-3.778471,-5.251386,4.047700
1,-4.324124,-4.445543,4.555000
1,-4.160400,-6.216412,4.385555
1,-2.711600,-5.175419,4.295322

Compound 2.9

E(B3LYP)	H(B3LYP)	G(B3LYP)
-1049.528904	-1049.239236	-1049.309078

6,1.535191,-0.512705,-0.373596
6,0.836137,-1.697440,-0.015759
6,1.265017,-2.927689,-0.526652
6,2.380788,-3.008434,-1.360309
6,3.094043,-1.858256,-1.700670
6,2.653064,-0.641211,-1.207098
1,0.723197,-3.828486,-0.256796
1,2.698023,-3.972695,-1.745612
1,3.963445,-1.888178,-2.348615
6,0.931246,0.727437,-0.024199
6,-0.192871,1.239964,0.057066
6,-1.570331,1.021064,-0.257730
6,-2.356415,1.999522,-0.889752
6,-2.106634,-0.274882,-0.029822
6,-3.631345,1.694028,-1.351647
1,-1.938684,2.992149,-1.021853
6,-3.405266,-0.547154,-0.483253
6,-4.151557,0.410202,-1.164489

1,-4.220872,2.455924,-1.854395
1,-3.830781,-1.521580,-0.268596
1,-5.147285,0.164542,-1.522592
6,-1.528887,-1.314674,0.912916
7,-0.188311,-1.689730,0.991909
8,-2.317112,-1.816597,1.711312
6,0.107112,-2.552545,2.151922
1,-0.288106,-3.567359,2.025644
1,1.189886,-2.593686,2.281361
1,-0.357377,-2.124578,3.041175
1,4.090336,3.582883,1.036392
6,3.613275,2.876468,0.347664
7,2.334502,2.399980,0.887501
1,4.247786,1.997287,0.246087
1,3.497276,3.343555,-0.637008
7,1.377851,3.197782,0.933142
7,0.237381,3.391471,0.884777
9,3.322903,0.481404,-1.553420

Compound 2.10

E(B3LYP)	H(B3LYP)	G(B3LYP)
-1128.16509899	-1127.816686	-1127.895753

6,-0.005861,0.001088,-0.004426
6,-0.005669,0.003235,1.413563
6,1.211442,0.003348,2.099335
6,2.431513,0.026787,1.417257
6,2.409477,0.037846,0.016894
6,1.218535,0.011531,-0.709358
1,1.202289,-0.005967,3.185899
1,3.352088,0.044621,-0.526836
6,-1.282177,-0.226225,-0.602266
6,-2.294974,-0.930998,-0.493919
6,-2.806597,-2.014754,0.285991
6,-3.438853,-3.120787,-0.304665
6,-2.556282,-2.002086,1.686298
6,-3.760984,-4.215000,0.480198
1,-3.659050,-3.125726,-1.365845
6,-2.932520,-3.125489,2.437968
6,-3.503663,-4.247815,1.847673
1,-2.787257,-3.097206,3.512254
1,-3.775515,-5.123014,2.427867
6,-2.190711,-0.780441,2.508574
7,-1.219968,0.160424,2.173991
8,-2.858059,-0.591727,3.524655

6,-1.233618,1.347065,3.048301
1,-0.847839,1.129632,4.051428
1,-0.622139,2.122023,2.582491
1,-2.260635,1.698205,3.159571
1,-2.435152,3.135877,-1.247797
6,-1.807589,2.775816,-2.071442
7,-1.917917,1.325204,-2.262591
1,-0.760698,2.972077,-1.834041
1,-2.063261,3.318274,-2.989046
7,-3.065594,0.831319,-2.325392
7,-3.788387,-0.037412,-2.079229
9,-4.344439,-5.283150,-0.099874
6,3.739619,0.062966,2.171758
1,4.517854,-0.505456,1.651033
1,4.108448,1.091912,2.280143
1,3.632761,-0.352670,3.178924
6,1.236202,-0.069091,-2.215837
1,0.937350,-1.069750,-2.554317
1,0.530819,0.632507,-2.671209
1,2.237965,0.132067,-2.607747

Compound 2.11

E(B3LYP)	H(B3LYP)	G(B3LYP)
-1028.93152016	-1028.575697	-1028.653182

6,0.000357,0.000607,0.000587
6,0.002138,-0.001276,1.419111
6,1.219297,-0.007070,2.104375
6,2.439465,0.015600,1.421910
6,2.416358,0.031813,0.022127
6,1.224567,0.011208,-0.703862
1,1.210292,-0.020982,3.191061
1,3.358753,0.038265,-0.521946
6,-1.276181,-0.223151,-0.599052
6,-2.282258,-0.938158,-0.493713
6,-2.798307,-2.020968,0.285895
6,-3.425947,-3.135975,-0.295478
6,-2.553043,-2.001373,1.685780
6,-3.753326,-4.246348,0.474060
1,-3.634330,-3.116770,-1.360477
6,-2.919757,-3.123524,2.442010
6,-3.483682,-4.247963,1.845674
1,-2.775542,-3.088824,3.516682
1,-3.738652,-5.111573,2.453399
6,-2.197411,-0.769303,2.500021
7,-1.210699,0.158507,2.180937

8,-2.889000,-0.563664,3.496448
6,-1.226257,1.347924,3.051257
1,-0.864907,1.126709,4.062623
1,-0.593976,2.112992,2.597251
1,-2.250229,1.714145,3.140729
1,-2.449171,3.123015,-1.236068
6,-1.818897,2.775338,-2.063043
7,-1.916061,1.325512,-2.265438
1,-0.773667,2.979054,-1.824367
1,-2.079913,3.323417,-2.975914
7,-3.060094,0.822929,-2.330034
7,-3.775625,-0.052309,-2.084429
6,3.747015,0.046120,2.177893
1,4.549083,-0.436047,1.609125
1,4.066888,1.077352,2.380261
1,3.663275,-0.462713,3.143983
6,1.241818,-0.063106,-2.210674
1,0.925494,-1.056575,-2.554345
1,0.548873,0.652713,-2.663254
1,2.247097,0.122839,-2.601291
1,-4.221755,-5.108517,0.006978

Transition States: *Trans* lactam *syn* regioisomers

Compound 2.1

E(B3LYP)	H(B3LYP)	G(B3LYP)
-950.301943826	-950.004959	-950.071729

6,0.108137,-0.074294,0.112466
6,0.067874,-0.019728,1.535855
6,1.242458,0.102591,2.269771
6,2.473500,0.185128,1.615237
6,2.523241,0.160489,0.219807
6,1.353151,0.034409,-0.526435
1,1.179049,0.150454,3.352565
1,3.387898,0.285588,2.192973
1,3.478149,0.248440,-0.291129
1,1.385384,0.047288,-1.610411
6,-1.158166,-0.191686,-0.555227
6,-2.404008,-0.119276,-0.552925
6,-3.614372,0.199090,0.168419
6,-4.910060,0.050879,-0.351420
6,-3.464416,0.706467,1.490461
6,-6.022481,0.389467,0.416500
1,-5.032518,-0.326540,-1.359296
6,-4.584872,1.068694,2.235592
6,-5.865712,0.897359,1.708062

1,-7.018102,0.263632,-0.000222
1,-4.448904,1.490255,3.227733
1,-6.736260,1.171125,2.297625
6,-2.059190,0.987566,1.956439
7,-1.216758,-0.111023,2.168028
6,-1.738495,-1.462563,2.374616
1,-1.819137,-2.033652,1.440961
1,-1.071839,-1.997416,3.058875
1,-2.726380,-1.400744,2.835586
8,-1.645074,2.132321,2.030451
7,-3.000378,-0.881010,-2.569342
7,-1.934397,-1.207992,-2.901952
7,-0.716181,-1.132212,-2.609049
6,0.128239,-2.290453,-2.924639
1,0.341649,-2.344555,-3.998664
1,1.068469,-2.140978,-2.392405
1,-0.319175,-3.235575,-2.594899

Compound 2.2

E(B3LYP)	H(B3LYP)	G(B3LYP)
-1049.53458202	-1049.244954	-1049.313518

6,0.000000,0.000000,0.000000
6,0.000000,0.000000,1.425926
6,1.194322,0.000000,2.136970
6,2.393144,0.016998,1.431479
6,2.433431,0.047977,0.041809
6,1.234690,0.042155,-0.666985
1,1.192642,0.009617,3.221046
1,3.392109,0.084934,-0.464705
6,-1.286476,0.004015,-0.636863
6,-2.523383,0.164382,-0.594938
6,-3.688775,0.537566,0.172567
6,-5.005516,0.499343,-0.312684
6,-3.467110,0.981802,1.507089
6,-6.069450,0.884799,0.500598
1,-5.182300,0.170684,-1.329536
6,-4.537702,1.392309,2.298876
6,-5.841558,1.330808,1.804325
1,-4.345213,1.764576,3.301331
6,-2.033401,1.144752,1.938738
7,-1.268240,-0.020583,2.091818
6,-1.881026,-1.338507,2.267428
1,-2.033680,-1.865690,1.317218
1,-1.234371,-1.945825,2.908877

1,-2.846069,-1.221959,2.764419
8,-1.530605,2.250999,2.036760
7,-0.963858,-0.856277,-2.746289
7,-2.190710,-0.821115,-3.010254
7,-3.219834,-0.433661,-2.629995
6,-0.221068,-2.056868,-3.148516
1,0.734471,-2.019432,-2.623672
1,-0.740683,-2.981887,-2.872369
1,-0.024758,-2.058213,-4.227120
1,-7.082623,0.844515,0.110154
1,1.243453,0.096556,-1.749642
9,3.551919,0.015918,2.119874
1,-6.673790,1.641794,2.429562

Compound 2.3

E(B3LYP)	H(B3LYP)	G(B3LYP)
-1049.53497718	-1049.245401	-1049.314198

6,0.000000,0.000000,0.000000
6,0.000000,0.000000,1.425033
6,1.197960,0.000000,2.130473
6,2.415151,0.011718,1.445549
6,2.428073,0.039733,0.049406
6,1.233631,0.036489,-0.668372
1,1.165362,0.008668,3.215664
1,3.373962,0.072774,-0.484247
6,-1.287820,0.009973,-0.635964
6,-2.523717,0.177513,-0.595677
6,-3.687299,0.554383,0.170217
6,-5.003969,0.528214,-0.318975
6,-3.468303,0.989231,1.508899
6,-6.073002,0.911910,0.486056
1,-5.181677,0.207153,-1.337835
6,-4.533182,1.399210,2.306488
6,-5.820571,1.339576,1.785235
1,-4.372228,1.768517,3.313987
6,-2.032184,1.147004,1.943357
7,-1.272212,-0.017603,2.089442
6,-1.890572,-1.333176,2.261697
1,-2.048618,-1.855121,1.309488
1,-1.242788,-1.945716,2.896815
1,-2.852847,-1.217219,2.764600
8,-1.534810,2.255864,2.039843
7,-0.974930,-0.857378,-2.746405
7,-2.201908,-0.822142,-3.006531
7,-3.229919,-0.431307,-2.626683

6,-0.229572,-2.054163,-3.154514
1,0.731674,-2.009094,-2.641098
1,-0.740483,-2.981388,-2.869550
1,-0.046651,-2.057080,-4.235436
1,-7.093918,0.890795,0.119467
1,3.348576,0.016199,2.000994
1,1.240137,0.090854,-1.751418
9,-6.855090,1.717815,2.562116

Compound 2.4

E(B3LYP)	H(B3LYP)	G(B3LYP)
-1049.53466496	-1049.245133	-1049.314092

6,-2.010933,-0.071657,-0.216706
6,-1.843060,-1.405916,0.257453
6,-2.928458,-2.274603,0.308080
6,-4.193462,-1.857696,-0.109245
6,-4.336835,-0.561192,-0.590854
6,-3.279086,0.335184,-0.655864
1,-2.771036,-3.288178,0.662664
1,-5.051744,-2.520312,-0.083038
1,-3.430761,1.323666,-1.071649
6,-0.831387,0.746496,-0.248642
6,0.410524,0.865815,-0.215934
6,1.707001,0.232431,-0.146529
6,2.926321,0.926324,-0.093753
6,1.731714,-1.191247,-0.144577
6,4.132563,0.231166,-0.035195
1,2.916394,2.009357,-0.103728
6,2.946867,-1.872685,-0.116073
6,4.148068,-1.165380,-0.045911
1,2.947680,-2.958495,-0.154454
1,5.092099,-1.702072,-0.012784
6,0.415882,-1.896154,-0.348306
7,-0.532029,-1.801596,0.679099
6,-0.159645,-1.453360,2.051069
1,-0.225294,-0.375845,2.248731
1,-0.826076,-1.979660,2.742116
1,0.863261,-1.784268,2.241702
8,0.150140,-2.424344,-1.414700
7,-1.552052,2.925683,-0.195470
7,-0.380442,3.372112,-0.141329
7,0.740792,3.074266,-0.230824
6,-2.554159,3.547331,0.679307
1,-3.422817,2.887862,0.673303

1,-2.198031,3.655555,1.710498
1,-2.860170,4.527283,0.295049
9,-5.551877,-0.155175,-1.015911
1,5.066727,0.784188,0.010139

Compound 2.5

E(B3LYP)	H(B3LYP)	G(B3LYP)
-1049.53497762	-1049.245416	-1049.314297

6,0.000000,0.000000,0.000000
6,0.000000,0.000000,1.425048
6,1.199145,0.000000,2.128722
6,2.415306,0.013805,1.442068
6,2.427329,0.042854,0.045836
6,1.232248,0.037786,-0.670725
1,1.167864,0.008267,3.213887
1,3.349374,0.019372,1.996534
1,3.372814,0.077620,-0.488358
1,1.237233,0.091731,-1.753898
6,-1.288821,0.008265,-0.633539
6,-2.524401,0.175934,-0.593160
6,-3.684404,0.562038,0.174498
6,-4.995849,0.539482,-0.323140
6,-3.460877,1.004566,1.509949
6,-6.036430,0.947559,0.498952
1,-5.200651,0.217315,-1.335717
6,-4.530968,1.437338,2.291727
6,-5.835456,1.397608,1.799645
1,-4.340408,1.812733,3.292917
1,-6.682960,1.719116,2.395528
6,-2.028554,1.154313,1.951078
7,-1.270933,-0.015793,2.089553
6,-1.891853,-1.329567,2.264295
1,-2.056179,-1.853293,1.313941
1,-1.243517,-1.943904,2.897361
1,-2.851753,-1.209855,2.770649
8,-1.524096,2.258250,2.070059
7,-0.982855,-0.870495,-2.743201
7,-2.211295,-0.837521,-2.996044
7,-3.237448,-0.445217,-2.613140
6,-0.237752,-2.067892,-3.150005
1,0.727010,-2.018086,-2.643587
1,-0.744741,-2.994687,-2.856817
1,-0.062201,-2.075938,-4.232098
9,-7.294192,0.913018,0.011987

Compound 2.6

E(B3LYP)	H(B3LYP)	G(B3LYP)
-1148.76753447	-1148.485428	-1148.556397

6,-2.011553,-0.074064,-0.212788
6,-1.842059,-1.408886,0.259151
6,-2.926949,-2.278389,0.307511
6,-4.191433,-1.861678,-0.111327
6,-4.335923,-0.564544,-0.591192
6,-3.279110,0.333231,-0.652838
1,-2.769435,-3.292288,0.661004
1,-5.049061,-2.525221,-0.087235
1,-3.431424,1.322654,-1.066132
6,-0.832186,0.744343,-0.240750
6,0.409063,0.865703,-0.204781
6,1.704458,0.231660,-0.137837
6,2.917508,0.934490,-0.088214
6,1.731389,-1.192476,-0.140007
6,4.107698,0.222882,-0.041165
1,2.933956,2.016455,-0.094463
6,2.950399,-1.868813,-0.125438
6,4.153916,-1.167245,-0.058597
1,2.957051,-2.953900,-0.170879
1,5.112395,-1.674641,-0.034937
6,0.418933,-1.902257,-0.343004
7,-0.531423,-1.803242,0.682132
6,-0.162463,-1.460081,2.056403
1,-0.221763,-0.382820,2.257460
1,-0.835404,-1.983630,2.743136
1,0.857084,-1.798802,2.251128
8,0.157389,-2.441155,-1.405029
7,-1.546802,2.929771,-0.190626
7,-0.373574,3.369527,-0.131861
7,0.746575,3.066738,-0.216187
6,-2.553873,3.563650,0.669732
1,-3.429433,2.913587,0.653750
1,-2.209755,3.670540,1.705067
1,-2.844042,4.545720,0.278968
9,5.267263,0.909340,0.015608
9,-5.550575,-0.159364,-1.016727

Compound 2.7

E(B3LYP)	H(B3LYP)	G(B3LYP)
-1064.82562277	-1064.493204	-1064.565781

6,0.000039,0.000046,-0.000102
6,0.000030,-0.000271,1.425338
6,1.197798,-0.000156,2.131139
6,2.415788,0.009824,1.447558
6,2.428896,0.036067,0.051358
6,1.234831,0.034103,-0.667127
1,1.163966,0.008275,3.216342
1,3.375055,0.066993,-0.482161
6,-1.287615,0.012280,-0.634937
6,-2.523152,0.182742,-0.588015
6,-3.682628,0.561659,0.180279
6,-5.005810,0.544180,-0.299656
6,-3.465307,0.998335,1.513699
6,-6.062258,0.936740,0.506824
1,-5.192433,0.221643,-1.316800
6,-4.524268,1.421130,2.316859
6,-5.832244,1.379528,1.819626
1,-4.310240,1.789574,3.313466
6,-2.031694,1.149147,1.955868
7,-1.272045,-0.019078,2.089760
6,-1.893953,-1.334503,2.248374
1,-2.047410,-1.849916,1.291993
1,-1.251609,-1.952915,2.883739
1,-2.859724,-1.219448,2.744667
8,-1.532012,2.255110,2.078466
7,-0.981607,-0.860351,-2.745773
7,-2.209820,-0.825466,-3.002322
7,-3.236982,-0.433047,-2.621977
6,-0.240405,-2.061118,-3.148290
1,0.716053,-2.022444,-2.625243
1,-0.759151,-2.985913,-2.869379
1,-0.046463,-2.064760,-4.227466
1,-7.083462,0.920575,0.139349
1,1.242512,0.087516,-1.750384
1,3.348941,0.013455,2.003612
8,-6.938032,1.751997,2.520853
6,-6.766195,2.245320,3.841942
1,-6.145423,3.150204,3.855731
1,-7.767576,2.487535,4.201829
1,-6.317566,1.488791,4.498986

Compound 2.8

E(B3LYP)	H(B3LYP)	G(B3LYP)
-1064.82532747	-1064.492973	-1064.56593

6,-0.000062,0.000190,-0.000057

6,-0.000036,0.000229,1.420733
6,1.189598,0.000260,2.143623
6,2.414548,0.014801,1.464349
6,2.430992,0.040115,0.060502
6,1.244020,0.036236,-0.655530
1,1.132984,0.013093,3.225057
1,3.391219,0.074639,-0.444181
6,-1.283305,0.014048,-0.639727
6,-2.520625,0.173664,-0.604798
6,-3.686087,0.546652,0.161716
6,-5.001982,0.514330,-0.327142
6,-3.468114,0.984308,1.499403
6,-6.067769,0.898691,0.484035
1,-5.176212,0.190778,-1.346097
6,-4.541119,1.393282,2.289215
6,-5.843670,1.337786,1.790798
1,-4.350694,1.760691,3.293939
6,-2.036720,1.143357,1.941697
7,-1.271024,-0.022172,2.086801
6,-1.887186,-1.340365,2.245511
1,-2.044472,-1.855296,1.289364
1,-1.239214,-1.957917,2.876012
1,-2.850235,-1.229022,2.747850
8,-1.537977,2.249902,2.060798
7,-0.957655,-0.838096,-2.762730
7,-2.184541,-0.803644,-3.026134
7,-3.214126,-0.419477,-2.643002
6,-0.206154,-2.022607,-3.193402
1,0.754096,-1.984288,-2.677339
1,-0.712656,-2.958383,-2.928650
1,-0.020260,-2.003919,-4.273861
1,-7.079666,0.862799,0.089501
1,1.263494,0.090437,-1.738363
8,3.633198,0.016602,2.071186
6,3.680215,0.036887,3.490926
1,3.207838,-0.855590,3.921840
1,4.739385,0.046924,3.753541
1,3.195739,0.934323,3.896110
1,-6.677221,1.648056,2.414753

Compound 2.9

E(B3LYP)	H(B3LYP)	G(B3LYP)
-1049.5329982	-1049.243383	-1049.311908

6,-1.598537,0.135433,-0.118658
6,-1.554862,-1.199726,0.389444

6,-2.705476,-1.972290,0.493103
6,-3.934113,-1.455268,0.077630
6,-4.006308,-0.169429,-0.455700
6,-2.849756,0.592417,-0.555775
1,-2.622283,-2.983813,0.876461
1,-4.940501,0.251906,-0.811885
6,-0.356599,0.852455,-0.178039
6,0.892147,0.844481,-0.132083
6,2.122241,0.082829,-0.116106
6,3.406808,0.650514,-0.120686
6,2.008739,-1.336283,-0.111962
6,4.539207,-0.161272,-0.114764
1,3.506157,1.728397,-0.131975
6,3.149895,-2.135940,-0.134076
6,4.417236,-1.552523,-0.119675
1,3.039243,-3.216184,-0.168761
1,5.304043,-2.180099,-0.125726
6,0.626570,-1.911010,-0.259976
7,-0.275508,-1.700736,0.791012
6,0.161511,-1.364599,2.146598
1,0.200033,-0.282682,2.324032
1,-0.531863,-1.816559,2.863306
1,1.154599,-1.784773,2.317691
8,0.275437,-2.434845,-1.303877
7,-0.794387,3.115831,0.094995
7,0.415926,3.387672,0.249033
7,1.488741,2.938601,0.160483
6,-1.795594,3.874224,0.848288
1,-2.765102,3.477904,0.551824
1,-1.670456,3.762345,1.932718
1,-1.760621,4.938531,0.589343
9,-2.956412,1.823297,-1.099615
1,-4.833352,-2.059126,0.151685
1,5.524326,0.297216,-0.113915

Compound 2.10

E(B3LYP)	H(B3LYP)	G(B3LYP)
-1128.16646966	-1127.818224	-1127.895817

6,0.000930,0.000117,-0.000992
6,0.000815,-0.003802,1.426428
6,1.188552,-0.004547,2.141591
6,2.420411,0.021830,1.474422
6,2.412402,0.095953,0.077935
6,1.235206,0.107480,-0.679514

1,1.143814,0.002487,3.227087
1,3.362528,0.170473,-0.447327
6,-1.301620,-0.060396,-0.607771
6,-2.540327,0.092395,-0.557864
6,-3.669632,0.619596,0.172150
6,-4.973724,0.672295,-0.342501
6,-3.424998,1.116596,1.484212
6,-5.986964,1.207857,0.439222
1,-5.195251,0.300963,-1.334710
6,-4.467837,1.671065,2.226147
6,-5.765924,1.707464,1.718622
1,-4.257270,2.084304,3.208189
1,-6.591870,2.124238,2.284976
6,-1.992124,1.208114,1.937772
7,-1.273498,0.015160,2.086431
6,-1.925884,-1.273637,2.308291
1,-2.062516,-1.846037,1.382125
1,-1.318468,-1.864958,3.001871
1,-2.903874,-1.107725,2.764988
8,-1.451373,2.295841,2.055423
7,-1.165545,-1.722887,-2.232849
7,-2.412204,-1.787164,-2.365004
7,-3.398747,-1.238324,-2.071986
6,-0.390279,-2.963562,-2.211964
1,0.608464,-2.691704,-1.865139
1,-0.812084,-3.709958,-1.528336
1,-0.302455,-3.398054,-3.214949
9,-7.237726,1.247227,-0.065240
6,1.309362,0.333923,-2.170554
1,0.535202,-0.212956,-2.712492
1,1.161138,1.398887,-2.395136
1,2.291406,0.051503,-2.563921
6,3.716650,-0.008903,2.248247
1,3.673639,0.647429,3.124691
1,3.938096,-1.020600,2.613800
1,4.560907,0.308773,1.628346

Compound 2.11

E(B3LYP)	H(B3LYP)	G(B3LYP)
-1028.93336145	-1028.577688	-1028.653321

6,-0.001430,0.002903,-0.004403
6,-0.000703,-0.000322,1.422680
6,1.187272,-0.004102,2.137932
6,2.419053,0.017590,1.470978
6,2.410785,0.091220,0.074287

6,1.233463,0.106368,-0.682740
1,1.142312,0.003972,3.223439
1,3.361002,0.162768,-0.451364
6,-1.303839,-0.052745,-0.612196
6,-2.542200,0.104438,-0.562097
6,-3.672776,0.633285,0.166488
6,-4.981057,0.690674,-0.339814
6,-3.426427,1.128091,1.478349
6,-6.014672,1.218694,0.430764
1,-5.175604,0.317023,-1.338003
6,-4.467049,1.674634,2.228180
6,-5.764173,1.707242,1.715343
1,-4.252290,2.081945,3.212266
1,-6.572538,2.124192,2.309542
6,-1.990584,1.217400,1.925597
7,-1.274768,0.024268,2.083781
6,-1.932496,-1.261939,2.304794
1,-2.071828,-1.832180,1.377750
1,-1.327286,-1.856438,2.997585
1,-2.909800,-1.092388,2.761708
8,-1.445562,2.304735,2.026323
7,-1.165655,-1.727709,-2.221030
7,-2.412672,-1.796792,-2.352643
7,-3.399897,-1.245832,-2.065061
6,-0.389714,-2.967270,-2.179583
1,0.606029,-2.690272,-1.827974
1,-0.815719,-3.706201,-1.490357
1,-0.293307,-3.414014,-3.176499
6,1.306527,0.331910,-2.173952
1,0.546779,-0.233930,-2.717062
1,1.133013,1.392426,-2.401379
1,2.296006,0.071690,-2.563909
6,3.715625,-0.018218,2.244157
1,3.667989,0.620968,3.132884
1,3.945300,-1.035028,2.590204
1,4.557367,0.317466,1.630218
1,-7.021629,1.252355,0.023683

Transition States: *Cis* lactam *anti* regioisomers

Compound 2.1

E(B3LYP)	H(B3LYP)	G(B3LYP)
-950.295399122	-949.998459	-950.067786

6,0.017404,-0.024611,0.002694
6,-0.004337,-0.018435,1.422619
6,1.209414,-0.008182,2.116574

6,2.426553,0.029723,1.434224
6,2.443510,0.071461,0.038984
6,1.245822,0.041896,-0.670785
1,1.194861,-0.014449,3.202617
1,3.356969,0.037583,1.994951
1,3.388006,0.117645,-0.495846
1,1.240926,0.051579,-1.755987
6,-1.232471,-0.280022,-0.642762
6,-2.221062,-1.005047,-0.478792
6,-2.815291,-2.033440,0.309330
6,-3.443511,-3.159047,-0.252582
6,-2.610139,-1.970336,1.714168
6,-3.827212,-4.230325,0.544772
1,-3.598078,-3.184798,-1.326432
6,-3.024682,-3.057221,2.496823
6,-3.601952,-4.186734,1.923855
1,-4.297649,-5.099891,0.093803
1,-2.908451,-2.988308,3.573050
1,-3.896905,-5.021299,2.553545
6,-2.236565,-0.722598,2.496662
7,-1.223457,0.168301,2.169429
8,-2.946086,-0.473609,3.470681
6,-1.238720,1.395500,2.988695
1,-0.884187,1.213787,4.010206
1,-0.600059,2.136815,2.505985
1,-2.261088,1.770213,3.054617
7,-1.603404,0.852331,-2.658322
7,-2.637400,0.354600,-2.821788
7,-3.550050,-0.364261,-2.367726
6,-4.544854,-0.932880,-3.277916
1,-4.090926,-1.564011,-4.052385
1,-5.205660,-1.546530,-2.663414
1,-5.147125,-0.151445,-3.756152

Compound 2.2

E(B3LYP)	H(B3LYP)	G(B3LYP)
-1049.52796487	-1049.238438	-1049.310553

6,-0.005134,0.003477,0.002811
6,-0.000772,0.005753,1.423851
6,1.223453,0.017562,2.099456
6,2.408694,0.057963,1.374461
6,2.427673,0.102977,-0.014300
6,1.212145,0.071880,-0.691455
1,1.262781,0.012347,3.183223

1,3.374729,0.151450,-0.540813
6,-1.263631,-0.249516,-0.623750
6,-2.259945,-0.959655,-0.443446
6,-2.849883,-1.988242,0.347047
6,-3.500537,-3.102719,-0.210820
6,-2.616877,-1.937893,1.748007
6,-3.879497,-4.176190,0.585941
1,-3.676224,-3.117786,-1.281500
6,-3.027313,-3.026553,2.530596
6,-3.626883,-4.145816,1.960569
1,-2.889334,-2.967509,3.604793
6,-2.215064,-0.701930,2.534218
7,-1.201160,0.189130,2.196394
8,-2.896591,-0.458373,3.528313
6,-1.187284,1.400637,3.040083
1,-0.812113,1.195563,4.049650
1,-0.553735,2.146580,2.557908
1,-2.204871,1.781304,3.135165
7,-1.625943,0.854346,-2.650933
7,-2.665099,0.365103,-2.810084
7,-3.578644,-0.346942,-2.347965
6,-4.614889,-0.871748,-3.237742
1,-4.201115,-1.503780,-4.033599
1,-5.276027,-1.475907,-2.614249
1,-5.206960,-0.065993,-3.687378
1,1.188626,0.085949,-1.775895
1,-4.367736,-5.037251,0.137650
9,3.576829,0.068742,2.049373
1,-3.917990,-4.982090,2.589671

Compound 2.3

E(B3LYP)	H(B3LYP)	G(B3LYP)
-1049.52796874	-1049.23851	-1049.309849

6,-0.009129,0.003616,0.002668
6,-0.002559,-0.005307,1.422558
6,1.224038,-0.016384,2.093239
6,2.427990,0.013956,1.387498
6,2.417975,0.070534,-0.007342
6,1.206568,0.062999,-0.693971
1,1.230334,-0.033715,3.179309
1,3.352358,0.111160,-0.560022
6,-1.274393,-0.231937,-0.620634
6,-2.258516,-0.962549,-0.453924
6,-2.841165,-1.991251,0.341351
6,-3.475494,-3.118722,-0.211192

6,-2.614075,-1.932159,1.743756
6,-3.850512,-4.194179,0.583377
1,-3.647442,-3.146789,-1.281965
6,-3.014337,-3.013773,2.537531
6,-3.594975,-4.126777,1.950162
1,-2.901070,-2.969598,3.614284
6,-2.229209,-0.682792,2.522484
7,-1.204756,0.190237,2.194520
8,-2.939413,-0.425602,3.493371
6,-1.198856,1.417318,3.014825
1,-0.849230,1.226427,4.036178
1,-0.545445,2.146563,2.533999
1,-2.214208,1.811051,3.079483
7,-1.678932,0.934232,-2.607223
7,-2.714249,0.437432,-2.762827
7,-3.624126,-0.284291,-2.307366
6,-4.604464,-0.870292,-3.223208
1,-4.136360,-1.501100,-3.989446
1,-5.265194,-1.486507,-2.611202
1,-5.210029,-0.098162,-3.712022
1,1.180833,0.084233,-1.778698
1,3.369139,0.004961,1.929896
1,-4.326268,-5.075572,0.166354
9,-3.947969,-5.167745,2.731123

Compound 2.4

E(B3LYP)	H(B3LYP)	G(B3LYP)
-1049.52799869	-1049.238503	-1049.30975

6,1.920844,0.820338,-0.447548
6,2.244434,-0.508426,-0.060092
6,3.361865,-1.123541,-0.633116
6,4.173789,-0.451030,-1.547072
6,3.856660,0.862234,-1.874057
6,2.748045,1.507170,-1.346277
1,3.607440,-2.141987,-0.347641
1,5.042003,-0.924623,-1.992423
1,2.513238,2.523316,-1.641203
6,0.646393,1.306545,-0.020793
6,-0.505556,0.868850,0.088041
6,-1.368777,-0.250210,-0.100817
6,-2.634250,-0.143773,-0.704587
6,-0.836558,-1.533843,0.196624
6,-3.353352,-1.281055,-1.051295
1,-3.026484,0.845191,-0.918798

6,-1.592940,-2.663660,-0.144925
6,-2.823702,-2.547076,-0.784473
1,-1.206736,-3.640786,0.124667
1,-3.379387,-3.440741,-1.053748
6,0.352851,-1.806943,1.101688
7,1.582285,-1.166830,1.036658
8,0.165285,-2.633461,1.993372
6,2.468708,-1.484830,2.172630
1,2.882018,-2.497838,2.100687
1,3.282103,-0.757743,2.186308
1,1.899261,-1.424909,3.101227
7,0.524305,3.576054,0.559490
7,-0.610203,3.512524,0.784758
7,-1.627225,2.805974,0.932526
6,-2.952630,3.420626,0.838639
1,-3.116802,3.914677,-0.127243
1,-3.674055,2.609639,0.950214
1,-3.118430,4.142649,1.646689
9,4.643725,1.527855,-2.744138
1,-4.323256,-1.183084,-1.531289

Compound 2.5

E(B3LYP)	H(B3LYP)	G(B3LYP)
-1049.52879364	-1049.239295	-1049.310441

6,-0.005013,0.005377,-0.001625
6,-0.001346,0.003097,1.418252
6,1.225423,0.000964,2.089054
6,2.429531,0.034272,1.383597
6,2.421372,0.083876,-0.011492
6,1.210427,0.066717,-0.698553
1,1.232455,-0.012281,3.175109
1,3.370197,0.032349,1.926985
1,3.356104,0.126278,-0.563347
1,1.184716,0.082191,-1.783374
6,-1.267346,-0.240226,-0.625030
6,-2.263765,-0.953046,-0.455072
6,-2.844387,-1.984069,0.339802
6,-3.490495,-3.096320,-0.225494
6,-2.612012,-1.934473,1.741715
6,-3.861844,-4.152009,0.588939
1,-3.672802,-3.143135,-1.292487
6,-3.029421,-3.023027,2.522574
6,-3.628332,-4.145452,1.961058
1,-2.896306,-2.964312,3.597063
1,-3.935353,-4.992019,2.565650

6,-2.212532,-0.701383,2.531979
7,-1.205842,0.191312,2.187598
8,-2.890447,-0.465009,3.531302
6,-1.196278,1.408687,3.021588
1,-0.817057,1.214016,4.031709
1,-0.567554,2.153888,2.531733
1,-2.215476,1.785641,3.117028
7,-1.669017,0.920816,-2.615349
7,-2.706641,0.427284,-2.765996
7,-3.618747,-0.286716,-2.303343
6,-4.592210,-0.893382,-3.213644
1,-4.117366,-1.538542,-3.963443
1,-5.256152,-1.497941,-2.593777
1,-5.194966,-0.131703,-3.721728
9,-4.464675,-5.221965,0.032541

Compound 2.6

E(B3LYP)	H(B3LYP)	G(B3LYP)
-1148.76127652	-1148.47917	-1148.552296

6,1.924018,0.823679,-0.446666
6,2.247074,-0.504513,-0.057971
6,3.366802,-1.118374,-0.627797
6,4.180134,-0.444583,-1.539536
6,3.862937,0.868463,-1.867862
6,2.752031,1.512164,-1.343258
1,3.613269,-2.136449,-0.342024
1,5.050098,-0.917234,-1.982504
1,2.516438,2.527949,-1.638762
6,0.647124,1.306579,-0.024530
6,-0.504868,0.872414,0.096040
6,-1.365418,-0.248248,-0.094789
6,-2.634496,-0.127721,-0.685430
6,-0.833481,-1.535651,0.190481
6,-3.340095,-1.271449,-1.016736
1,-3.048528,0.848803,-0.906362
6,-1.601775,-2.660436,-0.146457
6,-2.838652,-2.546598,-0.771630
1,-1.218608,-3.640402,0.115366
1,-3.422867,-3.418585,-1.045170
6,0.359554,-1.823644,1.083483
7,1.580232,-1.163638,1.035789
8,0.184780,-2.677215,1.951944
6,2.466324,-1.489104,2.169992
1,2.898818,-2.492700,2.080712
1,3.266010,-0.747446,2.202600

1,1.890575,-1.457619,3.095993
7,0.522938,3.574992,0.547021
7,-0.611270,3.511058,0.773669
7,-1.626531,2.803505,0.926785
6,-2.954716,3.411184,0.819925
1,-3.118143,3.889001,-0.154054
1,-3.673412,2.599600,0.943550
1,-3.124110,4.145126,1.616183
9,-4.548924,-1.143993,-1.598990
9,4.651605,1.534305,-2.735618

Compound 2.7

E(B3LYP)	H(B3LYP)	G(B3LYP)
-1064.82010688	-1064.487709	-1064.562012

6,0.047755,-0.106429,-0.159411
6,-0.005476,-0.012040,1.260574
6,1.181482,0.065429,1.982574
6,2.425250,0.083354,1.332911
6,2.481570,0.039163,-0.064770
6,1.295821,-0.058640,-0.790874
1,1.166145,0.133342,3.065227
1,3.428679,0.069415,-0.590477
6,-1.171601,-0.432819,-0.822713
6,-2.188083,-1.115056,-0.634349
6,-2.773432,-2.116252,0.198399
6,-3.380734,-3.275463,-0.316841
6,-2.597689,-1.978975,1.601646
6,-3.767141,-4.308964,0.528676
1,-3.511262,-3.354658,-1.391418
6,-3.017531,-3.027870,2.432033
6,-3.570408,-4.192895,1.907855
1,-2.923334,-2.901688,3.505321
6,-2.252877,-0.688301,2.323070
7,-1.243254,0.199339,1.968103
8,-2.981307,-0.393971,3.270354
6,-1.288261,1.463496,2.727881
1,-0.960162,1.333286,3.765821
1,-0.642145,2.186481,2.227863
1,-2.314856,1.831881,2.749267
7,-1.558609,0.482340,-3.025776
7,-2.591940,-0.033000,-3.063211
7,-3.402264,-0.869454,-2.609614
6,-4.826102,-0.513425,-2.602839

1,-5.257883,-0.584446,-3.607926
1,-5.316915,-1.246536,-1.960787
1,-5.002210,0.490246,-2.198917
1,1.329070,-0.117604,-1.874061
1,-4.218523,-5.206273,0.113631
8,3.510582,0.160795,2.154409
6,4.800554,0.187919,1.562332
1,5.508187,0.243576,2.391317
1,4.995298,-0.721450,0.978863
1,4.928937,1.066092,0.915904
1,-3.868744,-4.997370,2.574089

Compound 2.8

E(B3LYP)	H(B3LYP)	G(B3LYP)
-1064.81902314	-1064.486736	-1064.561968

6,0.013292,0.050170,-0.011703
6,0.029099,0.043381,1.408115
6,1.259274,0.032344,2.071864
6,2.459461,0.061862,1.359334
6,2.440460,0.118036,-0.035409
6,1.225004,0.109874,-0.715239
1,1.271653,0.016170,3.157990
1,3.371539,0.158410,-0.593871
6,-1.257481,-0.188249,-0.623491
6,-2.224805,-0.934981,-0.429152
6,-2.807652,-1.950547,0.378173
6,-3.451110,-3.083800,-0.158269
6,-2.578883,-1.888456,1.776686
6,-3.829037,-4.143328,0.645289
1,-3.628087,-3.121409,-1.228189
6,-2.983279,-2.962335,2.583174
6,-3.581098,-4.094401,2.027649
1,-2.853009,-2.864817,3.653047
6,-2.173572,-0.643274,2.550712
7,-1.169790,0.241477,2.186691
8,-2.847791,-0.391290,3.549566
6,-1.156305,1.475119,2.995936
1,-0.769624,1.300817,4.007098
1,-0.530816,2.210176,2.487126
1,-2.174954,1.853821,3.090950
7,-1.662394,0.907796,-2.641965
7,-2.692278,0.397722,-2.794478
7,-3.596993,-0.323111,-2.326342
6,-4.584875,-0.913515,-3.230558
1,-4.124158,-1.556448,-3.991387

1,-5.245667,-1.519721,-2.608592
1,-5.189245,-0.144793,-3.726640
1,1.193115,0.129667,-1.799854
1,-4.313465,-5.022746,0.232903
1,3.403976,0.053140,1.895934
8,-3.978467,-5.186518,2.737405
6,-3.786354,-5.181679,4.145569
1,-4.346163,-4.368673,4.624828
1,-4.165290,-6.141693,4.500258
1,-2.723868,-5.090931,4.405706

Compound 2.9

E(B3LYP)	H(B3LYP)	G(B3LYP)
-1049.52628586	-1049.23672	-1049.307422

6,1.514419,1.100150,-0.369994
6,2.081077,-0.139766,0.026875
6,3.355974,-0.489818,-0.430861
6,4.082665,0.373921,-1.251419
6,3.550464,1.607636,-1.627514
6,2.280426,1.944122,-1.183693
1,3.782320,-1.441269,-0.129130
1,5.070822,0.085606,-1.596993
1,4.091803,2.299787,-2.263561
6,0.141276,1.327645,-0.060740
6,-0.909445,0.673980,-0.058999
6,-1.501277,-0.585218,-0.375619
6,-2.694801,-0.705111,-1.109120
6,-0.751017,-1.749317,-0.059346
6,-3.127871,-1.945168,-1.563160
1,-3.257898,0.194029,-1.338140
6,-1.222741,-2.990048,-0.510250
6,-2.381079,-3.091325,-1.275503
1,-4.044046,-2.019596,-2.142673
1,-0.674056,-3.882169,-0.227798
1,-2.713041,-4.063878,-1.627430
6,0.373399,-1.822195,0.959419
7,1.461421,-0.961363,1.032470
8,0.266880,-2.704198,1.809793
6,2.288123,-1.166052,2.237850
1,2.878260,-2.088101,2.179827
1,2.954897,-0.309452,2.345866
1,1.636885,-1.243674,3.109583
7,-0.474727,3.451037,0.787844
7,-1.578110,3.123087,0.901057
7,-2.431347,2.211144,0.892007

6,-3.830265,2.549320,0.620629
1,-3.956733,3.073077,-0.335228
1,-4.371135,1.602429,0.583315
1,-4.257829,3.158282,1.425718
9,1.744807,3.118983,-1.562536

Compound 2.10

E(B3LYP)	H(B3LYP)	G(B3LYP)
-1128.16488788	-1127.816459	-1127.895812

6,0.035889,-0.030069,-0.055829
6,-0.012839,0.012726,1.360071
6,1.178870,0.023117,2.088993
6,2.422358,0.017390,1.450551
6,2.448801,0.002333,0.050357
6,1.283511,-0.026421,-0.716318
1,1.130308,0.045967,3.174474
1,3.409666,-0.001290,-0.460544
6,-1.217317,-0.264105,-0.708229
6,-2.211096,-0.986951,-0.552803
6,-2.764945,-2.033056,0.244090
6,-3.351592,-3.179495,-0.318508
6,-2.573907,-1.951424,1.650165
6,-3.704442,-4.234581,0.505181
1,-3.501610,-3.254502,-1.389353
6,-2.973043,-3.039964,2.440166
6,-3.512157,-4.194646,1.883232
1,-2.873503,-2.956285,3.516804
1,-3.804340,-5.041781,2.494363
6,-2.242551,-0.685830,2.418825
7,-1.249190,0.218654,2.074476
8,-2.962338,-0.438269,3.385877
6,-1.290806,1.466864,2.857464
1,-0.931787,1.323873,3.883674
1,-0.668396,2.207500,2.352584
1,-2.321273,1.820762,2.912783
7,-1.904969,1.199405,-2.484126
7,-2.931498,0.669542,-2.561599
7,-3.748093,-0.143172,-2.081109
6,-4.756856,-0.752018,-2.950084
1,-4.312310,-1.268669,-3.809819
1,-5.290473,-1.478032,-2.334690
1,-5.477727,-0.007653,-3.307509
9,-4.248737,-5.337476,-0.048188
6,3.704318,0.058174,2.248637
1,4.484536,-0.554550,1.783746

1,4.097089,1.081416,2.320029
1,3.552189,-0.304961,3.270194
6,1.347345,-0.095759,-2.221937
1,0.977135,-1.061560,-2.588859
1,0.724074,0.676787,-2.683455
1,2.375245,0.027250,-2.576552

Compound 2.11

E(B3LYP)	H(B3LYP)	G(B3LYP)
-1028.93134921	-1028.575551	-1028.652899

6,0.000444,-0.004885,-0.000797
6,-0.000116,-0.003297,1.416732
6,1.215280,-0.002623,2.105641
6,2.436699,0.021914,1.426535
6,2.415723,0.047238,0.026511
6,1.225471,0.029638,-0.701359
1,1.202331,-0.010635,3.192361
1,3.358808,0.067454,-0.516242
6,-1.272433,-0.227957,-0.619324
6,-2.247373,-0.973076,-0.450621
6,-2.769583,-2.046279,0.332279
6,-3.356315,-3.191703,-0.234795
6,-2.538231,-1.995526,1.732919
6,-3.675331,-4.290518,0.554056
1,-3.530612,-3.211865,-1.306226
6,-2.890920,-3.108870,2.508322
6,-3.427975,-4.255292,1.929759
1,-2.757090,-3.049029,3.583224
1,-3.674285,-5.110752,2.552319
6,-2.198150,-0.740729,2.518177
7,-1.212469,0.172696,2.178474
8,-2.905077,-0.514005,3.499803
6,-1.239256,1.399165,2.995754
1,-0.866828,1.225998,4.012519
1,-0.621272,2.151686,2.503426
1,-2.267656,1.754656,3.075568
7,-2.035013,1.279458,-2.333463
7,-3.059146,0.742002,-2.388994
7,-3.848604,-0.094500,-1.903904
6,-4.902852,-0.665347,-2.742692
1,-4.506915,-1.139154,-3.649724
1,-5.398688,-1.422473,-2.133017
1,-5.645073,0.090909,-3.023936
6,3.743961,0.053354,2.183157
1,4.519466,-0.523309,1.667032

1,4.120281,1.080057,2.287093
1,3.632918,-0.356629,3.192309
6,1.239386,0.004842,-2.209681
1,0.869276,-0.954918,-2.592379
1,0.590715,0.781606,-2.627019
1,2.253112,0.152290,-2.594716
1,-4.113329,-5.174803,0.098928

Transition States: *Trans* lactam *anti* regioisomers

Compound 2.1

E(B3LYP)	H(B3LYP)	G(B3LYP)
-950.302430875	-950.005388	-950.071848

6,0.073128,-0.465110,0.117539
6,0.042232,0.096101,1.428132
6,1.222982,0.441527,2.076308
6,2.453968,0.234256,1.450464
6,2.497942,-0.321303,0.170610
6,1.321557,-0.665292,-0.492368
1,1.164990,0.877109,3.069206
1,3.373264,0.508017,1.960591
1,3.454423,-0.483412,-0.318730
1,1.356771,-1.087695,-1.489157
6,-1.196123,-0.754835,-0.501154
6,-2.442086,-0.702427,-0.440722
6,-3.657959,-0.324993,0.231167
6,-4.934757,-0.826828,-0.065432
6,-3.525794,0.626582,1.280878
6,-6.051854,-0.374591,0.635109
1,-5.034071,-1.584978,-0.834753
6,-4.653802,1.097578,1.948370
6,-5.918106,0.595504,1.631435
1,-7.032619,-0.778290,0.398670
1,-4.538737,1.852657,2.721252
1,-6.794110,0.957844,2.161985
6,-2.128109,1.136949,1.528332
7,-1.229555,0.218605,2.079968
6,-1.684236,-0.987301,2.777124
1,-1.793507,-1.848578,2.105348
1,-0.953853,-1.238143,3.552614
1,-2.643667,-0.790184,3.259269
8,-1.777532,2.243793,1.156016
1,-4.864227,-0.498478,-2.906128
6,-3.966803,-0.763328,-3.466196
7,-3.071847,-1.444874,-2.521155
1,-3.521173,0.151209,-3.874056

1,-4.253003,-1.428939,-4.288944
7,-1.881053,-1.612712,-2.883610
7,-0.780545,-1.635106,-2.507267

Compound 2.2

E(B3LYP)	H(B3LYP)	G(B3LYP)
-1049.53542498	-1049.24579	-1049.314311

6,-0.001325,0.006687,0.001949
6,-0.001153,-0.000464,1.428836
6,1.192823,-0.008620,2.140715
6,2.392157,-0.012946,1.436352
6,2.433235,-0.011556,0.046920
6,1.235663,0.001623,-0.663079
1,1.190542,-0.002595,3.224838
1,3.392224,-0.015210,-0.460278
6,-1.282720,0.052963,-0.652912
6,-2.524062,0.138243,-0.550760
6,-3.717023,0.281252,0.241712
6,-5.020276,0.005376,-0.199972
6,-3.530931,0.732196,1.578604
6,-6.109691,0.202294,0.647177
1,-5.162794,-0.380428,-1.203587
6,-4.629950,0.959538,2.403247
6,-5.920883,0.691031,1.942163
1,-4.472163,1.340297,3.408637
1,-6.774762,0.859836,2.592119
6,-2.106706,1.029034,1.975413
7,-1.261585,-0.079780,2.104874
6,-1.784542,-1.438113,2.278769
1,-1.946292,-1.954540,1.323857
1,-1.069279,-2.014408,2.873585
1,-2.729607,-1.395958,2.823388
8,-1.689595,2.171086,2.059891
1,-4.937403,1.401504,-2.700376
6,-4.051432,1.339746,-3.333118
7,-3.189082,0.306575,-2.743462
1,-3.564813,2.321479,-3.358318
1,-4.364831,1.060773,-4.345858
7,-2.008700,0.238154,-3.165594
7,-0.910880,0.017076,-2.850941
1,1.249877,0.010214,-1.745784
1,-7.111873,-0.022650,0.292691
9,3.549675,-0.021372,2.127027

Compound 2.3

E(B3LYP)	H(B3LYP)	G(B3LYP)
-1049.53507923	-1049.245439	-1049.314043

6,-0.001199,-0.000497,-0.001566
6,-0.000075,0.003078,1.424302
6,1.197718,0.001619,2.130364
6,2.415191,-0.009650,1.446476
6,2.427875,-0.019053,0.050688
6,1.234136,-0.011531,-0.668209
1,1.164290,0.014353,3.215560
1,3.373751,-0.027059,-0.483880
6,-1.284574,0.042381,-0.656290
6,-2.525933,0.130105,-0.555686
6,-3.718124,0.274957,0.236678
6,-5.021902,-0.003274,-0.204291
6,-3.534441,0.728486,1.573272
6,-6.116556,0.189859,0.635384
1,-5.165981,-0.390370,-1.206916
6,-4.627753,0.956067,2.403465
6,-5.902319,0.678207,1.920204
1,-4.501184,1.336789,3.411741
6,-2.108823,1.031776,1.968133
7,-1.263624,-0.071747,2.100319
6,-1.784457,-1.428800,2.287825
1,-1.945705,-1.954507,1.337862
1,-1.066154,-1.997983,2.885651
1,-2.728234,-1.386191,2.834946
8,-1.702458,2.178606,2.039709
1,-4.925305,1.429097,-2.679689
6,-4.042012,1.359888,-3.315582
7,-3.196313,0.303851,-2.741970
1,-3.538356,2.333226,-3.329316
1,-4.363439,1.099956,-4.330848
7,-2.016996,0.225679,-3.167680
7,-0.920356,-0.003104,-2.854794
1,1.245834,-0.010514,-1.751286
1,-7.127859,-0.028696,0.308870
9,-6.962892,0.882475,2.726560
1,3.348240,-0.008710,2.002800

Compound 2.4

E(B3LYP)	H(B3LYP)	G(B3LYP)
-1049.53519672	-1049.245642	-1049.314342

6,2.215503,0.446793,-0.150590
6,2.338785,-0.974473,-0.117340
6,3.593398,-1.568847,-0.026861
6,4.748756,-0.787866,0.024264
6,4.613566,0.595130,-0.016139
6,3.380357,1.226022,-0.098444
1,3.657700,-2.651747,0.008263
1,5.736021,-1.231231,0.097064
1,3.326241,2.306665,-0.117280
6,0.881356,0.987861,-0.200197
6,-0.348637,0.775656,-0.184787
6,-1.475575,-0.115768,-0.097991
6,-2.790618,0.206863,-0.467245
6,-1.205099,-1.422433,0.396235
6,-3.813931,-0.728395,-0.321765
1,-2.992515,1.187701,-0.884096
6,-2.242510,-2.334832,0.572271
6,-3.547232,-1.992762,0.209276
1,-2.025025,-3.315517,0.986501
1,-4.351571,-2.711504,0.337896
6,0.225973,-1.688804,0.791522
7,1.148196,-1.759061,-0.258299
6,0.730503,-2.008956,-1.640502
1,0.529593,-1.083521,-2.195700
1,1.526697,-2.558360,-2.152330
1,-0.169920,-2.626221,-1.643761
8,0.570842,-1.717282,1.960359
1,-2.997090,2.699614,0.917923
6,-2.176880,3.417699,0.887384
7,-1.210778,2.903620,-0.092987
1,-1.744164,3.504516,1.890508
1,-2.575655,4.389926,0.575263
7,-0.068936,3.425468,-0.098929
7,1.062979,3.205450,-0.250720
9,5.726011,1.357800,0.030973
1,-4.825669,-0.467071,-0.619484

Compound 2.5

E(B3LYP)	H(B3LYP)	G(B3LYP)
-1049.53523882	-1049.245654	-1049.314328

6,-0.000210,0.004288,0.000954
6,-0.000165,-0.001112,1.426924
6,1.197988,-0.002672,2.132492
6,2.415184,-0.005614,1.448085
6,2.428377,-0.007531,0.052180

6,1.234671,0.000202,-0.666593
1,1.164840,0.004011,3.217722
1,3.348364,-0.004121,2.004320
1,3.374358,-0.009668,-0.482195
1,1.246055,0.007573,-1.749635
6,-1.283909,0.048615,-0.653097
6,-2.525352,0.138764,-0.553318
6,-3.715666,0.281396,0.242619
6,-5.015365,0.008271,-0.208693
6,-3.530619,0.729438,1.581103
6,-6.085298,0.212762,0.651929
1,-5.186882,-0.374343,-1.207408
6,-4.632879,0.958246,2.401803
6,-5.926149,0.694799,1.946902
1,-4.479349,1.338866,3.407477
1,-6.797608,0.854471,2.572689
6,-2.107945,1.024681,1.983979
7,-1.263433,-0.083757,2.100617
6,-1.783756,-1.442717,2.271930
1,-1.938926,-1.960373,1.316397
1,-1.068960,-2.017307,2.869090
1,-2.731316,-1.405180,2.812702
8,-1.695305,2.167534,2.084062
1,-4.928417,1.420901,-2.689484
6,-4.049049,1.340771,-3.329288
7,-3.195329,0.300253,-2.738745
1,-3.548813,2.315106,-3.368075
1,-4.376072,1.056623,-4.336152
7,-2.016299,0.221390,-3.163583
7,-0.919323,-0.003708,-2.848582
9,-7.329961,-0.061303,0.207915

Compound2.61

E(B3LYP)	H(B3LYP)	G(B3LYP)
-1148.76786085	-1148.485748	-1148.556603

6,2.214978,0.444272,-0.143596
6,2.339198,-0.976932,-0.121970
6,3.594126,-1.570927,-0.033629
6,4.748194,-0.788882,0.027464
6,4.612030,0.594417,-0.001389
6,3.378431,1.224800,-0.081996
1,3.659540,-2.653965,-0.007489
1,5.735739,-1.231766,0.099368
1,3.323296,2.305475,-0.092343
6,0.880044,0.984077,-0.191766

6,-0.350361,0.773405,-0.175602
6,-1.473777,-0.121851,-0.090010
6,-2.787945,0.210891,-0.449730
6,-1.201129,-1.432223,0.394822
6,-3.790058,-0.737132,-0.293813
1,-3.021149,1.185524,-0.860734
6,-2.240619,-2.342589,0.573003
6,-3.549260,-2.006064,0.222615
1,-2.024941,-3.325401,0.982024
1,-4.371479,-2.703399,0.341881
6,0.229884,-1.705625,0.783047
7,1.148943,-1.760046,-0.270527
6,0.730506,-1.997297,-1.654721
1,0.524785,-1.067335,-2.200506
1,1.528564,-2.537733,-2.173052
1,-0.166732,-2.619083,-1.663356
8,0.578057,-1.755478,1.950116
1,-3.012161,2.731114,0.897065
6,-2.181540,3.436888,0.866024
7,-1.211734,2.900094,-0.099273
1,-1.756965,3.529939,1.872016
1,-2.564100,4.410243,0.538216
7,-0.069191,3.419464,-0.111137
7,1.062199,3.193939,-0.259934
9,-5.048751,-0.407908,-0.650815
9,5.723298,1.357357,0.055483

Compound 2.7

E(B3LYP)	H(B3LYP)	G(B3LYP)
-1064.82596067	-1064.493531	-1064.565951

6,-0.036238,-0.007322,0.029324
6,-0.048638,-0.010622,1.451120
6,1.133964,-0.010937,2.185616
6,2.365440,-0.011605,1.518323
6,2.395087,-0.019942,0.115063
6,1.215875,-0.013855,-0.613065
1,1.066881,-0.000264,3.266542
1,3.360124,-0.021964,-0.381548
6,-1.307991,0.040523,-0.640496
6,-2.550988,0.126742,-0.556391
6,-3.752298,0.269214,0.222190
6,-5.051275,-0.004484,-0.234624
6,-3.582596,0.716434,1.562878
6,-6.150530,0.190681,0.600094

1,-5.182507,-0.387301,-1.241030
6,-4.691482,0.941403,2.375036
6,-5.977339,0.675152,1.898891
1,-4.544768,1.319199,3.383310
6,-2.164591,1.012590,1.981991
7,-1.318039,-0.094523,2.115186
6,-1.842172,-1.454773,2.265775
1,-1.976879,-1.965202,1.303557
1,-1.140937,-2.033987,2.874702
1,-2.801668,-1.419271,2.785256
8,-1.753587,2.155649,2.087387
1,-4.922798,1.430310,-2.704198
6,-4.036486,1.364786,-3.336269
7,-3.188831,0.314741,-2.755999
1,-3.538242,2.340982,-3.349459
1,-4.351864,1.101785,-4.352848
7,-2.003120,0.248501,-3.164906
7,-0.909145,0.022058,-2.841253
1,1.249696,-0.008716,-1.695718
1,-7.148574,-0.032751,0.232742
8,3.577579,-0.007024,2.138157
6,3.610307,0.044258,3.557107
1,3.136958,-0.840192,4.003473
1,4.666777,0.063646,3.830138
1,3.118659,0.948596,3.937728
1,-6.838685,0.842350,2.539415

Compound 2.8

E(B3LYP)	H(B3LYP)	G(B3LYP)
-1064.82586785	-1064.493465	-1064.566093

6,0.032242,-0.010062,-0.027933
6,0.049806,-0.010677,1.398176
6,1.255602,-0.011347,2.090568
6,2.465623,-0.020958,1.393440
6,2.462136,-0.029304,-0.002466
6,1.260410,-0.020534,-0.707965
1,1.233960,-0.000491,3.176144
1,3.401923,-0.036884,-0.547876
6,-1.258770,0.036724,-0.666281
6,-2.497905,0.127250,-0.542294
6,-3.678068,0.281074,0.263990
6,-4.995460,0.020525,-0.155144
6,-3.480186,0.729079,1.595559
6,-6.069221,0.227261,0.697503
1,-5.161370,-0.365305,-1.155180

6,-4.559399,0.972073,2.443890
6,-5.862740,0.719371,1.996995
1,-4.367853,1.353584,3.440262
6,-2.050175,1.018769,1.982943
7,-1.206528,-0.090244,2.087317
6,-1.730498,-1.447638,2.258422
1,-1.888362,-1.963543,1.302733
1,-1.016492,-2.024503,2.854609
1,-2.677833,-1.407315,2.799623
8,-1.637125,2.162037,2.080345
1,-4.931065,1.415701,-2.659067
6,-4.054746,1.343488,-3.304181
7,-3.199053,0.296669,-2.729902
1,-3.555102,2.318731,-3.332570
1,-4.386713,1.073704,-4.313661
7,-2.025106,0.216135,-3.169691
7,-0.924799,-0.013577,-2.869867
1,1.260031,-0.017593,-1.791204
1,-7.086404,0.020782,0.379929
8,-6.986372,0.911355,2.741225
6,-6.845317,1.430493,4.056329
1,-6.370929,2.420065,4.049001
1,-7.858520,1.517166,4.452242
1,-6.262659,0.754498,4.695681
1,3.404990,-0.020310,1.939222

Compound 2.9

E(B3LYP)	H(B3LYP)	G(B3LYP)
-1049.5297086	-1049.240176	-1049.308904

6,-1.764144,0.465577,0.123777
6,-1.912898,-0.953141,0.220554
6,-3.161541,-1.561726,0.181900
6,-4.311702,-0.785155,0.032322
6,-4.205073,0.597659,-0.091219
6,-2.951096,1.196898,-0.054747
1,-3.217561,-2.642884,0.253201
1,-5.075598,1.230320,-0.228673
6,-0.431058,1.012123,0.159765
6,0.799488,0.775798,0.129563
6,1.904281,-0.152536,0.060383
6,3.234937,0.153868,0.389388
6,1.601512,-1.479789,-0.352398
6,4.236391,-0.808243,0.268165
1,3.467157,1.143546,0.765047
6,2.614908,-2.422988,-0.504408

6,3.935057,-2.091468,-0.193178
1,2.364564,-3.419582,-0.857528
1,4.721648,-2.832668,-0.302655
6,0.158981,-1.752301,-0.679106
7,-0.723574,-1.726302,0.406008
6,-0.272013,-1.869626,1.792055
1,-0.049747,-0.905407,2.266617
1,-1.058495,-2.370397,2.365330
1,0.623648,-2.492914,1.819766
8,-0.231698,-1.868558,-1.828152
1,3.369647,2.537778,-1.067487
6,2.603850,3.293241,-0.889758
7,1.750802,2.778537,0.193953
1,2.042539,3.456529,-1.817005
1,3.095771,4.226117,-0.591328
7,0.660616,3.390680,0.370370
7,-0.471082,3.232388,0.578031
1,-5.289112,-1.256923,-0.001269
1,5.258408,-0.552789,0.534542
9,-2.905225,2.529906,-0.211785

Compound 2.10

E(B3LYP)	H(B3LYP)	G(B3LYP)
-1128.16373834	-1127.815331	-1127.892478

6,-0.003528,-0.030578,-0.012187
6,-0.005674,0.009543,1.414675
6,1.173382,0.029039,2.144068
6,2.411262,0.037839,1.492034
6,2.412040,0.066085,0.095188
6,1.244085,0.042505,-0.676473
1,1.113935,0.066211,3.228221
1,3.366319,0.126050,-0.424281
6,-1.303080,-0.083495,-0.647037
6,-2.542449,0.086654,-0.558712
6,-3.702498,0.438467,0.226175
6,-5.031641,0.253022,-0.184161
6,-3.464620,0.995178,1.515165
6,-6.065838,0.658222,0.647874
1,-5.261947,-0.230167,-1.123602
6,-4.528181,1.421666,2.307967
6,-5.846940,1.253509,1.884859
1,-4.320528,1.882917,3.269101
1,-6.689959,1.566268,2.491484
6,-2.026746,1.188444,1.907522
7,-1.275210,0.022896,2.079156

6,-1.884263,-1.281956,2.337796
1,-2.056323,-1.858994,1.420371
1,-1.219130,-1.854657,2.992187
1,-2.836737,-1.143840,2.853277
8,-1.522956,2.298590,1.957696
1,-4.850713,0.737072,-3.039646
6,-4.019035,0.249652,-3.548818
7,-3.331632,-0.581200,-2.546409
1,-3.361600,1.020101,-3.968687
1,-4.421633,-0.367227,-4.360311
7,-2.223616,-1.068322,-2.906163
7,-1.150274,-1.285807,-2.509626
9,-7.335901,0.464178,0.233372
6,1.378876,0.149226,-2.177850
1,1.341263,-0.832156,-2.661272
1,0.577245,0.751776,-2.612961
1,2.335685,0.614996,-2.435272
6,3.700982,0.033708,2.276550
1,3.951443,-0.978277,2.622245
1,4.539994,0.389311,1.670061
1,3.630070,0.670058,3.165592

Compound 2.11

E(B3LYP)	H(B3LYP)	G(B3LYP)
-1028.93070735	-1028.574863	-1028.649822

6,-0.000148,-0.003491,-0.002056
6,-0.000514,0.001564,1.425471
6,1.178947,0.003456,2.154460
6,2.416525,0.027873,1.502443
6,2.416130,0.089862,0.106827
6,1.247421,0.086071,-0.664351
1,1.119843,0.014475,3.239264
1,3.370084,0.161900,-0.411737
6,-1.300789,-0.038948,-0.636974
6,-2.539698,0.128127,-0.538388
6,-3.701942,0.456076,0.255079
6,-5.035328,0.273057,-0.146476
6,-3.461700,0.981693,1.556053
6,-6.089198,0.644421,0.686566
1,-5.237003,-0.193500,-1.102421
6,-4.521629,1.380830,2.366864
6,-5.838930,1.212500,1.937255
1,-4.308693,1.816415,3.339226
1,-6.663137,1.514843,2.577116
6,-2.021466,1.167319,1.945121

7,-1.269099,-0.000745,2.092206
6,-1.878355,-1.311342,2.318827
1,-2.046583,-1.866375,1.387275
1,-1.215592,-1.898969,2.962396
1,-2.833104,-1.185353,2.833252
8,-1.517219,2.276616,2.009556
1,-4.840840,0.873484,-2.982224
6,-4.021203,0.394080,-3.518023
7,-3.333029,-0.474670,-2.549969
1,-3.360628,1.171048,-3.920739
1,-4.440141,-0.191321,-4.344767
7,-2.225888,-0.949397,-2.929182
7,-1.152160,-1.182810,-2.543073
6,1.381344,0.230706,-2.162653
1,1.340368,-0.737622,-2.671415
1,0.580413,0.846034,-2.580877
1,2.339038,0.700646,-2.409215
6,3.706605,0.006140,2.286286
1,3.948945,-1.010453,2.624163
1,4.548279,0.359840,1.682339
1,3.641459,0.636107,3.180441
1,-7.112328,0.487635,0.355641

Isomerization Transition States
Compound 2.1
E(B3LYP) H(B3LYP) G(B3LYP)
-746.19933519 -745.96006 -746.01331

6,0.000000,0.000000,0.000000
6,0.000000,0.000000,1.432644
6,1.268580,0.000000,2.047091
6,2.451815,0.046026,1.309565
6,2.431261,0.099163,-0.081710
6,1.199761,0.065071,-0.723421
1,1.354808,-0.037041,3.123553
1,3.397786,0.044804,1.844219
1,3.352140,0.148809,-0.654252
1,1.137263,0.069822,-1.807264
6,-1.250554,-0.201289,-0.624211
6,-2.391327,-0.610890,-0.727112
6,-3.505224,-1.173069,-0.043121
6,-4.496780,-2.010454,-0.563417
6,-3.458892,-0.885462,1.339588
6,-5.428406,-2.592025,0.296622
1,-4.522214,-2.210286,-1.630030
6,-4.410138,-1.460337,2.182740

6,-5.377530,-2.328283,1.666067
1,-6.193930,-3.250924,-0.103271
1,-4.406412,-1.219651,3.241532
1,-6.104343,-2.779853,2.335272
6,-2.569712,0.211160,1.930128
7,-1.164552,0.077021,2.257511
6,-0.897281,0.606780,3.614934
1,-0.341514,-0.134197,4.197476
1,-0.324256,1.539923,3.580557
1,-1.841679,0.802635,4.112995
8,-3.176583,1.160874,2.393745

Compound 2.10

E(B3LYP)	H(B3LYP)	G(B3LYP)
-924.069034062	-923.778283	-923.842331

6,-0.003763,0.001234,0.004457
6,0.001691,-0.005655,1.435095
6,1.268091,-0.006229,2.050187
6,2.460819,0.048214,1.322669
6,2.412703,0.103108,-0.072276
6,1.192470,0.069591,-0.739647
1,1.351514,-0.050801,3.126948
1,3.335680,0.153823,-0.644608
6,-1.257031,-0.206451,-0.607498
6,-2.404081,-0.594154,-0.731665
6,-3.510626,-1.166584,-0.044770
6,-4.503808,-1.992906,-0.578006
6,-3.459197,-0.895896,1.341974
6,-5.421085,-2.565700,0.294488
1,-4.556543,-2.199296,-1.640822
6,-4.415475,-1.473715,2.178318
6,-5.390008,-2.333489,1.664202
1,-4.412044,-1.244623,3.239300
1,-6.130859,-2.799289,2.304927
6,-2.569443,0.192996,1.944505
7,-1.162081,0.057633,2.263646
6,-0.894099,0.566987,3.629127
1,-0.330748,-0.179469,4.196925
1,-0.328381,1.504930,3.608914
1,-1.838012,0.746936,4.133906
8,-3.175615,1.133999,2.427038
9,-6.373664,-3.375940,-0.209116
6,1.122940,0.077464,-2.247008
1,0.670189,-0.846280,-2.628204
1,0.508119,0.907080,-2.615805

1,2.120464,0.172524,-2.685823
6,3.784491,0.081564,2.050430
1,4.084549,1.113023,2.279653
1,3.735511,-0.461026,3.000535
1,4.582883,-0.361939,1.446490

Compound 2.11

E(B3LYP)	H(B3LYP)	G(B3LYP)
-824.836269456	-824.538128	-824.600013

6,-0.001529,0.001627,-0.001184
6,-0.001071,-0.002430,1.429413
6,1.261961,-0.006837,2.051025
6,2.458546,0.042044,1.329333
6,2.416263,0.095018,-0.065724
6,1.198635,0.065229,-0.738728
1,1.338828,-0.049906,3.128524
1,3.341640,0.141921,-0.634699
6,-1.253820,-0.201067,-0.619154
6,-2.399648,-0.593822,-0.740366
6,-3.513134,-1.159928,-0.057390
6,-4.508911,-1.990630,-0.580379
6,-3.463321,-0.882176,1.327337
6,-5.439445,-2.576196,0.278475
1,-4.538504,-2.182875,-1.648333
6,-4.412808,-1.460750,2.169437
6,-5.383927,-2.323047,1.649621
1,-4.405243,-1.227715,3.230024
1,-6.109849,-2.777824,2.317662
6,-2.571202,0.212235,1.917425
7,-1.168611,0.069266,2.252114
6,-0.908744,0.592996,3.613163
1,-0.353951,-0.149268,4.194904
1,-0.337887,1.527788,3.586771
1,-1.856070,0.783665,4.108043
8,-3.174205,1.168043,2.373700
6,1.137065,0.072717,-2.246543
1,0.678100,-0.847096,-2.629794
1,0.531143,0.907435,-2.618841
1,2.137768,0.159180,-2.679916
6,3.779038,0.072375,2.063125
1,4.079663,1.102777,2.296526
1,3.725228,-0.472584,3.011672
1,4.579834,-0.370759,1.462027
1,-6.207882,-3.230194,-0.124040